KOOTENAY LAKE GEOTHERMAL PROJECT – PHASE TWO

GEOLOGICAL, GEOCHEMICAL AND GEOSPATIAL INVESTIGATIONS INTO THE GEOTHERMAL POTENTIAL OF THE EAST SHORE OF KOOTENAY LAKE – SUMMARY REPORT, JANUARY 2023

Geoscience BC Report 2023-06

Prepared For:

Geoscience BC

Prepared By:
Gordon MacMahon (1), **Robert McQuarrie** (2), **Daniel Gatto** (3), **& Stefan Humphries** (4)

On behalf of
South Kootenay Lake Community Services Society

Community Connections

Regional District Central Kootenay

Natural Sciences and Engineering Research Council of Canada
Canada

Colleges and Institutes Canada
Collèges et instituts Canada

Selkirk College

University of Victoria

KOOTENAY LAKE GEOTHERMAL PROJECT – PHASE TWO

Geological, Geochemical and Geospatial Investigations into the Geothermal Potential of the East Shore of Kootenay Lake – Summary Report, January 2023

TABLE OF CONTENTS

Contributors:

1. Gordon MacMahon, BSc, MA - Retired Geologist, Volunteer Project Lead, SKLCSS
2. Robert McQuarrie, BA, MSc – Instructor, Selkirk College
3. Daniel Gatto, BSc - Retired Geologist, Volunteer
4. Stefan Humphries, MSc, Hydrogeologist, Volunteer

1) Project Introduction

Geothermal research is generally motivated by geothermal energy's potential for stable baseload-power supply which could help meet Canadian greenhouse gas reduction measures (Grasby et al., 2012). In addition to higher temperature geothermal power developments, there is a spectrum of direct heat commercial applications for geothermal fluid temperatures in the range of 40-80°C. It is this range of geothermal temperatures which is the focus of this project.

The Kootenay Lake area (see Figure 1) is host to several hot spring occurrences, specifically Ainsworth, Dewar Creek, Riondel and Crawford Creek (see Figure 5). Ktunaxa First Nation's peoples have experienced the hot springs for millennia and have been welcoming guests since the early 1930s. In the historic Bluebell Mine at Riondel, temperatures of 40°C and inflow rates of 150 litres per second were encountered during mining operations (Desrochers, 1992). Surface temperatures measured at the Dewar Creek hot spring exceed 82°C (Grasby et al., 2000), making it the hottest known surface expression of geothermal water in British Columbia. In addition, geochemical analyses of several hot springs in the Kootenay Lake area indicate that at depths of 2-3 km, water temperatures may exceed 120°C (Grasby et al, 2000).

A preliminary evaluation of the Kootenay Lake area geology indicates that the East Shore of Kootenay Lake may be well suited to serve as a pilot project to test the feasibility of developing a geothermal direct heat source for renewable district heating. A successful geothermal project in the Kootenays could create a template for similar developments within the Columbia Basin region. A confirmed geothermal district heat source on the East Shore could bolster a local green economy, support local agri-business, and improve food security while increasing employment and augmenting economic resilience.

Phase One of this project saw a Selkirk College Bachelor of GIS student source and compile all available public domain open-file project geothermal related data in 2021 (report available on Geoscience BC website). The data collected included remote sensing data such as Light Detection and Ranging (LiDAR) and infrared imagery, as well as geological and geophysical data. The interpretation of this data set was promising, helping to better frame the numerous hydrothermal mineral deposits and forming the beginning of a local geologic model for geothermal energy.

Phase Two of the project saw the hiring of a fourth-year geology student from Simon Fraser University to carry out geological and geochemical field investigations across the area of interest. The area of field study extends from just north of Riondel, south to Gray Creek on the east shore of Kootenay Lake, British Columbia (see Figure 1). This also includes Pilot Peninsula, in the west, as well as

an area to the east up the Crawford Creek drainage. Preliminary results from this fieldwork identified an area on Crawford Creek for the drone-based evaluation conducted in the fall of 2022, at the end of Phase Two. The project study covers an area of between 350 and 400 km^2 on the east shore of Kootenay Lake and the area of interest for the GIS drone work is also highlighted in Figure 1 (below).

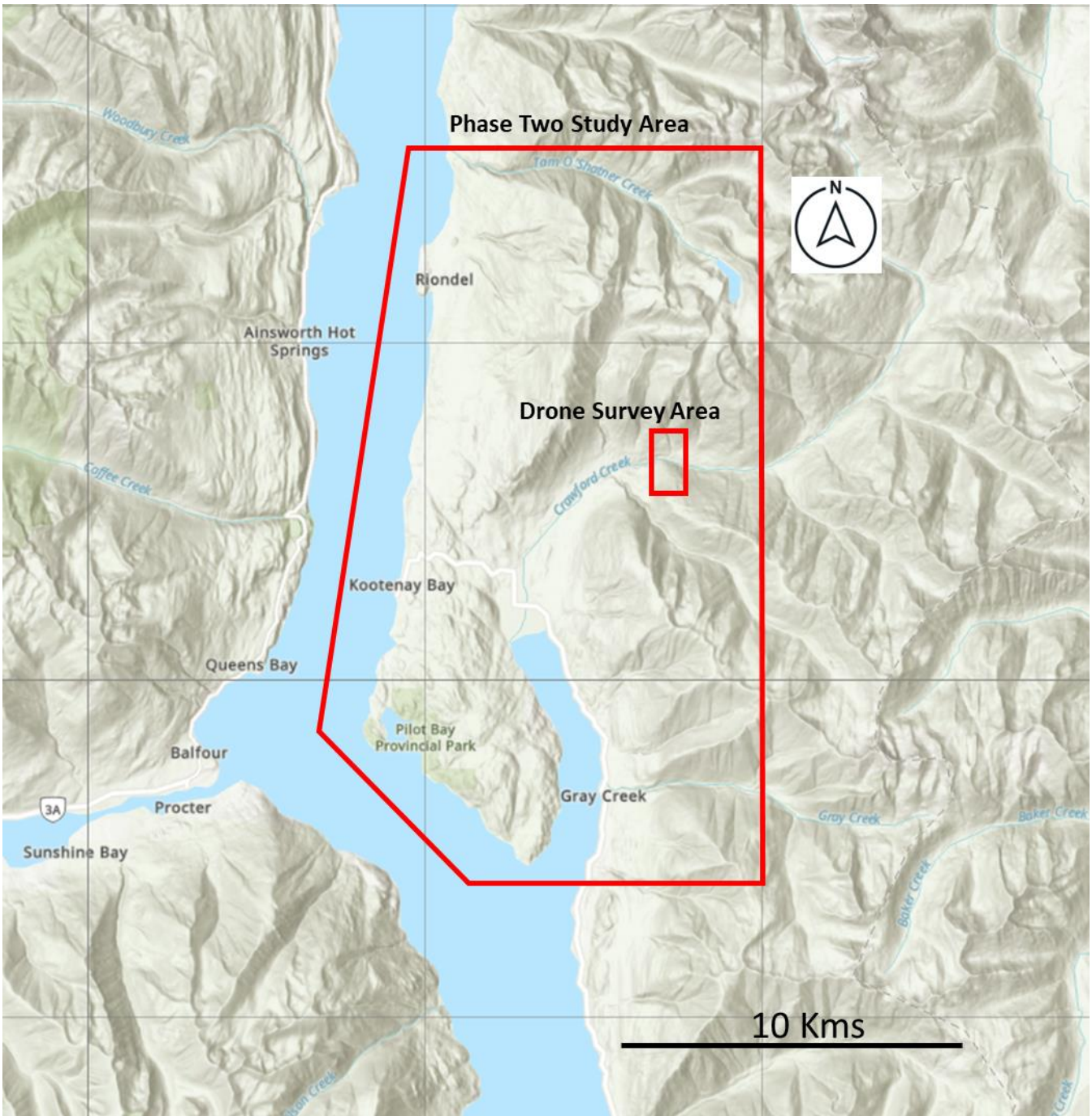

Figure 1 – Overview Map of Study Area

Geothermal heat and power have been pervasively developed around the globe, however, until recently, only modest levels of early-stage development have occurred thus far in Canada. Currently, there are 23 geothermal district heating (GDH) systems in the United States, with a capacity totaling more than 75 MW of thermal energy (MWth) (Robins et al, 2021). Most of these systems have been in operation for over 30 years and the oldest geothermal district heating installation in North America dates to 1892 in Boise, Idaho (Robins et al, 2021). Boise, Idaho is now the largest municipally operated geothermal system in the US, providing direct heat to over 90 buildings in downtown Boise. In a 2021 market report on geothermal energy in the US, the National Renewable Energy Laboratory (NREL) stated that the barrier to expansion of the geothermal direct heat sector was not technical, but rather political, social or economic. Other than hot springs/spas, there are currently just two small direct-heat geothermal projects active in Canada, one in Moosejaw, Saskatchewan. and the other in Springhill, Nova Scotia.

Rural communities play an important role in the economy, culture, and social fabric of British Columbia, while also being home to 10-20% of the provincial population. Demographic shifts, labour shortages, economic transition, and climate change are some of the major forces driving rural transition. Formulating strategies to support adaptive capacity within rural areas is critical to their resilience. To be most effective, this support must emerge from the specific context of the communities. By employing geological, geochemical, geophysical and geospatial technologies (and methodologies) in the Kootenay Lake area, geothermal resources in British Columbia and Canada may be better understood, laying the foundation for potential commercial-based geothermal direct heat developments.

2) Geological Setting

The Kootenay Lake region of Southeastern BC exhibits high heat flow. Deep, heat energy mapping shows that the modeled heat energy in the Kootenay Lake area is approximately 25-40% higher than the generalized background within BC (Figure 2).

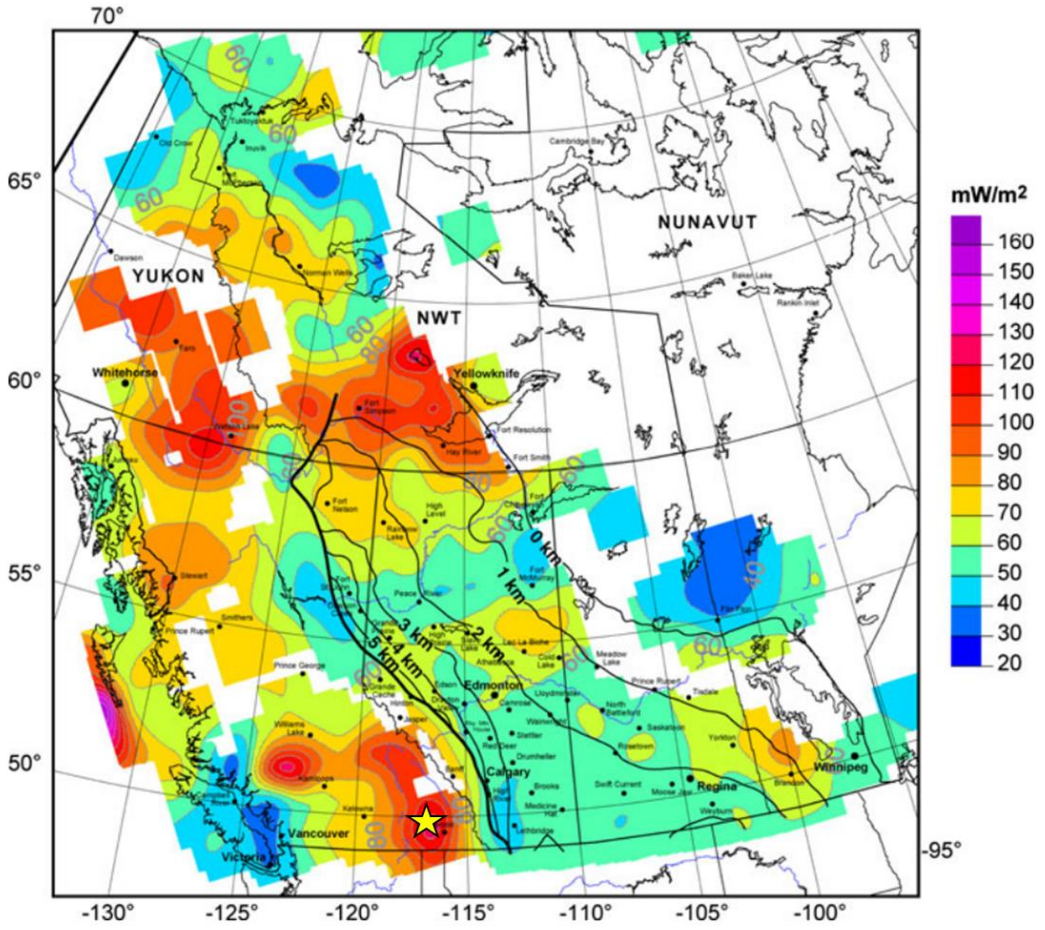

Figure 2 – Map showing averaged heat flow in western Canada. Approximate location of project area shown with a yellow star (Majorowicz & Grasby, 2010)

A major physiographic boundary within the Canadian Cordillera occurs at Kootenay Lake, with the Selkirk mountains lying to the west and the Purcell Mountains to the east of the lake. The eastern portion is represented by the Purcell Anticlinorium, a Cordilleran structure with some of the oldest rock (Proterozoic) exposures of the Cordillera at its core. Moving west the Purcell Anticlinorium transitions into the metamorphosed and deformed pericratonic / accreted island arc sequence of the Kootenay Arc (Rioseco & Pattison, 2018).

Monger et al (1982) originally framed the region as a highly metamorphosed suture zone between the thrusted strata of the Foreland Belt and the accreted terrains of the Intermontane Belt, an area known as the Omineca geomorphological belt. Figure 3 (below) is a simplified composite map showing the position of the geomorphological belts, from Webster (2016).

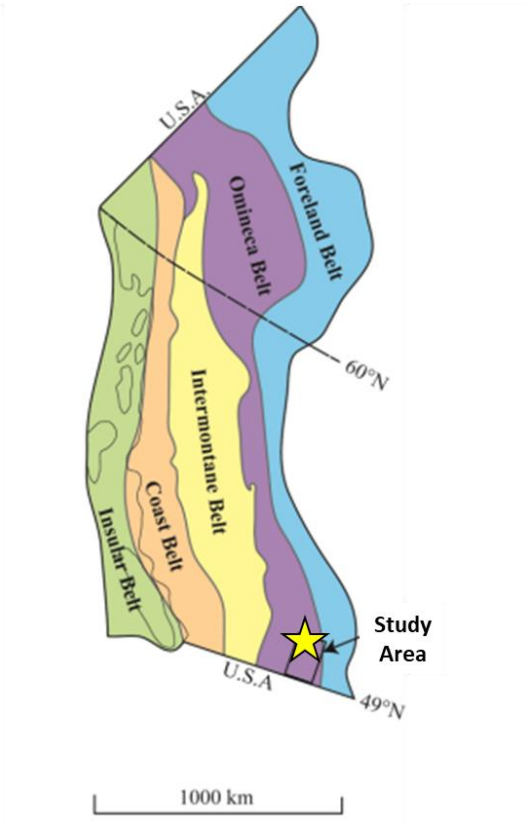

Figure 3 – The Canadian Cordillera showing the five geomorphological belts of the Canadian Cordillera. (Webster 2016)

The area of anonymously high heat flow depicted in Figure 2 (above) is essentially coincident with the location of the most highly metamorphosed rocks – proximal to Kootenay Lake. According to Moynihan & Pattison (2013), the area hosts rocks that were metamorphosed at approximately 25 kms depth and at temperatures of >650°C. Webster et al (2020) utilized Argon thermochronology to better understand the stages and timing of exhumation of this once deeply buried terrain. It was determined that final exhumation occurred during a period of regional extension along Eocene normal faults such as the Purcell Trench Fault. Webster et al also believed that the Eocene normal faults played a subsidiary role in the overall exhumation of the highest-grade metamorphic rocks in the Kootenay Lake area. Figure 4 below shows the main area of exhumation extending from Sandpoint, Idaho to Kootenay Lake near Crawford Bay which covers a period from 90-40 Ma.

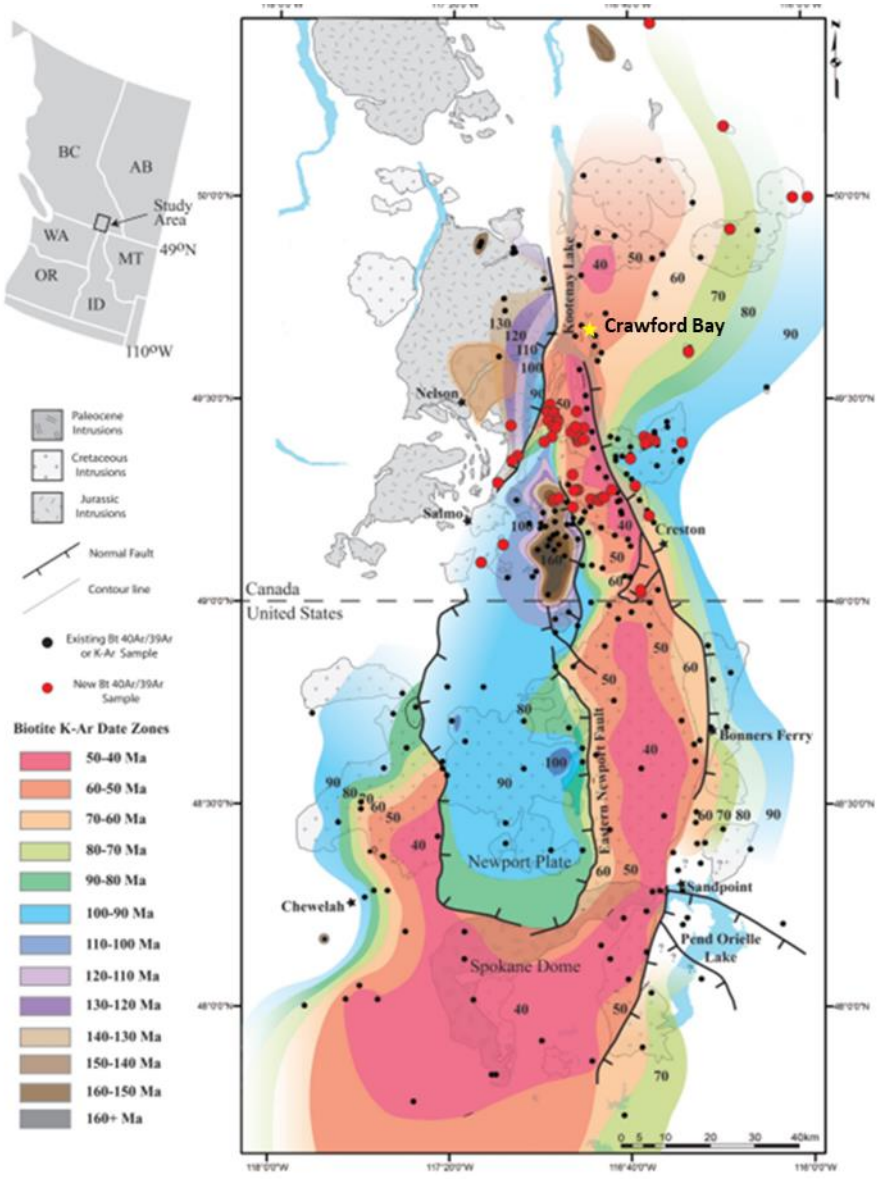

Figure 4 – Regional contours of K–Ar and 40Ar/39Ar biotite (Bt) dates. (Webster et al, 2020)

Geothermal activity is found throughout the area, in the form of hot springs at Ainsworth, Crawford Creek, Riondel and Dewar Creek (see Figure 5). Most thermal springs in BC occur proximal to major faults that share the common features of penetrating deeply into the crust (at least 5 km) and having a relatively recent (Eocene or younger) component of brittle deformation (mostly extensional) that is conducive to rapid fluid flow from great depths to the surface (Grasby & Hutcheon, 2001). Beaudoin et al (1992) indicated that these Eocene extensional

faults were first-order controls on channeling deep-seated thermal and mineralizing fluids towards upper crustal levels from depth. A subset of these Eocene and younger extensional faults has been mapped through the Kootenay Lake valley. See a simplified summary map in Figure 5 (below).

Finley et al (2020), found that the stress fields observed in the Kootenay's are consistent with the focal mechanisms of earthquakes which have occurred in the region, suggesting that transpressional strain has persisted from the Eocene to recent. The faulting and fracturing produced during this period are thought to maintain fault permeability.

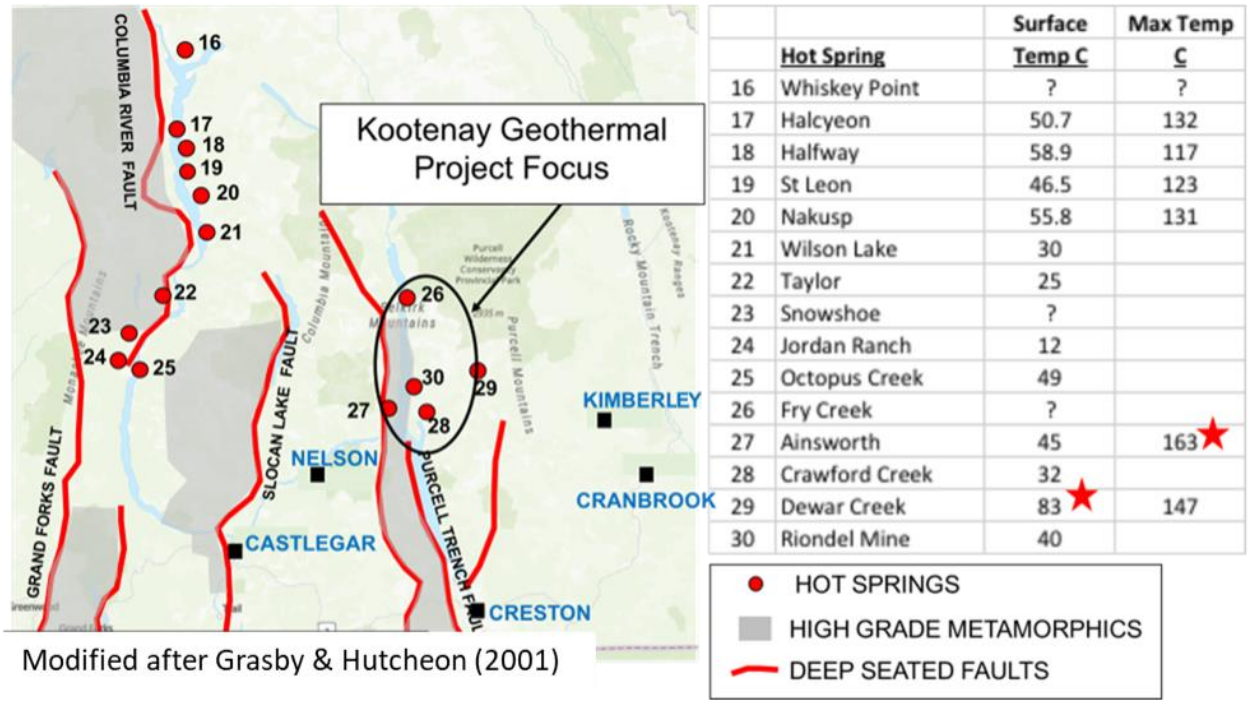

	Hot Spring	Surface Temp C	Max Temp C
16	Whiskey Point	?	?
17	Halcyeon	50.7	132
18	Halfway	58.9	117
19	St Leon	46.5	123
20	Nakusp	55.8	131
21	Wilson Lake	30	
22	Taylor	25	
23	Snowshoe	?	
24	Jordan Ranch	12	
25	Octopus Creek	49	
26	Fry Creek	?	
27	Ainsworth	45	163 ★
28	Crawford Creek	32	
29	Dewar Creek	83 ★	147
30	Riondel Mine	40	

Figure 5 – Summary overview map showing regional faults, hot spring locations and hot springs data as summarized from Grasby & Hutcheon (2001)

The major fault known as the Purcell Trench Fault (PTF), which is a 'down to the east' normal fault strikes south along the southern portion of Kootenay Lake and is mapped from Coeur D'Alene, Idaho, north, to Crawford Bay. Just west of the PTF is the Midge Creek / Gallagher Fault complex which extends from the Salmo area in the southwest to north of Kaslo on the west side of Kootenay Lake. Moynihan and Pattison (2013) interpreted the Midge Creek fault system, which dips down to the west, to be part of a larger Eocene fault complex that encompasses the Midge Creek, Gallagher, Lakeshore, and Josephine faults.

The bedrock sequence exposed in the study area was well defined by Höy (1980) during some of the earliest mapping in the region and is Cambrian to Neoproterozoic in age. Table 1 outlines a summary of Höy's geological divisions.

GROUP	FORMATION	MAP UNIT	EST THICKNESS (M)	DESCRIPTION
LARDEAU	INDEX	L4	Top not exposed	micaceous schist and gneiss
		L3	400-450	Calc-silicate gneiss, amphibole, schist; impure marble; amphibolite layer and pure white quartzite layer near base
		L2	700	Biotite-hornblende gneiss, amphibolite; minor calc-silicate gneiss, marble and schist
		L1	150	Micaceous schist
	BADSHOT	B	15-30	White crystalline calcite marble, dolomite
	MOHICAN	M	~50	Interlayered quartzite, calcareous and micaceous schist, limestone and dolomite
HAMILL		H4	230	Dark quartzite, dark fine-grained quartz rich schist
		H3	60-200	Massive white quartzite
		H2	2,000	Interbedded micaceous schist, quartzite and siltstone; minor amphibole
		H1	1,600	Massive white quartzite; gritty quartzite
HORSE-THIEF CK*	(part of the Windermere Supergroup)	HTC	base not exposed	Fine-grained light grey to green chlorite-muscovite schist and phyllite; rare white quartzite and marble

Table 1 - The primary geological divisions in the Riondel area (Höy, 1980).

The project area is characterized by three geographic regions representing somewhat different geological settings:

a) East side of the project area: East of the West Bernard Fault and east of Crawford Bay, lies the Lower Cambrian to Neoproterozoic Hamill Group quartzites and schists which overlie the Three Sisters Formation and the Windermere Supergroup. This area is host to the Crawford Creek hot spring (32°C), and a number of potentially deep-seated more regional faults and mineral showings of galena, pyrrhotite and pyrite (Jackass claim on the SE side of Mount Crawford), (Greene 1981).

b) West side approaching Kootenay Lake: A broad region of the mostly west dipping Lardeau Group - Index Formation, composed of gneisses with interbeds of quartzite and higher degrees of metamorphism encountered closer to Kootenay Lake (Sillimanite/K-spar zone – Moynihan & Pattison, 2013). Höy (1980) interpreted the area to represent a broad nappe structure, overturned to the west with west dipping Lardeau exposed at the surface and the older Badshot and Hamill eroded (with the exception of the Riondel peninsula where the Hamill overlies younger Badshot and Lardeau). This area is also marked by a chain of Cretaceous intrusions known as the Lakeshore

Intrusives. In the north of the project area is the Bluebell Mine at Riondel where geothermal fluids up to 41°C were encountered.

c) Area sandwiched between the above two regions: A band of tightly folded rocks comprised of Lardeau, Lower Cambrian Badshot marble and Hamill quartzite. This section is bounded on the west by the so-called Bluebell Mountain Fault (Crosby 1968) and on the east by the West Bernard Fault. One or both faults could be of a deep-seated nature capable of bringing geothermal fluids closer to the surface.

Hot geothermal fluids have been encountered in two of the above three regions with potentially deep-seated faults bordering all three regions of interest. Detailed geological mapping for the project area is shown in Figure 6 where two map sheets have been merged to display the mapping over the project area.

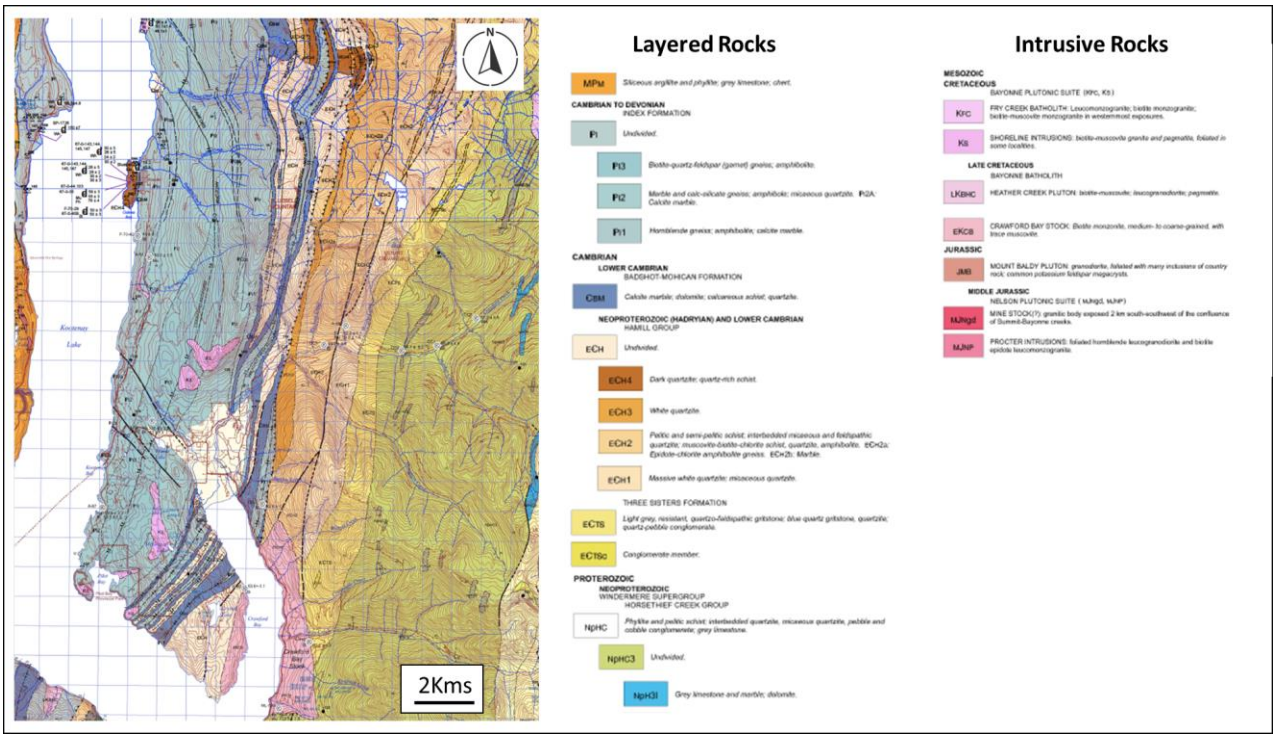

Figure 6 – Area geology map (merged Crawford Bay and Kaslo map sheets) Brown, D.A., et al (2011) Geological Survey of Canada, Open Files 6306 and 6307

The occurrence of thermal fluids in the now-abandoned Bluebell Mine in Riondel has attracted interest in the geothermal potential of the east shore of Kootenay Lake, first assessed by Desrochers (1992). In mine workings at a depth of 300 m, miners encountered hot waters of up to 40˚C flowing out of cracks and cavities. Inflow rates ranged from 45 - 1,000 litres/sec (6,000-13,500 Imp gpm), (Desrochers

1992). To prevent the mine workings from flooding, pumps worked 24 hours a day, complicating mine development and eventually contributing to the mine closure in 1972. The depth of the geothermal zone is approximately 200m elevation (above sea level) or about 330m below lake level (Desrochers, 1992). Figure 7 (below) illustrates the relationship between WNW fractures and the location of mapped ore bodies.

According to Moynihan & Pattison (2011), WNW faulting responsible for ore placement and the existence of hydrothermal fluid in the mine at Riondel, occurred later than the NW trending faults (red dashed lines in Figure 7).

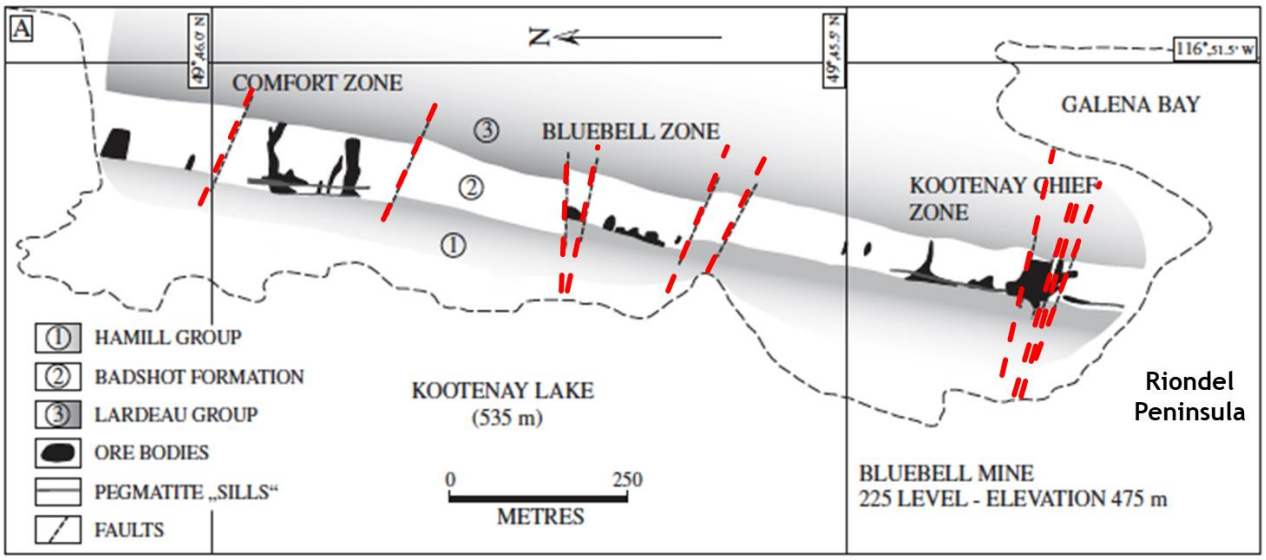

Figure 7 – Plan of the 225m level of the Bluebell Mine at Riondel. The outline of the Riondel peninsula is also shown. Figure from Moynihan & Pattison (2011)

The fieldwork conducted in the summer of 2022 has further highlighted the pervasive nature of WNW jointing throughout the study area. This will be discussed further in Section 4 – Results and Preliminary Interpretation.

3) Phase Two – Scope of Work

Key observations emerged from Phase 1 of this project regarding area fault orientation, the relative timing of faults and their potential relationship to both mineral deposition and geothermal activity. The objective of Phase 2 has been to conduct a multifaceted geotechnical survey, focused on the position and structural orientation of faults and related fracture systems. Data gathered in the field will help foster an understanding of the relative timing of different fracture sets and how they may connect to more regional, deep-rooted fault systems, capable of bringing heated geothermal fluids in closer proximity to the surface.

A. Bedrock Geology and Structure

A Simon Fraser University geology student conducted fieldwork during the summer of 2022 to collect geological and geochemical data. The structure and fracture orientation data gathered was used to construct stereonet projections leading to the creation of a structural model for the areas of interest. Understanding the nature and distribution of distinct fracture sets, as well as their geological setting, orientation, and quality, will be required to properly characterize subsurface geothermal reservoirs leading to the development of a hydrogeological model.

Bedrock measurements were collected using Stereonet Mobile Version 4.0.X (Allmendinger, 2022) on an iPhone SE running iOS 15.6. This app allowed for the collection of many data points across a broad area of interest during a relatively short field season. Structural measurements were taken for jointing, bedding or foliation planes while noting lithology and documenting any fault surfaces observed. A total of over 1,750 surfaces (bedding, faults, and joints) were measured during the field program. The data were also assigned to broad categories such as rock type or geographic location.

Stereonet 'beach-ball' projections were created for each measurement and displayed by rock type and geographic area in the geological report prepared by C. Vandenbrink (2022), see Appendix (A). Mapping of geology and geochemistry for this report was performed using ArcGIS Pro Version 3.0 software (Esri Inc., 2022).

B. Geochemistry

The chemical signature from field samples may highlight potential geothermal fluid flow pathways and potential similarities between samples derived from a range of locations in the project area. The analysis of these samples may also assist in further high-grading of a prospective target for drilling and testing in a future phase.

To establish an initial understanding of surface water properties, water from over 100 sites was tested in the field. Water chemistry data was collected, with the aid of an Oakton PCTSTestr 50 multiparameter meter, a single unit capable of measuring temperature, pH, conductivity, total dissolved solids (TDS), and salinity.

Depending on surface measurements, some seeps, creeks, or springs encountered during fieldwork were flagged to be sampled for laboratory analysis, with all data integrated into the project data platform (ArcGIS) for interpretation. A total of 20 sample locations were selected for laboratory analysis. These samples were collected over two days, adhering to accepted sampling methodologies. Samples were collected by carefully 'spoon feeding' water into the sample bottles provided. There was no filtering done in the field. Samples were delivered to CARO Analytical Services in Kelowna on August 31, 2022.

The water samples collected were analyzed for concentrations of major ions, namely: sodium, calcium, potassium, magnesium, chloride, carbonate /bicarbonate and sulphate. In addition, the following analyzed parameters may also prove invaluable in interpreting the water chemistry and assessing its suitability for geothermal exchange: lithium, boron, bromide, fluoride, silicon, iron, manganese, aluminum, arsenic, sulphide and uranium. (Please note silicon (Si) was not collected separately and was run from the same bottle and at the same time as all other metals via Inductively Coupled Plasma Mass Spectrometry or ICPMS). The CARO sample bottles are manufactured by Systems Plus and come pre-charged with the required preservatives.

Laboratory analysis results were received on October 31, 2022, with the resultant data input into the AqQa Version 1.5.0 software (Rockware) for review and analysis. This software was utilized to evaluate results, facilitating unit conversion, ion balance, sample mixing, basic fluid properties calculations, water chemistry diagrams (Piper, Stiff) and more.

C. Geospatial Evaluation

The drone-based remote sensing program targeted an area around Crawford Creek, where several compelling observations have been made, including a hot spring (32°C) which is located near the valley bottom. This hot spring is proximal to a mapped regional fault known as the Orebin Creek Fault (OCF), a near-vertical fault striking south from Orebin Creek toward the Crawford Bay Stock which is located on the east shore of Crawford Bay (Kootenay Lake) (Brown et al, 2011). The fault itself is well presented in a quarry along a forest service road where very fractured Hamill Formation quartzites are exposed (see Figure 13).

Although LiDAR coverage is not available locally over the Crawford Creek hot spring, there are several distal indications of cross-cutting faults which may contribute to the vertical movement of geothermal fluids at this location near the OCF. The Phase Two drone-based LiDAR coverage partially fills a gap in the open file database at this location. The Advanced Spaceborne Thermal Emission and Reflection Radiometer (ASTER) data from Phase One was of limited value. In Phase Two, Thermal Infrared (TIR) data was acquired closer to the ground in a focused manner and over an existing hot spring, to provide potential insights into fluid flow proximal to the above-mentioned faults, highlighting any thermal patterns with respect to its location and the extent of its surface expression.

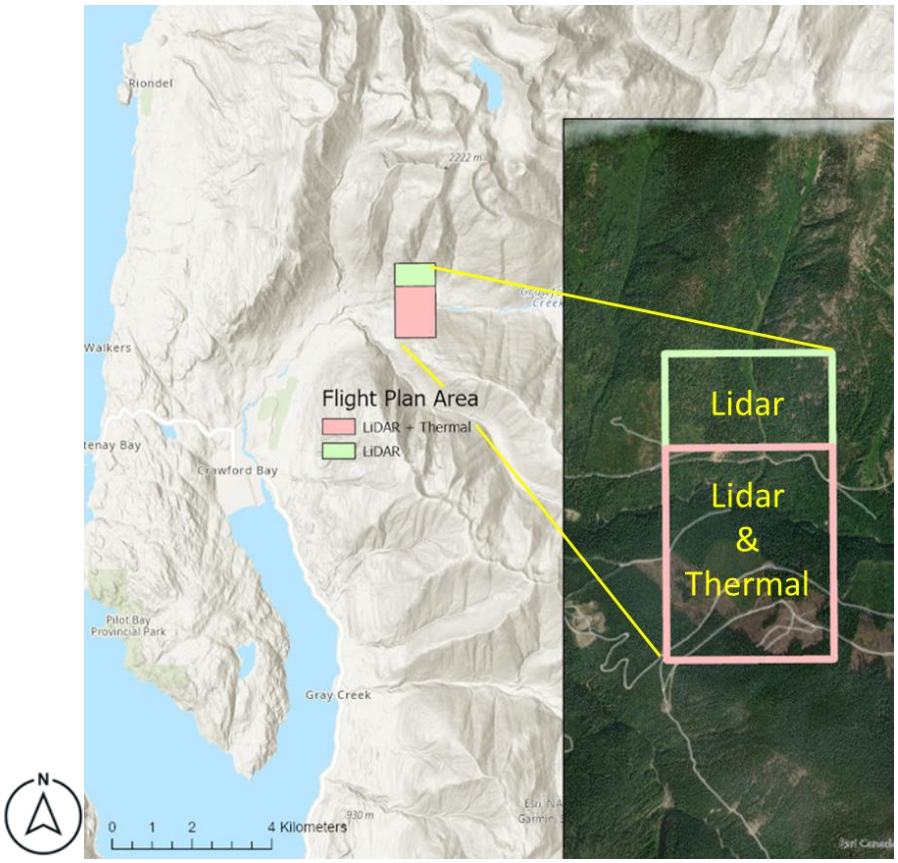

Figure 8 – Drone based evaluation, area of investigation.

A spatial analysis of the thermal imaging results can determine surface thermal energy locations and proximity to geological features or other geothermal indicators such as hot springs. This could also be used to analyze a change in surface temperature over time if additional data are collected in the future. If the planned drone-based infrared survey is successful, it may

provide a template for how a hot spring is expressed in an area known to have high annual precipitation, such as the Central Kootenays of BC. This template could be utilized on future projects and in other regions.

The drone-based evaluation was carried out by Selkirk College over two separate periods in October 2022. The aerial imagery was collected using Zenmuse L1 (LiDAR) and Zenmuse H20T (thermal) sensors equipped on the DJI Matrice 300 RTK UAV. An area of approximately 2.5 sq km was surveyed over the Crawford Creek hot spring which is situated northeast of the Crawford Bay Community (see Figure 8).

Approximately 100% of the LiDAR data was successfully collected, however, only about two-thirds of the thermal imagery was acquired before early snowfall caused a halt to the field acquisition (see areas highlighted in Figure 8, previous page).

4) Results and Preliminary Interpretation

Geology and Structure

Geological mapping was conducted from mid-June until late August 2022. The area is generally rugged and heavily vegetated with forest cover throughout and interspersed with private land. Therefore, the area of interest offered restricted and limited access, being generally confined to road cut outcrops and along a network of forest service roads. Local hiking trails in areas like Pilot Peninsula provided additional access.

Figure 9 shows the locations where geological data was collected with the different rock types identified (granite, gneiss, marble, quartzite, schist, gritstone, phyllite).

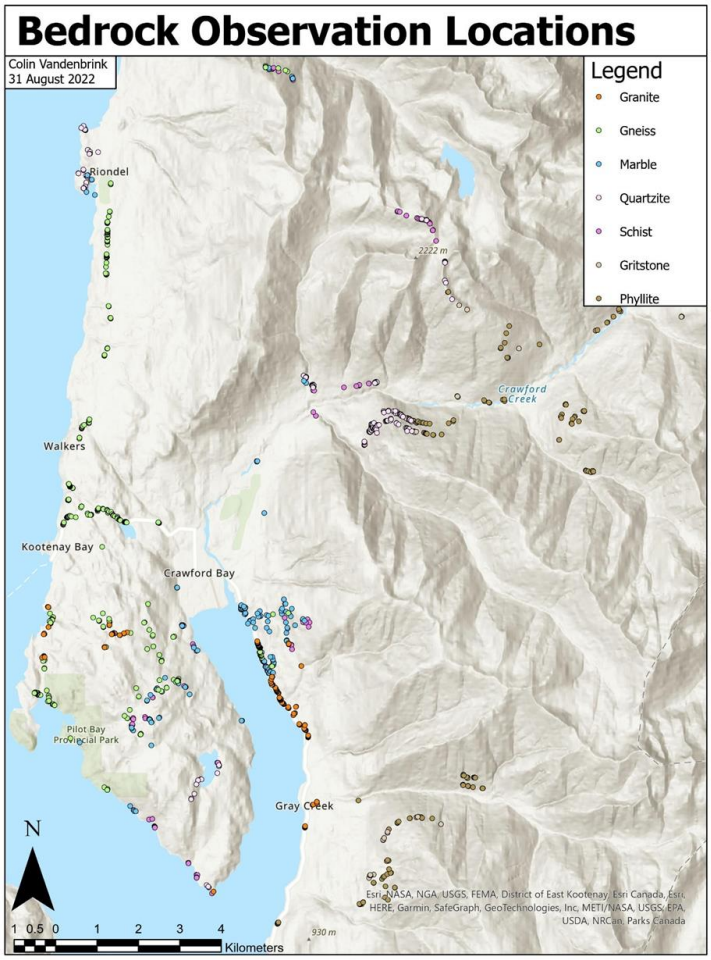

Figure 9 – Map showing locations where bedrock observations were recorded (Vandenbrink, 2022)

In addition to the identification of rock types, structural features including faulting, jointing, and bedding/foliation surfaces were also measured (faulting and bedding measurement locations shown in Figure 10). Structural data including stereonet plots depicting planes, poles, and contoured poles for faults, joints, and bedding/foliation surfaces were completed and provided in some detail within the report by C. Vandenbrink (2022), included in Appendix (A).

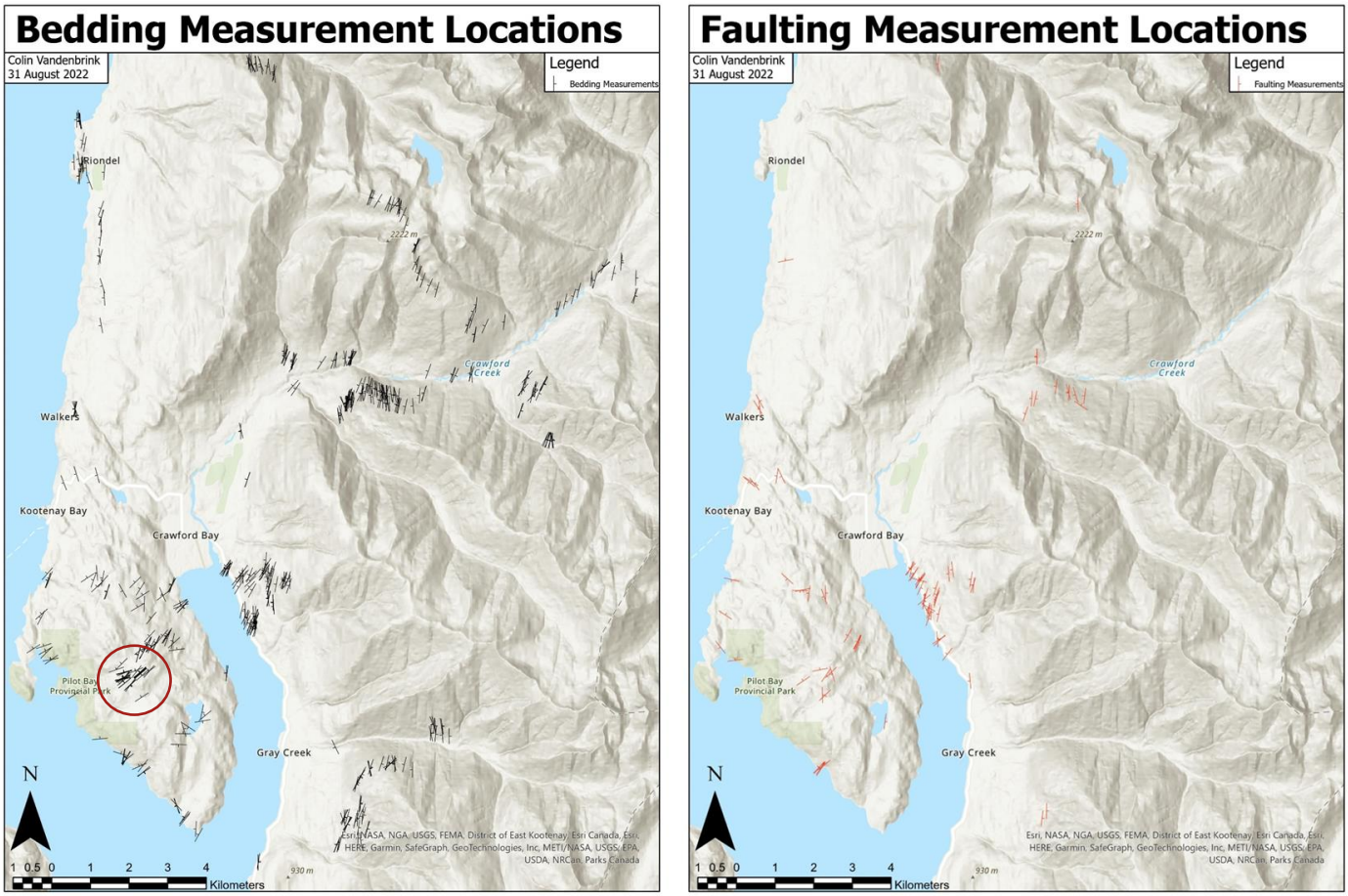

Figure 10 – Maps showing locations where bedding and fault attitudes were recorded (bedding planes in black, fault planes in red). Red circle highlights location of bedding strike change on Pilot Peninsula. (Vandenbrink 2022)

Below are a series of summary stereoplots depicting the structural elements measured across the project area. Separate plots were generated and divided both by both rock type and geographic region within the project. The rose diagrams shown by rock type in Figures 11 and 12 (below) provide the relative abundance of planar features by strike angle (bin size = 10°). Further detailed displays by region are provided in the Vandenbrink report (2022).

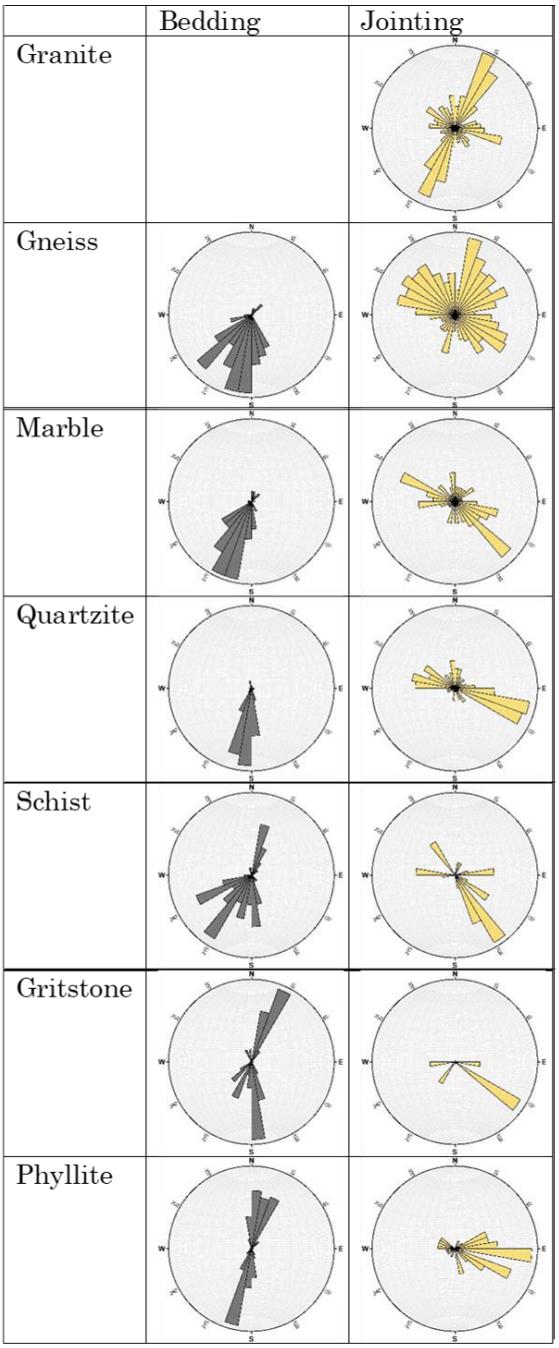

Figure 11 – Rose diagrams from planes, measured and displayed by rock type (Vandenbrink 2022)

A review of the above rose diagrams suggests some structural similarities by rock type in both bedding and jointing. The general bedding trend is predominantly NS, except for the southern end of Pilot Peninsula where bedding begins to strike more in an EW direction, with bedding there plunging to the north instead of west (see Figure 10). The jointing measured generally trends WNW in all rock types except granite.

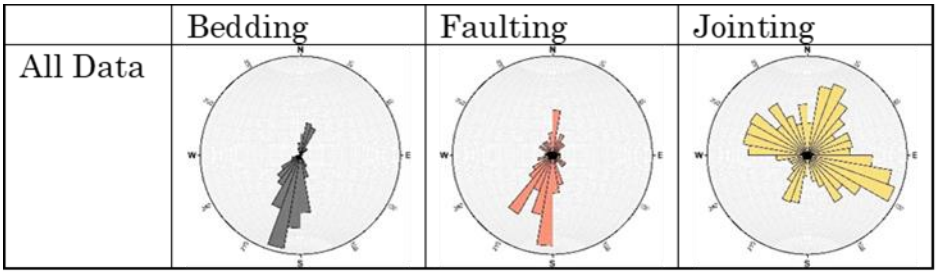

Figure 12 – Rose diagrams of planes from all areas, all data (Vandenbrink 2022)

Five major faults were interpreted within the study area (Figure 14) using LiDAR imagery and structural measurements. The most obvious of these faults is the Orebin Creek Fault (OCF), which is well exposed just north of Crawford Creek in an old quarry. It is a near-vertical normal fault which is mapped to strike south from Crawford Creek towards the Crawford Bay Stock.

Figure 13 – Hamill quartzite exposure along the Orebin Creek Fault, Fault gouge zone shown on the right (Strike 180° (yellow), Dip 86° West; Joint set Strike 118° (red), Dip 69-73°)

The Crawford Creek hot spring (32°C) is situated down slope and to the east from the trace of the Orebin Creek Fault (OCF) pictured in Figure13 (previous page). Hypothetically, this fault may have acted as a conduit for hydrothermal fluids. A summary of all faults directly mapped or inferred are shown in Figure 14. WNW jointing is prevalent through the Hamill quartzite at the OCF location, represented by a distinctive brittle fabric. The location of the Crawford Creek hot spring proximal to a potentially deep-seated fault such as the OCF, makes this a compelling area for direct-use geothermal potential, and worthy of further investigation.

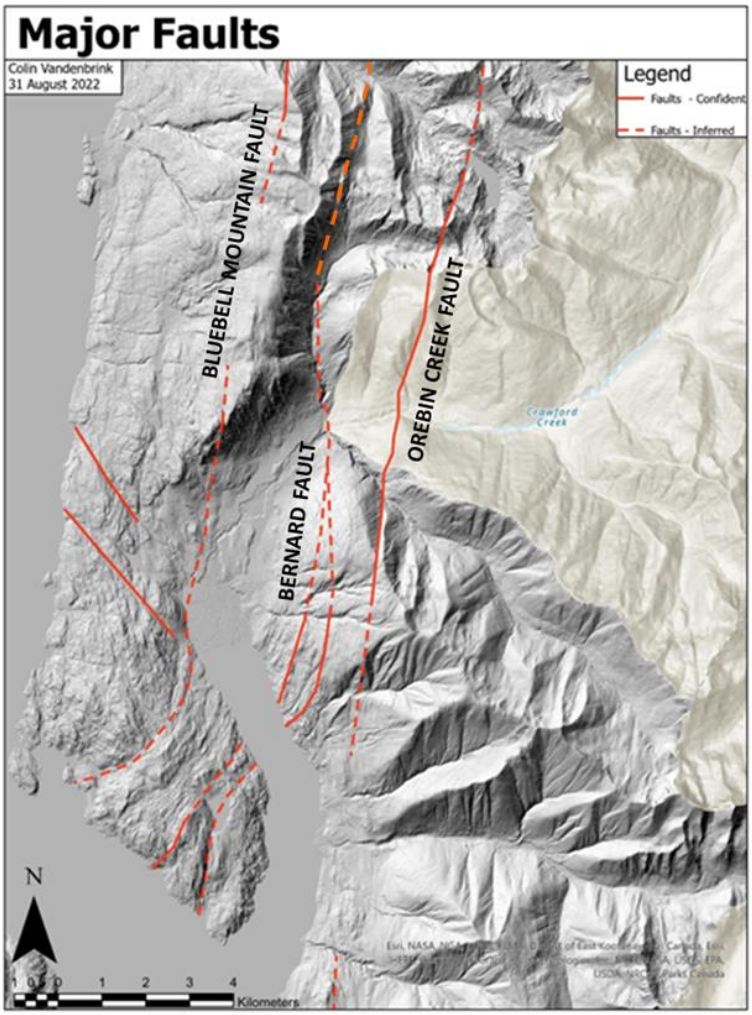

Figure 14 – Map showing major fault zones within the study area, underlain by open file LiDAR imagery where available (Vandenbrink 2022).

A second fault, the Bernard Fault (also evidenced as a steeply dipping fault) is mapped to occur approximately 1.5 km west of the Orebin Creek Fault and strikes

essentially north at this location. Although the fault is not exposed (west of Orebin Creek), there is evidence of the fault farther south approaching the Crawford Bay Stock. Höy (1980) mapped the Bernard Fault as a thrust fault and separated it into West and East Bernard Faults particularly north from Crawford Creek, however, this could not be verified due to the highly vegetated nature of the terrain and persistent presence of glacial till within the valley bottom in this area.

A third pronounced fault was located and directly measured high up the Tam O'Shanter Creek forest service road, north of Riondel (labelled Bluebell Mountain Fault in Figure 14). The road cut at this location exposes a broad section on both sides of the fault with very good vertical relief. This fault is also interpreted as a steeply dipping normal fault and is mapped to strike south towards Crawford Bay before bending southwest across the Pilot Peninsula. Here LiDAR shows good evidence of a major lineament with rock of distinctly different structural fabric evident on either side of the interpreted fault. This is also the location of the observed change in the strike of bedding mentioned previously. Although this fault was not mapped by Höy and is not shown on the GSC geology maps, Crosby (1968) had interpreted a fault at this location which he called the Bluebell Mountain Fault.

Geochemistry

As discussed previously, surface water bodies were tested using an Oakton PCTSTestr 50 multiparameter meter for pH, salinity, conductivity, TDS and temperature. When reviewing the properties of local area hot springs, it was observed that they were all acidic. The hot springs closer to Nakusp, on the other hand, are all basic in nature. Table 2 (below) shows the properties of area hot springs as well as the geothermal fluids sampled from the Bluebell Mine in Riondel; note the difference in pH highlighted (light blue – acidic, yellow – basic) by area. Given that the hot springs in the immediate area are all slightly acidic, including the Crawford Creek hot spring, pH was used as the first criteria in selecting sites for water sampling and analysis – targeting waters with low pH. Secondly, any site that demonstrated properties that were anomalously high (i.e., TDS or conductivity) were also selected for sampling.

			Hot Springs**					
	Units	**Rondel at 525ft level ***	**Ainsworth HS**	**Crawford Ck**	**Dewar Ck**	**Nakusp HS**	**Halcyon**	**Halfway**
Calcium	mg/L	430	142	4.4	27.9	59.57	52.1	158
Iron	mg/L	< 1	0.2 - 0.8			0.02	0.01	0.028
Magnesium	mg/L	280	0.4 to 5	2.8	0.3	0.36	0.6	0.1
Manganese	mg/L		0.45			0.011	0.01	0.009
Potassium	mg/L	60	20.3	1.159	10.9	4.75	7.1	3.8
Sodium	mg/L	440	238	2.2	206	82.35	164	72
Bicarbonates	mg/L		984	19.5	149	30.6	38.3	19
Chlorides	mg/L	80	48.65	0.5	54	1.69	5.6	4.7
Fluorides	mg/L	2	3.55	0.088		1.62	7.36	2.2 to 4.1
Sulfates	mg/L	280	48.6	12.8	287	273	426	490
Lithium	mg/L		0.68	0.5	0.907		0.64	0.062
Zinc	mg/L	2	0.01			0.03		0.033
Arsenic	mg/L		0.015	0.02		0.004		
pH		Acidic	6.34	6.4	6.4	7.98	7.7	8.2
TDS	ppm	3300	1739	45.8		546	788	805
Conductivity								
Note that 1mg/L equals 1000 Micrograms/L and no units were provided with the Geochemistry data base								
* Riondel Feasibility study, Desrochers 1992								
** Geoscience BC, Appendix F (2016)								

Table 2 – Summary of mineralogy and water properties available from area hot spring occurrences.

	Temp. (°C)	**pH**	**Conductivity (µS/cm)**	**TDS (ppm)**	**Salinity (ppt)**
Range Measured	7.7 - 30.1	6.59 - 8.44	25.6 - 605	7 - 424	0.0 - 0.3

Table – 3 Range of water properties measured using multi-parameter meter, from over 100 sites during the summer of 2022 (Vandenbrink, 2022)

Generally, the surface water temperatures were received with some uncertainty as to how representative they are due to the hot dry conditions that persisted during the field testing. In retrospect, documenting ambient air temperatures at the time the water was tested would have provided some context on the data gathered. Table 3 above, shows the data range for each criteria tested in the field (See Appendix (E) for full multiparameter meter testing results). A few specific sites will be revisited during Phase Three, retested and potentially sampled for analysis. Figure 15 (next page) shows the distribution and range of pH tested in-situ with the multiparameter meter. Groundwater measurements were shown to correlate with host bedrock with noticeable increases in properties such as conductivity and TDS observed near major fault zones.

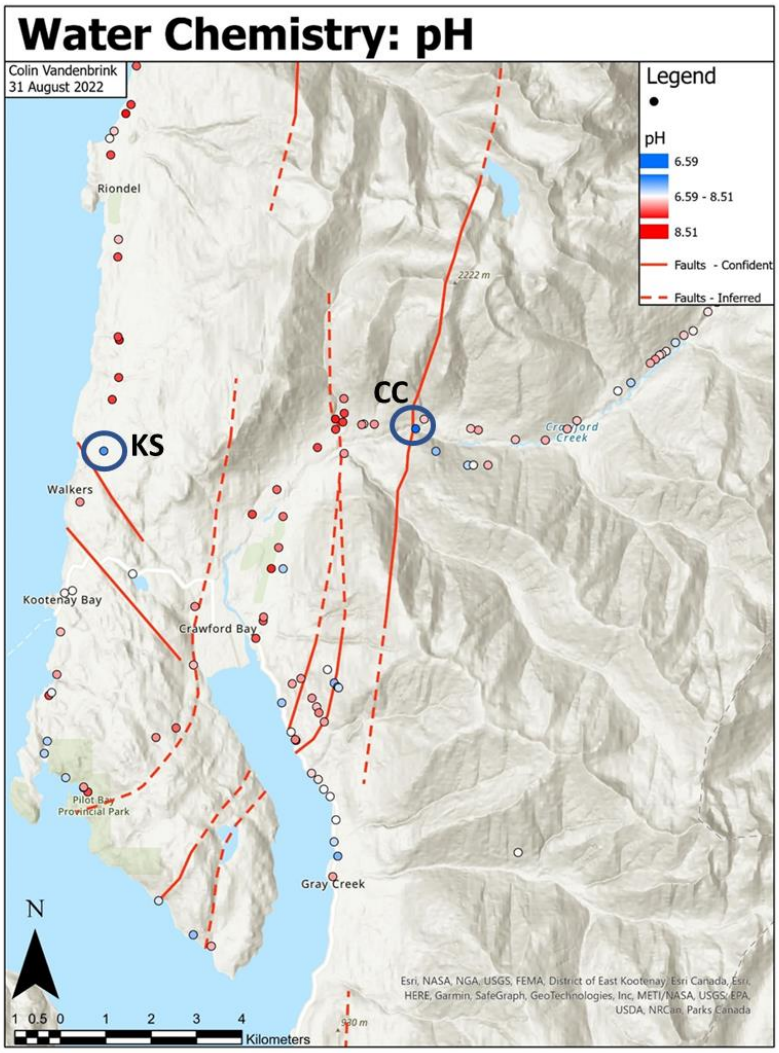

Figure 15 – Water chemistry sample points symbolized according to pH (blue = lower, red = higher), compared to assumed major fault locations. Lowest pH readings encountered were CC – Crawford Creek hot spring and KS – Krishna Spring (Vandenbrink 2022)

Figure 16 (next page) shows the sites that were selected for sampling and analysis. The Phase Two budget facilitated the analysis of twenty samples. A review of results indicates the need for detailed testing and sampling in certain focus areas such as Crawford Creek, plus additional follow-up work during Phase Three. A summary of the laboratory analysis results can be found in Appendix (D).

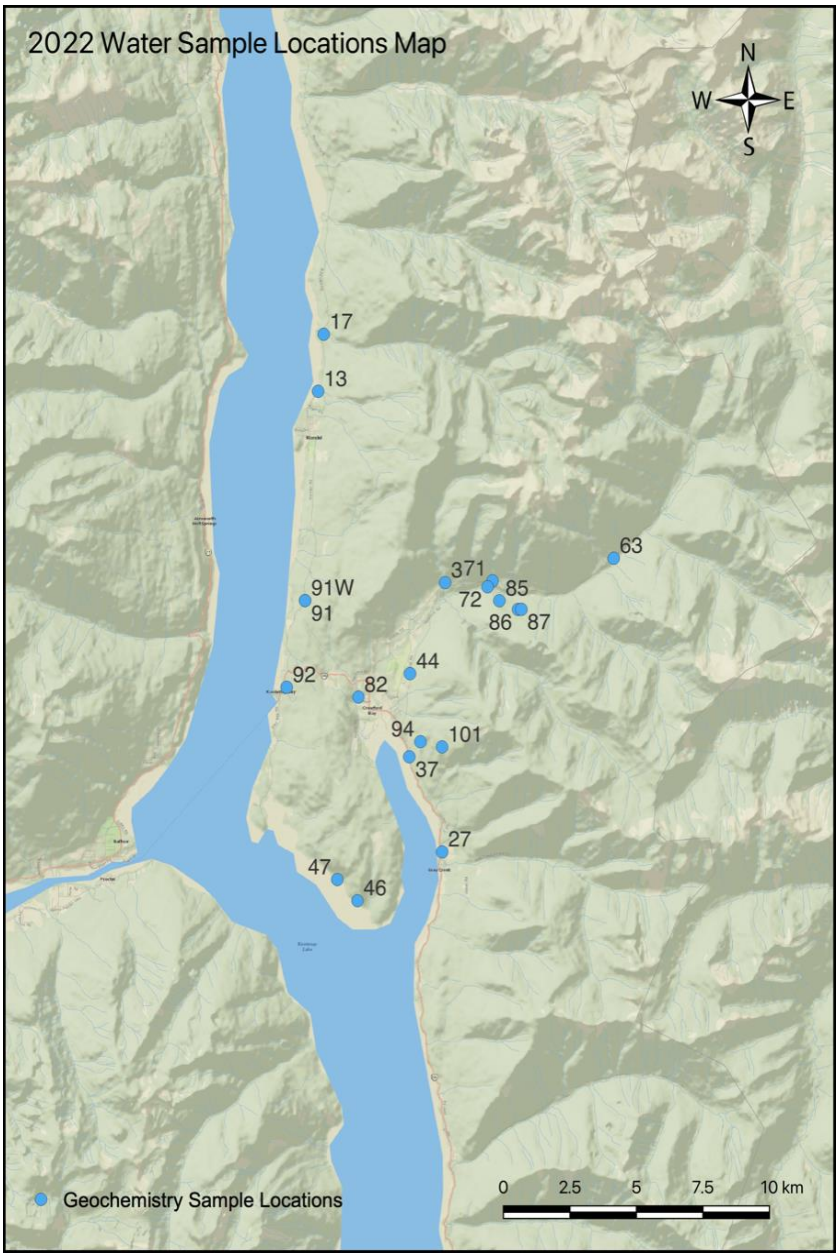

Figure 16 – Location of sites selected for water sampling and analysis (McQuarrie, 2022)

The geochemistry dataset for this project including ion concentrations of each sample was analyzed using AqQA software by Rockware. Geochemical data considered for area hot springs, in the above analysis (Table 2), was derived from Grasby, 2000, (Ainsworth and Dewar Creek) and Desrochers, 1992, (Riondel), while results for the twenty locations sampled in this Phase Two are from the CARO lab report (Appendix D).

Stiff diagrams can provide a quick visual comparison of the characteristics of water derived from different sources. A stiff diagram is essentially a polygon based on the abundance of a suite of cations and anions – magnesium (Mg), calcium (Ca), and sodium (Na) + potassium (K) cations on the left side of the diagram, and sulphate (SO_4), bicarbonate (HCO_3) plus carbonate (CO_3), and chloride (Cl)anions on the right side of the diagram.

Figure 17 shows the locations of water samples that received detailed laboratory analysis along with corresponding Stiff diagrams for each sample location. The Stiff diagrams are colour coded to represent the host rock at the location the water was sampled except for Ainsworth and Dewar Creek which are shown as black.

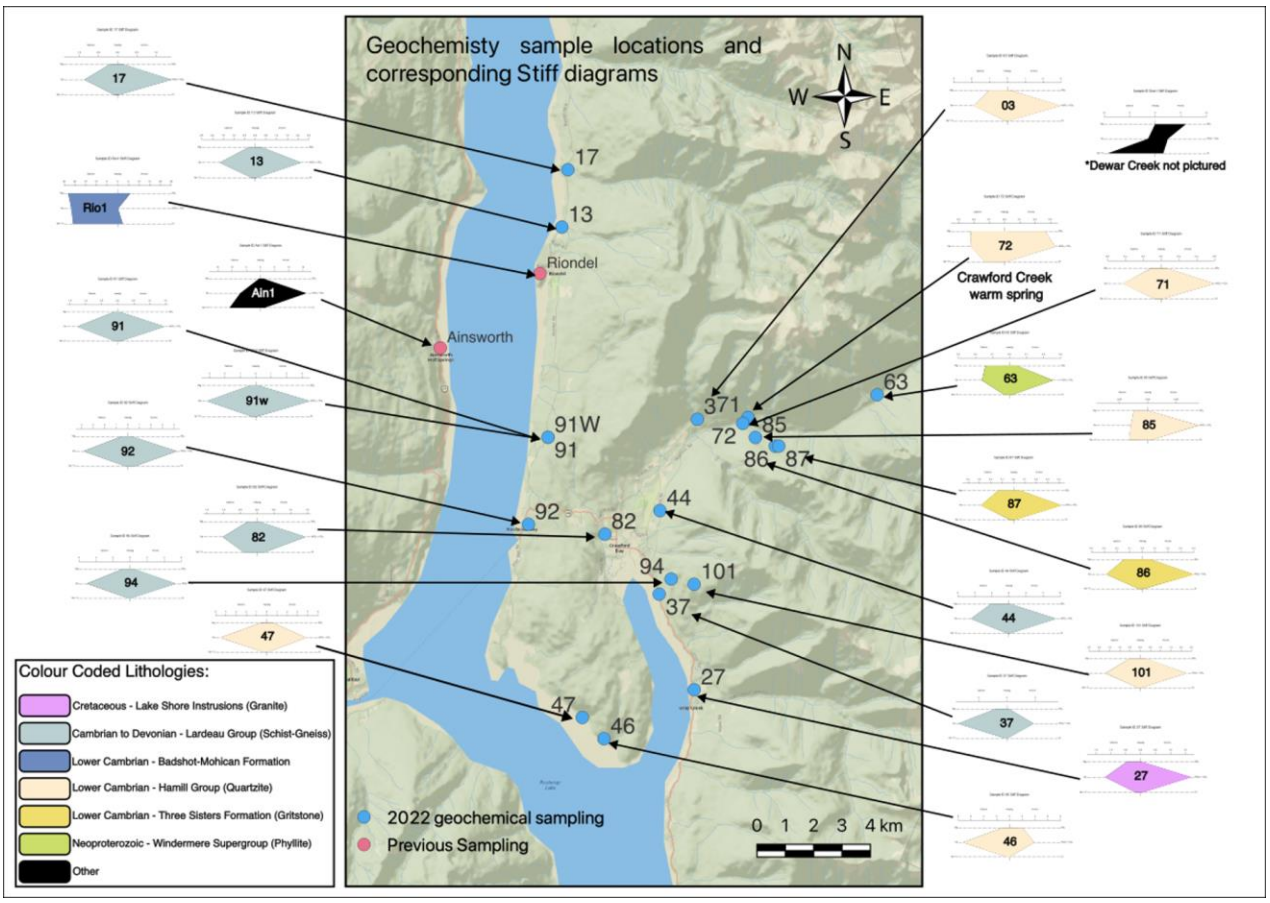

Figure 17 – Geochemistry sample locations with associated ion concentrations represented by Stiff Diagrams. Produced using QGIS software and AqQA software by Rockware. Sample 72 is the Crawford Bay warmspring sample. (McQuarrie, 2022)

When the Stiff diagram for the Crawford Creek hot spring sample is compared to the Stiff diagrams for Riondel and Ainsworth some similarities emerge (Figure 18). Crawford Creek and Riondel have an elevated level of magnesium, while Ainsworth, Riondel and Crawford Creek all have elevated levels of sodium / potassium. The Stiff diagram for Dewar Creek (location not shown on Figure 17) is similar to Crawford Creek in that they each have higher levels of both sulphate and sodium / potassium.

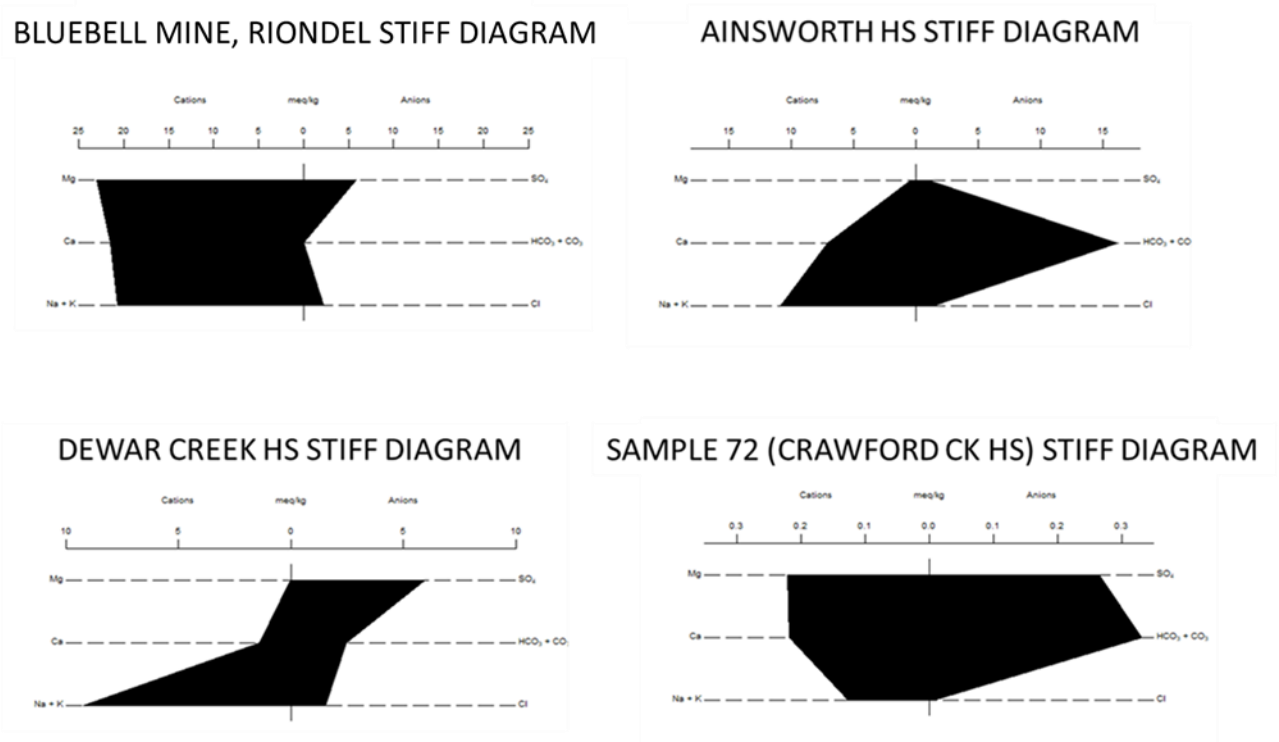

Figure 18 – Geochemistry Stiff Diagrams from four area hot springs. Produced using QGIS software and AqQA software by Rockware. (McQuarrie, 2022)

When comparing the details of the Stiff diagrams for all area hot springs it appears that Crawford Creek and Dewar Creek both have higher SO_4 and all four appear to have elevated levels of Na + K. In addition, Crawford Creek and Riondel both have higher levels of Mg.

Some similarities between area hot springs and Crawford Creek (Sample 72) are further evidenced on the Piper diagram displayed in Figure 19 below. A Piper diagram is a graphical representation of the chemistry of the water samples showing the cations and anions on separate ternary plots. The apexes of the cation plot are calcium, magnesium and sodium plus potassium cations and the apexes of the anion plot are chloride, sulphate, and carbonate plus bicarbonate anions.

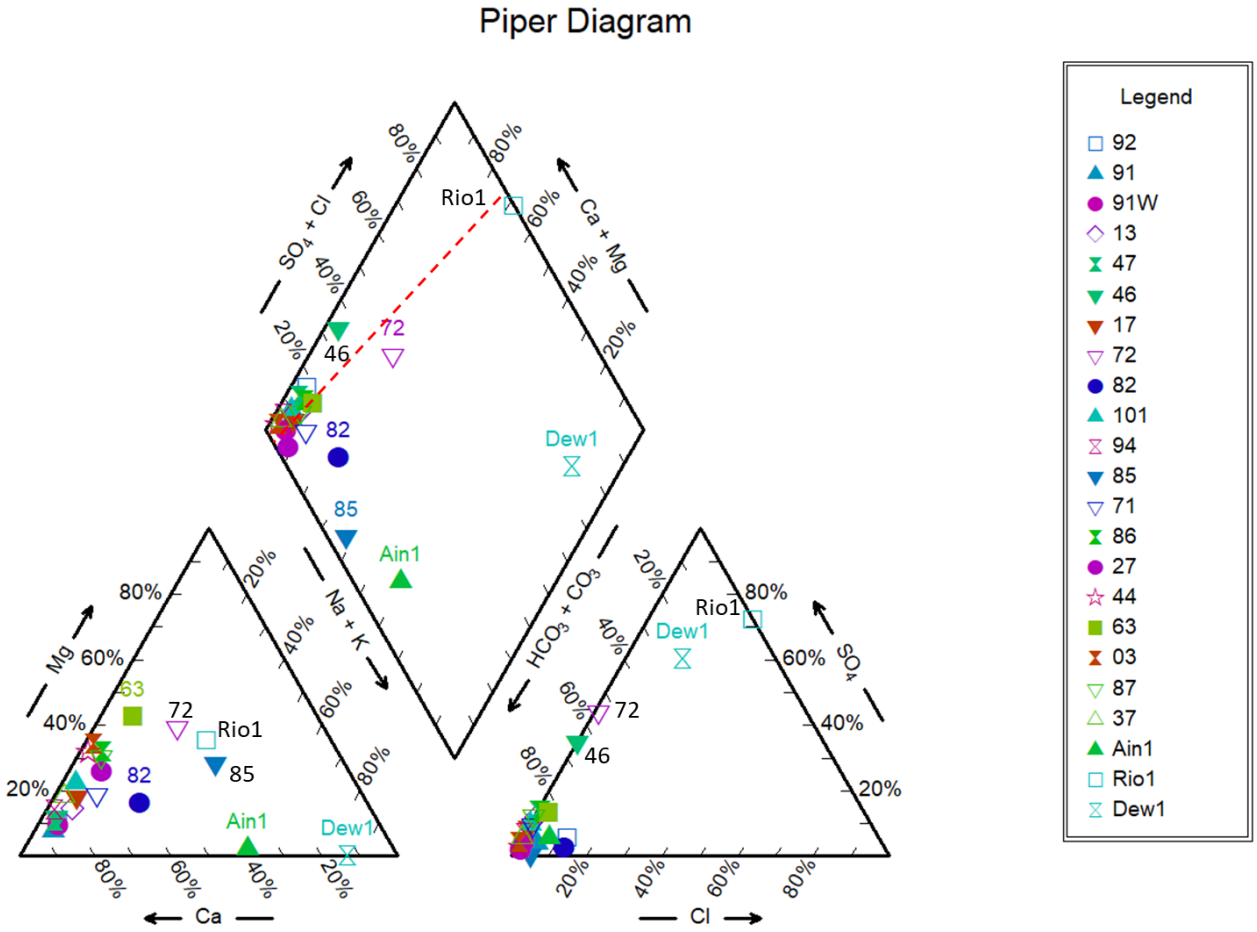

Figure 19 – Piper diagram for all 20 samples plus three area hot springs (Ain1, Rio1 and Dew1). Produced using QGIS software and AqQA software by Rockware. Sample 72 is the Crawford Creek hot spring sample with implied correlation trend bicarbonate rich surfical water and Riondel shown in dashed red line.

Examination of data point groupings on each of the above Piper diagrams indicate that in addition to Sample 72 (Crawford Creek), Sample 46, Sample 63, Sample 82 and Sample 85 are separate from the main cluster of data points in the bottom left corner of each plot and hold some similarity to the different hot springs (see Figure 16 or 17 for sample locations).

Sample 72 was collected from the Crawford Creek hot spring. The Piper diagram indicates that Sample 72 has a geochemically distinct water type, similar to the hot springs at Ainsworth, Riondel and Dewar Creek. However, the concentrations of major ions are much lower and the water from Sample 72 is much less mineralized. The Durov diagram demonstrates this well (Figure 20).

A Durov diagram is like a Piper diagram in that it is based on the percentage of major ion milliequivalents of the samples plotted. The cation and anion values are plotted on separate triangular panels with the data points projected onto a square grid at the base of each triangle. Unlike a Piper diagram, a Durov diagram allows the comparison of pH and the total dissolved solids (TDS).

The elevated temperature and lower pH also highlight that Sample 72 is different than the majority of other samples. The low mineralization of Sample 72 suggests either there has been significant dilution of a deeper thermal water due to mixing with relatively fresh water or the water has had a relatively short flow path with little interaction with any rock. The location of the sample site near the valley bottom within a glaciofluvial deposit would suggest the former is most likely. There is a potential straight-line correlation between bicarbonate-rich surficial waters (bottom left, Figure 19, above) and the Riondel sample, with Sample 72 lying near the projected correlation trend. This may again imply that Sample 72 is potentially a 'diluted' version of the waters encountered at Riondel. Sample 46 also lies near this projected trend.

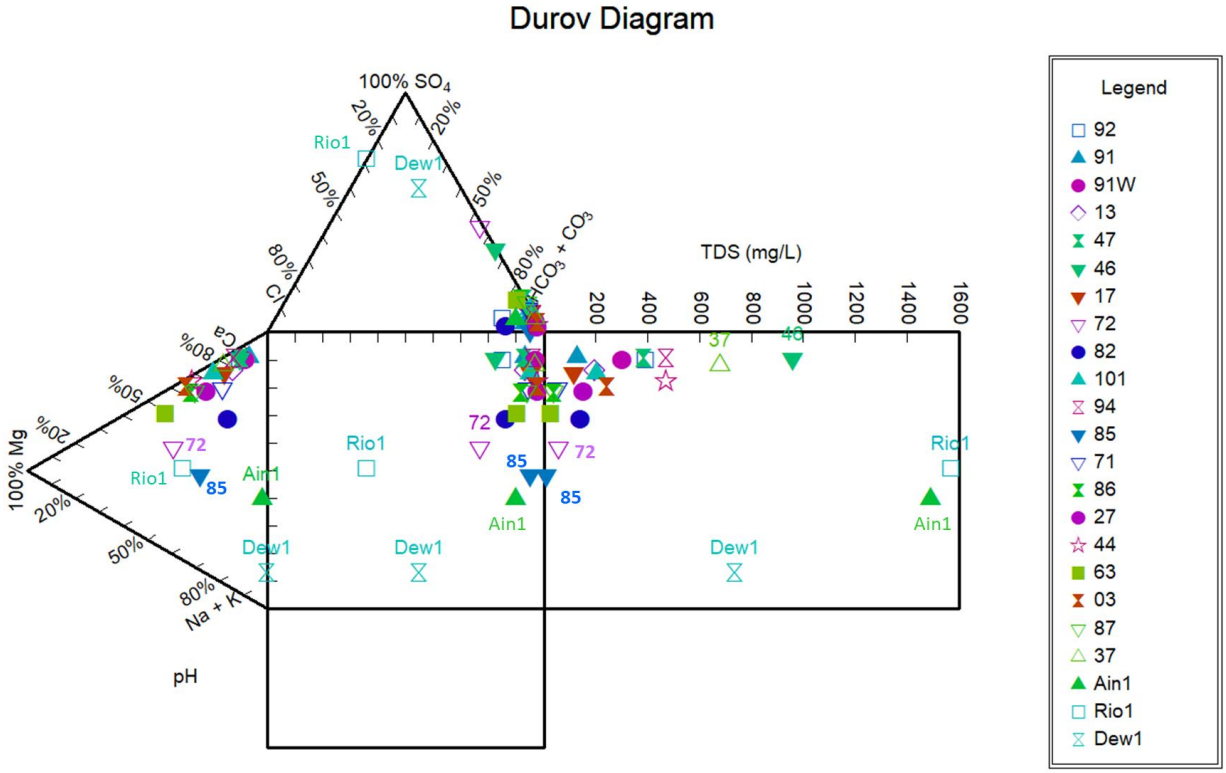

Figure 20 – Durov Diagram for all 20 samples plus three area hot springs (Ain1, Rio1 and Dew1). Produced using QGIS software and AqQA software by Rockware. Sample 72 is the Crawford Bay hot spring sample.

Sample 85 is interesting in that it is located within the Hamill H1 quartzite and was taken from a seep approximately 650 meters southeast of the Crawford Creek hot spring. It is also the site of a small fault where a two-meter-wide gouge zone was identified with a moderate amount of water flowing from it (rate not measured). The fault was measured to have a strike of 187° (the OCF has a strike of 180°) and a dip of 61°. Sample 85 plots close to Sample 72 on the Durov diagram above, however Sample 85 has very low mineralization with virtually no sulphate. Sulphate may have been diluted in Sample 85, however, it also has almost no chloride. These differences combined with the fact that there is a surface temperature of 20.4°C between the two samples, make it difficult to interpret Sample 85 having the same subsurface source as Sample 72.

Sample 46 is located near the south end of Pilot Peninsula about 350m northwest of an inferred fault (interpreted from LiDAR, Figure 14), where schist is mapped (possibly Hamill H2). A fault trace is mapped at this location on the GSC Geology Map for Crawford Bay (Open File 6306). The water was sampled from a seep that created iron staining, with high levels of iron as well as magnesium, manganese, sulphur and zinc measured in the analysis. Although highly mineralized the temperature measured at this site was only 9.5°C. Given the mineralization observed here and its location proximal to a potentially regional fault, this site should be considered for further follow up work in Phase Three.

Sample 63 is the farthest east sample data point. The sample was taken from a seep above Crawford Creek, in an area mapped as phyllite from the Windermere Supergroup. No faults were observed or interpreted near this sample point. Given that the temperature observed at this location was only 8.2°C and that the water had very low TDS (23.4 ppm) and low conductivity (33µS/cm), there are currently no plans to follow up on this area.

Sample 82 plots proximal to some of the other data points mentioned above, as well as Riondel and Ainsworth, for two of the three Piper diagrams. This sample was collected from a stream called Beaver Creek located below Fraser Lake at the north end of Pilot Peninsula. This lake falls on a well-defined NW trending fault evident on LiDAR and parallel to two other NW trending faults mapped on the GSC Geology Map for Crawford Bay (Open File 6306). When Fraser Lake was tested using the multiparameter meter it recorded a temperature of 25°C, the second warmest surface temperature measured after Crawford Creek hot spring. In the heat of the summer, warmer water was measured during the heat of the afternoon, however this test occurred late in the morning when ambient air temperature was 22°C and the air temperature the previous evening had fallen to 13°C overnight, so the measured temperature of 25°C is deemed representative.

While the overall mineralogy of Sample 82 is generally low, it was noted to have a high level of chloride (7.61 mg/L). This was the highest level measured from all twenty samples. Chloride is generally considered an indicator of groundwater age with older groundwater having high levels of chloride (Humphries, personal communication). Chloride measured at Ainsworth and Dewar Creek was in the range of 48-54 mg/L.

One other sample worth commenting on is **Sample 37**, given the elevated levels of certain metals evident in the analysis, including aluminum, iron, magnesium, manganese, sodium, sulphur, titanium, tungsten, vanadium, and zinc. The bedrock consists of diopside which is quite unique for the area. The metamorphism to massive diopside from a dolostone would likely have taken place during the Cretaceous, however, Pattison et al (2020) suggest that the localization of the alteration to just this unit indicates that it was potentially a significant hydrothermal event. The silica rich fluids of this event would have likely carried the heavy metals observed in the sample. The Stiff diagram for Sample 37, however, does not appear anomalous and seems to resemble many of the other sample points located across the study area.

There was a water test site located approximately 850m southeast along Crawford Bay (site number 35). This site is in Badshot marble and tested a surface water temperature of 24.8°C, in addition, the water had high TDS (340ppm) and conductivity (480µS/cm). Generally, this area appears to have undergone significant structuring and deformation with some 15-20 faults observed in the field over a two-kilometer distance. An extension of the Bernard Fault is inferred to be present in this area (Figure 14) and potentially be part of the identified fault network mapped in the field. This area will be considered for additional geological mapping and potentially additional geochemical work within Phase Three.

Geospatial Evaluation

Field operations and data collection for the project at Crawford Creek focus area took place on October 6 and 27, 2022 to collect LiDAR, Thermal and Red Green Blue (RGB) Imagery. A DJI M300 drone was flown using a DJI Zenmuse L1 LiDAR sensor, and a DJI Zenmuse H20T Thermal and RGB sensor.

The surveys were flown using a Stonex S900 GNSS receiver Base Station, and ground control points/targets location measured using Trimble Geo7x GNSS devices. For the thermal survey, hot packs were used to help identify the targets in the thermal images as much of this survey was flown after dark. The purpose of doing night flights was to maximize the temperature differential between ambient air and ground surface temperatures.

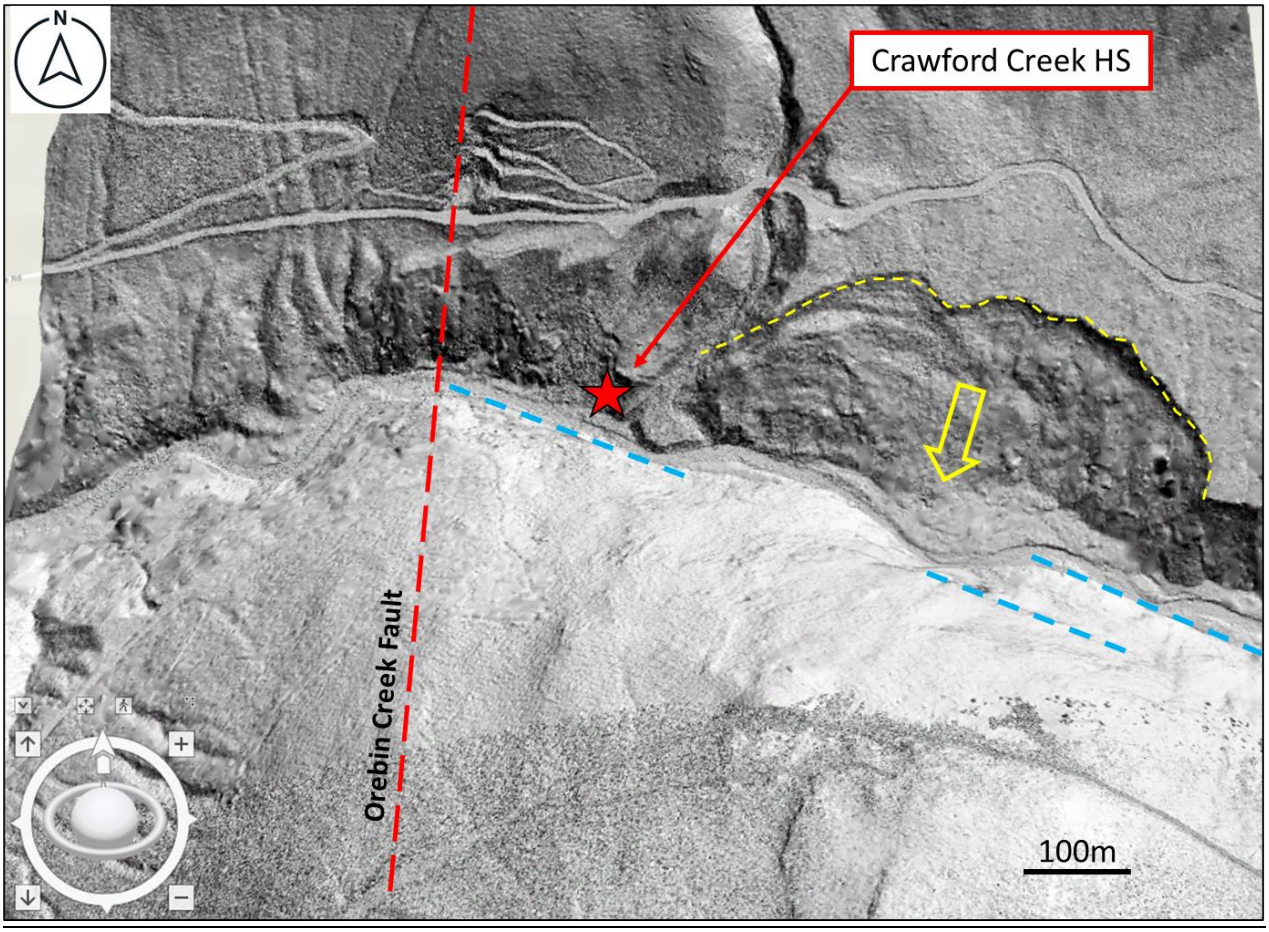

Figure 21 – Preliminary LiDAR image over the Crawford Creek area of interest, WNW striking lineaments highlighted in blue and slump feature highlighted in yellow.

LiDAR surveys were flown at a height of 120m, and thermal surveys were flown at 100m due to the lower resolution of the thermal sensor. The surveys were broken into multiple flights to allow for battery changes. Terrain following was implemented to ensure a consistent elevation and to maintain the ground sampling distance (which minimizes error in data processing). Since much of the area was densely forested, an overlap of 90% was used between flight lines.

LiDAR point clouds were downloaded off the L1 sensor and converted into LAS files. The LAS files were categorized into ground and all-point layers for production of a digital elevation model (DEM) and digital surface model (DSM) respectively. The DEM strips away all vegetation to allow a visualization and analysis of the bare ground. Data were processed using CloudCompare.

Thermal images were downloaded off the H20T sensor in a raw JPG format. The images were converted to a geotiff format which allowed for relative

temperatures to be converted to radiometric temperatures. The images were then stitched together in a mosaic using Correlator 3D.

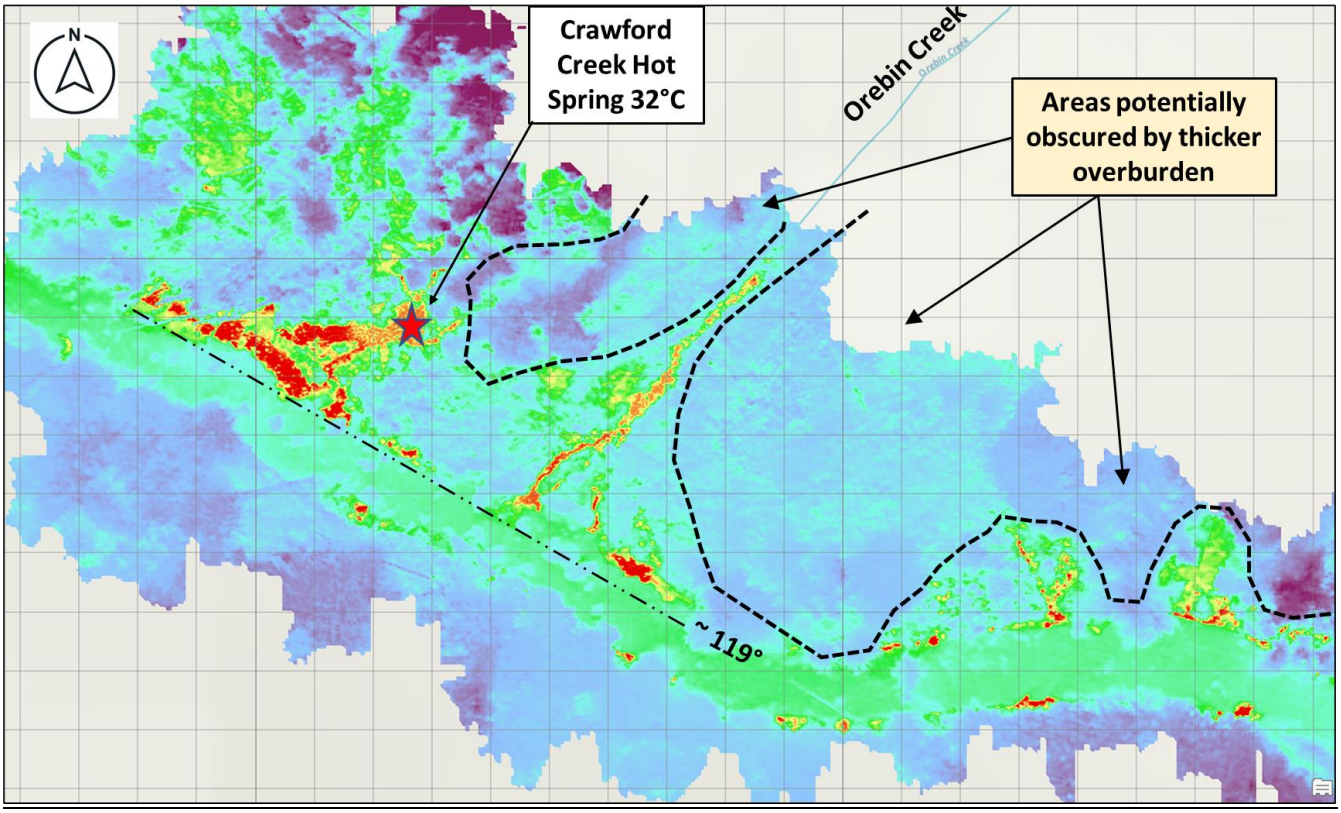

Figure 22 – Preliminary (partial) Total Infrared (TIR) thermal image mosaic over the Crawford Creek area of interest. Area of anomalous thermal signature extends across an area of approximately 190m by 55m. The grid shown is 10m by 10m.

Comparing the measured trends from the thermal image in Figure 22 to the structural measurements from outcrop taken in the field, the strike of Crawford Creek at this location (119°) fits within the data range for jointing measured in the Orebin Creek area (See Figure 24 below). When comparing the LiDAR image with the thermal image it appears that much of the area east of the Crawford Creek hot spring is beneath the slump feature identified in Figure 20 (in whole or in part). Small thermal features close to the valley bottom and on the easterly edge of the mosaic appear to be seeps situated along, or proximal to, the down slope edge of this slump feature.

Close examination of individual thermal anomalies, within the mosaic, suggest that the relative strength (or measured relative temperature) of each feature decreases upslope. This could be a function of overburden thickening away from

the valley bottom with the thermal water measured being deeper within the overburden and therefore less evident to the thermal sensors (Figure 22 detail below).

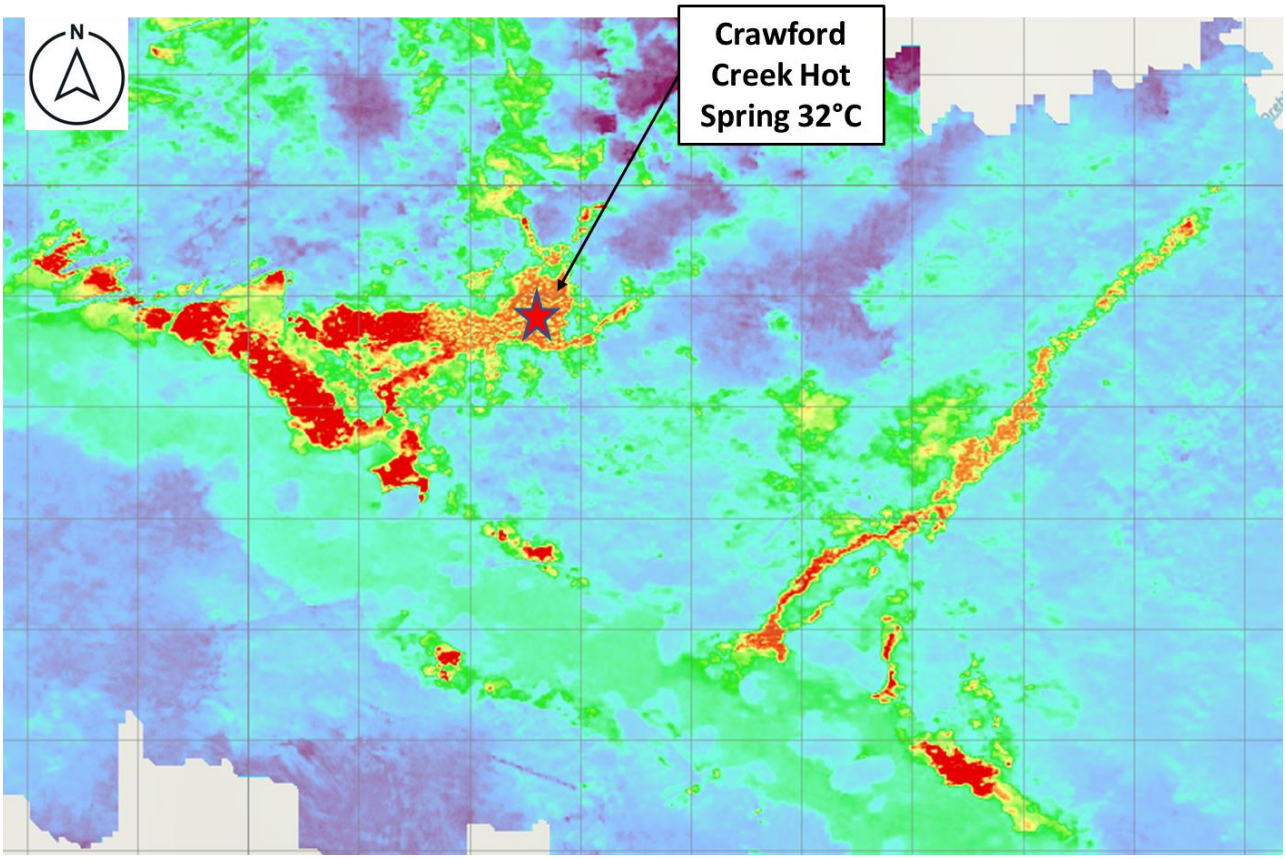

Figure 23 – Preliminary (partial) TIR thermal image mosaic, zoomed in over the Crawford Creek hot spring and upslope area above the spring. The grid shown is 10m by 10m.

There is also a linear thermal feature associated with the bottom of the Orebin Creek drainage. It appears there may be a point source beneath the creek or in the adjacent slope which elevates creek temperatures through the final 50 meters of its decent, before emptying into Crawford Creek.

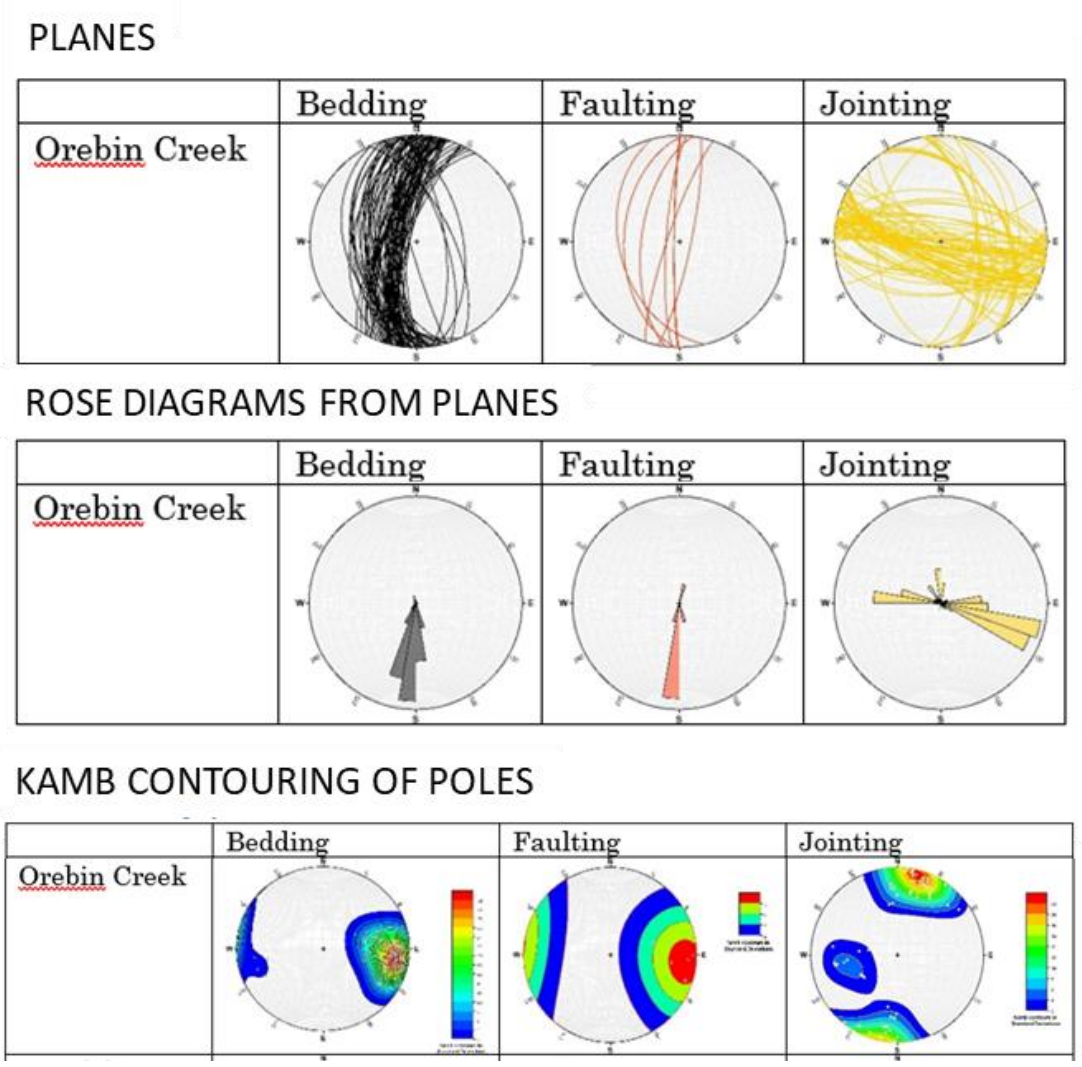

Figure 24 – Summary of structural measurements for the Orebin Creek area taken in the summer of 2022 (Vandenbrink, 2022)

A review of only a small portion of the thermal data has occurred thus far and the preliminary indications are encouraging. The overburden (glacial till and fluvial fill) appears to mask the potential extent and full expression of the thermal anomalies observed. In addition, the underlying structural trends and their relationship to the thermal features are obscured. Less than 5% of the total thermal mosaic has been received (at the time of writing); the work to date already highlights specific areas where further work in Phase Three can be directed.

Topographic Map

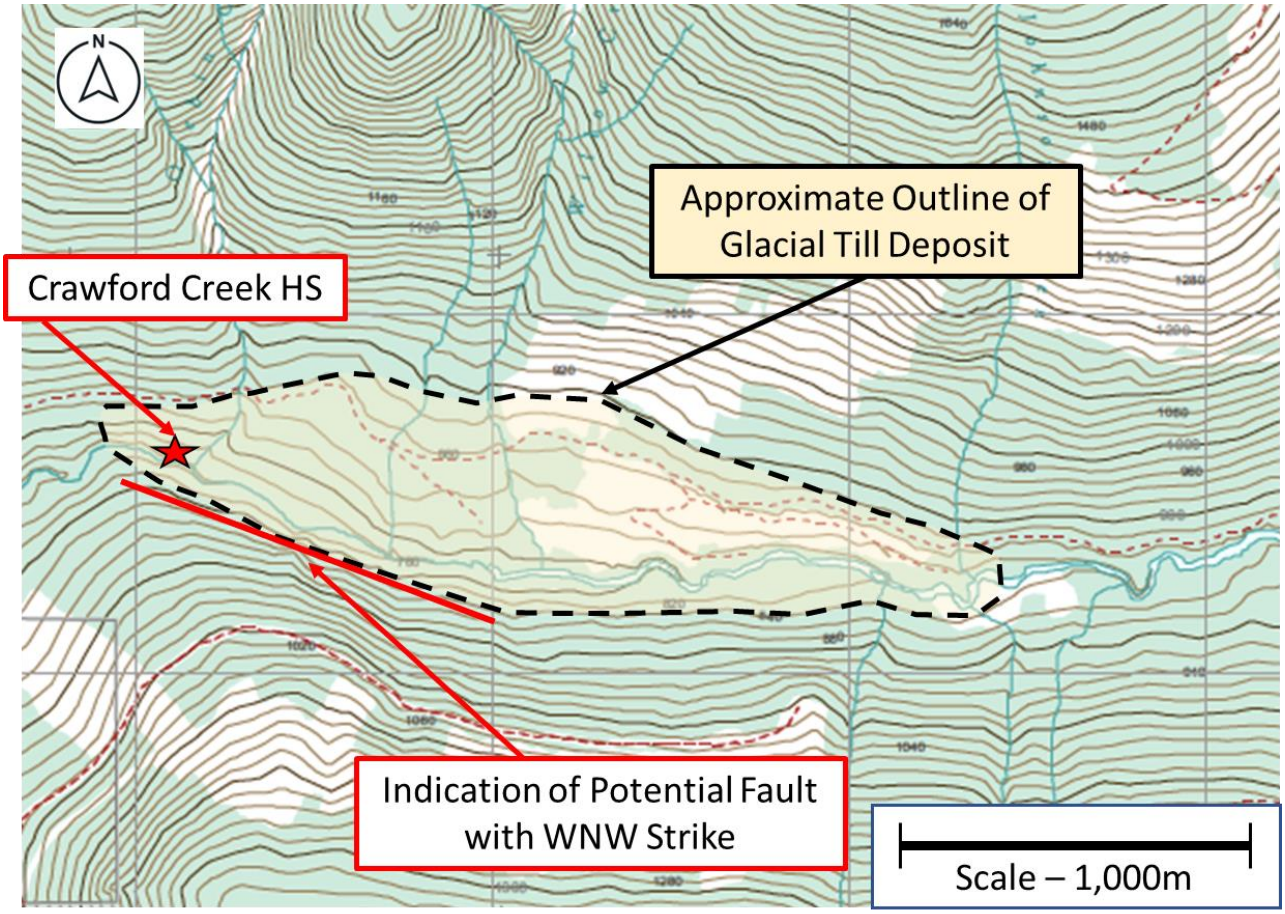

Figure 25 – Approximate position of glaciofluvial lobe extending along Crawford Creek to the Crawford Creek hot spring in the east. Modified from BC Ministry of Environment Soil Resources Map, Nelson Area.

The glaciofluvial till sediments deposited in the Crawford Creek valley bottom have previously been mapped (BC Ministry of the Environment, 1980). When this mapping is compared to LiDAR and topographic maps, the lobe of glaciofluvial deposits occur where the topographic contour spacing broadens, thinning where tight topographic contours suggest the near surface presence of bedrock (Figure 25). On the south side of Crawford Creek, the edge of glaciofluvial deposits may have been controlled in part by potential WNW faulting, as evidenced by a tightening of contours and a change in strike of the valley floor observed there.

In addition to the Crawford Creek hot spring focus area, several other areas of interest emerged as field results were integrated into the project. Figure 26 (below) shows the location of the top three leads. Lead #1, located on the east side of Crawford Bay is the most compelling lead thus far, after Crawford Creek.

The area is host to Badshot marble and is highly faulted with two major faults identified and mapped, one most likely being the Bernard Fault. In the outcrop, the Bernard Fault zone was measured to be approximately 50m wide, iron-stained, brittle, and highly chloritized.

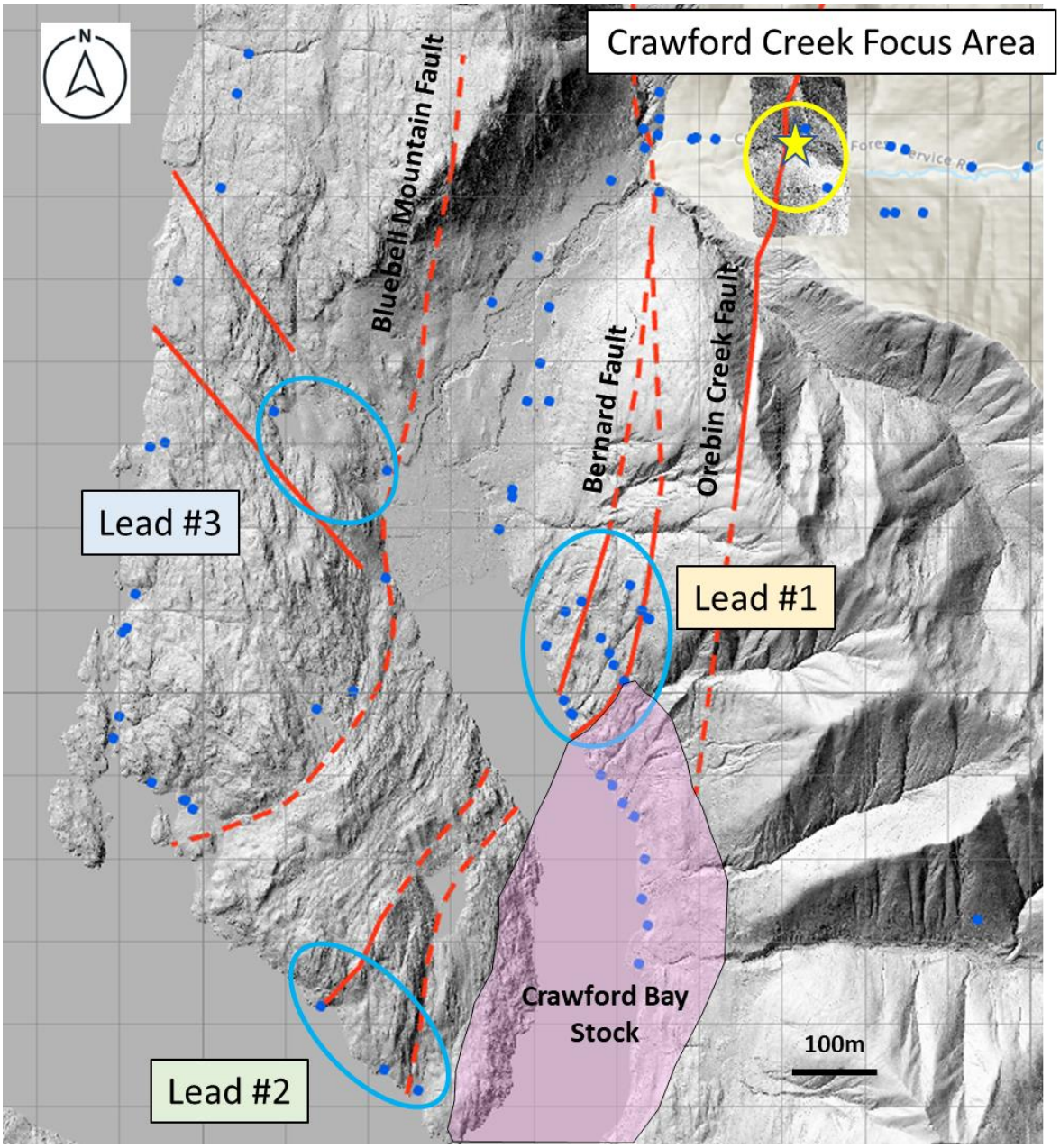

Figure 26 – Location of key areas of interest for further work. Crawford Creek hot spring to the north on Crawford Creek. Leads 1 and 3 near Crawford Bay and Lead 2 at the south end of Pilot Peninsula (blue dots are water test sites, solid red lines are mapped faults and dashed red lines are inferred faults).

Surface waters tested in this area had elevated TDS (up to 424 ppm) and conductivity levels up to 597 µS/cm, with three sites exhibiting temperatures ranging from 19-24.8°C. The site which had the highest temperature was proximal to a 10m wide chloritized fault zone and directly offsetting the Crawford Bay Stock to the south. Lead #1 will be targeted for geological and geochemical follow-up in Phase Three.

5) Recommendations for Further Work, Phase Three (2023)

A preliminary plan for Phase Three is summarized here within the following categories:

Detailed Geology and Geochemistry – Focusing on the Orebin Creek area as a priority, detailed geological mapping of all available outcrops is planned. A more focused geological program will allow for close examination of folding, joint sets and any related mineralization or alteration. A detailed geochemistry program will test and appropriately sample any seeps and springs, particularly those evidenced from the 2022 thermal survey. There will be multiple measurements and samples surrounding the location of Crawford Creek hot spring and along Crawford and Orebin Creeks, to further characterize the hydro-geothermal system and to increase the confidence in the measurements received. This detailed Geochem program may include sampling for dissolved silica (SiO_2) as well as sampling for δD (deuterium) and δ O (oxygen) isotopes. This isotope analysis may provide a way to estimate the proportion of meteoric water in the samples. The flow rate of each spring identified within the Crawford Creek system will be measured in-situ using a flow probe or alternate method. This will help quantify the hydrothermal / geothermal system.

Additional geochemical related work being considered is sampling for dissolved silica for geothermometry calculations. Also, should Lead #1 continue to validate geothermal potential there, sampling for helium isotopes (3He/4He ratios) could be done to determine if a radiogenic heat source related to the Crawford Bay Stock is potentially involved in this area.

Given that much of the thermal survey area has still to be processed, the scope of work will likely expand beyond what the current mosaic covers and potentially highlight other thermal anomalies which will need similar detailed follow-up work as part of Phase Three.

Geospatial and Geophysical – This will involve another thermal survey including a Multi-Spectral Infrared survey, a thermal video of a broader area, and potentially a UAV Magnetometer survey. Consideration will be given to conducting up to three drone-based thermal assessments, each in different seasons – summer, fall and winter to observe any seasonal changes to the discharge of thermal fluids related to the Crawford Creek system.

The surface expression of thermal features appear to be related to a WNW structure following Crawford Creek, or parallel to it, and outflows of thermal water are either related to these structures or Hamill H1 bedding-parallel structures. In either case, the full extent of the Crawford Creek thermal anomaly is likely masked by overburden. An Electrical Resistivity Tomography (ERT) survey could effectively

map overburden thickness and indirectly map underlying bedrock, identifying any structures or trends and how these features relate to the thermal anomalies identified thus far. Depending on the survey geometry it is possible to image resistivity structure, which is controlled mostly by groundwater saturation levels. This could assist in delineating spring flow pathways.

Figure 25 shows the approximate extent of the main glacial deposit around the Crawford Creek hot spring. The eastern end of this deposit is covering and partially masking the geothermal surface expression and represents an area requiring an alternative technology such as ERT to provide further definition of overburden, as well as variations in subsurface fluid saturation. A UAV Magnetometer survey could also define overburden thickness and over a broader area, providing context to the ERT survey.

3D Geological and Geothermal Modelling – A key priority in Phase Three will be to build a detailed and fully integrated 3D model, showing bedrock lithology, bedding, jointing, and faulting, with the thermal anomalies measured at surface projected to depth. If possible, the model could help provide an estimate of the flow rate for the entire system including observed seeps. This would constrain the hydrogeological model further, knowing the volume and heat content being emitted from the system.

This 3D model would be used to guide the drill planning process, as directional drilling to encounter enhanced fracturing will be considered. Modelling of this nature will require the use of software programs such as Leapfrog by Sequent.

Drilling Test Well(s) – Depending on how well the above three elements continue to corroborate and support the presence of a geothermal reservoir proximal to the surface, a test well or wells will be considered for early 2024. The aim in drilling these test wells will be to confirm suitable fluid temperature at depth, establish a geothermal gradient and to determine sustained fluid flow rates.

Potential Future Commercial Opportunities – When field investigations from Phase Three of the Kootenay Lake Geothermal Project have been successfully concluded, a predictive geological and geothermal model will be developed leading to the quantification of a geothermal reservoir target for drilling. A geothermal reservoir that yields sufficient heat content and fluid flow rates will present a range of Direct Heat applications prospective for the Kootenay Lake area, along with numerous low carbon opportunities that would lend themselves to sustainable economic community development.

Cold weather climates in the northern hemisphere such as Alaska, Iceland and the Netherlands have demonstrated geothermal derived heat can sustainably grow agricultural products year-round. In 1992, the Desrochers feasibility

assessment for the geothermal energy of the Bluebell Mine in Riondel envisioned nine Quonset style greenhouses, each 7 x 60m (3,780 sq m) for a 100% capacity (year-round) greenhouse complex. Geothermal direct heat applications have expanded greatly in recent years, providing many examples of how worldwide best practices approaches can be applied in the Central Kootenay's region.

6) Conclusion

The Phase Two field program conducted over the Kootenay Lake project area has provided a valuable geological and geochemical framework which has highlighted the geothermal potential of the local area and the Crawford Creek valley specifically. Crawford Creek is the site of an existing hot spring (32°C), which is proximal to the Orebin Creek Fault (OCF), a south striking, steeply dipping normal fault. This is a fault which could act as a conduit for the movement of geothermal fluids from depth.

The Crawford Creek hot spring has water chemistry which is similar to other area hot springs. These hot springs are known to be slightly acidic and demonstrate elevated levels of sulphate, magnesium and sodium or potassium in particular. While the Crawford Creek hot spring does not exhibit the same high concentrations, it does have levels which are elevated beyond most background levels observed in most of the remaining samples analyzed in 2022. The host reservoir of the Crawford Creek hot spring is the Hamill H1, which is a massive, white quartzite. This quartzite is highly fractured in the immediate vicinity of the OCF with persistent WNW jointing (strike ~ 119°, dip 70°). Steeply dipping bedding with frequent jointing within a brittle quartzite suggests the potential for enhanced permeability with improved movement of geothermal fluids from depth in the immediate area.

The drone-based evaluation of the area surrounding the Crawford Creek hot spring and along the Orebin Creek Fault have further accentuated the area's potential. Preliminary thermal mapping shows a surface geothermal expression which extends beyond the hot spring, up and down the valley for a total of 400 metres and upslope from the valley bottom over 55 metres distance. The detailed LiDAR acquired in this area shows a well-defined overburden slump feature extending east from the hot spring. This slump of glaciofluvial till material appears to be responsible for masking and potentially supressing a broader geothermal surface expression in the immediate vicinity. With only a small portion of the thermal data processed and compiled in the mosaic at the time of writing, the thermal anomaly could expand further from the current footprint.

The work currently planned for Phase Three of this project will target the Crawford Creek and Orebin Creek areas, surrounding the Crawford Creek hot spring, with the objective of gathering remaining geotechnical data to allow generation of a geothermal model and to identify a drilling location. This work will allow for the drilling of a test well, or wells, within the subsequent 12-18 months. Encountering geothermal fluids in the 40-80°C range, with substantial and sustained flow rates, could lead to the development of a commercial-based, pilot geothermal demonstration project within two years.

7) Acknowledgments

Phase Two of this project was made possible through the initial funding support of The Regional District of Central Kootenay – Community Sustainable Living Advisory Committee (CSLAC), Economic Development Commission (EDC) and a Community Development grant. Additional funds were later made available through CICan – The Colleges and Institutes Canada, Geoscience BC and The Natural Sciences and Engineering Research Council of Canada (NSERC).

Funding for this initiative has been provided in part by the Government of Canada through Natural Resources Canada's Green Jobs – Science and Technology Internship Program, as part of the Youth Employment and Skills Strategy (*Le financement de cette initiative est fourni par le gouvernement du Canada par l'entremise du Programme de stages en sciences et technologie - Emplois verts)*.

This project would not have been possible without the support of these groups.

Countless hours of open and ongoing geological discussions with retired area geologist, Sonni Greene, (Kootenay Bay, BC) were incredibly valuable; advancing an understanding of observed geological phenomena and in helping to mature the most appropriate geological / geothermal model for the area.

Technical research support followed by broad technical and business-related discussions were generously provided by another retired geologist, Dan Gatto, who lives in Harrop, BC.

Fourth-year geology student, Colin Vandenbrink (Simon Fraser University) was hired to conduct our summer field program. Colin's ability to work independently in a technically challenging environment was greatly appreciated. Colin also brought numerous new innovative approaches to the fieldwork which enabled him to cover a lot of ground, collecting volumes of data, in a relatively short field season.

Fourth-year geology student, Aidan McQuarrie from the University of Victoria supported the project through his direct studies program, visiting the field and supporting the initial drone operation. He has since conducted a literature review and completed an assessment of the structural geology data gathered, integrating this data with geochemistry results from the summer fieldwork. Aidan's technical advisor at the University of Victoria is Theron Finley. Theron's structural geology background and his firsthand experience working on geothermal systems in the Kootenay's was greatly appreciated.

Significant hands-on efforts by Alec Kvarnstrom and Marcus Friesen (fourth-year Selkirk College students) and the ongoing mentorship provided by GIS instructor,

Robert McQuarrie as well as drone pilot David Greaves, drove the GIS initiative forward and made the final data acquisition outcomes possible.

Finally, Stefan Humphries, a hydrogeologist based in Nelson, BC assisted in the review of geochemistry results and guided the preliminary interpretation of these results, in addition to providing suggestions for the Phase Three geochemistry program.

8) References

Allmendinger R. (2022) Stereonet Mobile App
http://www.geo.cornell.edu/geology/faculty/RWA/programs/stereonet.html

Andrews, G.D.M. and Russell, J.K., (2007) Cover Thickness across the Southern Interior Plateau, British Columbia (NTS 092O, P; 093A, B, C, F): Constraints from Water-Well Records. in Geoscience BC Summary of Activities 2007, Geoscience BC Report 2008-1, p.11-20.

BC Ministry of the Environment (1980), Soil Resources of the Nelson Map Area, RAB Bulletin 20.

Beaudoin, G. Roddick, J.C., and Sangster, D.F., (1992), Eocene age for Ag-Pb-Zn-Au vein and replacement deposits of the Kokanee Range, southeastern British Columbia, Canadian Journal of Earth Sciences, 29(1): p. 3-14.

Blewitt, G., Coolbaugh, M., Holt, W., Kreemer, C., Davis, J., & Bennett, R., (2002), Targeting of potential geothermal resources in the Great Basin from regional relationships between geodetic strain and geological structures: Geothermal Resources Council Transactions, v. 26, p. 523–526.

Brown, D.A., MacLeod, R.F., and Wagner, C.L. (comp.), 2011. Geology, Kaslo, British Columbia; Geological Survey of Canada, Open File 6306

Brown, D.A., Wagner, C.L., and Chow, W., (2011). Geology, Crawford Bay, British Columbia; Geological Survey of Canada, Open File 6307

Canadian Geothermal Energy Association, (2013) Geothermal Technology Roadmap: Global Best Practices Summary, Exploration through Generation, Calgary, Alberta

Chen, Y. et al (2019) Seismic evidence for a mantle suture and implications for the origin of the Canadian Cordillera, Nature Communications

Colpron, M. and Price, P.A. (1995) Tectonic Significance of the Kootenay Terrane, Southeastern Canadian Cordillera: An Alternative Model, Geology; January 1995; v. 23; no. 1.

Cook, F.A., (2016) Merging Geological, Seismic Reflection and Magnetotelluric Data in the Purcell Anticlinorium, Southeastern British Columbia, Geoscience BC Report 2016-001

Crosby P., (1968), Tectonic, Plutonic, and Metamorphic History of the Central Kootenay Arc, British Columbia, Canada: Geological Society of America, Special paper 99, 94p.

Desrochers, D.T., (1992) Geothermal Feasibility Study for the Use of Hot Water Near Riondel, British Columbia, Geological Survey of Canada Open File 2502

Doughty, P.T., and Price, R.A., (2000) Geology of the Purcell Trench Rift Valley and Sandpoint Conglomerate: Eocene En-echelon Normal Faulting and Synrift Sedimentation Along the Eastern Flank of the Priest River Metamorphic Complex, northern Idaho, GSA Bulletin; September 2000; v. 112; no. 9; p. 1356–1374;

Erkan, K., Holdman, G., Blackwell, D. and Benoit, W., (2007) Thermal Characteristics of the Chena Hot Springs, Alsaka Geothermal System, Proceedings, Thirty-Second Workshop on Geothermal Reservoir Engineering Stanford University, Stanford, California

Faulds, J., Coolbaugh, M., Bouchot, V., Moeck, I., and Oğuz, K., (2010) Characterizing Structural Controls of Geothermal Reservoirs in the Great Basin, USA, and Western Turkey: Developing Successful Exploration Strategies in Extended Terranes, Proceedings World Geothermal Congress 2010 Bali, Indonesia

Faulds, J. E. and Hinz, N.H., (2015) Favorable Tectonic and Structural Settings of Geothermal Systems in the Great Basin Region, Western USA: Proxies for Discovering Blind Geothermal Systems, Proceedings World Geothermal Congress, Melbourne, Australia, 19-25 April 2015

Finley, T (2020) Fault-hosted geothermal systems in southeastern British Columbia, MSc Thesis University of Alberta

Finley T., Johnston S, Unsworth, M., Banks J, and Dinu-Ion, P. (2022) Modern Dextral Strain Controls Active Hydrothermal Systems in the Southeastern Canadian Cordillera, to be published.

Fyles, J.T., (1967) Geology of the Ainsworth-Kaslo Area, British Columbia, BC Department of Mines and Petroleum Resources, Bulletin No. 53, Victoria BC.

Georgsson, L. S., (2009) Geophysical Methods Used in Geothermal Exploration, United Nations University Geothermal Training Programme, Reykjavik, Iceland

Geoscience BC, (2016) Report 2015-11: An Assessment of the Economic Viability of Selected Geothermal Resources in British Columbia; BC Hydro Technical Supplement, October 2016, URL

https://www.bchydro.com/content/dam/BCHydro/customer-portal/documents/corporate/regulatory-planning-documents/integrated-resource-plans/current-plan/rou-characterization-geothermal-technical-supplement-201610.pdf (February 2023)

Ghomshei, M. (2010). "A presentation at the Canadian Geothermal Energy Association Annual Conference 2010". New Frontiers in Geothermal Energy. Vancouver: CanGEA.

Grasby, S.E., I. Hutcheon and H.R. Krouse, (2000) The Influence of Water-Rock Interaction on the Chemistry of Thermal Springs in Western Canada. Applied Geochemistry, Vol. 15, p. 439-454.

Grasby, S.E. and I. Hutcheon, (2001) Controls on the Distribution of Thermal Springs in the Southern Canadian Cordillera. Canadian Journal of Earth Sciences, Vol. 38, p. 427-440.

Gradsby, S.E., et al (2012) Geothermal Energy Resource Potential of Canada, Geological Survey of Canada Open File 6914

Greene, S. A., (1981) Geological Report Jackass Claims, Barefoot Groups, Prepared for Springpoint Resources Ltd., Calgary Alberta

Höy, Trygve, (1980) Geology of the Riondel Area Central Kootenay Arc Southeastern British Columbia, Bulletin 73 – Ministry of Energy Mines and Petroleum Resources, Victoria, BC

Jessop, A.M., (1986) Catalogue of Boreholes 2 – Geothermal Energy Holes. Report for British Columbia Hydro and Power Authority, Internal Report No. 86-2, January 1986, 58 p.

Kerr Wood Leidal, Consulting Engineers, (2016) An Assessment of the Economic Viability of Selected Geothermal Resources in British Columbia - Revised final (R1) report; Geoscience BC, Report 2015-11, 131 p., URL https://cdn.geosciencebc.com/project_data/GBCReport2015-11/GBC2015-11_KWL_Geothermal%20Economics_Project_Report_27Sep16.pdf (February 2023)

Kimball, Sarah, (2010) Favourability Map of British Columbia Geothermal Resources, Masters of Applied Science Thesis, Faculty of Graduate Studies, UBC, Vancouver

Leclair, A.D. (1988) Polyphase Structural and Metamorphic Histories of the Midge Creek Area, Southeast British Columbia: Implications for Tectonic Processes in the Central Kootenay Arc. Ph.D. thesis, Queen's University, 264 p.

Majorowicz & Grasby, (2010) High Potential Regions for Enhanced Geothermal Systems in Canada, Natural Resources Research, Vol. 19, No. 3, September 2010

Monger, J. W. H., Price, R. A., & Tempelman-Kluit, D. J. (1982). Tectonic accretion and the origin of the two major metamorphic and plutonic welts in the Canadian Cordillera. *Geology*, *10*(2), 70-75.

Moynihan, D. & Pattison, D.R.M. (2008). Origin of the Kootenay Lake Metamorphic High, Southeastern British Columbia. *British Columbia Geological Survey Geological Fieldwork, 2008-1,* 147–158.

Moynihan, D.P., and Pattison D.R.M., (2013) Barrovian Metamorphism in the Central Kootenay Arc, British Columbia: Petrology and Isograd Geometry, Canadian Journal of Earth Science 50: 769–794

Moynihan, D.P., and Pattison D.R.M., (2011) The Origin of Mineralized Fractures at the Bluebell Mine Site, Riondel British Columbia, Society of Economic Geologists, Inc., Economic Geology, v. 106, pp. 1043–1058

Pattison, D.R.M., Moynihan, D.P., McFarlane, C.R.M., Simony, P.S. & Cubley, J.F. (2020) Field guide to the geology, metamorphism and tectonics of the Foreland and Omineca belts of SW Alberta and SE British Columbia. Geological Association of Canada Field Guide Series 2020-A, 257 pages

Peters, J. (2012) Late Pleistocene Evolution of Glacial Lake Purcell: A Potential Floodwater Source to the Channeled Scabland, MSc Thesis Simon Fraser University Vancouver BC

Rioseco, N.A. and Pattison, D.R.M. (2018): Preliminary investigations of the metamorphic and thermochronological interface between the Purcell Anticlinorium and the Kootenay Arc, southeastern British Columbia (NTS 082F, G); in Geoscience BC Summary of Activities 2017: Minerals and Mining, Geoscience BC, Report 2018-1, p. 47–56.

Robins, J., Kolker, A., Flores-Espino, F., Pettitt, W., Beckers, K. Pauling, H. and Anderson, B. (2021) 2021 U.S. Geothermal Power Production and District Heating Market Report, National Renewable Energy Laboratory (NREL)

Smith, Jerome, (2015) Geothermal Development for Colorado, Economics of Heat vs. Power Only, Advances in Geothermal Direct-Use Workshop. NREL 2015,

URL https://www.energy.gov/sites/prod/files/2015/07/f24/03-The-Importance-of-Shifting-Exploration-Models---Jerry--Smith_0.pdf

Smith, M.T. and Gehrels, G.E., (1992) Structural Geology of the Lardeau Group Near Trout Lake, British Columbia: Implications for the structural evolution of the Kootenay Arc, Department of Geosciences, University of Arizona, Tuscon Az.

Turner, R.J.W., Anderson, R.G., Franklin, R., Anderton, L., and Fowler, F. (2009) Geotour Guide for the West Kootenay's BC, Geological Survey of Canada Open File 6135

Tuya Terra Geo Corp., (2016) Direct-use Geothermal Resources in British Columbia Report 2016-07 (Section A), Burnaby, BC

Webster, E. (2016). Tectonothermal Evolution of the Southern Omineca Belt, Southeastern British Columbia (Unpublished doctoral thesis). University of Calgary, Calgary, AB.

Webster, E.R. and Pattison, D.R.M., (2013) Metamorphism and Structure of the Southern Kootenay Arc and Purcell Anticlinorium, Southeastern British Columbia (Parts of NTS 082F/02, /03, /06, /07); in Geoscience BC Summary of Activities 2012, Geoscience BC, Report 2013-1, p. 103–118.

Webster, E.R. and Pattison, D. R. M., University of Calgary, (2018) Spatially Overlapping Episodes of Deformation, Metamorphism, and Magmatism in the Southern Omineca Belt, Southeastern British Columbia, Canadian Journal of Earth Science 55: 84–110

Webster, E.R., Archibald, D.A., Pattison, D.R.M., Pickett, J.A. and Jensen, J.C. (2020) Tectonic Domains and Exhumation History of the Omineca Belt in Southeastern British Columbia from 40/Ar/39Ar Thermochronology, Canadian Journal of Earth Sciences 57: 918-946, 2020

9) Appendix

A. Geology Summer Student Report – C. Vandenbrink, 2022
(Attached as a separate file)

B. University of Victoria, Student Report – A. McQuarrie, 2022
(Attached as a separate file)

C. Laboratory analysis summary – CARO Labs, Kelowna

CARO Analytical Services	**Client** South Kootenay Lake Community Services Society																							
FINAL Analytical Testing R	**Attention** Gary Sly																							
Work Order: 22I0019	**Project** Analytical Testing																							
Report Date: 2022-10-31 1	**Project Info** [none]																							
Note: This is not the original data. Please refer to PDF / Hardcopy report.																								
LAB ID					22I0019-01	22I0019-02	22I0019-03	22I0019-04	22I0019-05	22I0019-06	22I0019-07	22I0019-08	22I0019-09	22I0019-10	22I0019-11	22I0019-12									
CLIENT ID					52	51	91W	13	47	46	17	72	82	101	94	85								
DATE SAMPLED					2022-08-29	2022-08-29	2022-08-29	2022-08-29	2022-08-29	2022-08-29	2022-08-29	2022-08-30	2022-08-30	2022-08-30	2022-08-30	2022-08-30									
DATE RECEIVED					2022-08-31	2022-08-31	2022-08-31	2022-08-31	2022-08-31	2022-08-31	2022-08-31	2022-08-31	2022-08-31	2022-08-31	2022-08-31	2022-08-31									
MATRIX					Water	Water	Water	Water	Water	Water	Water	Water	Water	Water	Water	Water								
General Method	**Analyte**	**Units**	**MRL**	**Std (CDWQG)**																				
Anions	Bromide	mg/L	0.1	N/A	<0.10	<0.10	<0.10	<0.10	<0.10	<0.10	<0.10	<0.10	<0.10	<0.10	<0.10	<0.10								
Anions	Chloride	mg/L	0.1	AO<=250	22	2.79	1.48	0.69	0.79	0.63	0.25	0.25	7.61	0.23	0.4	0.17								
Anions	Fluoride	mg/L	0.1	MAC=1.5	0.29	<0.10	0.36	<0.10	0.15	0.7	<0.10	<0.10	<0.10	<0.10	<0.10	<0.10								
Anions	Sulfate	mg/L	1	AO<=500	13.5	2.9	7.6	13.8	29	96.9	6.3	12.7	2	11.7	19.2	<1.0								
Calculated Parameters	Hardness, Total (as CaCO3)	mg/L	0.5	None Required	217	68.7	175	97.5	256	413	53.4	22	65.2	110	295	2.73								
General Parameters	Alkalinity, Total (as CaCO3)	mg/L	1	N/A	255	88.7	212	129	232	233	84.8	20.2	87.7	137	322	5.4								
General Parameters	Alkalinity, Phenolphthalein (a	mg/L	1	N/A	<1.0	<1.0	<1.0	<1.0	<1.0	<1.0	<1.0	<1.0	<1.0	<1.0	<1.0	<1.0								
General Parameters	Alkalinity, Bicarbonate (as CaC	mg/L	1	N/A	255	88.7	212	129	232	233	84.8	20.2	87.7	137	322	5.4								
General Parameters	Alkalinity, Carbonate (as CaCO	mg/L	1	N/A	<1.0	<1.0	<1.0	<1.0	<1.0	<1.0	<1.0	<1.0	<1.0	<1.0	<1.0	<1.0								
General Parameters	Alkalinity, Hydroxide (as CaCO	mg/L	1	N/A	<1.0	<1.0	<1.0	<1.0	<1.0	<1.0	<1.0	<1.0	<1.0	<1.0	<1.0	<1.0								
General Parameters	Sulfide, Total	mg/L	0.02	AO<=0.05	<0.020	<0.020	<0.020	<0.020	<0.020	<0.020	<0.020	<0.020	<0.020	<0.020	<0.020	<0.020								
Total Metals	Aluminum, total	mg/L	0.005	OG<0.1	<0.0050	0.0131	<0.0050	0.0265	0.0375	20	0.045	<0.0050	0.0446	0.0937	0.0119	0.0175								
Total Metals	Antimony, total	mg/L	0.0002	MAC=0.006	<0.00020	<0.00020	<0.00020	<0.00020	<0.00020	<0.00040	<0.00020	<0.00020	<0.00020	<0.00020	<0.00020	<0.00020								
Total Metals	Arsenic, total	mg/L	0.0005	MAC=0.01	<0.00050	<0.00050	<0.00050	<0.00050	<0.00050	<5.10	<0.00050	0.0015	<0.00050	<0.00050	<0.00050	<0.00050								
Total Metals	Barium, total	mg/L	0.005	MAC=2	0.0582	0.0063	<0.0050	0.0436	0.0432	0.156	0.0205	0.0155	0.0291	0.0097	0.0138	0.0416								
Total Metals	Beryllium, total	mg/L	0.0001	N/A	<0.00010	<0.00010	<0.00010	<0.00010	<0.00010	0.0247	<0.00010	<0.00010	<0.00010	<0.00010	<0.00010	<0.00010								
Total Metals	Bismuth, total	mg/L	0.0001	N/A	<0.00010	<0.00010	<0.00010	<0.00010	<0.00010	<0.00020	<0.00010	<0.00010	<0.00010	<0.00010	<0.00010	<0.00010								
Total Metals	Boron, total	mg/L	0.05	MAC=5	<0.0500	<0.0500	<0.0500	<0.0500	<0.0500	<0.100	<0.0500	<0.0500	<0.0500	<0.0500	<0.0500	<0.0500								
Total Metals	Cadmium, total	mg/L	1E-05	MAC=0.005	<0.000010	<0.000010	<0.000010	<0.000010	0.000045	0.00389	<0.000010	0.0002	<0.000010	0.000024	<0.000010	0.000017								
Total Metals	Calcium, total	mg/L	0.2	None Required	76.6	25.3	63	33	90.7	145	17.3	4.36	20.5	33.8	101	0.6								
Total Metals	Chromium, total	mg/L	0.0005	MAC=0.05	<0.00050	<0.00050	<0.00050	<0.00050	<0.00050	0.00732	<0.00050	0.00064	<0.00050	<0.00050	<0.00050	<0.00050								
Total Metals	Cobalt, total	mg/L	0.0001	N/A	<0.00010	0.00023	<0.00010	<0.00010	0.00029	0.261	<0.00010	<0.00010	<0.00010	0.00018	<0.00010	<0.00010								
Total Metals	Copper, total	mg/L	0.0004	MAC=2	<0.00040	0.00075	0.00071	0.00042	0.00153	0.284	<0.00040	<0.00040	0.00077	0.00075	0.0006	<0.00040								
Total Metals	Iron, total	mg/L	0.01	AO<=0.3	<0.010	0.169	0.403	0.033	0.073	302	0.063	<0.010	0.042	0.081	0.02	<0.010								
Total Metals	Lead, total	mg/L	0.0002	MAC=0.005	<0.00020	<0.00020	<0.00020	<0.00020	<0.00020	0.0192	<0.00020	<0.00020	<0.00020	<0.00020	<0.00020	<0.00020								
Total Metals	Lithium, total	mg/L	0.0001	N/A	0.00831	0.00108	0.00907	0.00296	0.00325	0.0269	0.00103	0.00301	0.00125	0.00072	0.00254	0.00031								
Total Metals	Magnesium, total	mg/L	0.01	None Required	6.2	1.33	4.16	3.68	6.98	12.1	2.47	2.69	3.37	6.22	10.3	0.298								
Total Metals	Manganese, total	mg/L	0.0002	MAC=0.12	0.00041	0.0254	0.0992	0.00131	0.00402	5.4	0.00284	0.00081	0.00507	0.0104	0.00297	0.00066								
Total Metals	Molybdenum, total	mg/L	0.0001	N/A	0.00052	0.00022	0.00032	0.00169	0.00107	0.00026	0.00044	0.00034	0.00028	0.00065	0.0007	<0.00010								
Total Metals	Nickel, total	mg/L	0.0004	N/A	<0.00040	0.00084	<0.00040	<0.00040	0.00146	1.07	<0.00040	0.00114	0.00053	0.00044	<0.00040	<0.00040								
Total Metals	Phosphorus, total	mg/L	0.05	N/A	<0.050	<0.050	<0.050	<0.050	<0.050	0.459	<0.050	<0.050	<0.050	<0.050	<0.050	<0.050								
Total Metals	Potassium, total	mg/L	0.1	N/A	2.58	1.34	1.76	3.62	4.73	4.72	1.67	1.2	2.69	1.33	2.83	0.49								
Total Metals	Selenium, total	mg/L	0.0005	MAC=0.05	<0.00050	<0.00050	<0.00050	<0.00050	<0.00050	<0.00100	<0.00050	<0.00050	<0.00050	<0.00050	<0.00050	<0.00050								
Total Metals	Silicon, total	mg/L	1	N/A	7.7	5.4	7.9	4.4	6.4	96.3	2.7	10.7	7.7	6	6.5	2.9								
Total Metals	Silver, total	mg/L	5E-05	None Required	<0.000050	<0.000050	<0.000050	<0.000050	<0.000050	0.000283	<0.000050	<0.000050	<0.000050	<0.000050	<0.000050	<0.000050								
Total Metals	Sodium, total	mg/L	0.1	AO<=200	3.23	1	3.78	1.06	2.01	5.07	0.62	2.19	7.57	1.17	1.53	0.47								
Total Metals	Strontium, total	mg/L	0.001	MAC=7	0.609	0.0313	0.128	0.0894	0.162	0.252	0.042	0.0397	0.0881	0.0576	0.175	0.0063								
Total Metals	Sulfur, total	mg/L	3	N/A	3.2	<3.0	<3.0	4.8	10.1	35.5	<3.0	4.2	<3.0	4	6.7	<3.0								
Total Metals	Tellurium, total	mg/L	0.0005	N/A	<0.00050	<0.00050	<0.00050	<0.00050	<0.00050	<0.00100	<0.00050	<0.00050	<0.00050	<0.00050	<0.00050	<0.00050								
Total Metals	Thallium, total	mg/L	2E-05	N/A	<0.000020	<0.000020	<0.000020	<0.000020	<0.000020	0.00061	<0.000020	<0.000020	<0.000020	<0.000020	<0.000020	<0.000020								
Total Metals	Thorium, total	mg/L	0.0001	N/A	<0.00010	<0.00010	<0.00010	<0.00010	<0.00010	0.00087	<0.00010	<0.00010	<0.00010	<0.00010	<0.00010	<0.00010								
Total Metals	Tin, total	mg/L	0.0002	N/A	<0.00020	<0.00020	<0.00020	<0.00020	<0.00020	<0.00040	<0.00020	<0.00020	<0.00020	<0.00020	<0.00020	<0.00020								
Total Metals	Titanium, total	mg/L	0.005	N/A	<0.0050	<0.0050	<0.0050	<0.0050	<0.0050	0.195	<0.0050	<0.0050	<0.0050	<0.0050	<0.0050	<0.0050								
Total Metals	Tungsten, total	mg/L	0.0002	N/A	<0.0002	<0.0002	0.0012	<0.0002	<0.0002	<0.0004	<0.0002	<0.0002	<0.0002	<0.0002	<0.0002	<0.0002								
Total Metals	Uranium, total	mg/L	2E-05	MAC=0.02	0.00167	0.000095	0.000504	0.00143	0.00103	0.00307	0.000415	0.00014	0.000495	0.000292	0.00129	0.000027								
Total Metals	Vanadium, total	mg/L	0.005	N/A	<0.0050	<0.0050	<0.0050	<0.0050	<0.0050	0.011	<0.0050	<0.0050	<0.0050	<0.0050	<0.0050	<0.0050								
Total Metals	Zinc, total	mg/L	0.004	AO<=5	<0.0040	<0.0040	0.0046	<0.0040	0.0045	1.41	<0.0040	0.0188	<0.0040	<0.0040	<0.0040	<0.0040								
Total Metals	Zirconium, total	mg/L	0.0001	N/A	<0.00010	<0.00010	<0.00010	<0.00010	<0.00010	0.00115	<0.00010	<0.00010	<0.00010	<0.00010	<0.00010	<0.00010								
CDWQG - Guidelines for Canadian Drinking Water Quality (Health Canada, June 2019)																								

CARO Analytical Services	**Client**	South Kootenay Lake Community Services Society										
FINAL Analytical Testing Report	**Attention**	Gary Sly										
Work Order: 22I0035	**Project**	Analytical Testing										
Report Date: 2022-10-31 11:06:09	**Project Info**	[none]										
Note: This is not the original data. Please refer to PDF / Hardcopy report.												
LAB ID					22I0035-01	22I0035-02	22I0035-03	22I0035-04	22I0035-05	22I0035-06	22I0035-07	22I0035-08
CLIENT ID					71	86	27	44	63	03	87	37
DATE SAMPLED					2022-08-30	2022-08-30	2022-08-30	2022-08-30	2022-08-30	2022-08-30	2022-08-30	2022-08-30
DATE RECEIVED					2022-08-31	2022-08-31	2022-08-31	2022-08-31	2022-08-31	2022-08-31	2022-08-31	2022-08-31
MATRIX					Water	Water	Water	Water	Water	Water	Water	Water
General Method	**Analyte**	**Units**	**MRL**	**Std (CDWQG)**								
Anions	Bromide	mg/L	0.1	N/A	<0.10	<0.10	<0.10	<0.10	<0.10	<0.10	<0.10	<0.10
Anions	Chloride	mg/L	0.1	AO<=250	0.26	0.2	1.02	2.27	0.36	0.17	<0.10	0.31
Anions	Fluoride	mg/L	0.1	MAC=1.5	<0.10	<0.10	0.16	<0.10	<0.10	<0.10	<0.10	<0.10
Anions	Sulfate	mg/L	1	AO<=500	3	3.1	1.5	7.2	1.9	6.2	2.7	13.5
Calculated Parameters	Hardness, Total (as CaCO3)	mg/L	0.5	None Required	26.8	21.3	82.5	327	15.1	143	21	527
General Parameters	Alkalinity, Total (as CaCO3)	mg/L	1	N/A	36.1	24	102	335	15.4	181	25.3	283
General Parameters	Alkalinity, Phenolphthalein (as CaCO3)	mg/L	1	N/A	<1.0	<1.0	<1.0	<1.0	<1.0	<1.0	<1.0	<1.0
General Parameters	Alkalinity, Bicarbonate (as CaCO3)	mg/L	1	N/A	36.1	24	102	335	15.4	181	25.3	283
General Parameters	Alkalinity, Carbonate (as CaCO3)	mg/L	1	N/A	<1.0	<1.0	<1.0	<1.0	<1.0	<1.0	<1.0	<1.0
General Parameters	Alkalinity, Hydroxide (as CaCO3)	mg/L	1	N/A	<1.0	<1.0	<1.0	<1.0	<1.0	<1.0	<1.0	<1.0
General Parameters	Sulfide, Total	mg/L	0.02	AO<=0.05	<0.020	<0.020	<0.020	<0.020	<0.020	<0.020	<0.020	<0.100
Total Metals	Aluminum, total	mg/L	0.005	OG<0.1	0.0087	0.0211	1.31	0.0134	0.0724	0.0301	0.0437	48.8
Total Metals	Antimony, total	mg/L	0.0002	MAC=0.006	<0.00020	<0.00020	<0.00020	<0.00020	<0.00020	<0.00020	<0.00020	0.00098
Total Metals	Arsenic, total	mg/L	0.0005	MAC=0.01	<0.00050	<0.00050	<0.00115	<0.00050	<0.00050	<0.00050	<0.00050	<0.00650
Total Metals	Barium, total	mg/L	0.005	MAC=2	<0.0050	<0.0050	0.0255	0.0206	<0.0050	0.0214	<0.0050	0.668
Total Metals	Beryllium, total	mg/L	0.0001	N/A	<0.00010	<0.00010	0.00019	<0.00010	<0.00010	<0.00010	<0.00010	0.00295
Total Metals	Bismuth, total	mg/L	0.0001	N/A	<0.00010	<0.00010	<0.00010	<0.00010	<0.00010	<0.00010	<0.00010	0.00698
Total Metals	Boron, total	mg/L	0.05	MAC=5	<0.0500	<0.0500	<0.0500	<0.0500	<0.0500	<0.0500	<0.0500	<0.0500
Total Metals	Cadmium, total	mg/L	1E-05	MAC=0.005	<0.000010	<0.000010	0.000024	0.00001	0.000016	<0.000010	<0.000010	0.00224
Total Metals	Calcium, total	mg/L	0.2	None Required	8.45	5.62	23.7	88.8	3.23	37.2	5.68	171
Total Metals	Chromium, total	mg/L	0.0005	MAC=0.05	<0.00050	<0.00050	0.00172	<0.00050	<0.00050	<0.00050	<0.00050	0.0519
Total Metals	Cobalt, total	mg/L	0.0001	N/A	<0.00010	<0.00010	0.00101	<0.00010	0.00027	<0.00010	<0.00010	0.0882
Total Metals	Copper, total	mg/L	0.0004	MAC=2	<0.00040	0.00045	0.00536	0.00042	0.00149	<0.00040	0.00057	0.481
Total Metals	Iron, total	mg/L	0.01	AO<=0.3	<0.010	0.014	1.51	0.015	0.09	0.033	0.036	49
Total Metals	Lead, total	mg/L	0.0002	MAC=0.005	<0.00020	<0.00020	0.00376	<0.00020	<0.00020	<0.00020	<0.00020	0.101
Total Metals	Lithium, total	mg/L	0.0001	N/A	0.00017	0.00014	0.00338	0.0019	0.00046	0.00033	0.00026	0.104
Total Metals	Magnesium, total	mg/L	0.01	None Required	1.37	1.75	5.64	25.6	1.71	12.2	1.65	24.1
Total Metals	Manganese, total	mg/L	0.0002	MAC=0.12	0.00078	0.00042	0.0318	0.00189	0.0249	0.00416	0.00264	4.48
Total Metals	Molybdenum, total	mg/L	0.0001	N/A	0.00014	<0.00010	0.00218	0.00052	<0.00010	0.00039	<0.00010	0.00304
Total Metals	Nickel, total	mg/L	0.0004	N/A	<0.00040	<0.00040	0.00285	<0.00040	0.00326	<0.00040	0.00046	0.253
Total Metals	Phosphorus, total	mg/L	0.05	N/A	<0.050	<0.050	0.089	<0.050	<0.050	<0.050	<0.050	1.97
Total Metals	Potassium, total	mg/L	0.1	N/A	0.7	0.19	1.29	3.03	0.15	1.69	0.11	8.18
Total Metals	Selenium, total	mg/L	0.0005	MAC=0.05	<0.00050	<0.00050	<0.00050	<0.00050	<0.00050	<0.00050	<0.00050	0.00445
Total Metals	Silicon, total	mg/L	1	N/A	3.7	2.5	9.6	6	3.6	3.6	2.6	62.8
Total Metals	Silver, total	mg/L	5E-05	None Required	<0.000050	<0.000050	<0.000050	<0.000050	<0.000050	<0.000050	<0.000050	0.000951
Total Metals	Sodium, total	mg/L	0.1	AO<=200	1.14	0.52	2.9	1.84	0.56	0.73	0.61	2.29
Total Metals	Strontium, total	mg/L	0.001	MAC=7	0.0162	0.0092	0.154	0.0981	0.0129	0.0472	0.0093	0.411
Total Metals	Sulfur, total	mg/L	3	N/A	<3.0	<3.0	<3.0	<3.0	<3.0	<3.0	<3.0	8.9
Total Metals	Tellurium, total	mg/L	0.0005	N/A	<0.00050	<0.00050	<0.00050	<0.00050	<0.00050	<0.00050	<0.00050	<0.00050
Total Metals	Thallium, total	mg/L	2E-05	N/A	<0.000020	<0.000020	<0.000020	<0.000020	<0.000020	<0.000020	<0.000020	0.000934
Total Metals	Thorium, total	mg/L	0.0001	N/A	<0.00010	<0.00010	<0.00010	<0.00010	<0.00010	<0.00010	<0.00010	0.0007
Total Metals	Tin, total	mg/L	0.0002	N/A	<0.00020	<0.00020	<0.00020	<0.00020	<0.00020	<0.00020	<0.00020	0.00663
Total Metals	Titanium, total	mg/L	0.005	N/A	<0.0050	<0.0050	0.0461	<0.0050	<0.0050	<0.0050	<0.0050	1.09
Total Metals	Tungsten, total	mg/L	0.0002	N/A	<0.0002	<0.0002	<0.0002	<0.0002	<0.0002	<0.0002	<0.0002	0.0032
Total Metals	Uranium, total	mg/L	2E-05	MAC=0.02	0.000034	0.000032	0.00299	0.00131	0.000102	0.000275	0.000028	0.0171
Total Metals	Vanadium, total	mg/L	0.005	N/A	<0.0050	<0.0050	<0.0050	<0.0050	<0.0050	<0.0050	<0.0050	0.0691
Total Metals	Zinc, total	mg/L	0.004	AO<=5	<0.0040	<0.0040	0.0053	<0.0040	<0.0040	<0.0040	<0.0040	0.46
Total Metals	Zirconium, total	mg/L	0.0001	N/A	<0.00010	<0.00010	0.00022	<0.00010	<0.00010	<0.00010	<0.00010	0.00699
CDWQG - Guidelines for Canadian Drinking Water Quality (Health Canada, June 2019)												

D. Stiff Diagrams from AqQa by Rockware

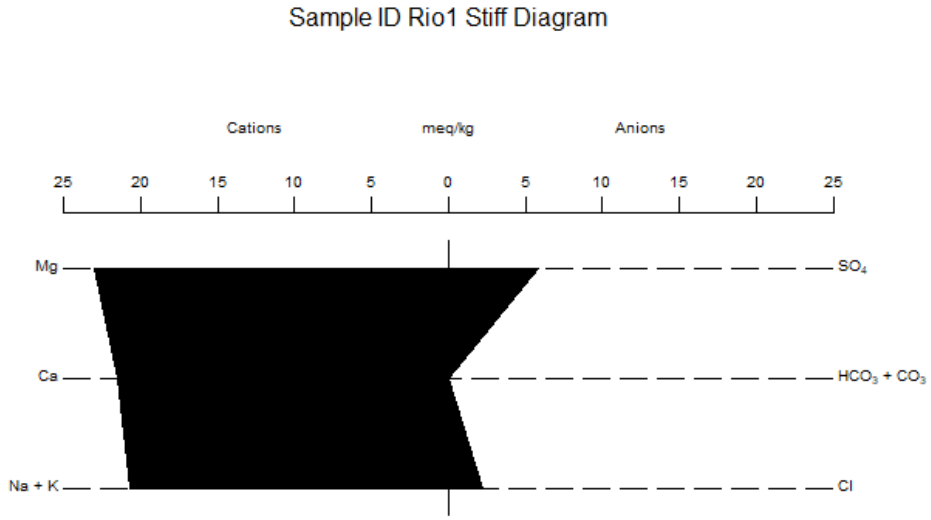

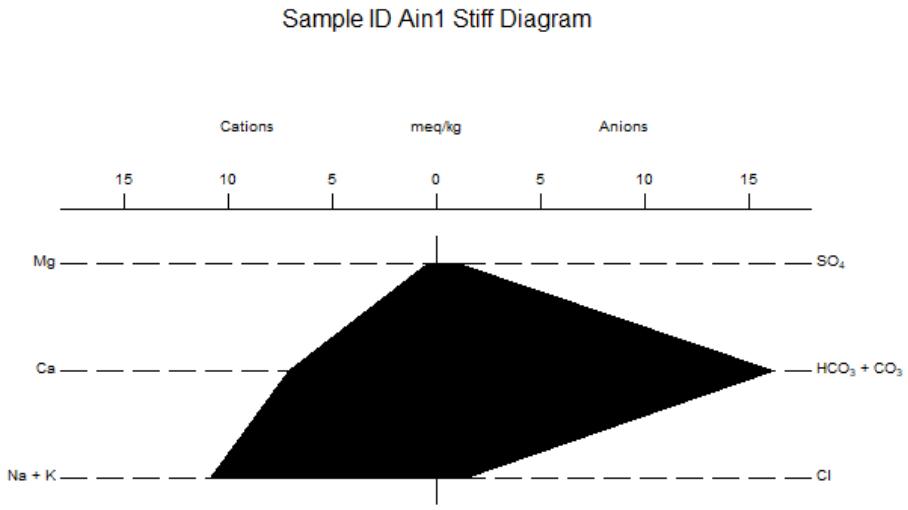

Sample ID Dew1 Stiff Diagram

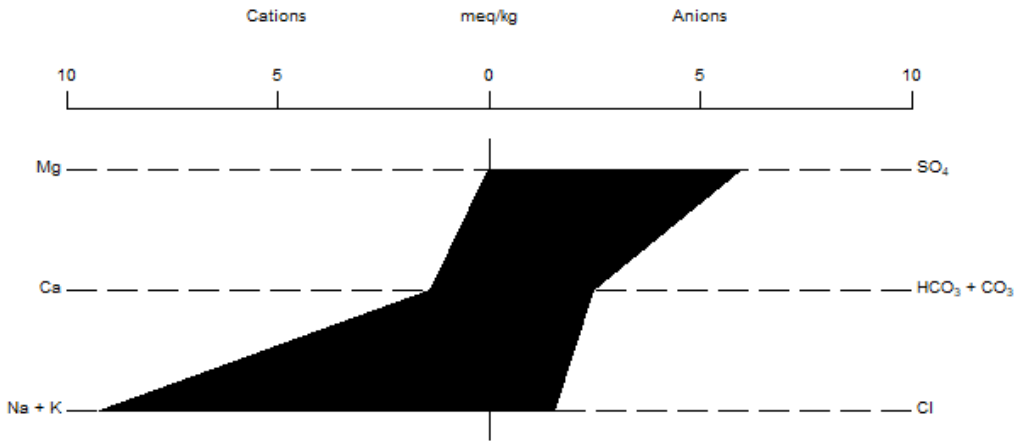

Sample ID 72 Stiff Diagram

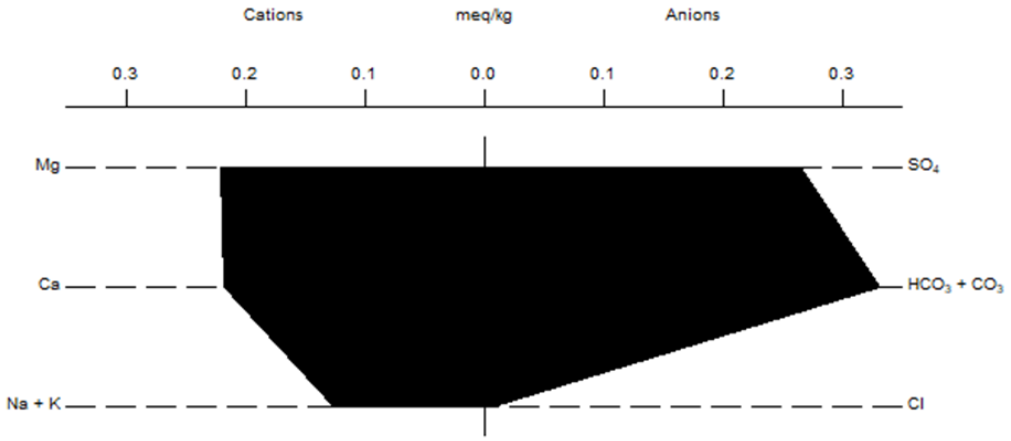

Sample ID 101 Stiff Diagram

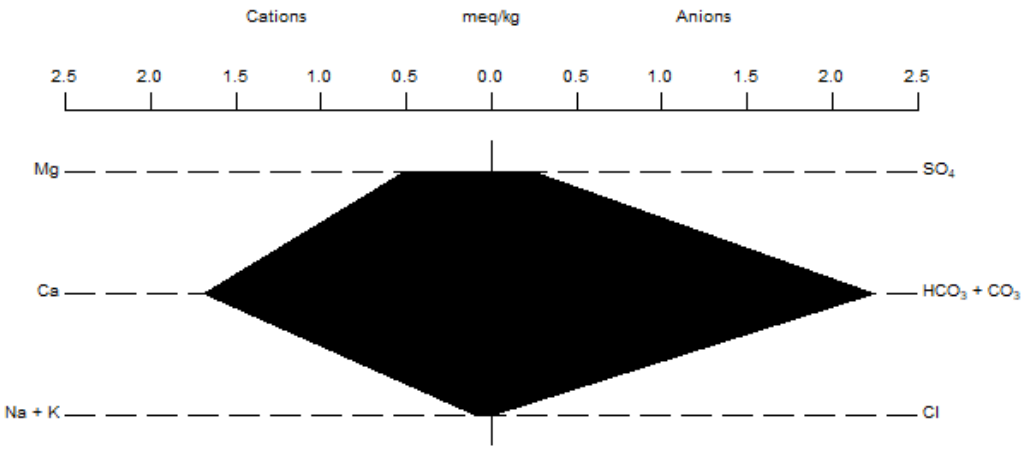

Sample ID 94 Stiff Diagram

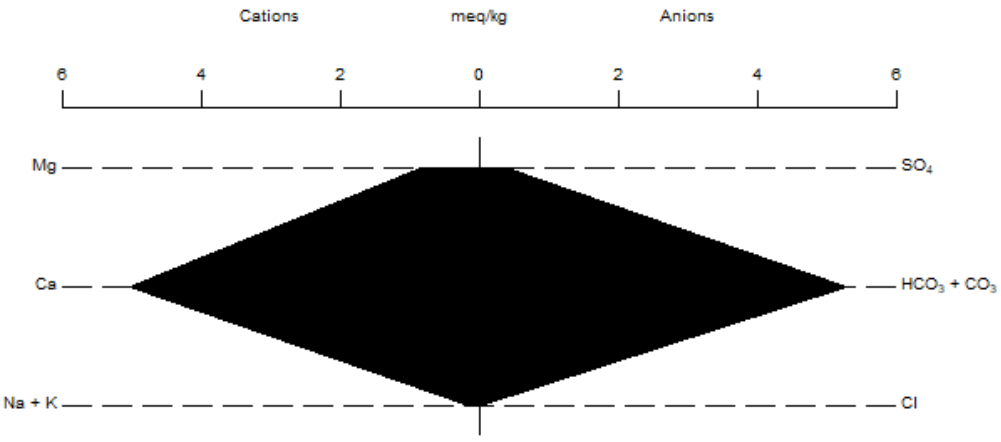

Sample ID 92 Stiff Diagram

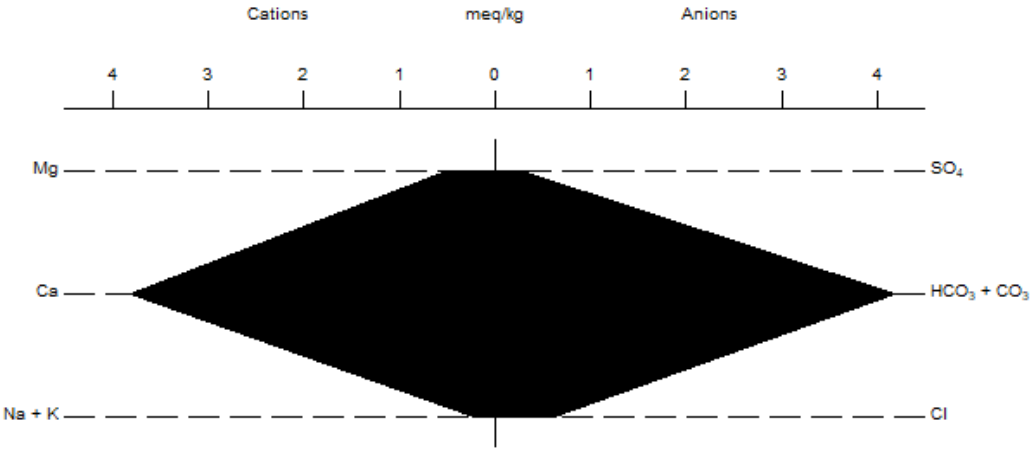

Sample ID 91W Stiff Diagram

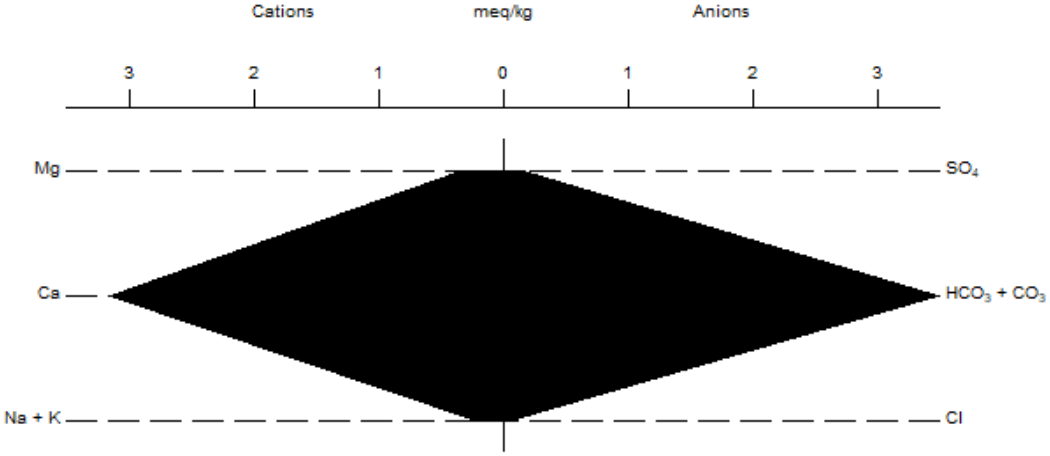

Sample ID 91 Stiff Diagram

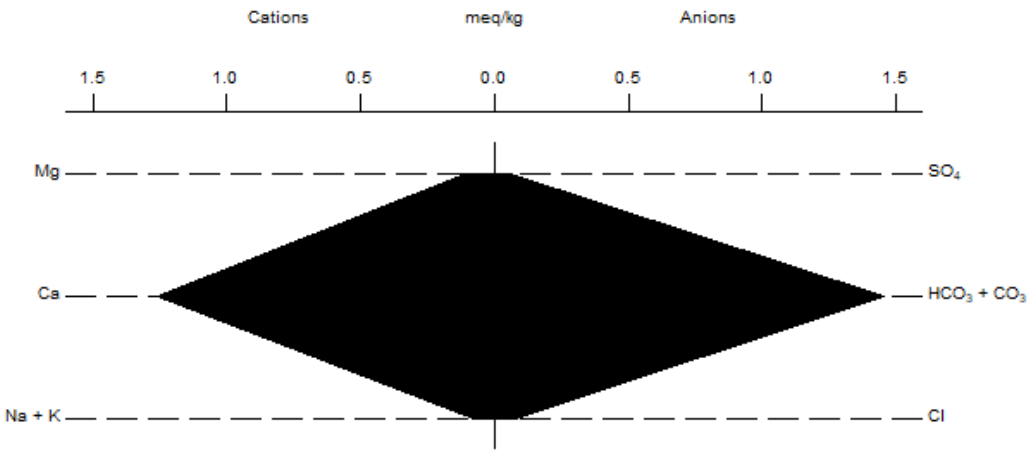

Sample ID 86 Stiff Diagram

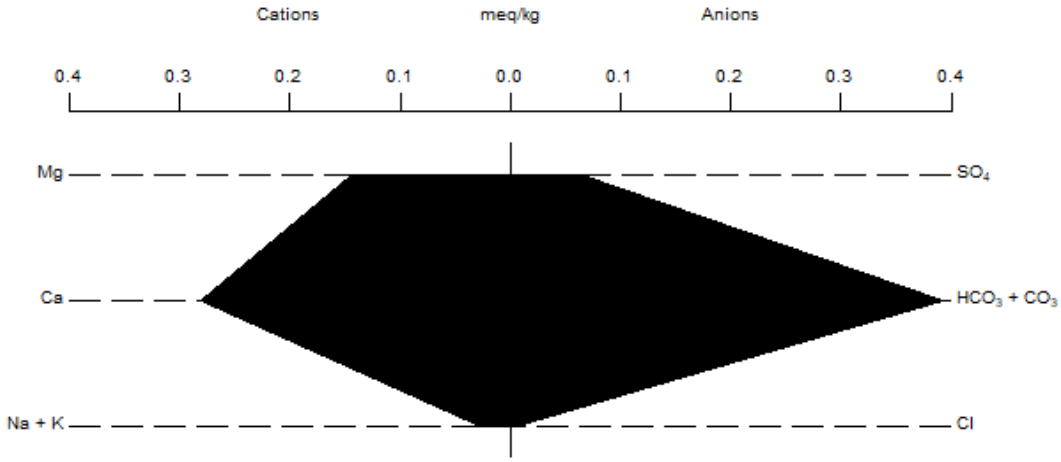

Sample ID 87 Stiff Diagram

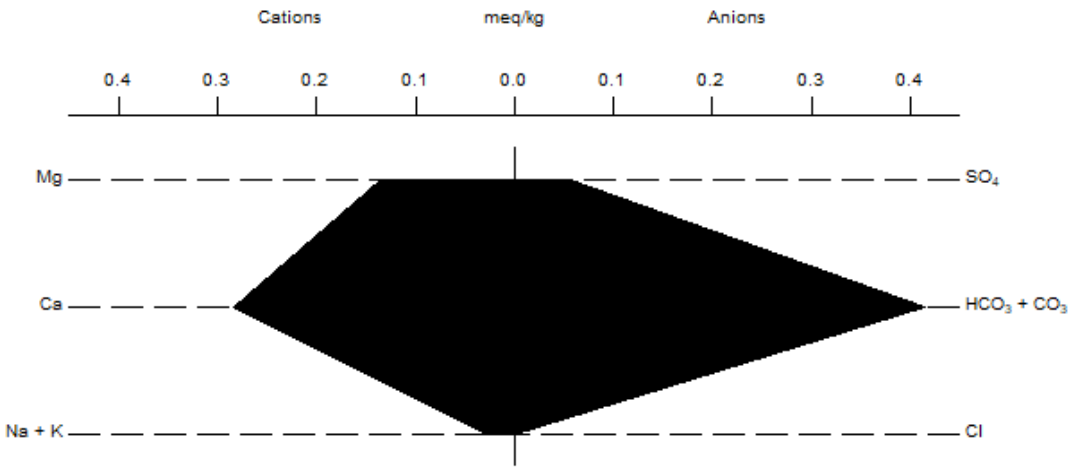

Sample ID 82 Stiff Diagram

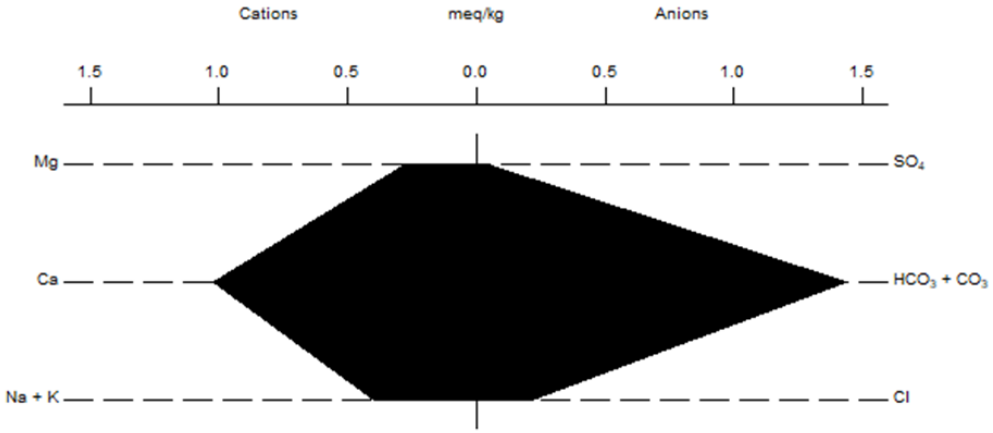

Sample ID 63 Stiff Diagram

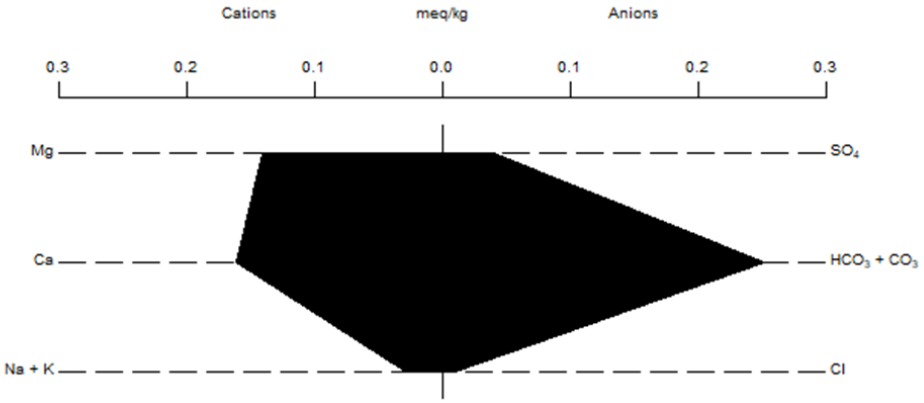

Sample ID 71 Stiff Diagram

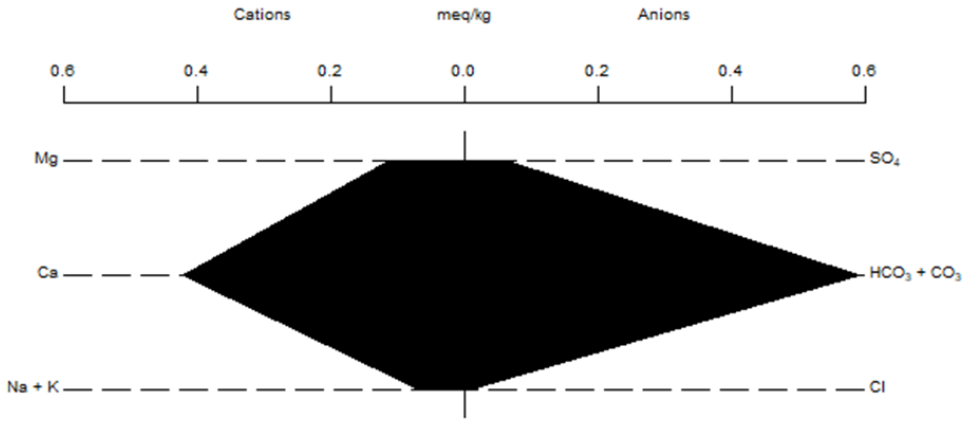

Sample ID 13 Stiff Diagram

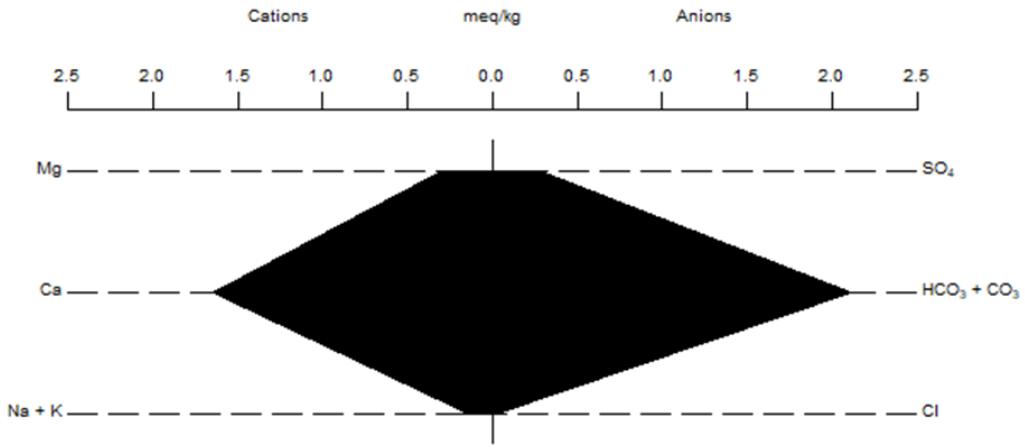

Sample ID 85 Stiff Diagram

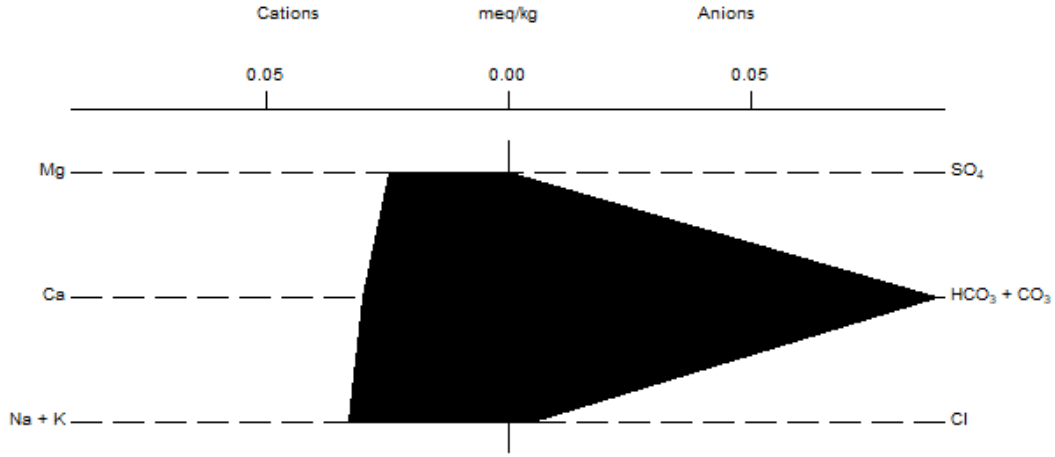

Sample ID 27 Stiff Diagram

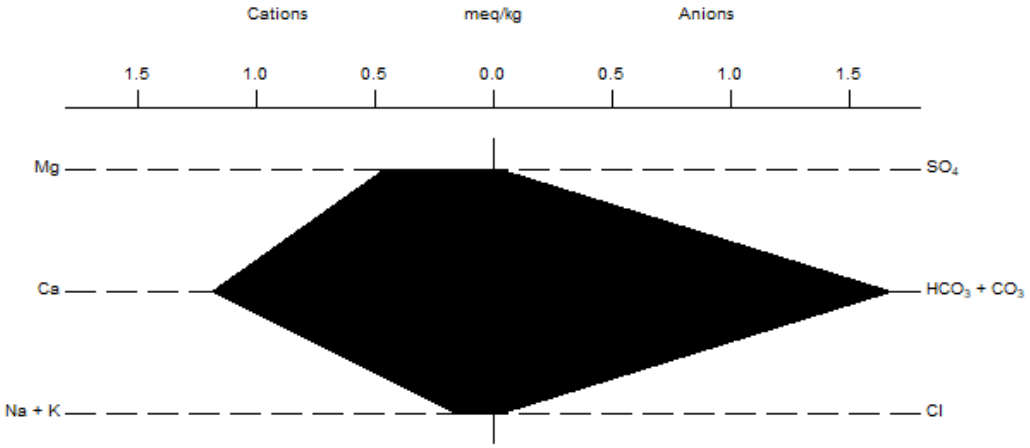

Sample ID 17 Stiff Diagram

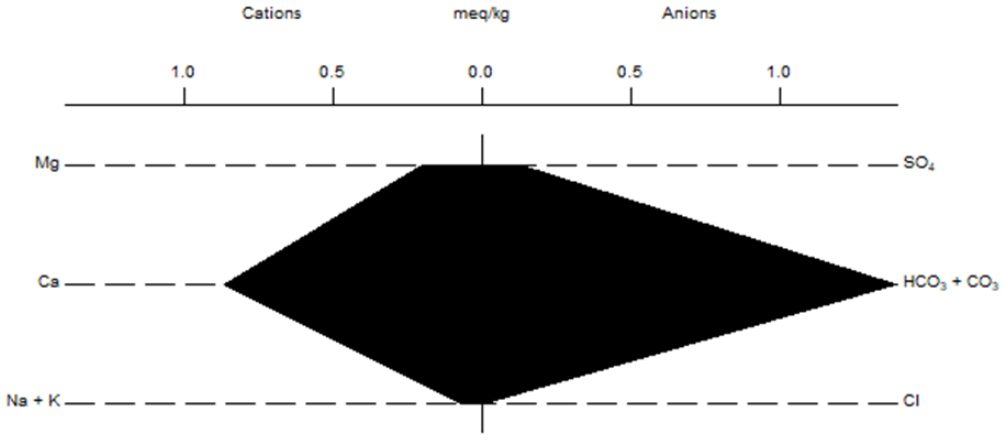

Sample ID 37 Stiff Diagram

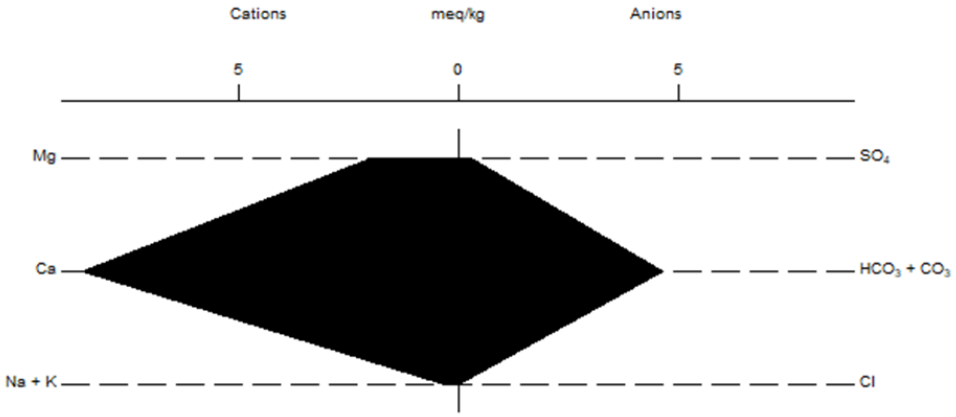

Sample ID 03 Stiff Diagram

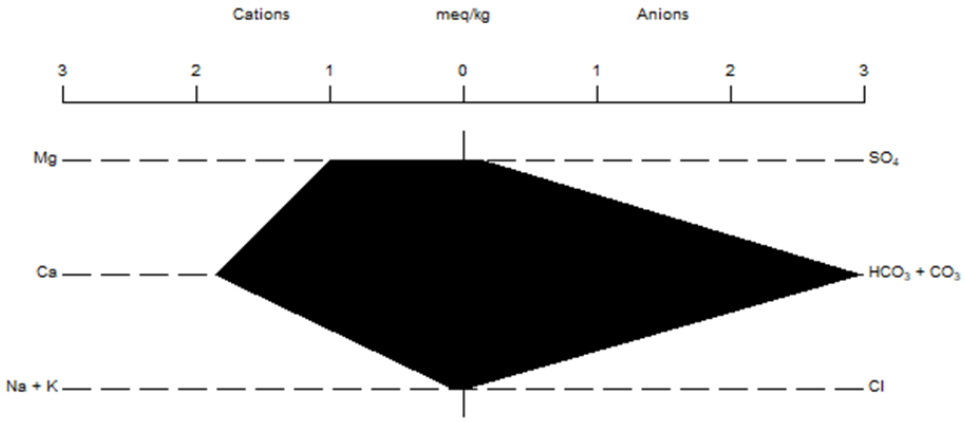

Sample ID 47 Stiff Diagram

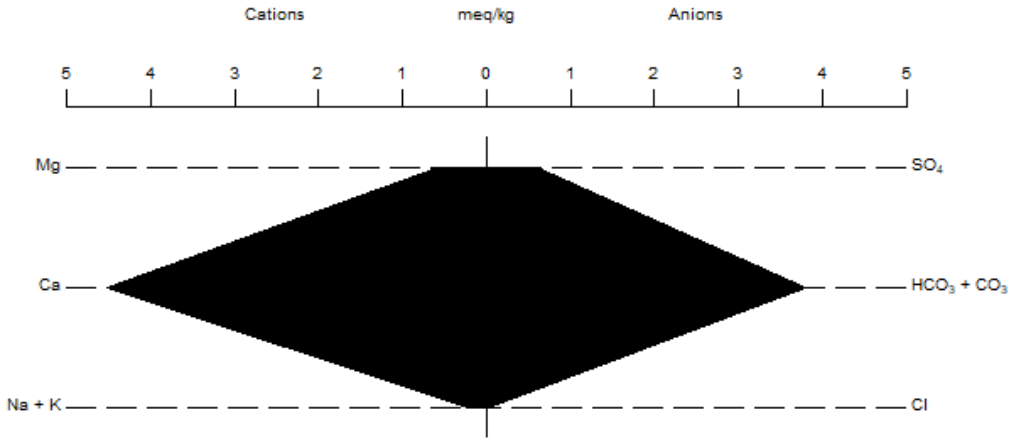

Sample ID 44 Stiff Diagram

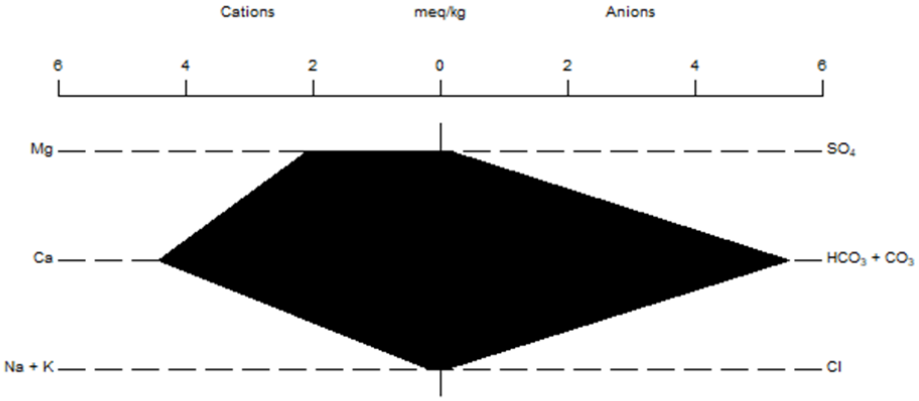

Sample ID 46 Stiff Diagram

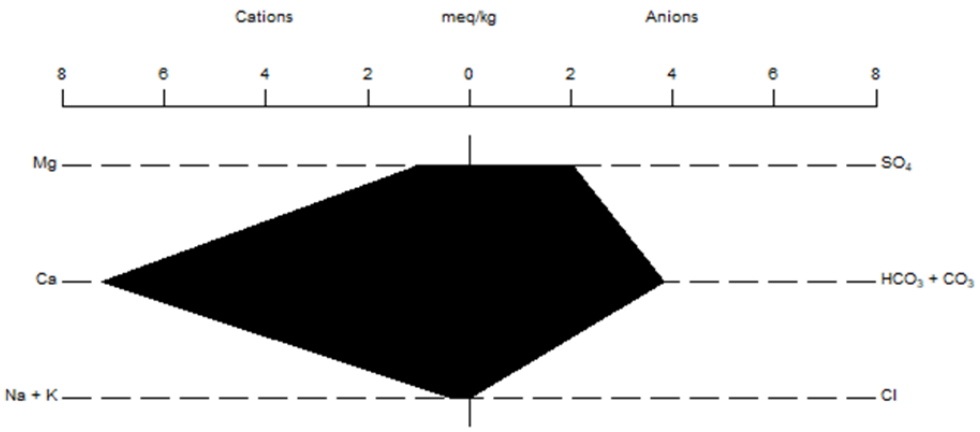

E. Multiparameter Testing Results Summary

ID	Type	Easting	Northing	Temperature (øC)	pH	Conductivity (æS/cm)	TDS (ppm)	Salinity (ppt)
1	2	515335	5506584	10.8	8.29	121	85.9	0
2	1	515332	5506811	8.1	8.43	205	146	0
3	1	515496	5506744	13.2	8.32	279	201	0.1
4	2	510414	5507241	12.6	8.29	95.8	67.9	0
5	2	510557	5507726	12	8.27	117.6	85.9	0
6	2	510571	5508551	10.9	8.42	158.3	112	0
7	2	510543	5508622	13.3	8.27	151.5	110	0
8	2	510538	5510379	12.6	8.23	235	167	0.1
9	2	510552	5510765	11.5	7.8	205	146	0.1
10	2	510381	5512625	11.5	8.25	167.2	119	0
11	1	510358	5512987	14.4	7.61	318	222	0.1
12	1	510456	5513149	12.7	7.76	348	248	0.1
13	2	510715	5513534	9.8	8.44	208	148	0.1
14	1	510828	5513733	13.8	8.3	374	268	0.1
15	1	510948	5514583	21.6	8.17	384	279	0.2
16	1	510920	5514875	15.3	8.51	264	193	0.1
17	2	510928	5515558	11.6	8.25	103.6	73.5	0
18	2	508919	5499451	13.9	7.25	243	171	0.1
19	1	508985	5499721	13.8	7.25	133.4	94.9	0
20	1	509021	5500727	13.8	8.28	261	185	0.1
21	1	509080	5500790	10.7	7.46	123.5	88.7	0
22	2	509196	5501188	12.4	7.94	123	87.3	0
23	2	509276	5502127	11.5	7.82	80.5	57.3	0
24	2	509365	5502981	15	7.59	131.3	92.9	0
25	1	519356	5497270	16.1	7.59	152.5	108	0
26	2	515273	5496740	11.7	7.92	88.4	63	0
27	2	515384	5497190	11.6	7.06	160.2	114	0
28	2	515302	5497506	11.6	7.32	56.4	40.5	0
29	2	515344	5497988	15.2	7.54	46.5	33.1	0
30	2	515215	5498503	10.1	7.57	84.4	59.9	0
31	2	515074	5498662	12.1	7.5	25.6	18.3	0
32	2	514952	5498880	14.6	7.66	117.3	83.7	0
33	2	514806	5499015	10.8	7.72	50.2	35.7	0
34	2	514462	5499735	13.8	8.2	283	201	0.1
35	1	514446	5499758	24.8	8.03	480	340	0.2
36	1	514355	5499922	19.7	7.55	515	364	0.2
37	1	514150	5500565	13.9	7.19	470	330	0.2
38	2	513577	5501984	11.5	8.2	168.6	118	0
39	1	513740	5502368	17.7	8.16	192.3	136	0.1
40	1	513749	5502453	12.8	8.01	169.1	120	0
41	1	513919	5503520	17.7	8.36	440	312	0.1
42	1	514081	5503982	22.5	8.07	509	360	0.2
43	1	514178	5504667	14.3	8.09	226	160	0.1
44	1	514178	5503515	7.7	7.24	605	428	0.3
45	2	512598	5495209	9.7	7.85	294	209	0.1
46	1	512201	5495458	9.5	7.14	626	442	0.3
47	1	511437	5496208	16.2	7.4	517	370	0.2
48	2	509877	5498604	14.6	8.25	385	273	0.2
49	2	509783	5498698	13.2	8.12	318	227	0.1
50	2	509786	5498712	13.8	7.93	271	192	0.1
51	1	509389	5498918	13.9	7.31	299	209	0.1
52	2	523823	5509460	9.5	7.71	92.6	65.8	0

ID	Type	Easting	Northing	Temperature (øC)	pH	Conductivity (æS/cm)	TDS (ppm)	Salinity (ppt)
53	2	523735	5509381	9.7	7.81	67.6	48.4	0
54	1	523538	5509170	8.9	7.67	242	172	0.1
55	2	523213	5508751	11	7.62	118.2	83.8	0
56	2	523009	5508655	12.1	7.76	97.4	69.2	0
57	1	522822	5508494	7.1	7.36	59.6	42.2	0
58	1	522618	5508302	9.1	7.66	104.8	74.1	0
59	1	522521	5508236	8.5	7.68	118.8	87.6	0
60	2	522471	5508214	7.7	7.71	171.1	121	0
61	2	522380	5508125	7.6	7.92	129.3	91.8	0
62	2	522269	5508042	9.6	7.85	102.3	72.6	0
63	1	521841	5507610	8.2	7.27	33	23.4	0
64	2	521554	5507429	12.5	7.55	60.9	43.2	0
65	2	520652	5506775	11	7.77	114.1	81.2	0
66	1	520440	5506592	13.6	7.84	128.9	91.7	0
67	2	519956	5506346	14.6	7.86	69.5	49.2	0
68	2	519296	5506358	13.2	7.81	89.1	63.4	0
69	2	518480	5506568	13.4	7.9	106	74.7	0
70	2	518312	5506601	10.9	7.78	81	57.3	0
71	2	517286	5506808	11.2	7.78	63.7	44.8	0
72	1	517100	5506597	30.1	6.59	68.8	49.1	0
73	2	516188	5506697	15.2	7.95	115.4	80	0
74	2	515957	5506701	11.6	7.71	238	167	0.1
75	2	515911	5506688	12.8	7.96	230	164	0.1
76	2	514936	5506184	9.4	8.26	196.1	139	0
77	2	514042	5505259	12.7	8.1	201	142	0.1
78	2	513499	5504715	12.3	8.27	221	157	0.1
79	2	511378	5499802	21.6	7.99	171.1	122	0
80	1	511821	5500013	12.5	8.14	325	240	0.1
81	1	512205	5501398	13.9	7.81	210	149	0.1
82	2	512236	5502684	14.4	7.98	174.1	123	0
83	2	510866	5503403	24.6	7.55	143.1	101	0
84	2	515525	5506054	12.9	7.93	66.7	47.3	0
85	1	517544	5506102	9.7	7.13	9.9	7	0
86	1	518246	5505794	11.7	7.3	43.3	30.9	0
87	2	518371	5505797	12.8	7.58	46.7	33.2	0
88	1	518693	5505797	13	7.85	87.6	62.2	0
89	1	515519	5507260	11	8.03	324	229	0.1
90	2	515526	5506938	11.5	8.29	273	195	0.1
91	1	510228	5506108	11.3	6.86	150.4	108	0
92	1	509536	5503034	11.1	7.58	459	325	0.2
93	1	514380	5500984	13	7.89	515	365	0.2
94	1	514571	5501100	8.6	7.93	597	424	0.3
95	1	514814	5500669	12.6	7.94	486	345	0.2
96	1	514919	5500477	20.3	7.8	432	305	0.2
97	1	514968	5500346	9.1	8.02	281	201	0.1
98	1	515085	5500146	11.3	7.91	210	148	0.1
99	1	515156	5501296	16.3	7.55	201	141	0.1
100	1	515304	5501001	18.5	7.11	88.7	63.1	0
101	1	515382	5500915	12.4	7.28	221	156	0.1
102	1	515402	5500897	11	7.35	235	166	0.1
103	1	509703	5504985	16	7.97	332	229	0.1

Structural and Water Chemistry Considerations for Geothermal Potential in Crawford Bay and Surrounding Area: Field Work 2022

Colin Vandenbrink

Submitted 31 August 2022

Client: South Kootenay Lake Community Service Society

Executive Summary

This report presents the results of geothermal exploration field work conducted in the region surrounding Crawford Bay, British Columbia. The primary objectives of this report are to determine the major structural features in the region, and determine a chemical signature within surface water bodies indicative of geothermal fluid input. Structural and water chemistry data were collected and used in the construction of a series of maps and stereoplots that serve to elucidate the objectives above. The principle finding of this report are that low pH anomalies tend to occur within thermal springs and along south-striking, steeply dipping normal faults in the region. The trends of major faults mapped by this report curve sharply to the west towards the south of the study area, suggesting that geothermal activity in this region may be the result of a transitional zone between two larger regional fault zones in the north and south of Kootenay Lake, which both terminate near Crawford Bay.

The optimal location for further geothermal exploration is that around Orebin Creek, where a major fault system, a thermal spring, favourable water chemistry, and highly permeable rock all coincide. Steeply dipping bedding and jointing planes in this region intersect to provide an ideal mechanism for the transport of geothermal fluids from depth. The ideal trend and plunge for a well wishing to perpendicularly intersect these weakness planes is 073.6/23.2.

Table of Contents

Introduction

This report presents the findings of fieldwork and data analysis conducted in summer 2022 by Colin Vandenbrink, retained by the South Kootenay Lake Community Service Society to perform a feasibility study of geothermal energy resource potential surrounding the town of Crawford Bay, British Columbia. The specific objectives of this report include determining the nature of the large geologic structures in the region such as folds and faults as conduits for geothermal fluids, and assessing surface water chemistry to attempt to determine a chemical signature of geothermal fluid input within creeks and springs. The findings of this report help to further constrain possible areas of interest for future geothermal energy exploration.

Study Area Description

This study covers an area of approximately 400 km^2 on the east shore of Kootenay Lake, extending from the town of Riondel in the north to that of Grey Creek in the south, encompassing the entirety of Crawford Bay and extending inland up to Canyon Creek (Figure 1). Kootenay Lake itself acts as a major structural boundary within the Canadian Cordillera, separating the Selkirk mountains on the west from the Purcell Mountains to the east, with major regional faults running the length of the lake. This region also hosts a history of geothermal activity in the form of hot springs at Ainsworth, Crawford Creek, and Riondel. More broadly, this region lies within the Omineca geomorphologic belt, which acts as a highly metamorphosed suture zone between the thrusted strata of the Foreland belt and the accreted terrains of the Intermontane belt (Monger et al., 1982).

Figure 1 - Overview map of the area studied in this report.

Background Information and Previous Work

Previous Work

This study represents phase two of a three phase endeavor to determine the geothermal potential of this region, building off work done in phase one to access and integrate necessary geospatial data for the project, and succeeded by phase three, which will involve the drilling of one or two geothermal test wells in locations of greatest geothermal potential.

The data accessed and organized during phase one by Sabutsch (2021) included numerous spatial analysis assets such as previous geological mapping information, well locations, advanced spaceborne thermal emission and reflection radiometer (ASTER) data for numerous chemical compounds, thermal imaging, digital elevation models, and other miscellaneous information. Also generated in this previous phase was numerous maps showing the extent of previous mapping and areas of interest given the data provided, making specific reference to thermal anomalies and lineaments within the study area.

Evidence for Geothermal Activity

The primary driver of geothermal energy interest has historically been the inflow of hot fluids into the now-abandoned Bluebell mine in Riondel B.C. These fluids, first assessed for their geothermal potential by Desrochers (1992), exited fractures in the mine at a depth of 300 m with a temperature of approximately 38° C and at a rate of 90 – 1000 L/sec. This geothermal occurrence, combined with other proximal surface geothermal expressions such as Ainsworth hot spring and Crawford creek warm spring, create a compelling narrative for the presence of a significant geothermal resource in the region. Geoscience BC (2016) reports the waters within the Crawford Creek, Ainsworth, and even the further afield Dewar Creek springs to all have acidic pH levels, while other hot springs such as those near Nakusp B.C. are much more basic, suggesting that acidic water may be an important indicator of geothermal influence within the Kootenay Lake region.

In the Canadian Cordillera, the main control on the movement of geothermal fluids is major fault systems (Grasby & Hutcheson, 2001). Specifically, structurally complex areas of fault interaction provide the greatest degree of geothermal potential, with these key structural settings outlined by Faulds and Hinz (2015; Figure 2). Evidence also exists that thermal spring occurrences are associated with modern seismicity, suggesting that neotectonic strain is a factor controlling the surface expression of geothermal activity, and explaining why some major faults do not display any surface geothermal presence (Finley, 2020). Kootenay Lake is host to one of the major fault systems of the Canadian Cordillera, demarcated by the normal east-dipping Purcell Trench fault in the south and terminating near Crawford Bay around the "kink in the lake", and the normal west-dipping Lakeshore, Josephine and Gallagher faults continuing just northwest of Crawford Bay. It is thought that these two fault systems are likely related (Moynihan & Pattison, 2008), and interaction between these faults may serve as the mechanism for increased geothermal activity. Identifying the structural style of the geothermal system around Kootenay lake, and comparing that to other developed projects elsewhere, is key for de-risking this project.

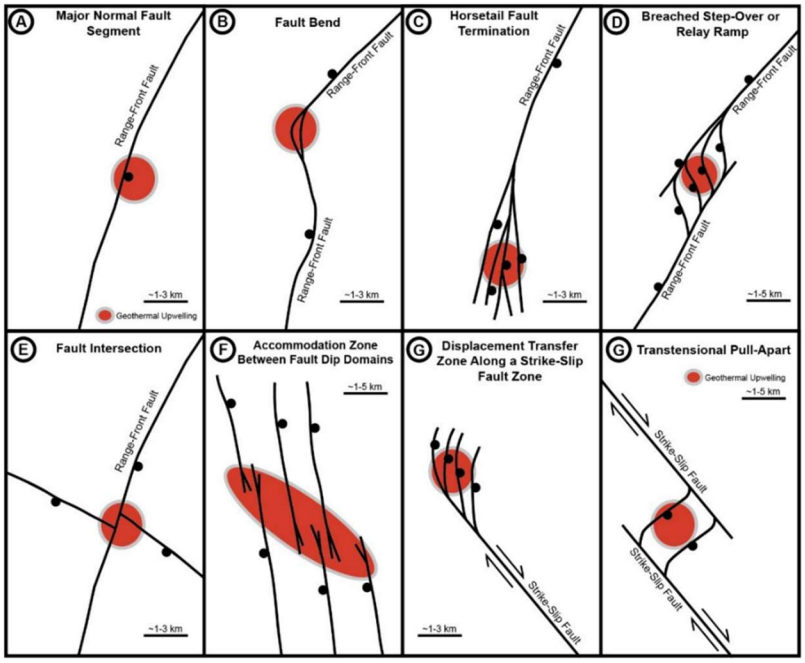

Figure 2 - Common structural settings for geothermal systems in Nevada (Faulds & Hinz, 2015).

Geological Divisions and Common Substitutions

The rock packages within the study area are mapped wildly different by various sources, however this report considers the mapping of Höy (1980) to be the most definitive and correct (Figure 3). Common legacy substitutions of these divisions within the literature that continue to persist include exclusively referring to the gneisses of the Index Formation as the Lardeau, while separating out the Badshot and Mohican Formations and lumping both calcareous packages together as Badshot. Additionally, the gritty quartzite at the base of the Hamill Group is commonly separated as the Three Sisters Formation. Refer to Livingstone (1968) and Walker (1934) for further elaboration on these substitutions. It should also be noted that the chlorite-muscovite schist and phyllite of the Horse-thief Creek Group forms part of the larger Windermere Supergroup, which spans much of the area east of the study area. Finally, the figure below does not list the Crawford Bay Stock, a large intrusive granitic body spanning the width of Crawford Bay.

Group	Formation	Map Unit	Estimated Thickness *metres*	Description
Lardeau	Index	L4	top not exposed	micaceous schist and gneiss
		L3	400 — 450	calc-silicate gneiss, amphibolite, schist; impure marble; amphibolite layer and pure white quartzite layer near base
		L2	700	biotite-hornblende gneiss, amphibolite; minor calc-silicate gneiss, marble, and schist
		L1	150	micaceous schist
	Badshot	B	15 — 30	white crystalline calcite marble, dolomite
	Mohican	M	~50	interlayered quartzite, calcareous and micaceous schist, limestone, and dolomite
Hamill		H4	230	dark quartzite, dark fine-grained quartz-rich schist
		H3	60 — 200	massive, white quartzite
		H2	2 000	interbedded micaceous schist, quartzite, and siltstone; minor amphibolite
		H1	1 600	massive, white quartzite; gritty quartzite
Horse-thief Creek		HTC	base not exposed	fine-grained, light grey to green chlorite-muscovite schist and phyllite; rare white quartzite and marble near top

Figure 3 - The primary geological divisions in the Riondel area (Höy, 1980).

Geologic History

The following is a high-level summary of the geologic history of the Canadian Cordillera presented by Monger (2008), making specific reference to events affecting the Kootenay Lake region:

Neoproterozoic – Earliest Cambrian (750 – 540 Ma): The breakup of the Rodinian supercontinent causes erosion from elevated continental rift margins, creating the sediment supply needed for the formation of the Windermere Supergroup.

Early Cambrian – Early Devonian (520 – 390 Ma): The newly formed Panthalassa Ocean creates the depositional environment necessary for the formation of the craton margin deposits (Lardeau, Badshot, Hamill), which are represented as off-shelf facies in the Kootenay Lake region, transitioning into near-shore facies further east in the Rocky Mountains.

Middle and Late Devonian (390 – 360 Ma): The initiation of subduction and arc magmatism along the west coast of paleo North America creates tuff horizons within the continental margin deposits.

Carboniferous and Permian (360 – 250 Ma): Back-arc extension forms the Slide Mountain Ocean between the magmatic arc and the continental margin. This has a minimal effect on the already deposited continental margin strata around Kootenay Lake.

Triassic (250 – 200 Ma): Arc rotation causes the westmost terranes to fold in on themselves, though this has a minimal effect on the much more eastward Kootenay Lake region.

Early Jurassic (200 – 175 Ma): Arc rotation closes on the west coast, while the breakup of Pangea begins in the east.

Early Cretaceous (175 – 100 Ma): Southeast oblique subduction of Pacific oceanic crust causes sinistral transpression of the emergent Cordillera (left-lateral strike-slip faulting) while continued opening of the Atlantic Ocean causes westward

motion of the North American continent. Magmatism generated by this compressive episode causes the intrusion of granites into the pericratonic terranes, including those around Kootenay Lake.

Mid Cretaceous to earliest Paleogene (100 – 60 Ma): Pacific oceanic crust switches to northeast oblique subduction causing dextral transpression of the emergent Cordillera (right-lateral strike-slip faulting). Thrust sheets generated during this compressive episode form the Rocky Mountains.

Paleogene (60 – 23 Ma): Overthickening of the continental crust combined with far-field forces from changing plate motions cause orogenic collapse, creating a period of dextral transtension and extension in the Cordillera. This extension created the network of north-northeast trending normal faults that dominate the Kootenay Lake region today, and exhumed the Monashee Mountains, exposing cratonic basement rocks at the surface.

Neogene (23 – 0 Ma): Cordillera as it is known today, with minimal changes to the Kootenay Lake region.

Scope of Work

The following deliverables were created for this report:

Bedrock Mapping

- Collection of surficial geology data within the study area.
- Maps of surficial bedrock geology.
- Interpretation of the geology of the region.

Structural Mapping

- Collection of structural data within the study area.
- Maps of surface structural features including faulting, jointing, and bedding/foliation surfaces.
- Stereoplot figures showing planar features, rose diagrams of these planar features, poles to these planes, and Kamb contouring of these poles for each geologic material
- Stereoplot figures showing planar features, rose diagrams of these planar features, poles to these planes, and Kamb contouring of these poles for a selection of different geographic regions.
- Interpretation of this structural analysis and a discussion of the structural controls on a geothermal system in this region

Groundwater Chemistry

- Collection of temperature, pH, conductivity, total dissolved solids, and salinity data from surface water bodies including lakes, streams, springs, and seeps.
- Maps showing surficial trends in temperature, pH, conductivity, total dissolved solids, and salinity.
- Interpretation of how water chemistry may be influenced by the movement of hydrothermal fluids.
- Collection of water samples from promising or anomalous areas for future lab analysis.

Methodology

Collection of Structural and Bedrock Geology Data

Structural measurements were collected using Stereonet Mobile Version 4.0.X (Allmendinger, 2022) using an iPhone SE running iOS 15.6. Stereonet Mobile is an all-in-one structural geology app that gathers the structural attitude of any planar surface the mobile device is set upon, automatically georeferencing the datum in the process, among other features. Using a mobile device for the gathering of structural information has some caveats when compared with traditional methods of gathering structural data and are further explained in Allmendinger et al. (2017), however the efficiency at which a large number of data points can be collected using mobile devices far outweighs any limitations present in this emerging technology.

Within Stereonet Mobile there is the option to record a note for any given measurement. For this study, this note section was used to record the bedrock geology surrounding any given joint, bedding, or foliation plane into broad categories of geologic material allowing the data to be queried and analysed by rock type. As this study is focused on conduits for geothermal fluid more so than the material that these fluids pass through, the bedrock geology was greatly simplified into seven categories:

- Granite – corresponding to the Crawford Bay Stock and related intrusions.
- Gneiss – corresponding to the Index Formation within the Lardeau Group.
- Marble – corresponding to the Badshot and Mohican Formations within the Lardeau Group.
- Quartzite – corresponding to the Hamill Group.
- Schist – corresponding to the Hamill Group.
- Gritstone – corresponding to the Three Sisters Formation or lower Hamill Group.
- Phyllite – corresponding to the Horse-thief Creek Group, part of the Windermere Supergroup.

For this simplification, minor intrusive rocks and heterogeneity within rock types (such as leucocratic versus melanocratic gneisses) have been ignored so that regional trends are not muddled by many similar rock types.

For faults, the notes field was instead used to describe the size and pervasiveness of the structure, including any other relevant information (mineralization, evidence of movement, etc.), this means that it is not possible to query faults by the rock type(s) that they intersect, however this trade-off was made to better determine where major fault lines traversed during spatial analysis, so that minor or low-confidence faults were not considered in this process.

Collection of Water Chemistry Data.

Water chemistry data was collected using an Oakton PCTSTestr 50 multiparameter meter, a single unit capable of measuring temperature, pH, conductivity, total dissolved solids (TDS), and salinity. UTM coordinates for each sample point were collected using a Garmin inReach Explorer+ GPS device. Each sample point was given a basic description and separated into two categories, one for springs, seeps, and wells which likely have a greater groundwater component, and a second for creeks, rivers and lakes which are likely to have much greater meteoric influence. After analysis, areas of interest were revisited to collect water samples for further lab analysis.

Analysis of Structural and Bedrock Geology Data

The data collected using Stereonet Mobile could only be exported as SQLite database files, so DB Browser for SQLite Version 3.12.2 (SQLite Browser, 2021) was used to parse and clean up the data. DB Browser for SQLite presents SQLite database files in an editable spreadsheet format, while also allowing for SQL queries to single out data with specific attributes. The dataset was queried for each of the seven rock types described above (granite, gneiss, marble, quartzite, schist, gritstone, phyllite) as well as by geographic region, roughly corresponding to key landforms within the study area. The seven regions chosen were bounded as follows and are shown in Figure 4:

- Grey Creek: 514000 – 520000 E, 5493000 – 5499000 N
- Lower Crawford Creek: 513000 – 519000 E, 5499000 – 5515000 N
- Lower Peninsula: 508000 – 514000 E, 5494000 – 5500000 N
- Orebin Creek: 516000 – 518000 E, 5505000 – 5507000 N
- Riondel: 509000 – 511000 E, 5511000 – 5514000 N
- Riondel Road: 508000 – 513000 E, 5500000 – 5511000 N
- Upper Crawford Creek: 519000 – 525000 E, 5504000 – 5510000 N

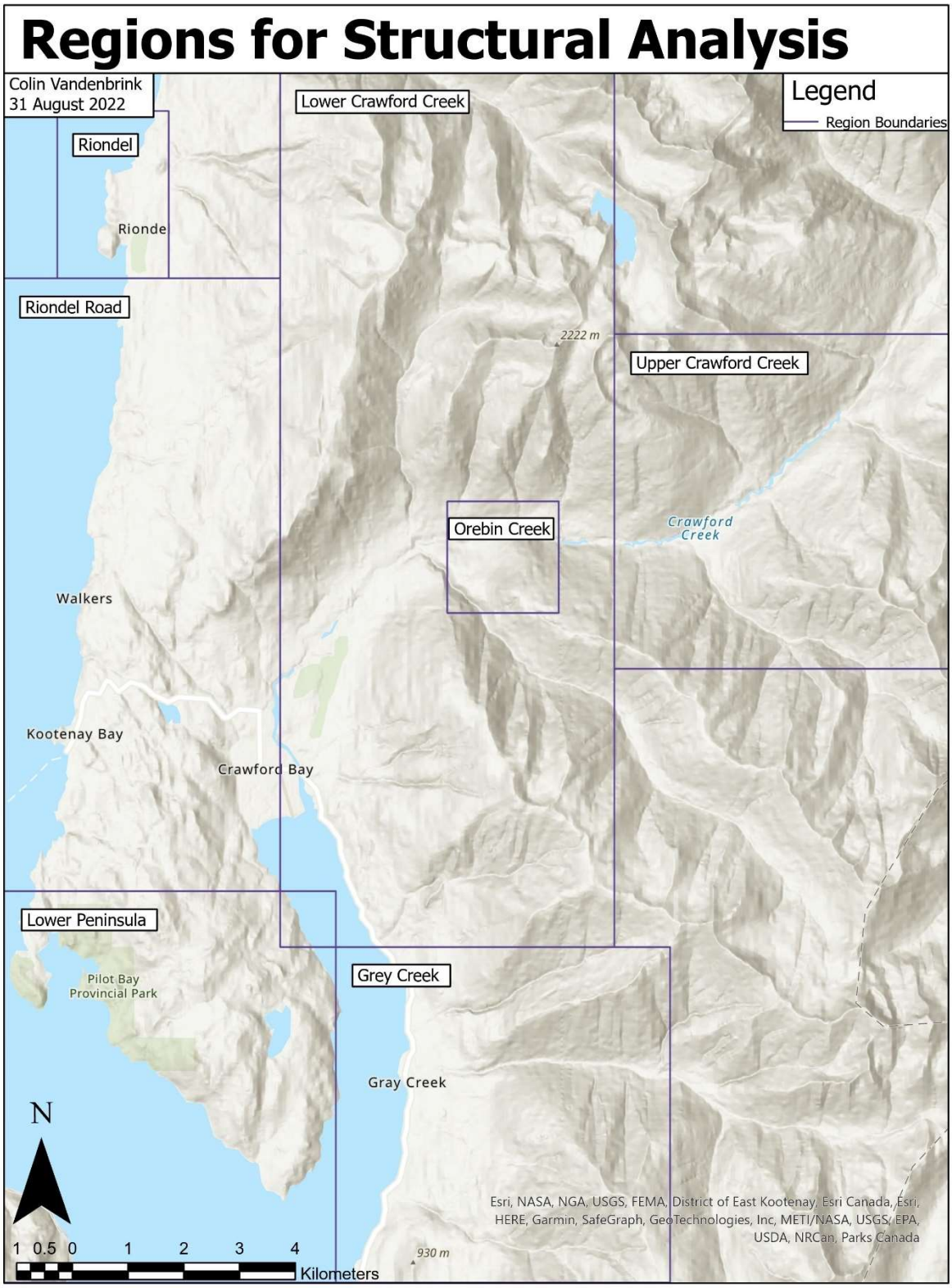

Figure 4 - Map of the geographic regions used to parse and analyse structural data.

Results of these queries were copied into empty SQLite database files and imported into Stereonet Version 11.4.X (Allmendinger, 2020), the desktop companion software to Stereonet Mobile, allowing for further analysis and the export of figures in PDF or image format. For each rock type or geographic region, figures were created showing planes, rose diagrams from these planes, poles to these planes, and Kamb contouring of these poles for bedding/foliation, faulting, and jointing data. It should be noted that due to the foliation planes in foliated rocks being largely the same as adjacent bedding planes in non-foliated rocks, the terms foliation and bedding were largely conflated for the purposes of this study.

Kamb contours, first proposed by Kamb (1959), contour poles based on their variation from a normal distribution. Kamb contours generally occupy a larger area and smooth data more then other contouring methods, and is a common method for modern stereonet contouring applications. Further description of the algorithms used in Stereonet can be found in Almendinger et al. (2012) and Cardozo & Allmendinger (2013).

Spatial Analysis and Mapping

Mapping was performed using ArcGIS Pro Version 3.0 (Esri Inc., 2022). Planar data was plotted and symbolized using strike and dip symbology, with symbols rotated according to the strike measurement. From these, differences in the orientations of bedding planes were used to infer the locations of folds, while fault measurements were used to infer the locations of major fault traces. It should be noted that due to the recent extensional history of the area, all faulting was assumed to be normal unless proven otherwise.

Bedrock data was plotted and used to create polygons of the assumed extent of each rock type. Assuming that the west-dipping faults in the study area are largely normal, strata is shown to be younging westward across faults whenever possible.

Water chemistry data was plotted and symbolized using a colour gradient for each parameter measured (temperature, pH, conductivity, total dissolved solids, salinity). Anomalous values from this data were also used to help infer the trace of major faults, under the assumption that fluids travelling within faults affect surface water chemistry.

All layers described above, plus some other miscellaneous assets, as well as additional data collected by Sabutsch (2021), were used to create a series of maps to better visualize the data and inferences made by this report.

Results

Structural and Bedrock Data

The following maps show the locations where geological data was collected (Figures 5 – 8). Maps are provided for rock type (granite, gneiss, marble, quartzite, schist, gritstone, phyllite), as well as bedding, faulting, and jointing. Full page versions of these maps are available in Appendix A. A table of data used to produce these maps is available in Appendix C.

Figure 5 - Map showing locations where bedrock observations were recorded.

Figure 6 - Map showing locations where bedding attitudes were recorded.

Figure 7 - Map showing locations where faulting attitudes were recorded.

Figure 8 - Map showing locations where jointing attitudes were recorded.

Water Chemistry Data

The following maps show the locations where water chemistry data was collected (Figures 9 – 13). These data points have been symbolized separately for each parameter recorded (temperature, pH, conductivity, total dissolved solids, and salinity). Full page versions of these maps are available in Appendix A. A table of data used to create these maps is available in Appendix D.

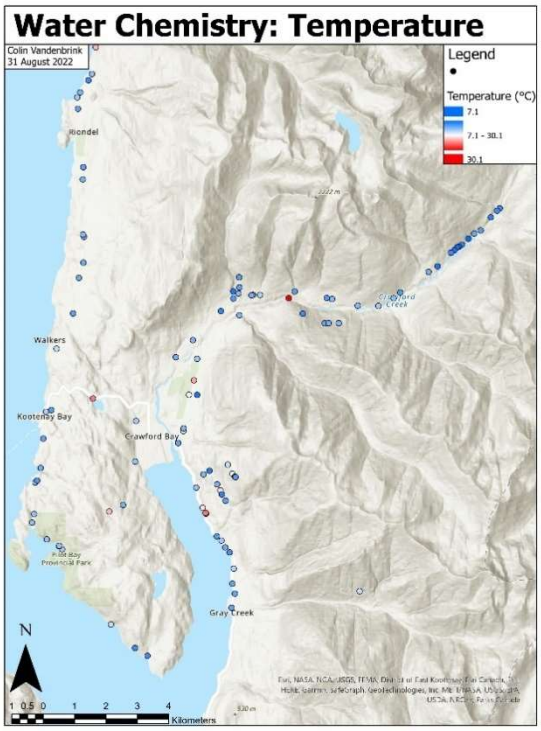

Figure 9 - Water chemistry sample points symbolized according to temperature (blue = lower, red = higher).

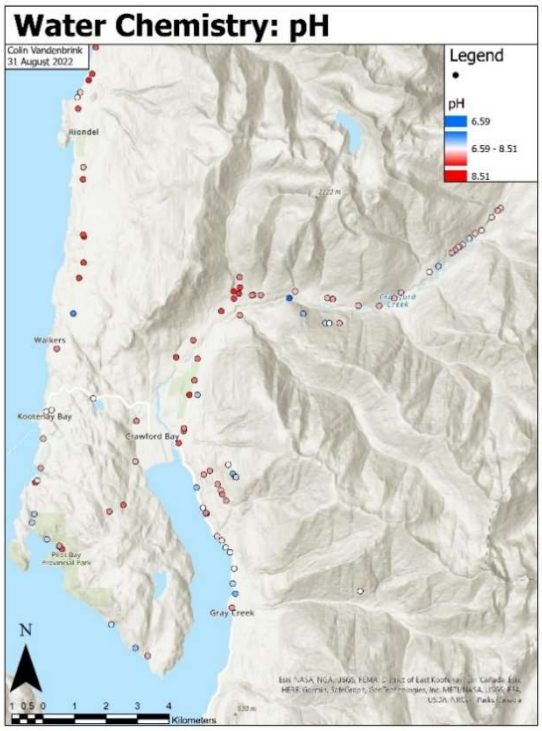

Figure 10 - Water chemistry sample points symbolized according to pH (blue = lower, red = higher).

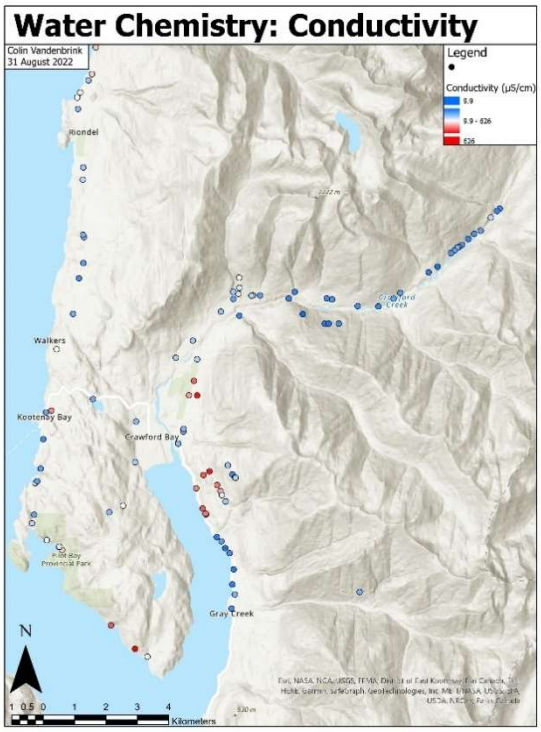

Figure 11 - Water chemistry sample points symbolized according to conductivity (blue = lower, red = higher).

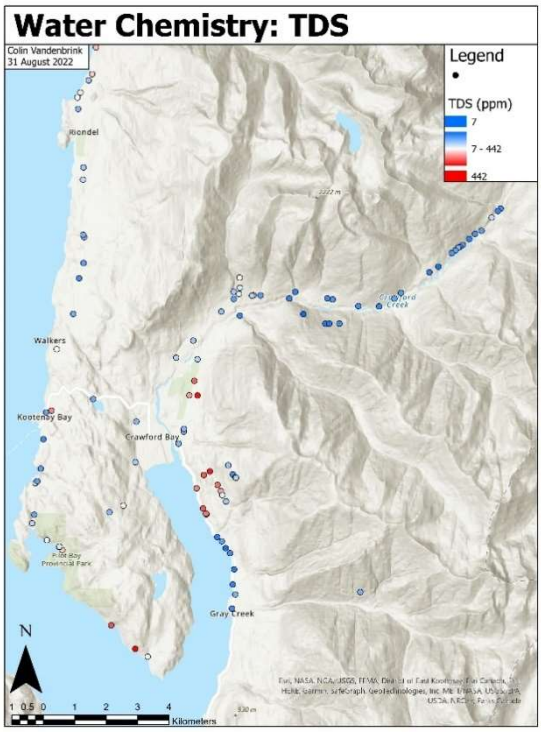

Figure 12 - Water chemistry sample points symbolized according to total dissolved solids (blue = lower, red = higher).

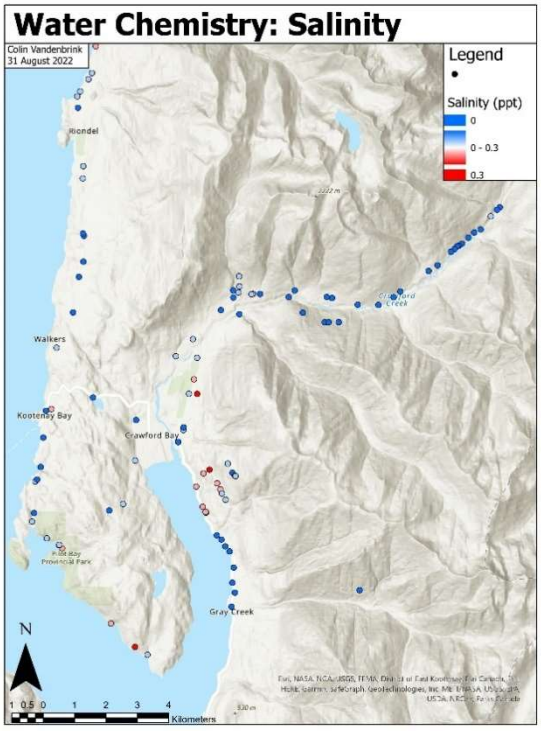

Figure 13 - Water chemistry sample points symbolized according to salinity (blue = lower, red = higher).

Structural Analysis

Below are a series of stereoplots capturing the structural geology of the study region. Plots are divided both by rock type (Figures 14 – 17) and by geographic location (Figures 18 – 21), with further plots of all data together following these (Figures 22 – 25). Rose diagrams show the relative abundance of planar features by strike angle (bin size = 10°), while Kamb contouring of poles to planes show the relative "tightness" of measurements, showing which materials or regions have much more regular structure, and which materials or regions are more varied. Plots purely showing planes and poles are primarily provided for reference. Full page versions of all plots including the sample size for each figure are provided in Appendix B.

Plots by Rock Type

Planes

	Bedding	Jointing
Granite		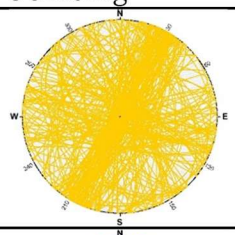
Gneiss	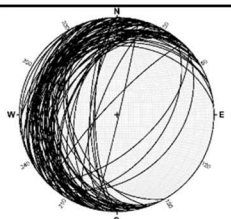	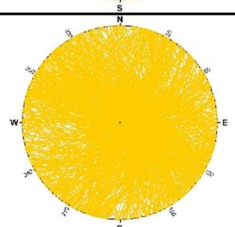
Marble	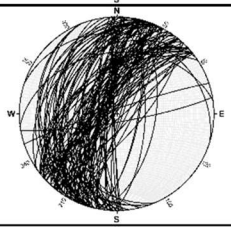	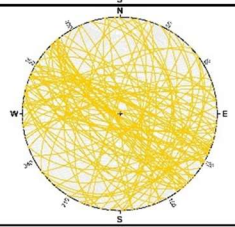
Quartzite	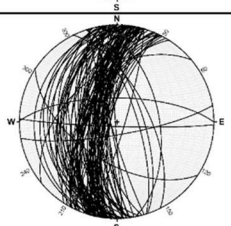	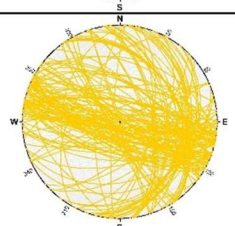
Schist	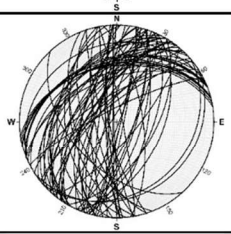	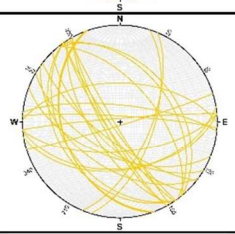
Gritstone	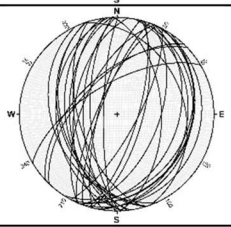	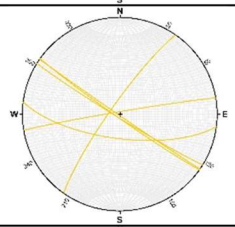
Phyllite	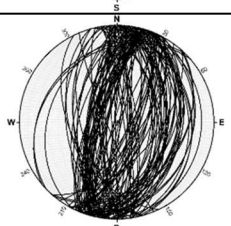	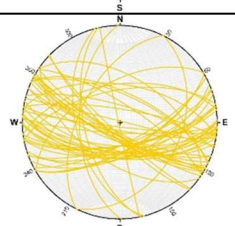

Figure 14 - Planes by rock type.

Rose Diagrams from Planes

	Bedding	Jointing
Granite		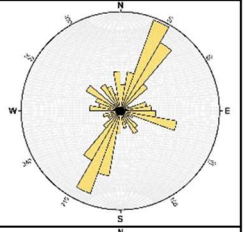
Gneiss	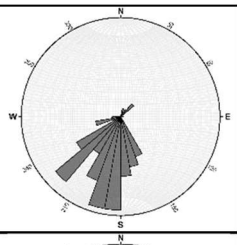	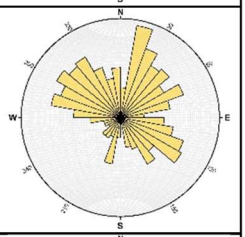
Marble	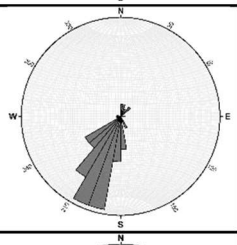	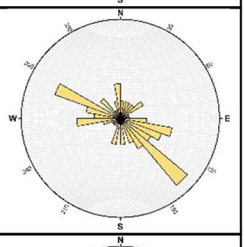
Quartzite	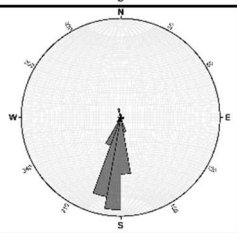	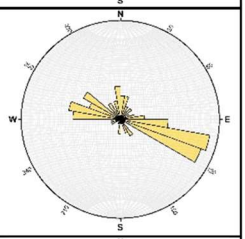
Schist	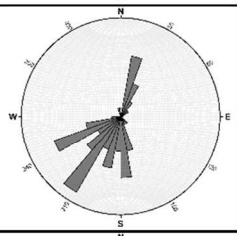	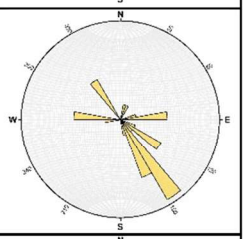
Gritstone	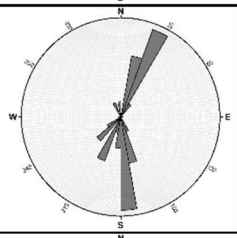	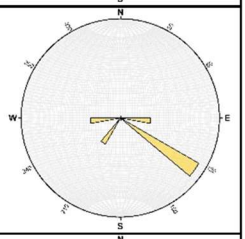
Phyllite	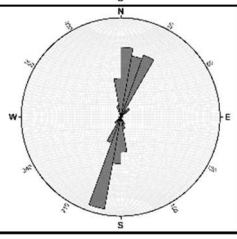	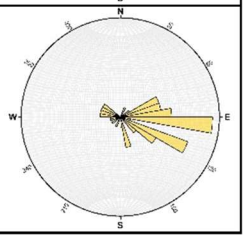

Figure 15 - Rose diagrams from planes by rock type.

Poles to Planes

	Bedding	Jointing
Granite		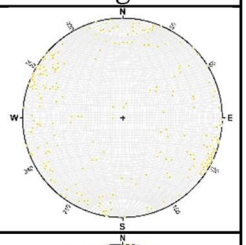
Gneiss	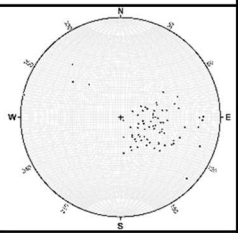	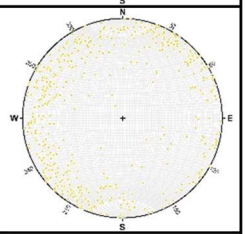
Marble	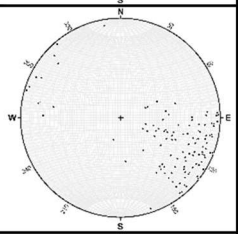	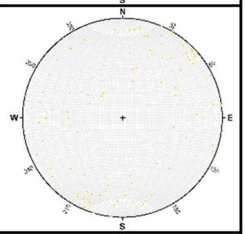
Quartzite	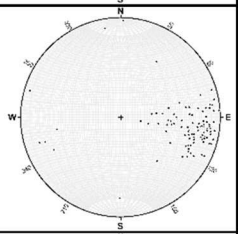	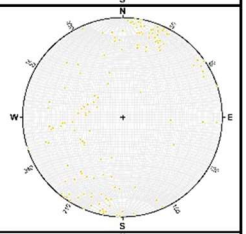
Schist	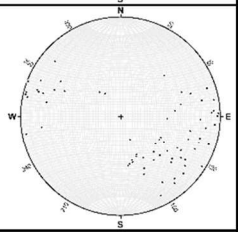	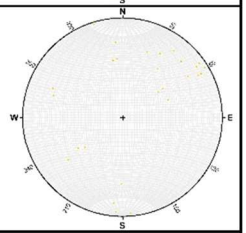
Gritstone	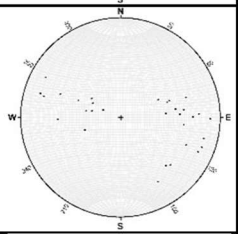	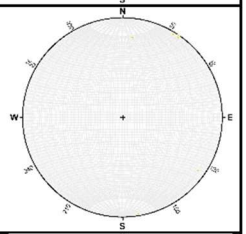
Phyllite	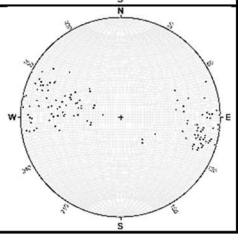	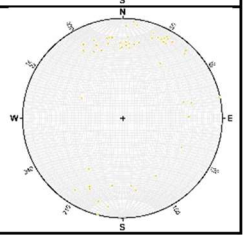

Figure 16 - Poles to planes by rock type.

Kamb Contouring of Poles

	Bedding	Jointing
Granite		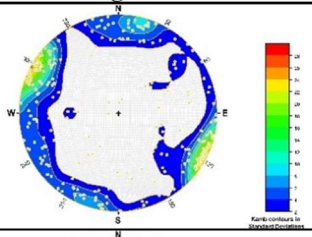
Gneiss	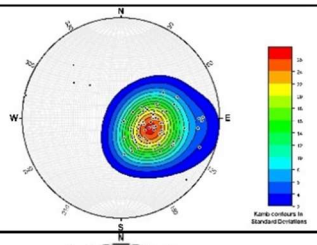	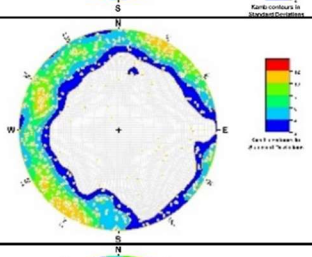
Marble	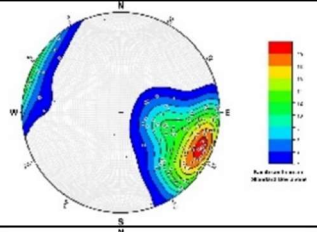	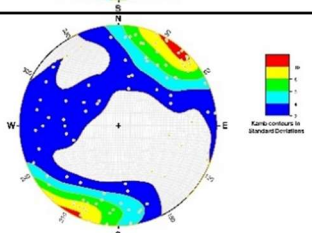
Quartzite	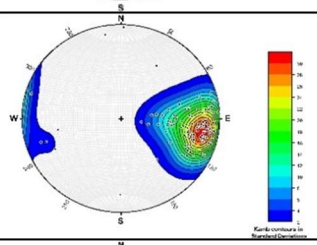	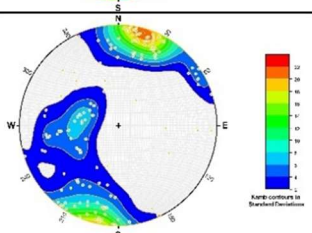
Schist	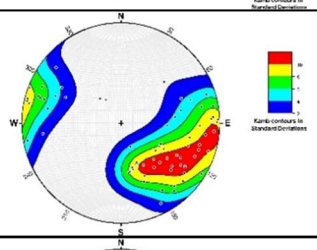	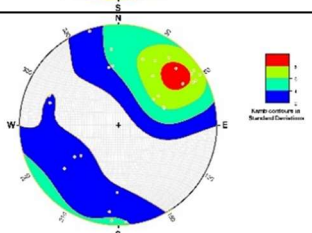
Gritstone	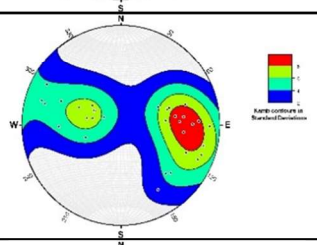	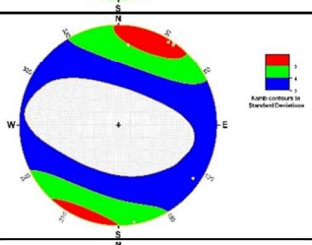
Phyllite	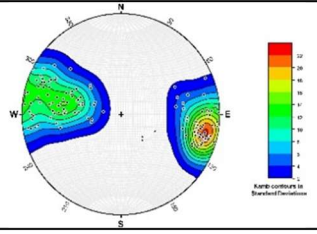	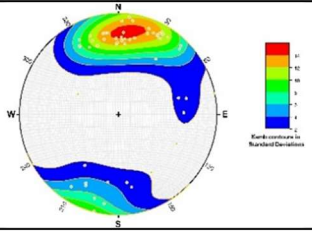

Figure 17 - Kamb contouring of poles by rock type.

Plots by Geographic Location

Planes

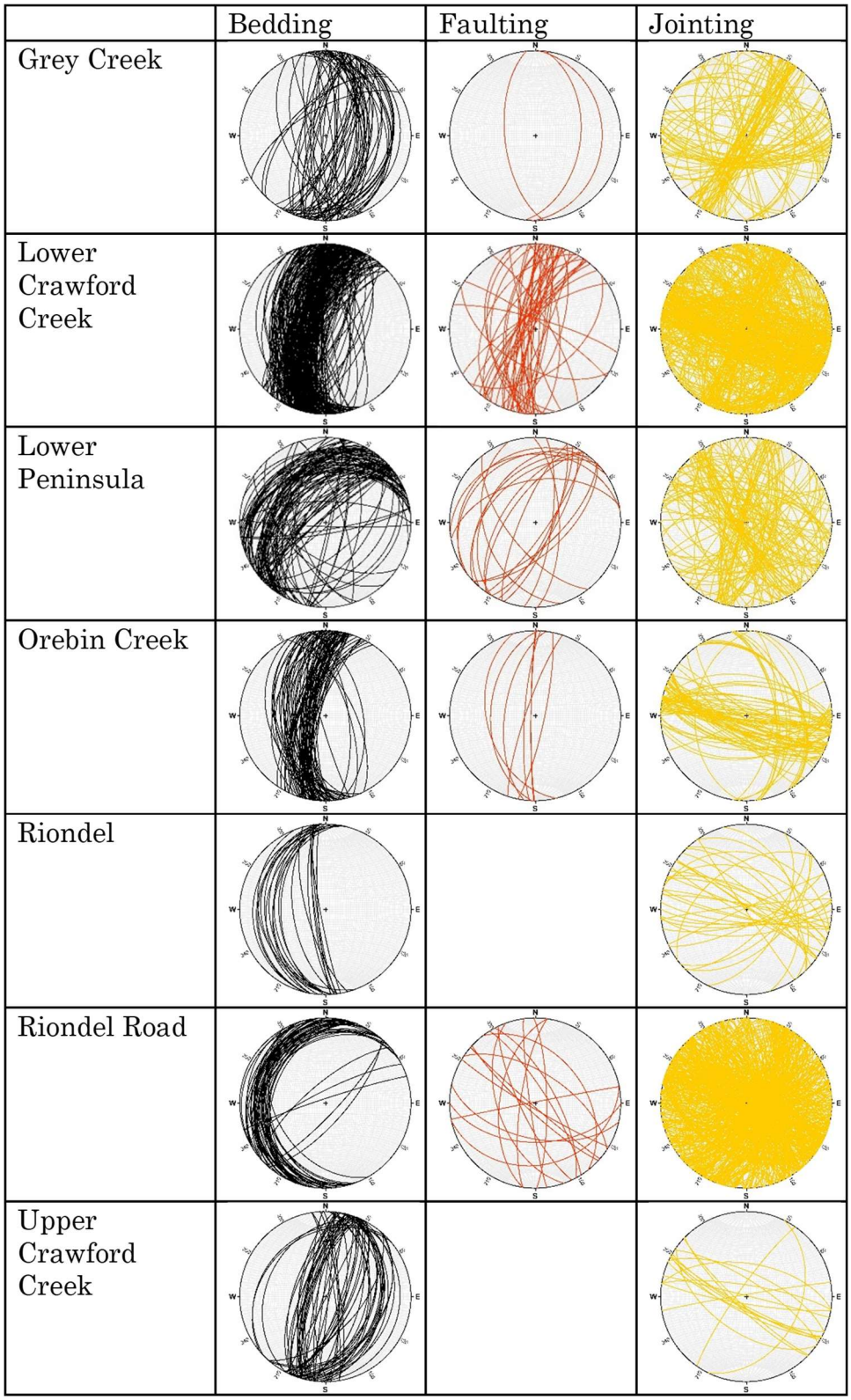

Figure 18 - Planes by geographic location.

Rose Diagrams from Planes

	Bedding	Faulting	Jointing
Grey Creek	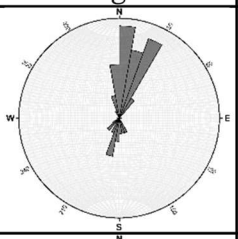	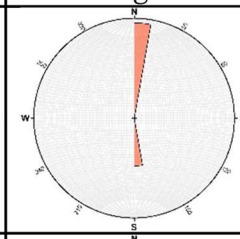	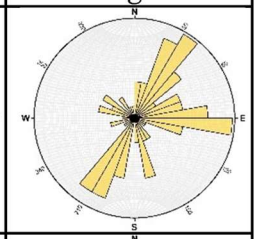
Lower Crawford Creek	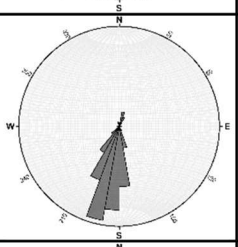	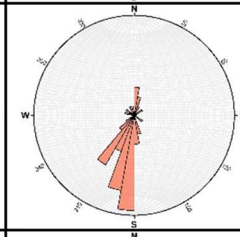	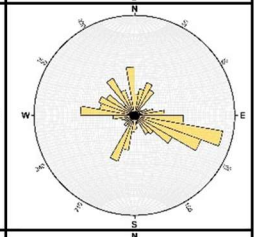
Lower Peninsula	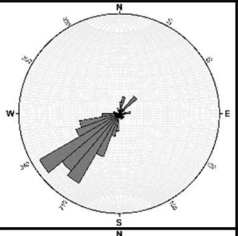	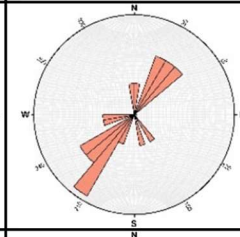	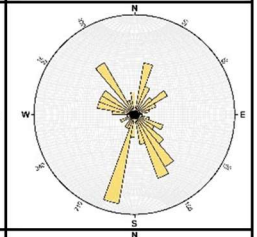
Orebin Creek	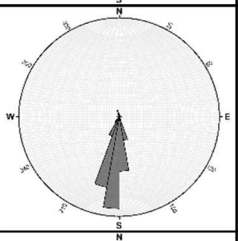	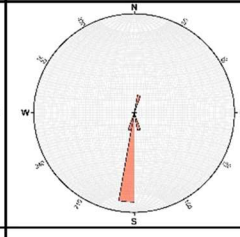	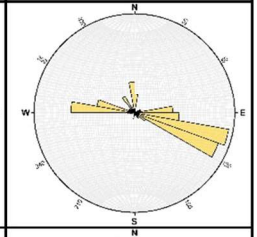
Riondel	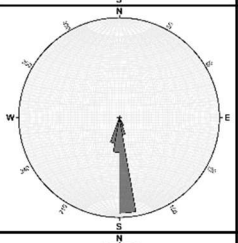		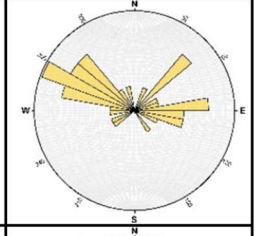
Riondel Road	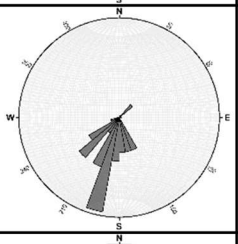	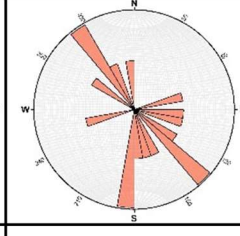	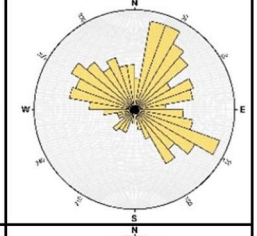
Upper Crawford Creek	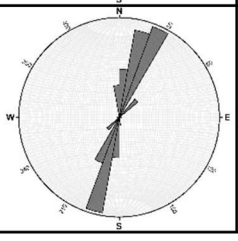		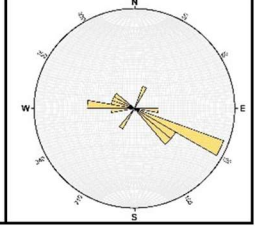

Figure 19 - Rose diagrams from planes by geographic location.

Poles to Planes

	Bedding	Faulting	Jointing
Grey Creek	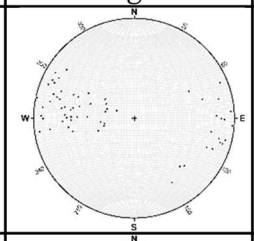	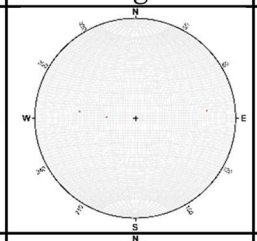	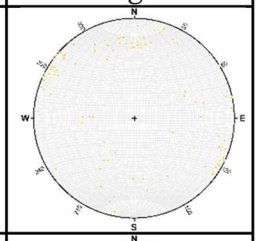
Lower Crawford Creek	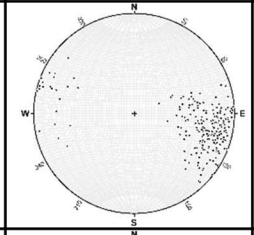	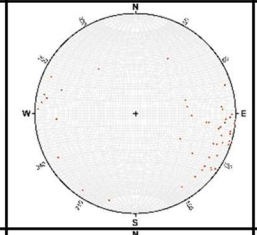	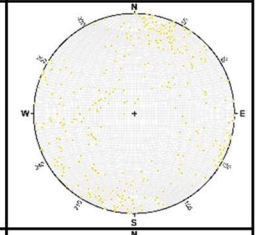
Lower Peninsula	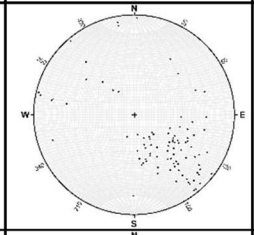	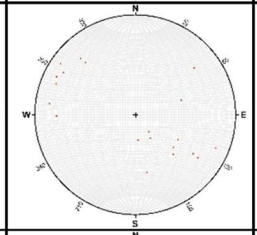	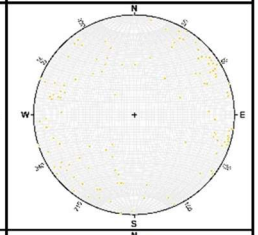
Orebin Creek	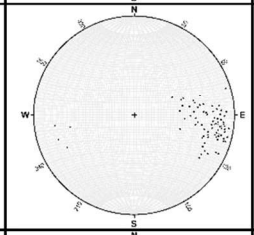	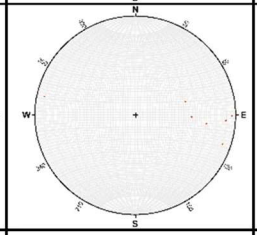	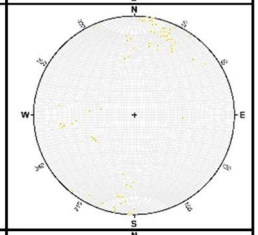
Riondel	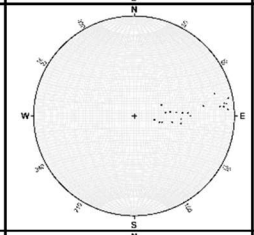		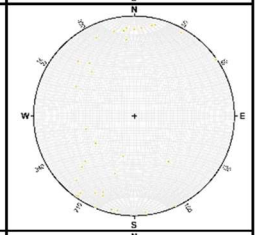
Riondel Road	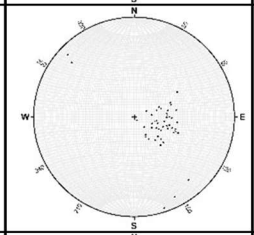	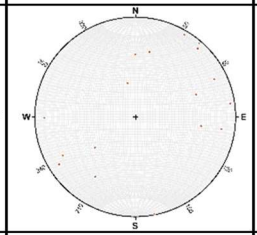	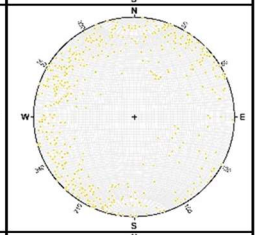
Upper Crawford Creek	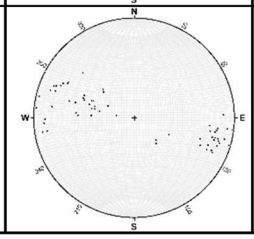		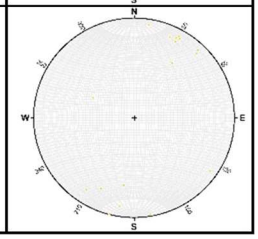

Figure 20 - Poles to planes by geographic location.

Kamb Contouring of Poles

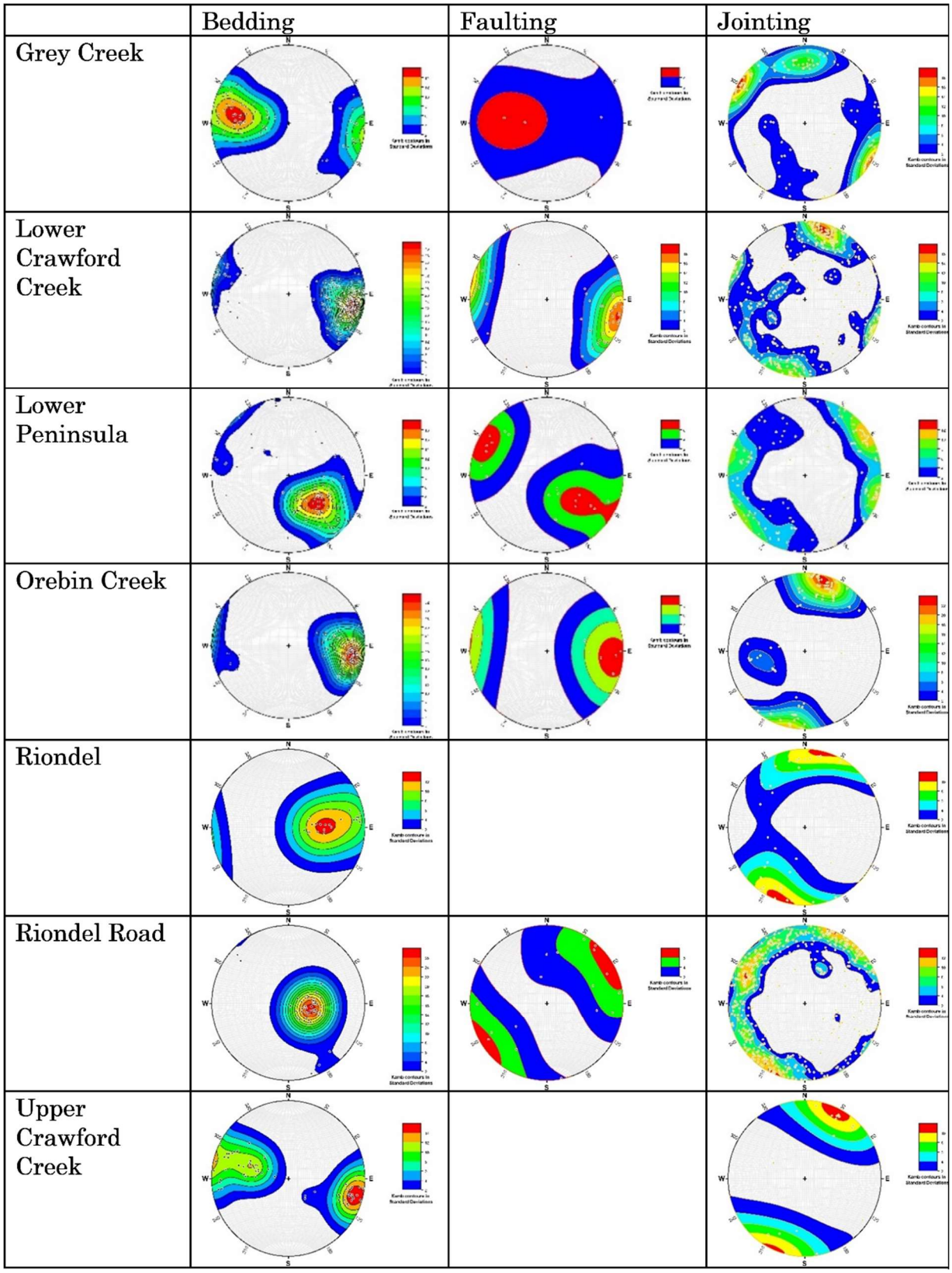

Figure 21 - Kamb contouring of poles by geographic location.

Plots for All Data

Planes

	Bedding	Faulting	Jointing
All Data	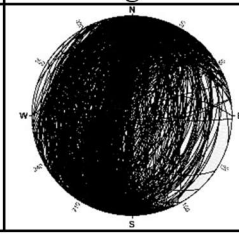	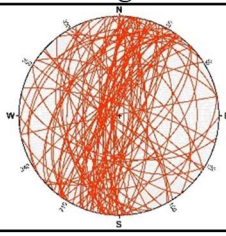	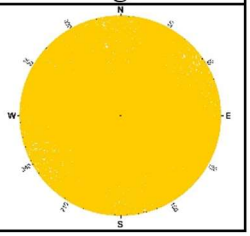

Figure 22 - Planes for all data.

Rose Diagrams from Planes

	Bedding	Faulting	Jointing
All Data	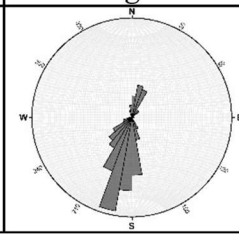	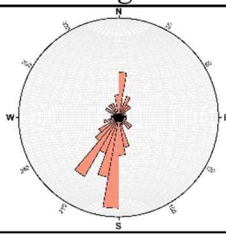	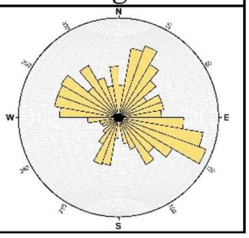

Figure 23 - Rose diagrams from planes for all data.

Poles to Planes

	Bedding	Faulting	Jointing
All Data	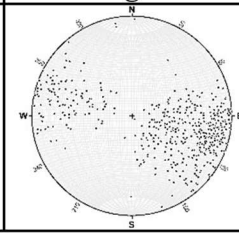	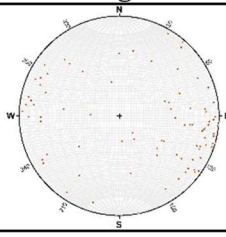	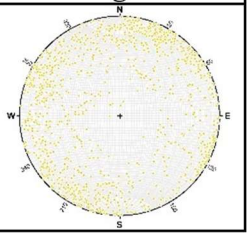

Figure 24 - Poles to planes for all data.

Kamb Contouring of Poles

	Bedding	Faulting	Jointing
All Data	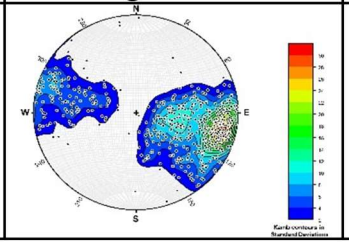	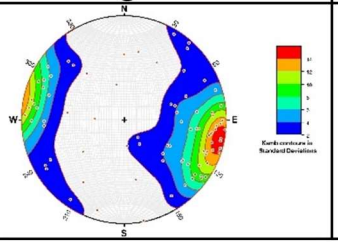	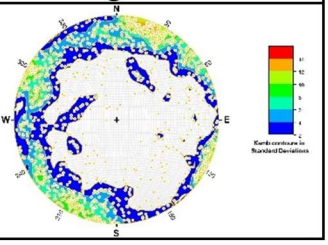

Figure 25 - Kamb contouring of poles for all data.

Discussion

Major Fault Zones

Using a combination of LiDAR imagery, structural measurements, stratigraphic displacement, and water chemistry, five major faults were interpreted within the study area (Figures 26 & 27). The most obvious of these structures is the Orebin Creek fault (Figure 28), a near-vertical normal fault striking south from Orebin Creek within the Crawford Creek drainage towards the Crawford Bay Stock. The Crawford Creek warm spring lies nearly along the trace of the Orebin Creek fault, thus it is assumed that this fault is a major conduit for hydrothermal fluids. A second fault, the West Bernard fault (Figure 29), is interpreted as a steeply dipping normal fault running 1.5 kilometers east of, and striking roughly parallel to, the Orebin Creek fault before curving westward, bifurcating, and travelling across Crawford Bay and the lower portion of the peninsula. Höy (1980) separates the West Bernard fault into the West and East Bernard faults to the north of Crawford Creek, however this bifurcation could not be verified. The trace of the West Bernard fault is largely determined from LiDAR, stratigraphy, and water chemistry, rather then direct structural measurements (except on the east shore of Crawford Bay), and it is possible, especially to the north of Crawford Creek, that this feature is instead the axis of a fold. The third fault is a previously unmapped fault directly measured approximately 4 kilometers up Tam O'Shanter Creek north of Riondel, and interpreted as a steeply dipping normal fault which strikes south towards Crawford Bay before curving across the northern end of the peninsula, following a major lineament. The final two faults are more minor faults in comparison, and follow major lineaments 1.5 and 3 kilometers north of Kootenay Bay, striking southeast. Given that the Orebin Creek fault is the most significant fault in the region and hosts direct evidence of geothermal fluids in the form of the Crawford Creek warm spring, it is interpreted by this report to be the best target for future geothermal exploration.

On a larger regional scale, the curving of fault traces towards the west suggests a likely intersection with the major fault system running through Kootenay Lake. It is possible that the major faults in the Crawford Bay area serve as a transitional zone between the Purcell Trench fault in the south and the Lakeshore, Josephine and Gallagher faults in the north, with a structure similar to the accommodation zone between fault dip domains, or the breached step-over structure described by Faulds and Hinz (2015).

Figure 26 - Map showing major fault zones within the study area.

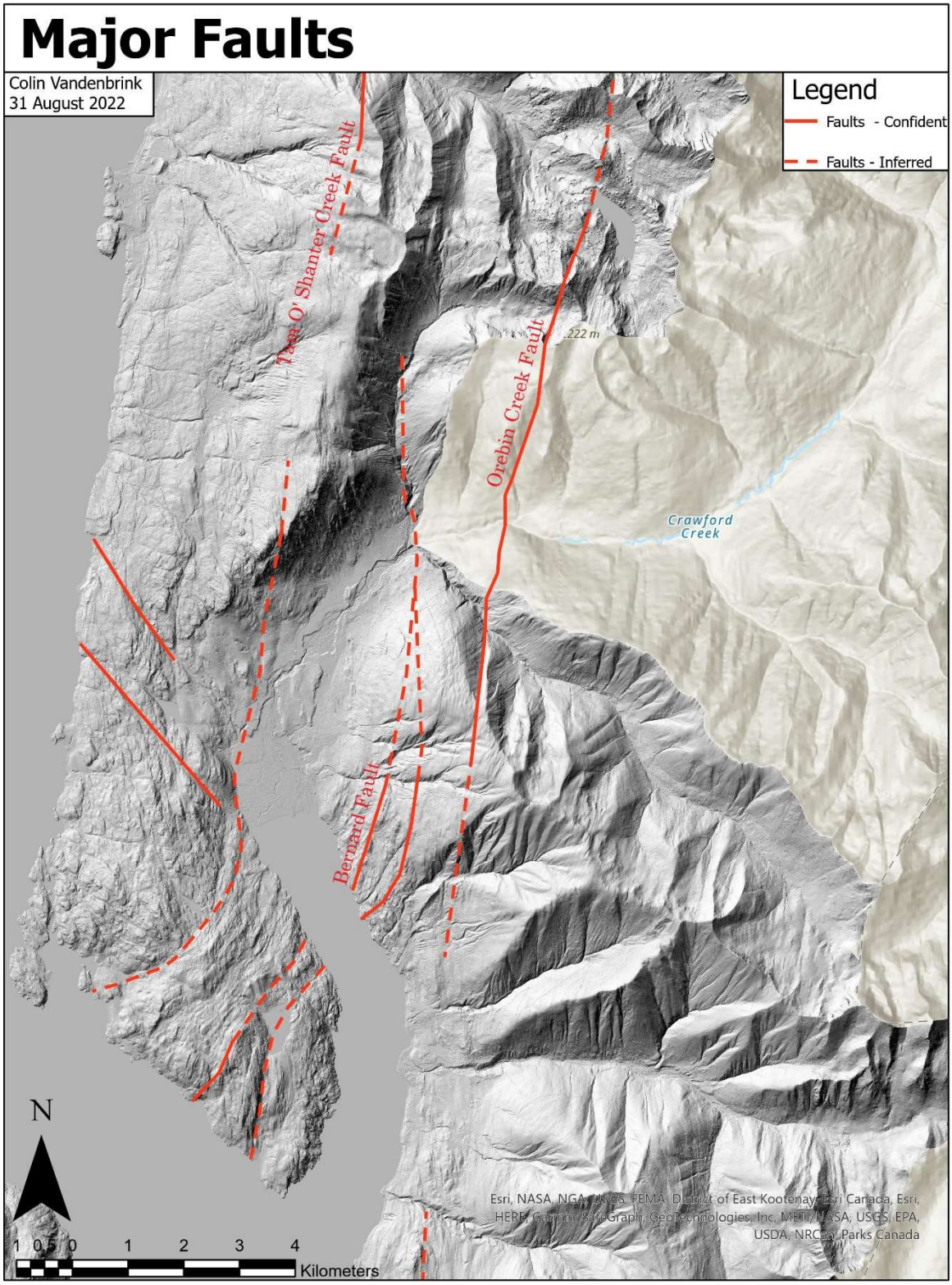

Figure 27 - Map showing major fault zones within the study area, underlain by LiDAR imagery where available.

Figure 28 - The surface expression of the Orebin Creek fault. View is approximately 25 meters across. Facing north. 517014 E, 5506814 N.

Figure 29 - A highly altered zone interpreted as a portion of the West Bernard fault, with water emerging from multiple locations along the exposure. View is approximately 25 meters across. Facing north-northwest. 511437 E, 5496208 N.

Bedrock Geology

The bedrock geology of the study area is complex and varied (Figure 30). In general, the geology can be divided into three major provinces: An unfolded, planar western zone principally composed of Lardeau gneiss, a highly deformed central zone composed of tight, isoclinal folds bounded by steeply dipping faults and principally composed of Badshot marble and Hamill quartzite and schist, and a broadly folded eastern zone containing large, kilometer scale folds within Windermere phyllites.

Western zone: The Lardeau gneisses in the region along Riondel Road have very consistent foliation planes typically striking south to southwest and dipping 36°, only differing as it approaches the trace of the Bluebell Mountain fault, where strikes shift further southwest and dips become shallower. These gneisses are also often intruded by a highly leucocratic pegmatite, which anecdotally becomes more prevalent moving east. The primary outlier within this otherwise consistent zone is that of the Riondel peninsula, which is composed of older Hamill quartzite overlying younger Badshot marble, and is interpreted as a displaced block of an overturned anticline.

Central zone: Alternating Lardeau gneiss, Badshot marble, and Hamill quartzite and schist is interpreted as isoclinal folds bounded by steeply dipping normal faults. On the lower peninsula, structural measurements only support this model in a few locations, and across Crawford Bay, frequent faulting is observed. A model of tightly spaced imbricate faults could also be valid, and may better agree with bedding measurements, however the folding model was chosen as it explains the stratigraphic succession better then normal faulting. Additionally, the frequent faulting on the east shore could not be correlated across the bay to the peninsula, and an isoclinal folding model better follows after the interpretation of Höy (1980). Near the peak of Mount Crawford, this folding model is much better supported by structural measurements. Near Preacher Creek, older Hamill quartzite is overlying younger Badshot marble, and is interpreted as the intersection of an overturned anticline and the West Bernard fault. It is possible that the West Bernard fault

runs along the axis of this fold, or is not a fault at all but merely a highly deformed fold axis. The West Bernard fault was interpreted instead to run along the base of the Badshot marble to maintain stratigraphic succession. The series of rocks seen in the Tam O'Shanter drainage are also interpreted as the east limb of an anticline to maintain this succession.

Eastern zone: Largely composed of rocks from the Windermere Supergroup, this zone is free from the intense faulting and folding further east, with the only major feature being a large, kilometer-scale fold, though the axis of this structure could not be precisely located and is only inferred.

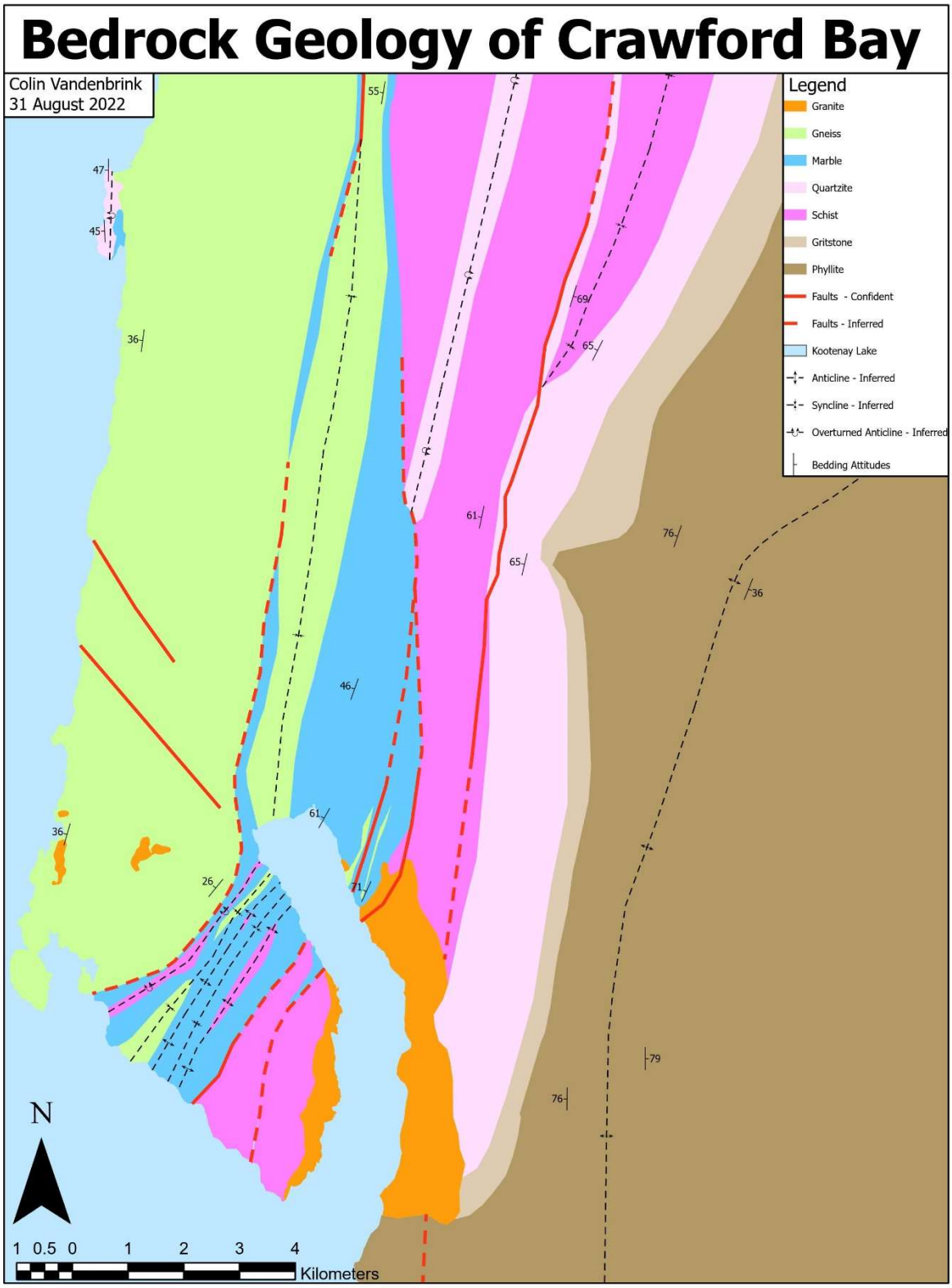

Figure 30 - Map of the interpreted bedrock geology within the study area.

Correlations Between Water Chemistry and Faulting

Groundwater measurements were shown to correlate both with underlying bedrock and with major fault zones, however as this report is primarily focussed on faults as vectors for geothermal fluids, only the latter is considered in detail. Below are maps of the water chemistry parameters shown above superimposed on the interpreted locations for major fault traces (Figures 31 – 35). Temperature is immediately dismissible as there are no sample locations with temperature values appreciably higher than the daytime air temperature, with the exception of the Crawford Creek warm spring (Figure 36). The only parameter of those tested that is similar near major faults and within the Crawford Creek warm spring is pH, with lower values coinciding with fault traces. The pH in the Crawford Creek warm spring was 6.59, with the only other acidic water source in the study area being the Krishna spring proximal to the two major liniments north of Kootenay Bay with a pH of 6.86 (Figure 37). Other water sources near major faults often had a pH just above 7, while most sources elsewhere had a pH between 7.5 and 8.5. These observations agree with the reporting from Geoscience B.C., confirming that acidic water is in fact an indicator of geothermal input in the Kootenay Lake region. Conductivity and total dissolved solids are highly correlated with each other, with salinity also correlated to a lesser degree. Although these three parameters are much higher near faults, they are extremely low within the Crawford Creek warm spring, therefore the waters in these locations are sourced by a different mechanism then the warm spring, or these elevated parameters have more to do with the marble bedrock they often coincide with, rather then any structural control.

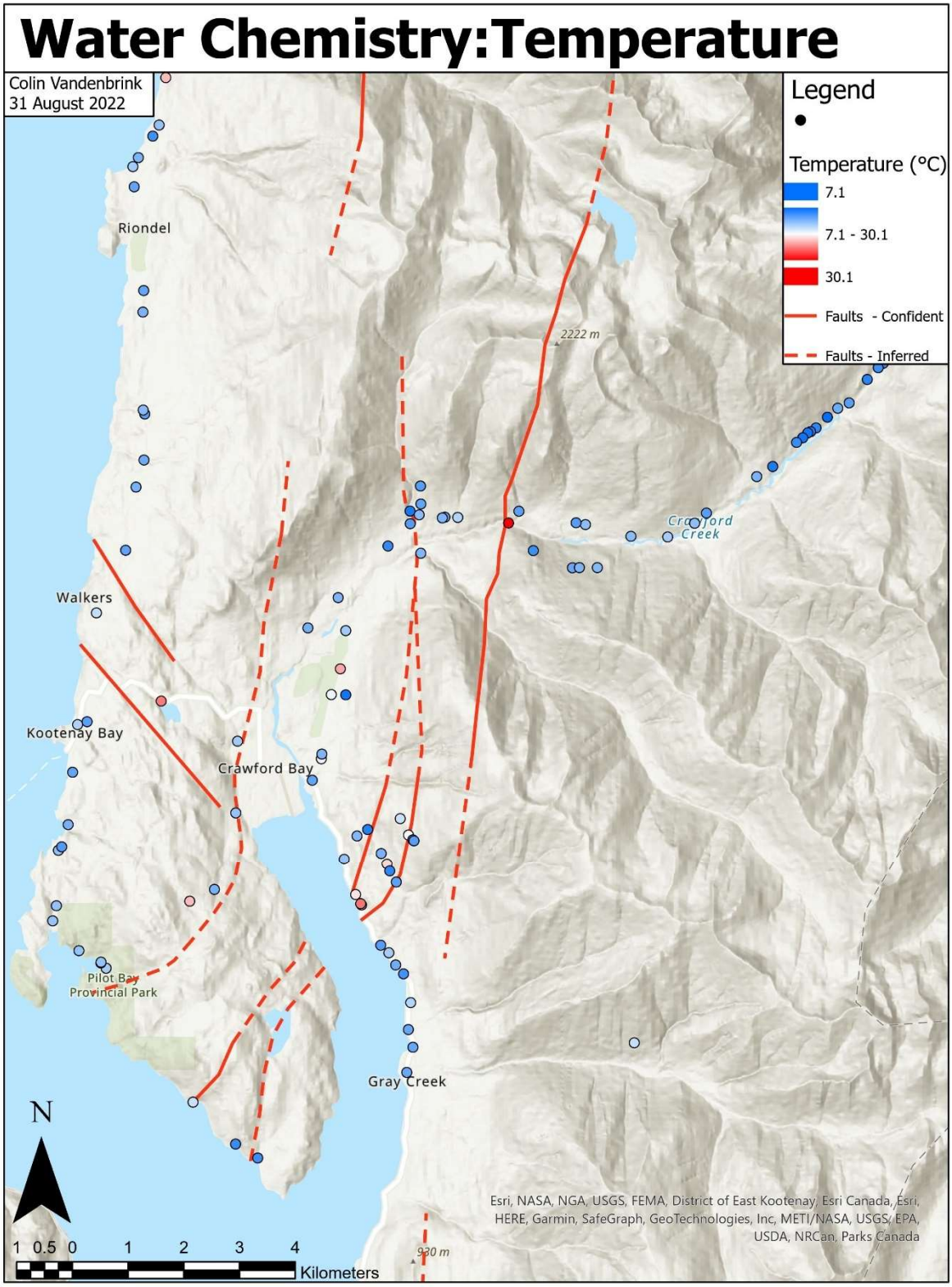

Figure 31 - Water chemistry sample points symbolized according to temperature (blue = lower, red = higher), compared to assumed major fault locations.

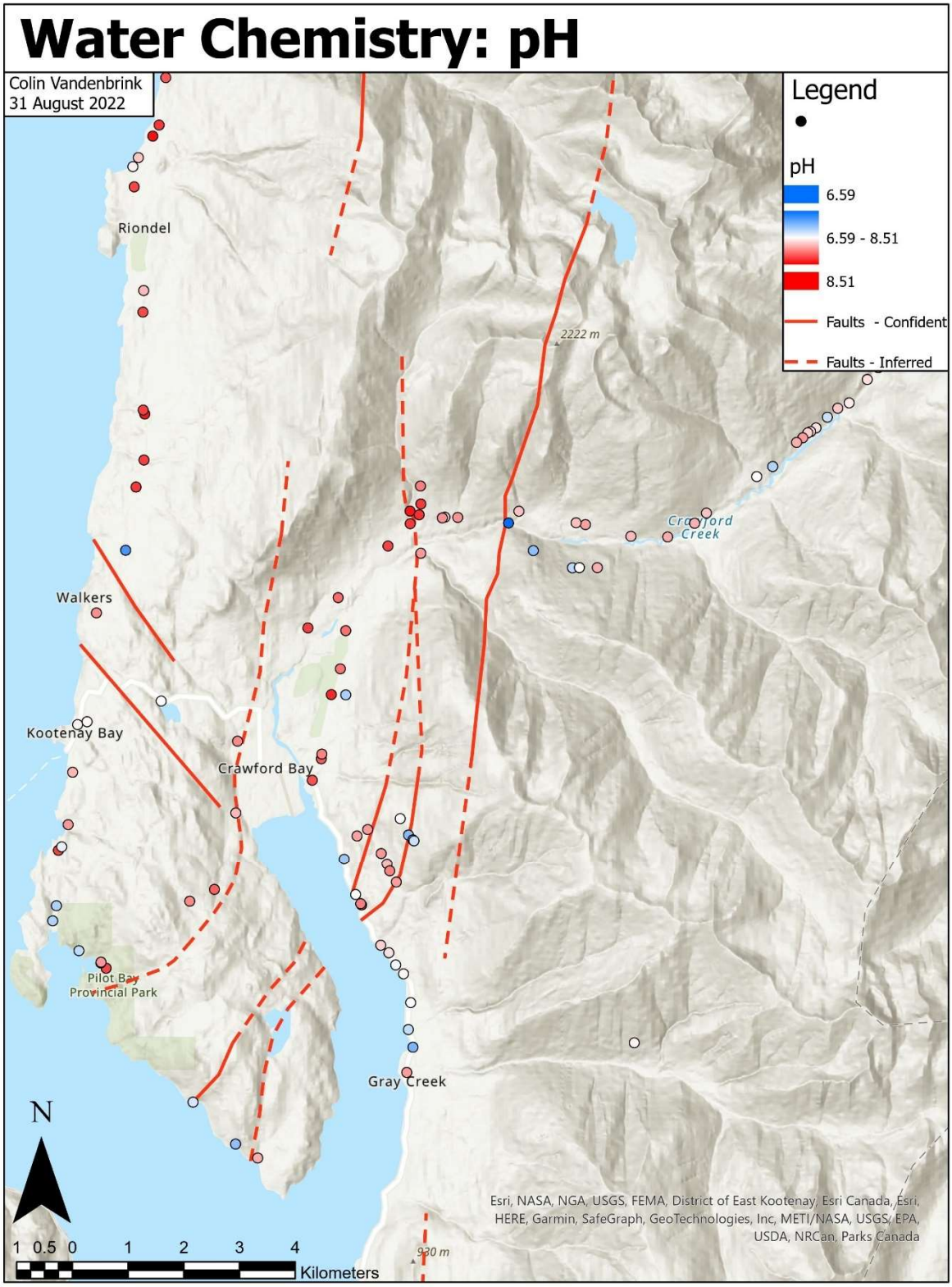

Figure 32 - Water chemistry sample points symbolized according to pH (blue = lower, red = higher), compared to assumed major fault locations.

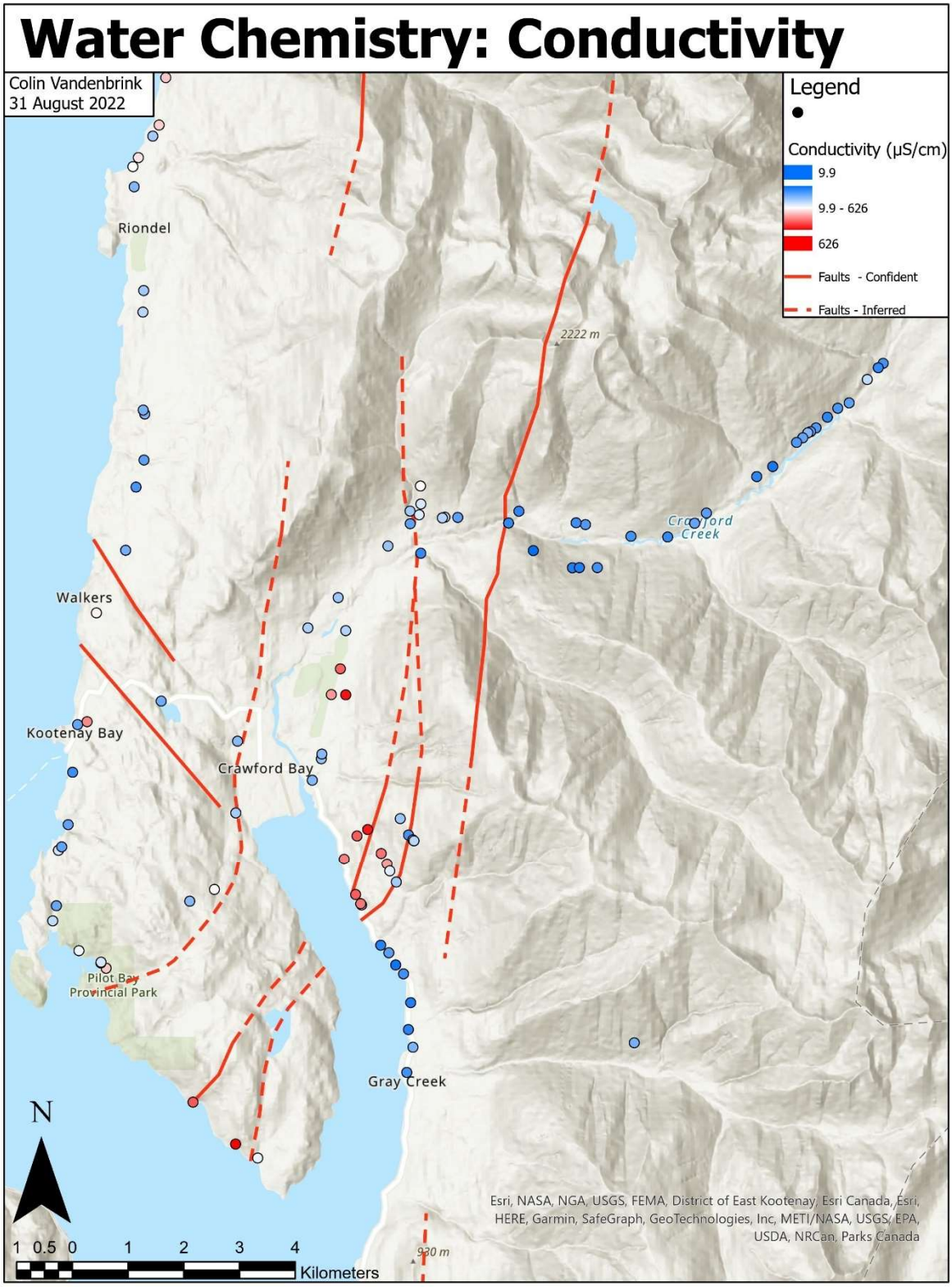

Figure 33 - Water chemistry sample points symbolized according to conductivity (blue = lower, red = higher), compared to assumed major fault locations.

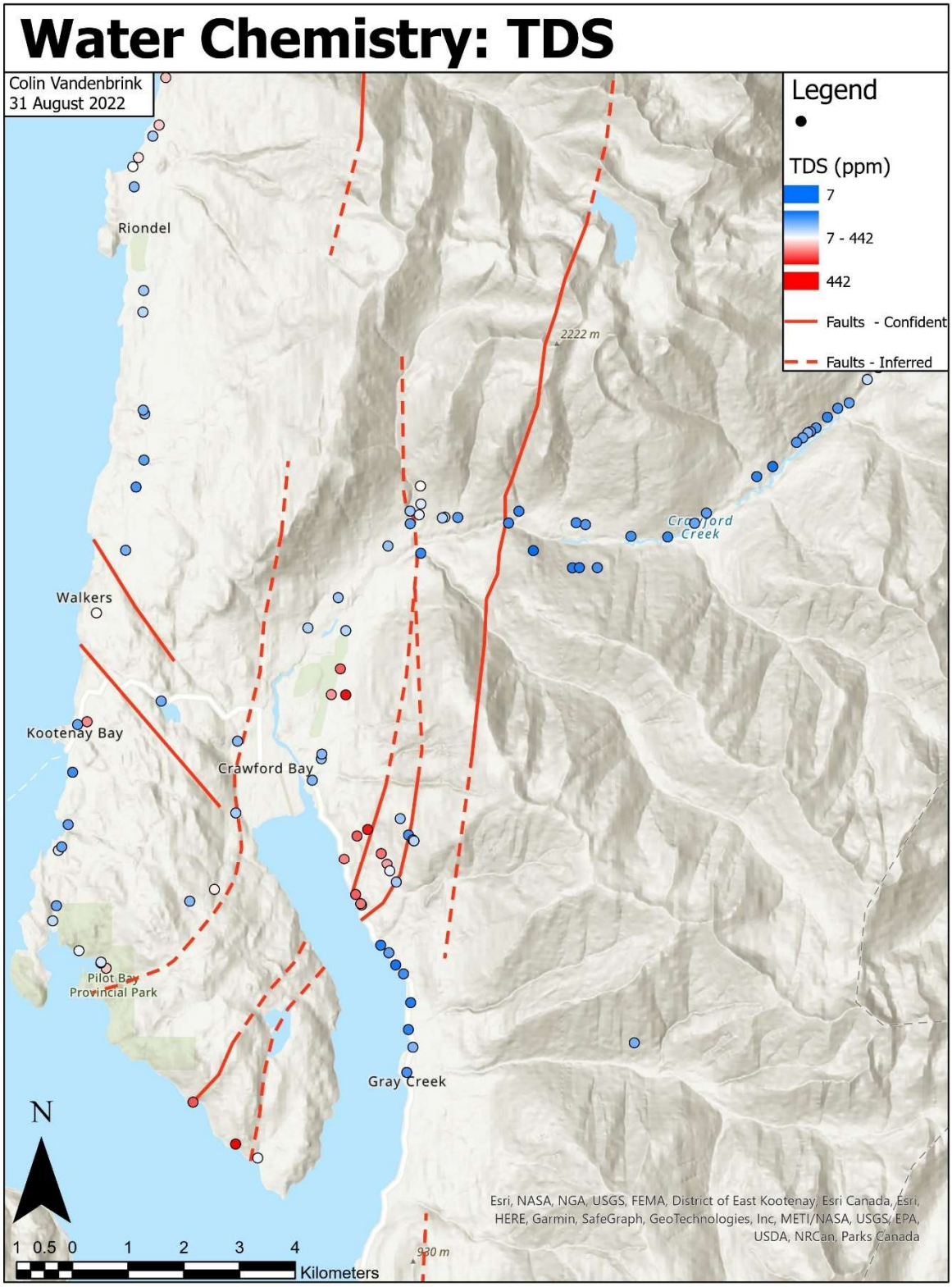

Figure 34 - Water chemistry sample points symbolized according to total dissolved solids (blue = lower, red = higher), compared to assumed major fault locations.

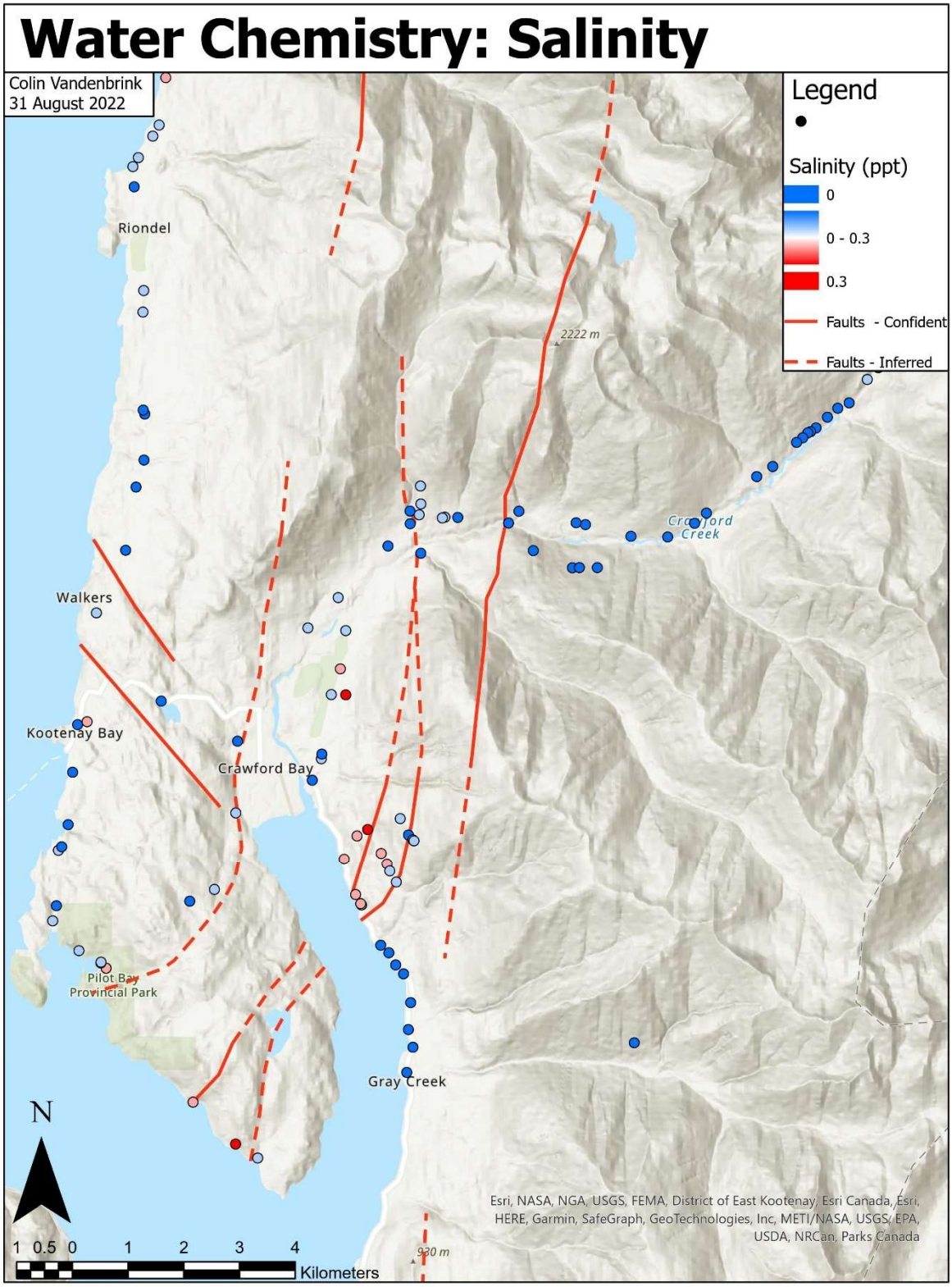

Figure 35 - Water chemistry sample points symbolized according to salinity (blue = lower, red = higher), compared to assumed major fault locations.

Figure 36 - A bathing pool at the Crawford Creek warm spring. The source of the spring is approximately 5 meters upslope, though it is largely obscured. Construction pails near the pool show scale. Facing west-southwest. 517100 E, 5506597 N.

Figure 37 - Krishna spring. Pool is approximately 2 meters across. Facing northeast. 510228 E, 5506108 N.

Implications of Structural Analysis

Many of the inferences previously discussed are further confirmed by structural analysis. For example, bedding planes largely dip to the southwest in most cases, with the notable exception of within the Windermere rocks, where large, kilometer scale folds are observed (Figure 38).

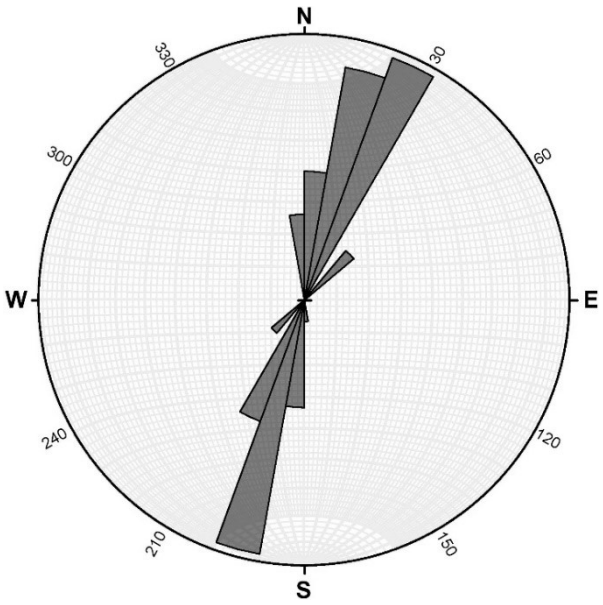

Figure 38 - Rose diagram of bedding planes for Upper Crawford Creek. N = 62.

Conversely, Kamb contouring demonstrates how both gneiss and quartzite demonstrate the most consistent foliation/bedding planes compared to every other rock type observed (Figures 39 – 40). The incredibly consistent foliation planes for gneiss across its extent suggest that these rocks only experienced a single stress regime, without undergoing later reorganization.

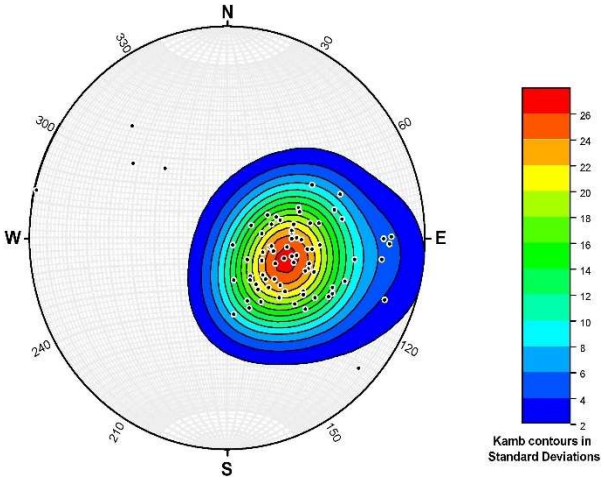

Figure 39 - Kamb contouring of bedding poles for gneiss. N = 78.

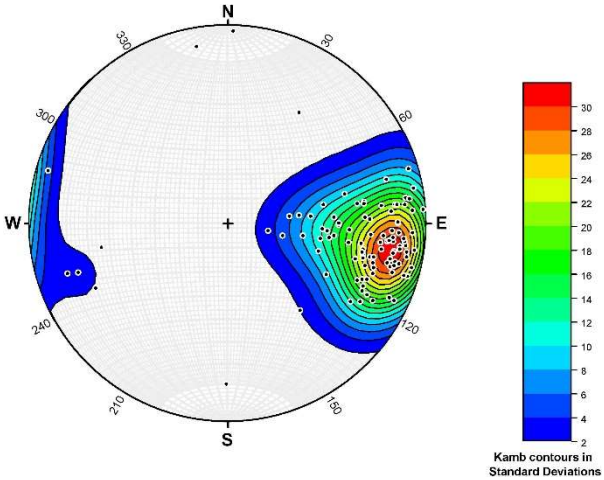

Figure 40 - Kamb contouring of bedding poles for quartzite. N = 104.

Bedding measurements in the Lower Crawford Creek region, as well as the Orebin Creek region more specifically, are analogous to fault measurements, suggesting that faults slip along bedding planes (Figures 41 – 44).

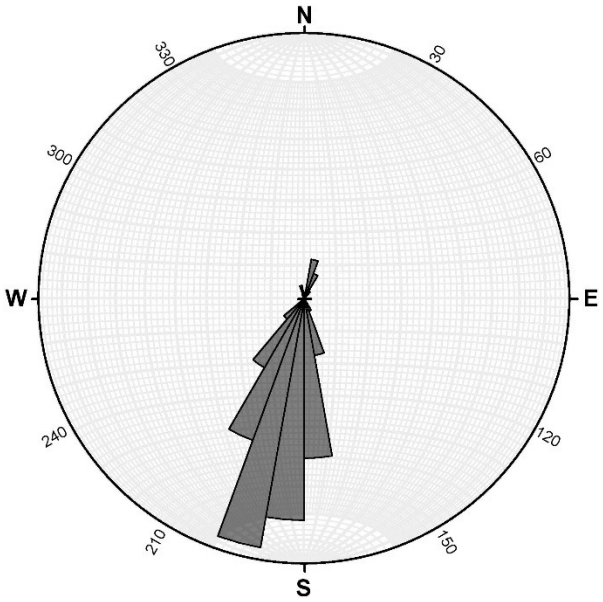

Figure 41 - Rose diagram of bedding planes for Lower Crawford Creek. N = 240.

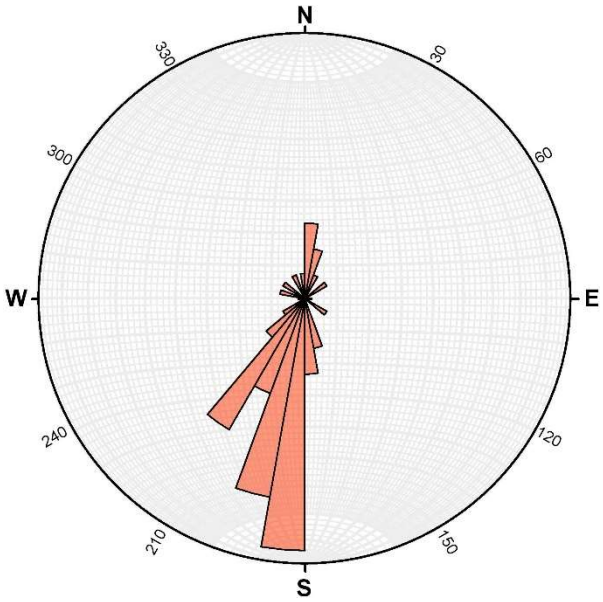

Figure 42 - Rose Diagram of Fault planes for Lower Crawford Creek. N = 48.

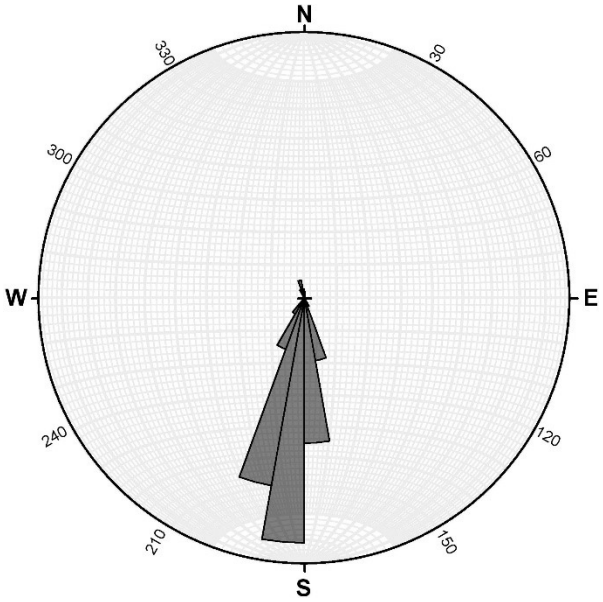

Figure 43 - Rose diagram of bedding planes for Orebin Creek. N = 84.

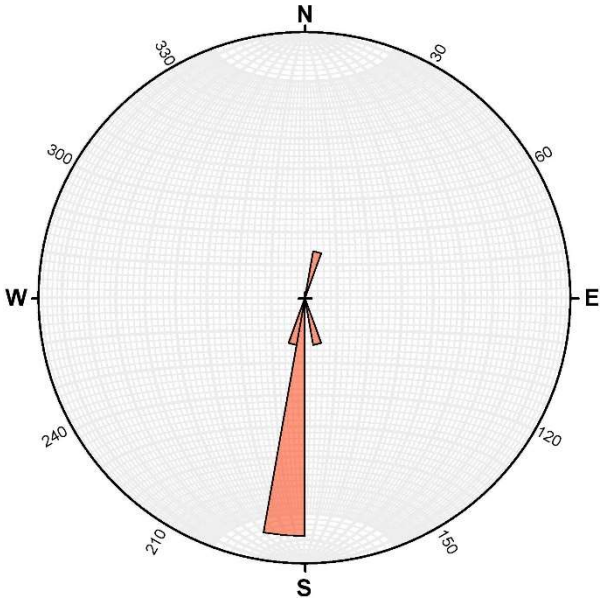

Figure 44 - Rose diagram of fault planes for Orebin Creek. N = 8.

A set of conjugate faults is observed in the Lower Peninsula region, suggesting the formation of faults along the axes of overturned folds, or perhaps the same faulting along bedding planes seen elsewhere, but applied to a highly folded environment (Figure 45).

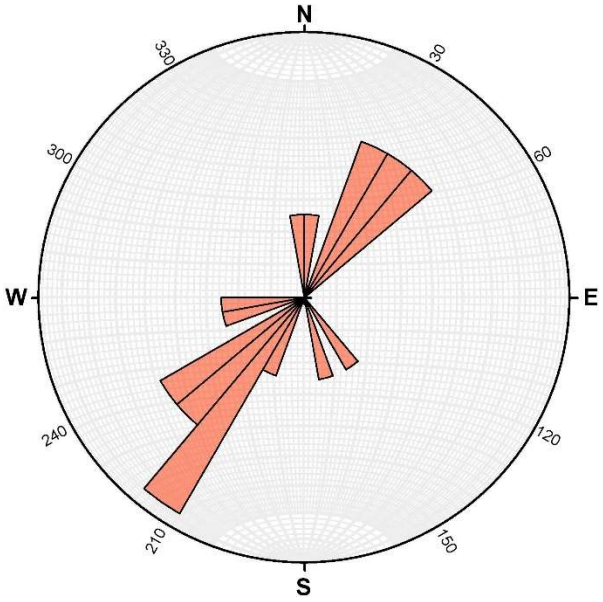

Figure 45 - Rose diagram of fault planes for Lower Peninsula. N = 20.

Joint planes also show interesting trends in the form of conjugate sets in granite, Badshot marble, and Hamill quartzite (Figures 46 – 49). Also seen is the west-northwest striking ore-bearing fracture set in the Riondel mine and its east-northeast conjugate set as described by Moynihan & Pattison (2011).

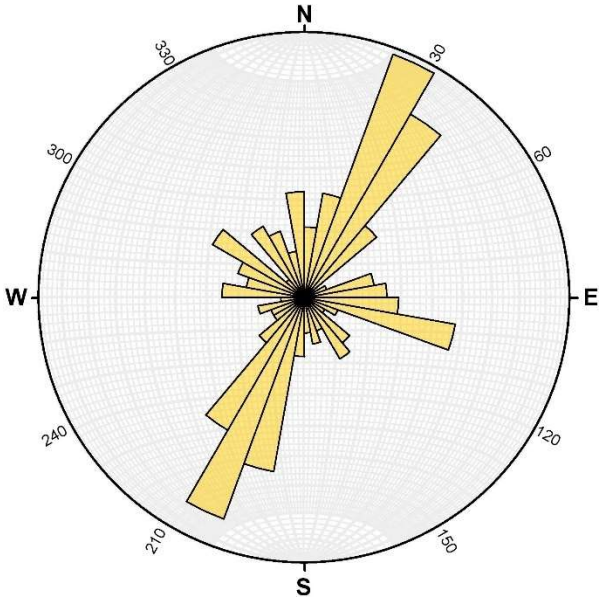

Figure 46 - Rose diagram of joint planes for granite. N = 251.

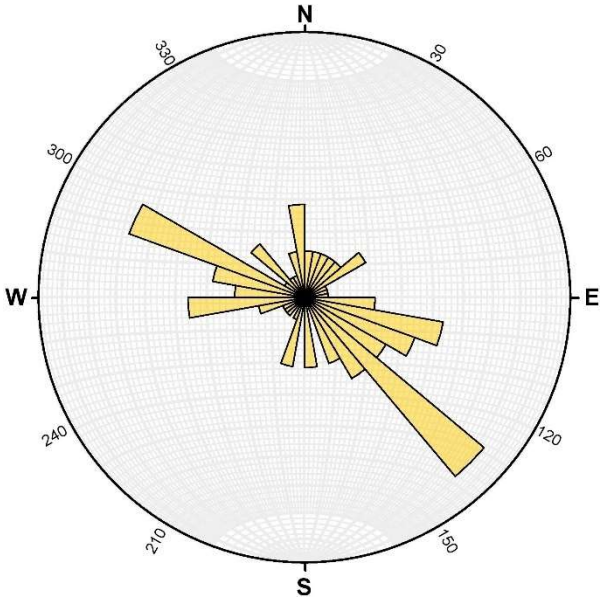

Figure 47 - Rose diagram of joint planes for marble. N = 95.

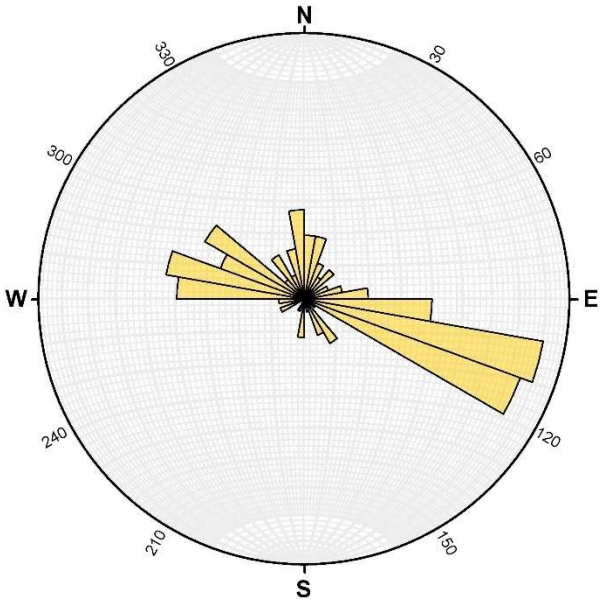

Figure 48 - Rose diagram of joint planes for quartzite. N = 149.

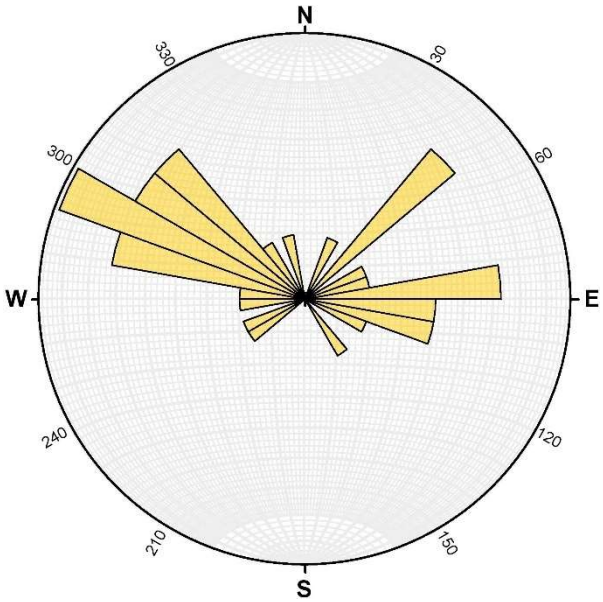

Figure 49 - Rose diagram of joint planes for Riondel. N = 34.

Joints also form conjugate sets with bedding planes, especially in the Orebin Creek region, where steeply dipping bedding planes intersect steeply dipping joint planes, providing an ideal environment for the propagation of hot fluids from depth (Figures 50 – 53). Both surfaces are frequent and highly regular, producing the most permeable region seen anywhere in the study area. The much more minor, shallow dipping joint set in the Orebin Creek quartzites were anecdotally the site of significant water flow from the rock faces, though this is likely due to their cross cutting of the other much steeper dipping planar features, rather then some innate higher fluid flow within this specific joint set.

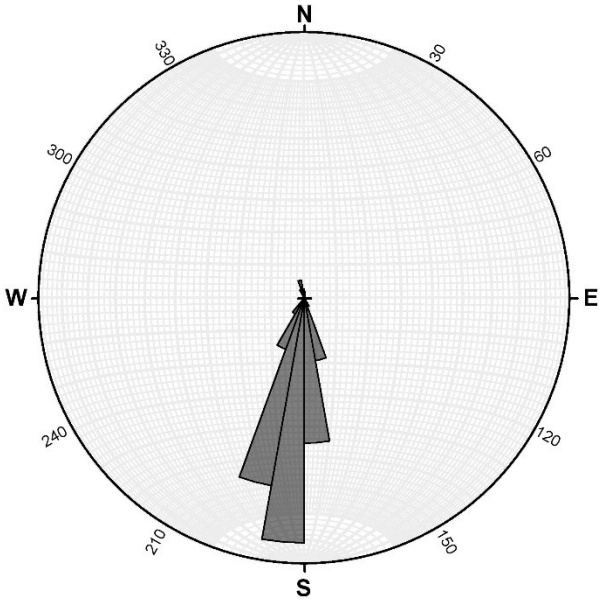

Figure 50 - Rose diagram of bedding planes for Orebin Creek. N = 84.

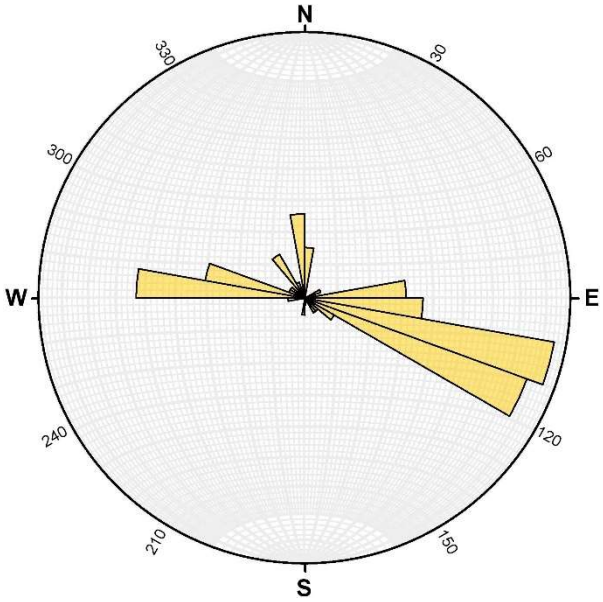

Figure 51 - Rose diagram of joint planes for Orebin Creek. N = 79.

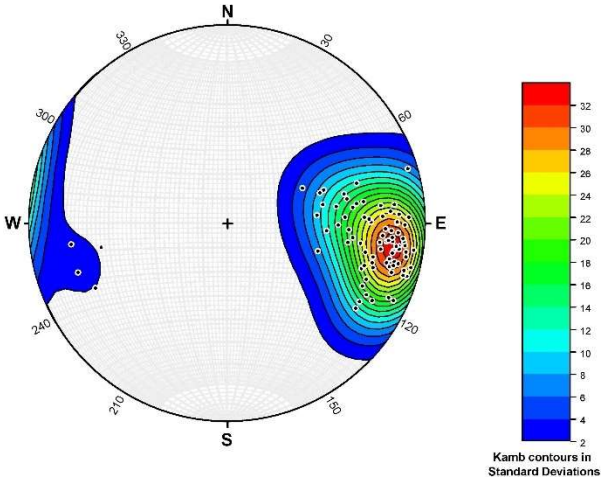

Figure 52 - Kamb contouring of bedding poles for Orebin Creek. N = 84.

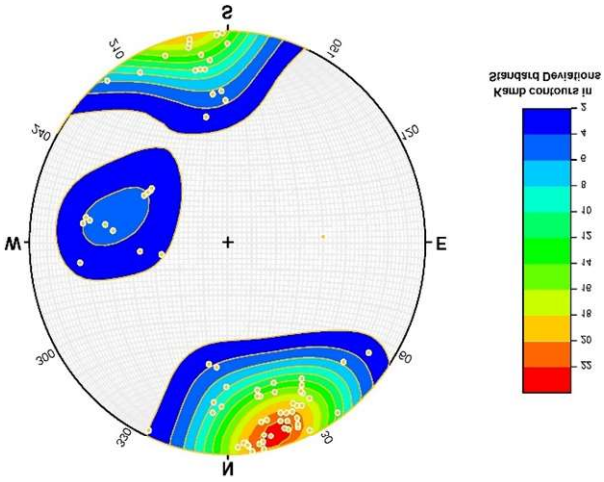

Figure 53 - Kamb contouring of joint poles for Orebin Creek. N = 79.

Areas of Greatest Geothermal Potential

By far, the region within the study area with the greatest geothermal potential is that around Orebin Creek. Not only does this region already host a pre-existing surficial expression of geothermal activity in the form of the Crawford Creek warm spring, it also hosts a major regional fault in the form of the Orebin Creek fault. Steeply dipping, very regular, near perpendicular sets of bedding and jointing planes also provide extensive permeability for transporting geothermal fluids from depth.

A geothermal well in this location would ideally intersect both bedding and jointing planes to maximize delivery of geothermal fluids to the well. This ideal angle can be geometrically determined from structural data (Figure 54). Assuming only bedding planes striking between 170 - 200°, and only jointing planes of the most pervasive, steeply dipping joint set striking between 90 - 120° to limit outliers, the average bedding attitude is 186.3/68.4, and the average jointing attitude is 107.1/76.7. These two planes intersect at a line with the attitude 253.6/66.8. The ideal angle for a well wishing to intersect both bedding and jointing planes at an ideal angle is therefore perpendicular to the line of their intersection, at 073.6/23.2.

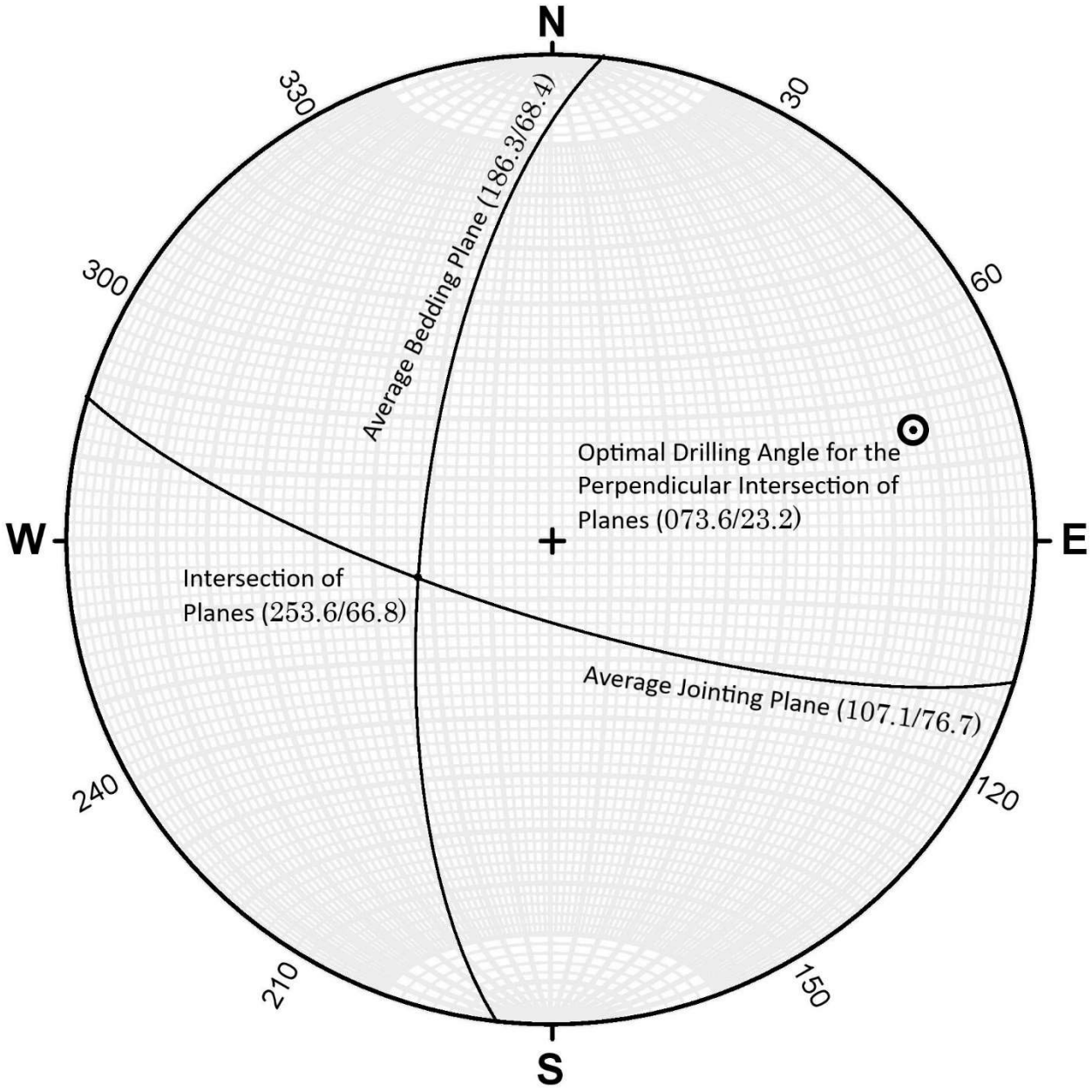

Figure 54 - Determination of the optimal orientation of a well for intersecting bedding and jointing planes near the Orebin Creek fault.

A second area of interest is that of the Krishna spring, proximal to the two major liniments north of Kootenay Bay. This is the only water source measured with an acidic pH besides the Crawford Creek warm spring, and the lineaments lying just to the south of the spring provide a mechanism for the transportation of geothermal fluids. Unfortunately, the Lardeau gneiss at this location is much less consistently

fractured then the quartzites around Orebin Creek, suggesting that permeability in this location would be substantially less.

Other areas of nominal interest include the east shore of Crawford Bay and the extreme south of the peninsula, where water sampling often reported pH values significantly below background levels (though not acidic), in localities proximal to major fault traces. The intense faulting and folding at these localities provide a potential mechanism for the movement of geothermal fluids. However, access to these areas is limited, and the structural and chemical indicators are simply not as strong as the two locations described above.

Conclusions and Future Work

Crawford Bay and the surrounding area shows significant geothermal potential. South striking, steeply dipping normal faults act as conduits for geothermal fluids in the region, expressed most prominently by the Crawford Creek warm spring. The trace of these faults curve sharply to the east towards the south of the study area, suggesting an accommodation zone or step-over between the two fault systems to the north and south of the study area within Kootenay Lake. Water chemistry sampling suggests that the best indicator of geothermal influence on a water body is an acidic pH, and pH values significantly below background levels are common near major fault traces.

Overall, the area of greatest geothermal potential is that of Orebin Creek, where significant faulting, a thermal spring in the form of the Crawford Creek warm spring, and favourable water chemistry all coincide. Frequent and consistent steeply dipping bedding and jointing planes within quartzite also greatly enhance permeability and the movement of geothermal fluids in this region. The ideal trend and plunge for a well wishing to perpendicularly intersect these planar features is 073.6/23.2.

Future work to be done includes improving LiDAR coverage for better determining the traces of major faults, an investigation into the broader structural context to determine the structural setting of the geothermal system, and further chemical analysis of water sources with anomalously low pH. A map with the locations of samples that were sent for further lab analysis is available in Appendix A. Test wells drilled proximal to the Orebin Creek fault would also provide significant insight into the potential for future operations.

References

Allmendinger, R. W., Siron, C. R., & Scott, C. P. (2017). Structural data collection with mobile devices: Accuracy, redundancy, and best practices. *Journal of Structural Geology*, *102*, 98–112. doi:10.1016/j.jsg.2017.07.011.

Allmendinger, R.W. (2020). *Stereonet* (Version 11.4.X) [computer software]. Retrieved from www.rickallmendinger.net/stereonet/.

Allmendinger, R.W. (2022). *Stereonet Mobile* (Version 4.0.X) [mobile app]. Retrieved from www.rickallmendinger.net/stereonet-mobile/.

Allmendinger, R. W., Cardozo, N., and Fisher, D. (2012). *Structural geology algorithms: Vectors and tensors in structural geology*. Cambridge University Press.

Cardozo, N., & Allmendinger, R. W. (2013). Spherical projections with OSXStereonet. *Computers & Geosciences*, *51*, 193–205. doi:10.1016/j.cageo.2012.07.021.

Desrochers, D. T. (1992). Geothermal feasibility study for the use of hot water near Riondel. *British Columbia: Geological Survey of Canada Open File*, *2502*. doi:10.4095/133452.

Esri Inc. (2022). *ArcGIS Pro* (Version 3.0) [computer software]. Retrieved from www.esri.com/en-us/arcgis/products/arcgis-pro/overview/.

Faulds, J., & Hinz, N. (2015). Favorable tectonic and structural settings of geothermal systems in the Great Basin region, western USA: Proxies for discovering blind geothermal systems. *Proceedings World Geothermal Congress, Melbourne, Australia, 19-25 April 2015* (No. DOE-UNR-06731-02). Nevada Bureau of Mines and Geology, University of Nevada, Reno.

Finley, T. (2020). *Fault-hosted geothermal systems in southeastern British Columbia* [Master's thesis, University of Alberta]. doi:10.7939/r3-r87x-jt83.

Geoscience BC. (2016). *Direct-use Geothermal Resources in British Columbia.* (Report 2016-07). Retrieved from https://www.geosciencebc.com/projects/2015-022/.

Grasby, S. E., & Hutcheon, I. (2001). Controls on the distribution of thermal springs in the southern Canadian Cordillera. *Canadian Journal of Earth Sciences*, *38*(3), 427-440. doi:10.1139/e00- 091.

Höy, T. (1980). *Geology of the Riondel area, central Kootenay Arc, southeastern British Columbia*. Ministry of Energy, Mines, and Petroleum Resources.

Kamb, W. B. (1959). Ice petrofabric observations from Blue Glacier, Washington, in relation to theory and experiment. *Journal of Geophysical Research*, *64*(11), 1891–1909. doi:10.1029/jz064i011p01891.

Livingstone, K. W. (1968). *Geology of the Crawford Bay map-area* [Doctoral dissertation, University of British Columbia].

Monger, J.W.H. (2008). Evolution of Canada's western mountains. *Geological Survey of Canada Open File, 5804*. doi:10.4095/225581.

Monger, J. W. H., Price, R. A., & Tempelman-Kluit, D. J. (1982). Tectonic accretion and the origin of the two major metamorphic and plutonic welts in the Canadian Cordillera. *Geology*, *10*(2), 70-75. doi: 10.1130/0091-7613(1982)10<70:taatoo>2.0.co;2.

Moynihan, D. & Pattison, D.R.M. (2008). Origin of the Kootenay Lake Metamorphic High, Southeastern British Columbia. *British Columbia Geological Survey Geological Fieldwork, 2008-1,* 147–158.

Moynihan, D. P., & Pattison, D. R. (2011). The origin of mineralized fractures at the Bluebell Mine site, Riondel, British Columbia. *Economic Geology*, *106*(6), 1043-1058. doi: 10.2113/econgeo.106.6.1043.

Sabutsch, J. (2021). *Community Geothermal Assessment 2021 Report*. Selkirk Innovates.

SQLite Browser (2021). *DB Browser for SQLite* (Version 3.12.2) [computer software]. Retrieved from www.sqlitebrowser.org/.

Walker, J. F. (1934). Geology and mineral deposits of Salmo Map-Area, British Columbia, Canada Dept. Mines, Geol. Survey, Mem, 172, 1-102.

Appendices

Appendix A: Maps

Full-size versions of maps used in the report above (Figures 55 – 75).

Geologic Mapping

Figure 55 - Overview map of the area studied in this report.

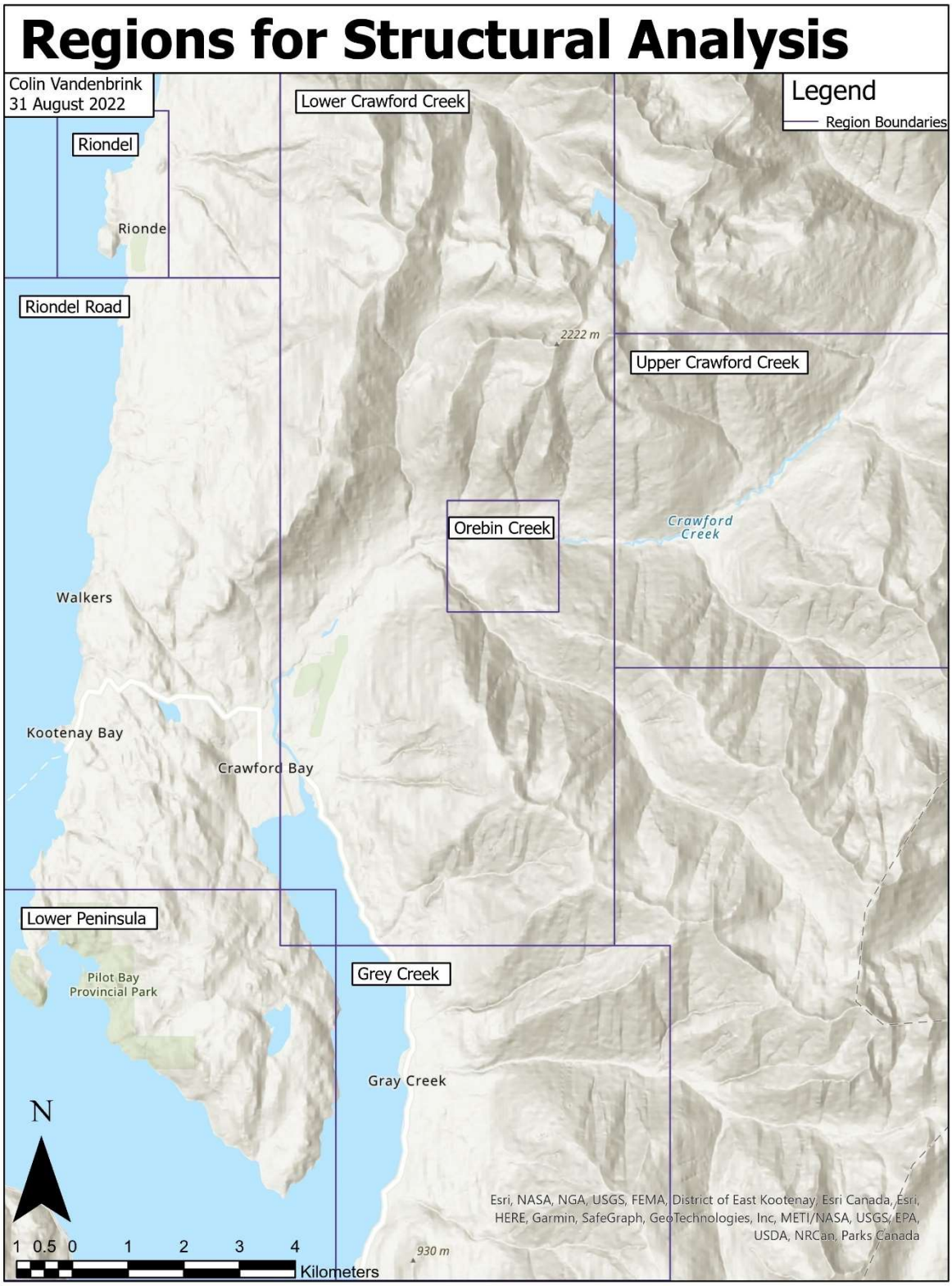

Figure 56 - Map of the geographic regions used to parse and analyse structural data.

Figure 57 - Map showing locations where bedding attitudes were recorded.

Figure 58 - Map showing locations where fault attitudes were recorded.

Figure 59 - Map showing locations where joint attitudes were recorded.

Figure 60 - Map of major fault zones within the study area.

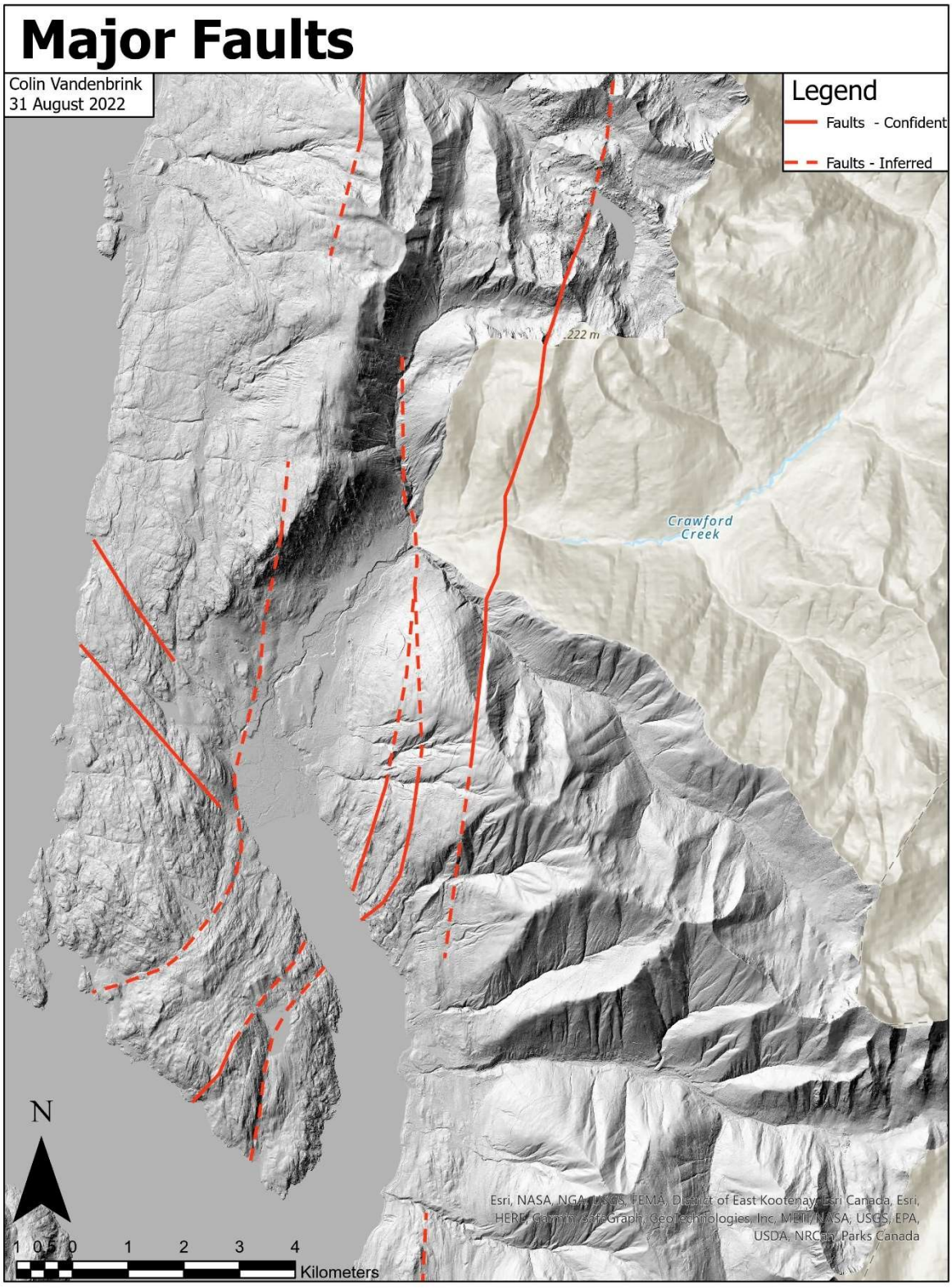

Figure 61 - Map showing major fault zones within the study area, underlain by LiDAR imagery where available.

Figure 62 - Map showing locations where bedrock observations were recorded.

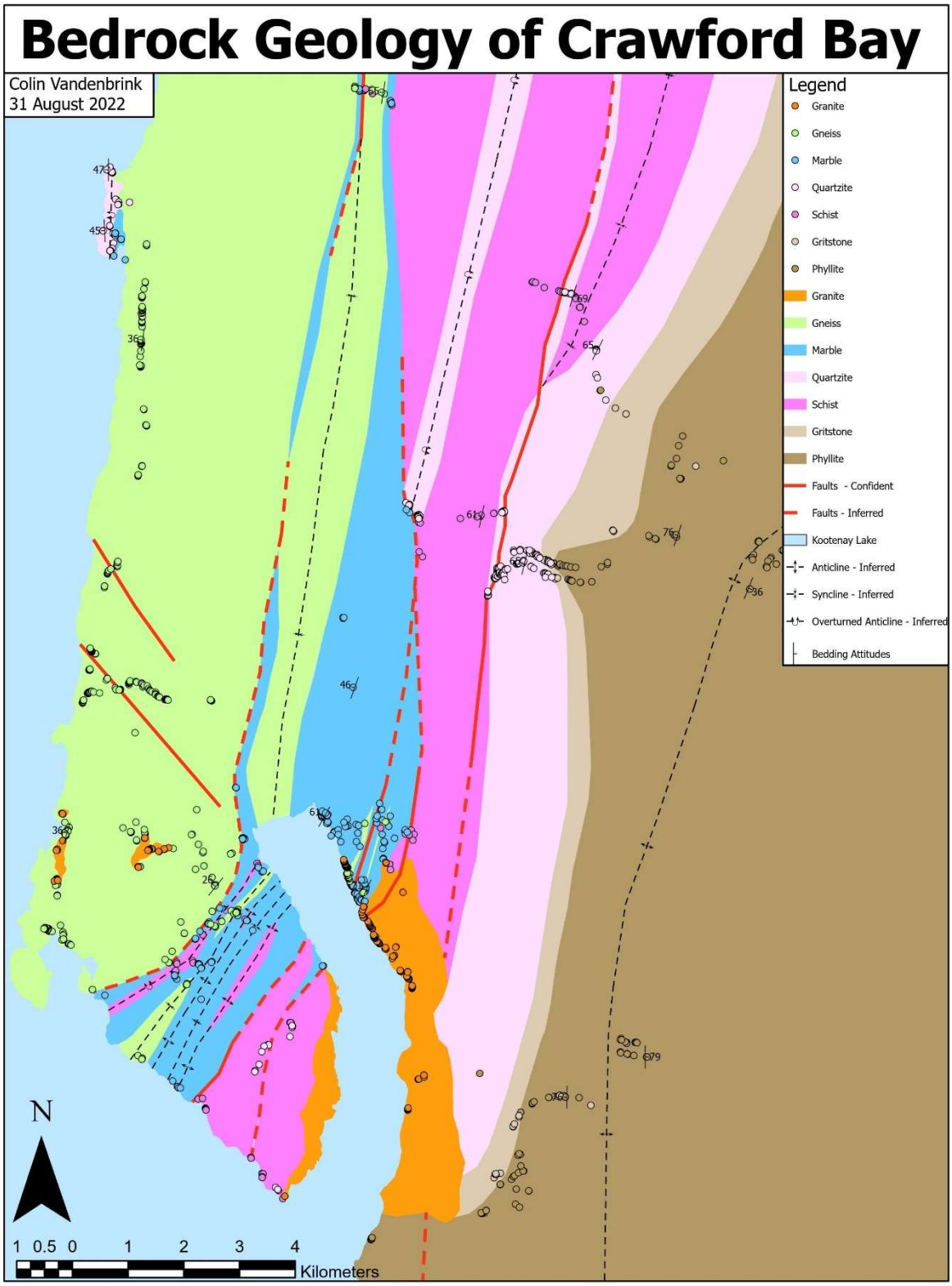

Figure 63 – Map of the interpreted bedrock geology within the study area, with data points for rock type.

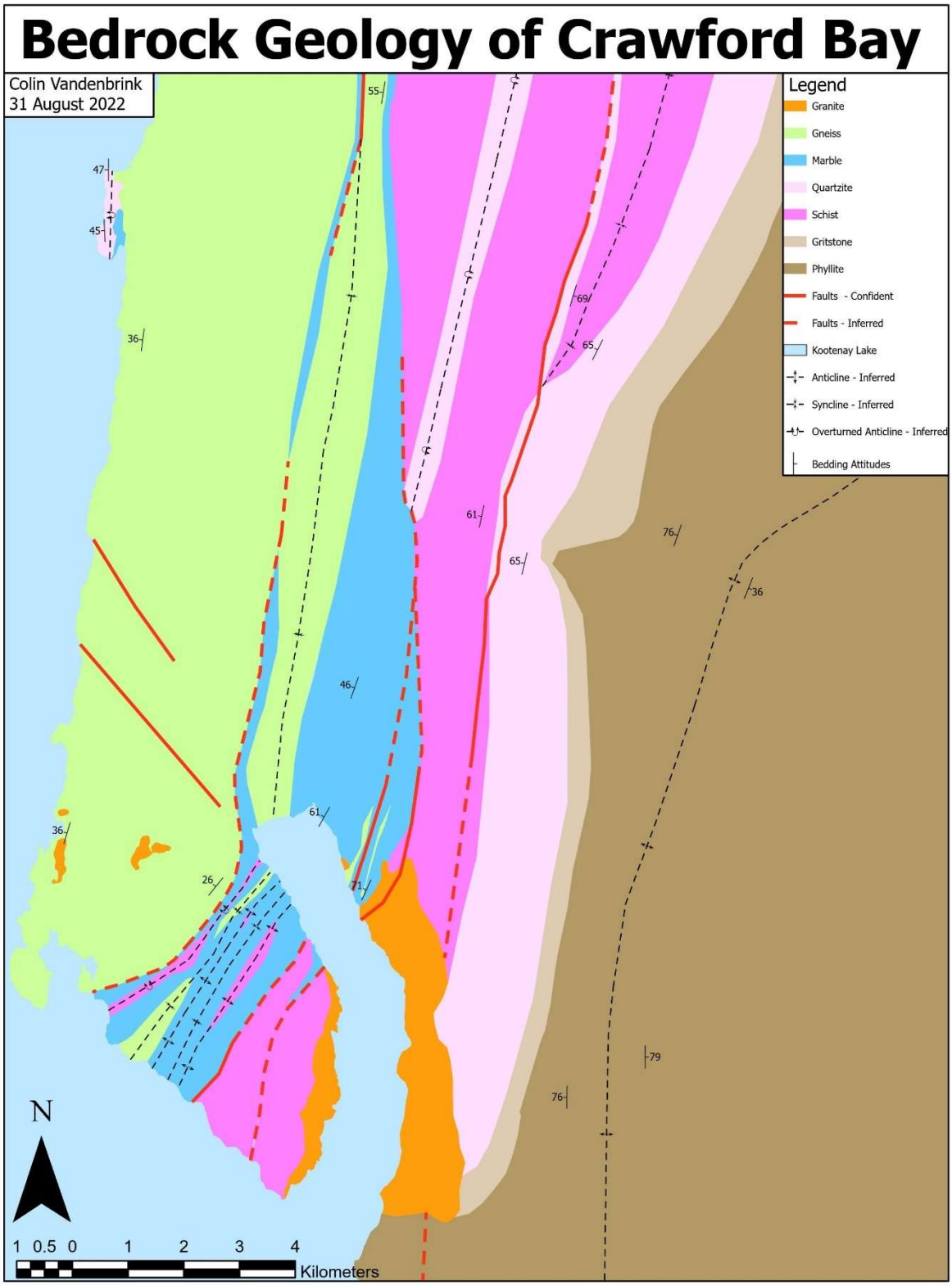

Figure 64 - Map of the interpreted bedrock geology within the study area.

Water Chemistry Mapping

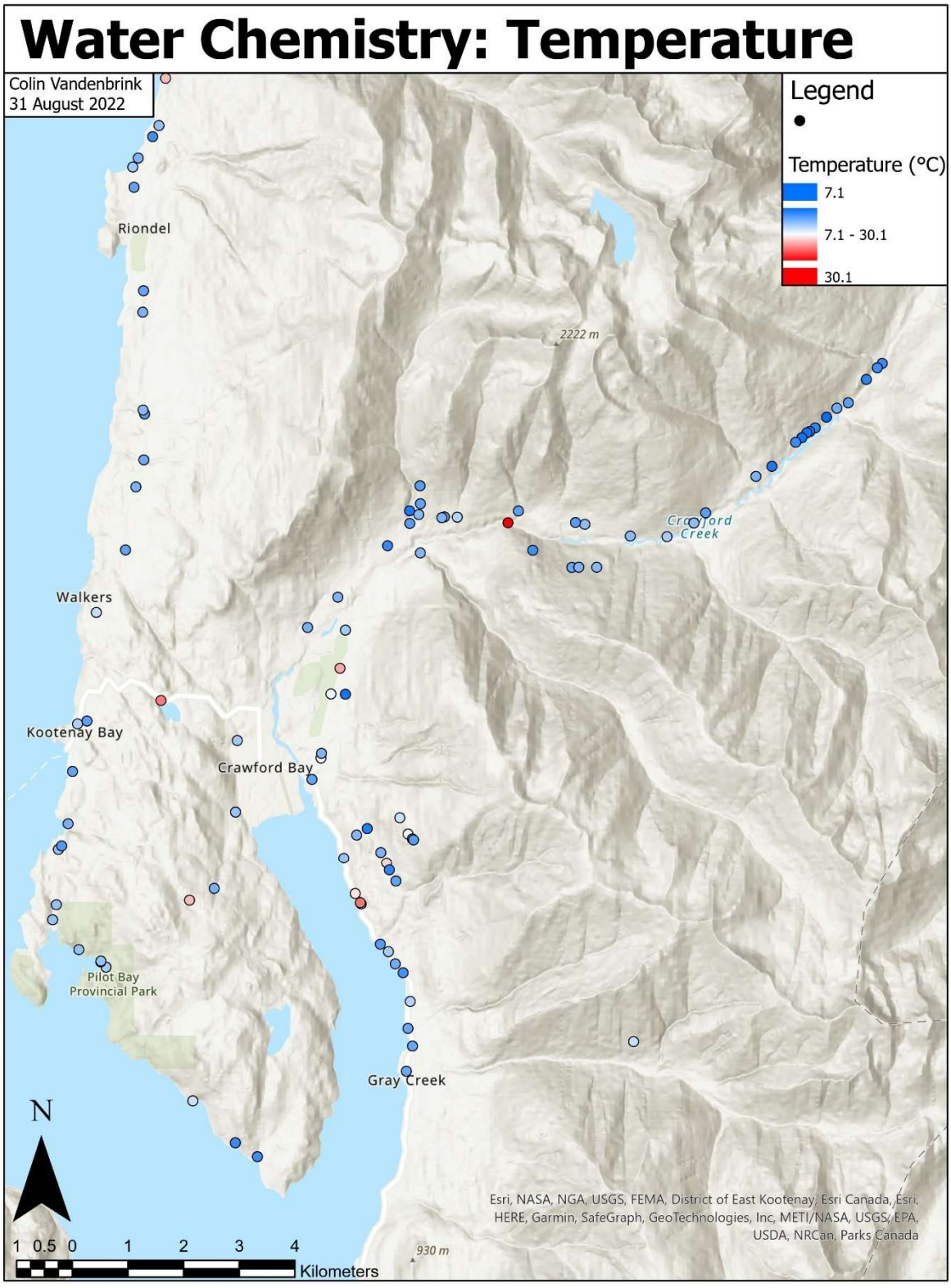

Figure 65 - Water chemistry sample points symbolized according to temperature (blue = lower, red = higher).

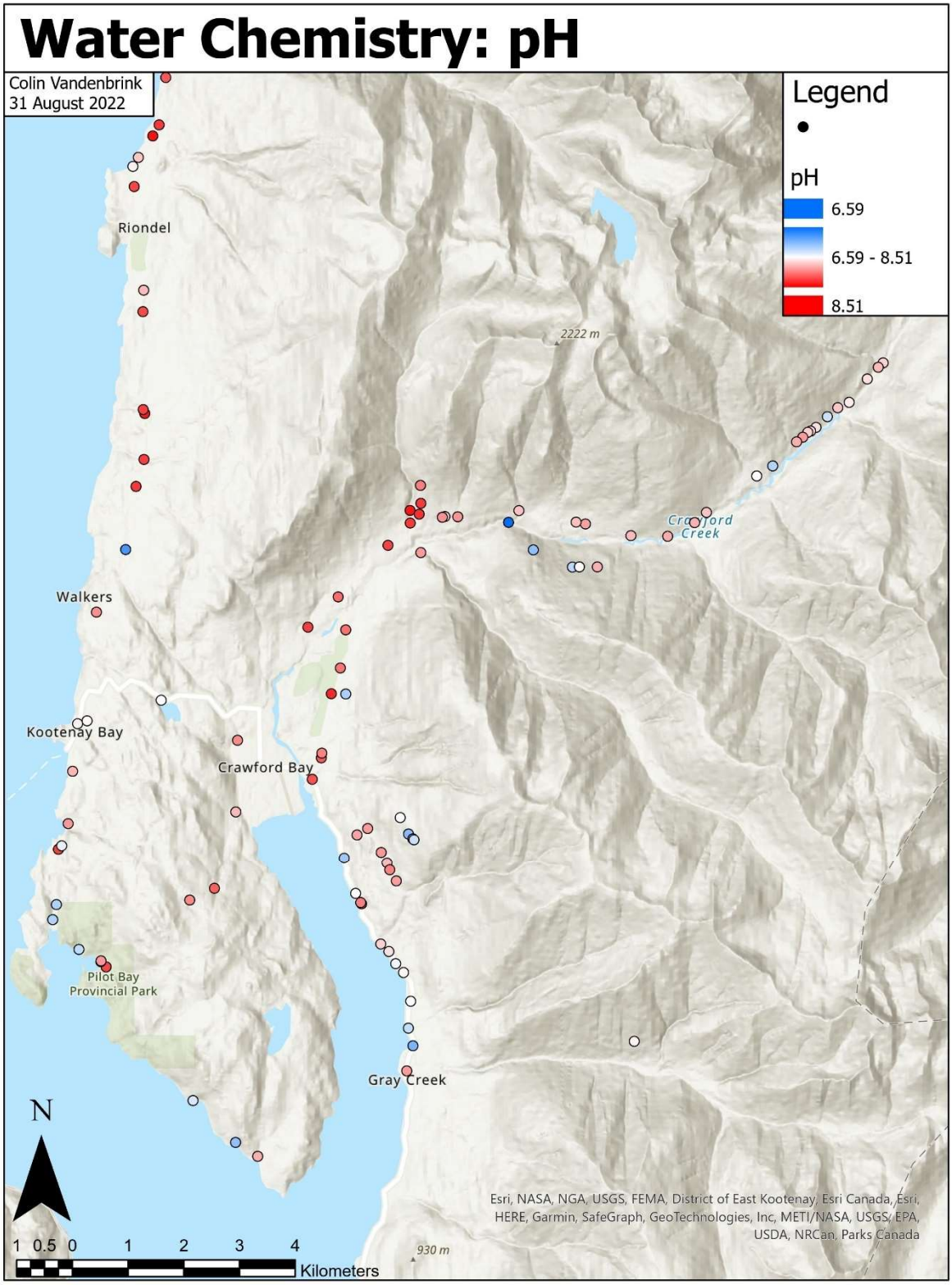

Figure 66 - Water chemistry sample points symbolized according to pH (blue = lower, red = higher).

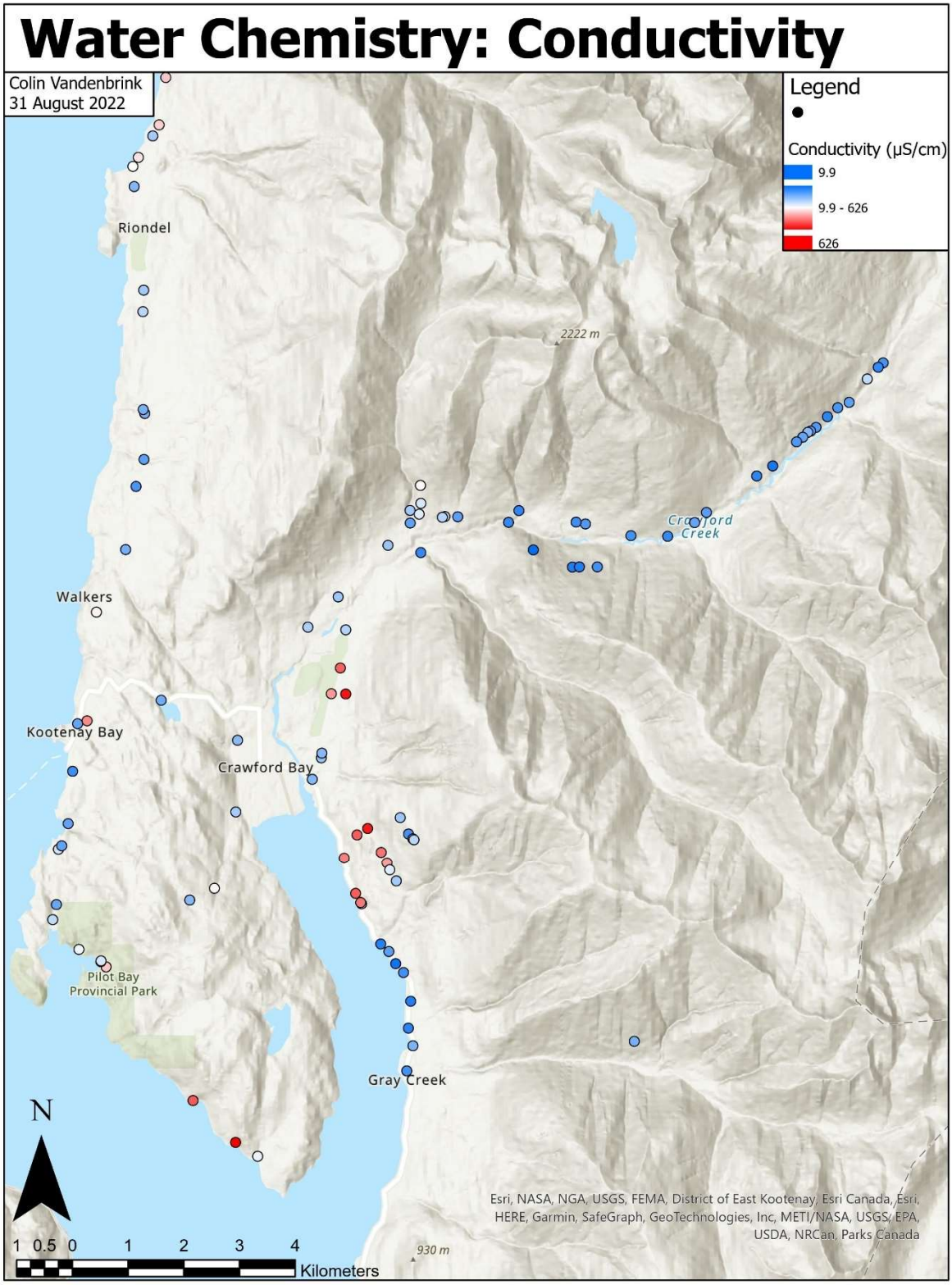

Figure 67 - Water chemistry sample points symbolized according to conductivity (blue = lower, red = higher).

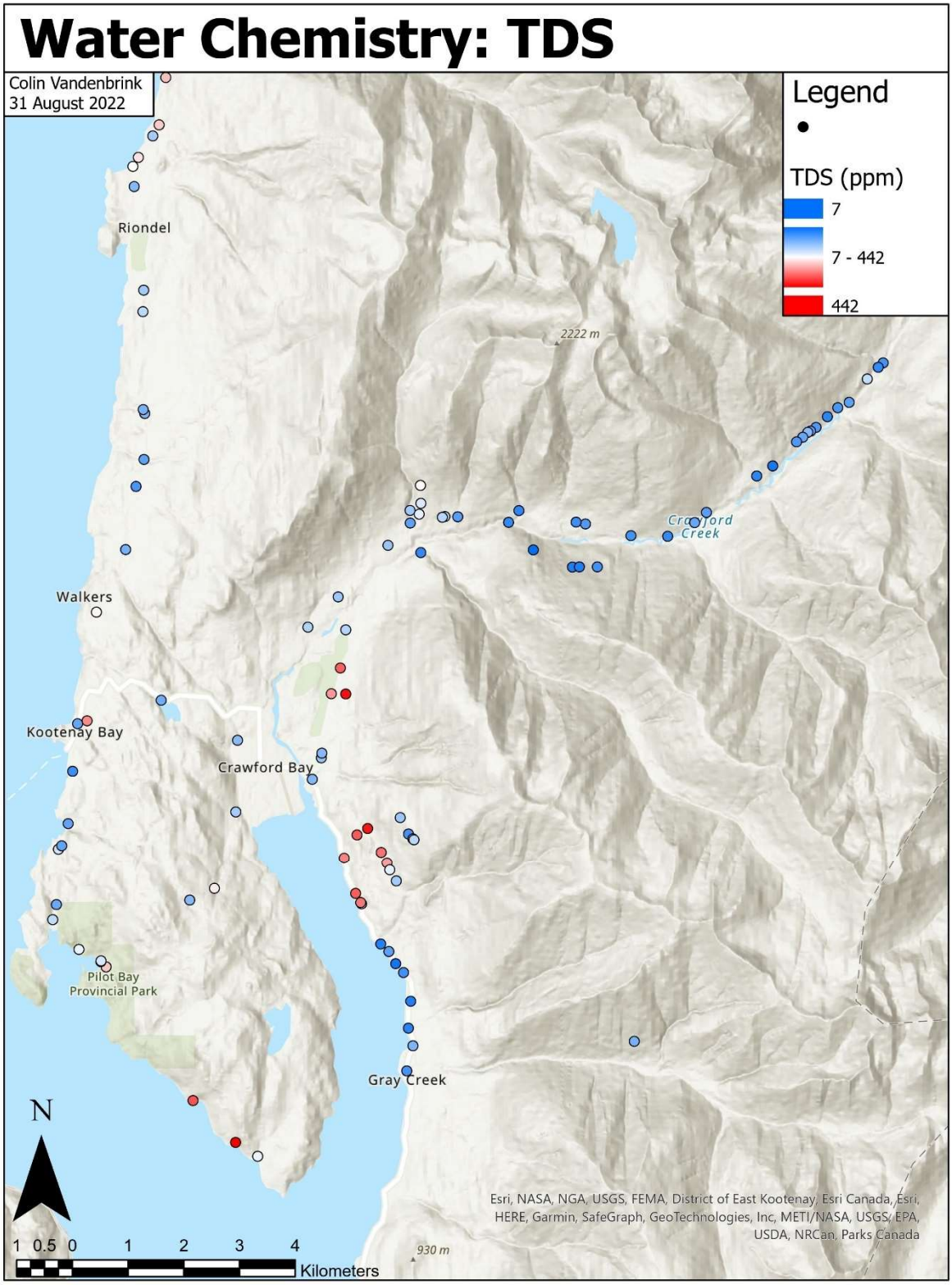

Figure 68 - Water chemistry sample points symbolized according to total dissolved solids (blue = lower, red = higher).

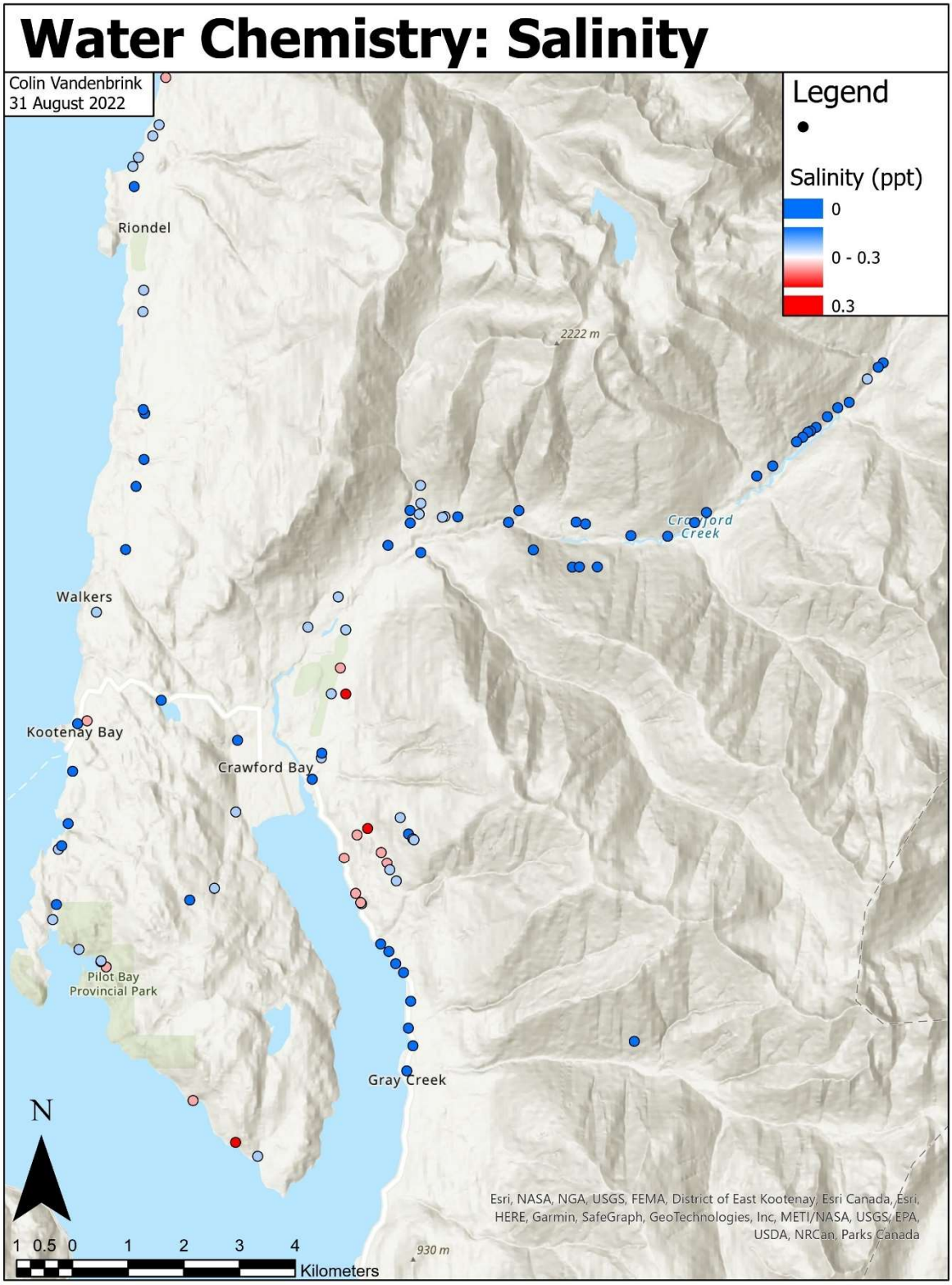

Figure 69 - Water chemistry sample points symbolized according to salinity (blue = lower, red = higher).

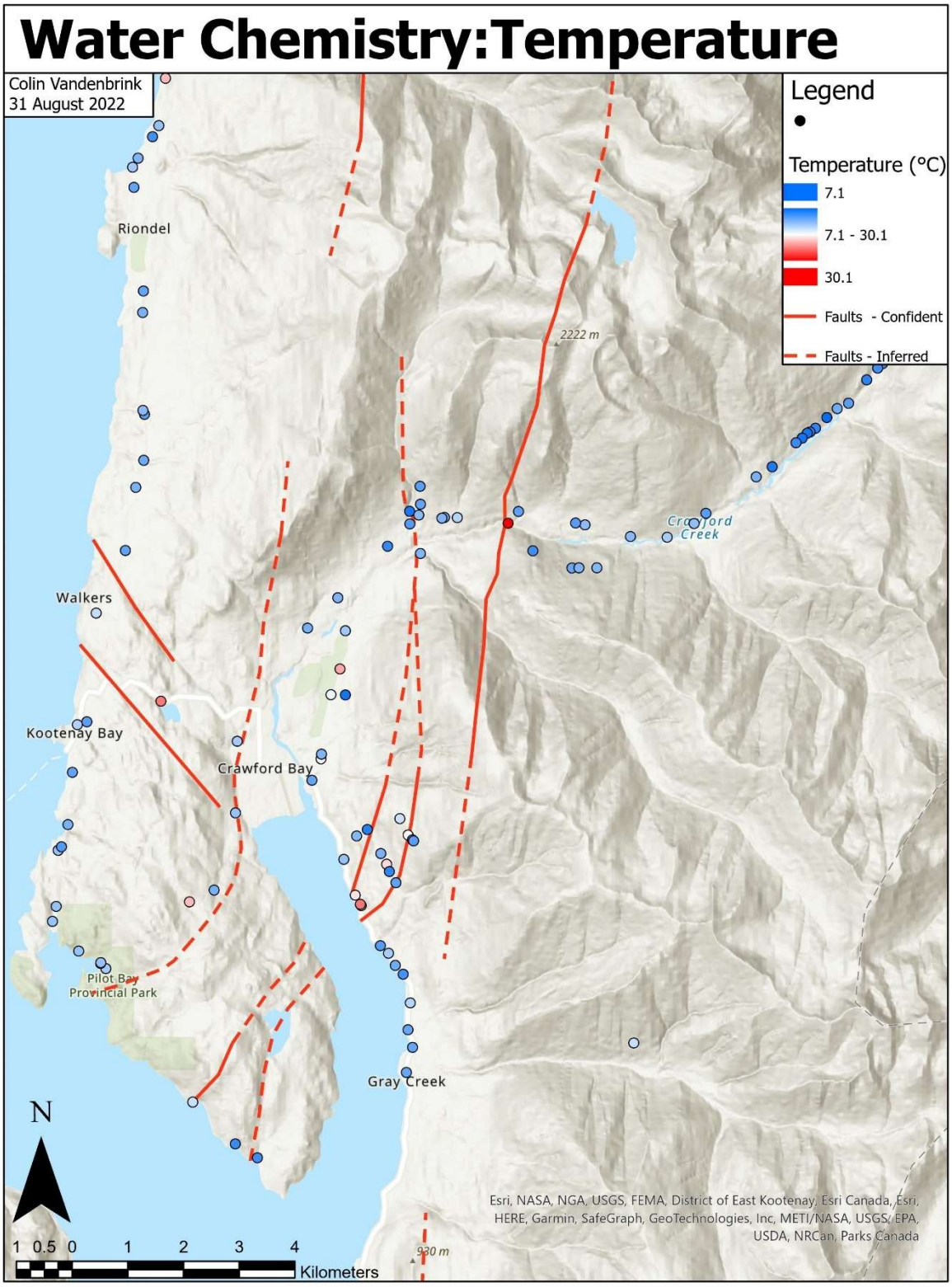

Figure 70 - Water chemistry sample points symbolized according to temperature (blue = lower, red = higher), compared to assumed major fault locations.

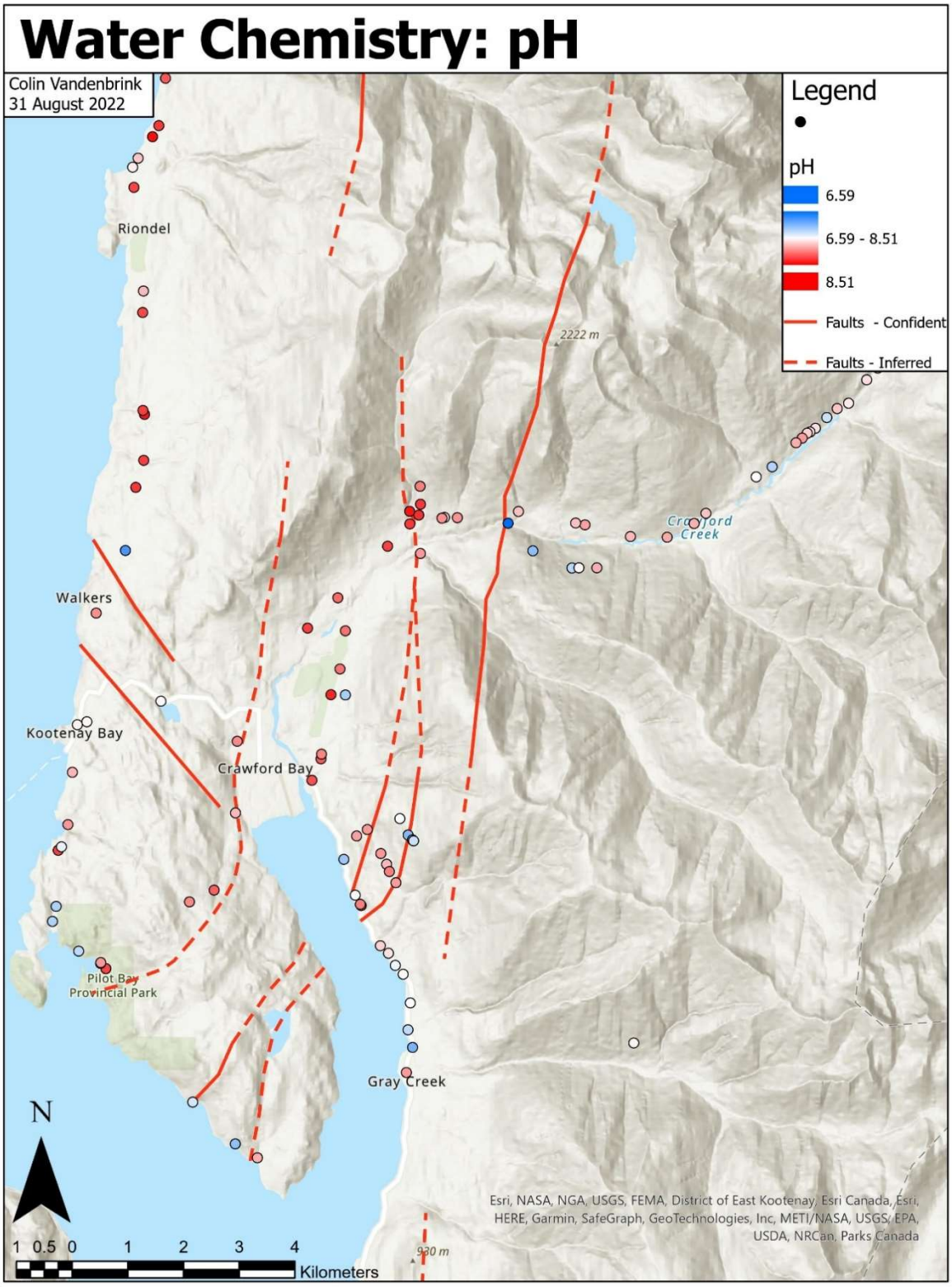

Figure 71 - Water chemistry sample points symbolized according to pH (blue = lower, red = higher), compared to assumed major fault locations.

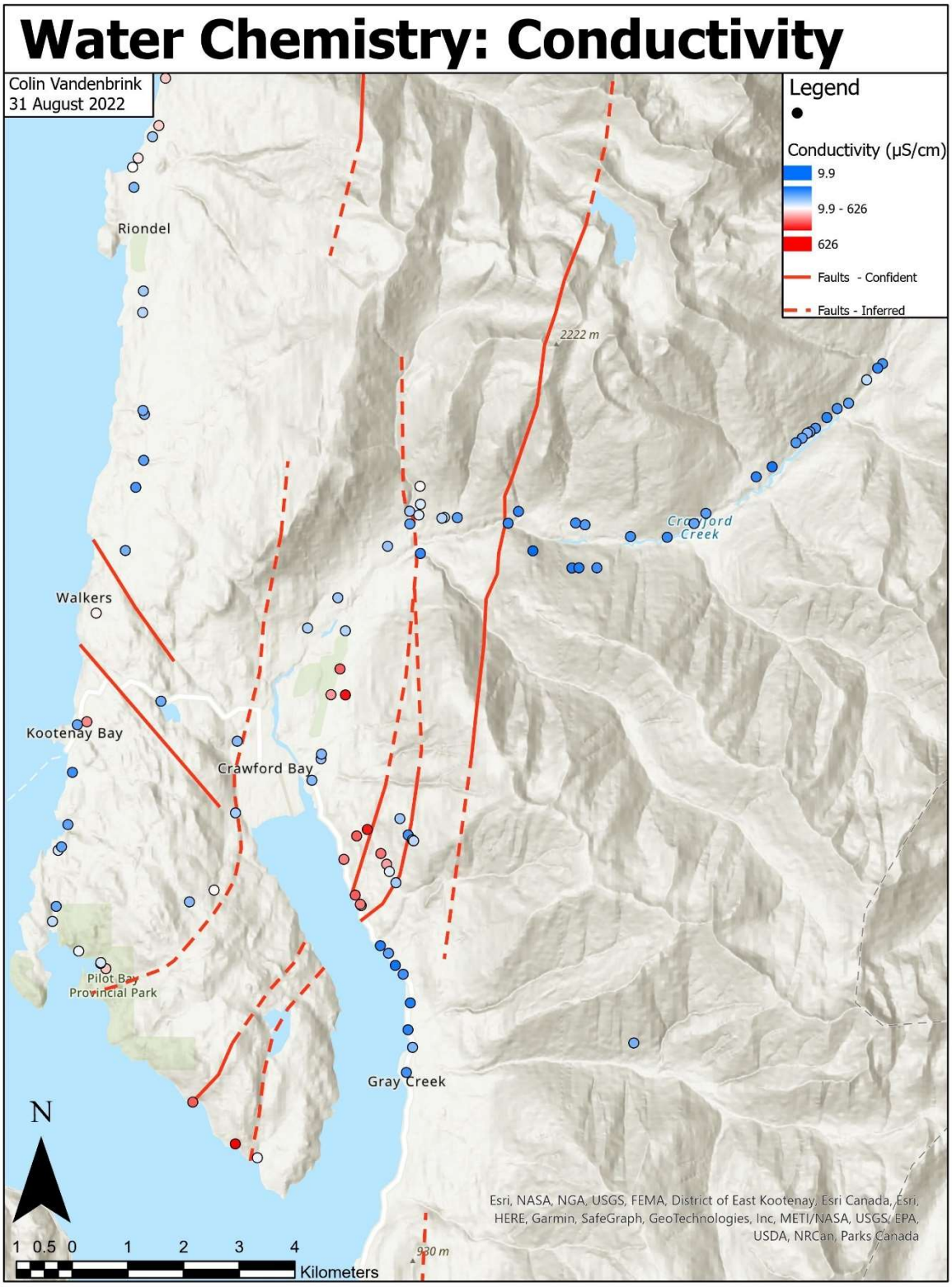

Figure 72 - Water chemistry sample points symbolized according to conductivity (blue = lower, red = higher), compared to assumed major fault locations.

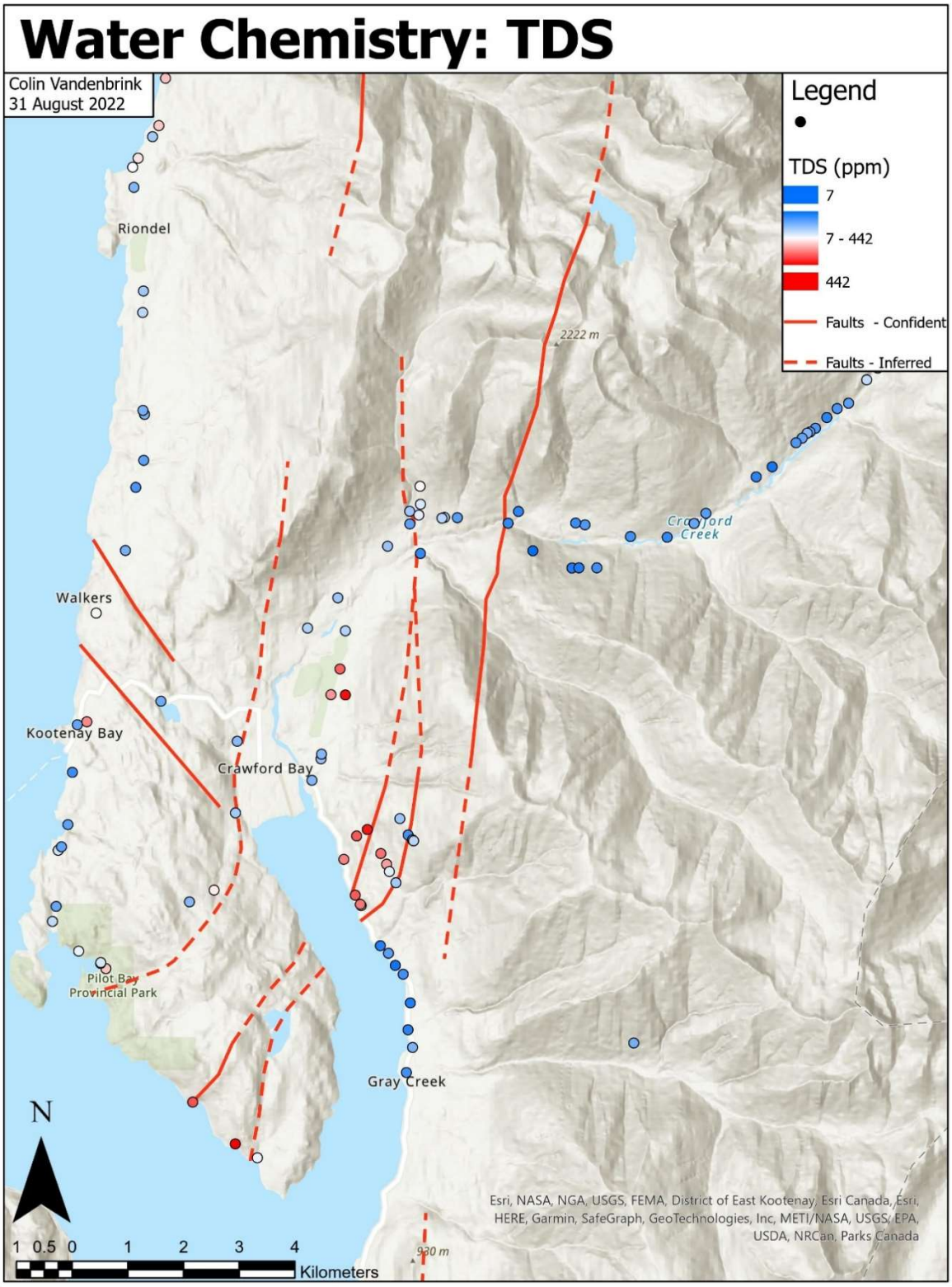

Figure 73 - Water chemistry sample points symbolized according to total dissolved solids (blue = lower, red = higher), compared to assumed major fault locations.

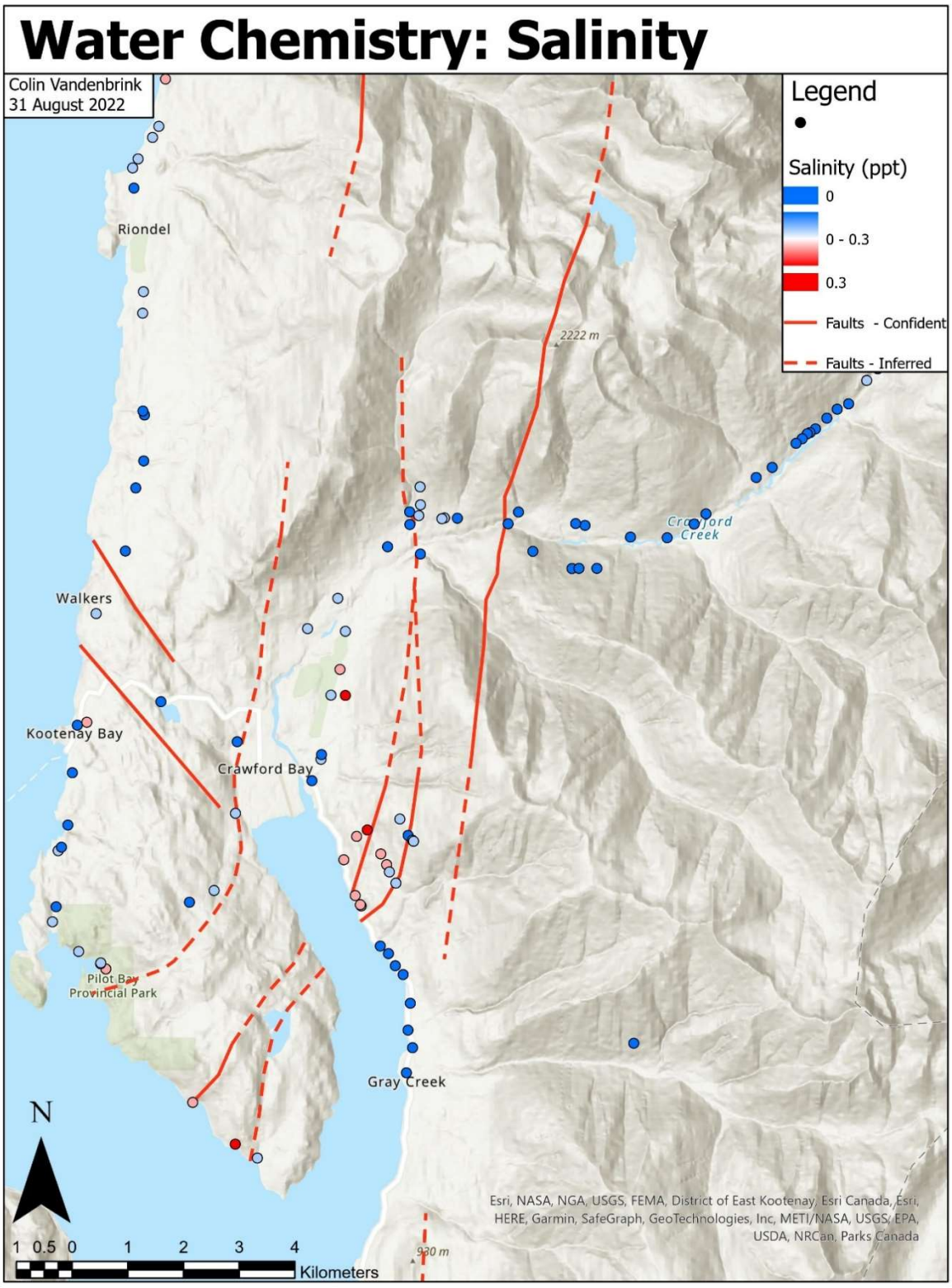

Figure 74 - Water chemistry sample points symbolized according to salinity (blue = lower, red = higher), compared to assumed major fault locations.

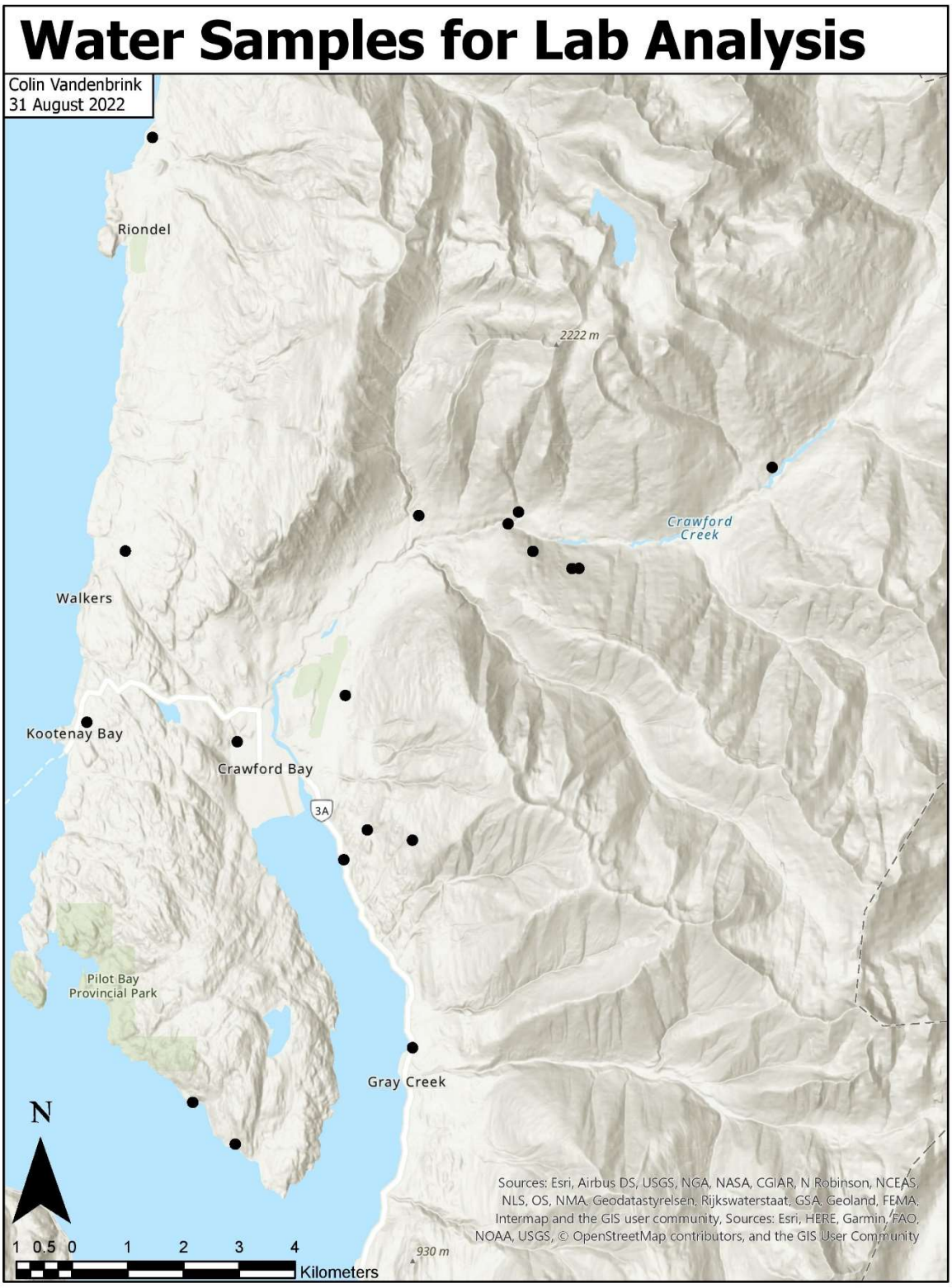

Figure 75 – Map showing the locations of samples that were sent for further lab analysis.

Appendix B: Stereoplots

Full-size versions of all stereoplots used in the report above (Figures 76 – 215)

Plots by Rock Type

Gneiss

Bedding

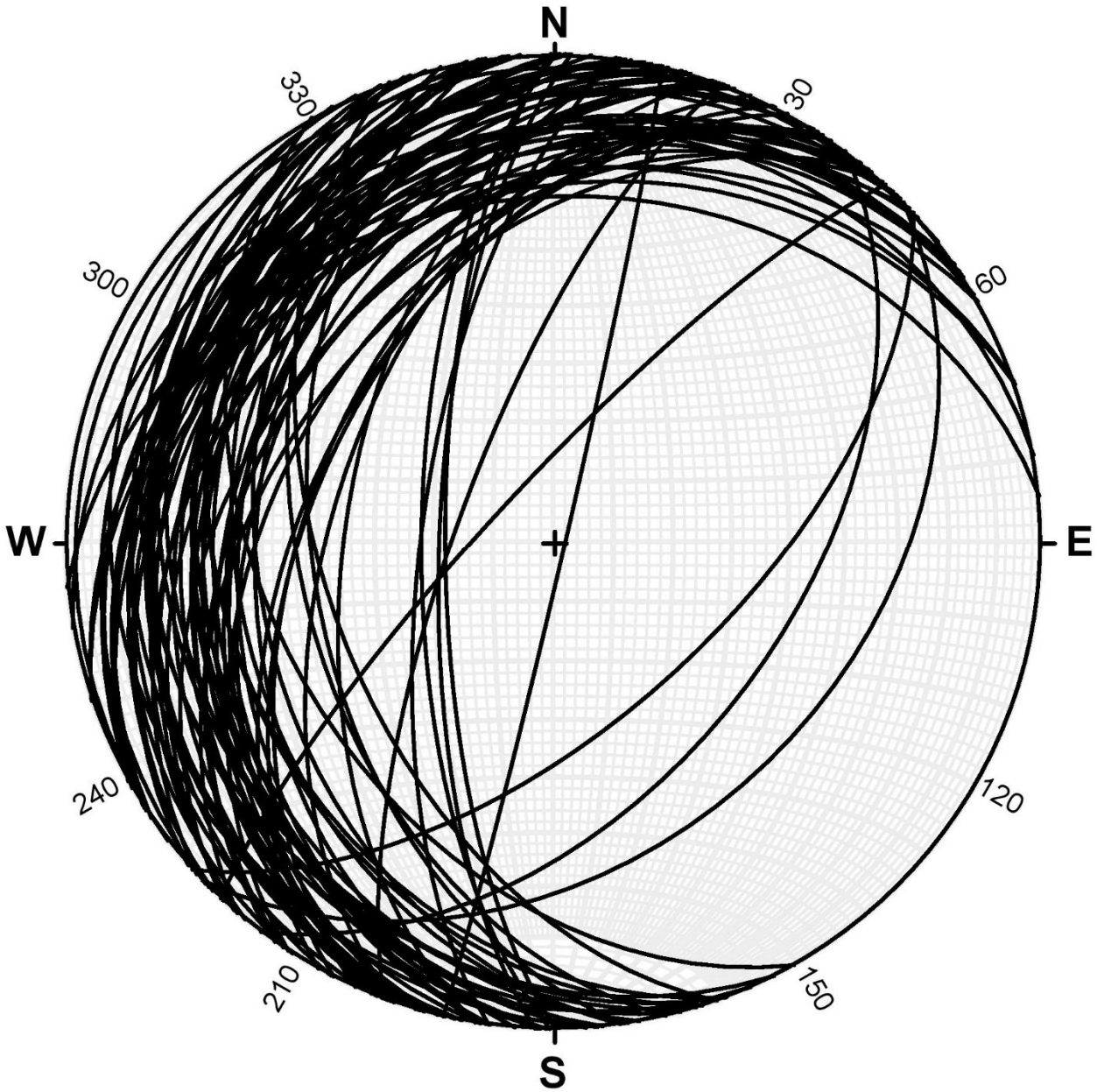

Figure 76 - Bedding planes for gneiss. N = 78.

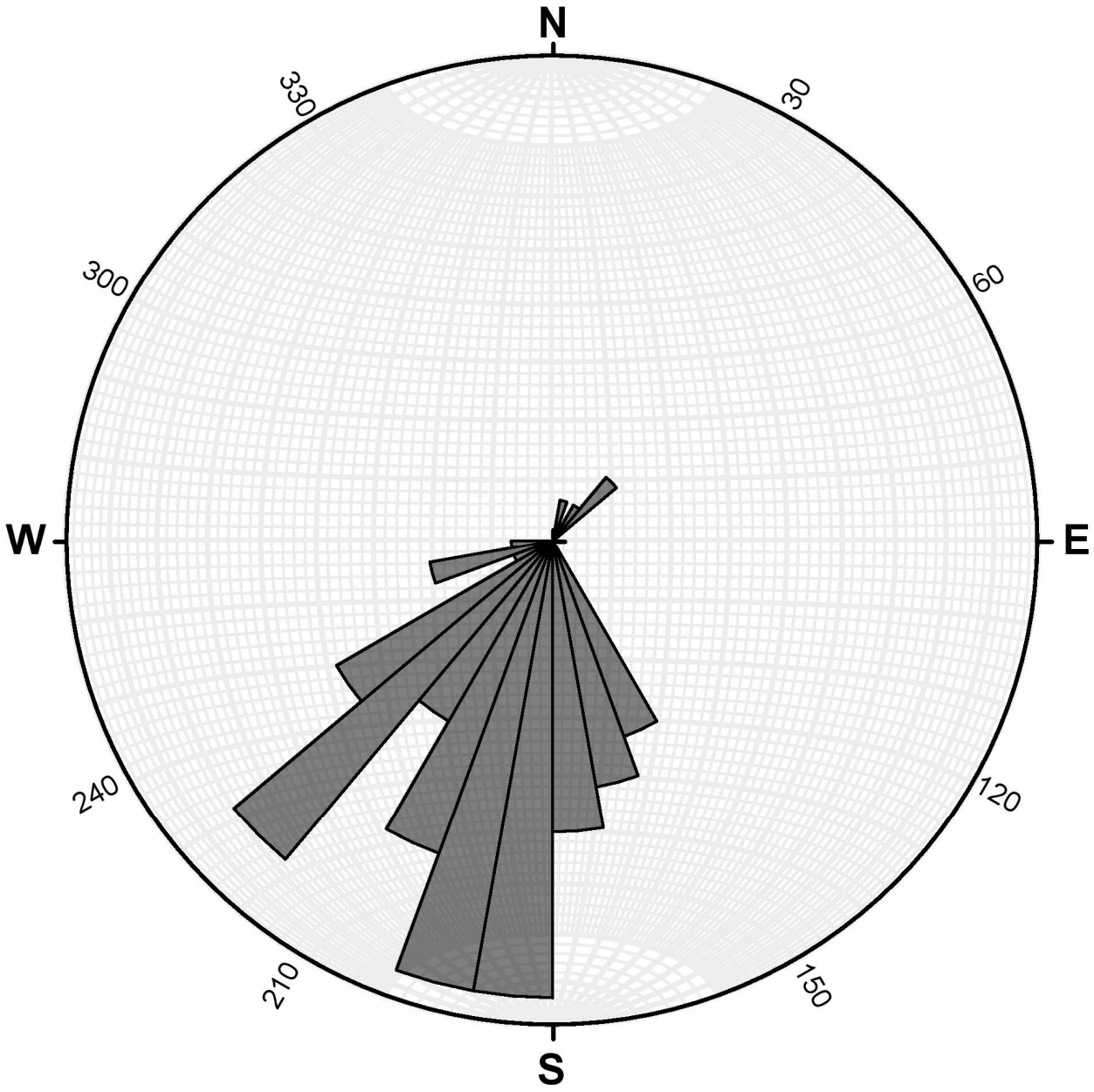

Figure 77 - Rose diagram of bedding planes for gneiss. N = 78.

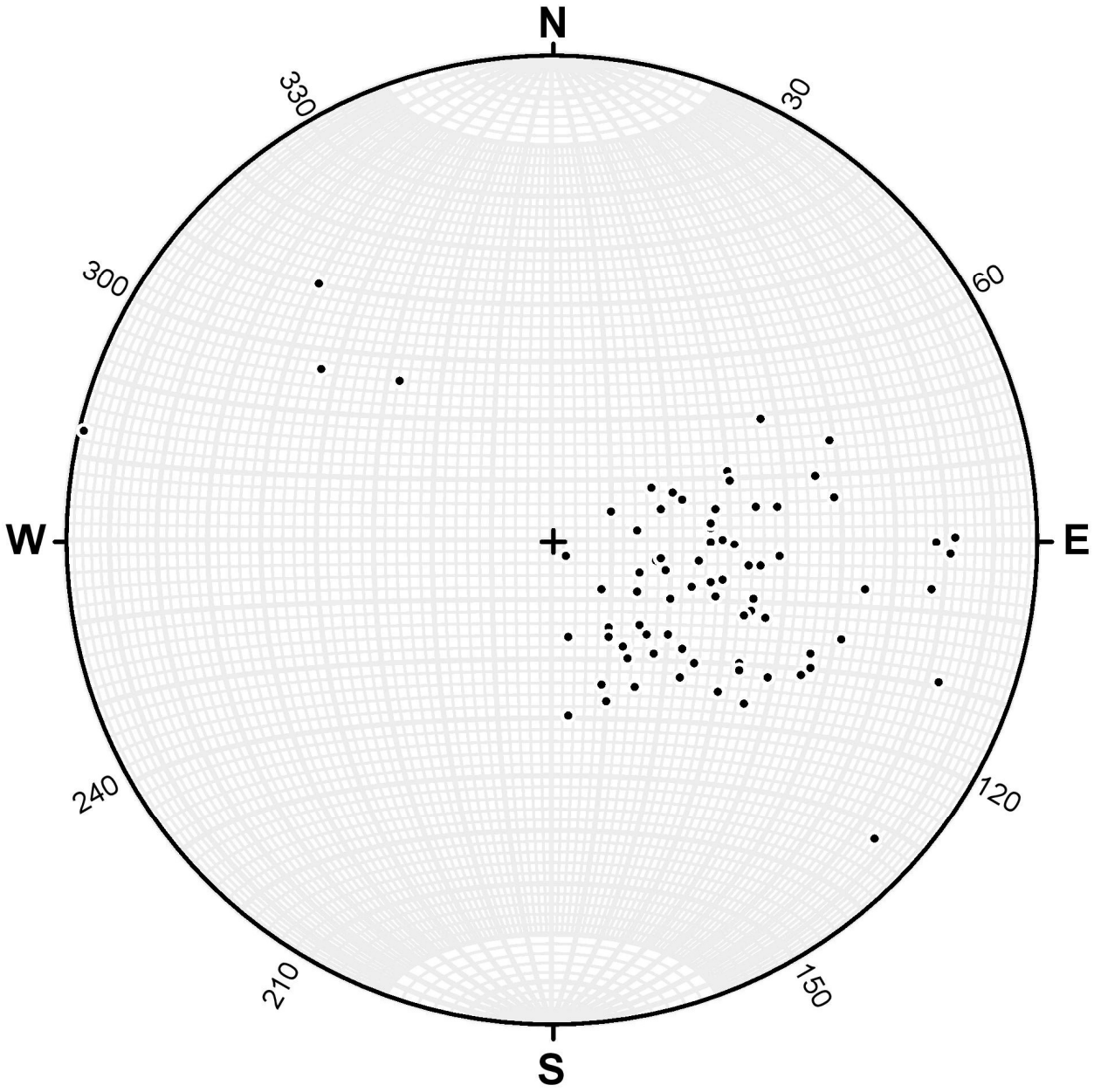

Figure 78 - Bedding poles for gneiss. N = 78.

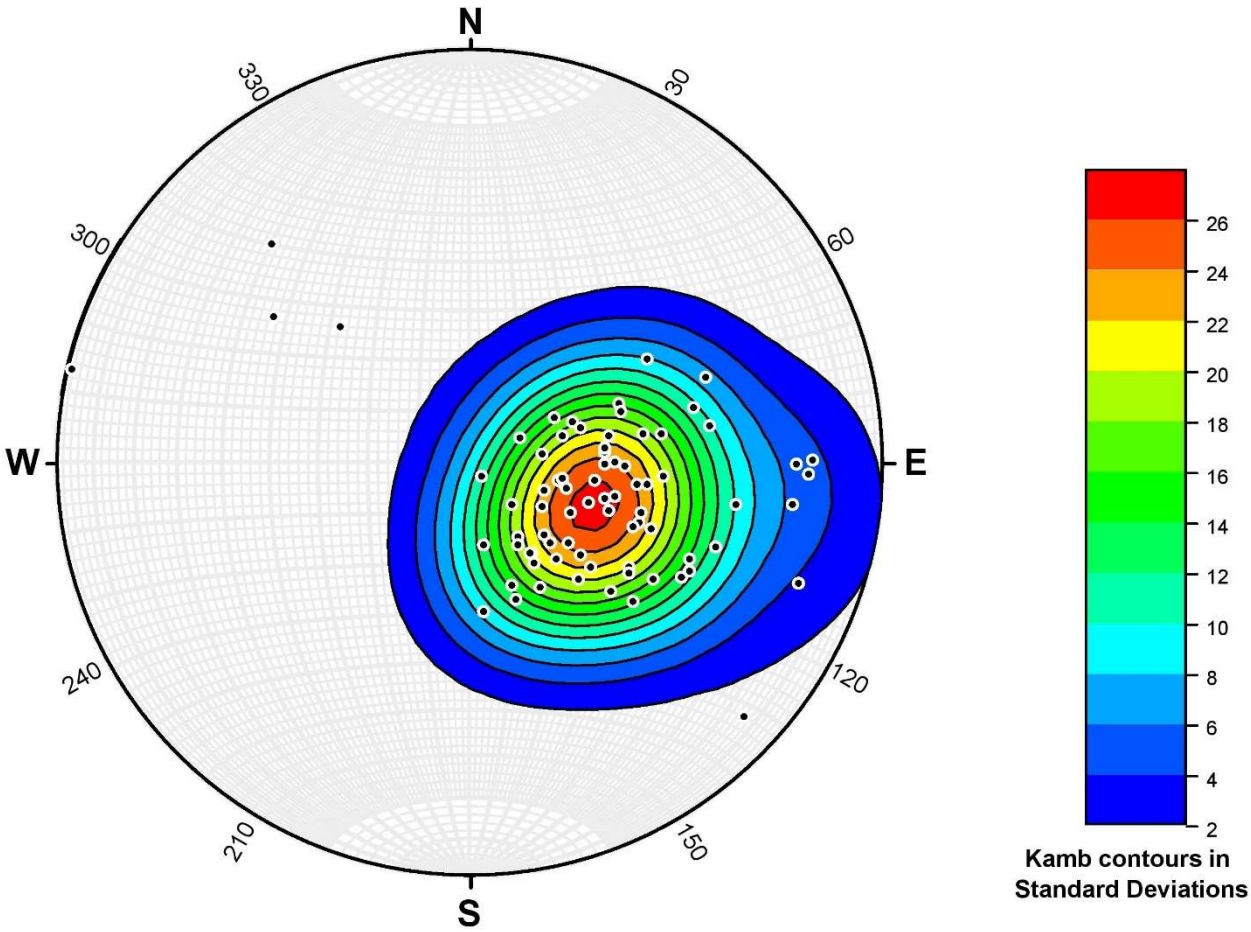

Figure 79 - Kamb contouring of bedding poles for gneiss. N = 78.

Jointing

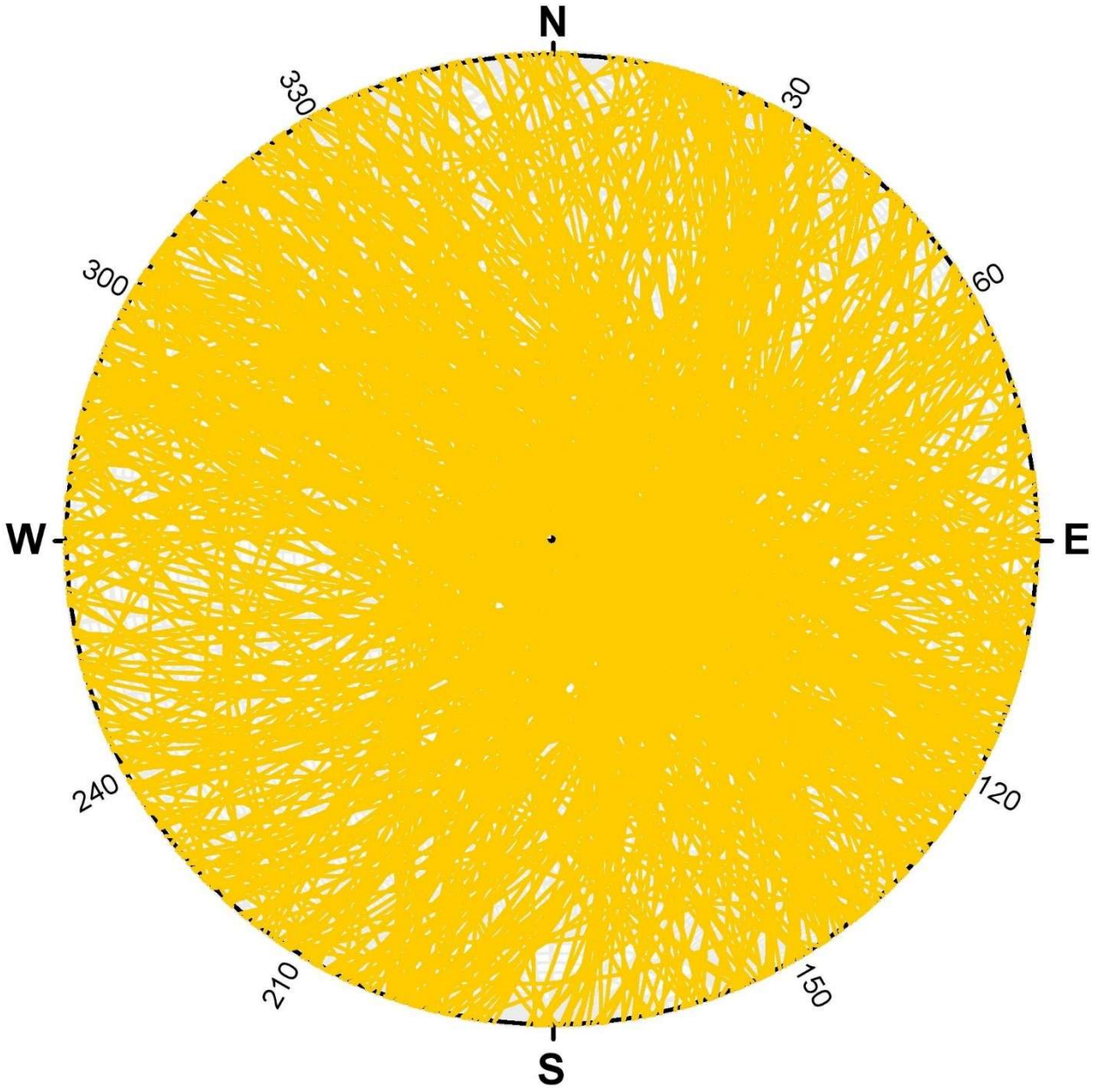

Figure 80 - Joint planes for gneiss. N = 495.

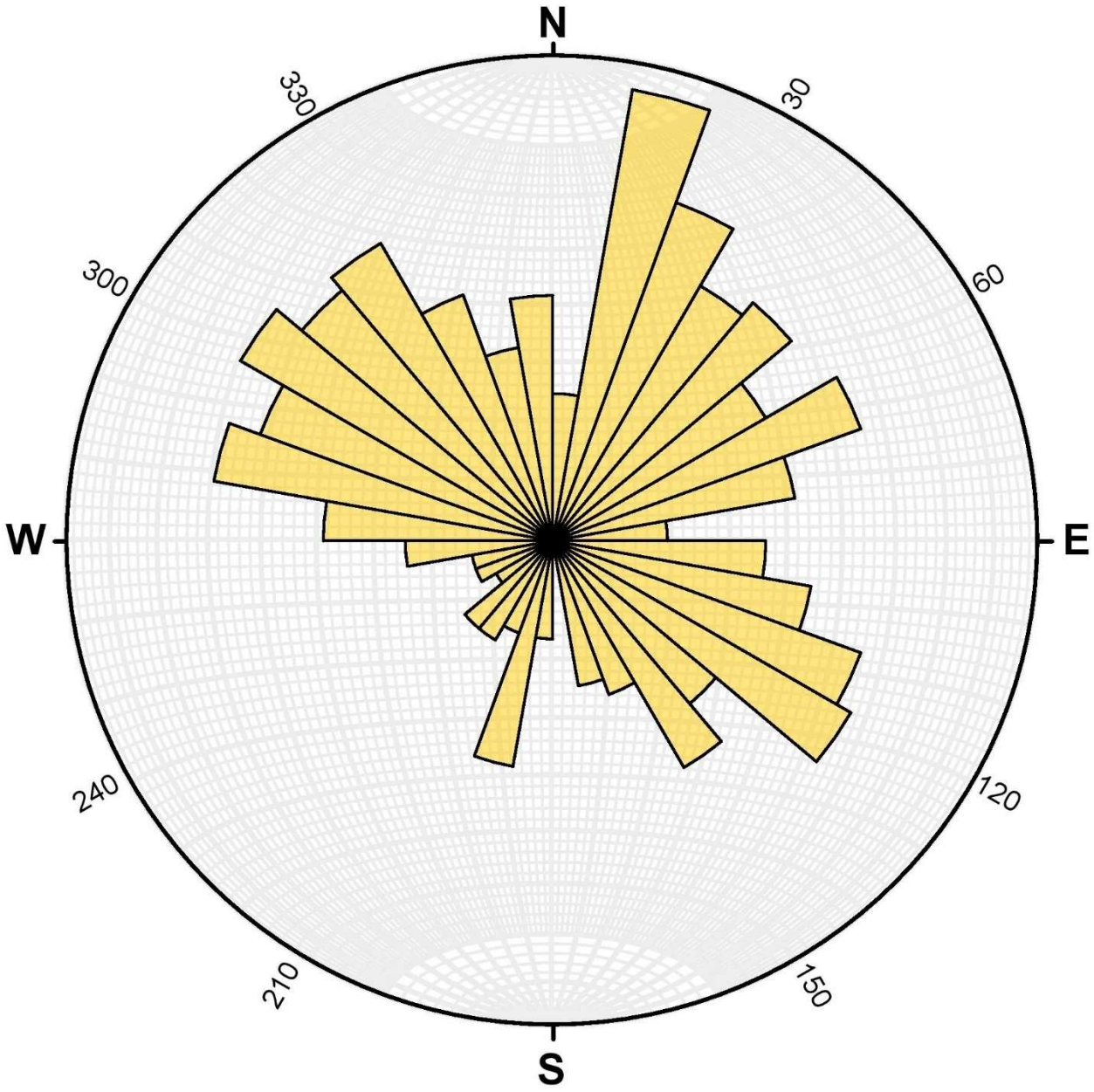

Figure 81 - Rose diagram of joint planes for gneiss. N = 495.

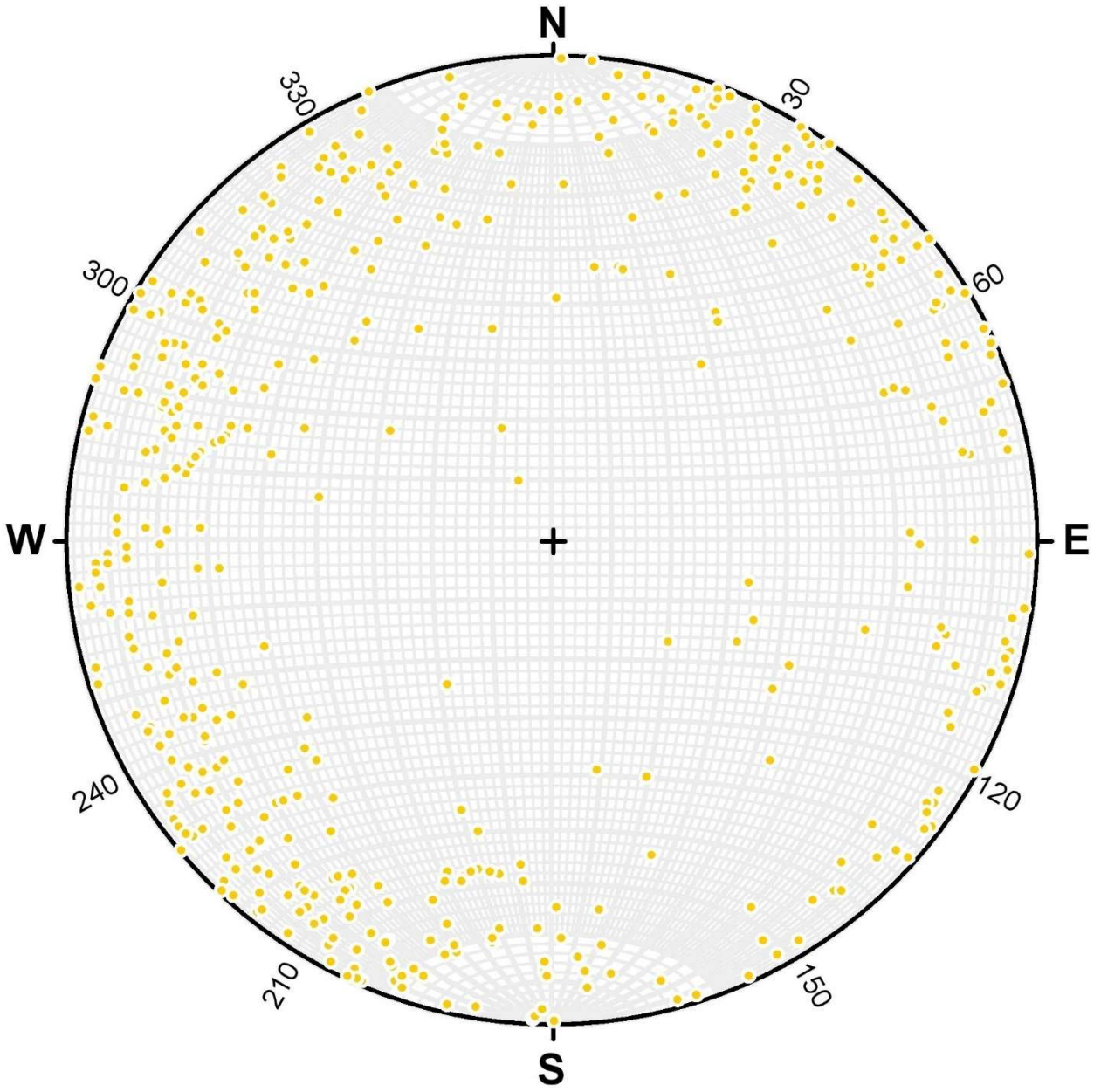

Figure 82 - Joint poles for gneiss. N = 495.

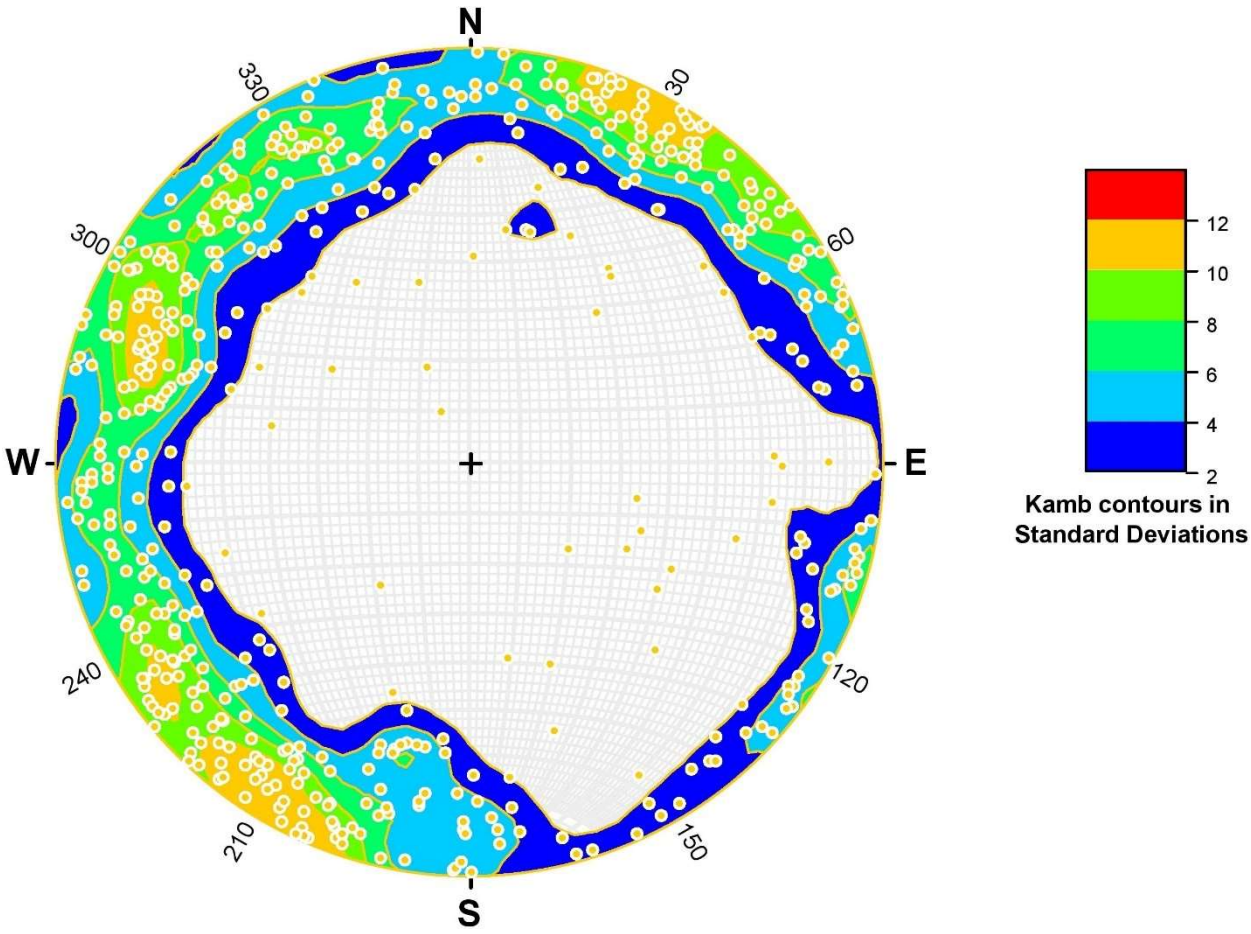

Figure 83 - Kamb contouring of joint poles for gneiss. N = 495.

Granite

Jointing

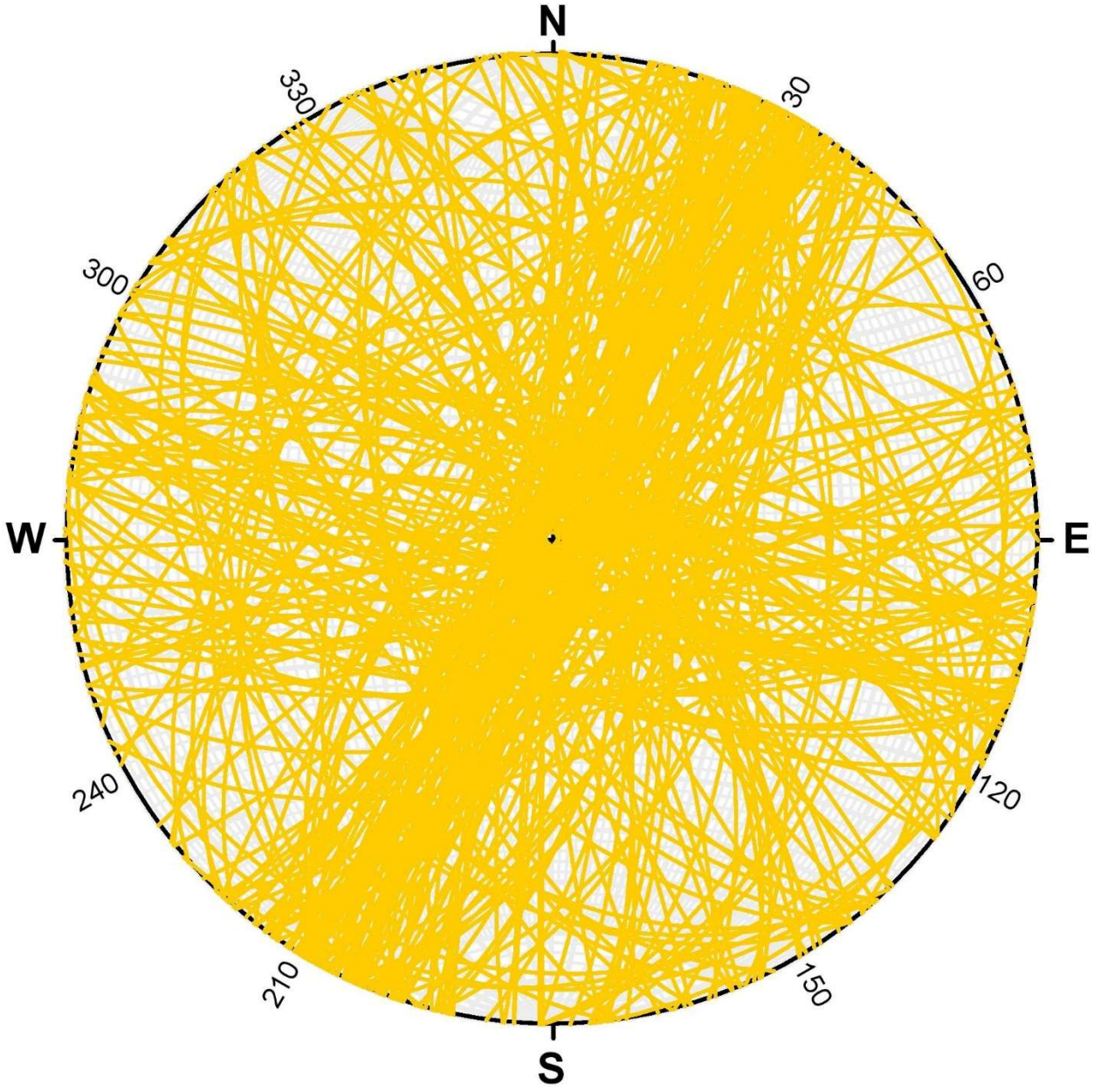

Figure 84 - Joint planes for granite. N = 251.

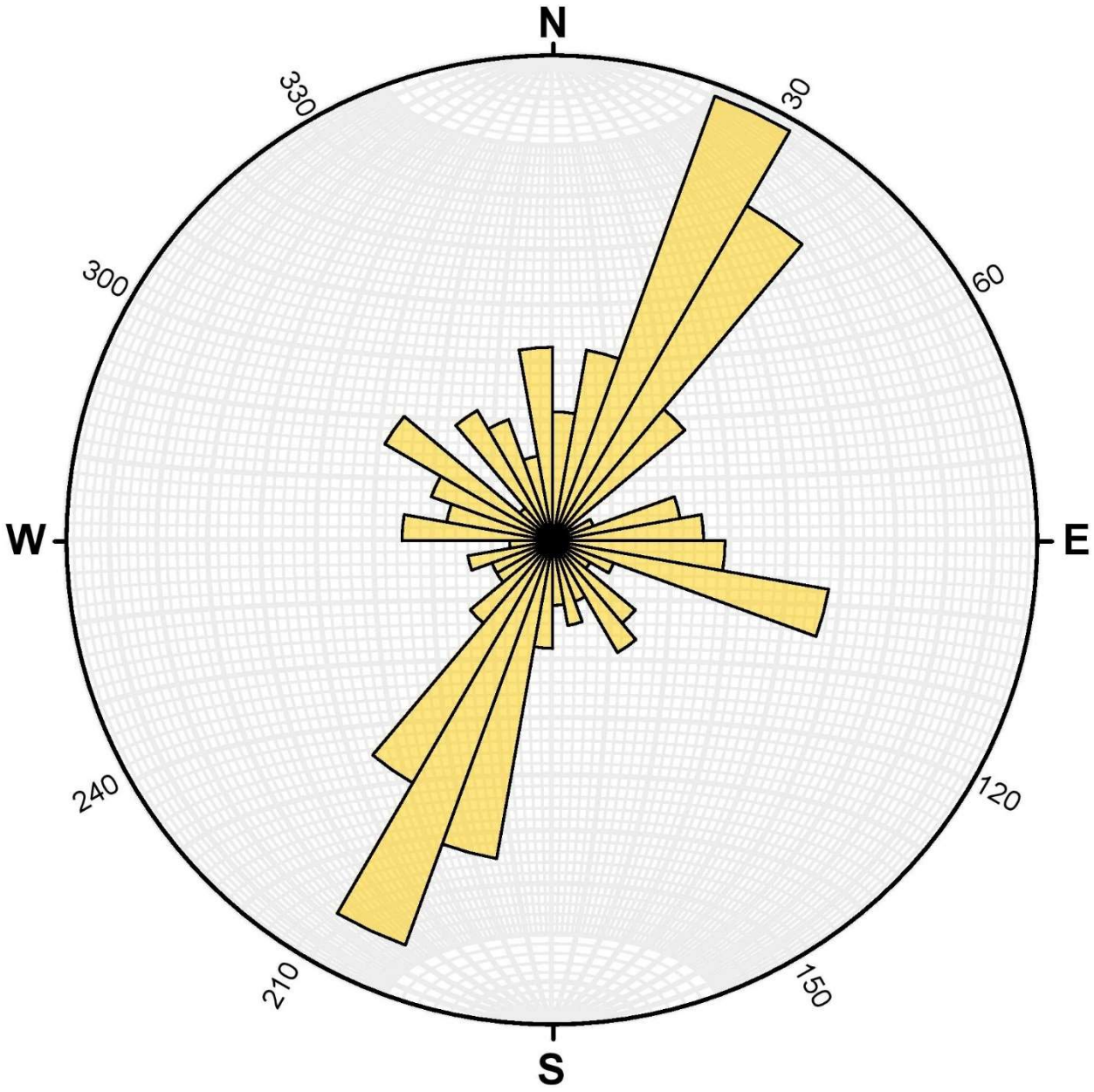

Figure 85 - Rose diagram of joint planes for granite. N = 251.

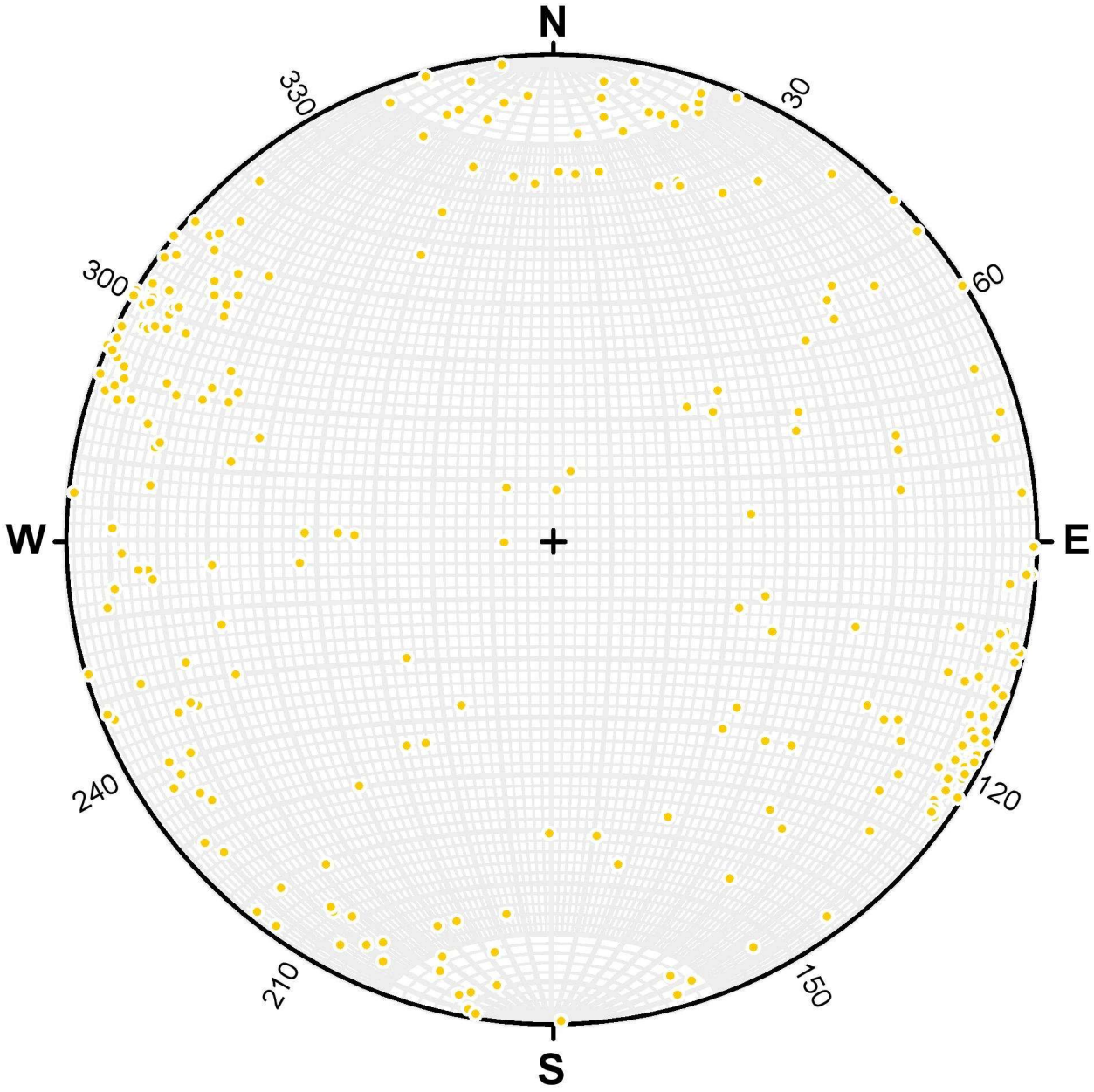

Figure 86 - Joint poles for granite. N = 251.

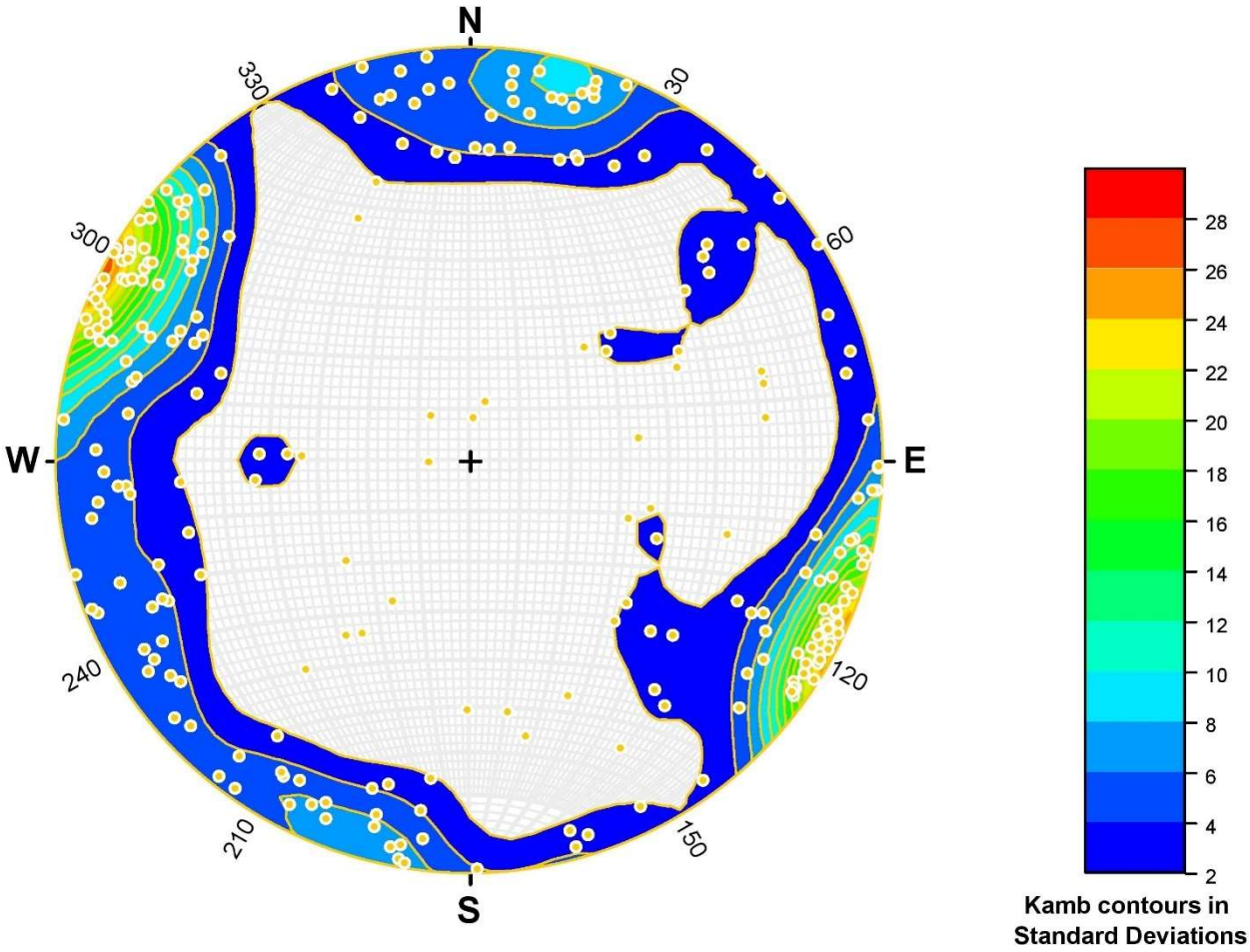

Figure 87 - Kamb contouring of joint poles for granite. N = 251.

Gritstone

Bedding

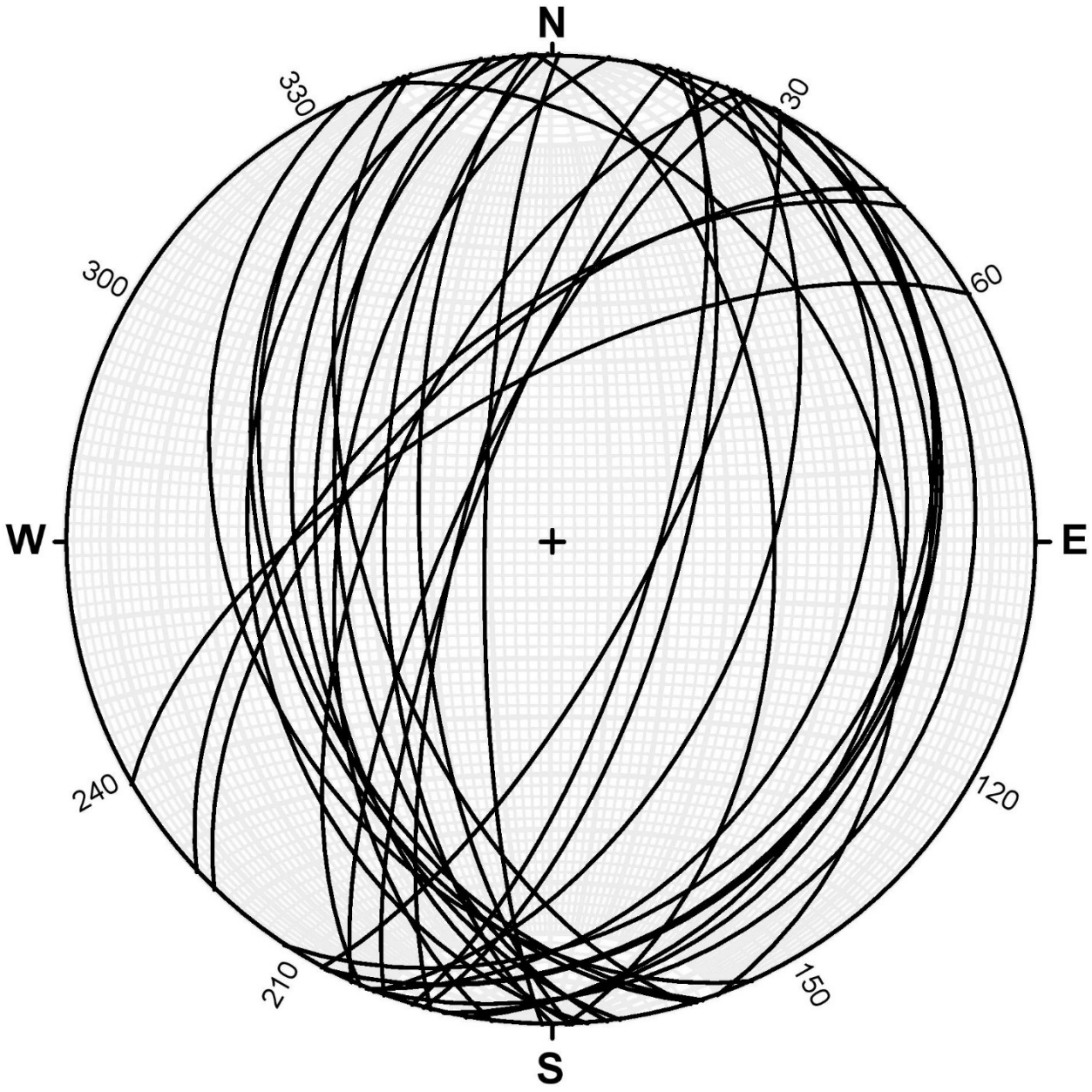

Figure 88 - Bedding planes for gritstone. N = 32.

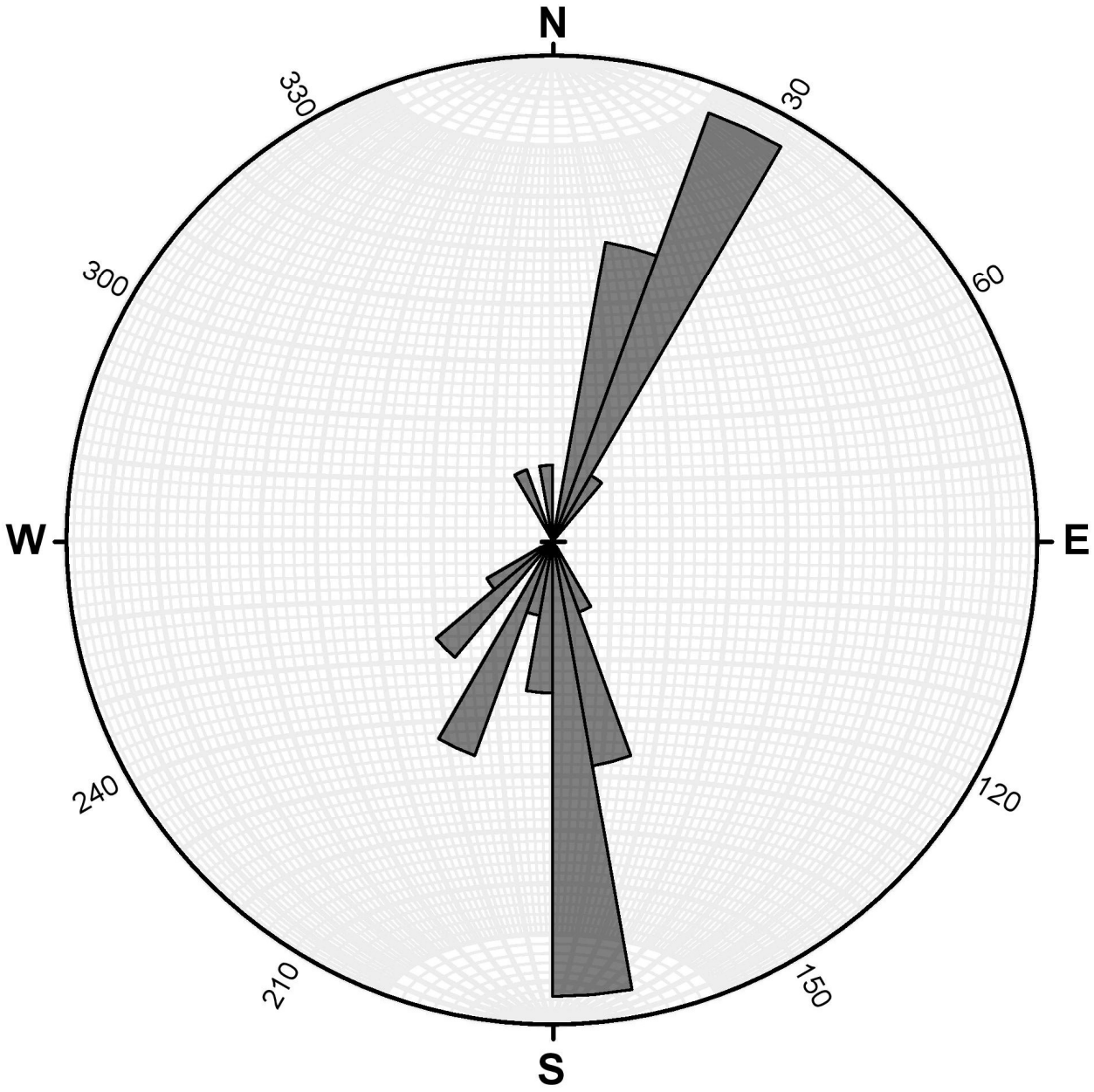

Figure 89 - Rose diagram of bedding planes for gritstone. N = 32.

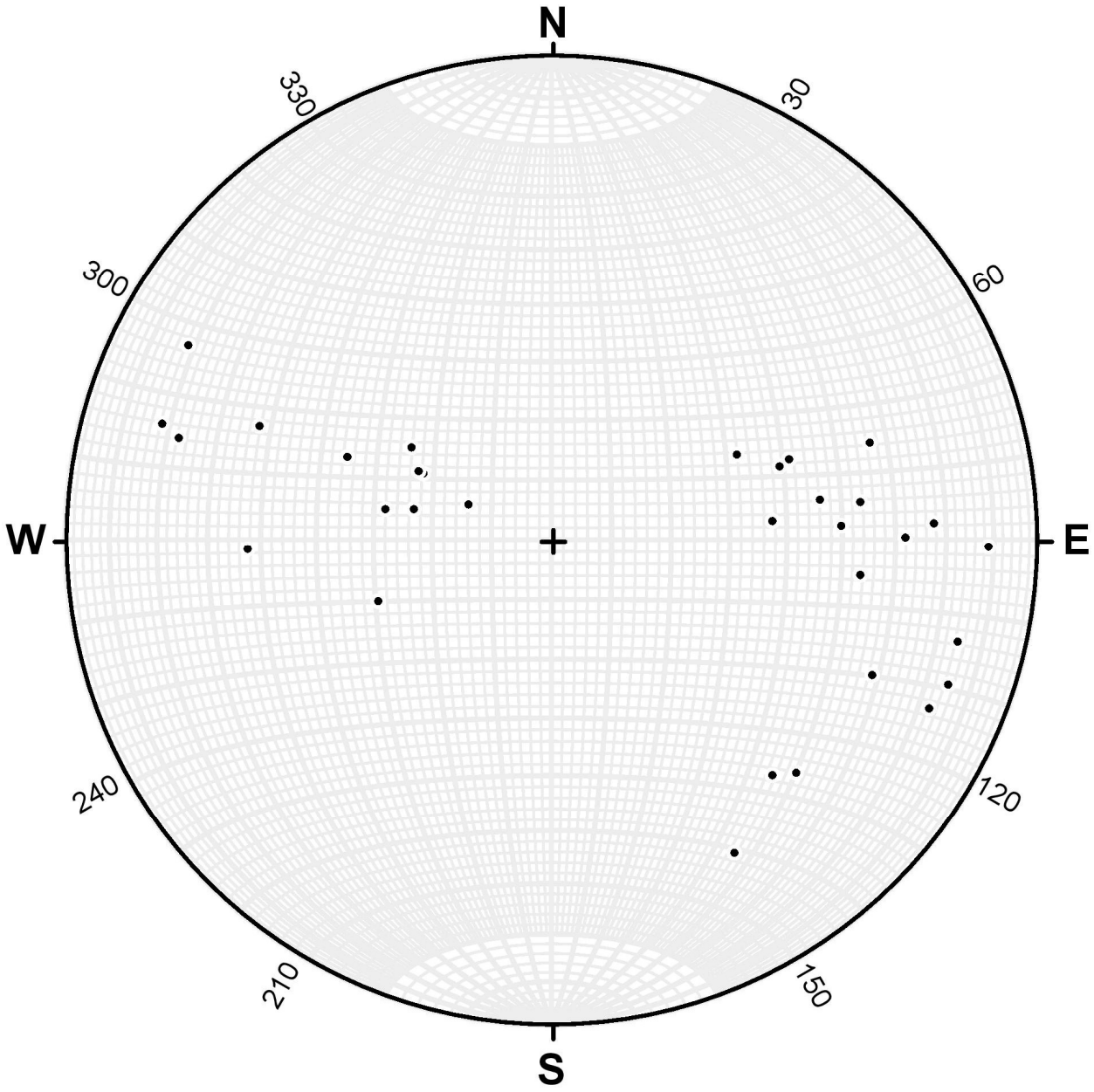

Figure 90 - Bedding poles for gritstone. N = 32.

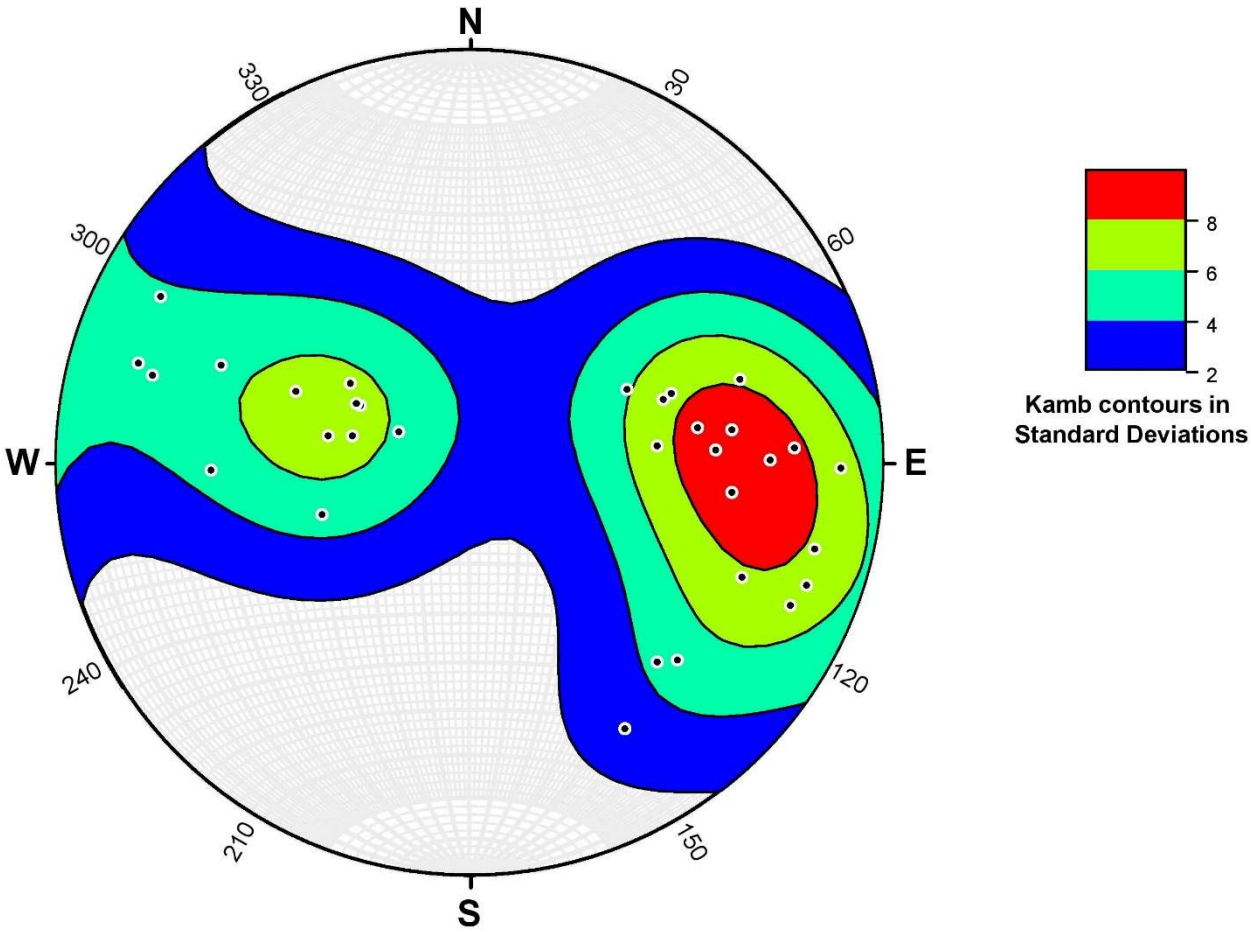

Figure 91 - Kamb contouring of bedding poles for gritstone. N = 32.

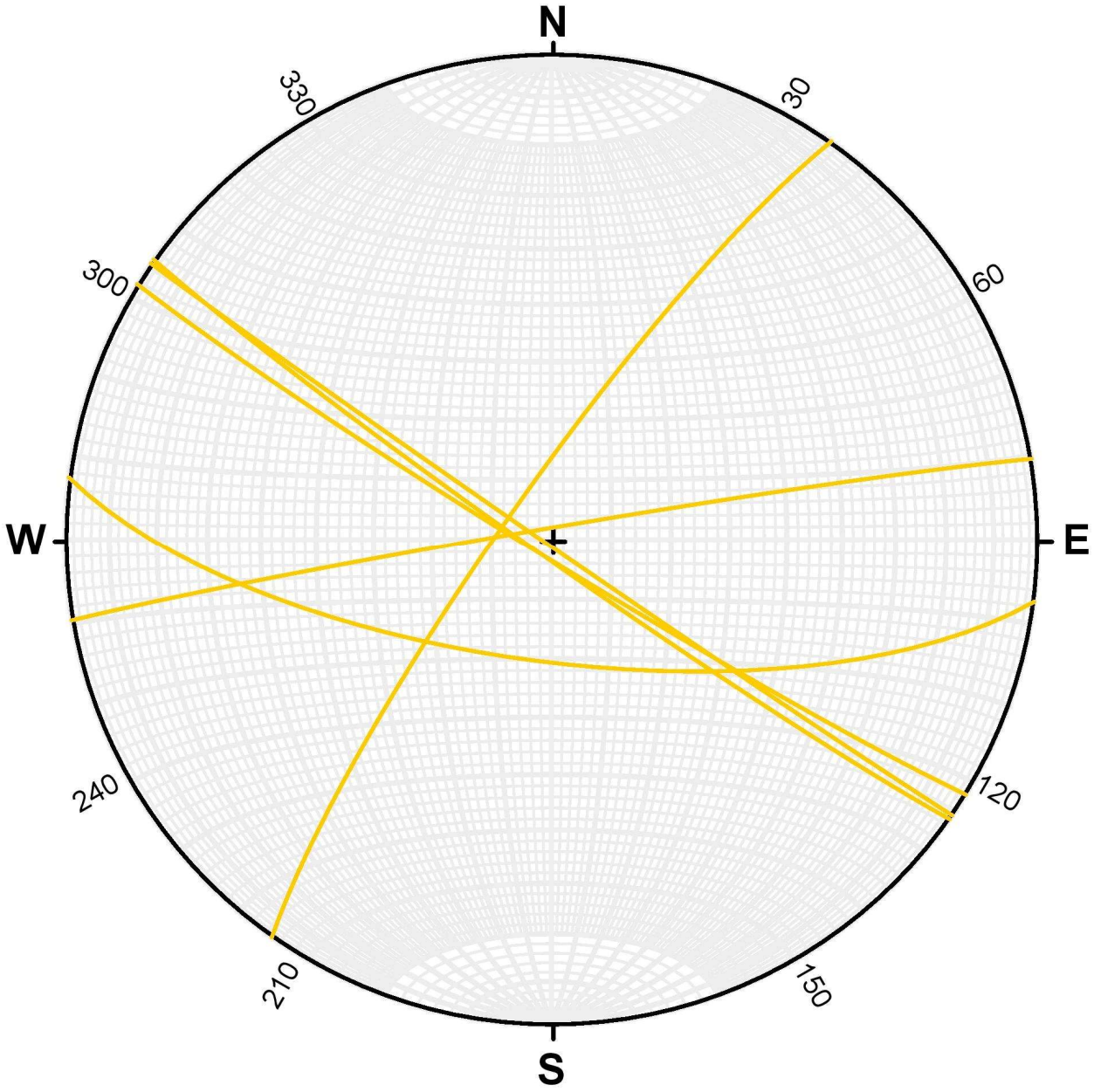

Figure 92 - Joint planes for gritstone. N = 6.

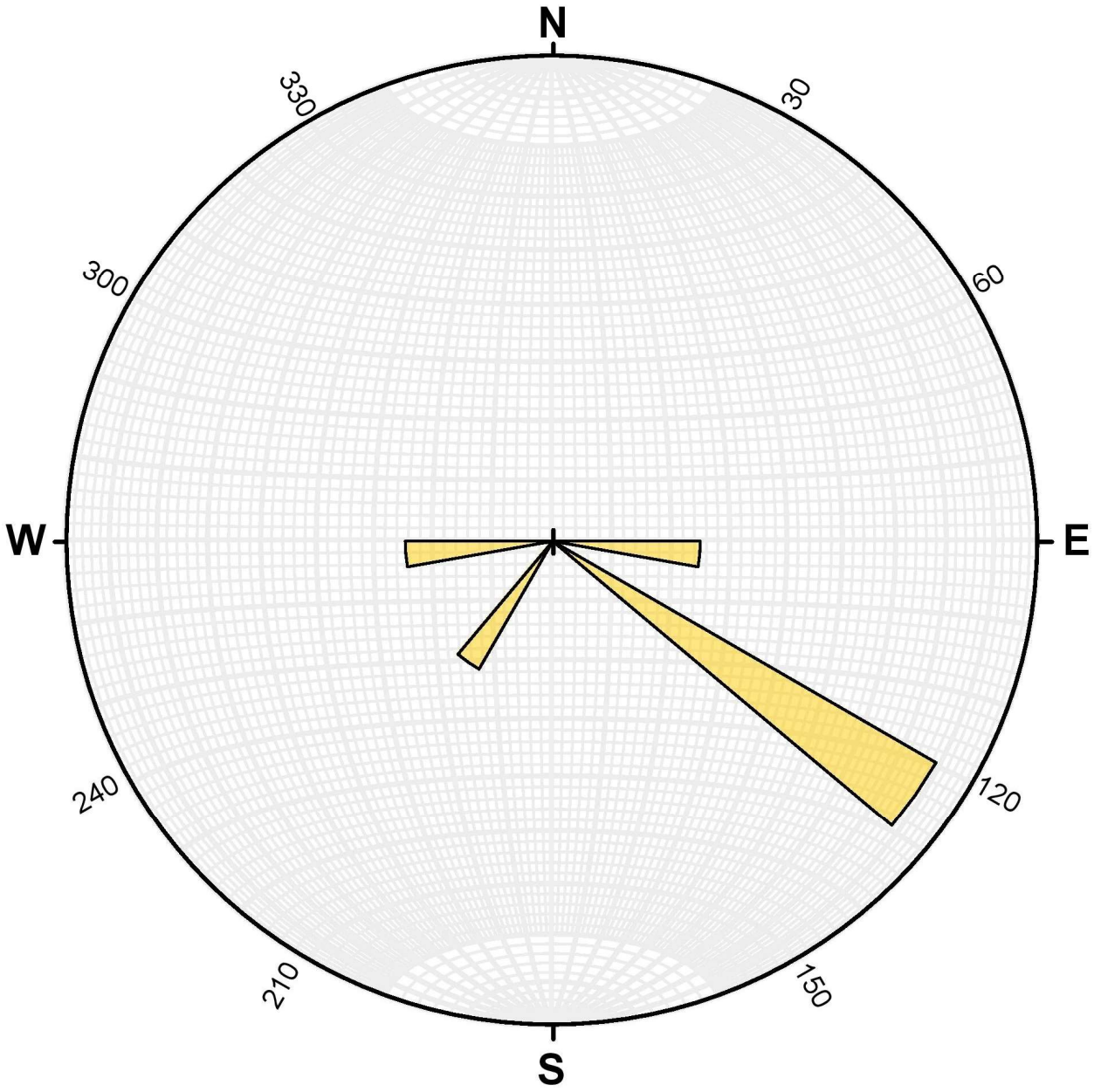

Figure 93 - Rose diagram of joint planes for gritstone. N = 6.

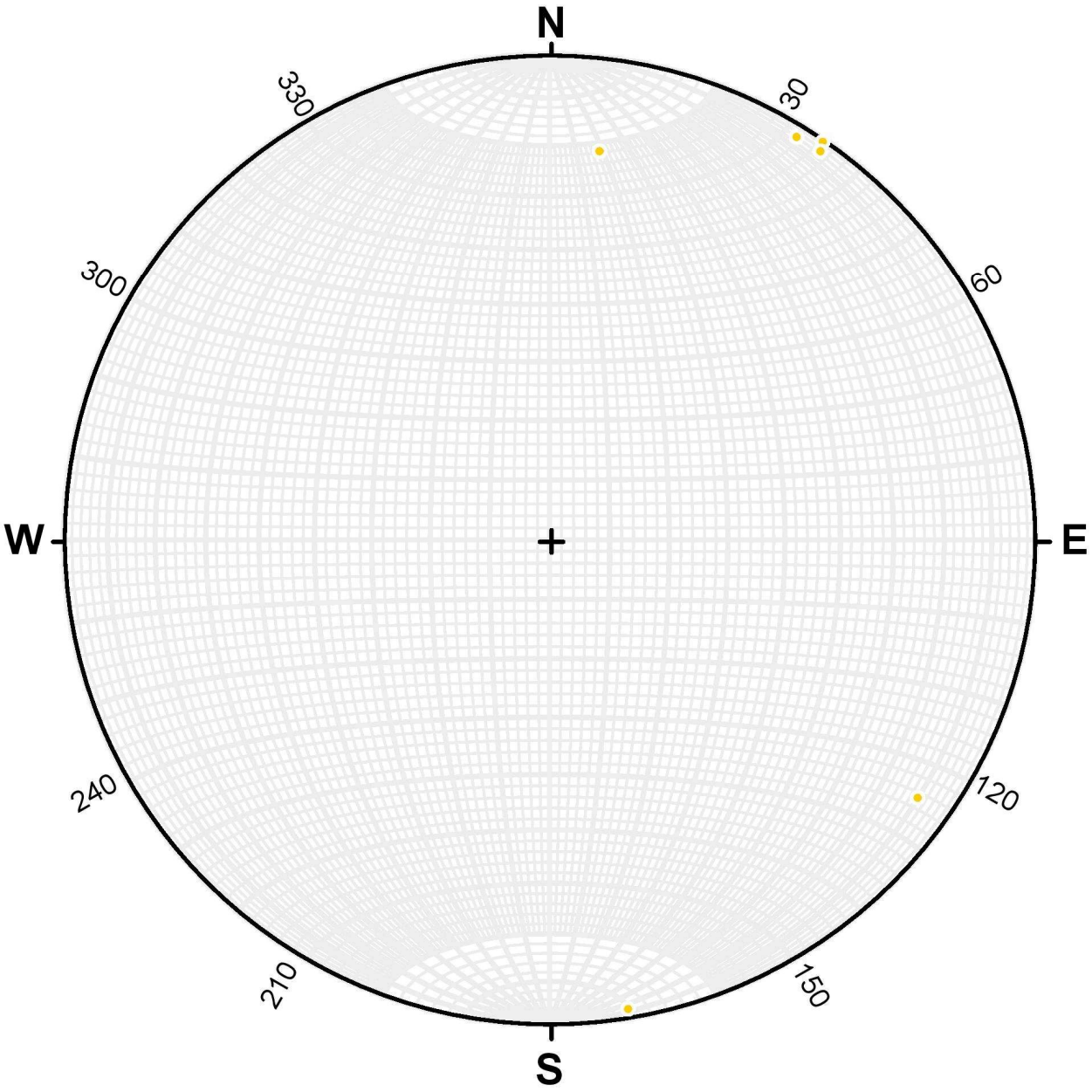

Figure 94 - Joint poles for gritstone. N = 6.

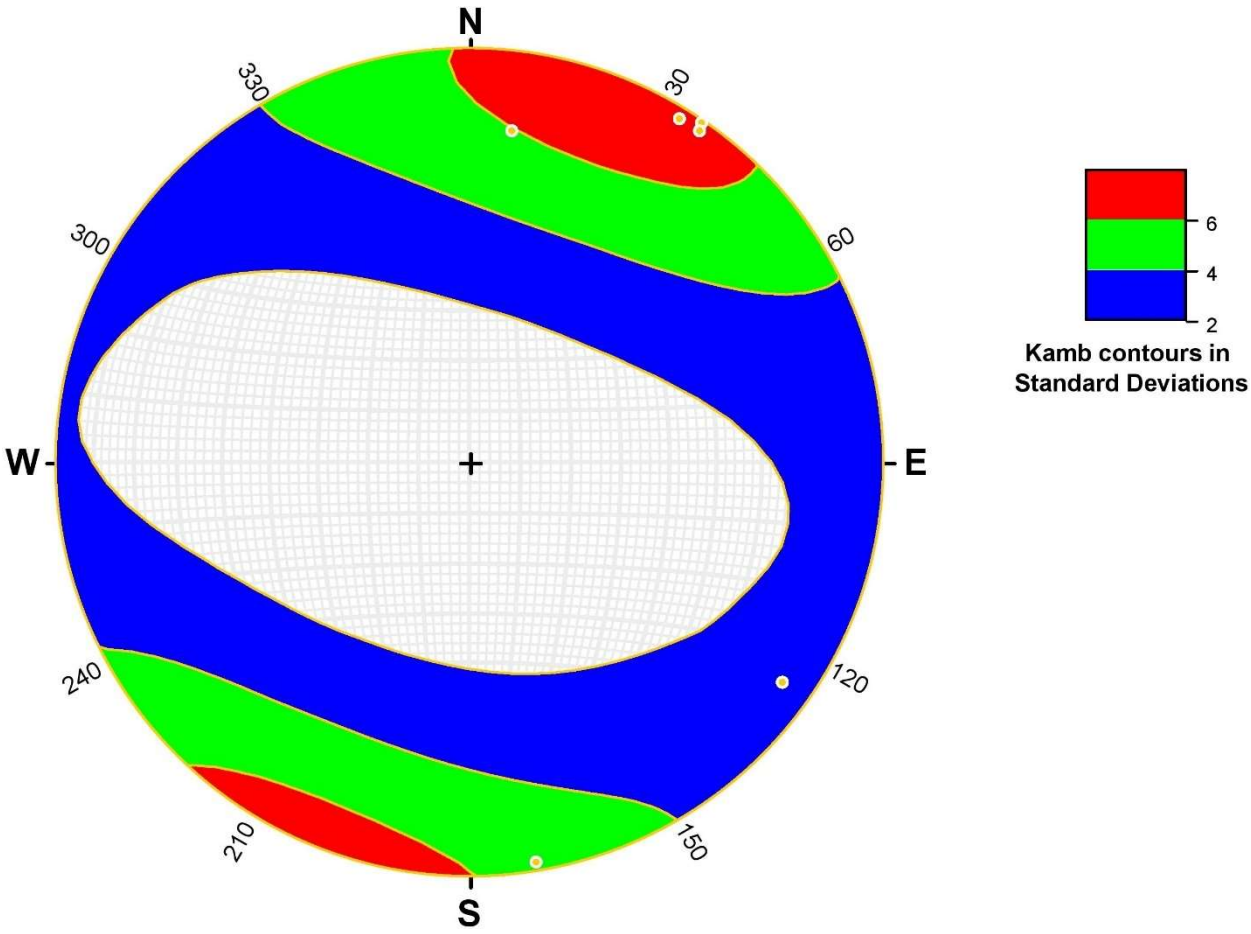

Figure 95 - Kamb contouring of joint poles for gritstone. N = 6.

Marble

Bedding

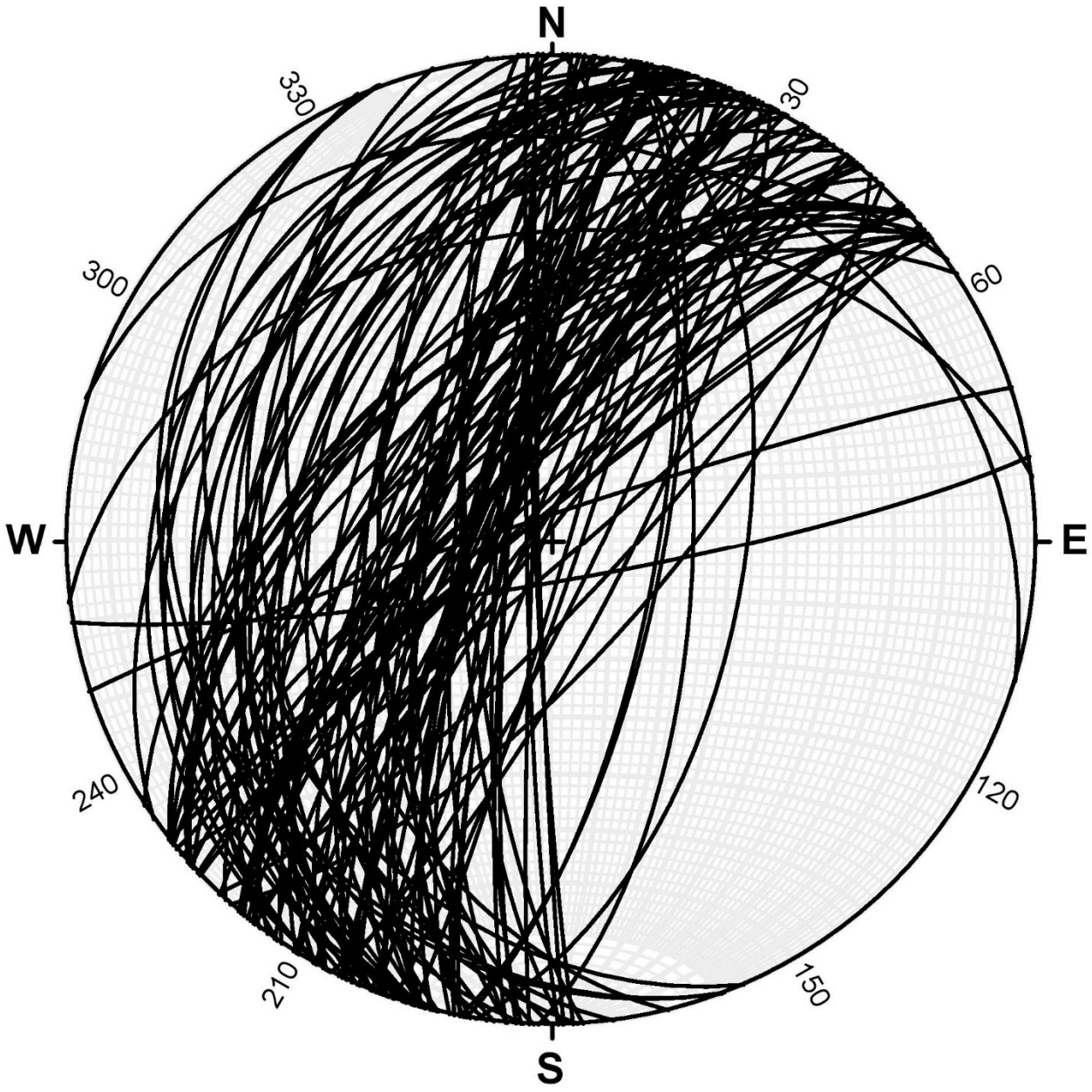

Figure 96 - Bedding planes for marble. N = 121.

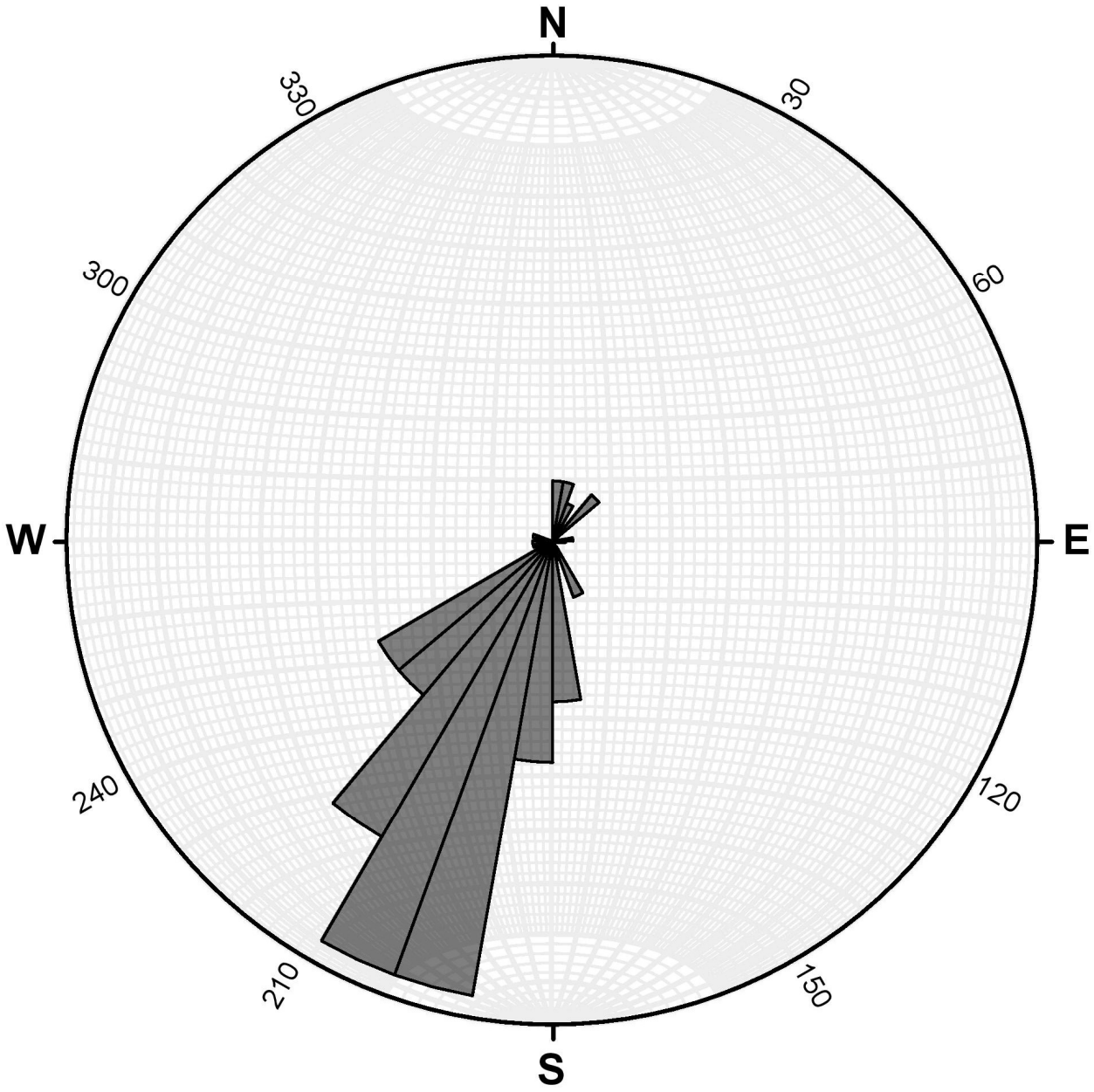

Figure 97 - Rose diagram of bedding planes for marble. N = 121.

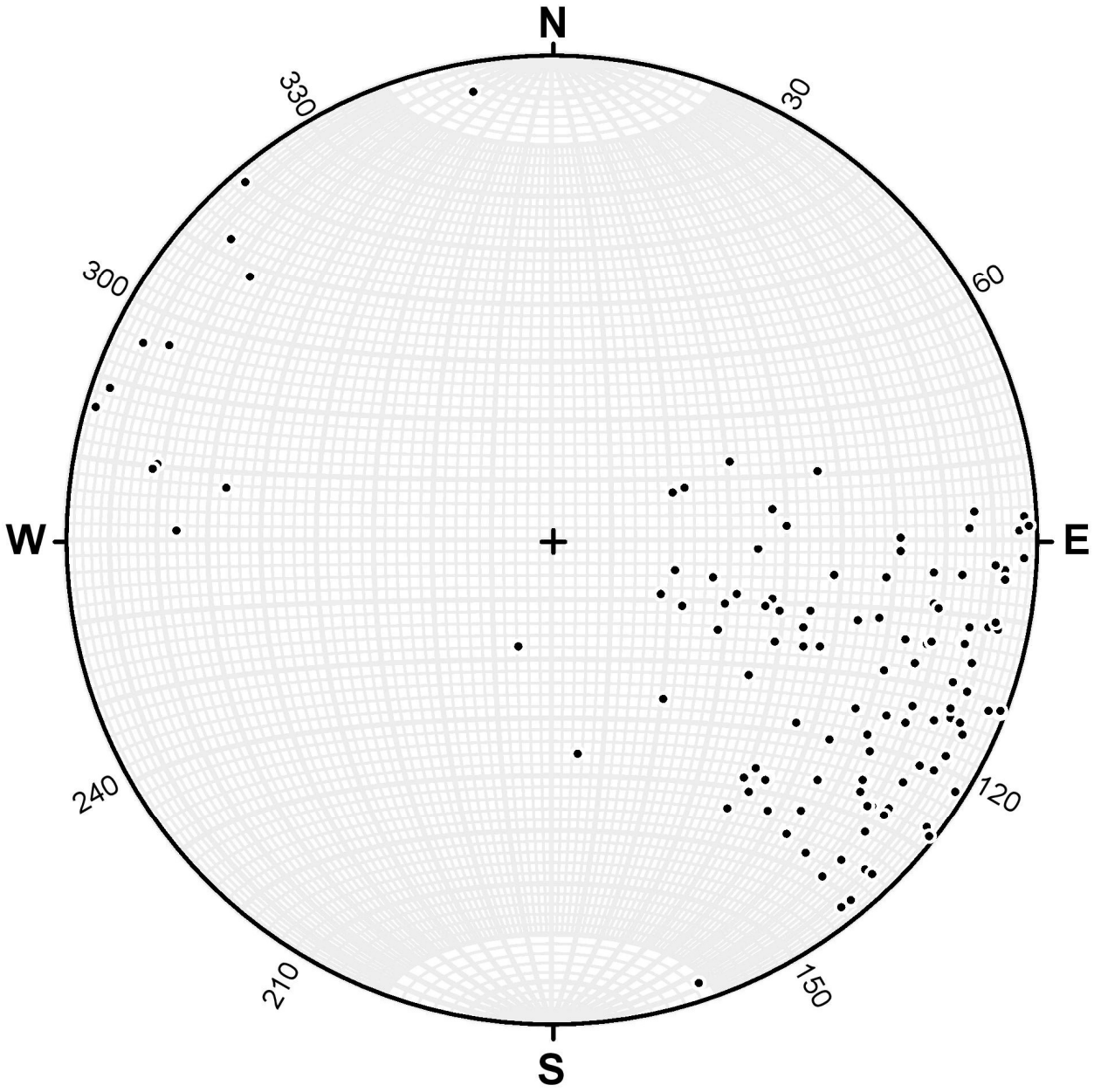

Figure 98 - Bedding poles for marble. N = 121.

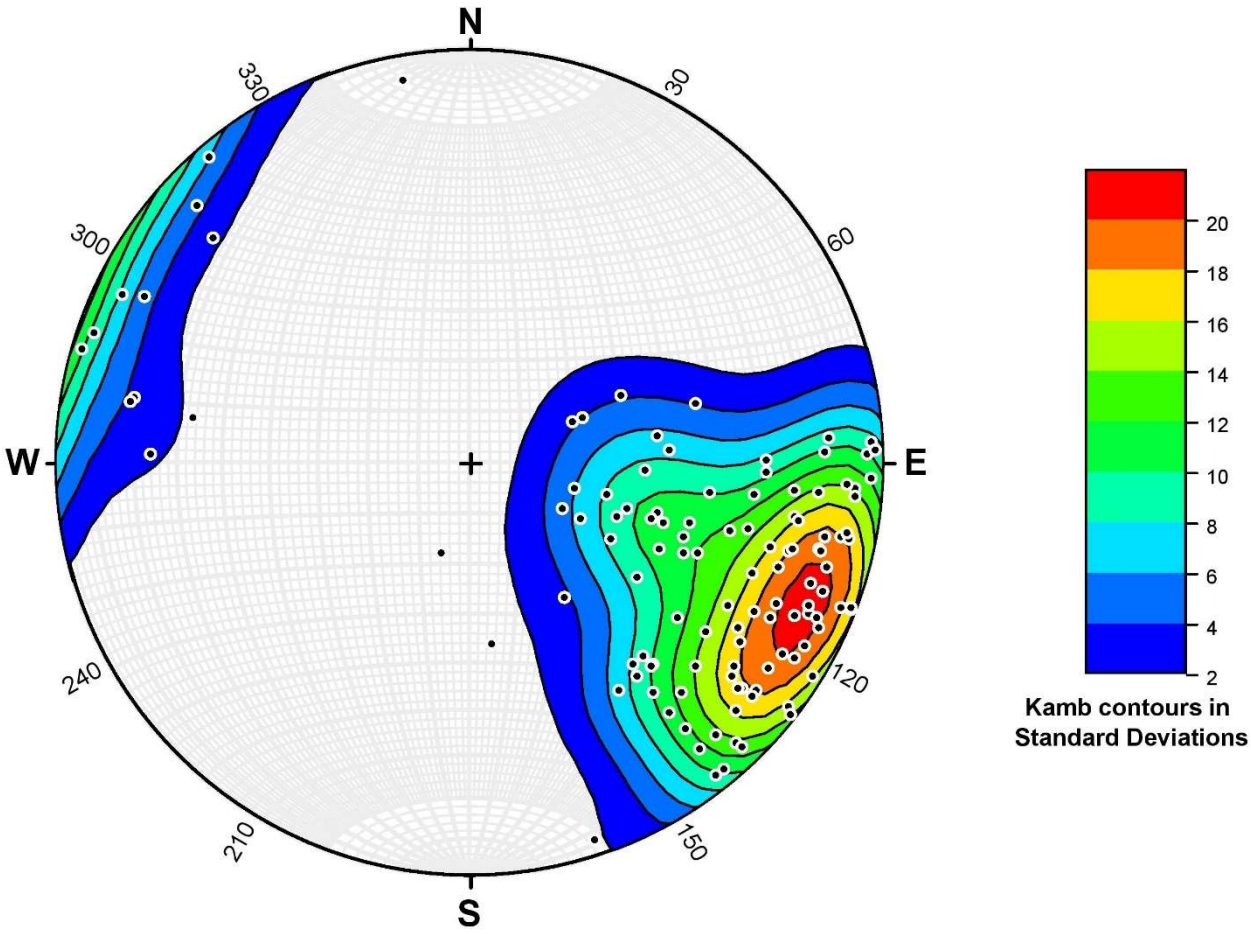

Figure 99 - Kamb contouring of bedding poles for marble. N = 121.

Jointing

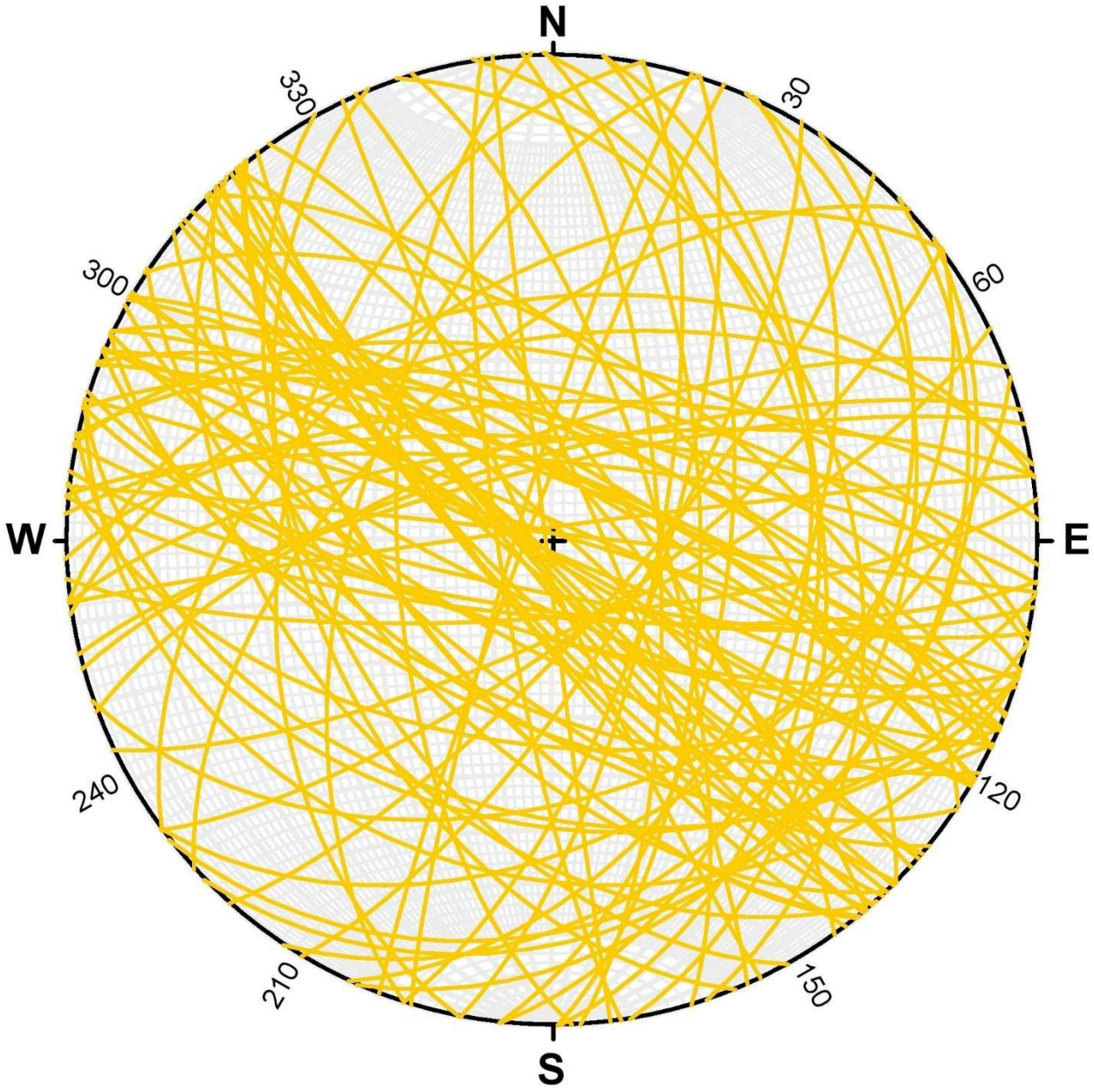

Figure 100 - Joint planes for marble. N = 95.

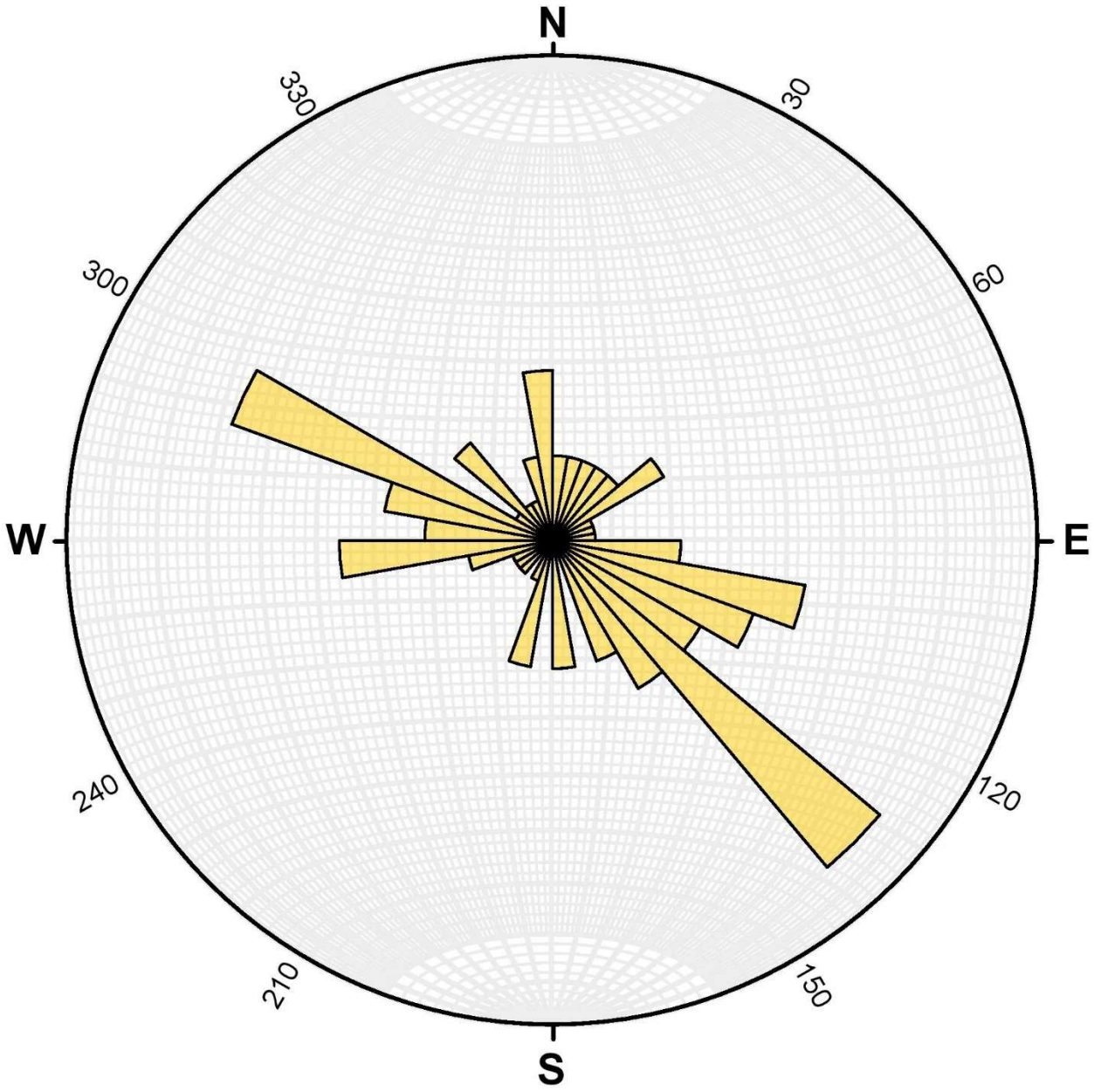

Figure 101 - Rose diagram of joint planes for marble. N = 95.

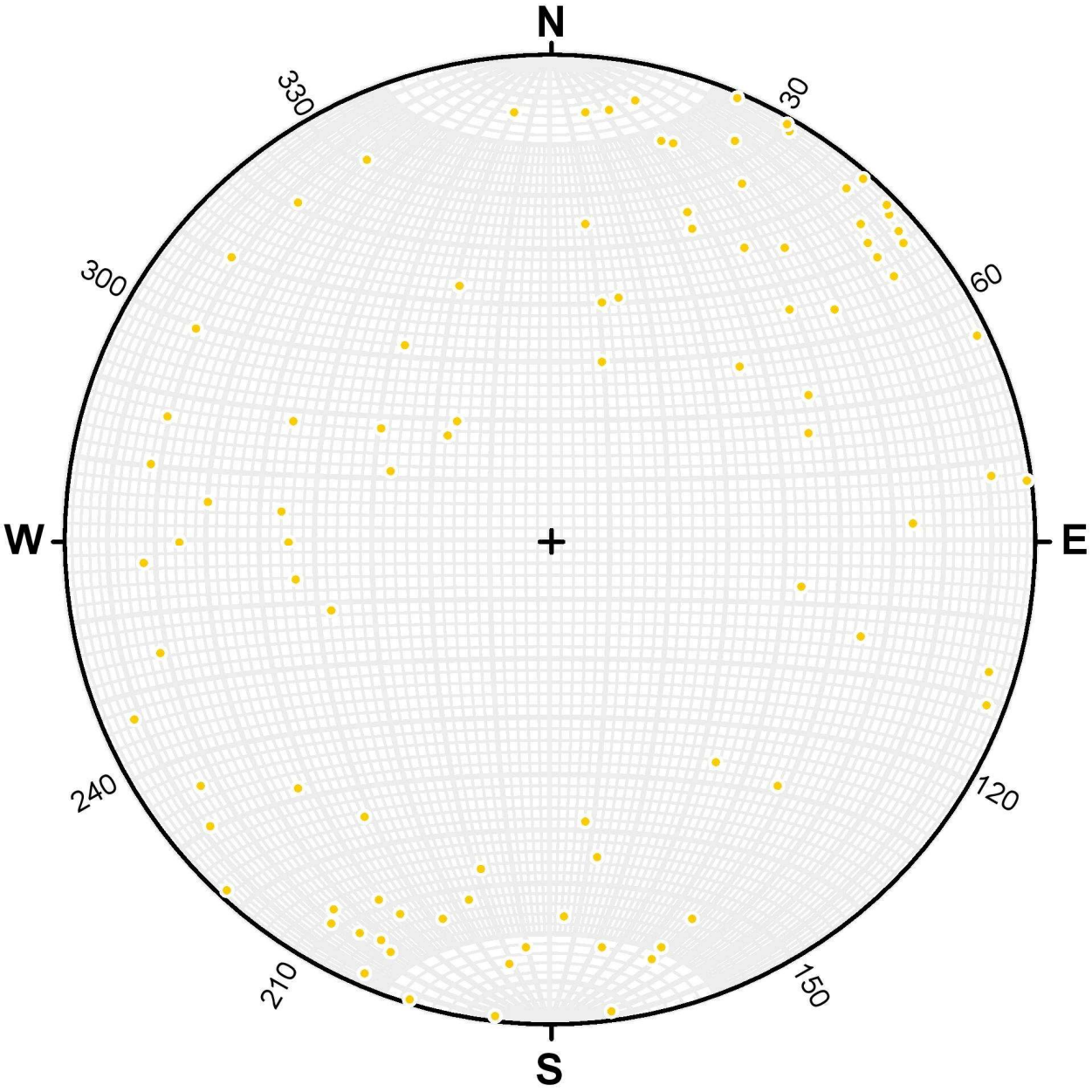

Figure 102 - Joint poles for marble. N = 95.

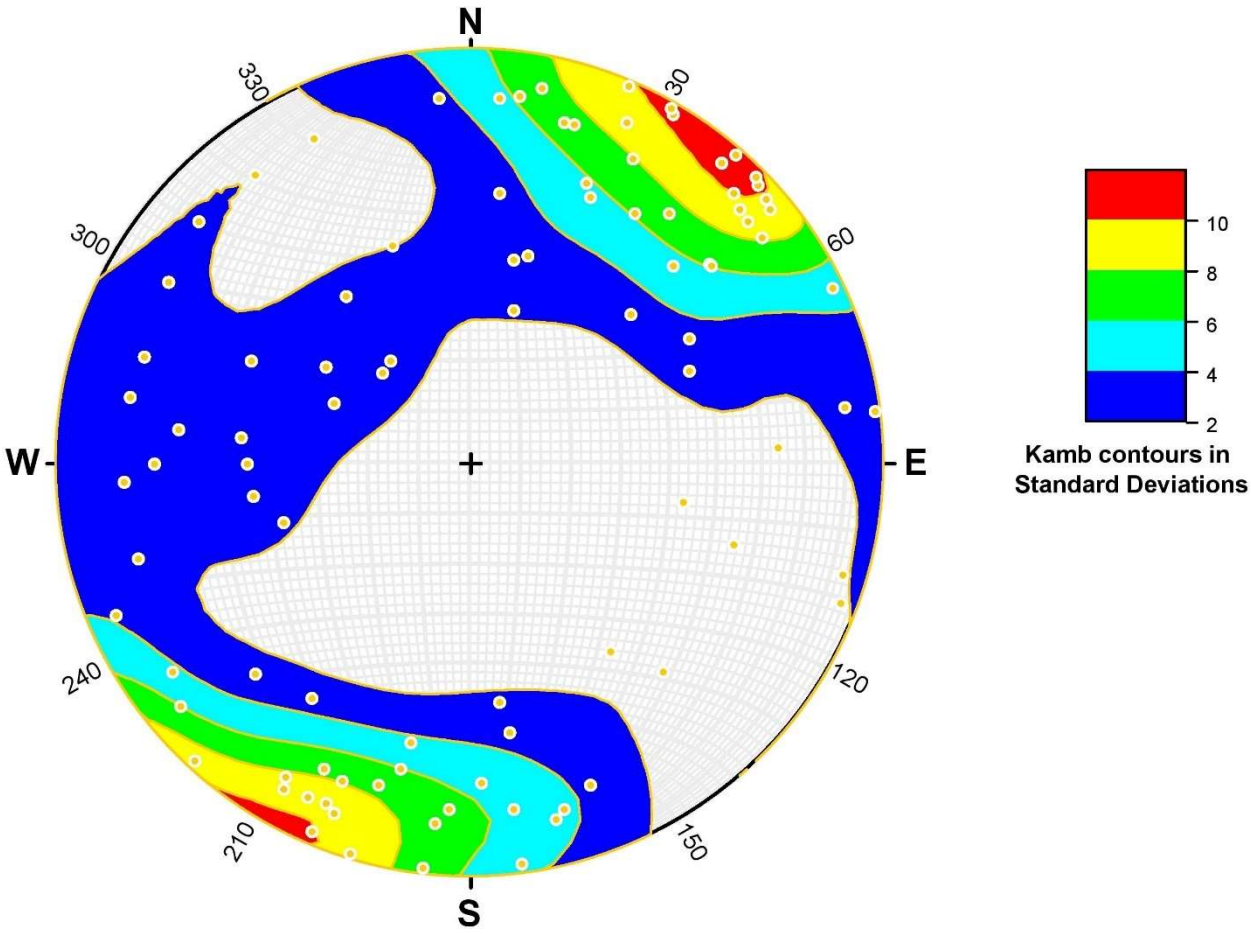

Figure 103 - Kamb contouring of joint poles for marble. N = 95.

Phyllite

Bedding

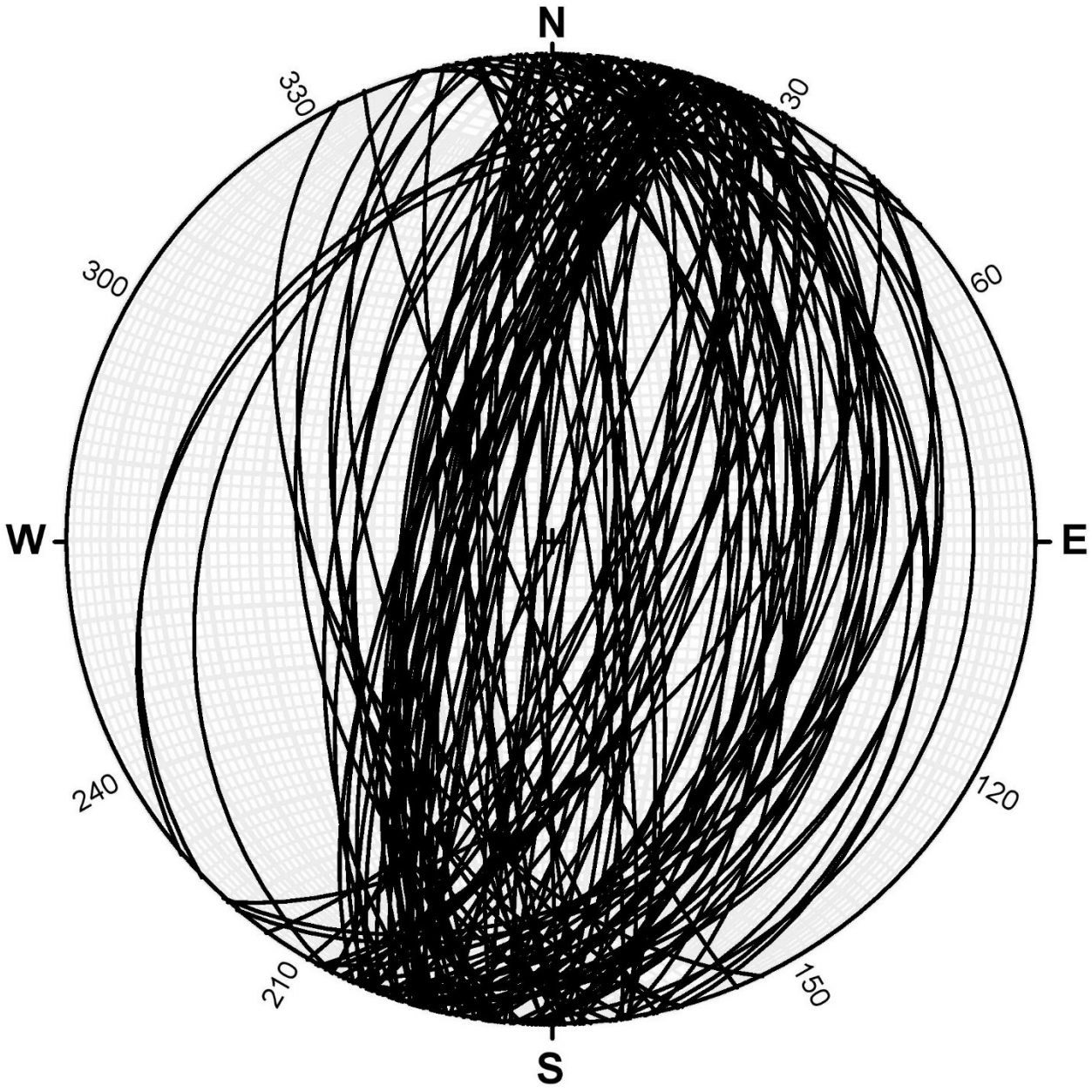

Figure 104 - Bedding planes for phyllite. N = 128.

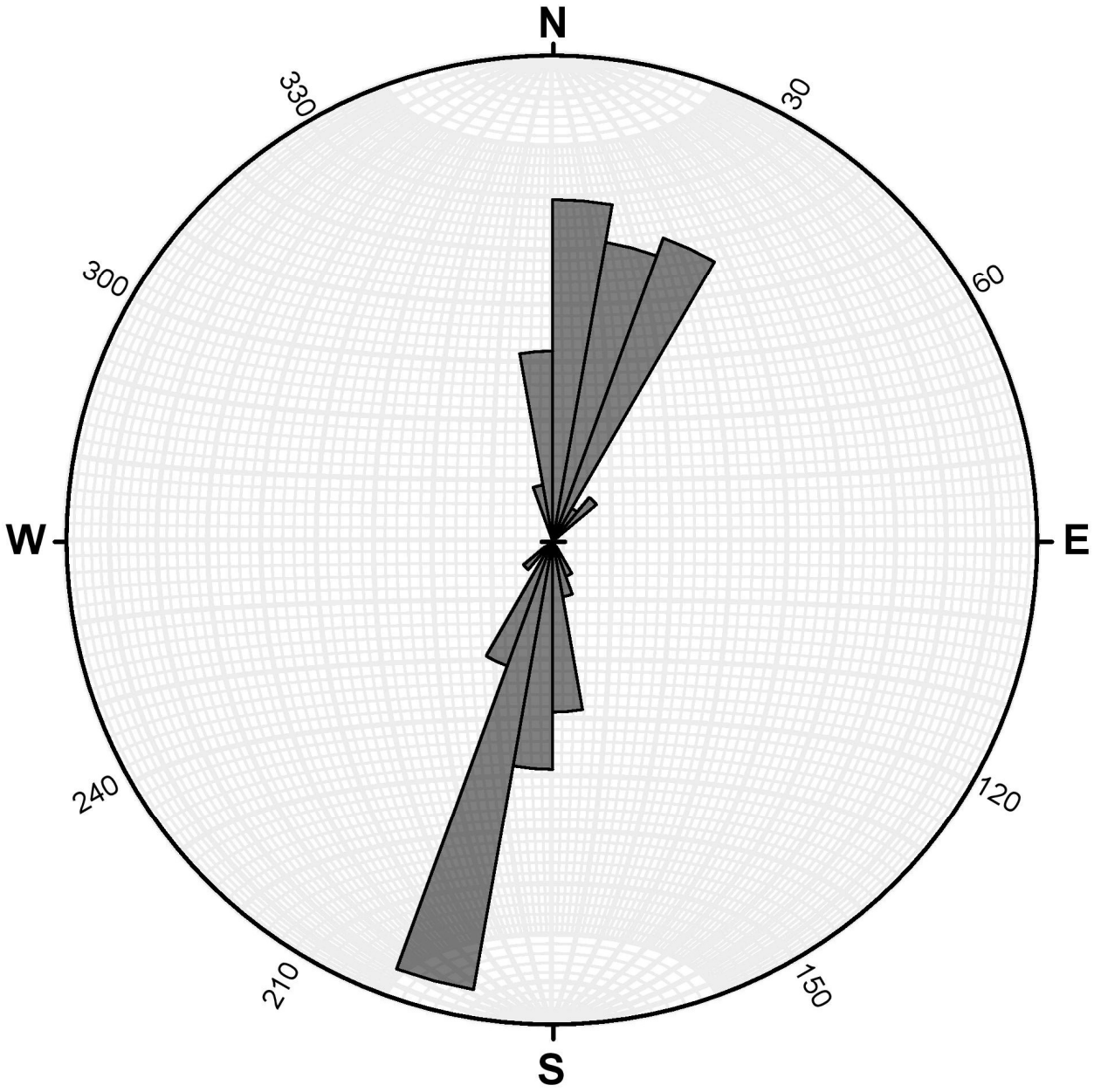

Figure 105 - Rose diagram of bedding planes for phyllite. N = 128.

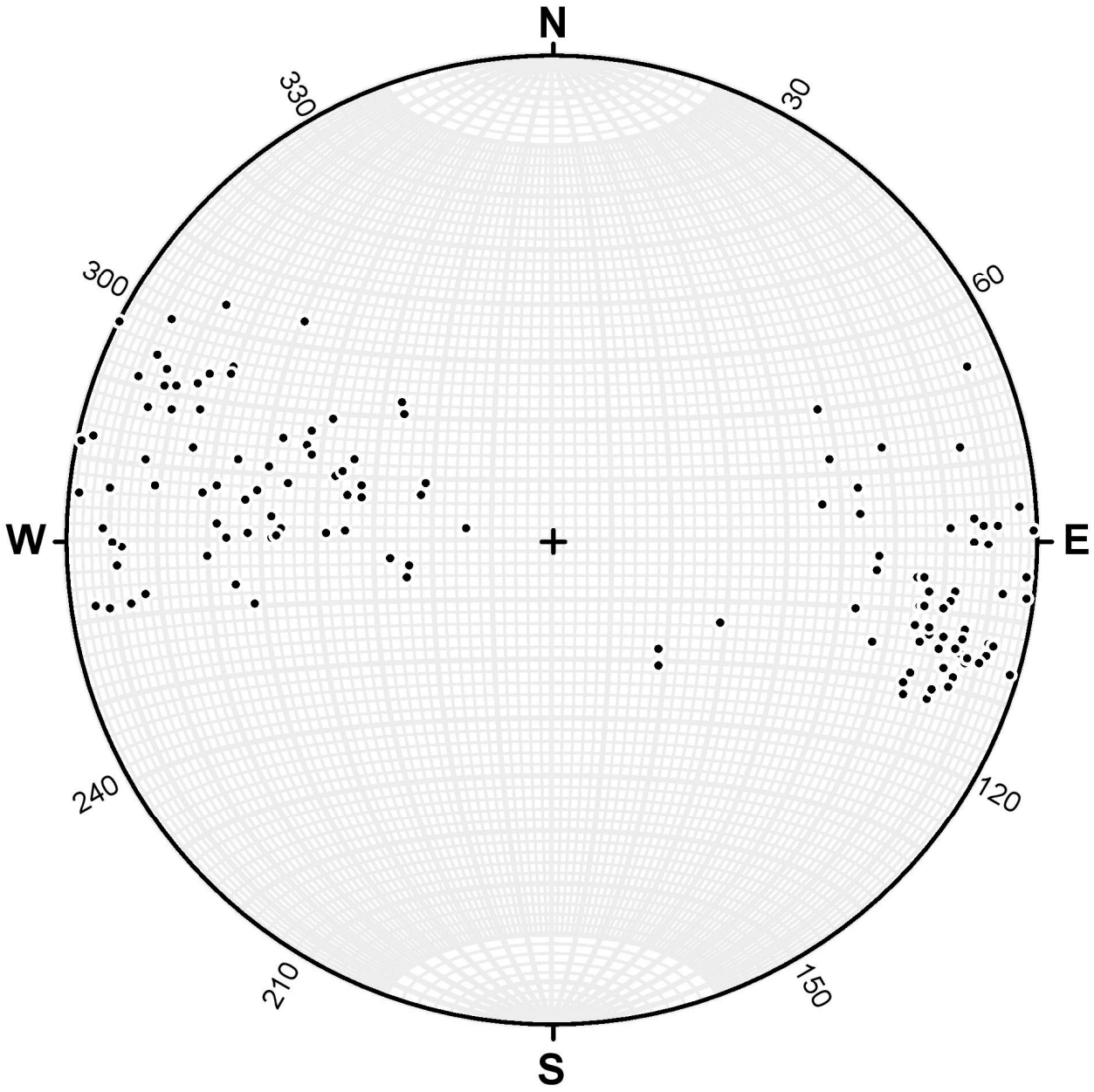

Figure 106 - Bedding poles for phyllite. N = 128.

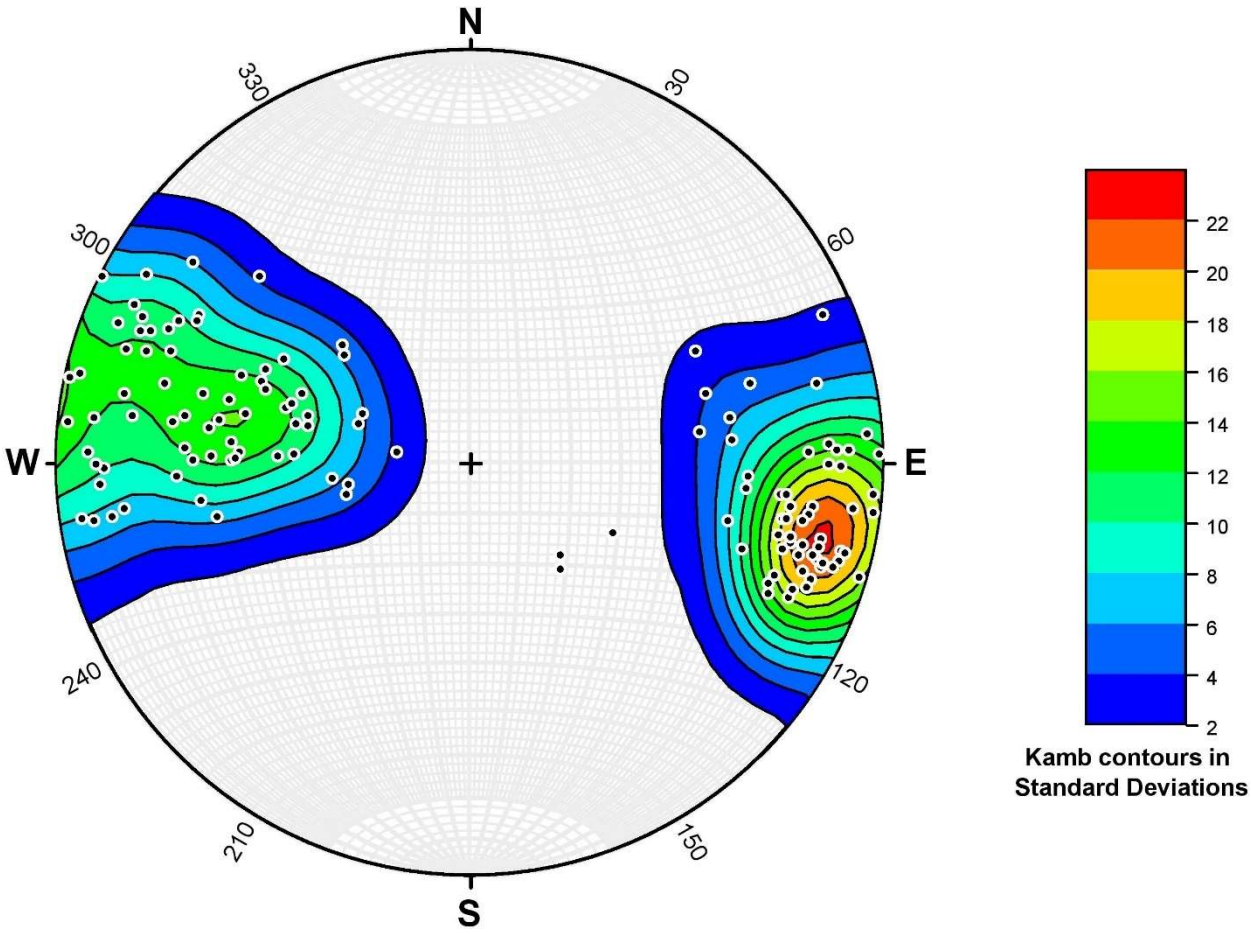

Figure 107 - Kamb contouring of bedding poles for phyllite. N = 128.

Jointing

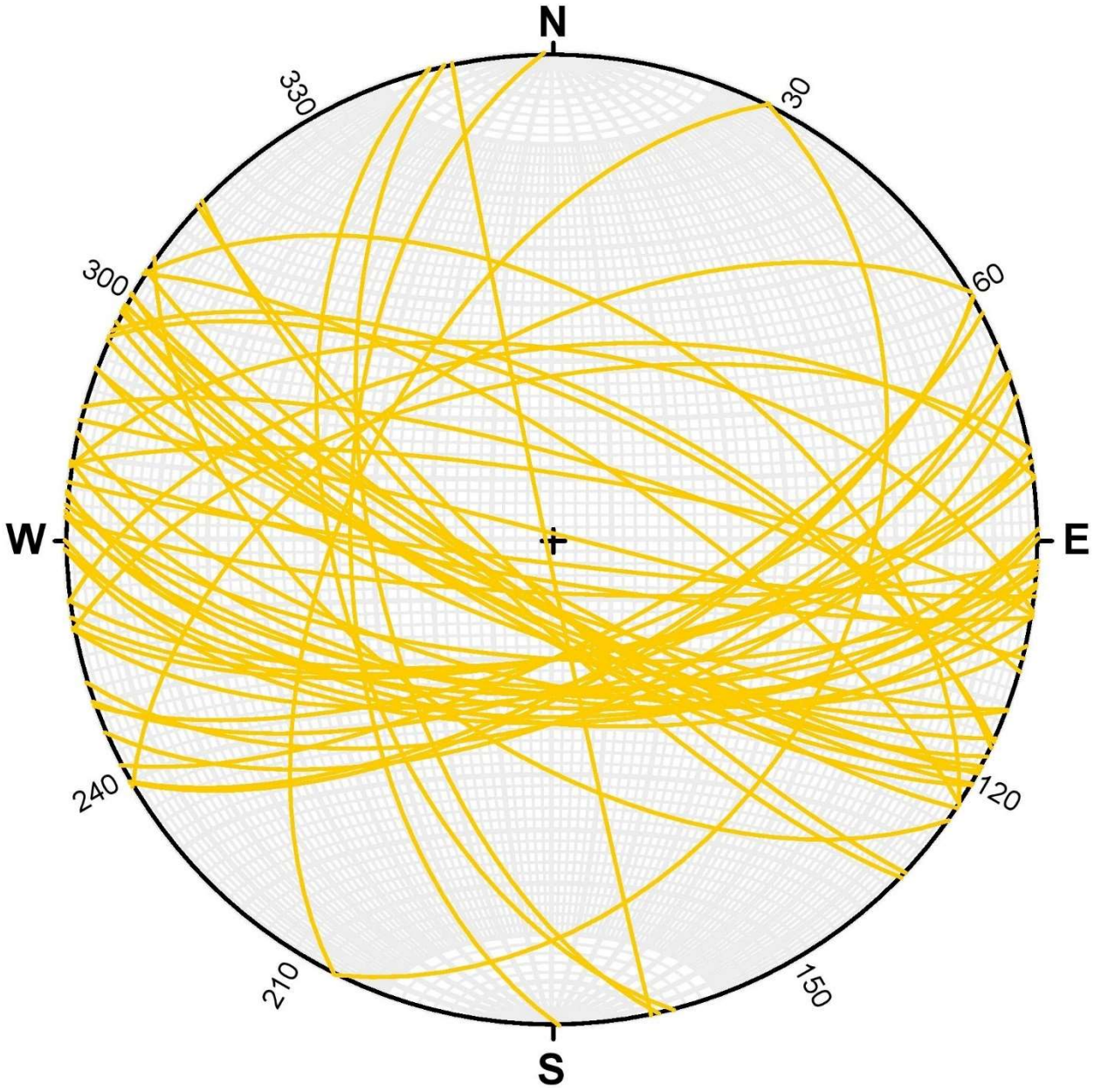

Figure 108 - Joint planes for phyllite. N = 54.

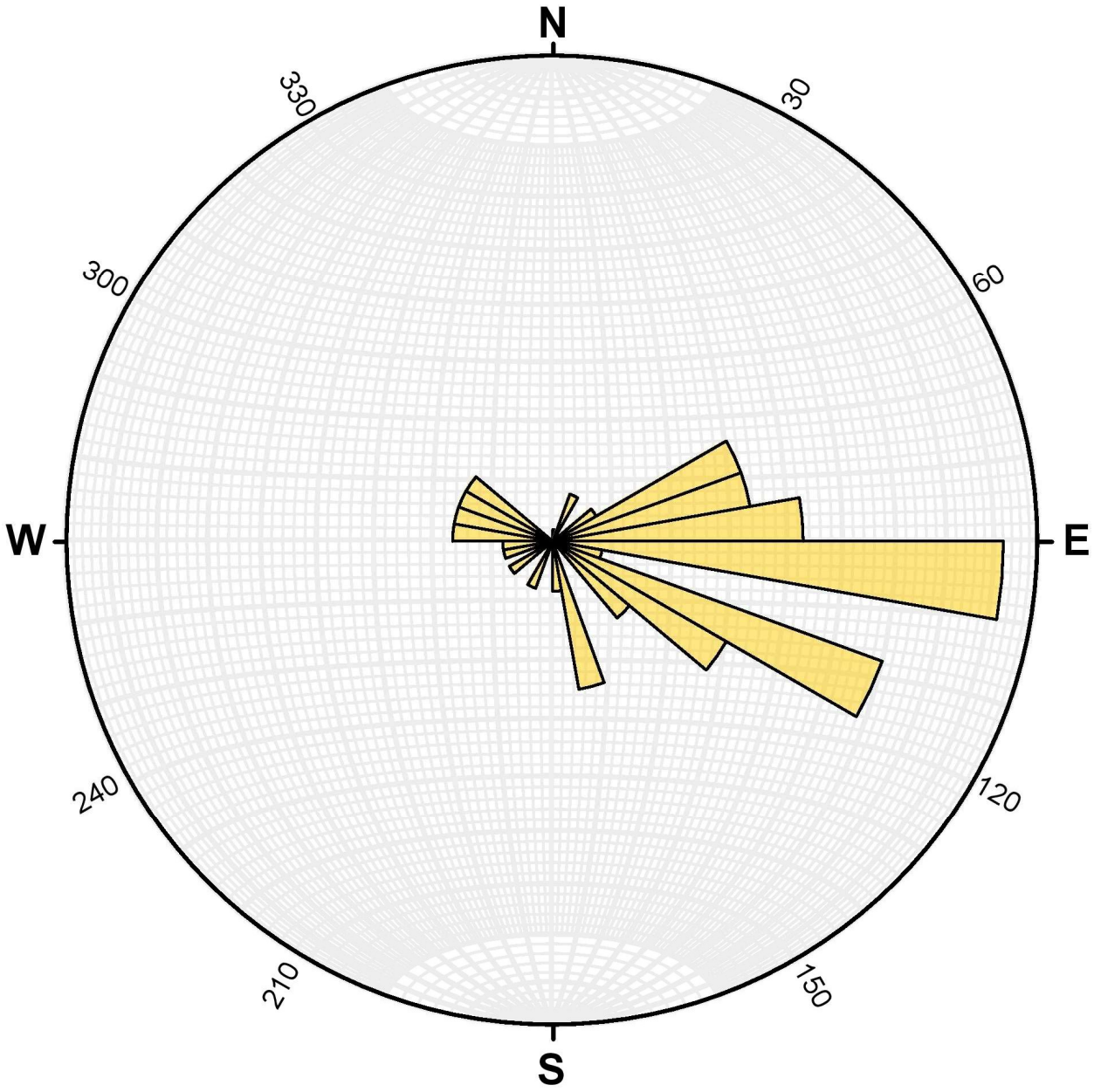

Figure 109 - Rose diagram of joint planes for phyllite. N = 54.

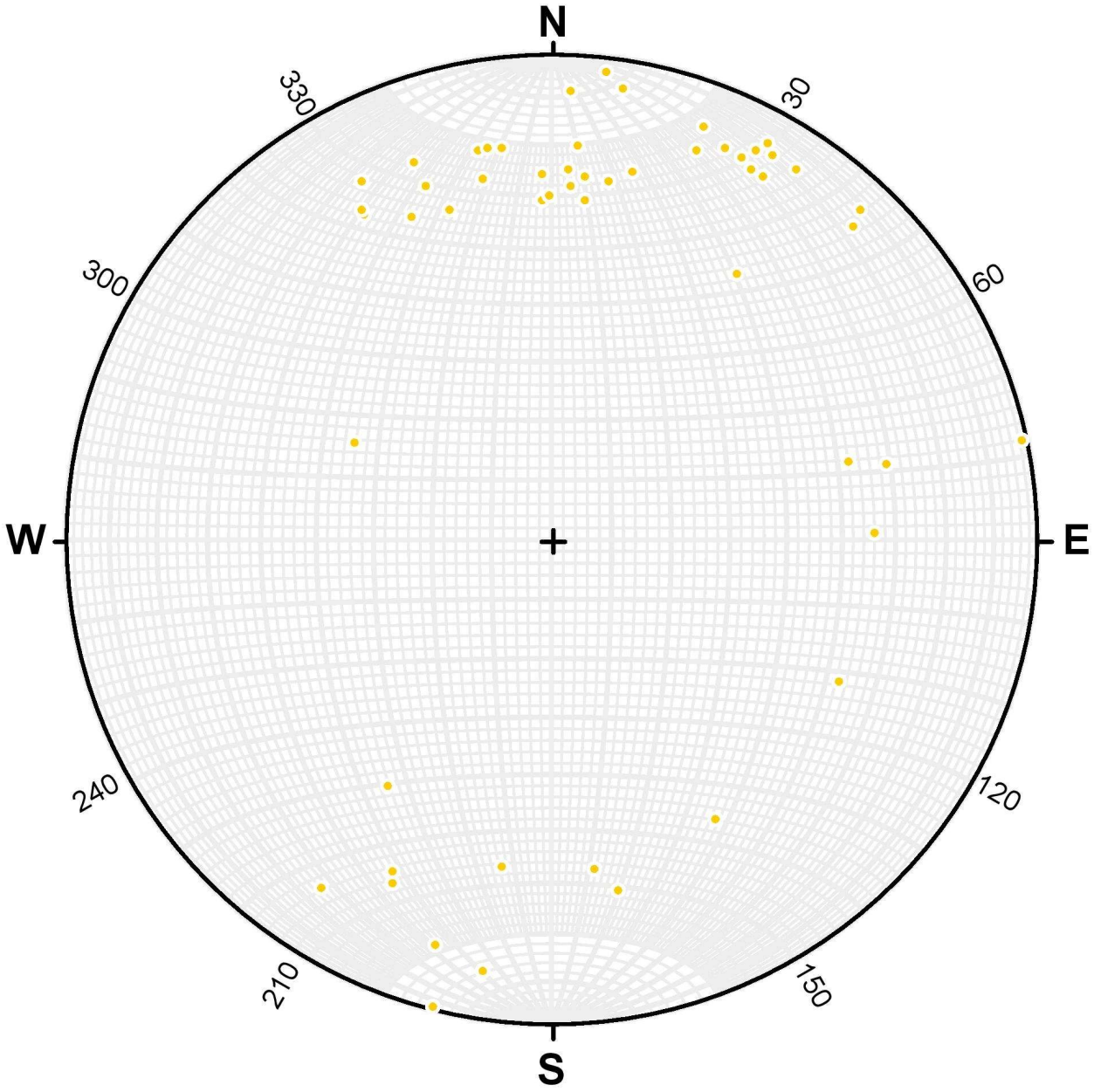

Figure 110 - Joint poles for phyllite. N = 54.

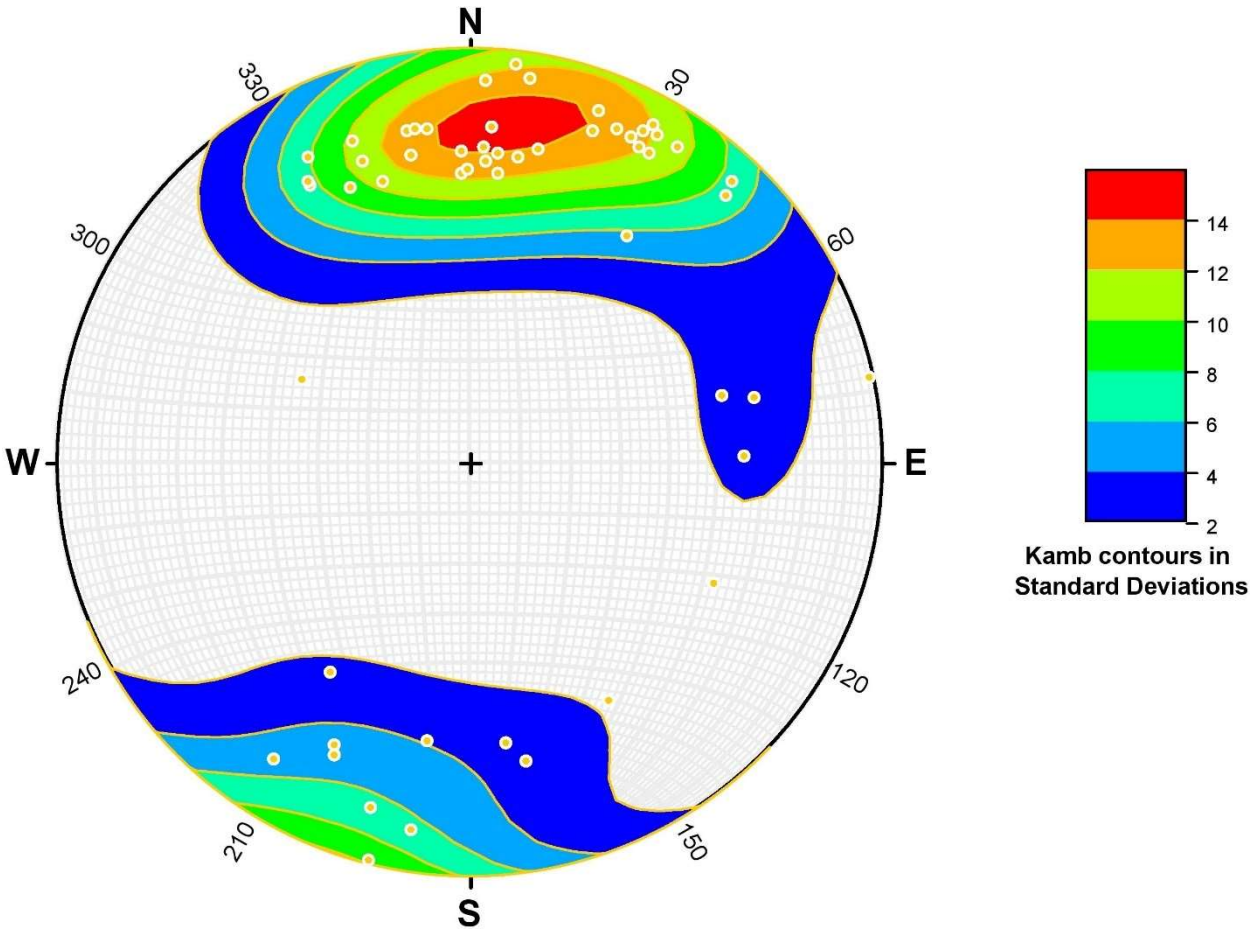

Figure 111 - Kamb contouring of joint poles for phyllite. N = 54.

Quartzite

Bedding

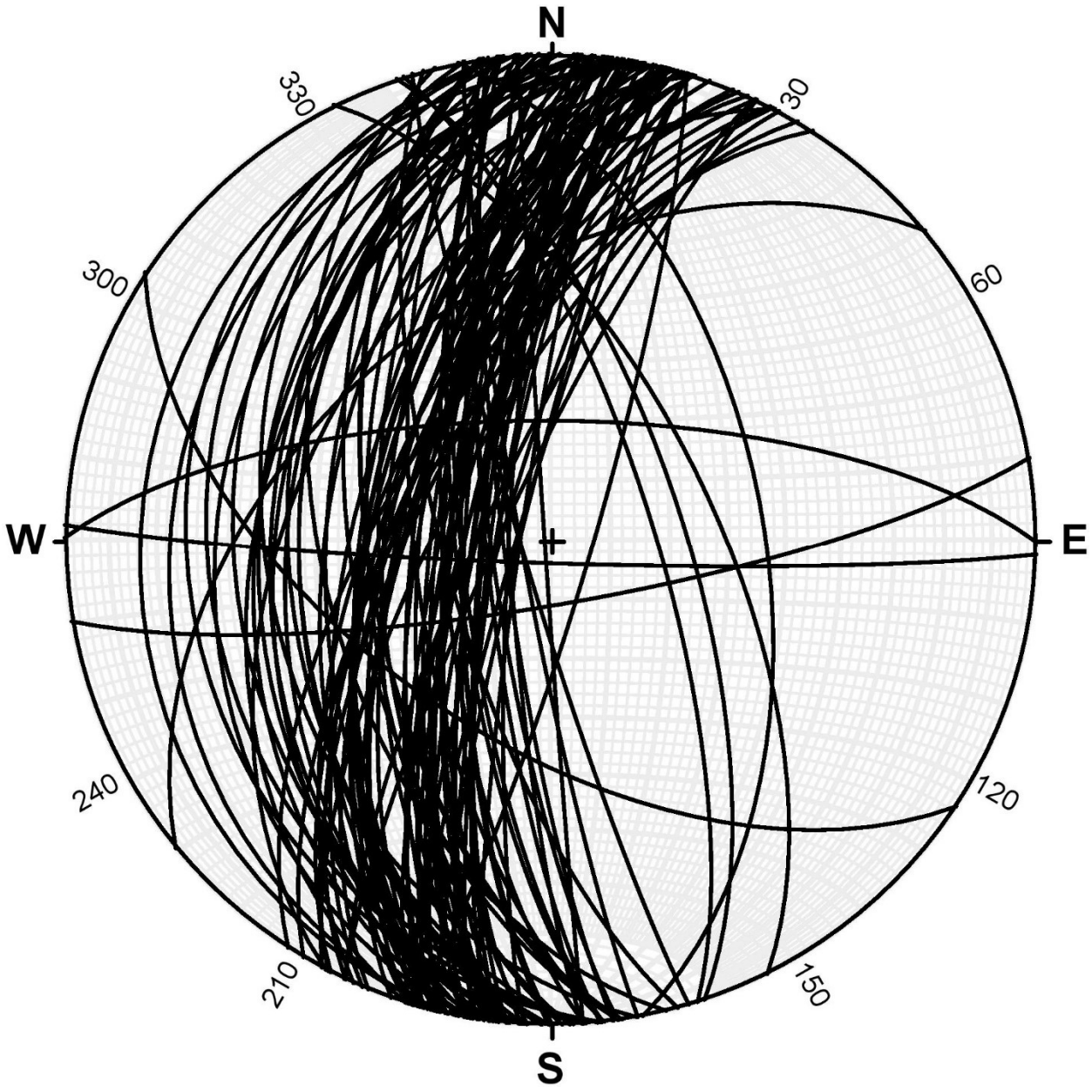

Figure 112 - Bedding planes for quartzite. N = 104.

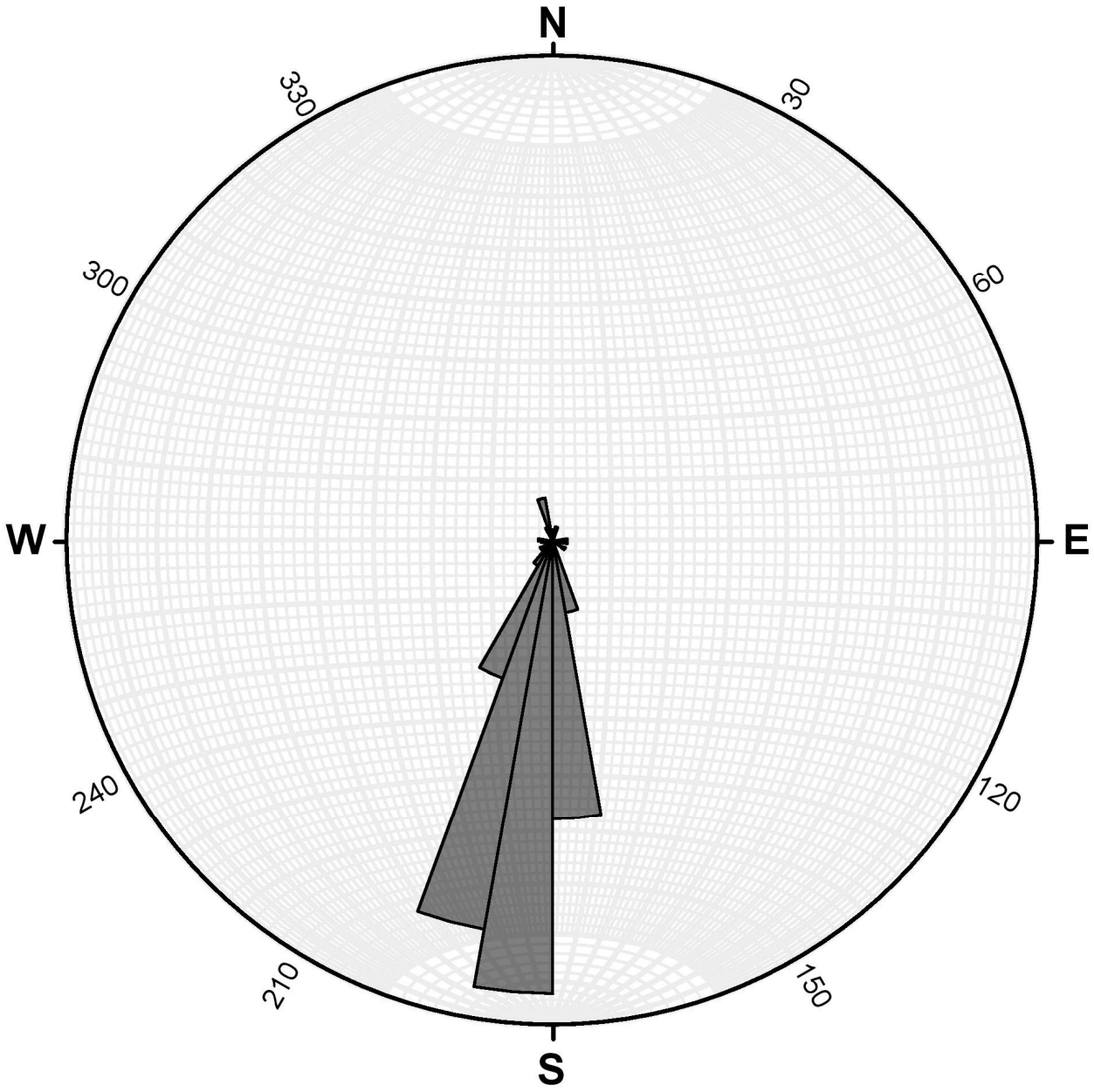

Figure 113 - Rose diagram of bedding planes for quartzite. N = 104.

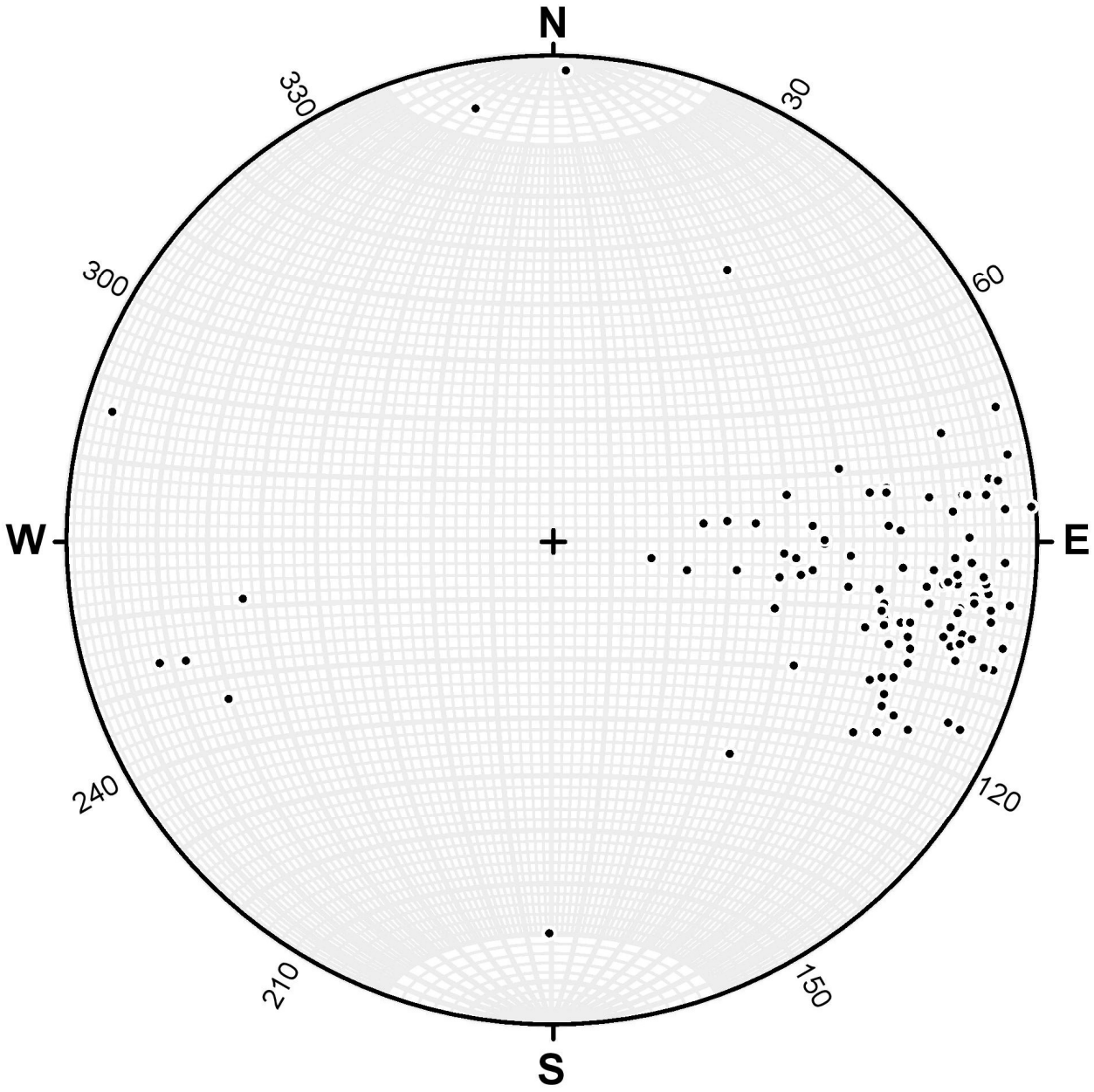

Figure 114 - Bedding poles for quartzite. N = 104.

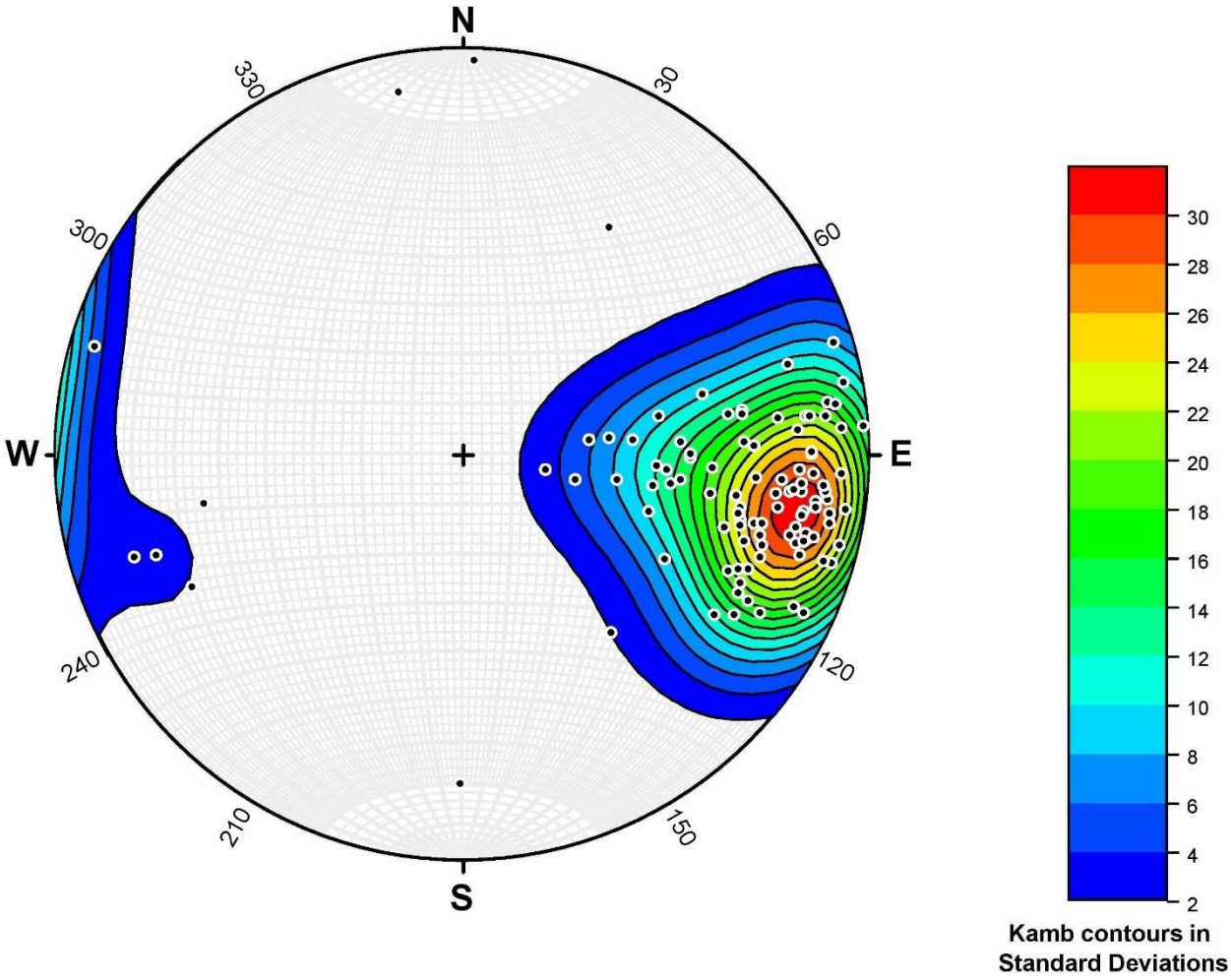

Figure 115 - Kamb contouring of bedding poles for quartzite. N = 104.

Jointing

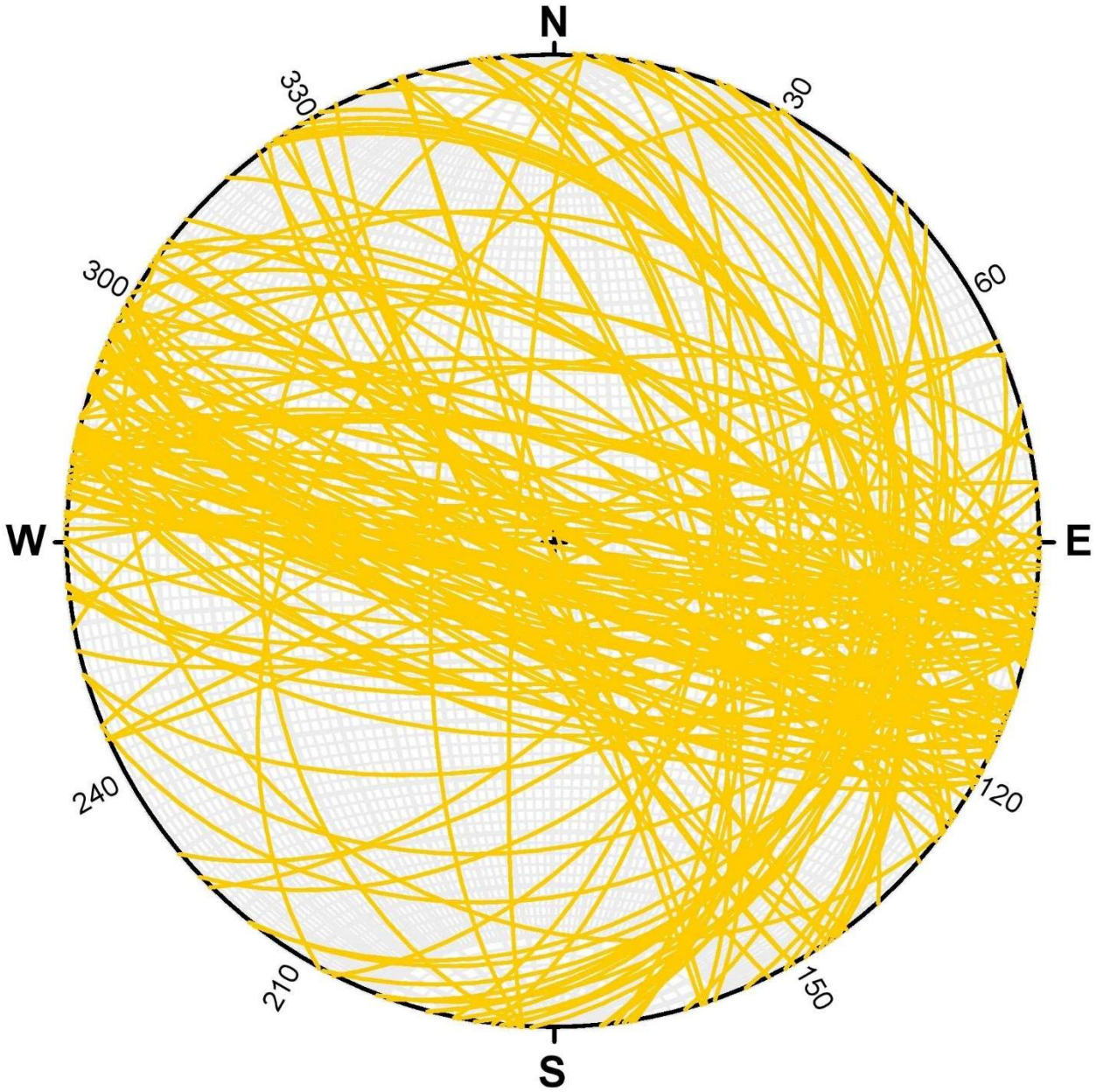

Figure 116 - Joint planes for quartzite. N = 149.

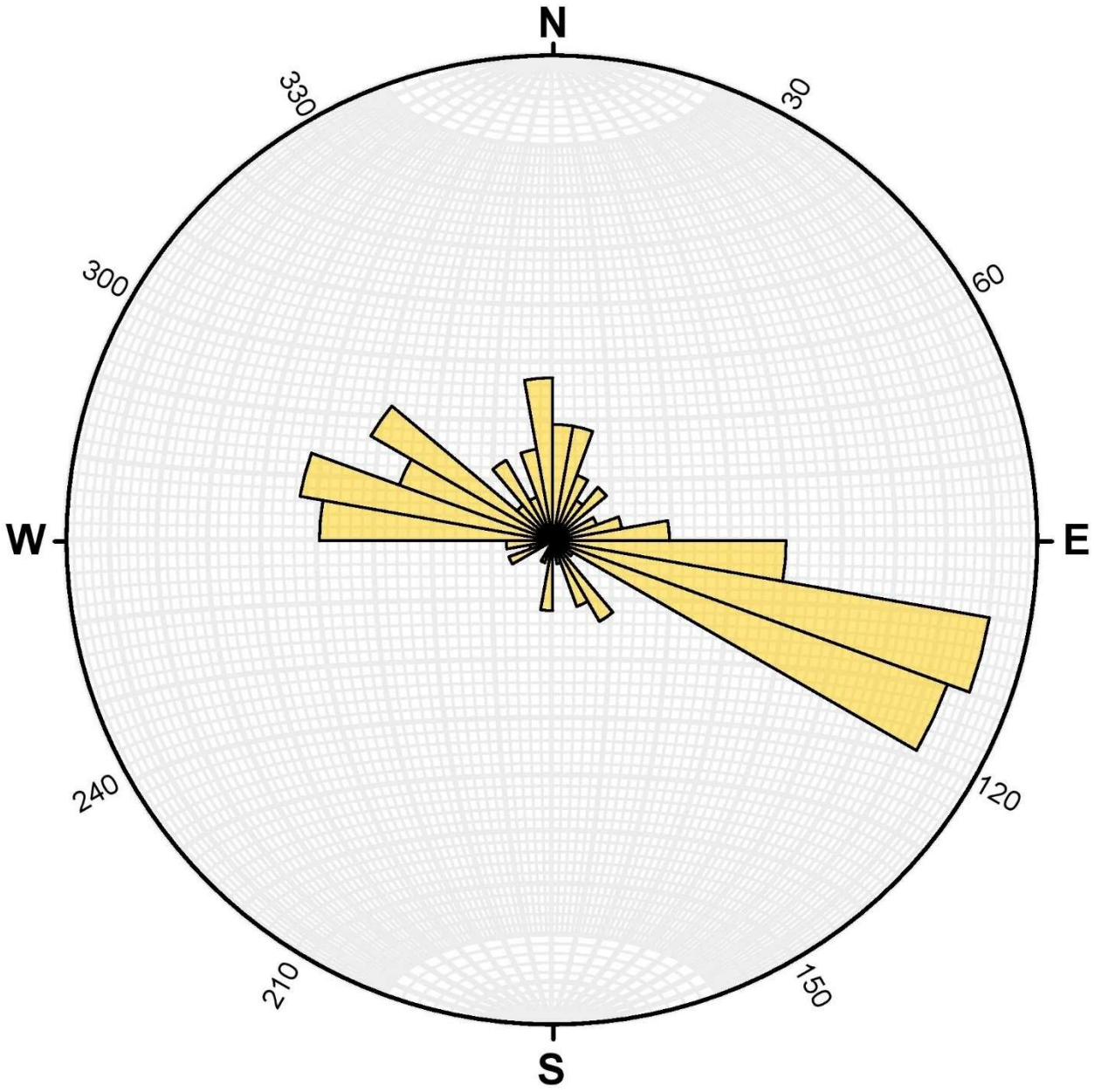

Figure 117 - Rose diagram of joint planes for quartzite. N = 149.

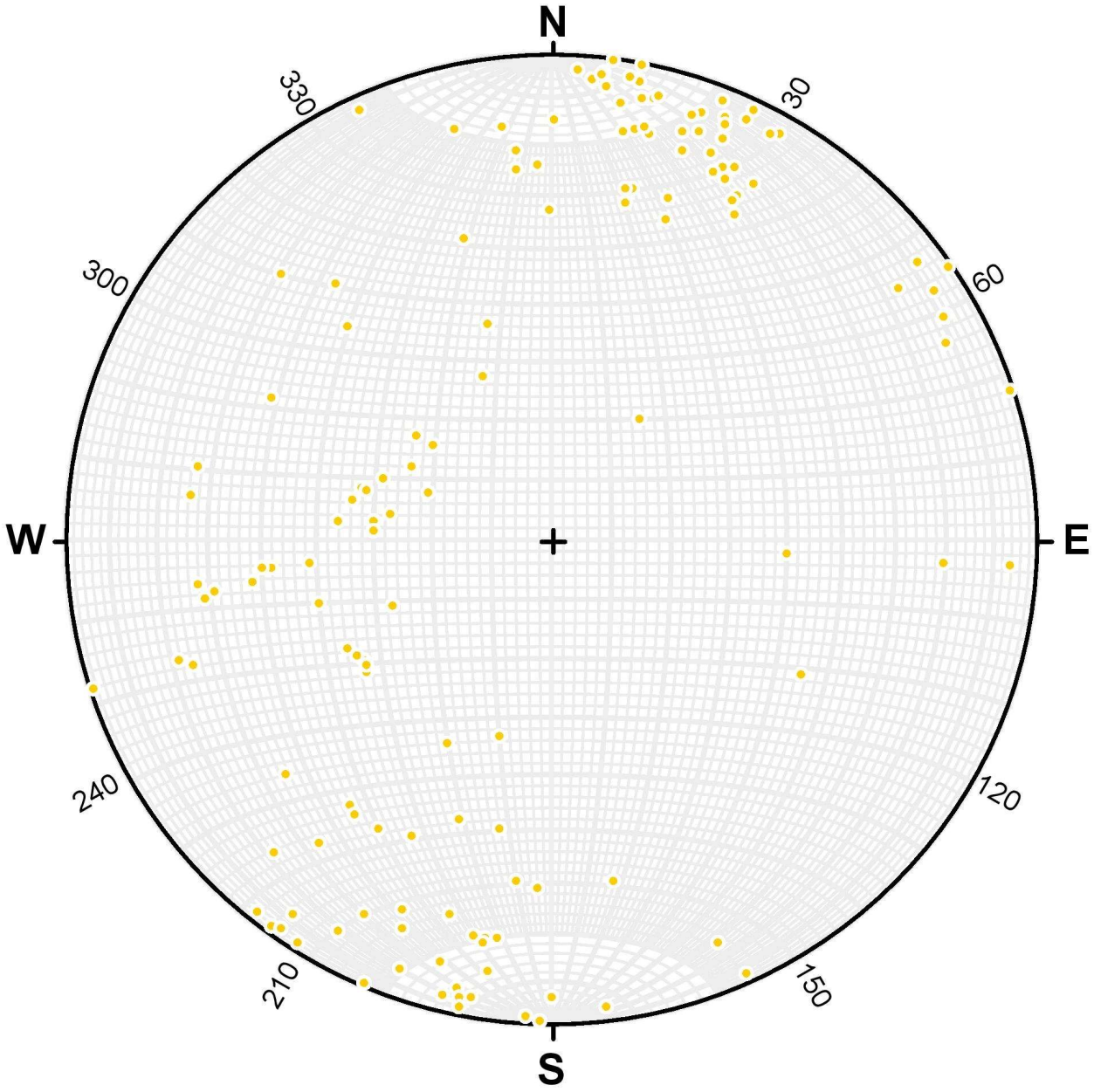

Figure 118 - Joint poles for quartzite. N = 149.

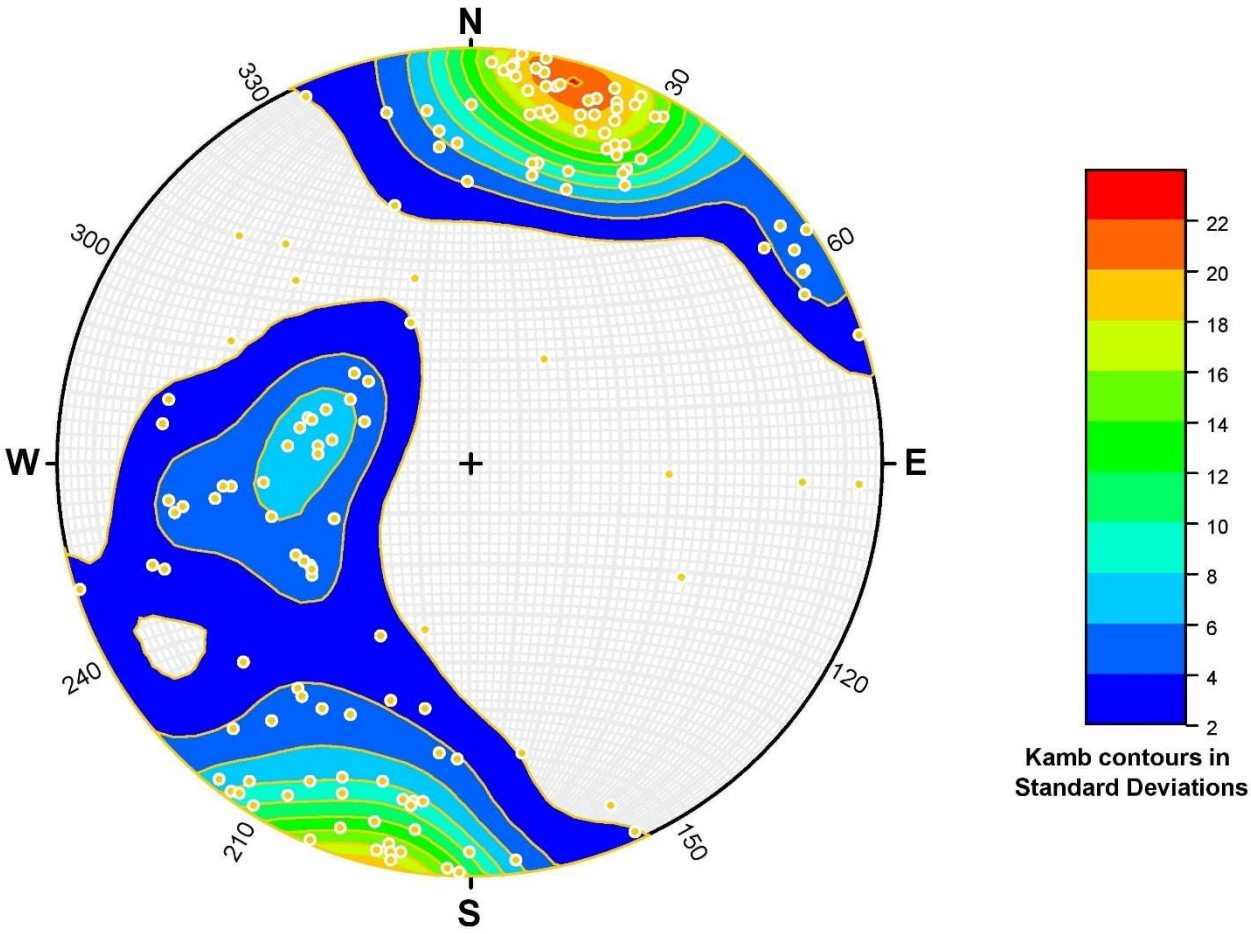

Figure 119 - Kamb contouring of joint poles for quartzite. N = 149.

Schist

Bedding

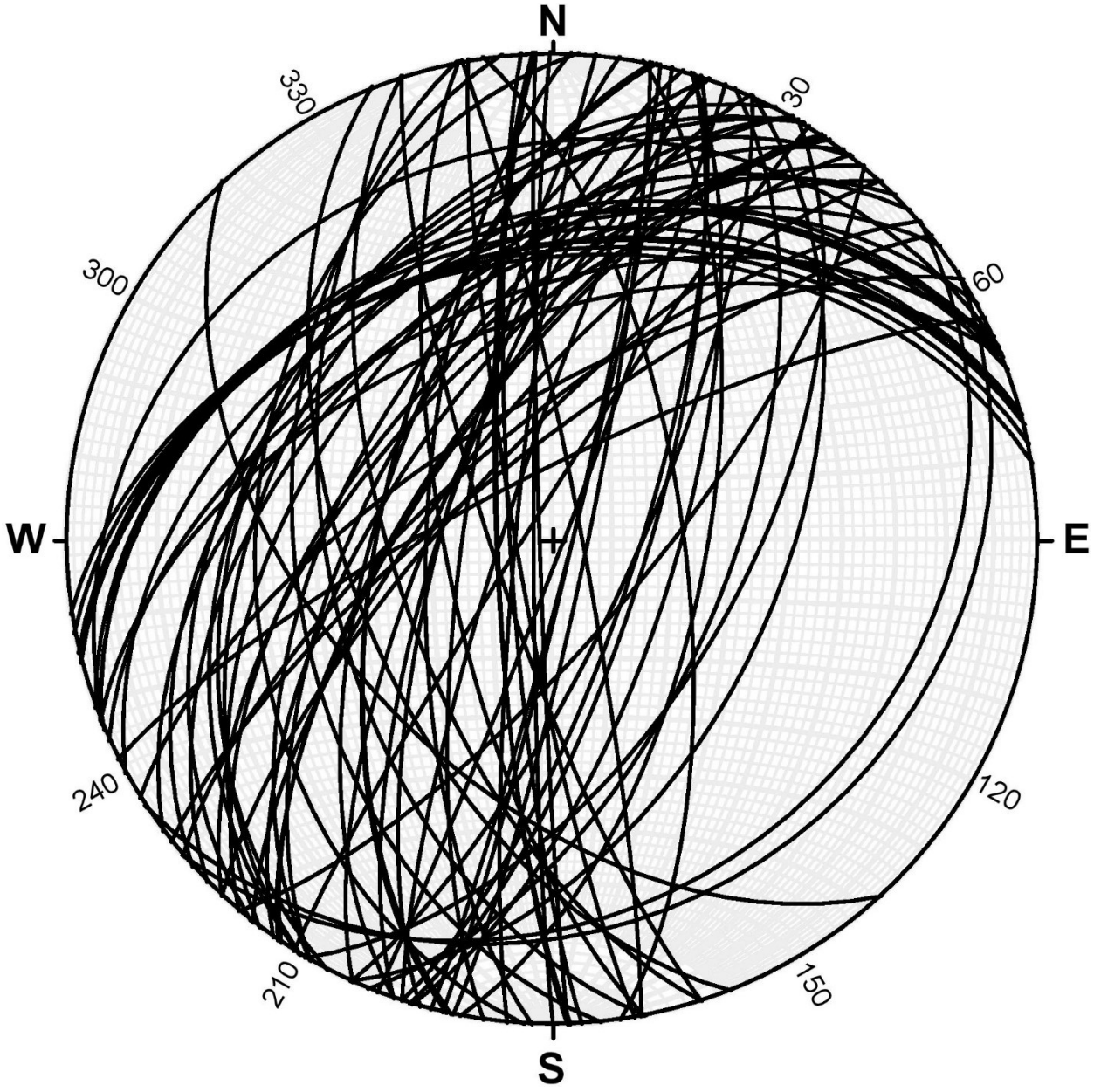

Figure 120 - Bedding planes for schist. N = 75.

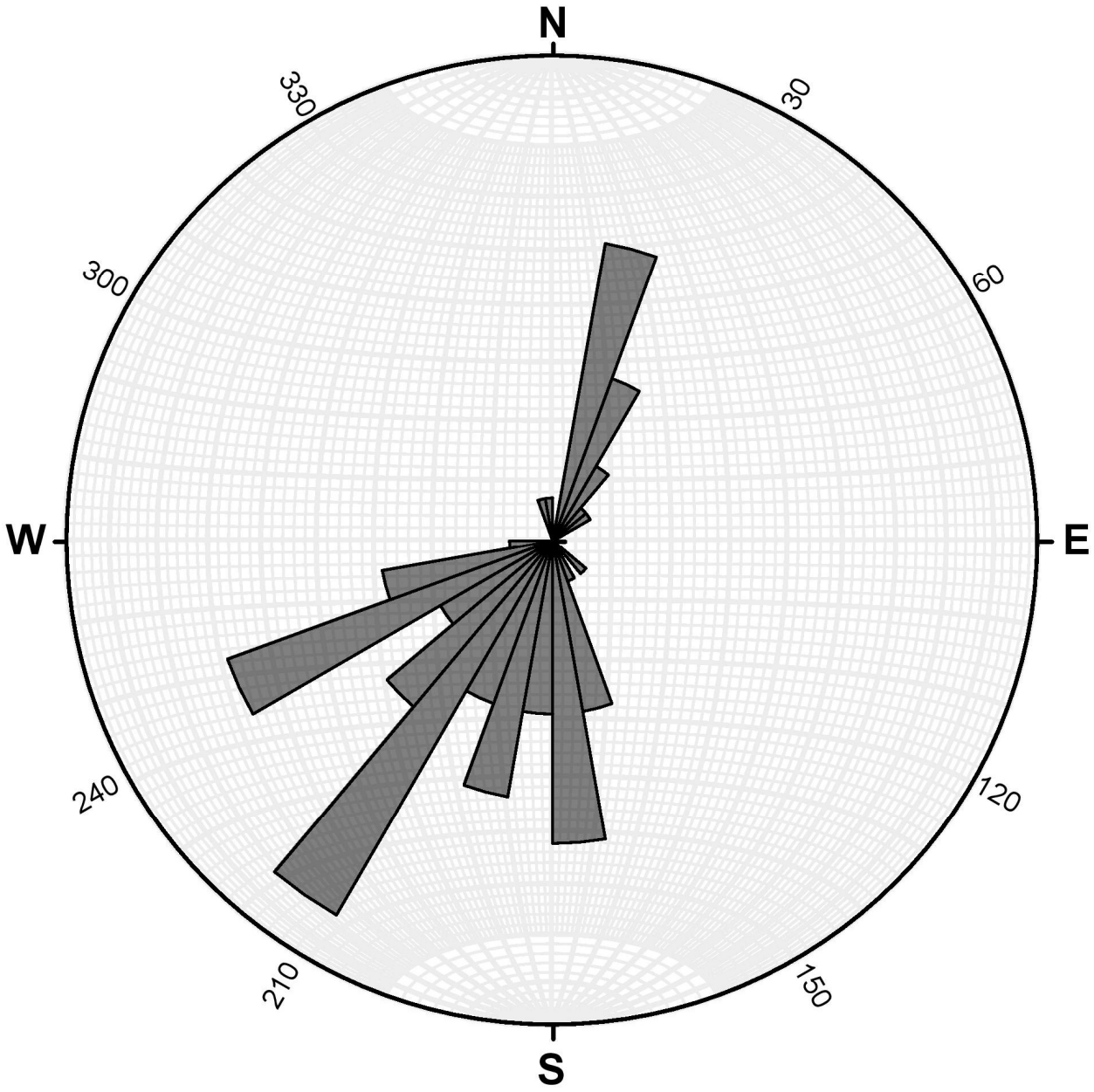

Figure 121 - Rose diagram of bedding planes for schist. N = 75.

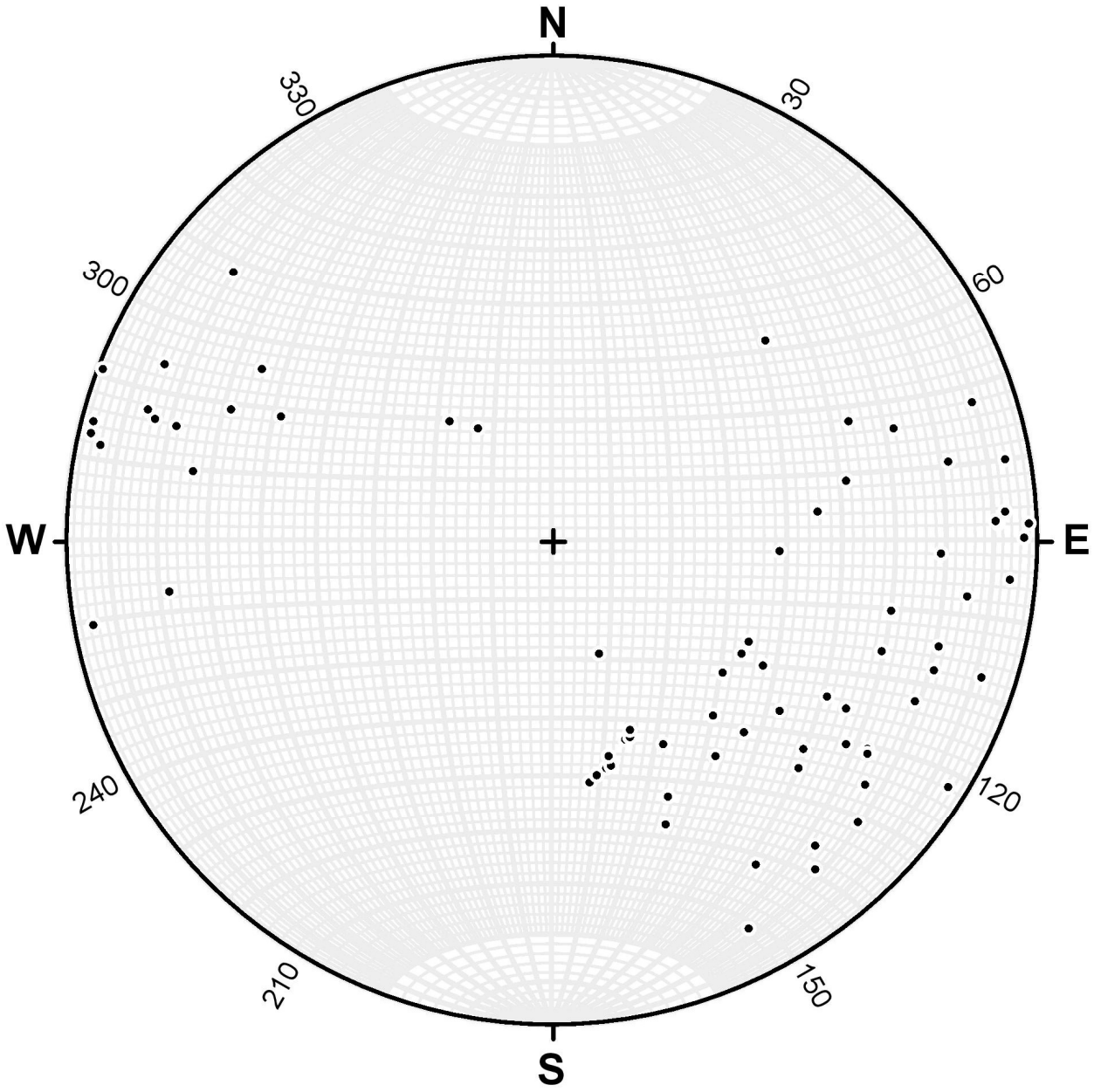

Figure 122 - Bedding poles for schist. N = 75.

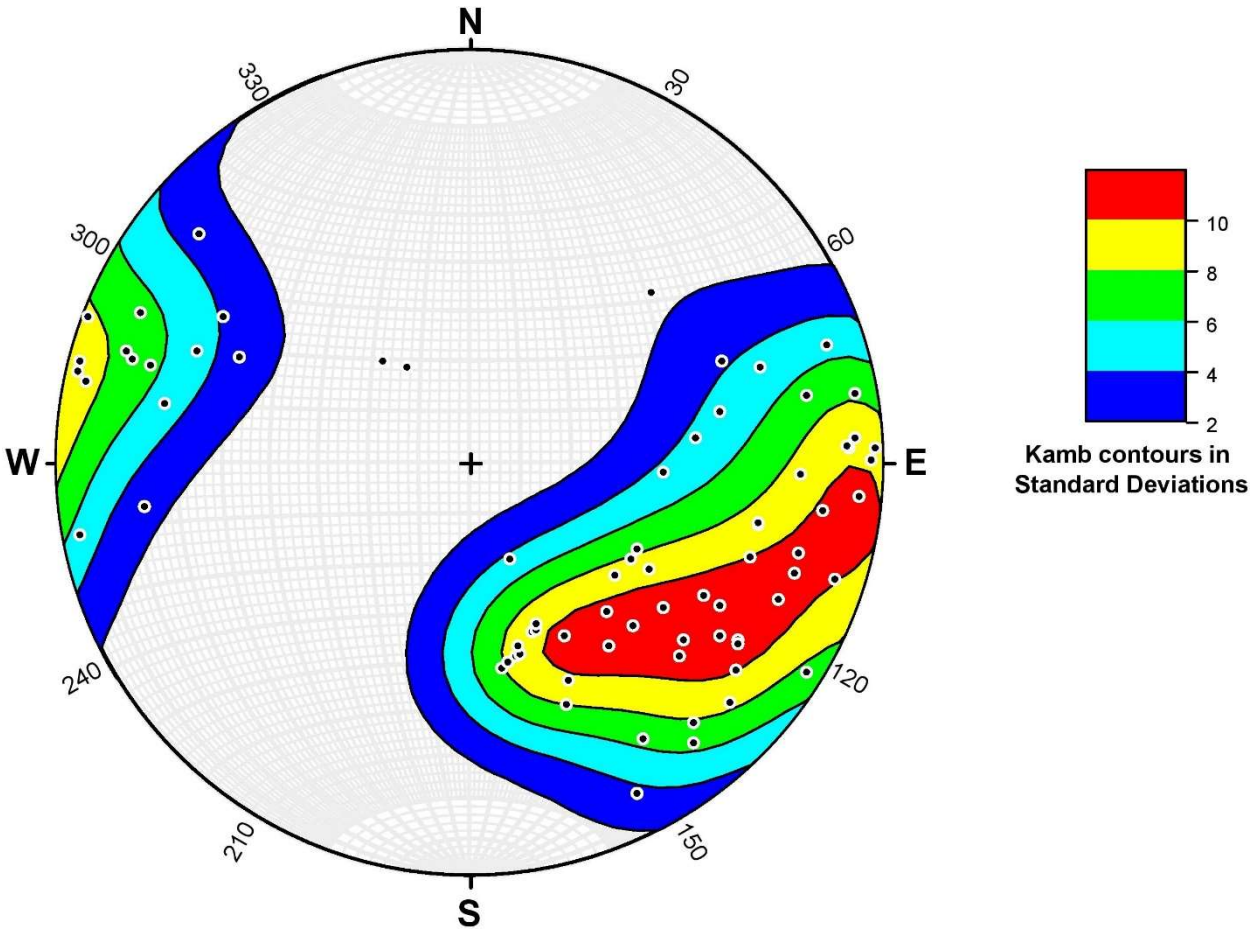

Figure 123 - Kamb contouring of bedding poles for schist. N = 75.

Jointing

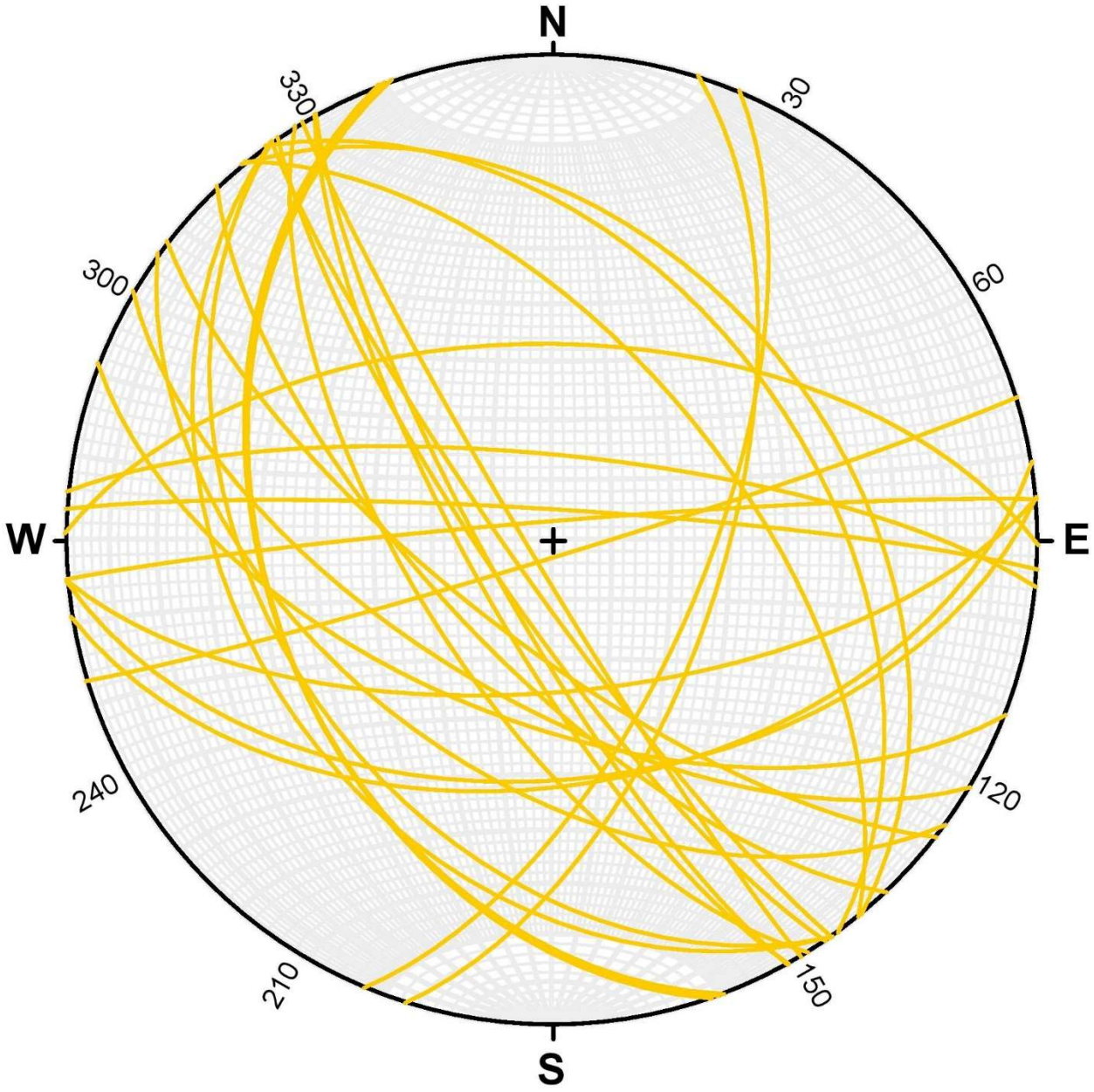

Figure 124 - Joint planes for schist. N = 29.

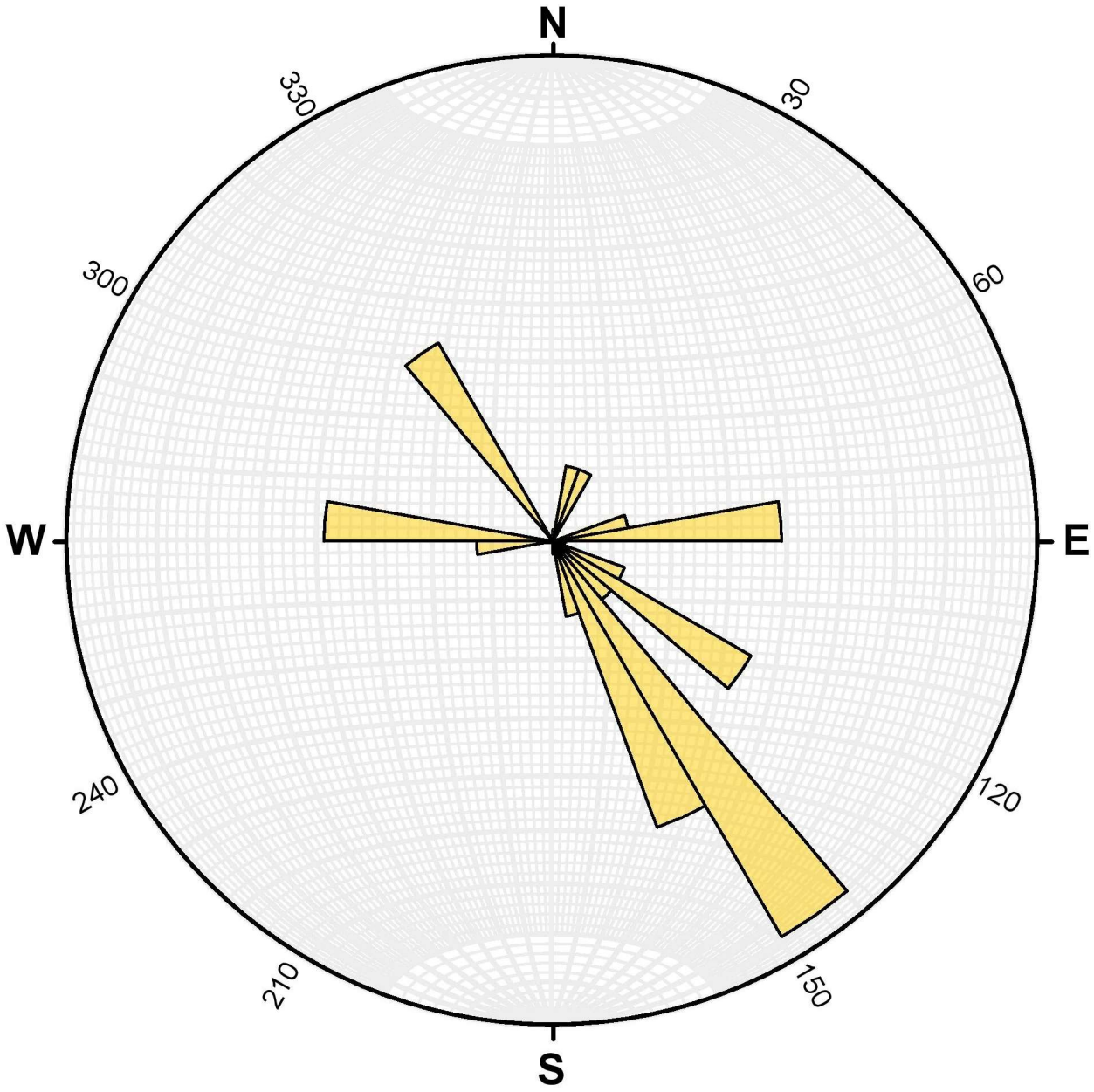

Figure 125 - Rose diagram of joint planes for schist. N = 29.

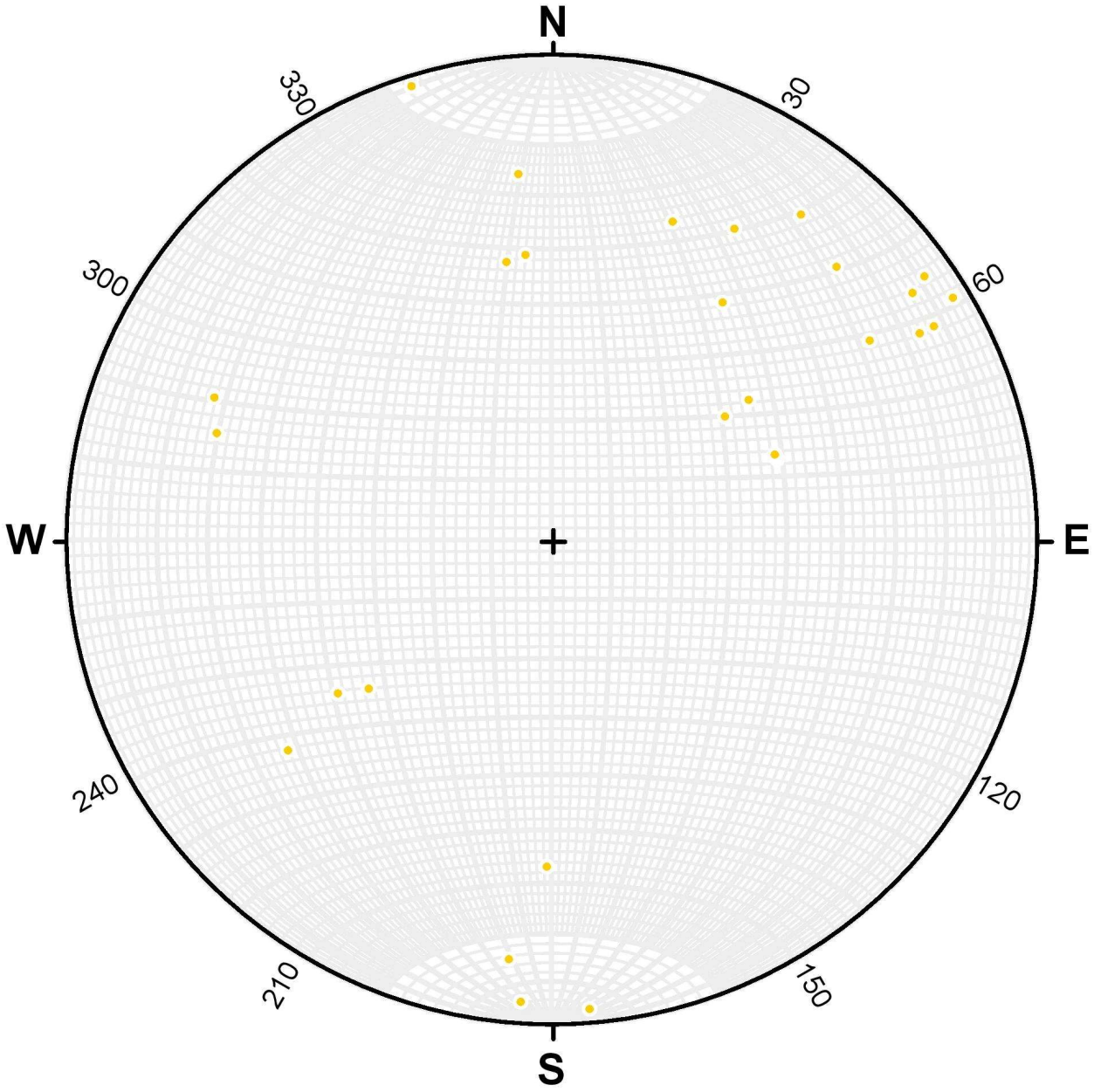

Figure 126 - Joint poles for schist. N = 29.

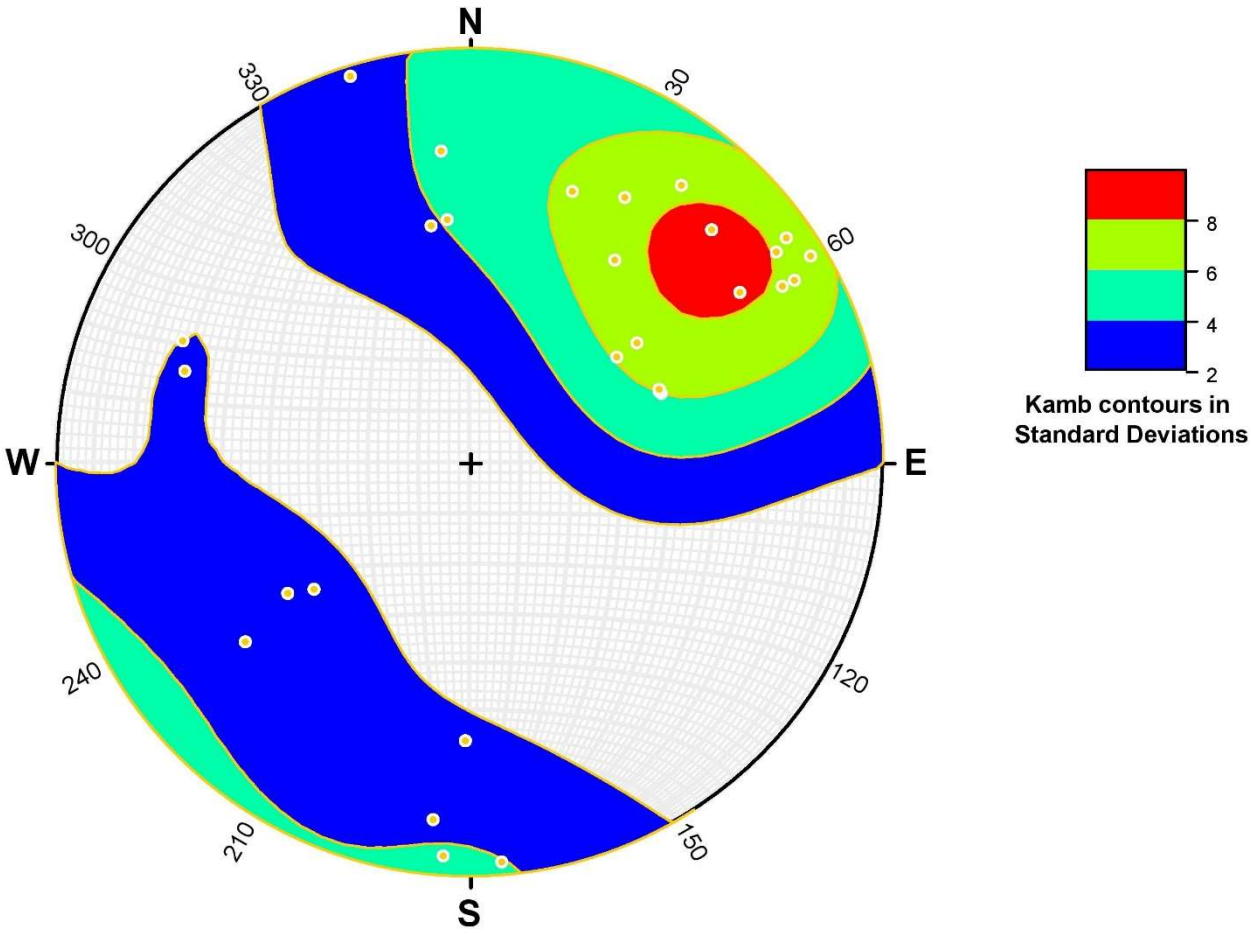

Figure 127 - Kamb contouring of joint poles for schist. N = 29.

Plots by Geographic Location

Grey Creek

Bedding

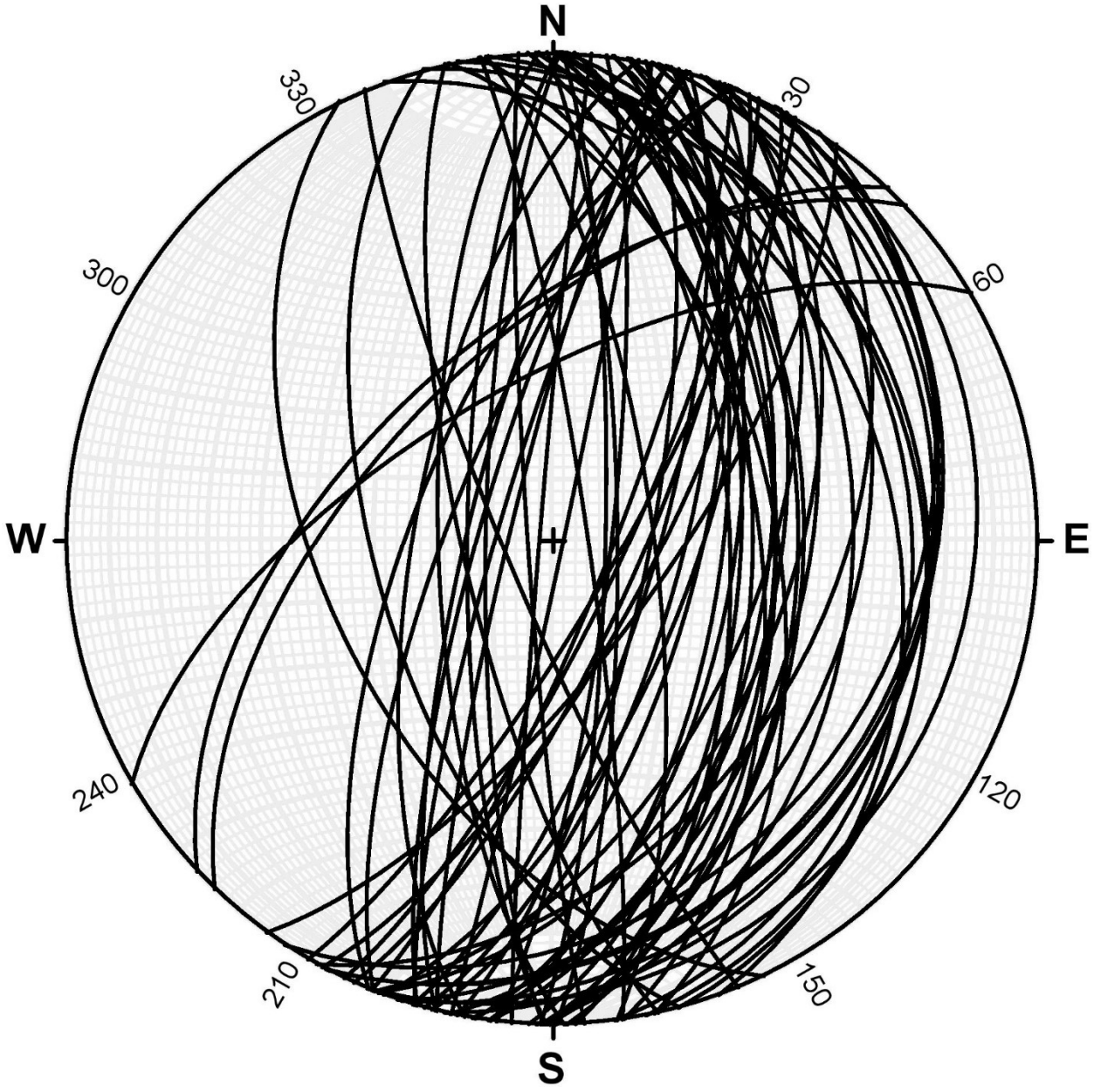

Figure 128 - Bedding planes for Grey Creek. N = 65.

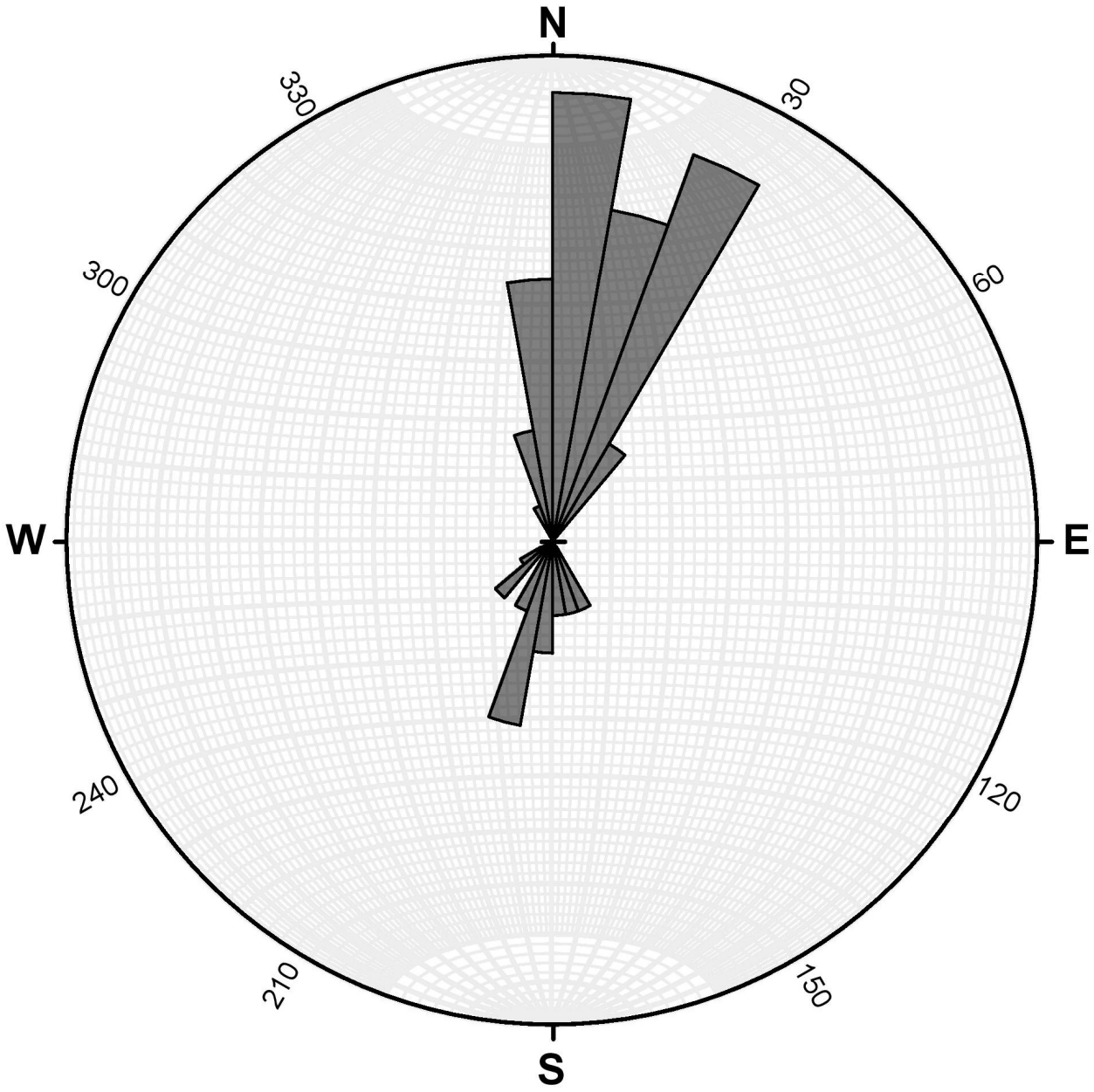

Figure 129 - Rose diagram of bedding planes for Grey Creek. N = 65.

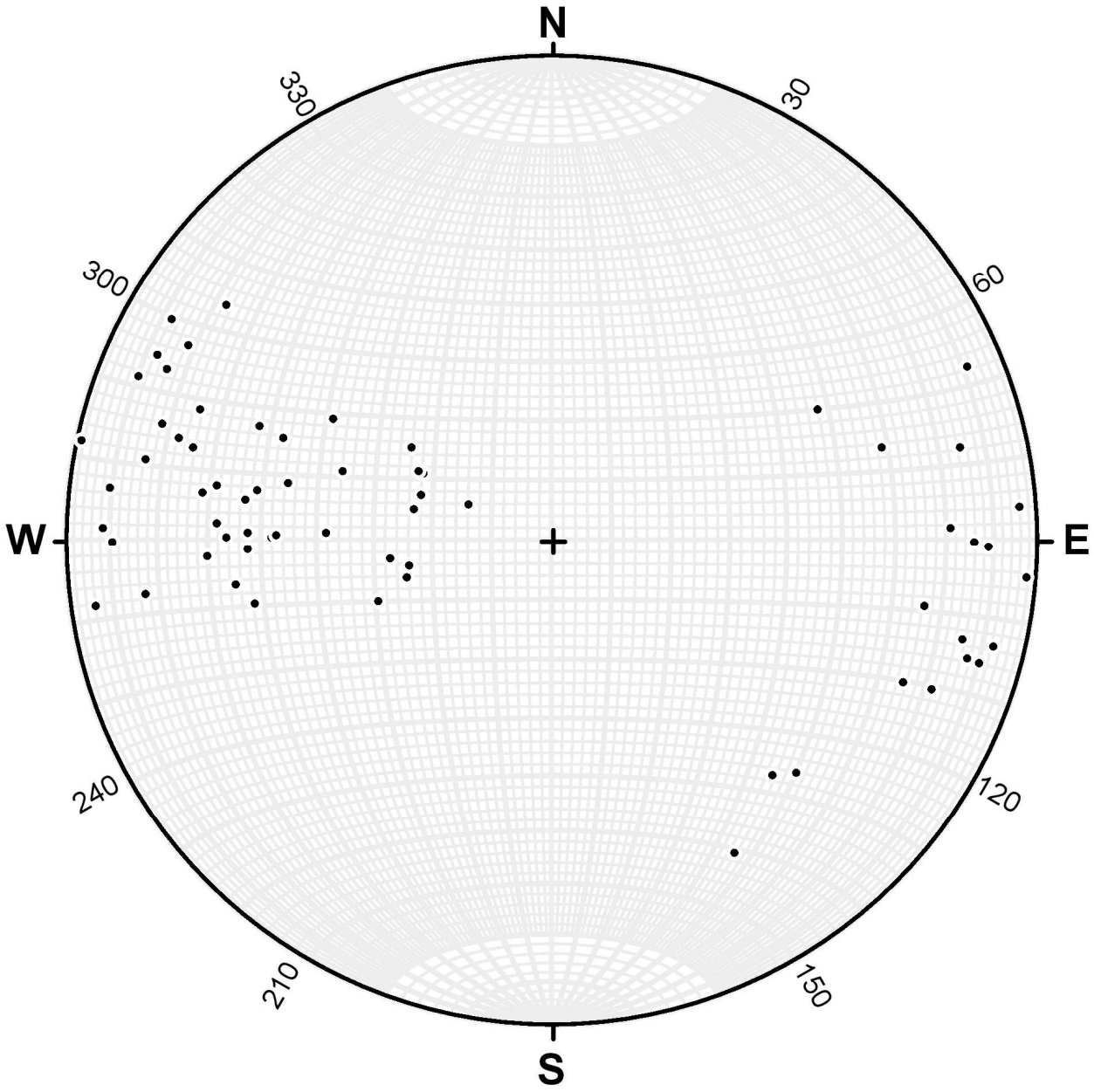

Figure 130 - Bedding poles for Grey Creek. N = 65.

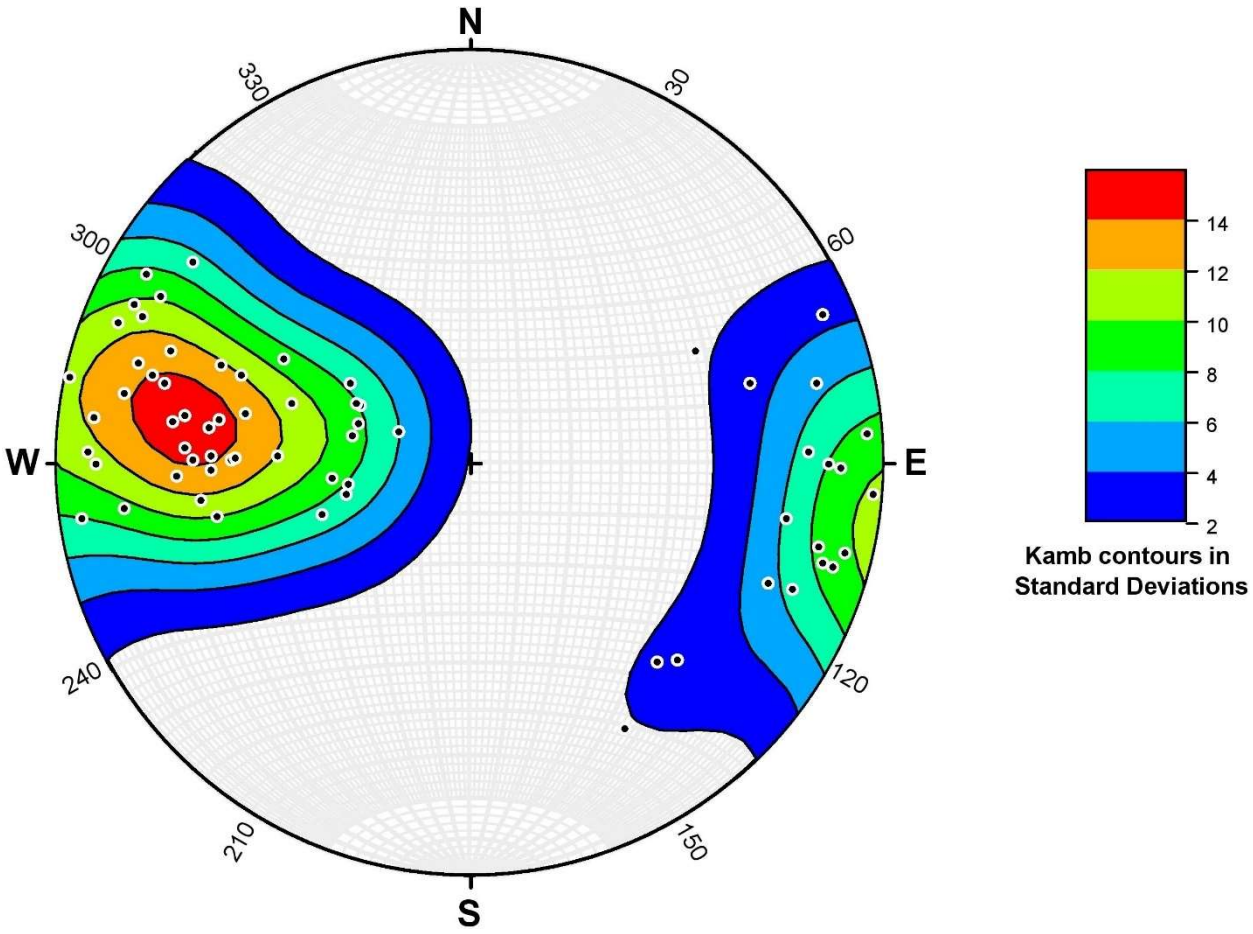

Figure 131 - Kamb contouring of bedding poles for Grey Creek. N = 65.

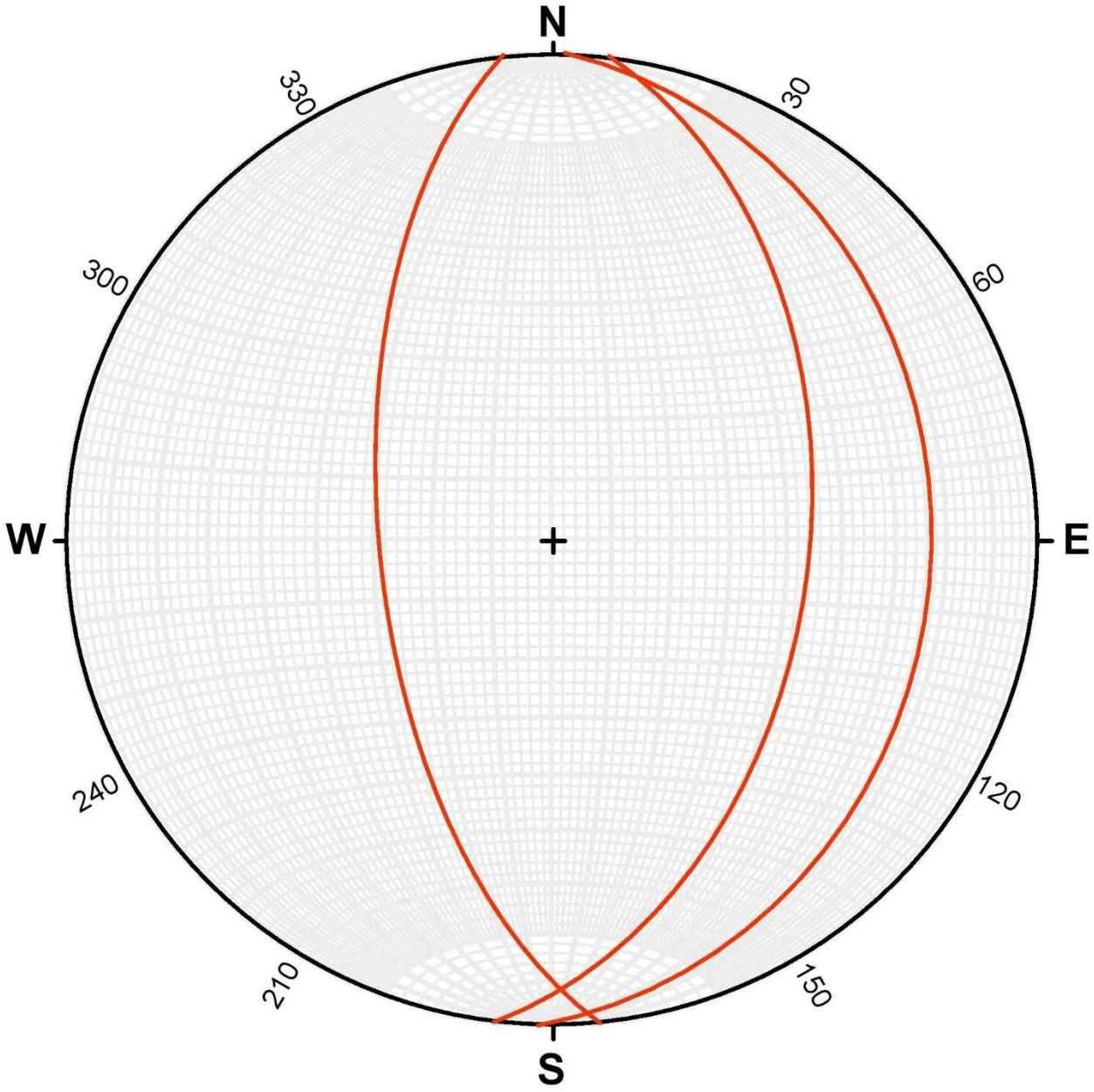

Figure 132 - Fault planes for Grey Creek. N = 3.

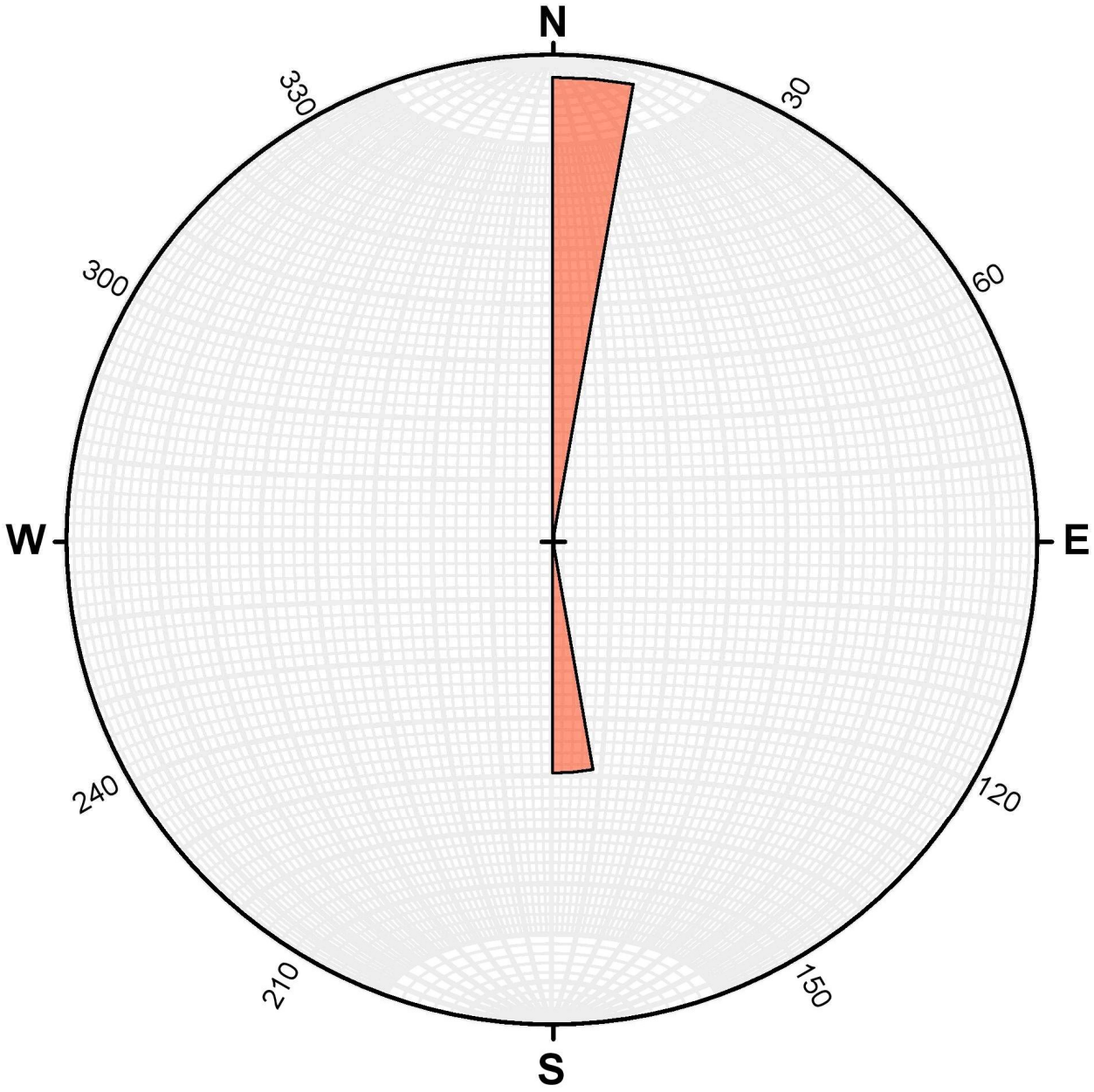

Figure 133 - Rose diagram of fault planes for Grey Creek. N = 3.

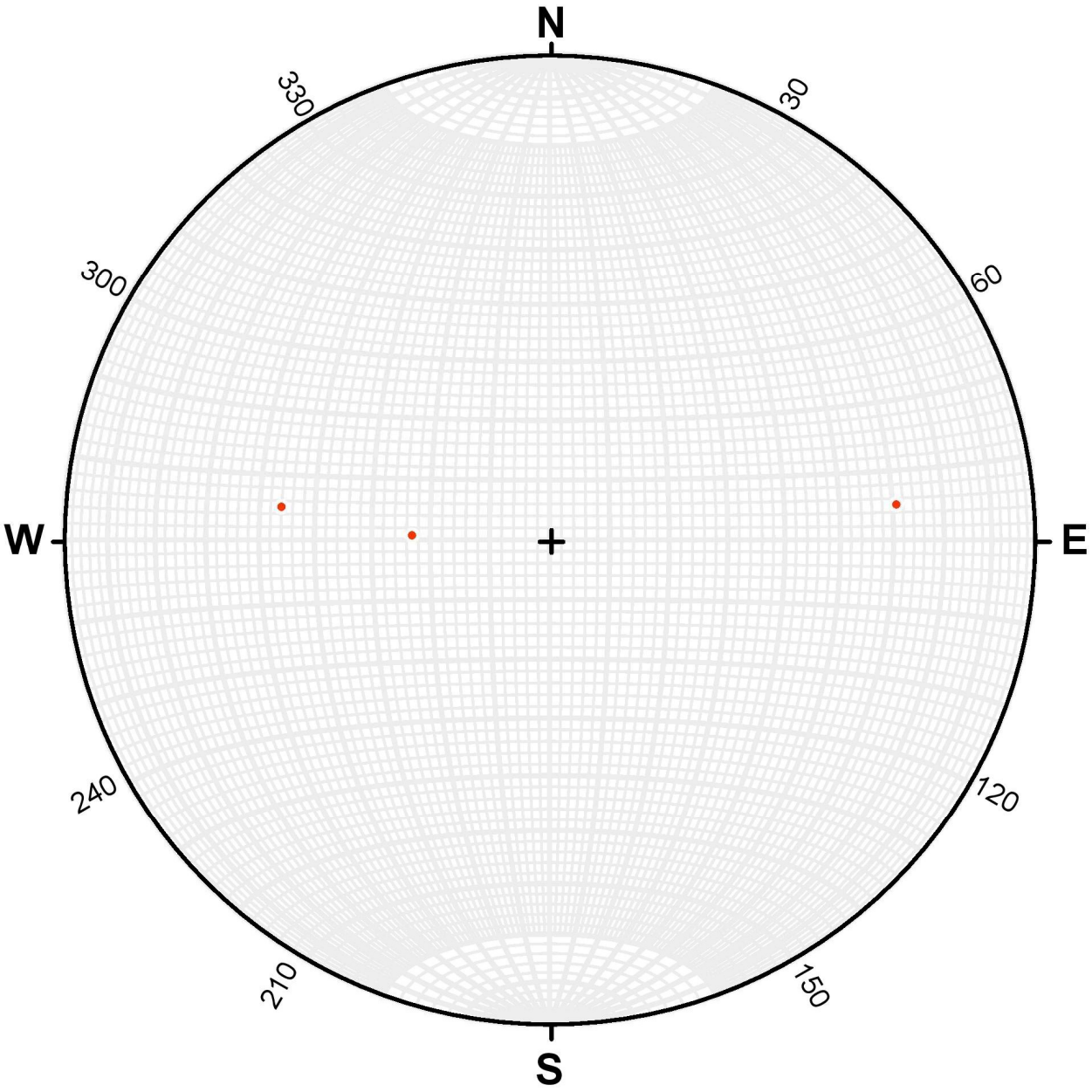

Figure 134 - Fault poles for Grey Creek. N = 3.

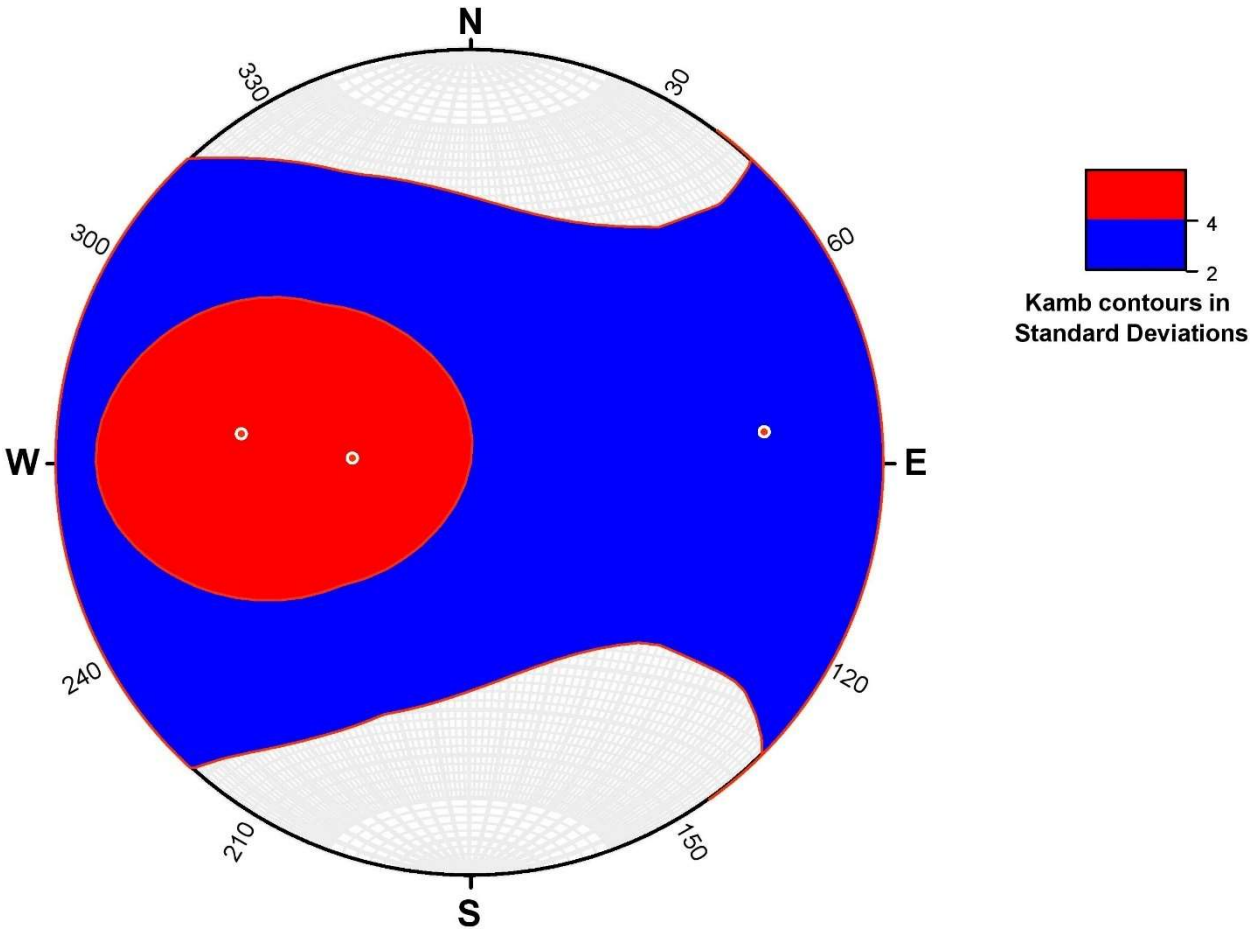

Figure 135 - Kamb contouring of fault poles for Grey Creek. N = 3.

Jointing

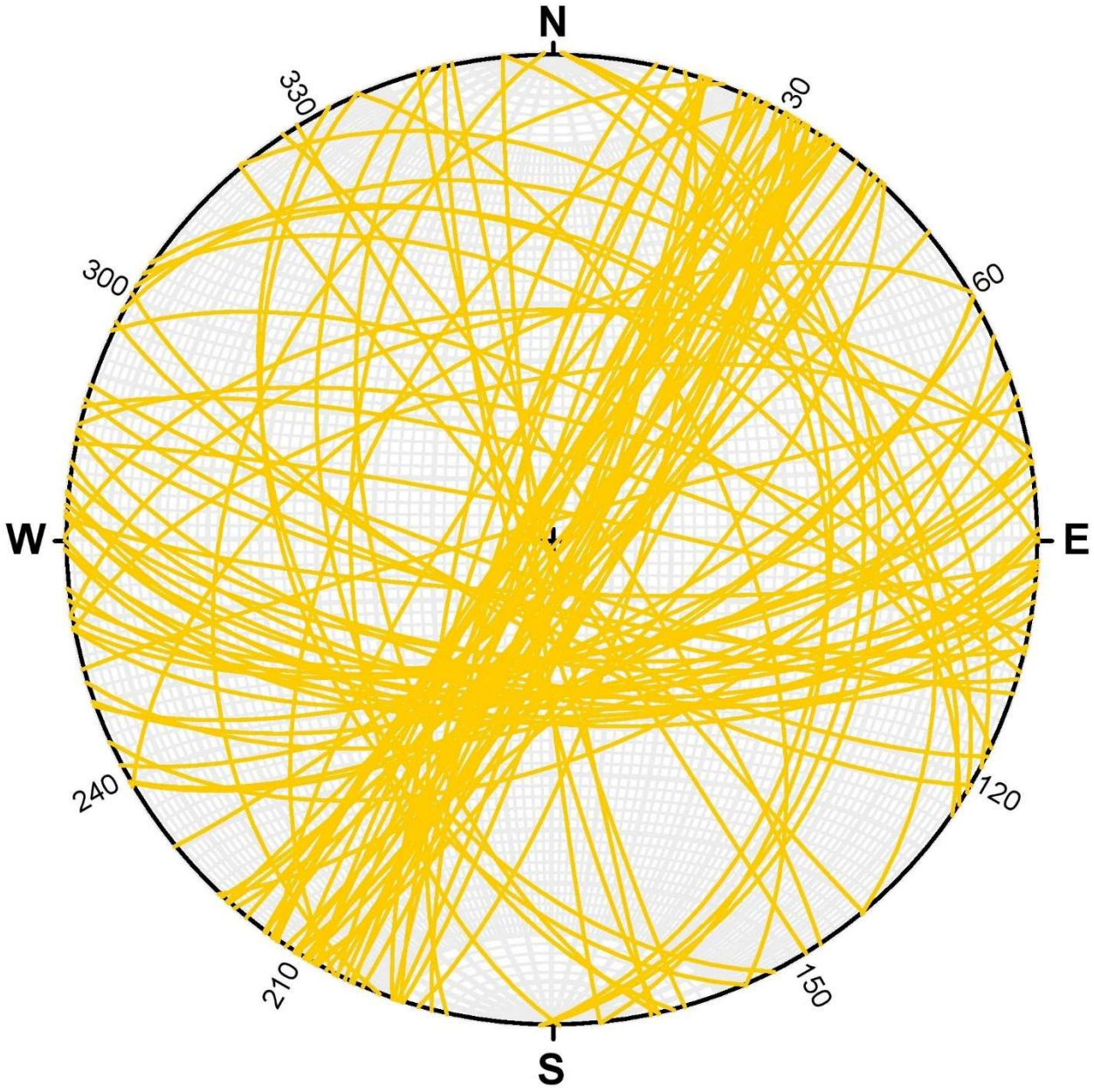

Figure 136 - Joint planes for Grey Creek. N = 103.

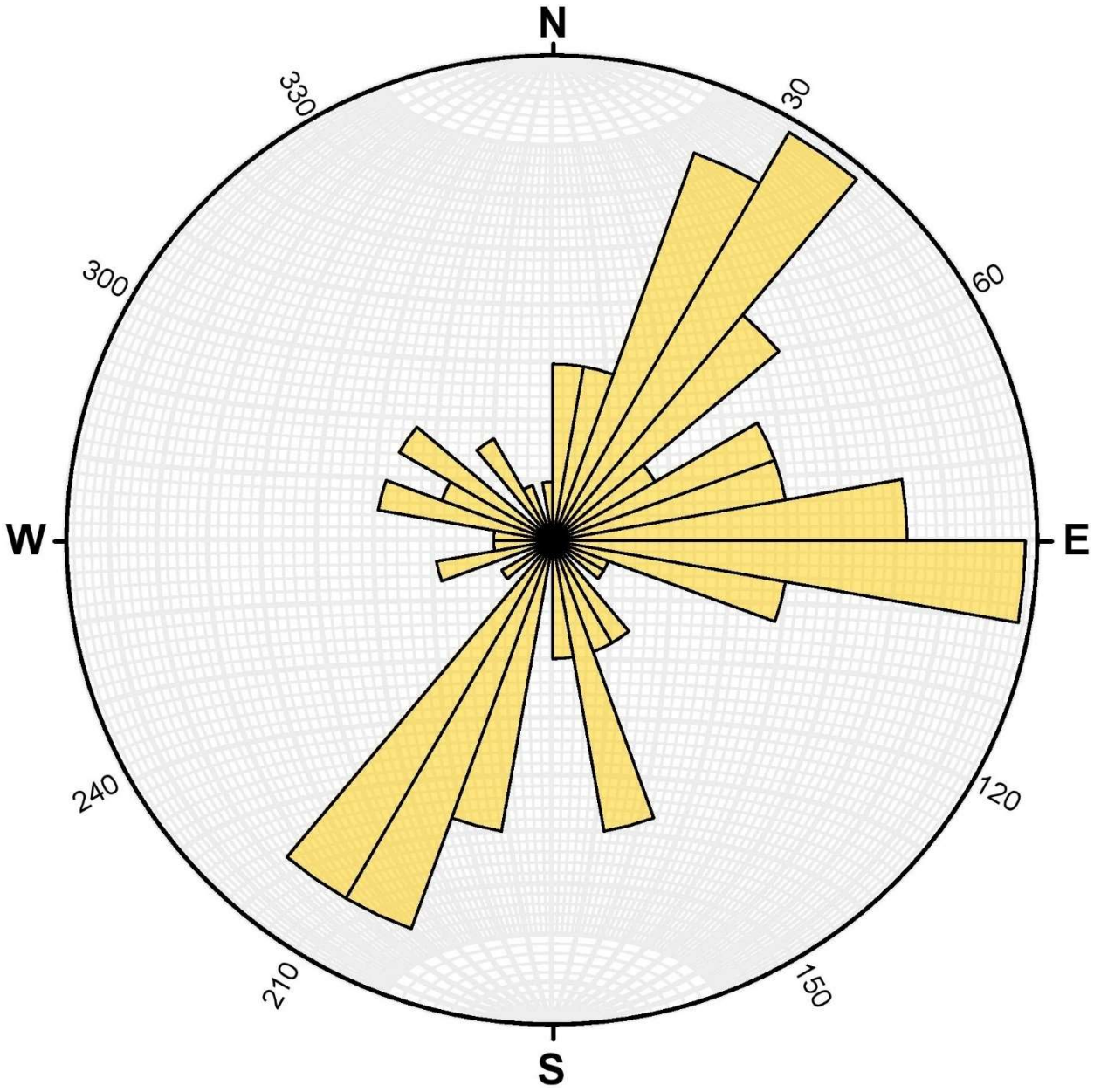

Figure 137 - Rose diagram of joint planes for Grey Creek. N = 103.

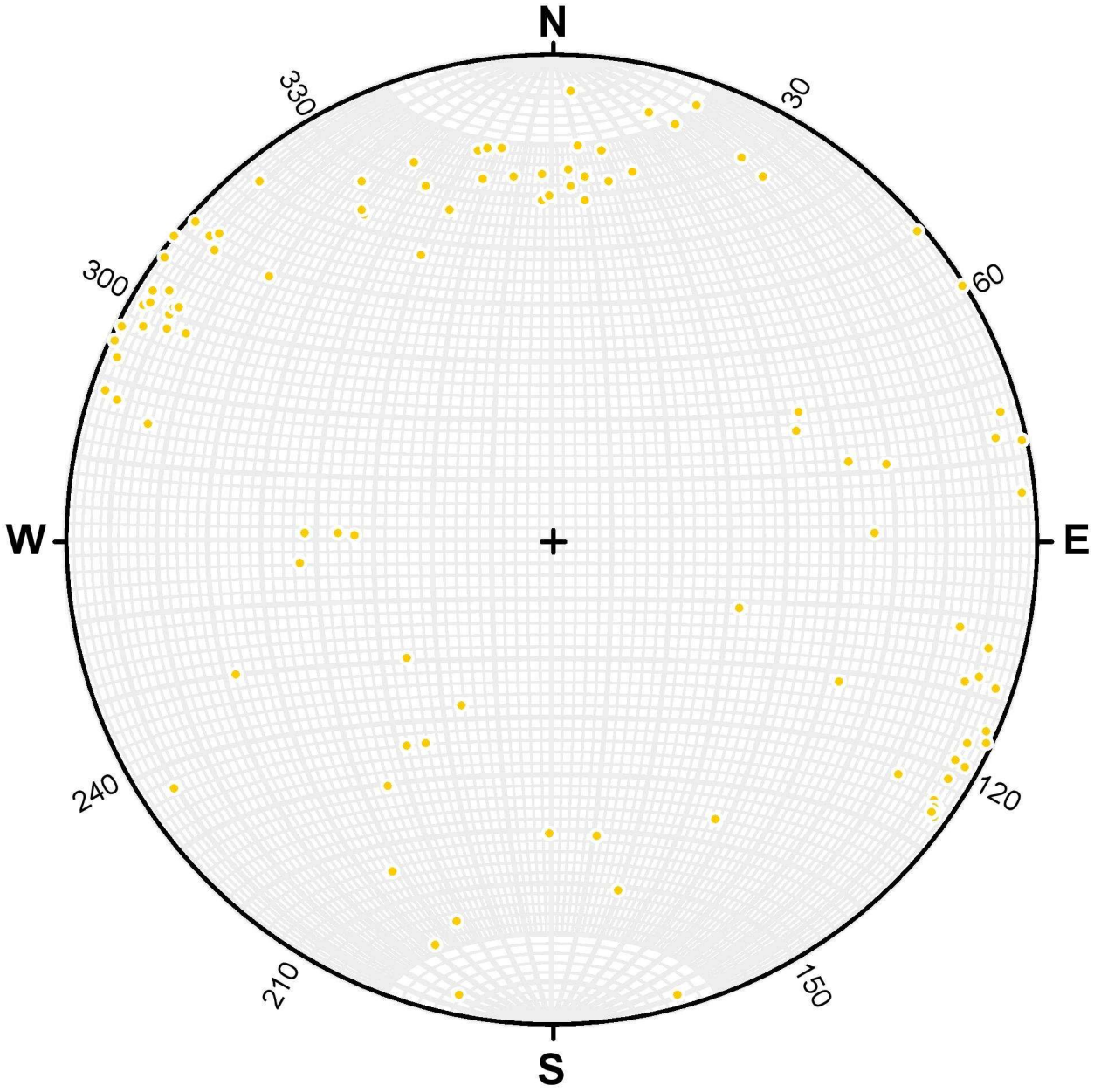

Figure 138 - Joint poles for Grey Creek. N = 103.

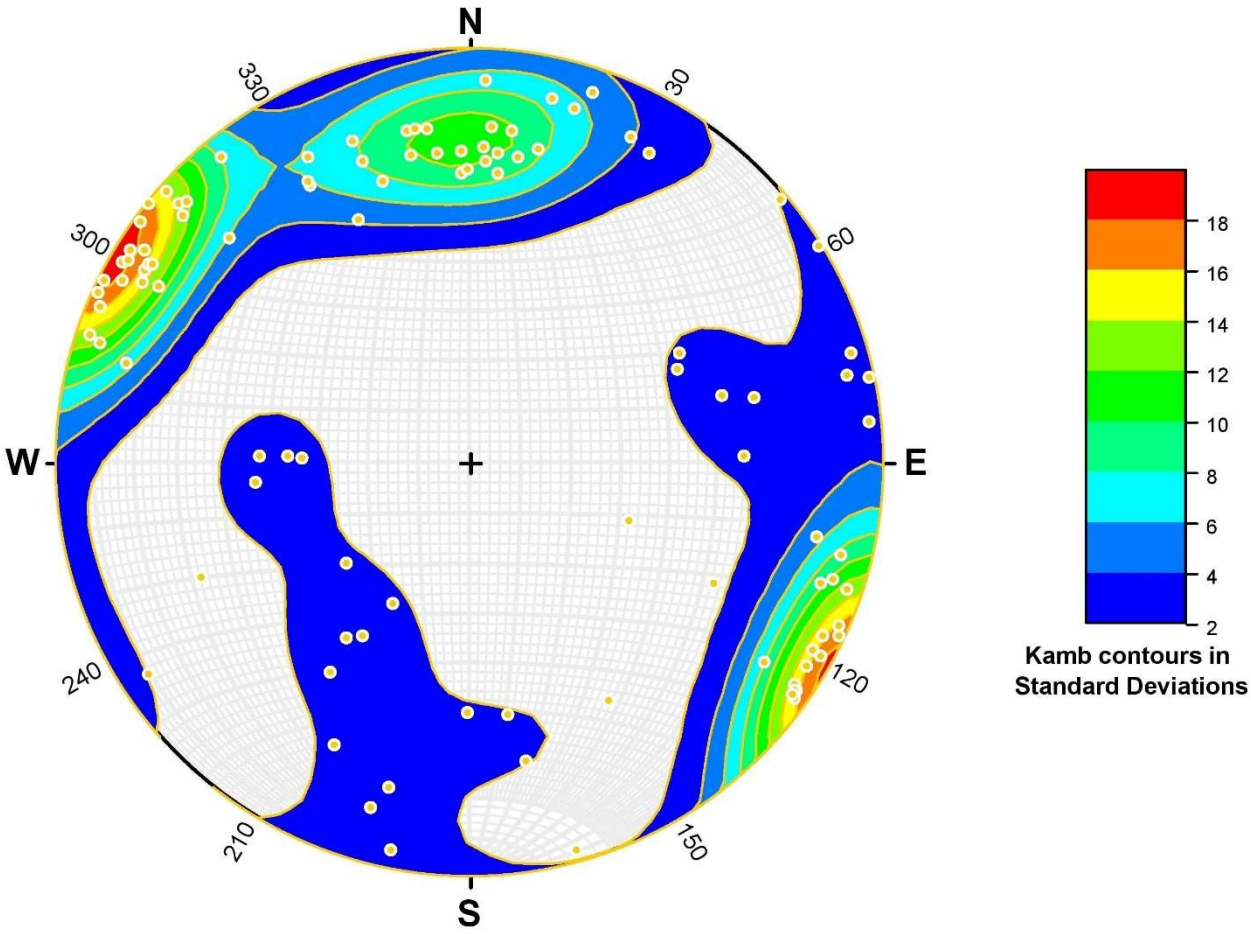

Figure 139 - Kamb contouring of joint poles for Grey Creek. N = 103.

Lower Crawford Creek

Bedding

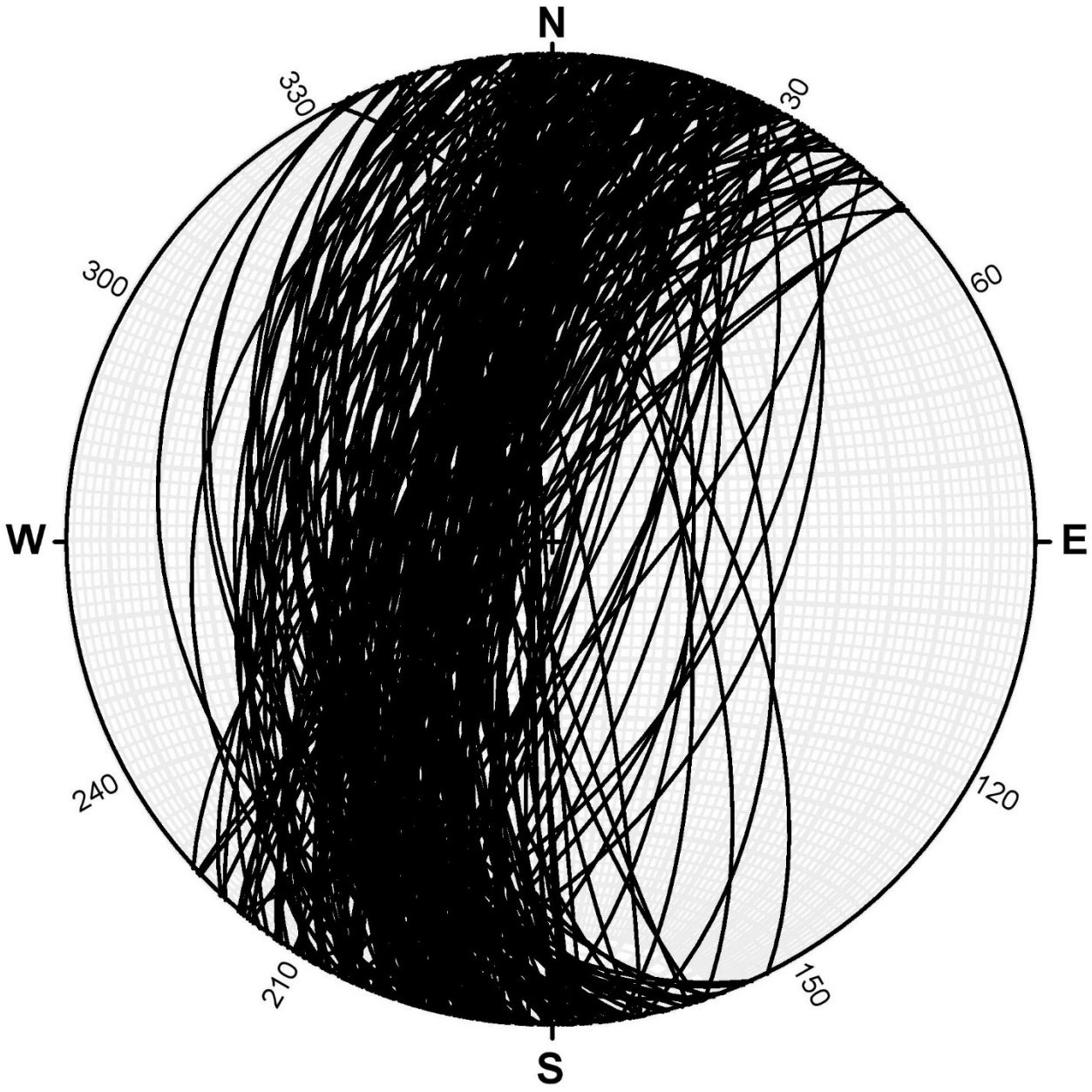

Figure 140 - Bedding planes for Lower Crawford Creek. N = 240.

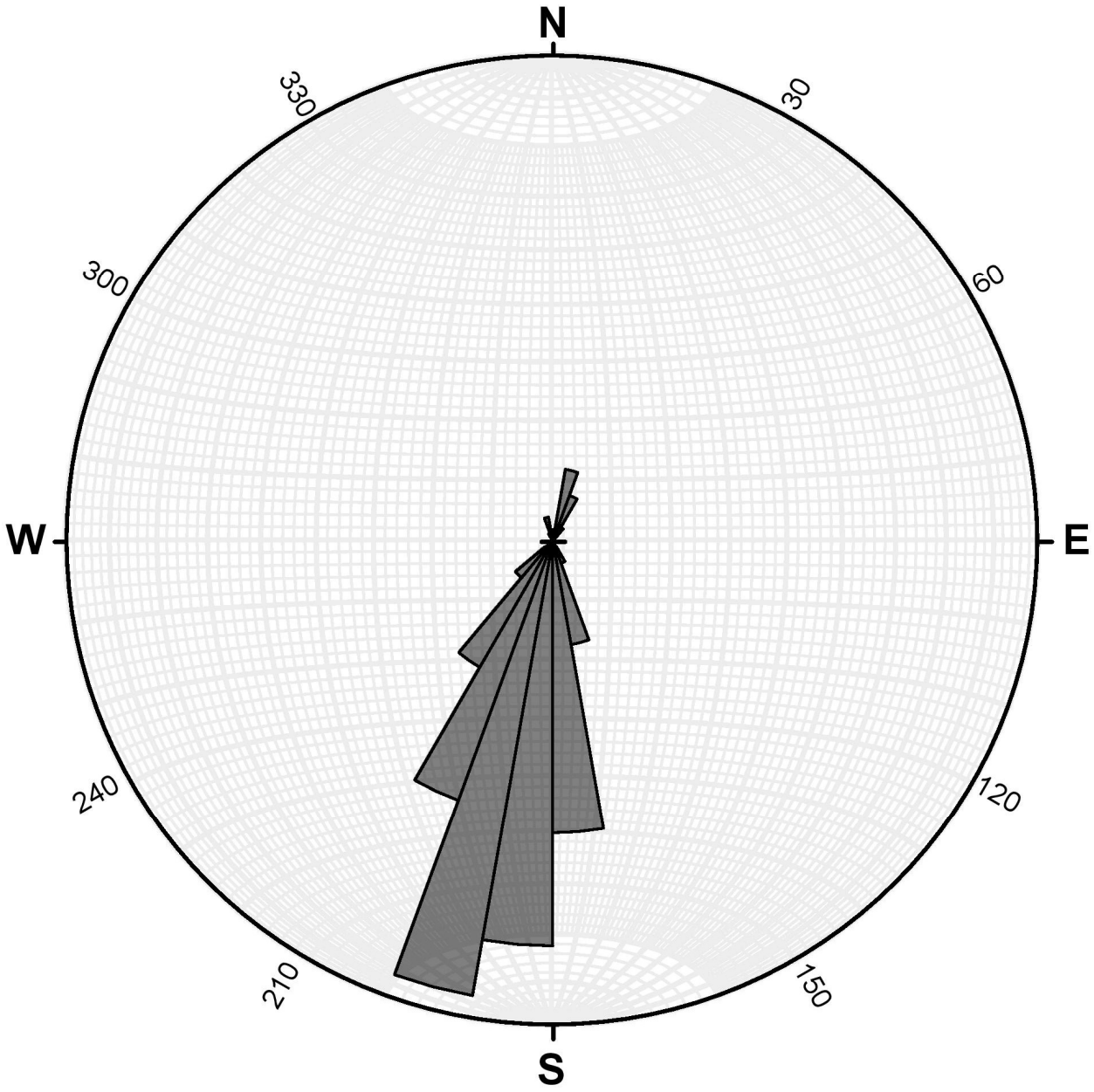

Figure 141 - Rose diagram of bedding planes for Lower Crawford Creek. N = 240.

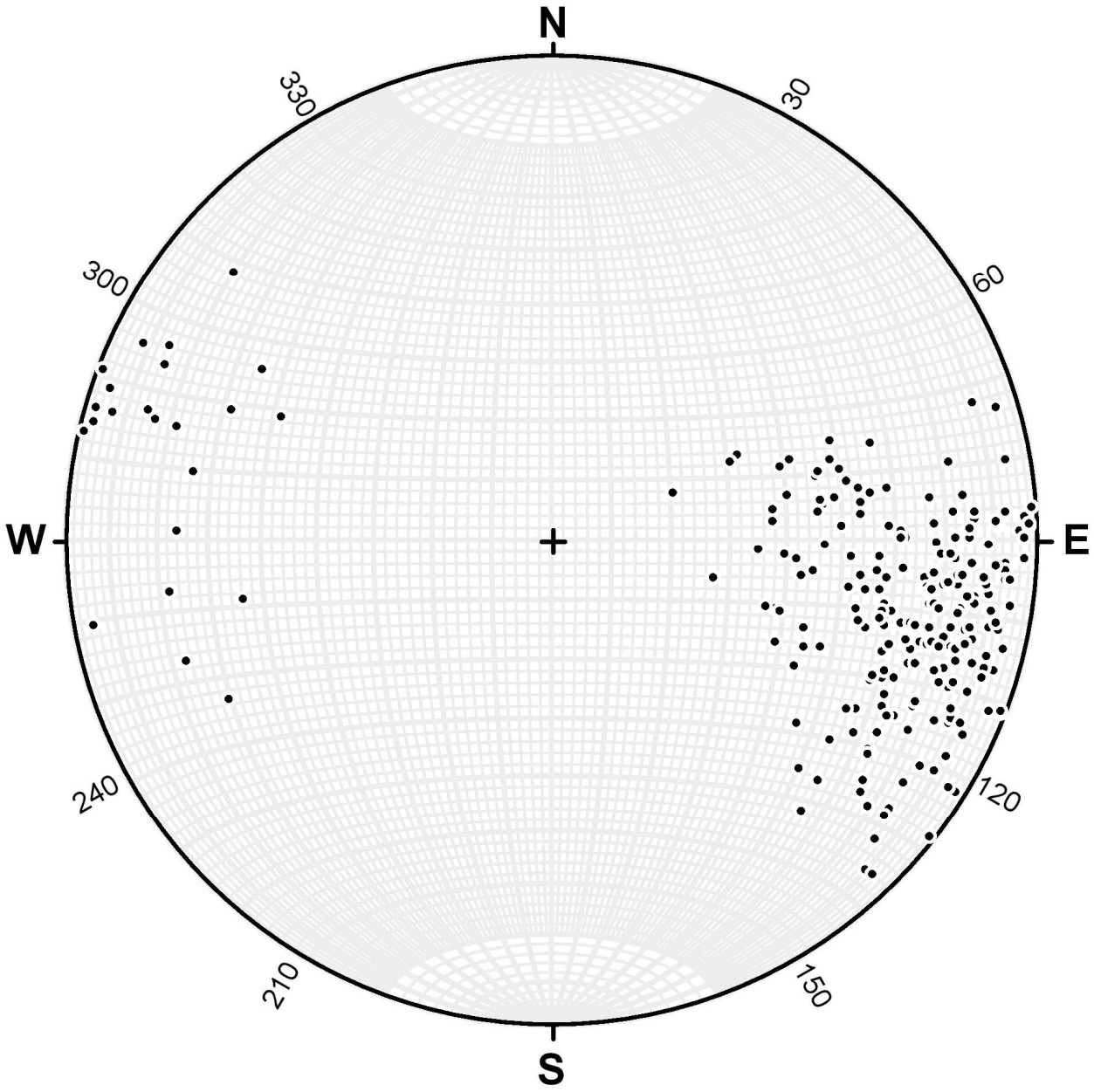

Figure 142 - Bedding poles for Lower Crawford Creek. N = 240.

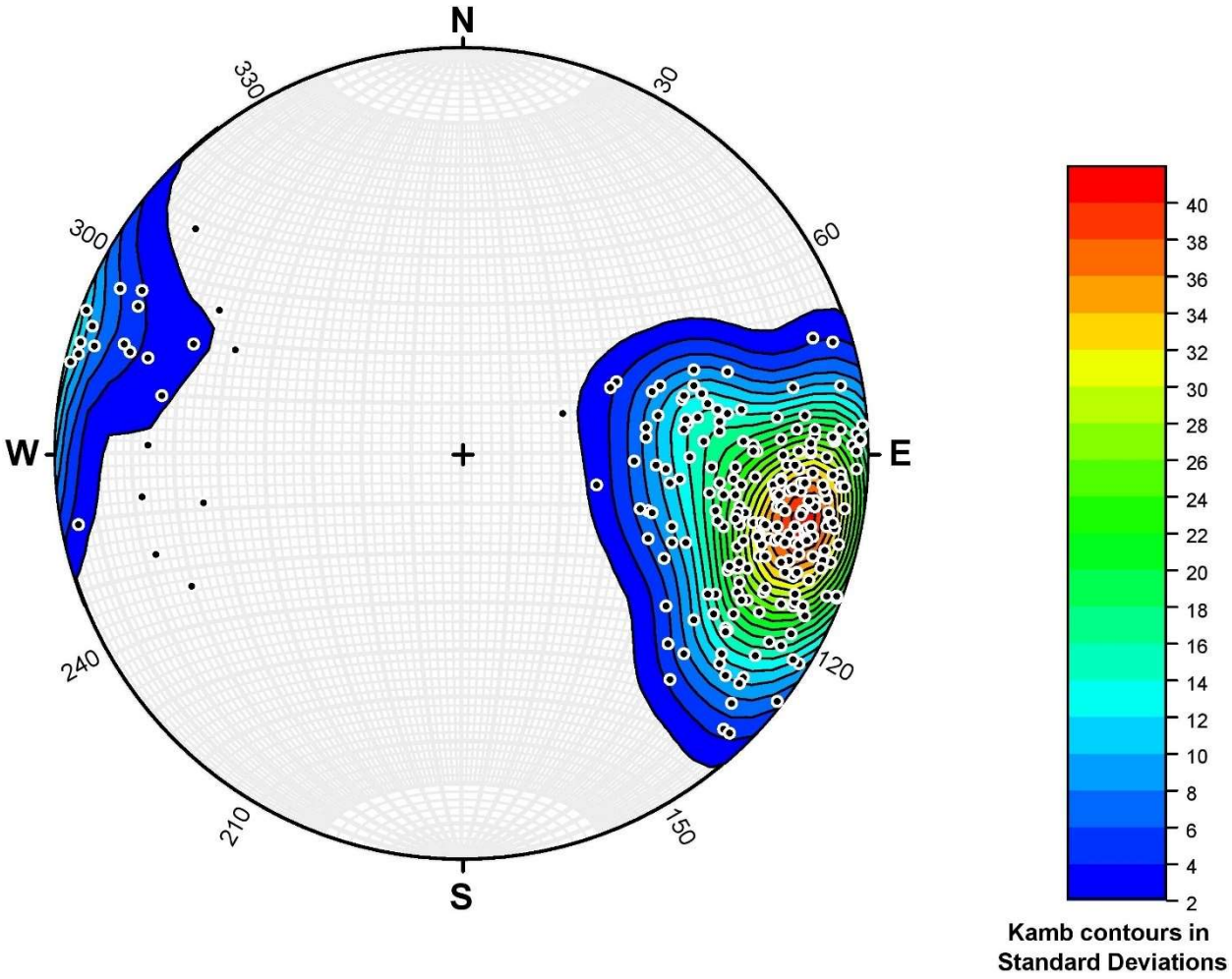

Figure 143 - Kamb contouring of bedding poles for Lower Crawford Creek. N = 240.

Faulting

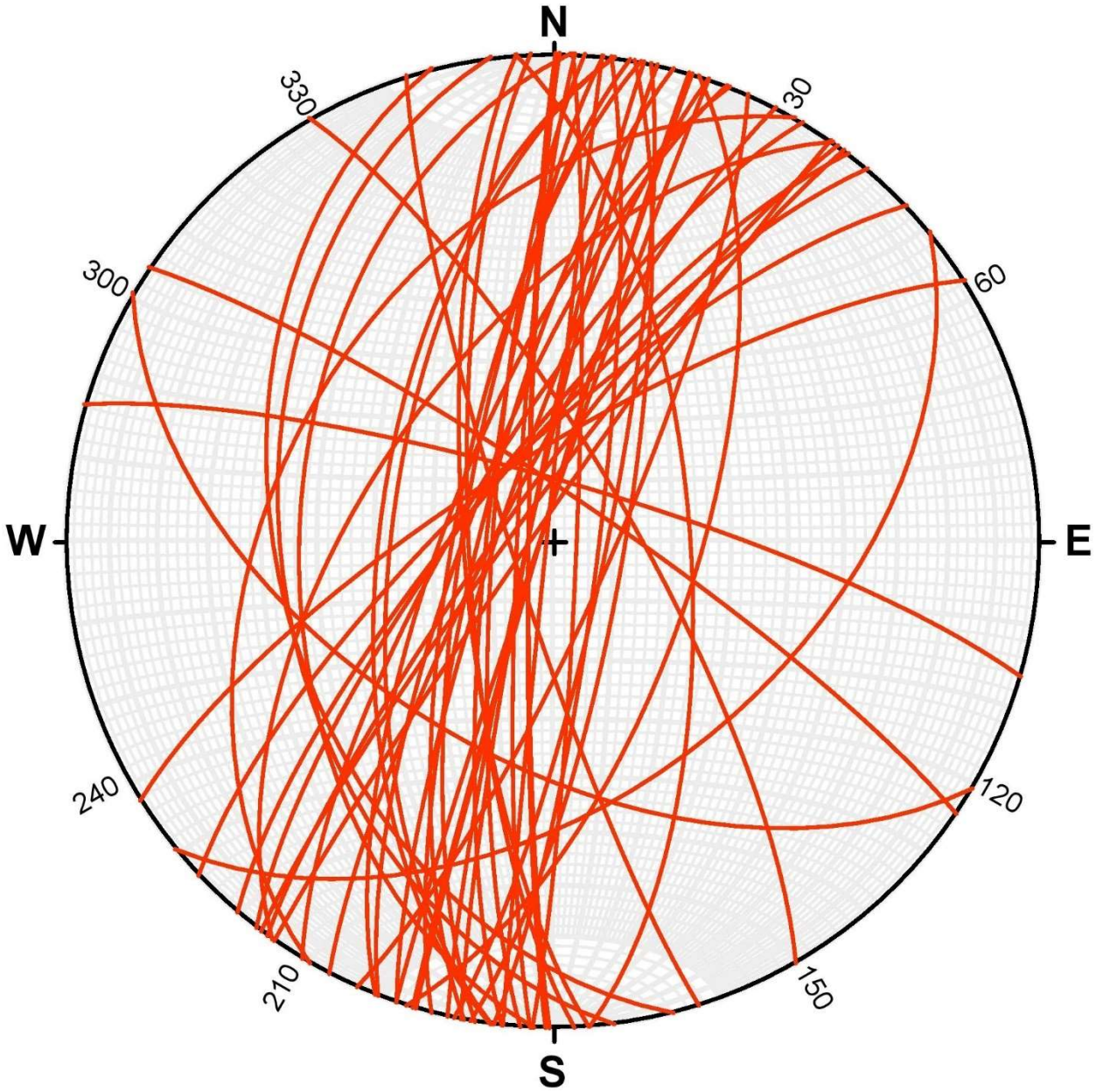

Figure 144 - Fault planes for Lower Crawford Creek. N = 48.

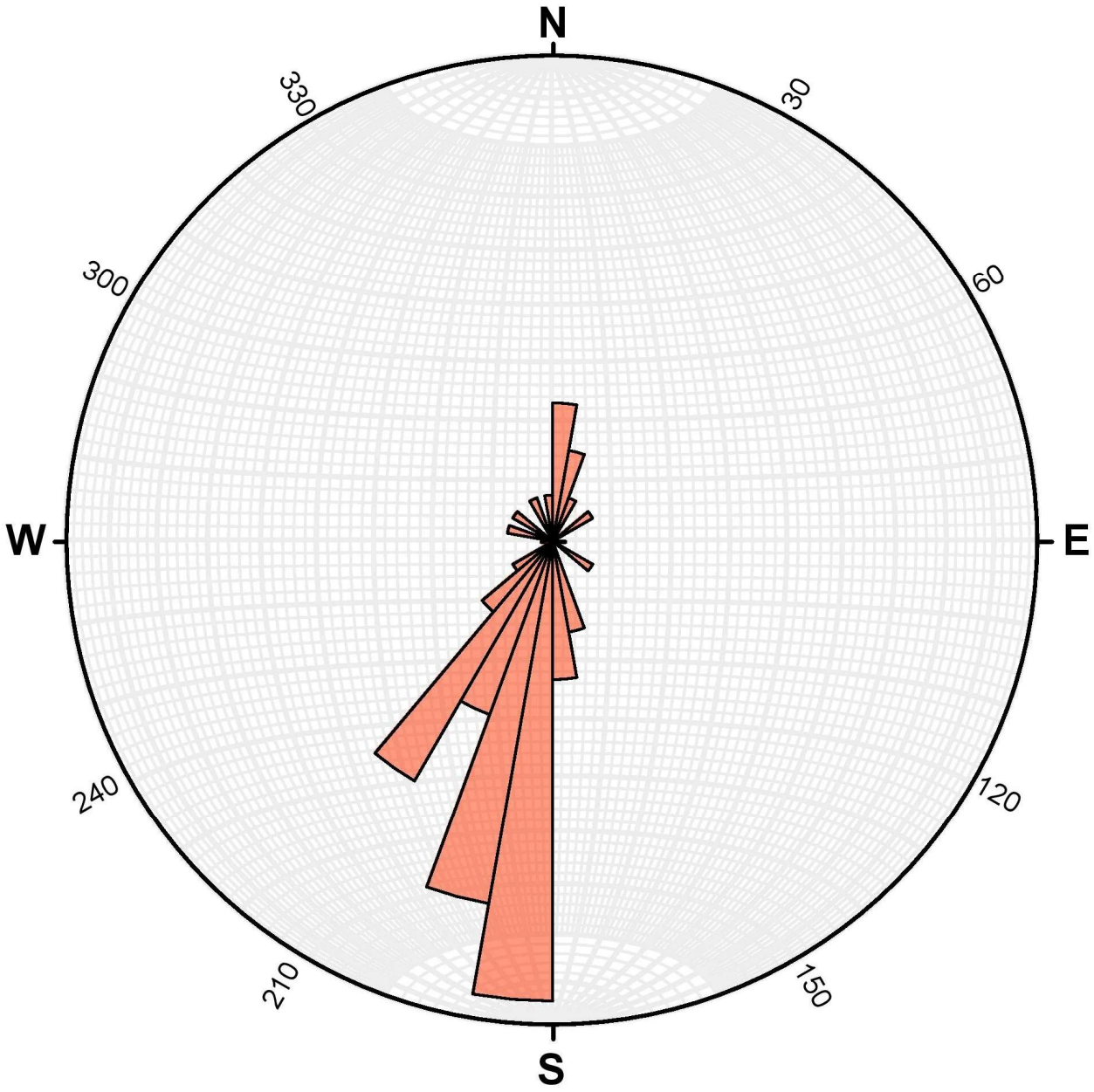

Figure 145 - Rose Diagram of Fault planes for Lower Crawford Creek. N = 48.

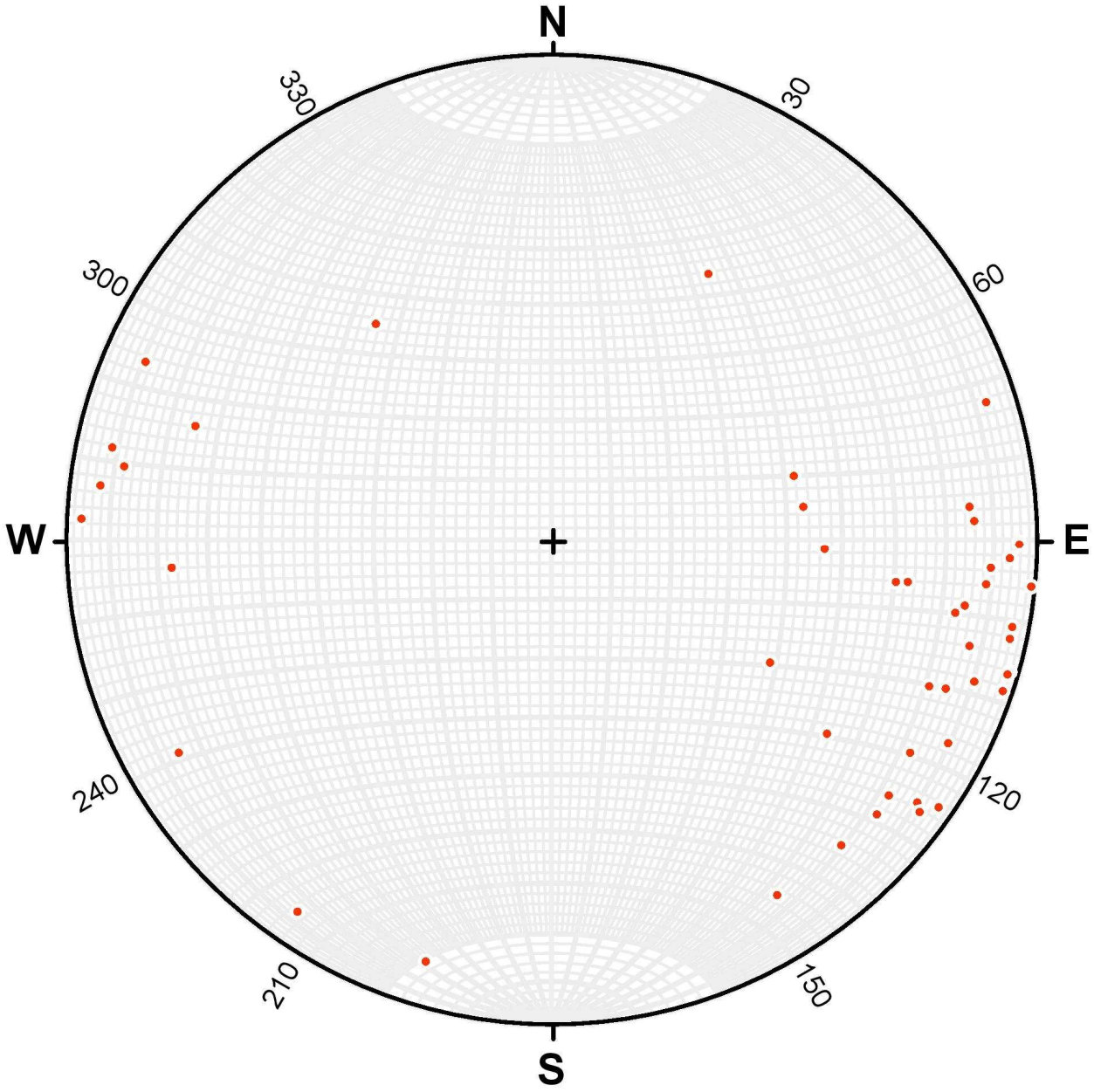

Figure 146 - Fault poles for Lower Crawford Creek. N = 48.

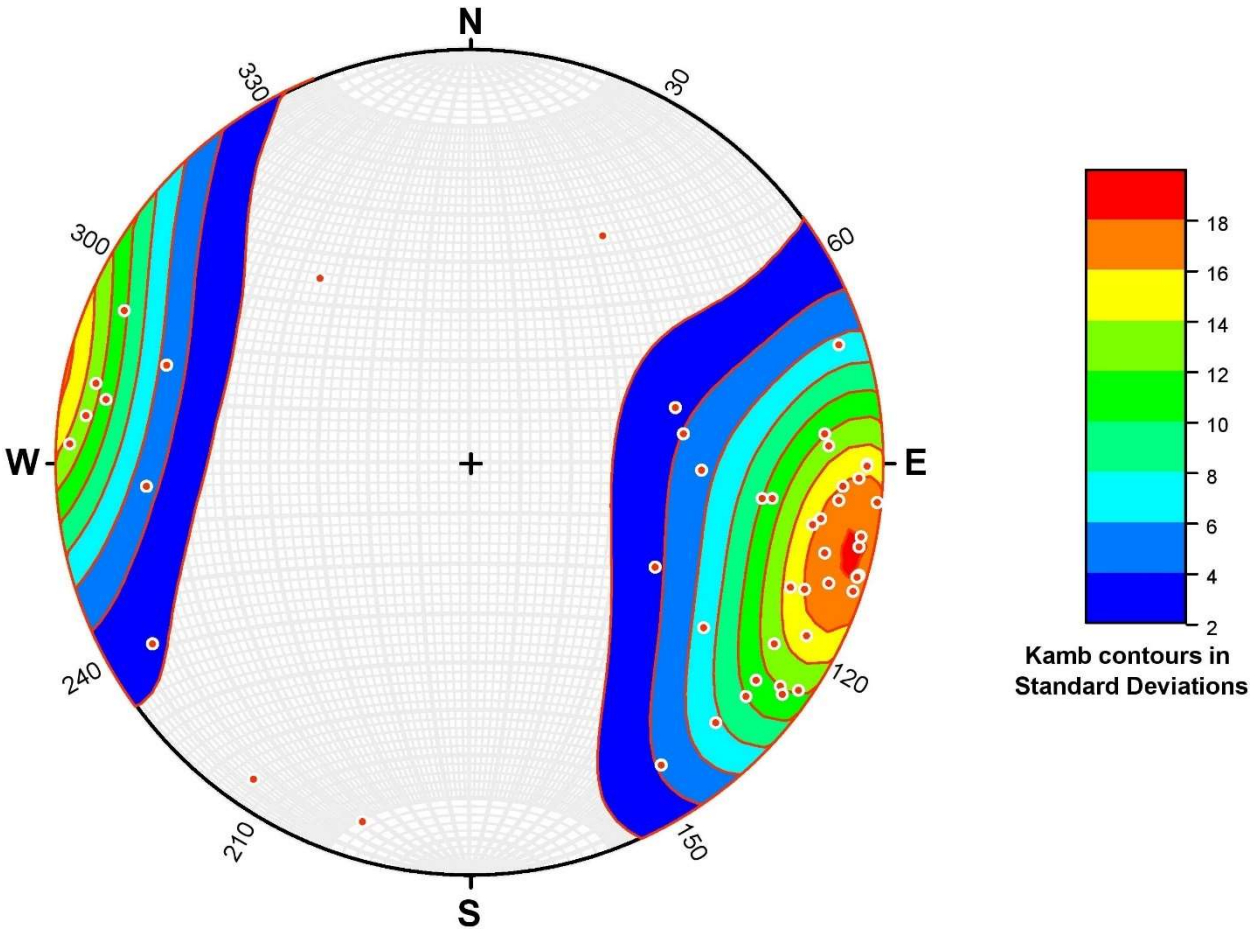

Figure 147 - Kamb contouring of fault poles for Lower Crawford Creek. N = 48.

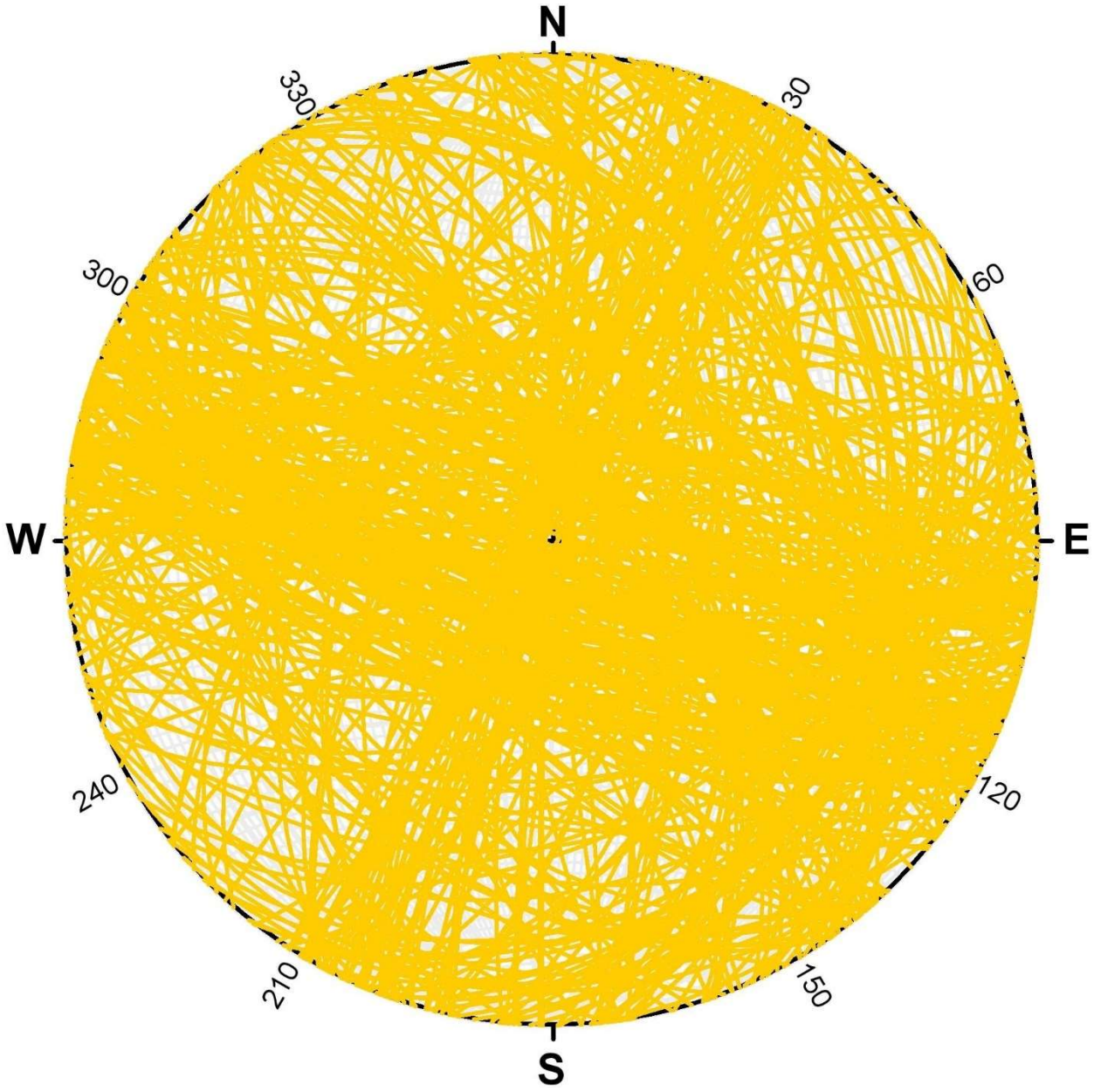

Figure 148 - Joint planes for Lower Crawford Creek. N = 371.

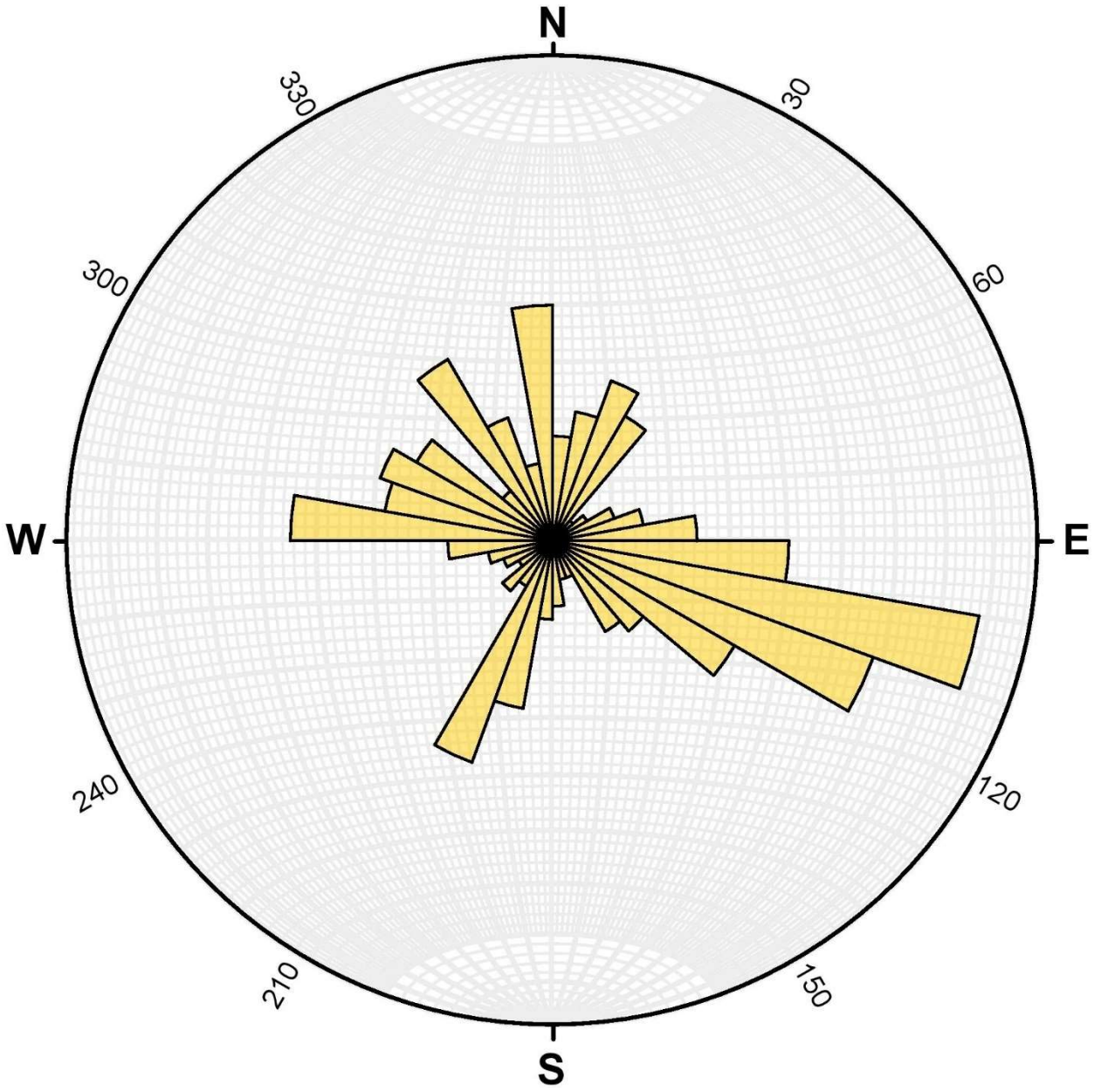

Figure 149 - Rose diagram of joint planes for Lower Crawford Creek. N = 371.

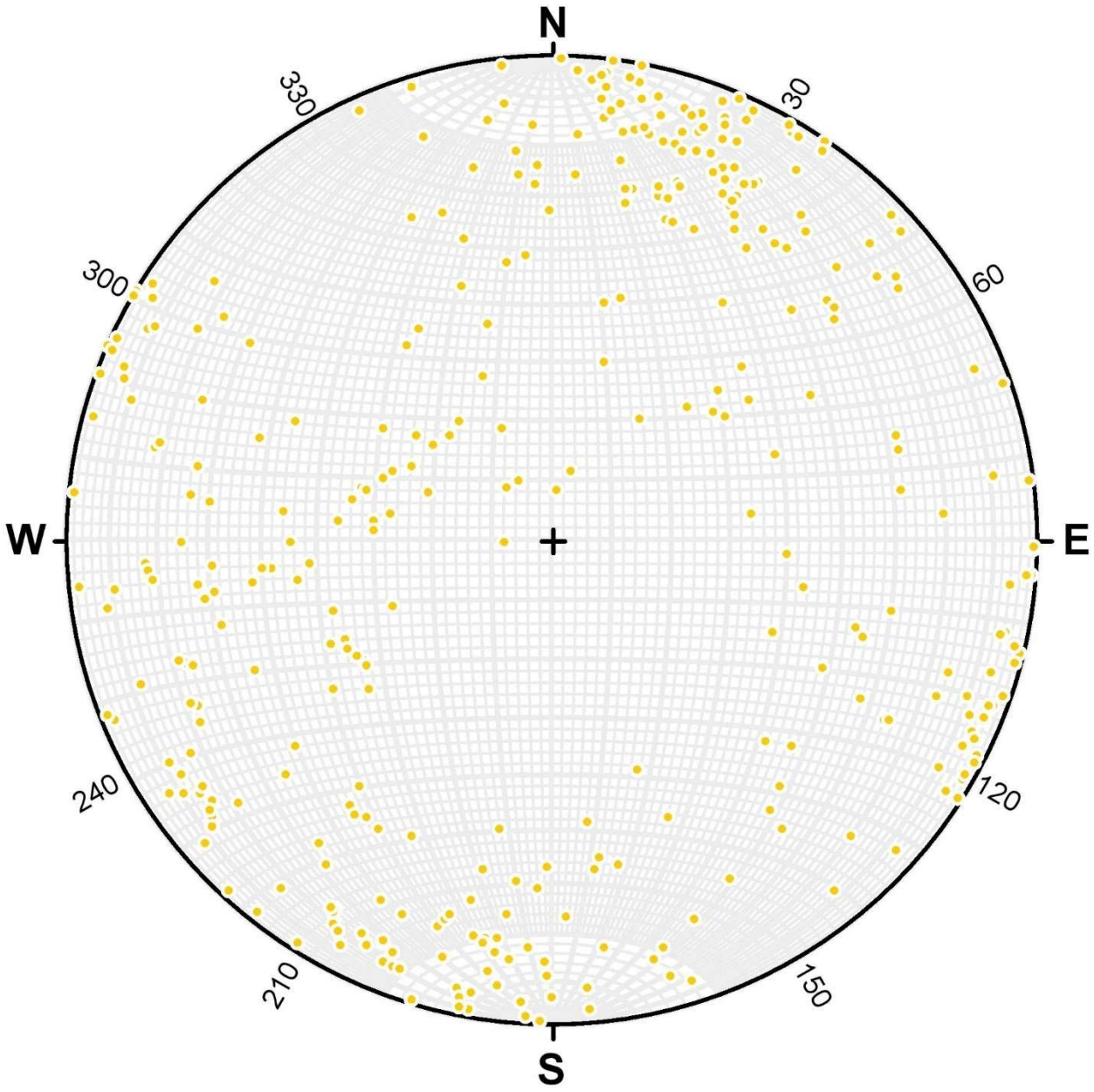

Figure 150 - Joint poles for Lower Crawford Creek. N = 371.

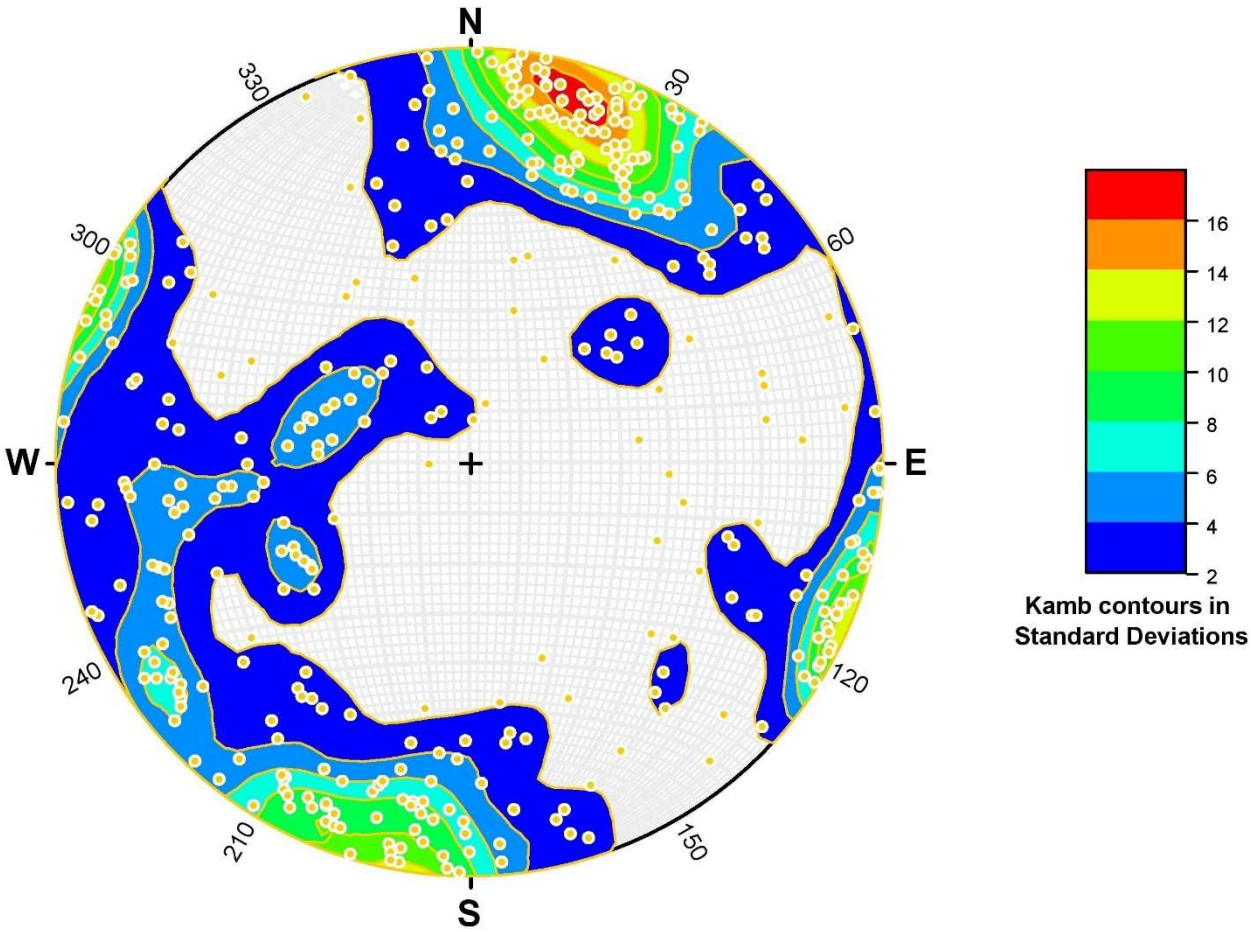

Figure 151 - Kamb contouring of joint poles for Lower Crawford Creek. N = 371.

Lower Peninsula

Bedding

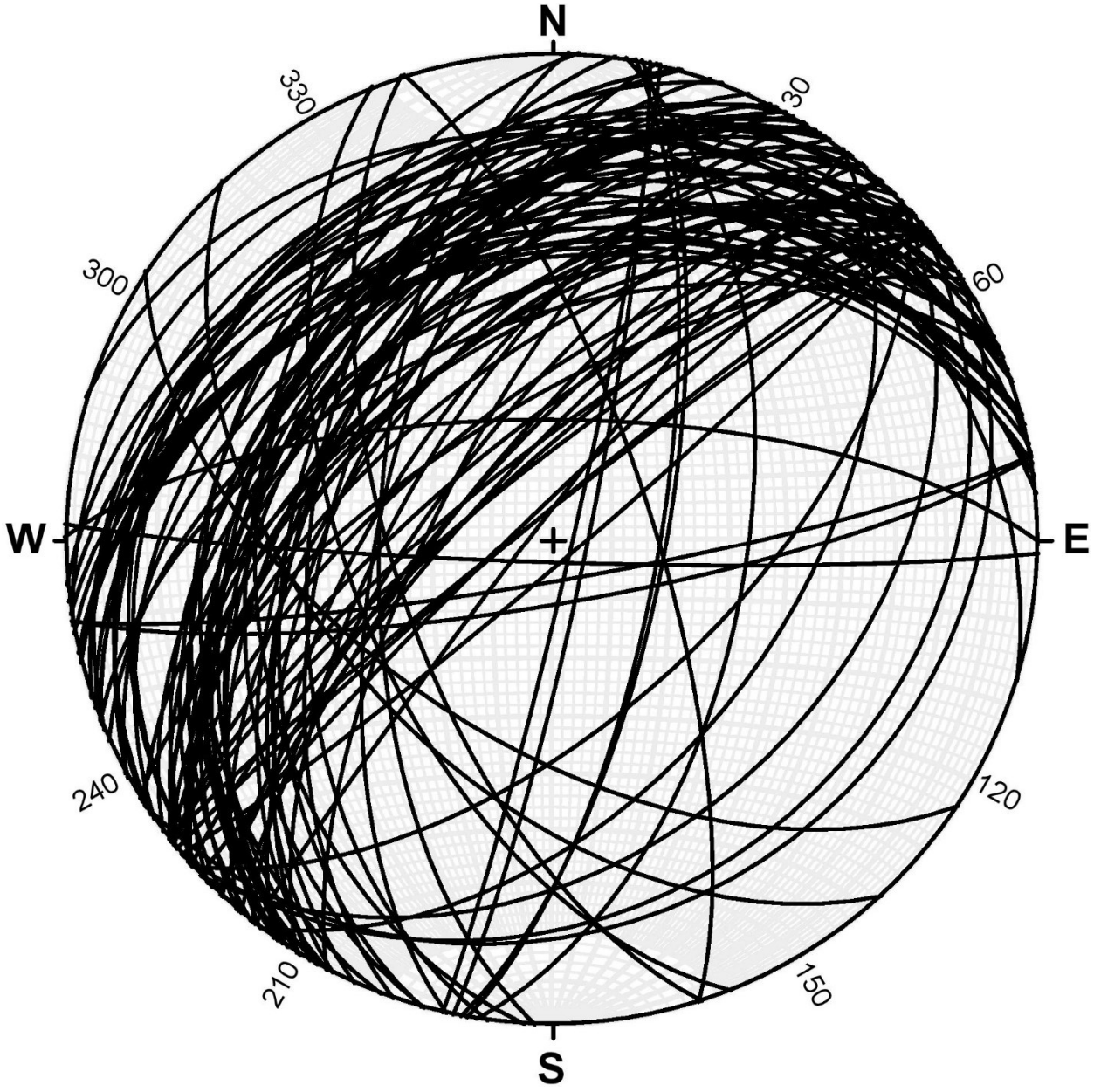

Figure 152 - Bedding planes for Lower Peninsula. N = 97.

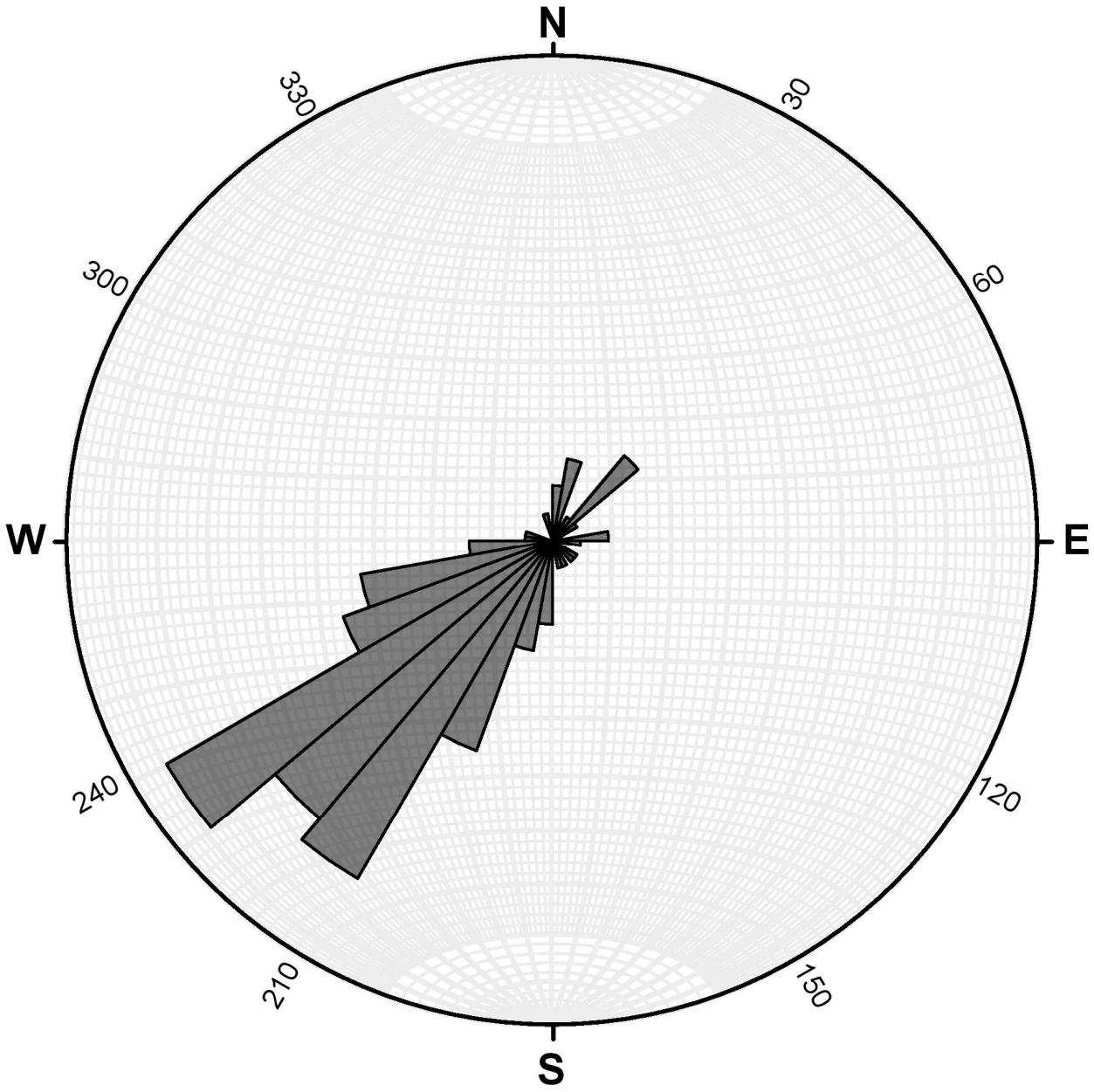

Figure 153 - Rose diagram of bedding planes for Lower Peninsula. N = 97.

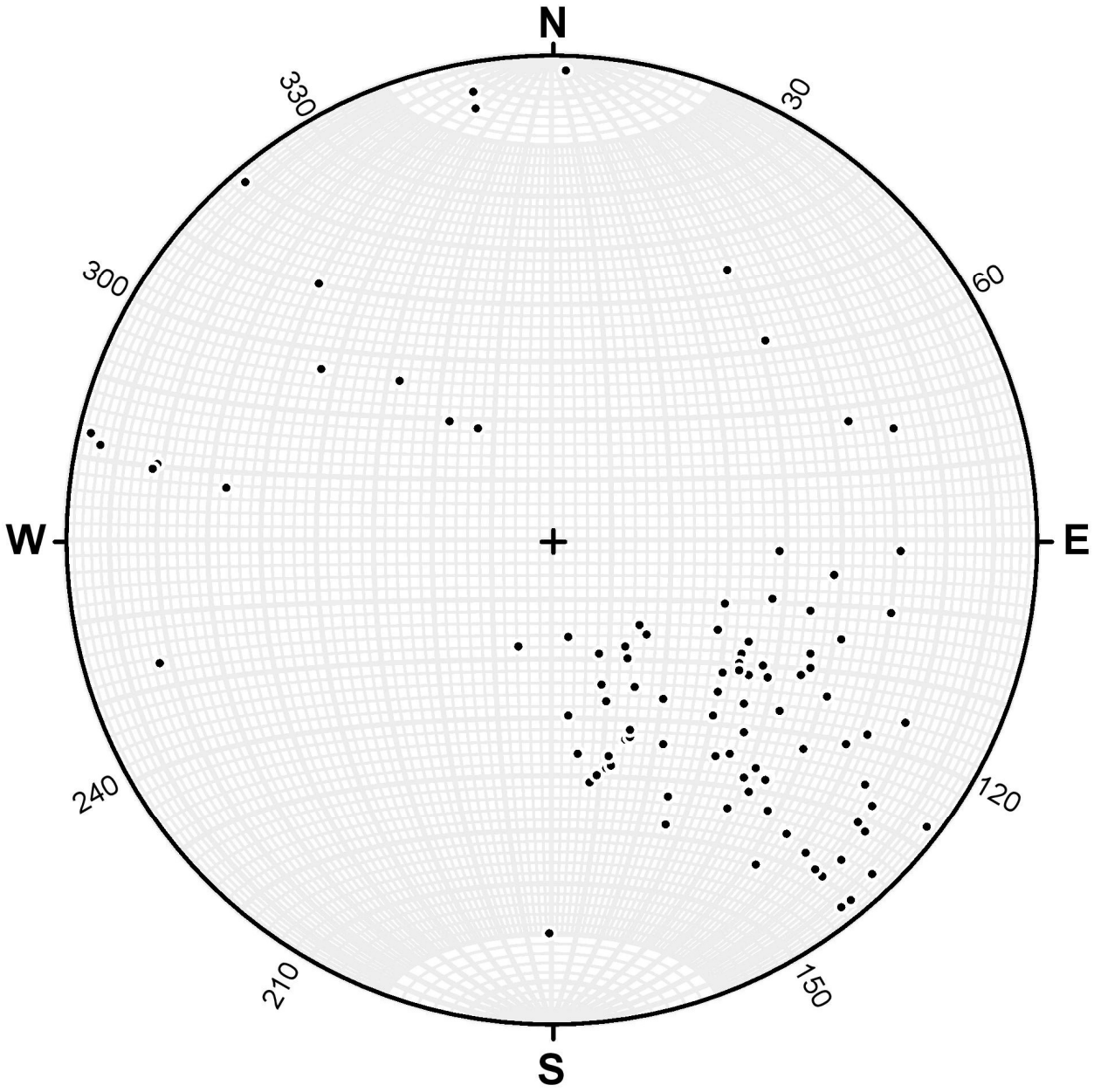

Figure 154 - Bedding poles for Lower Peninsula. N = 97.

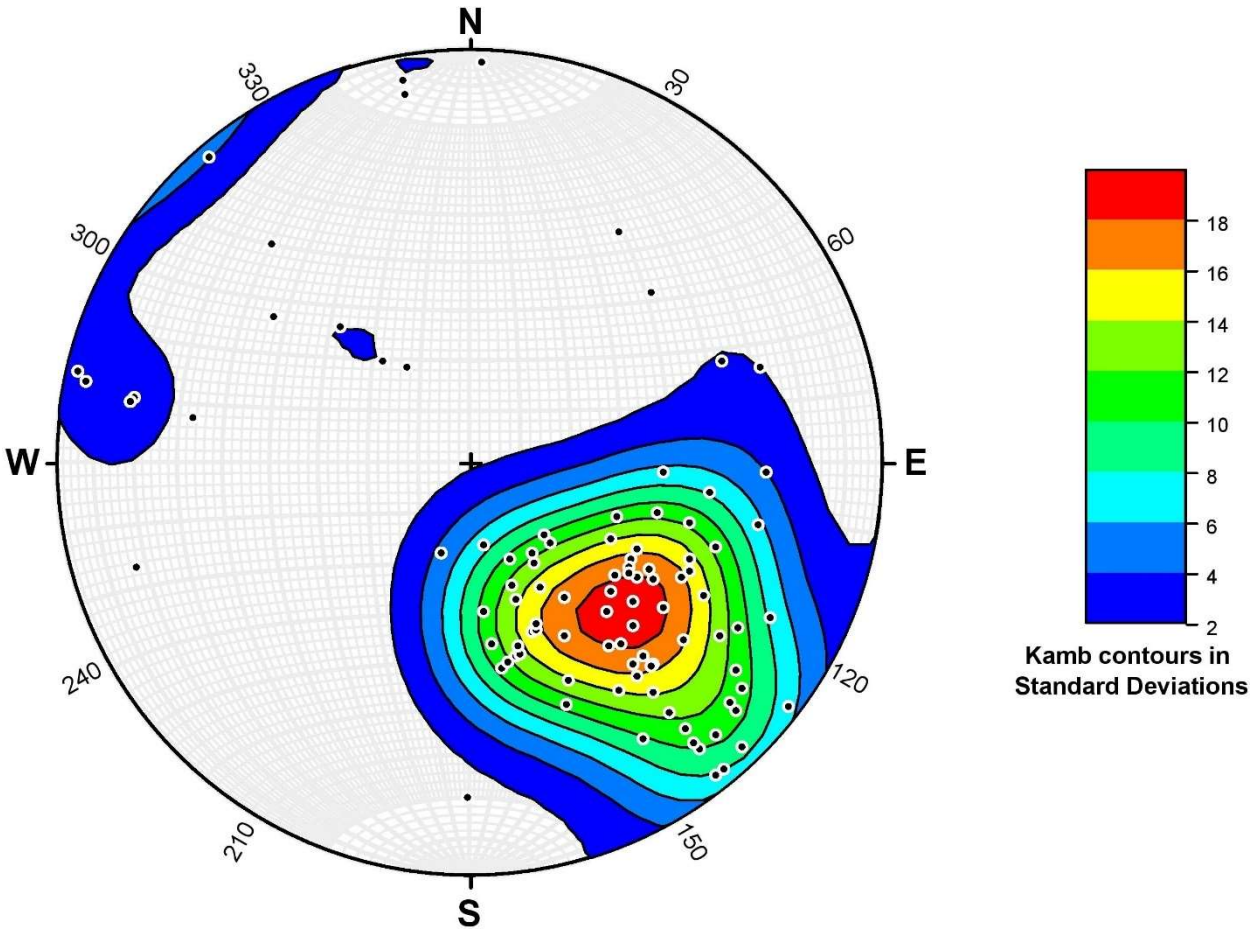

Figure 155 - Kamb contouring of bedding poles for Lower Peninsula. N = 97.

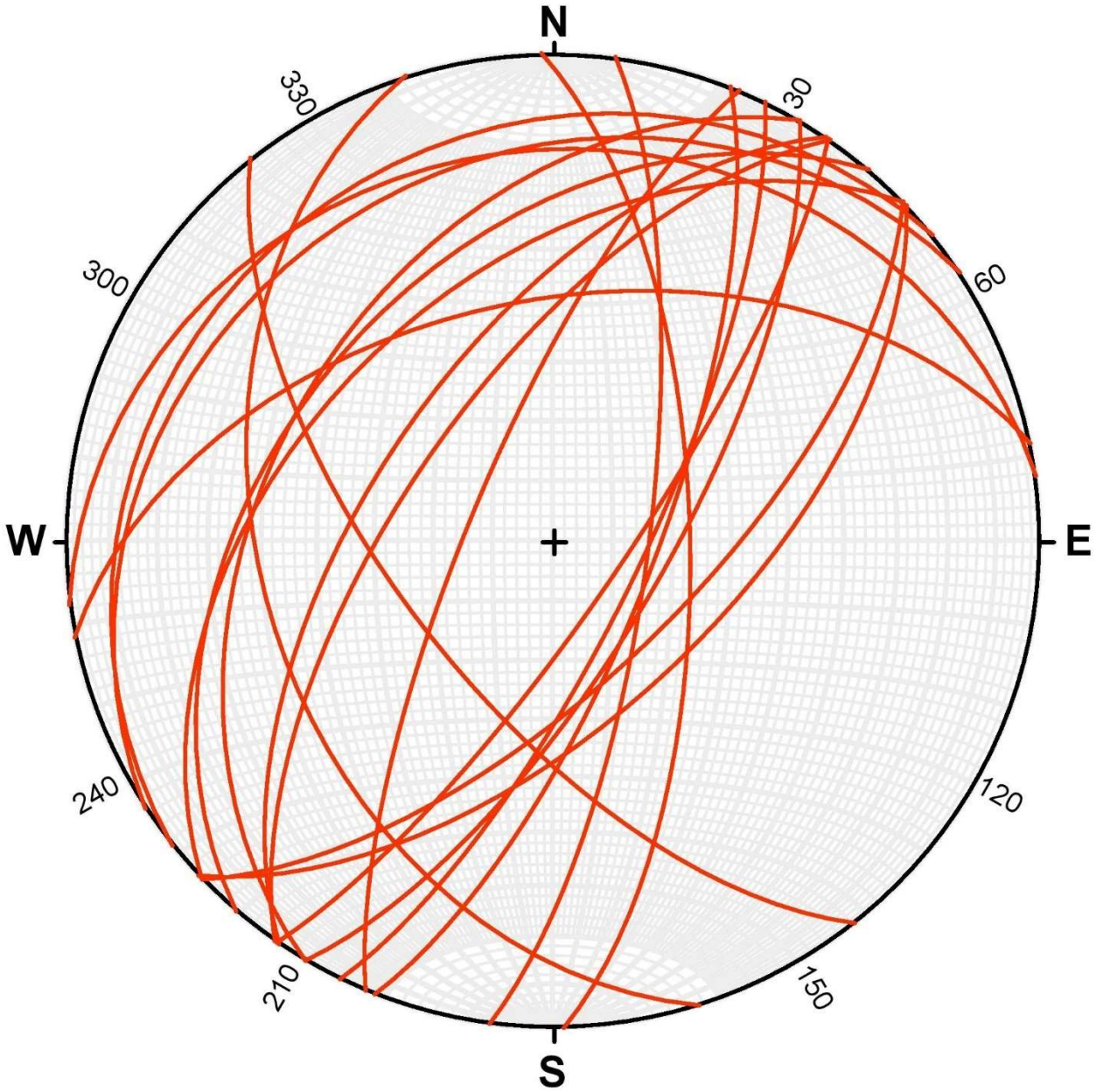

Figure 156 - Fault planes for Lower Peninsula. N = 20.

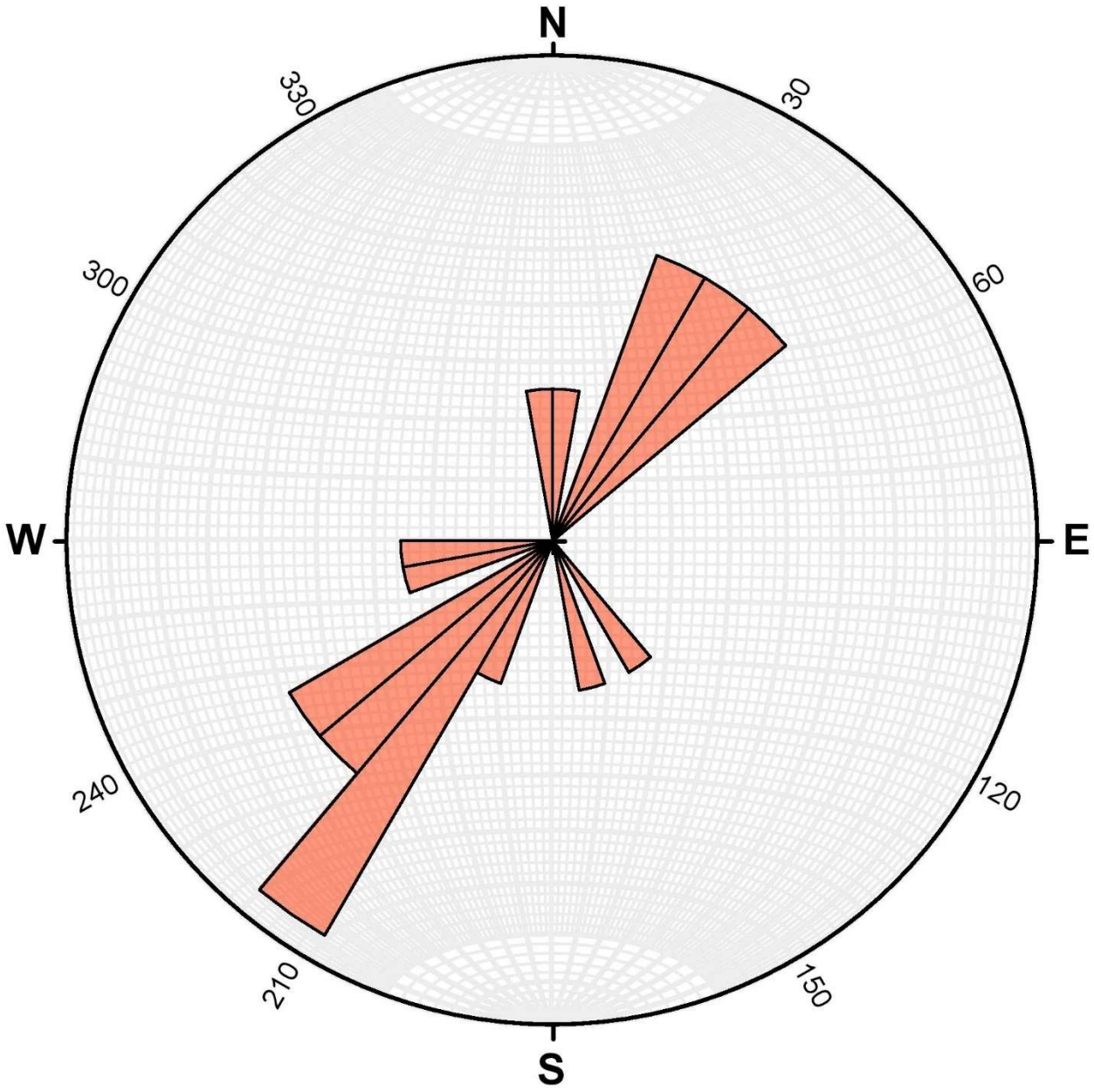

Figure 157 - Rose diagram of fault planes for Lower Peninsula. N = 20.

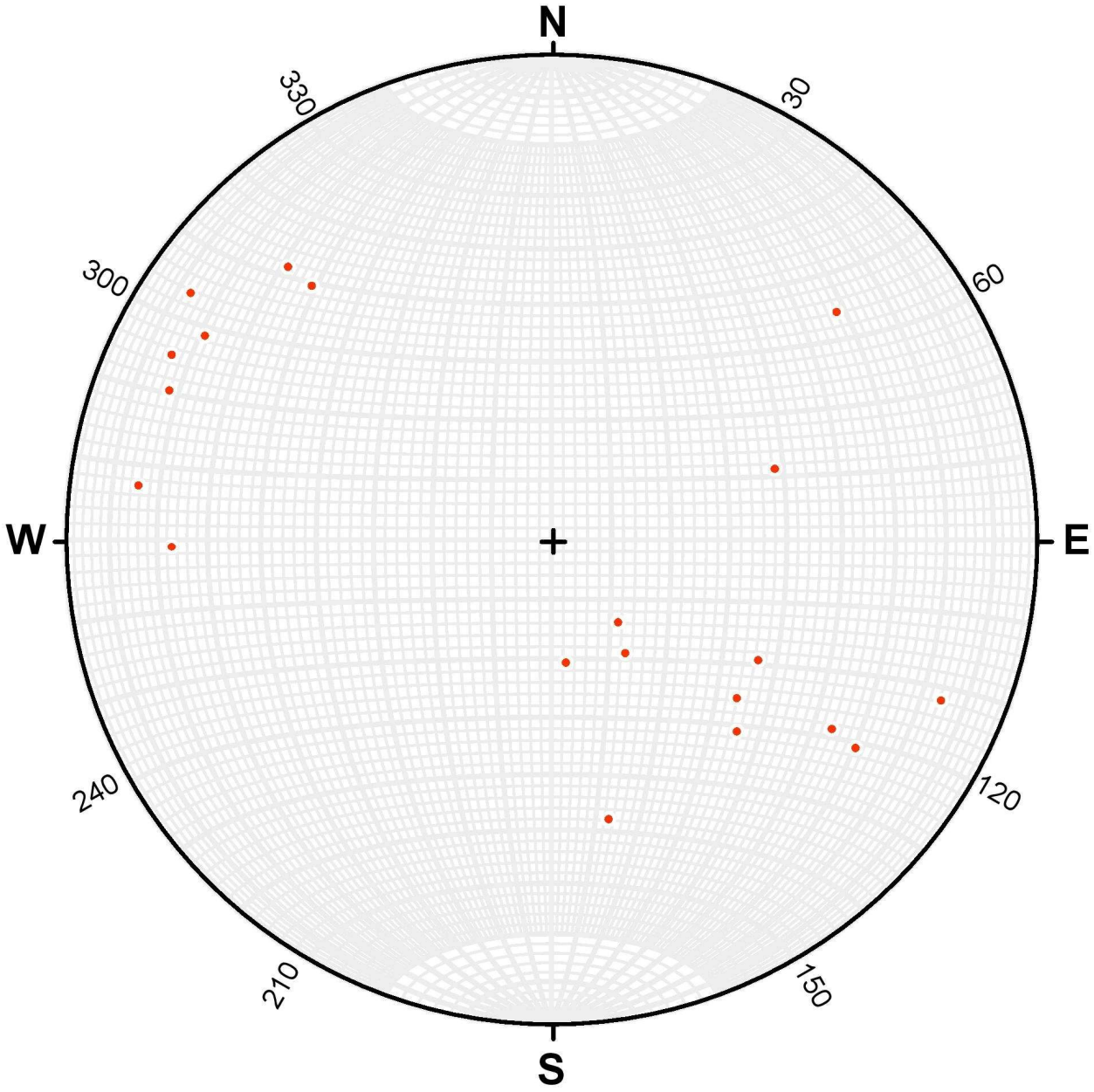

Figure 158 - Fault poles for Lower Peninsula. N = 20.

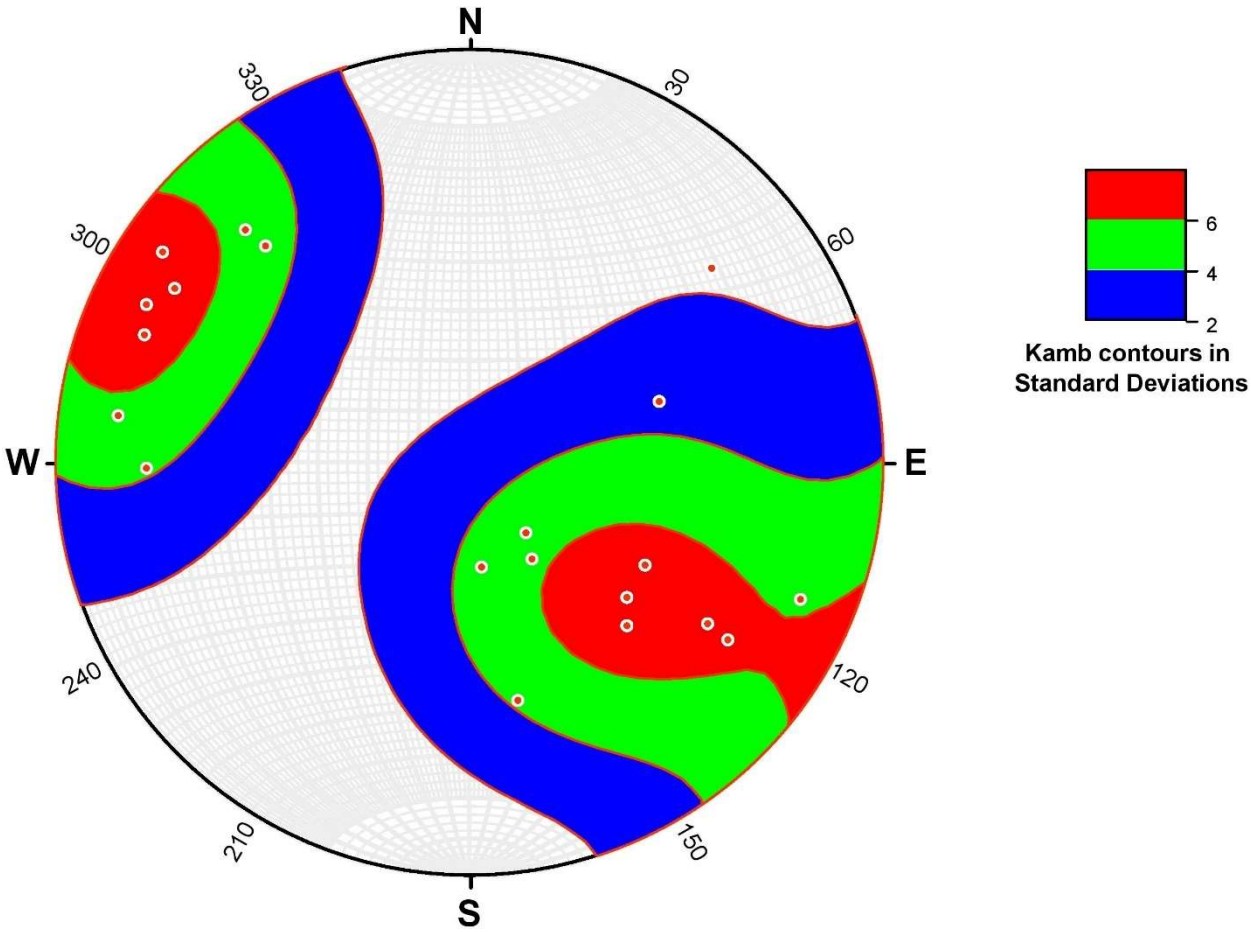

Figure 159 - Kamb contouring of fault poles for Lower Peninsula. N = 20.

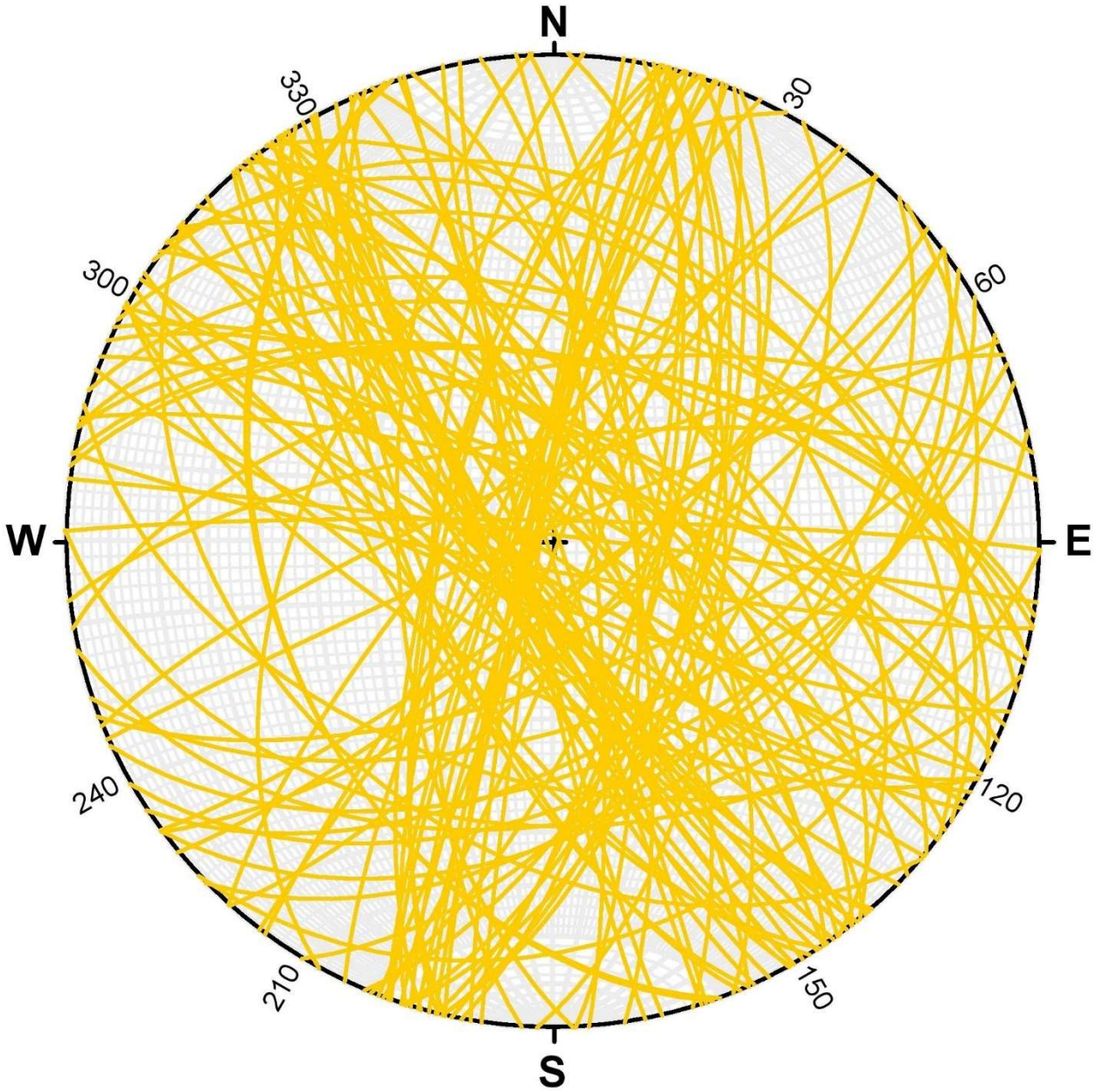

Figure 160 - Joint planes for Lower Peninsula. N = 121.

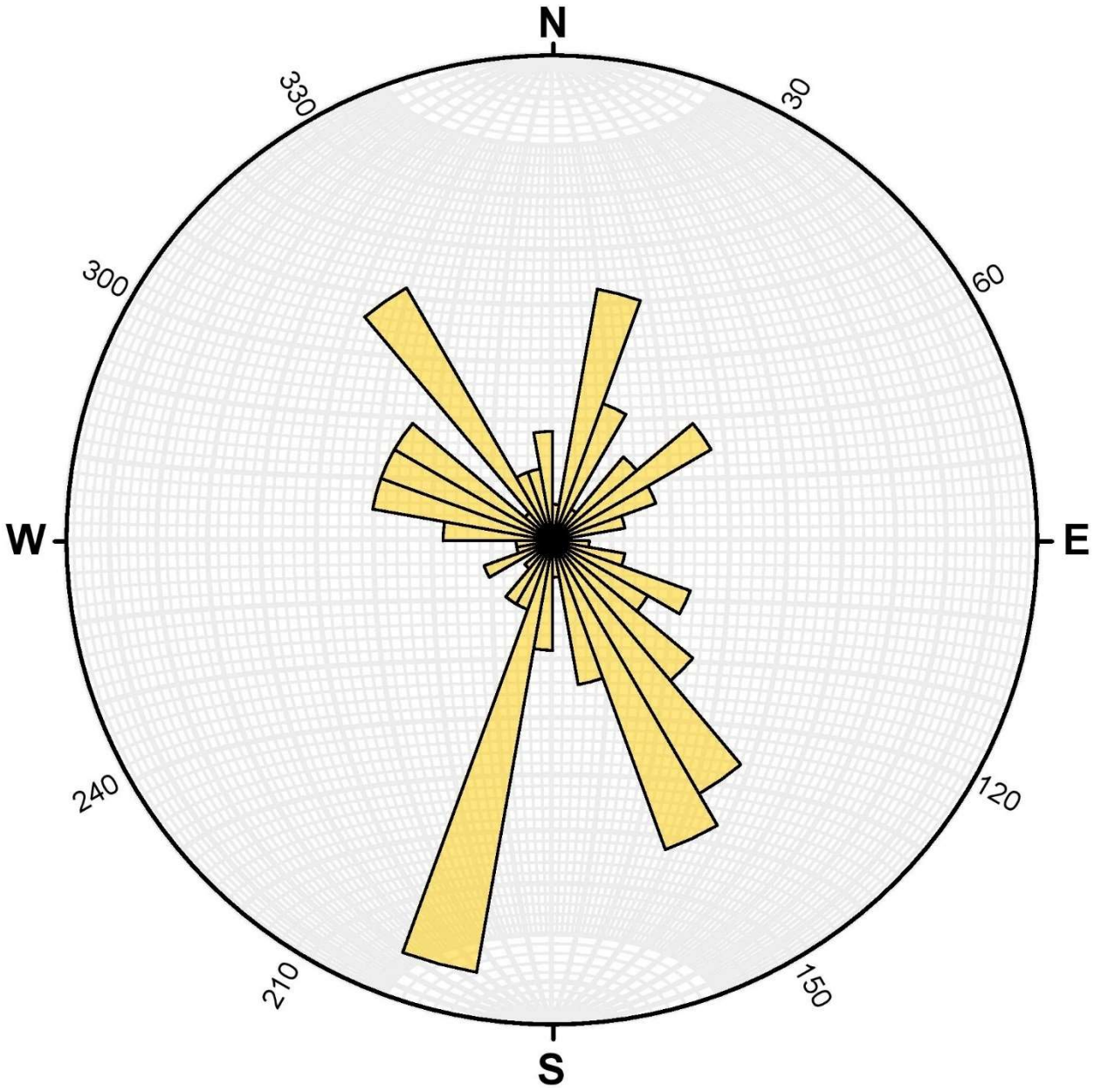

Figure 161 - Rose diagram of joint planes for Lower Peninsula. N = 121.

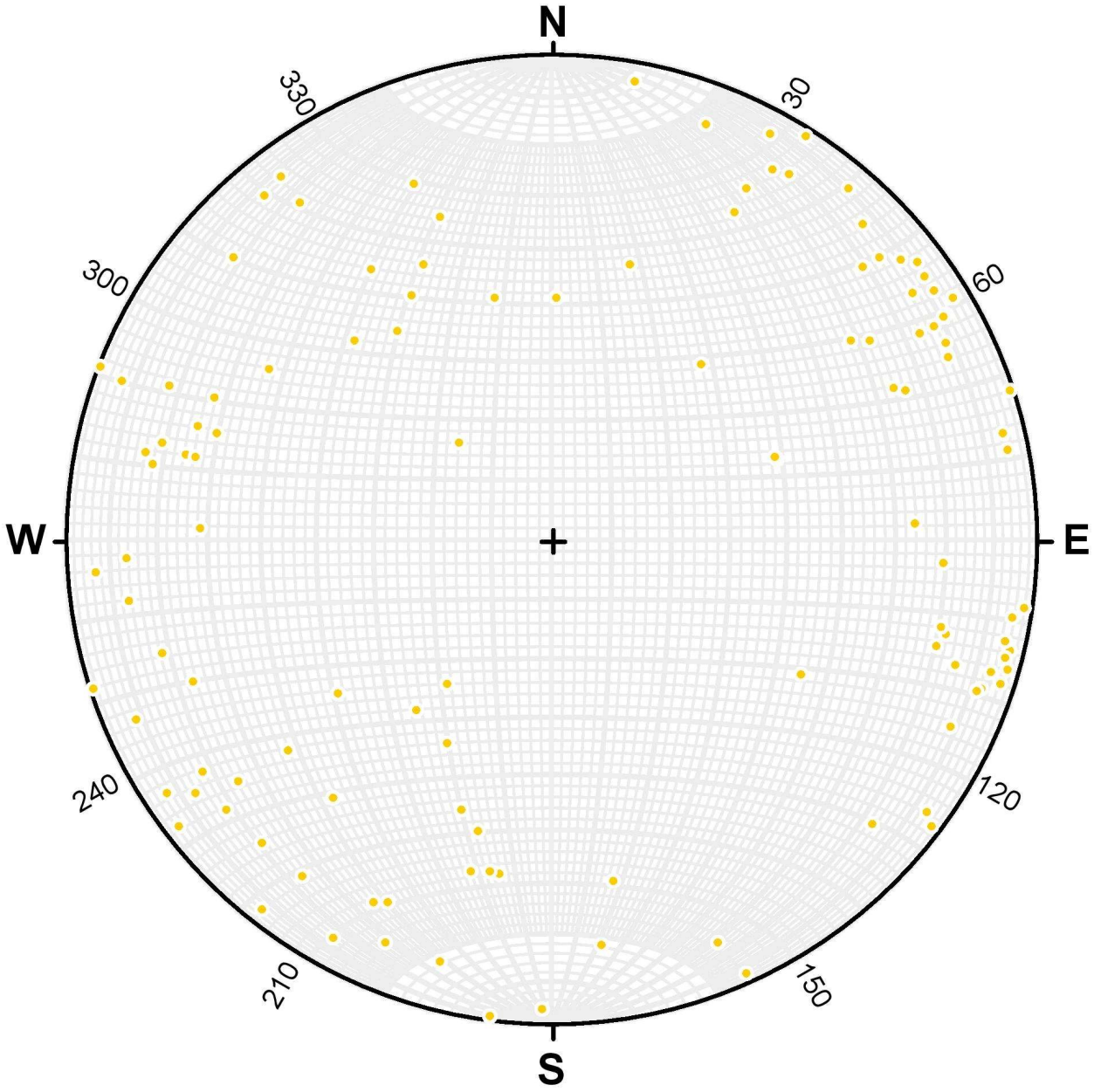

Figure 162 - Joint poles for Lower Peninsula. N = 121.

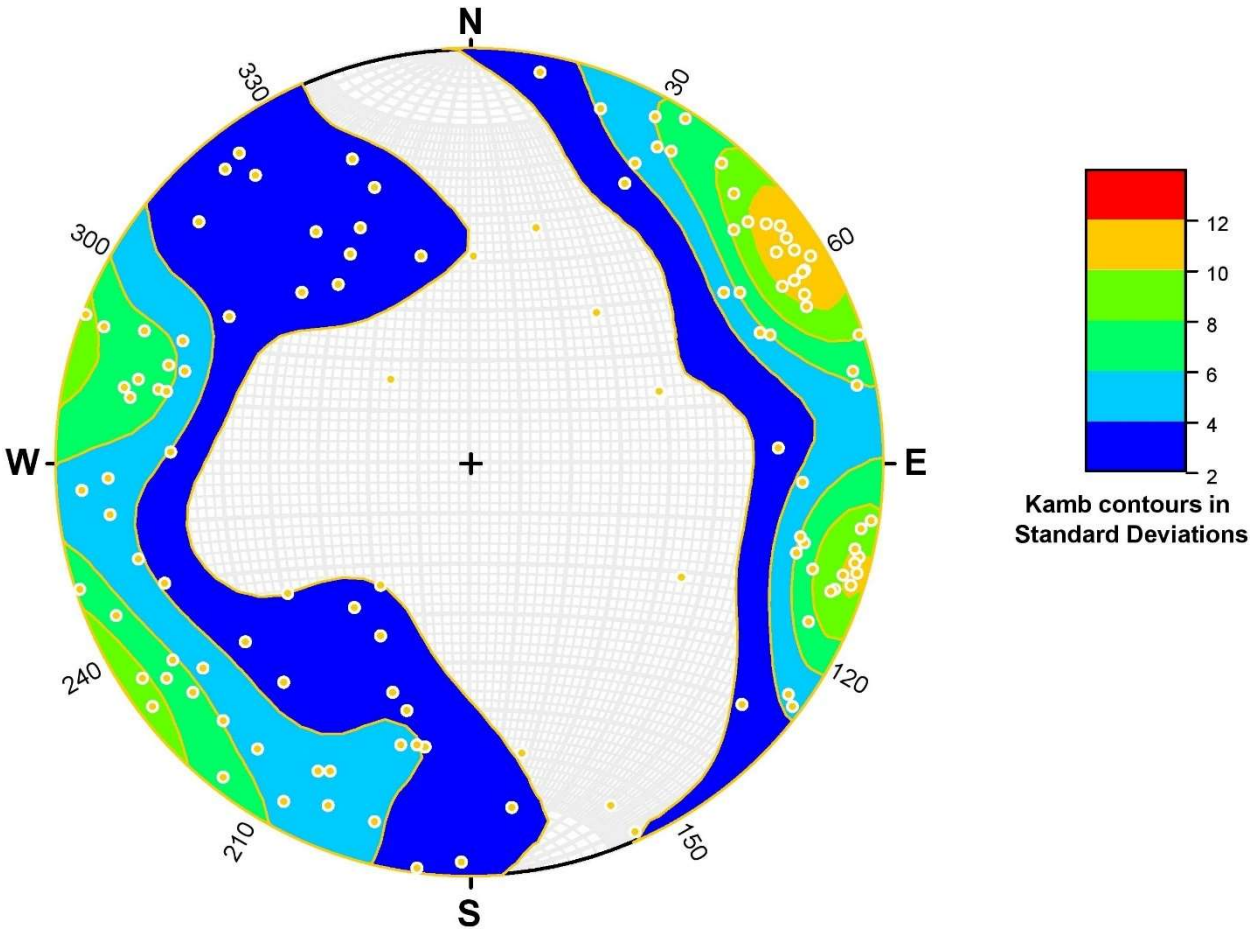

*Figure 163 - Kamb contouring of joint poles for Lower Peninsula. N = 121. *

Orebin Creek

Bedding

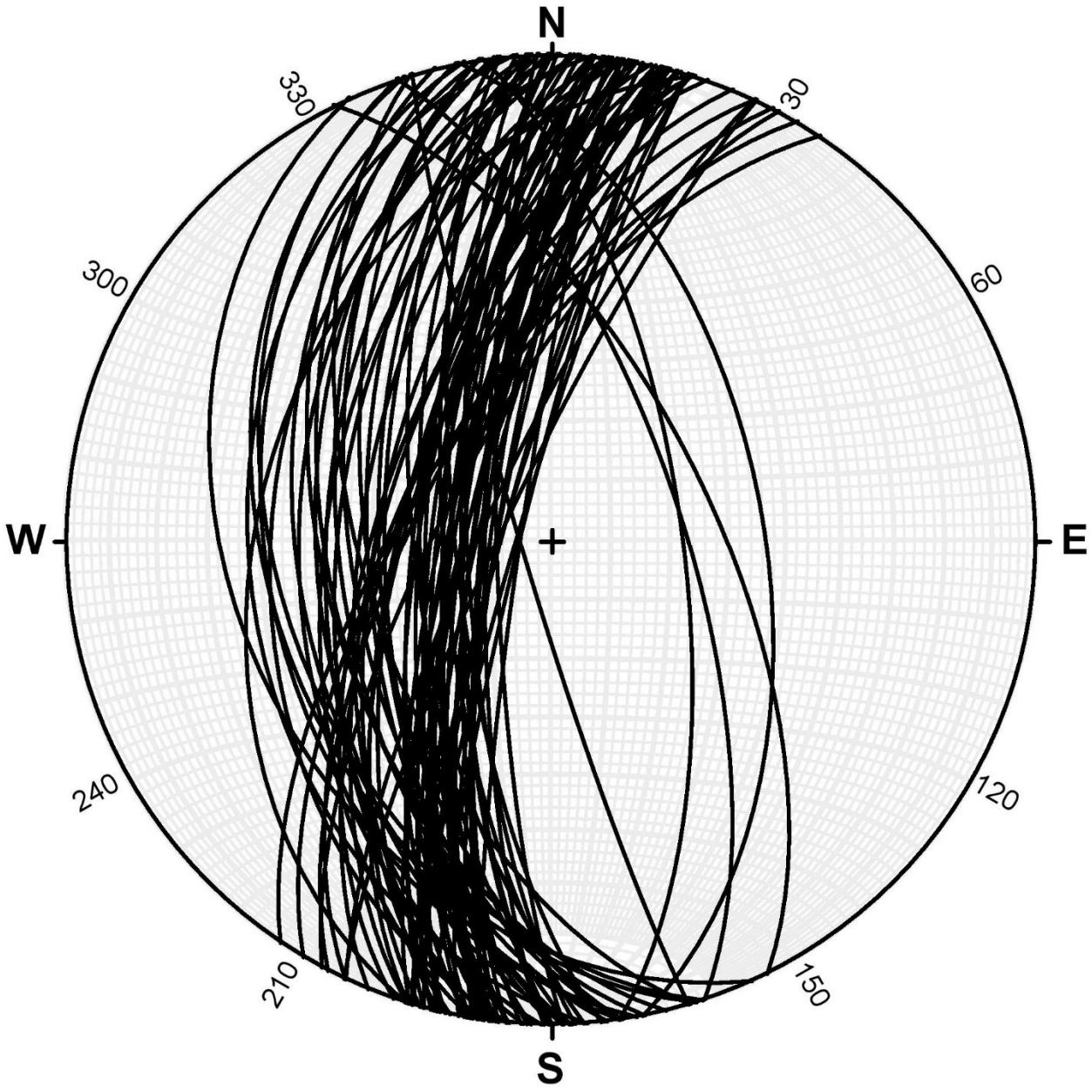

Figure 164 - Bedding planes for Orebin Creek. N = 84.

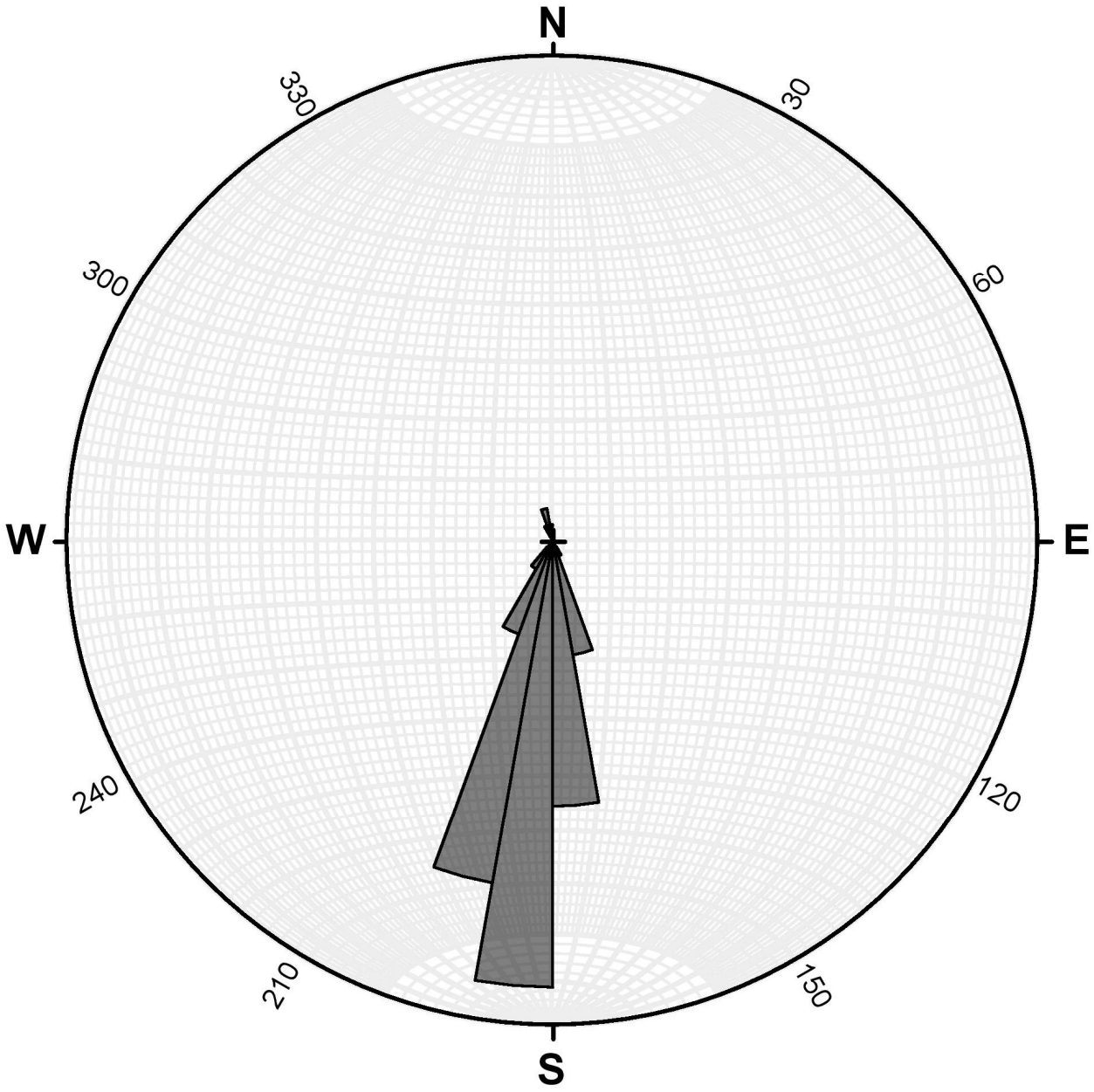

Figure 165 - Rose diagram of bedding planes for Orebin Creek. N = 84.

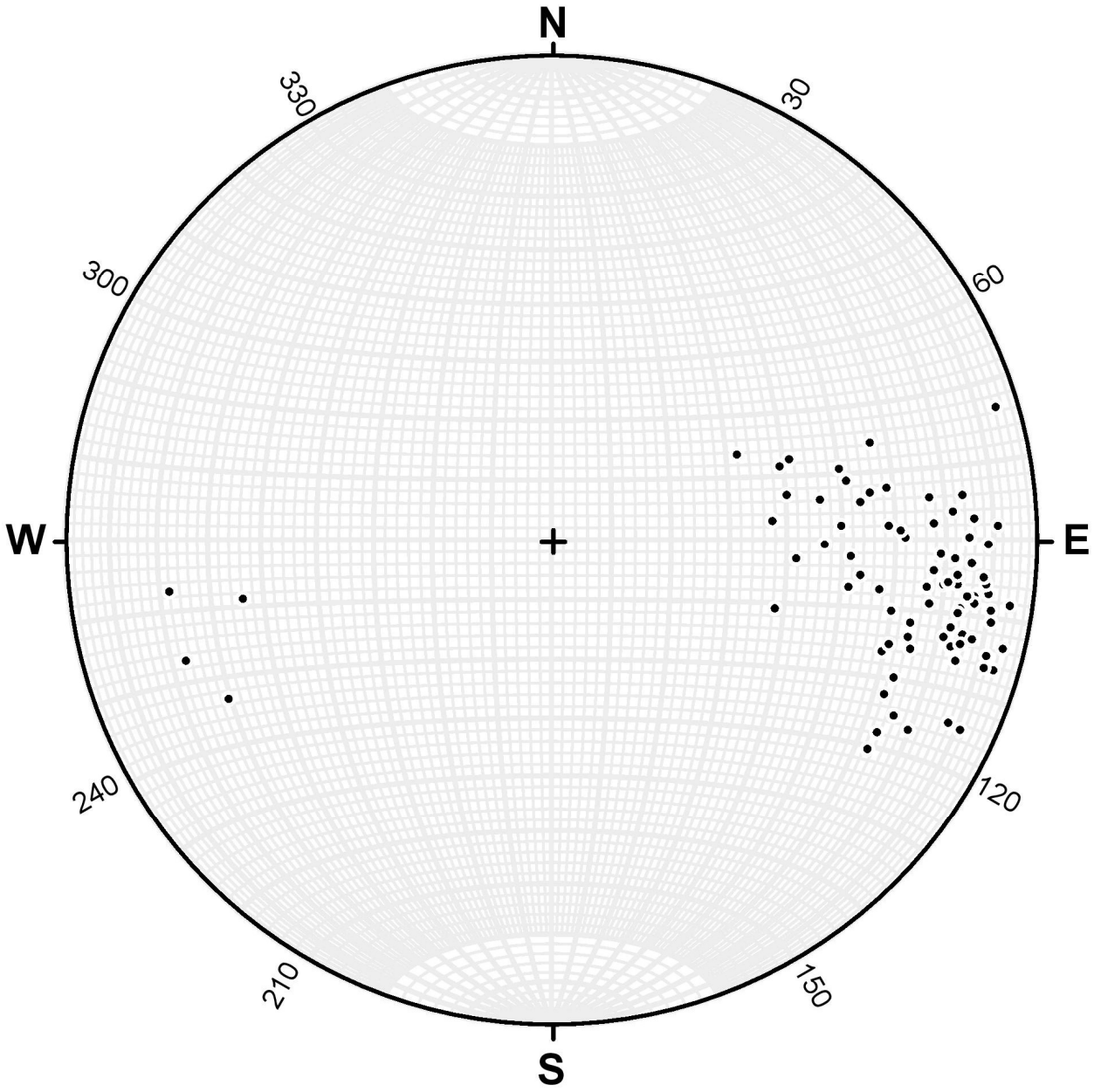

Figure 166 - Bedding poles for Orebin Creek. N = 84.

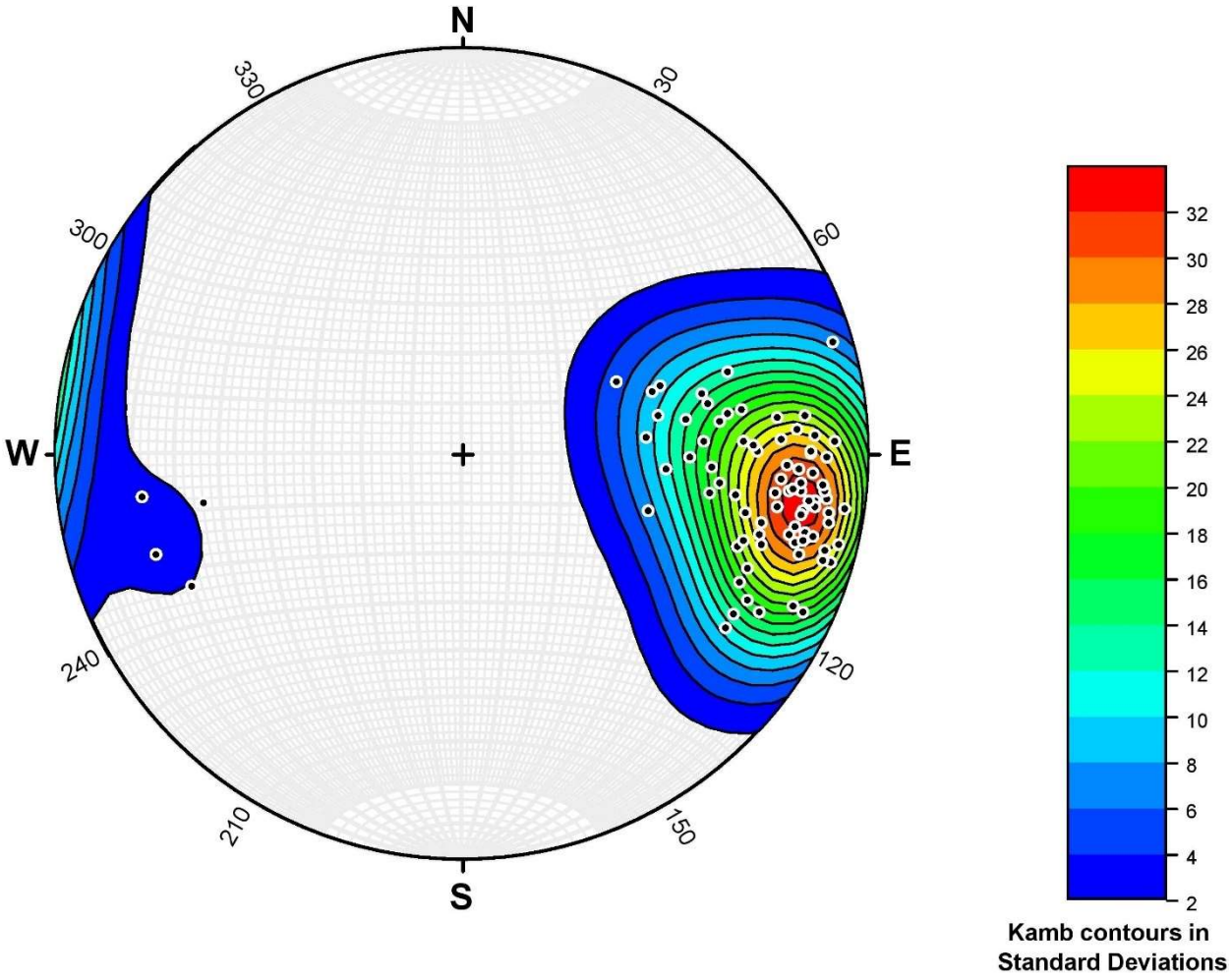

Figure 167 - Kamb contouring of bedding poles for Orebin Creek. N = 84.

Faulting

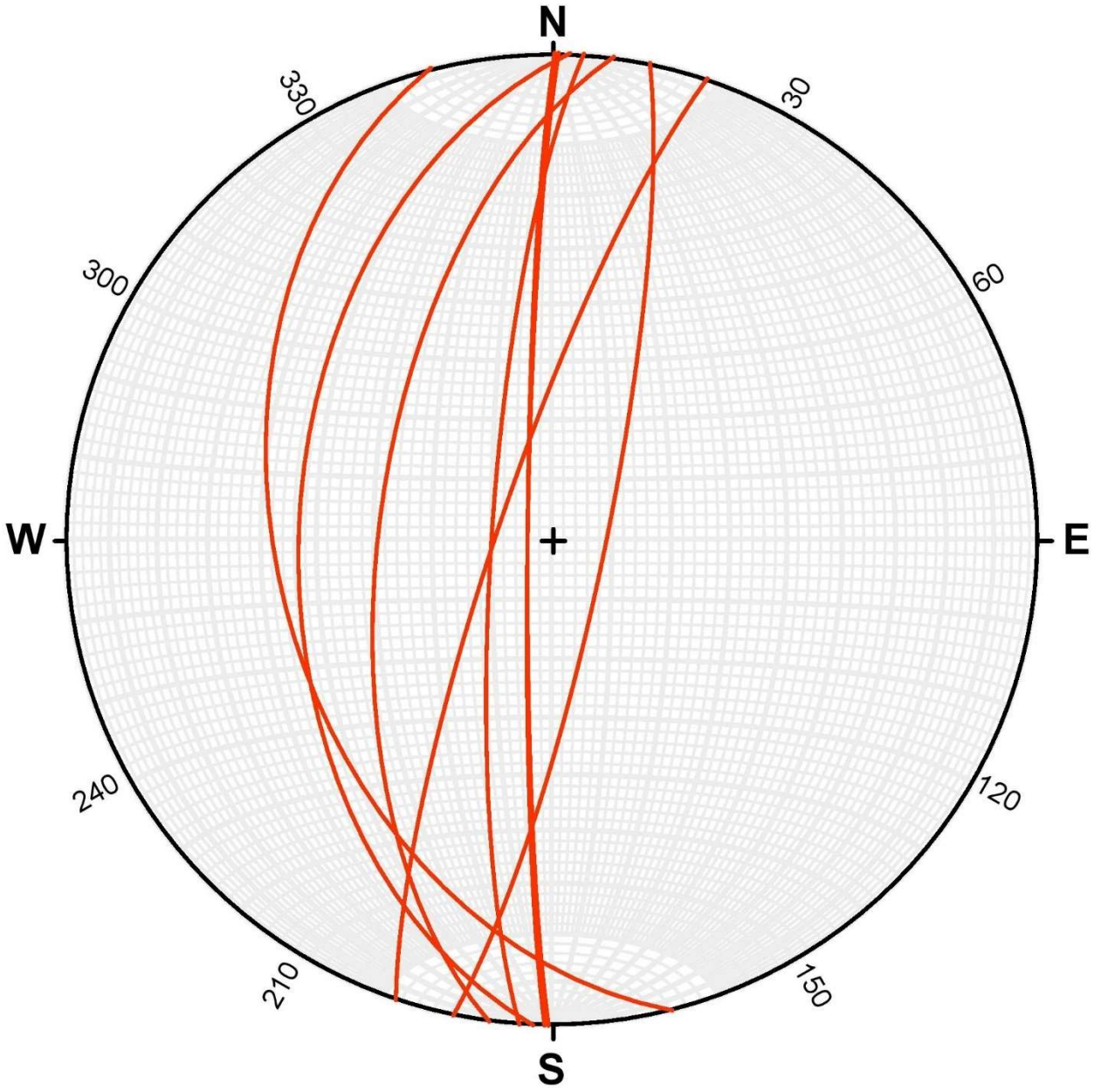

Figure 168 - Fault planes for Orebin Creek. N = 8.

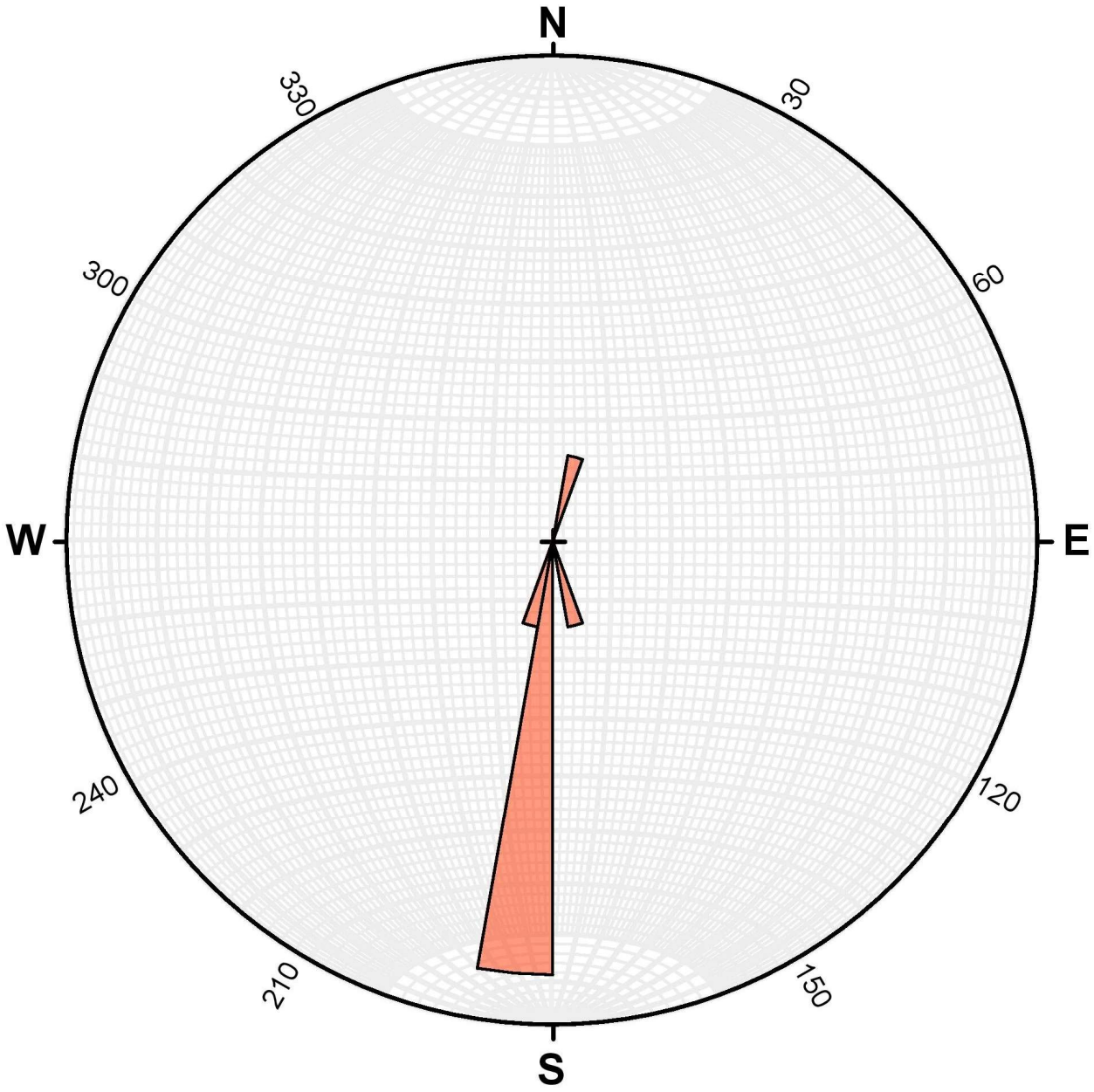

Figure 169 - Rose diagram of fault planes for Orebin Creek. N = 8.

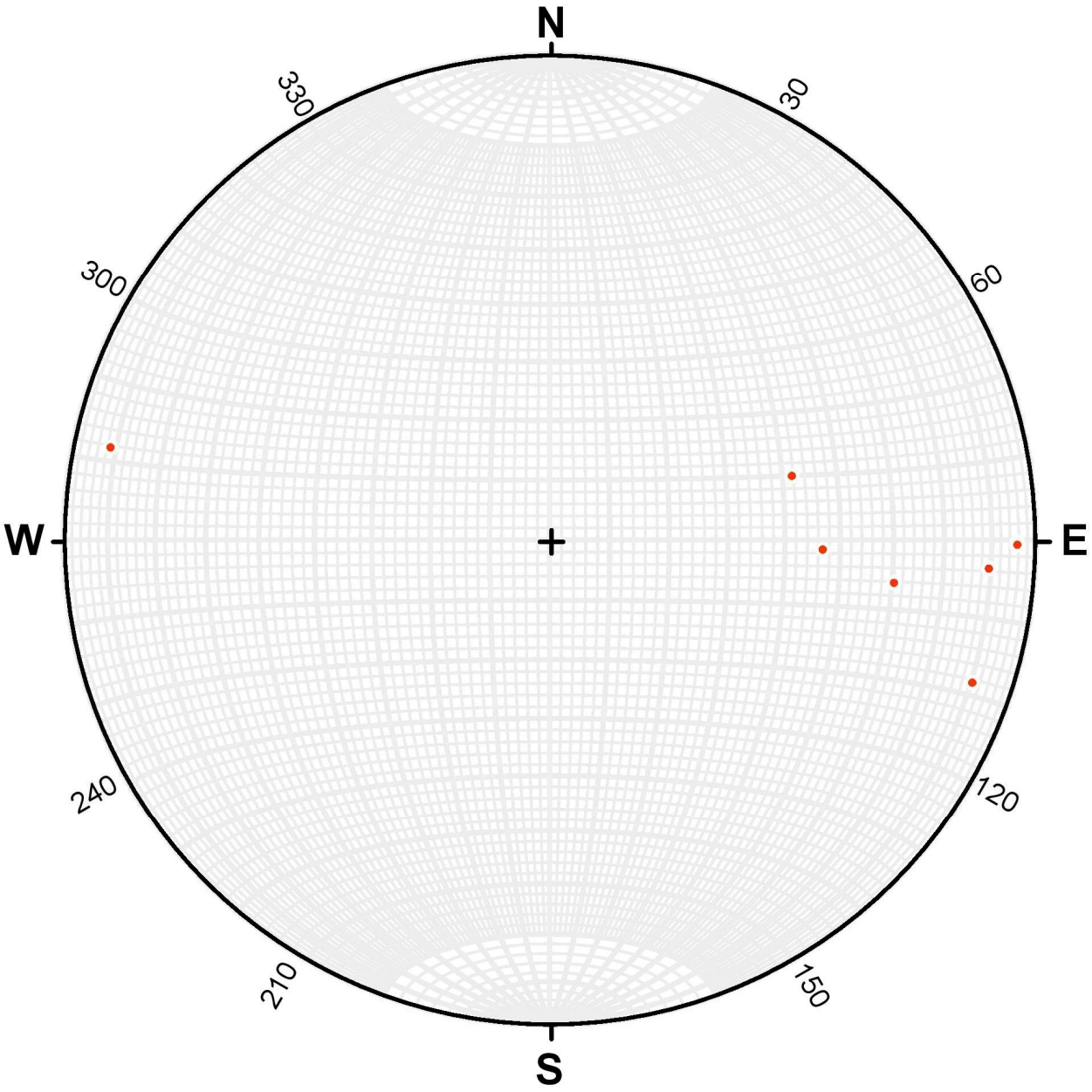

Figure 170 - Fault poles for Orebin Creek. N = 8.

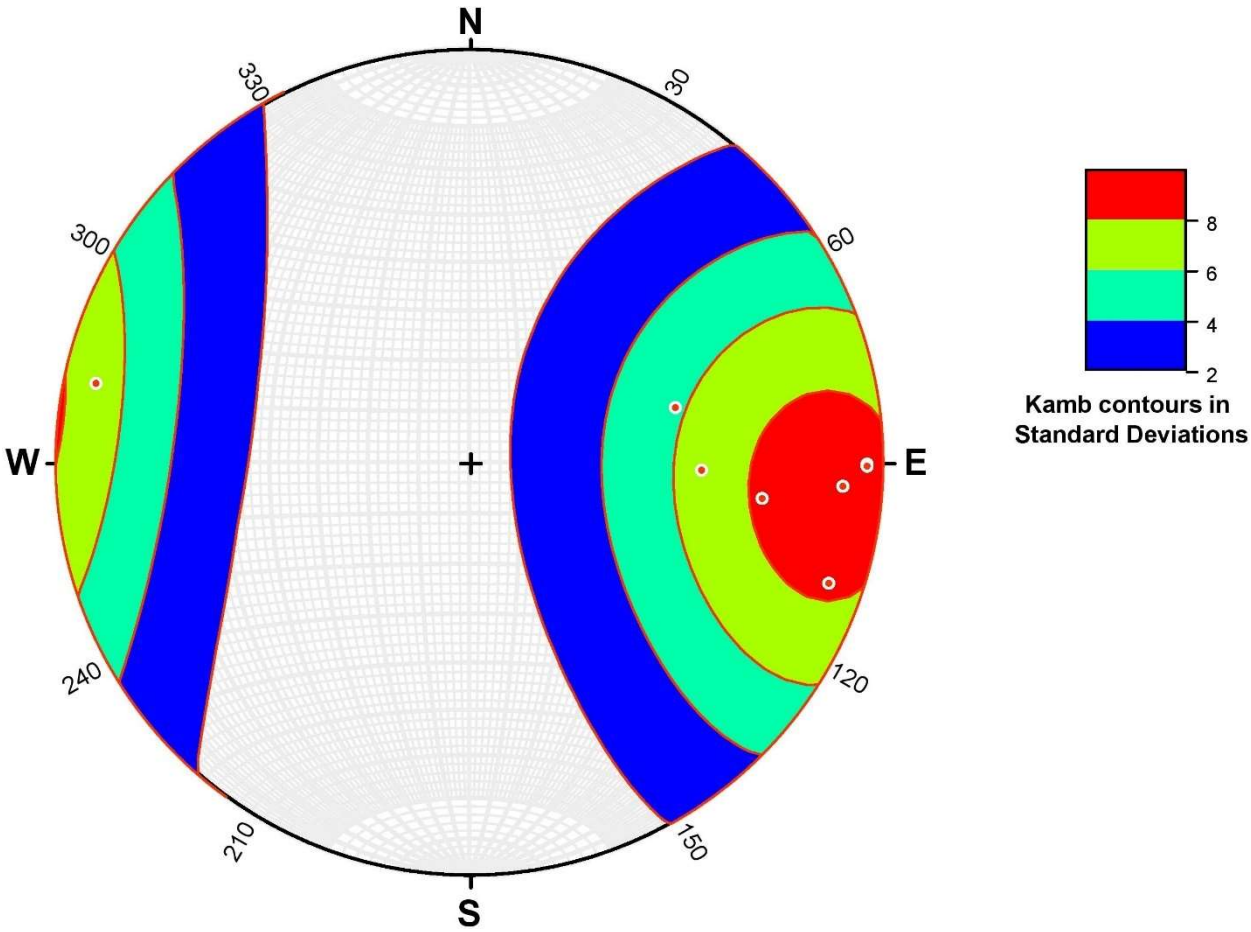

Figure 171 - Kamb contouring of fault poles for Orebin Creek. N = 8.

Jointing

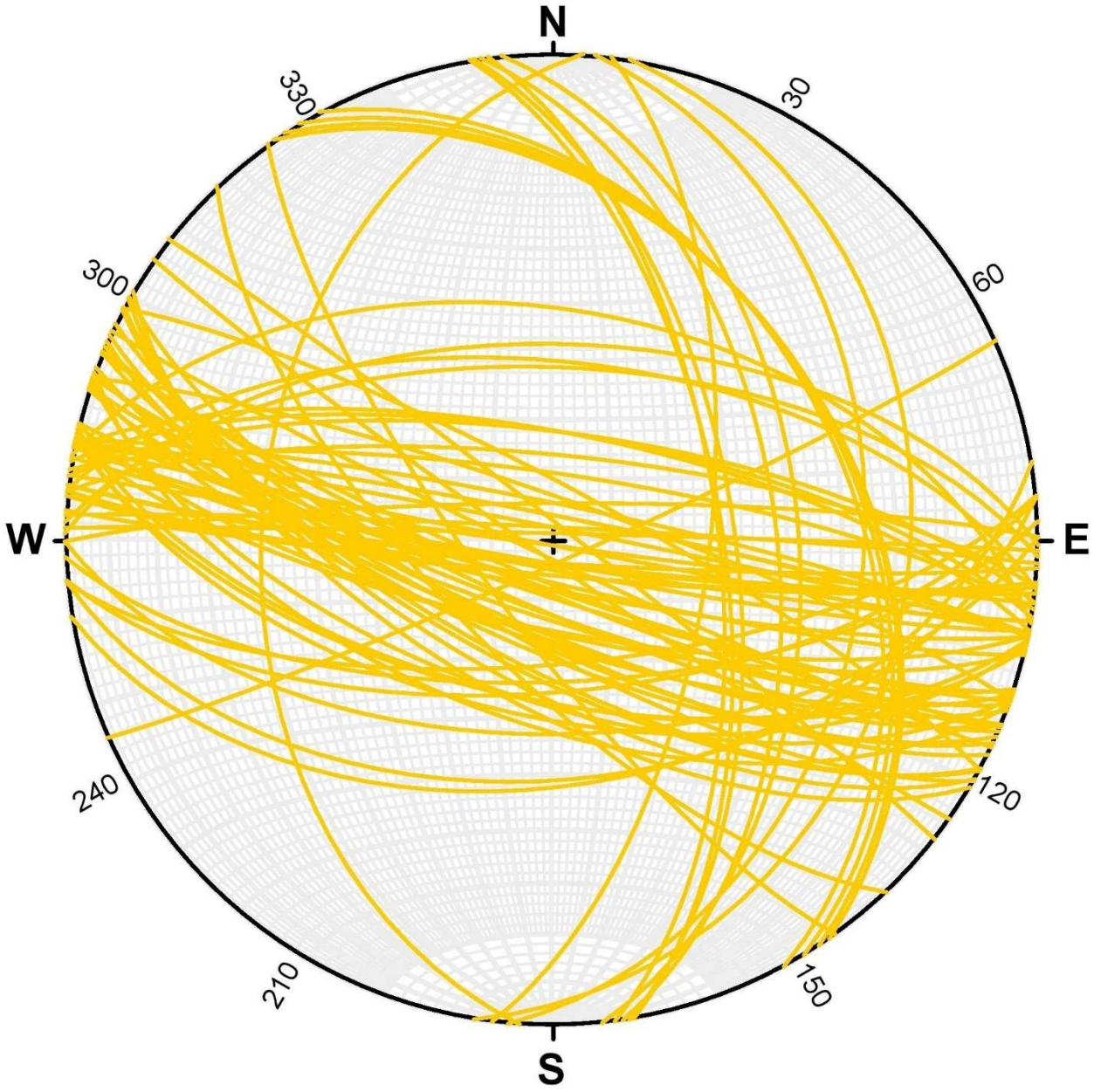

Figure 172 - Joint planes for Orebin Creek. N = 79.

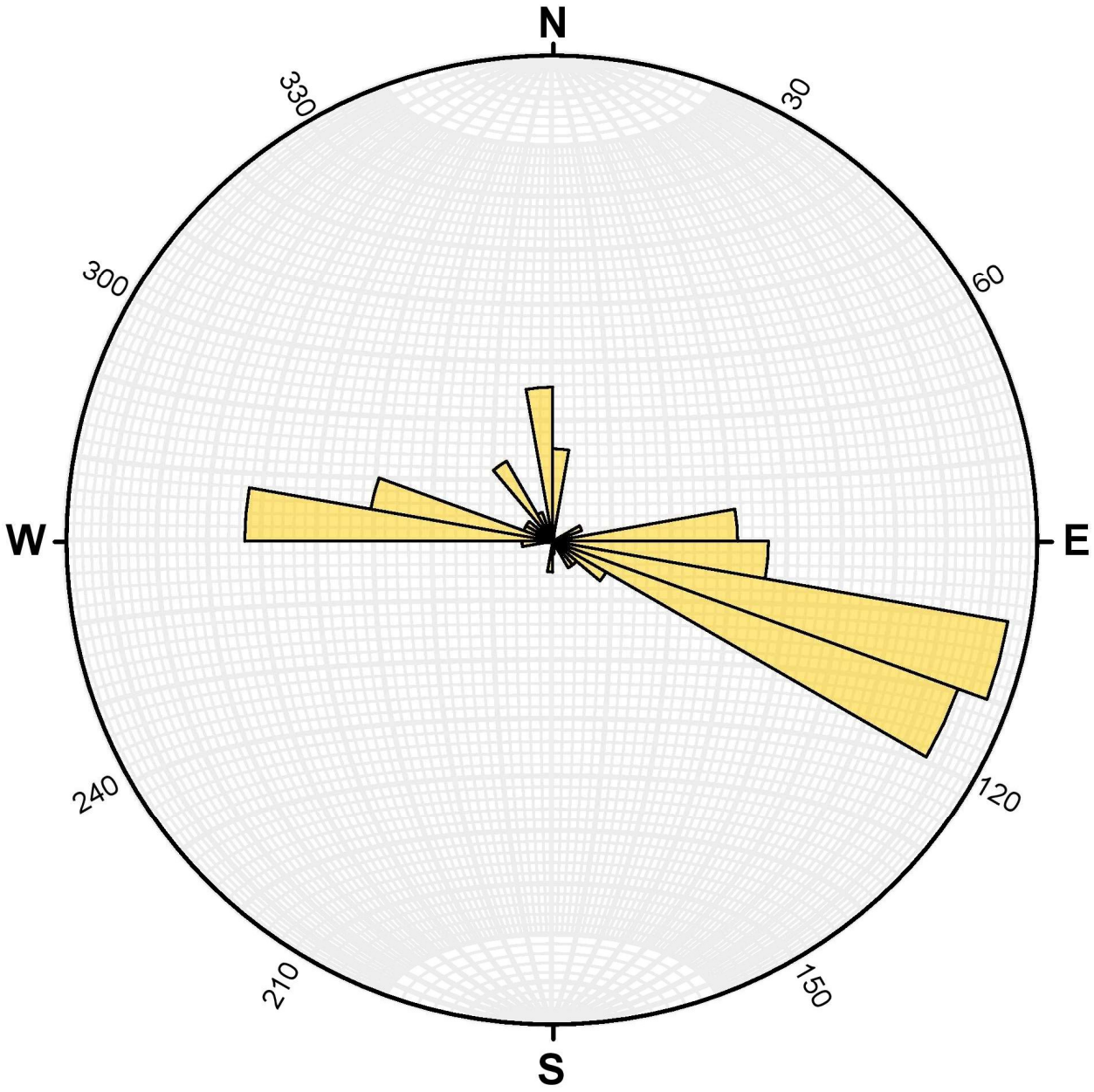

Figure 173 - Rose diagram of joint planes for Orebin Creek. N = 79.

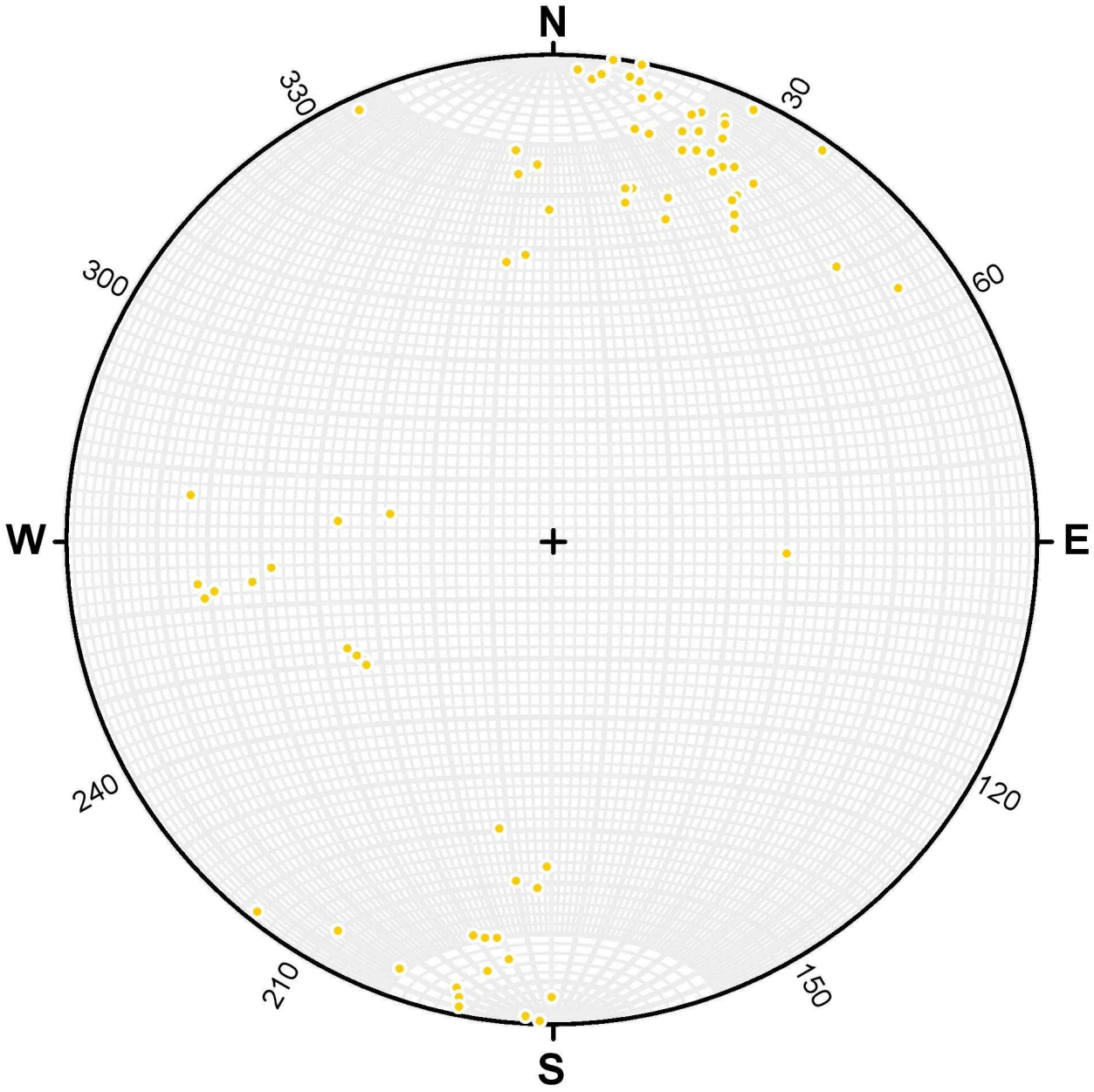

Figure 174 - Joint poles for Orebin Creek. N = 79.

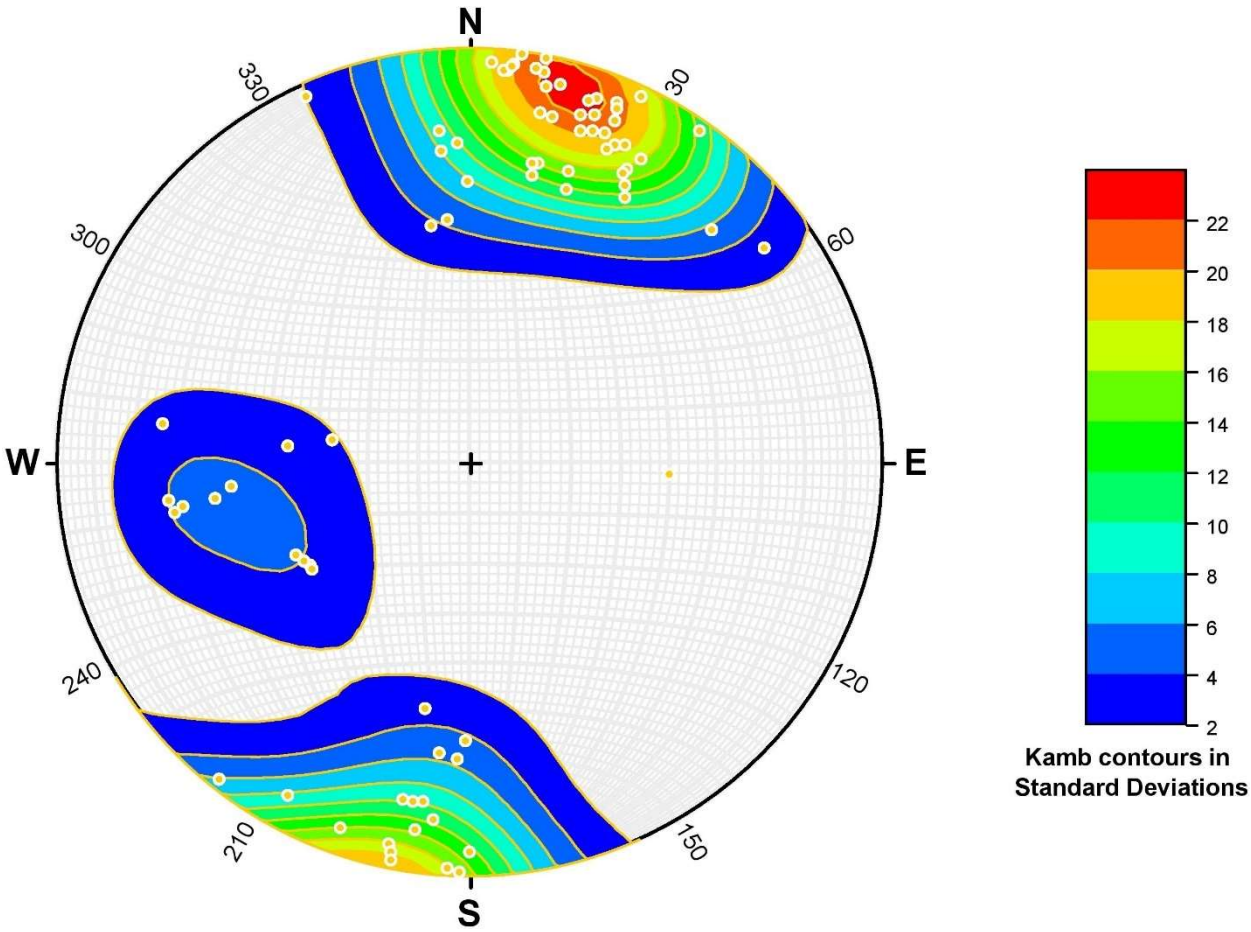

Figure 175 - Kamb contouring of joint poles for Orebin Creek. N = 79.

Riondel

Bedding

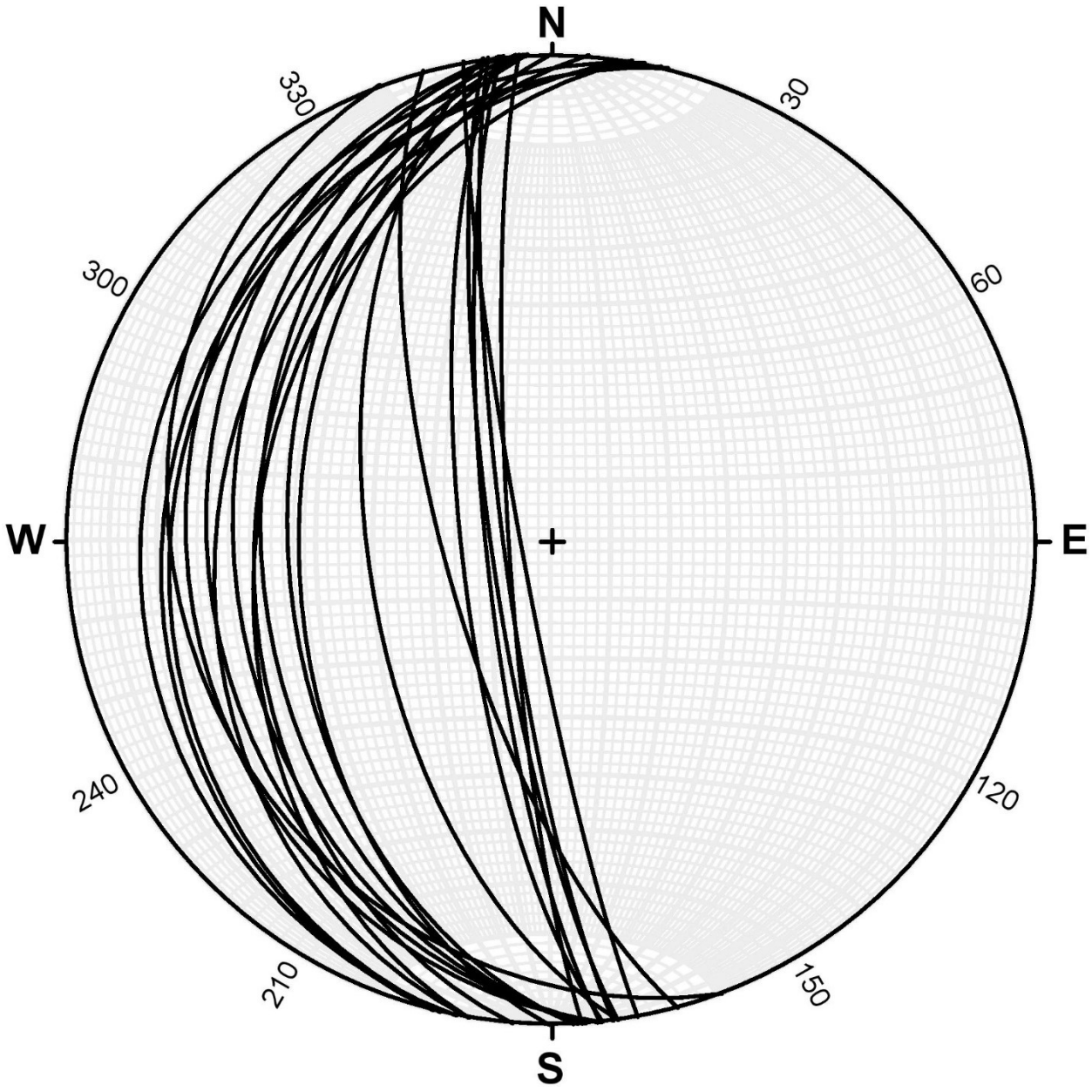

Figure 176 - Bedding planes for Riondel. N = 21.

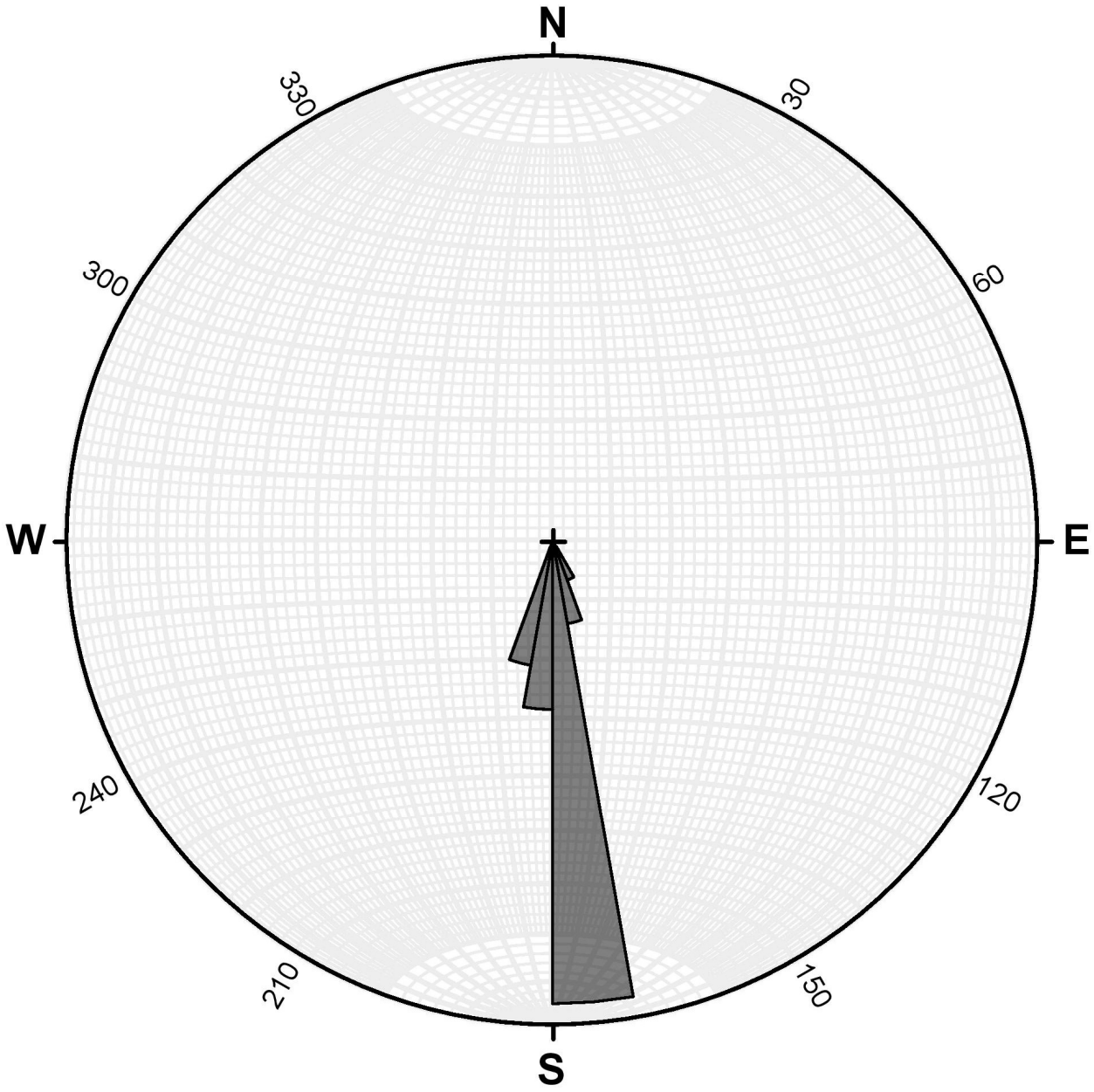

Figure 177 - Rose diagram of bedding planes for Riondel. N = 21.

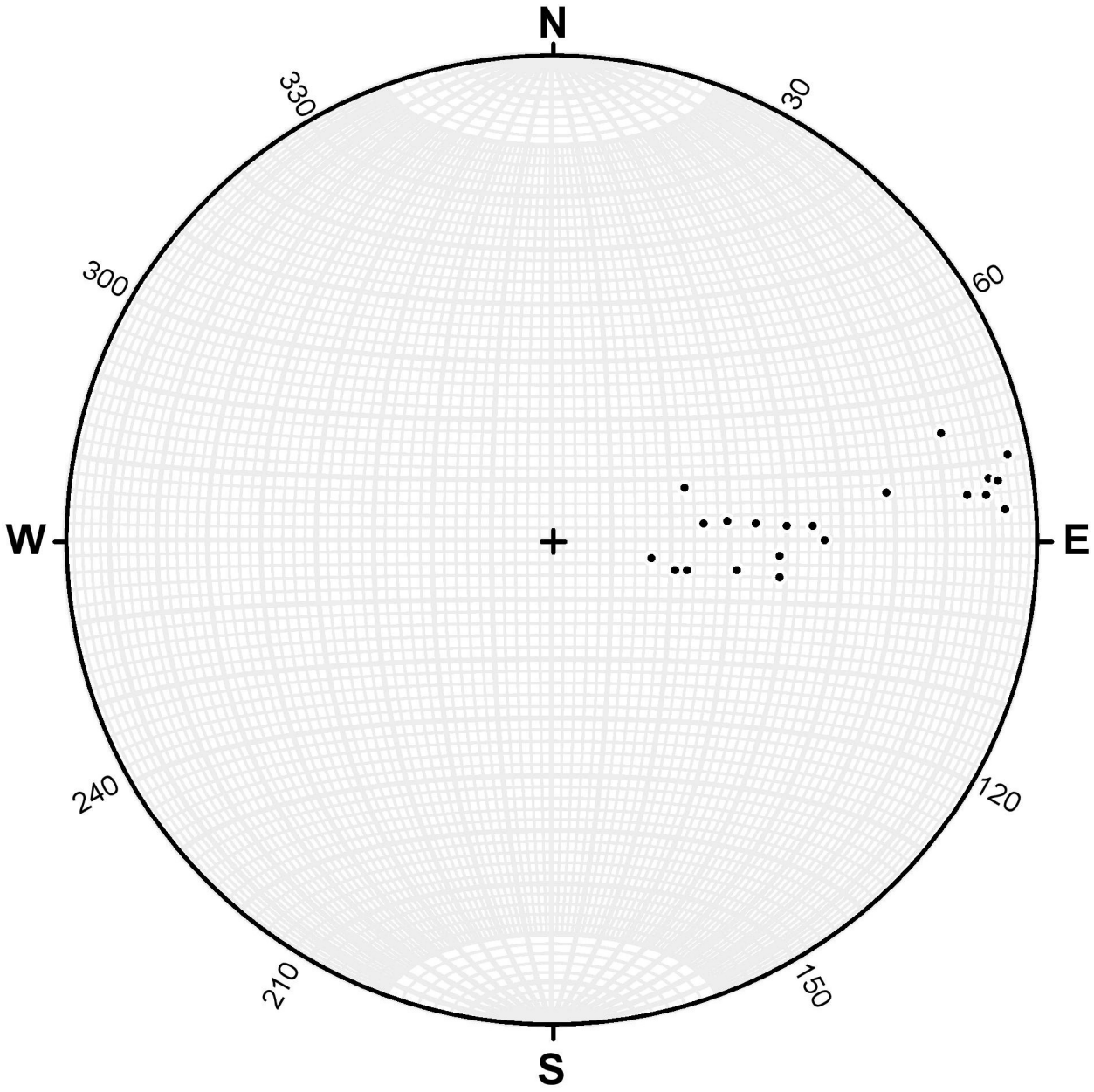

Figure 178 - Bedding poles for Riondel. N = 21.

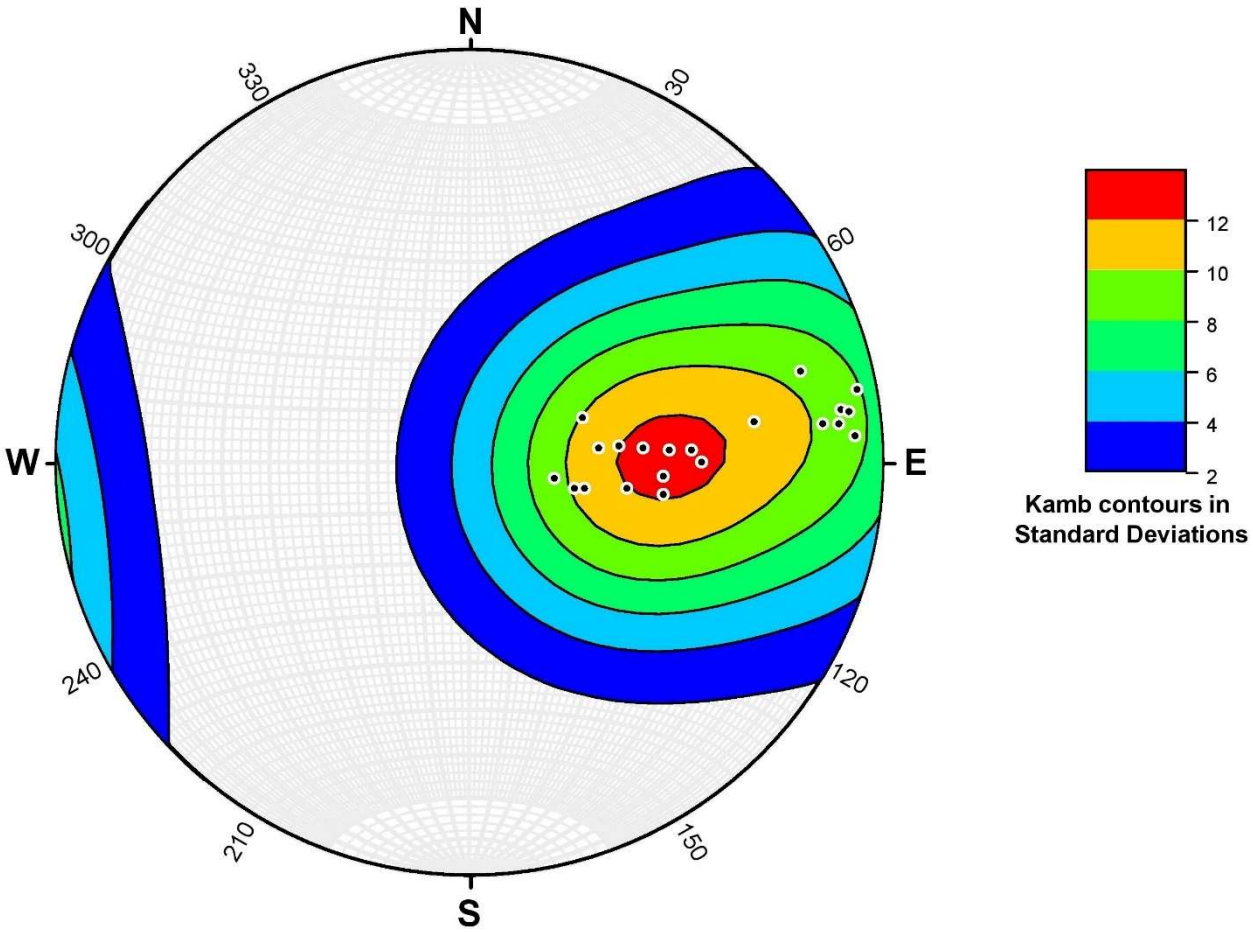

Figure 179 - Kamb contouring of bedding poles for Riondel. N = 21.

Jointing

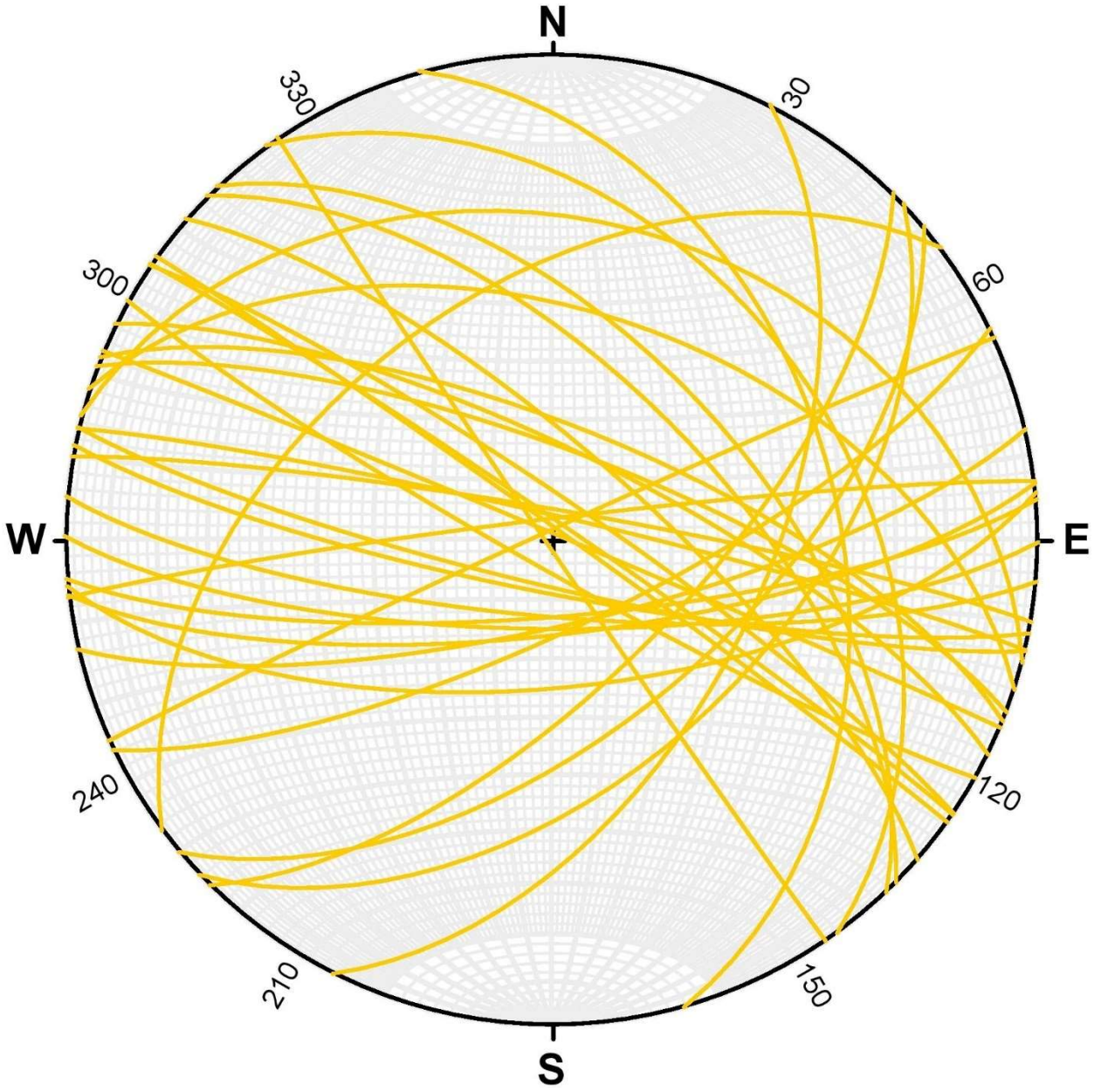

Figure 180 - Joint planes for Riondel. N = 34.

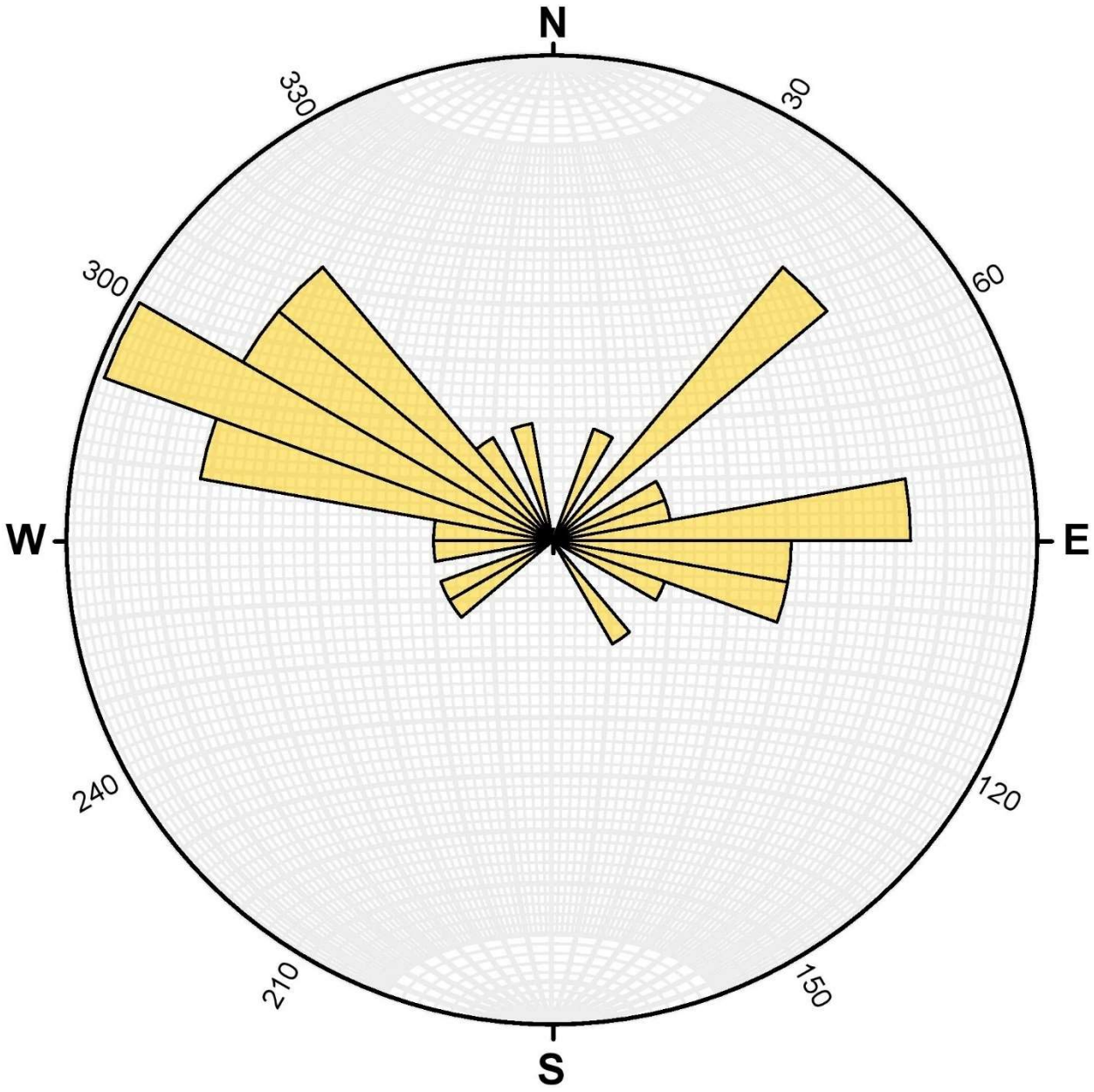

Figure 181 - Rose diagram of joint planes for Riondel. N = 34.

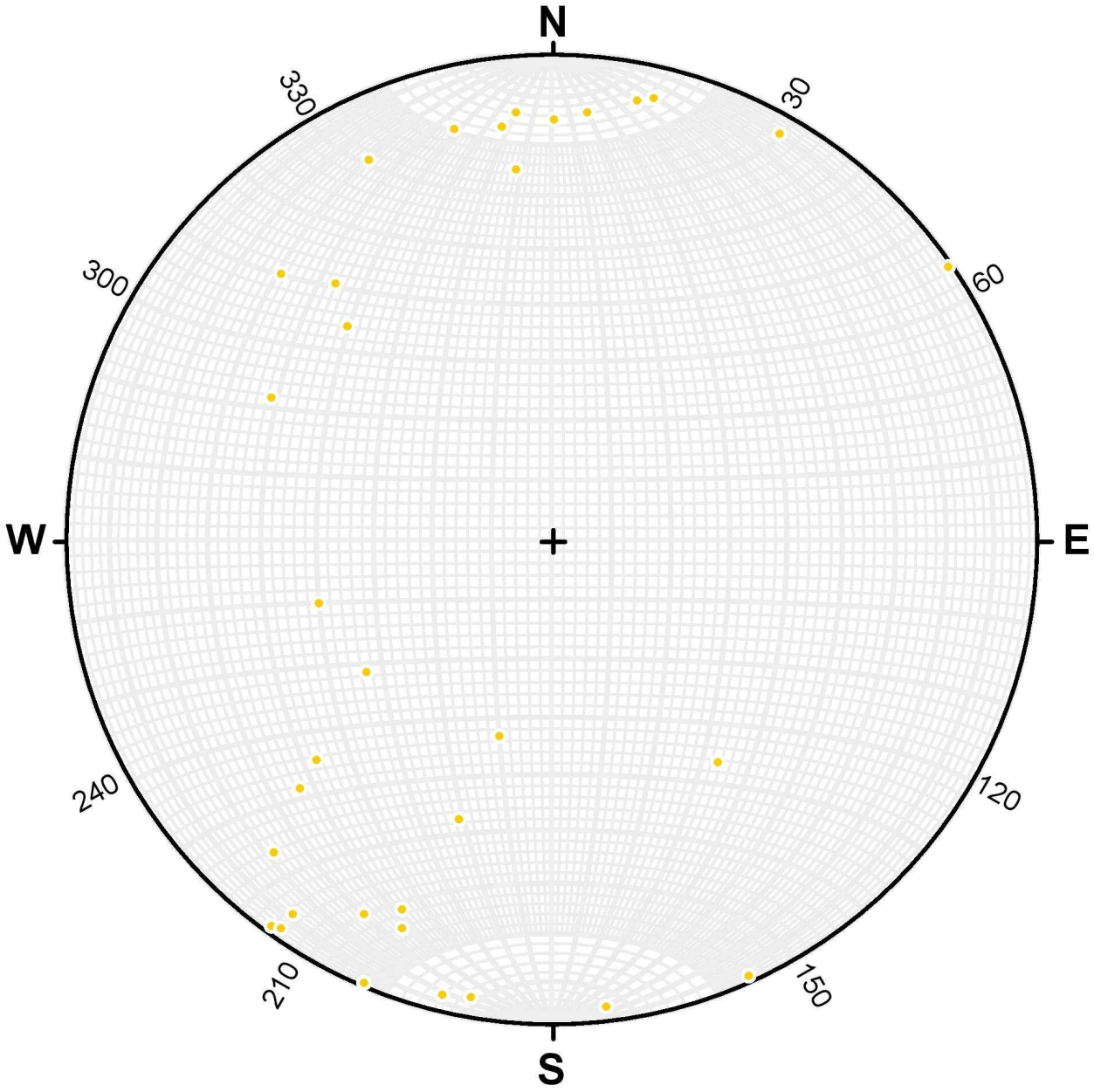

Figure 182 - Joint poles for Riondel. N = 34.

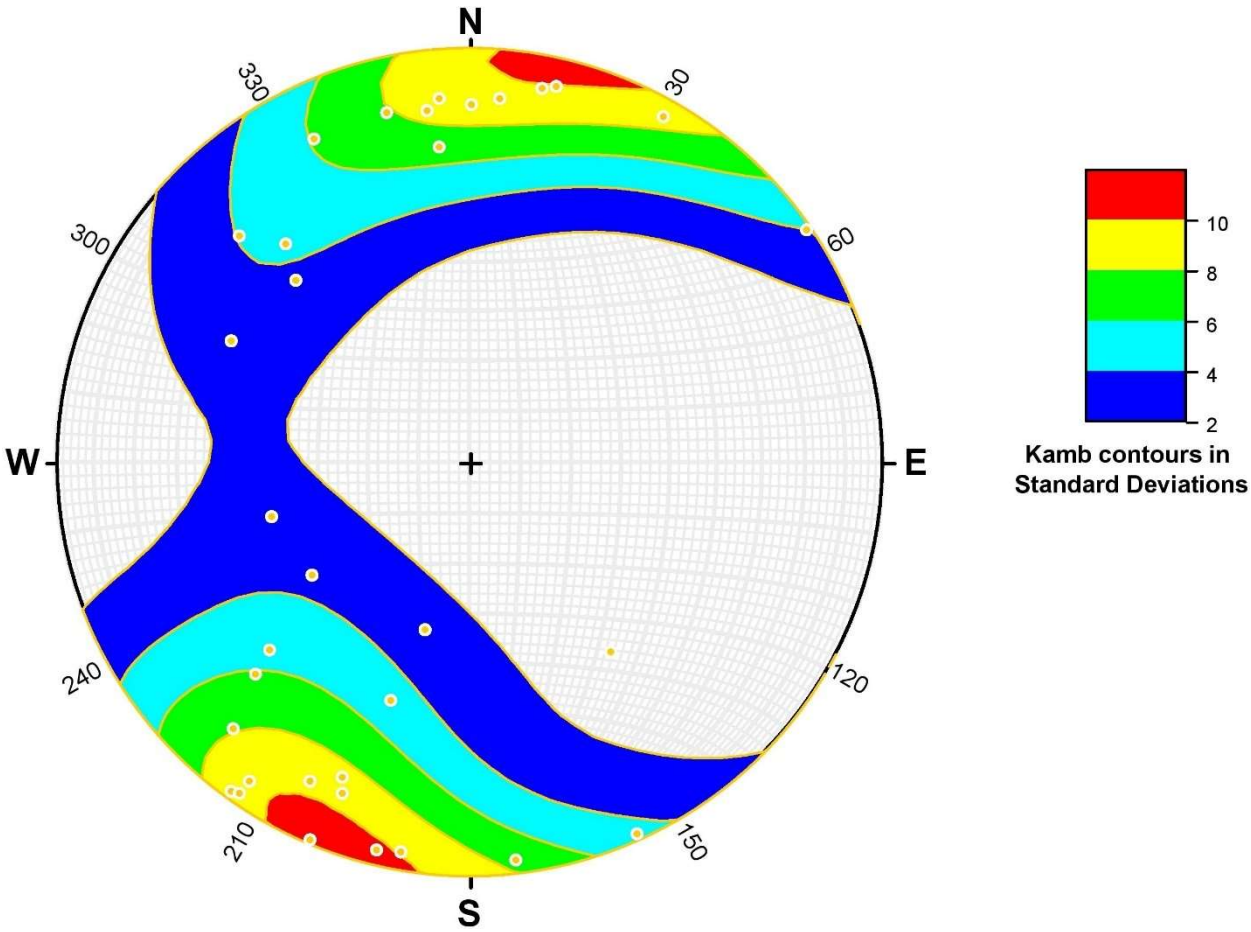

Figure 183 - Kamb contouring of joint poles for Riondel. N = 34.

Riondel Road

Bedding

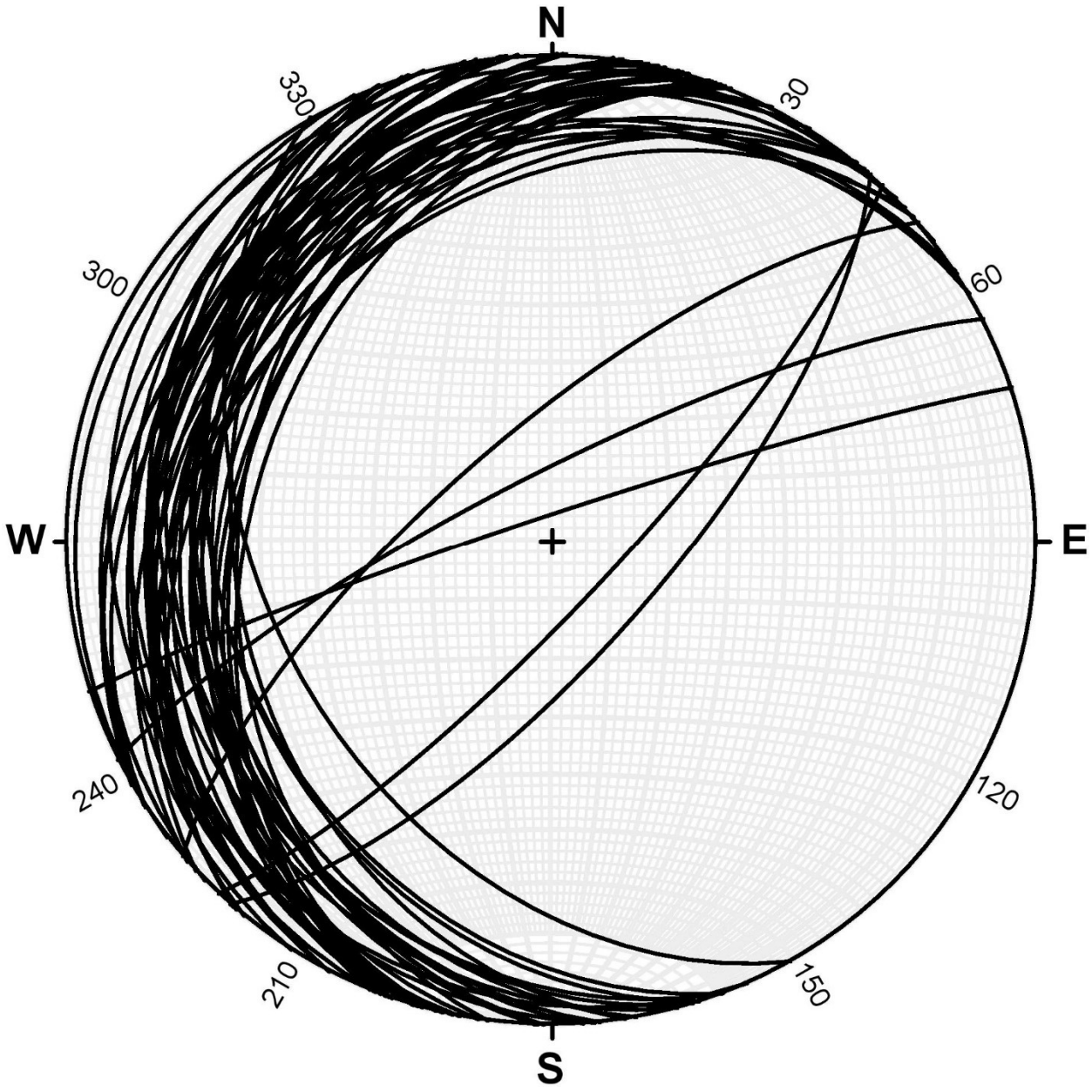

Figure 184 - Bedding planes for Riondel Road. N = 50.

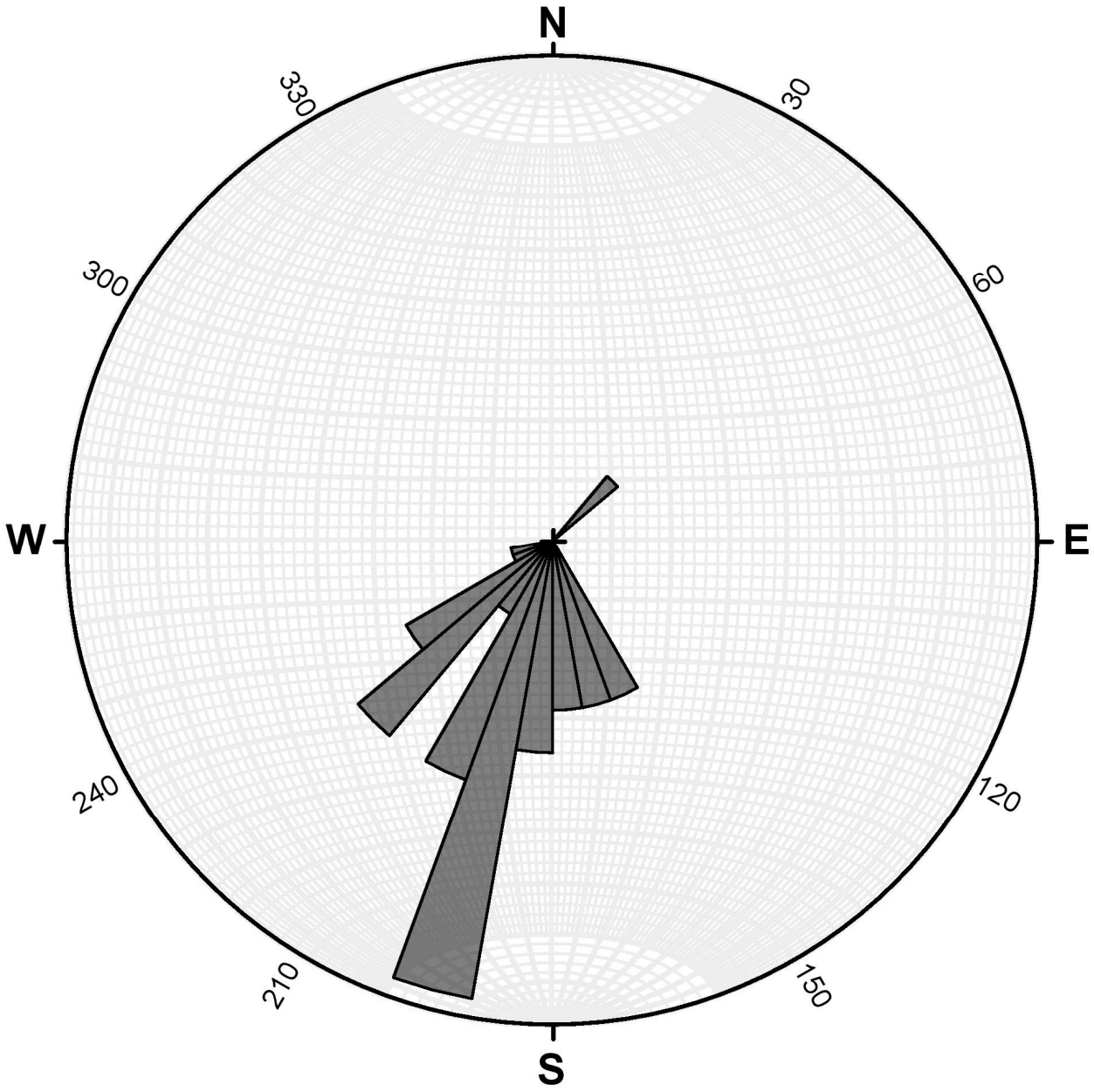

Figure 185 - Rose diagram of bedding planes for Riondel Road. N = 50.

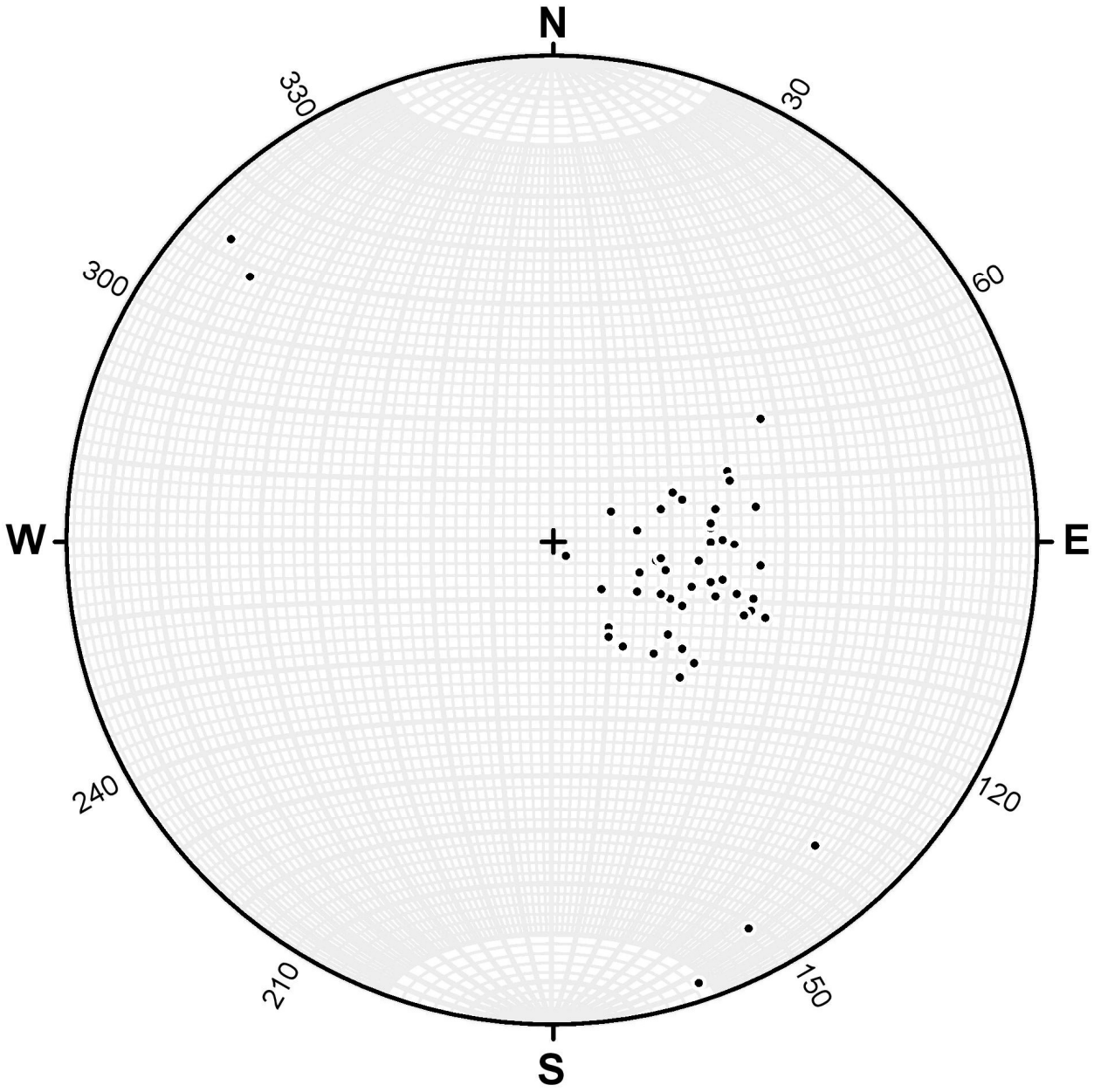

Figure 186 - Bedding poles for Riondel Road. N = 50.

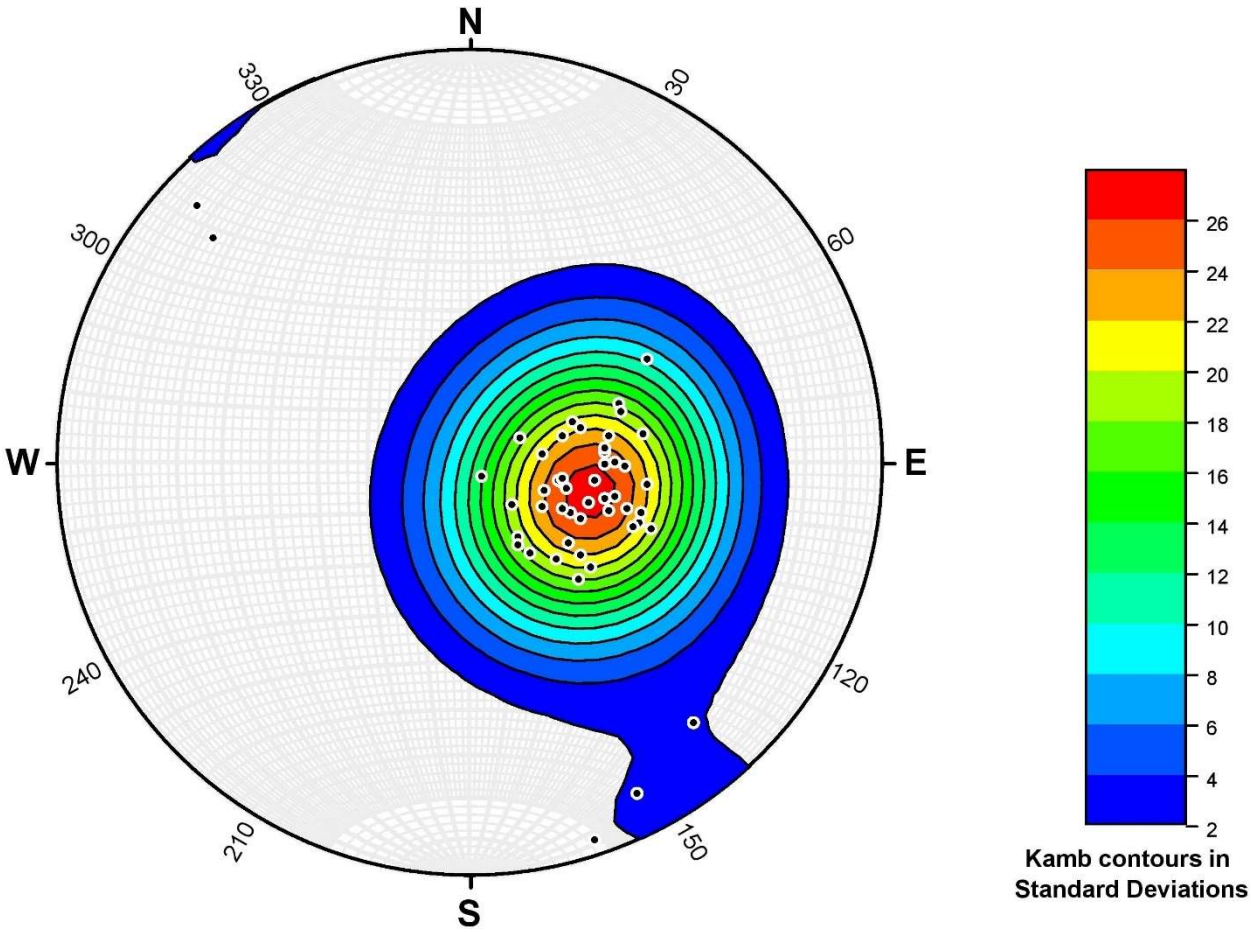

Figure 187 - Kamb contouring of bedding poles for Riondel Road. N = 50.

Faulting

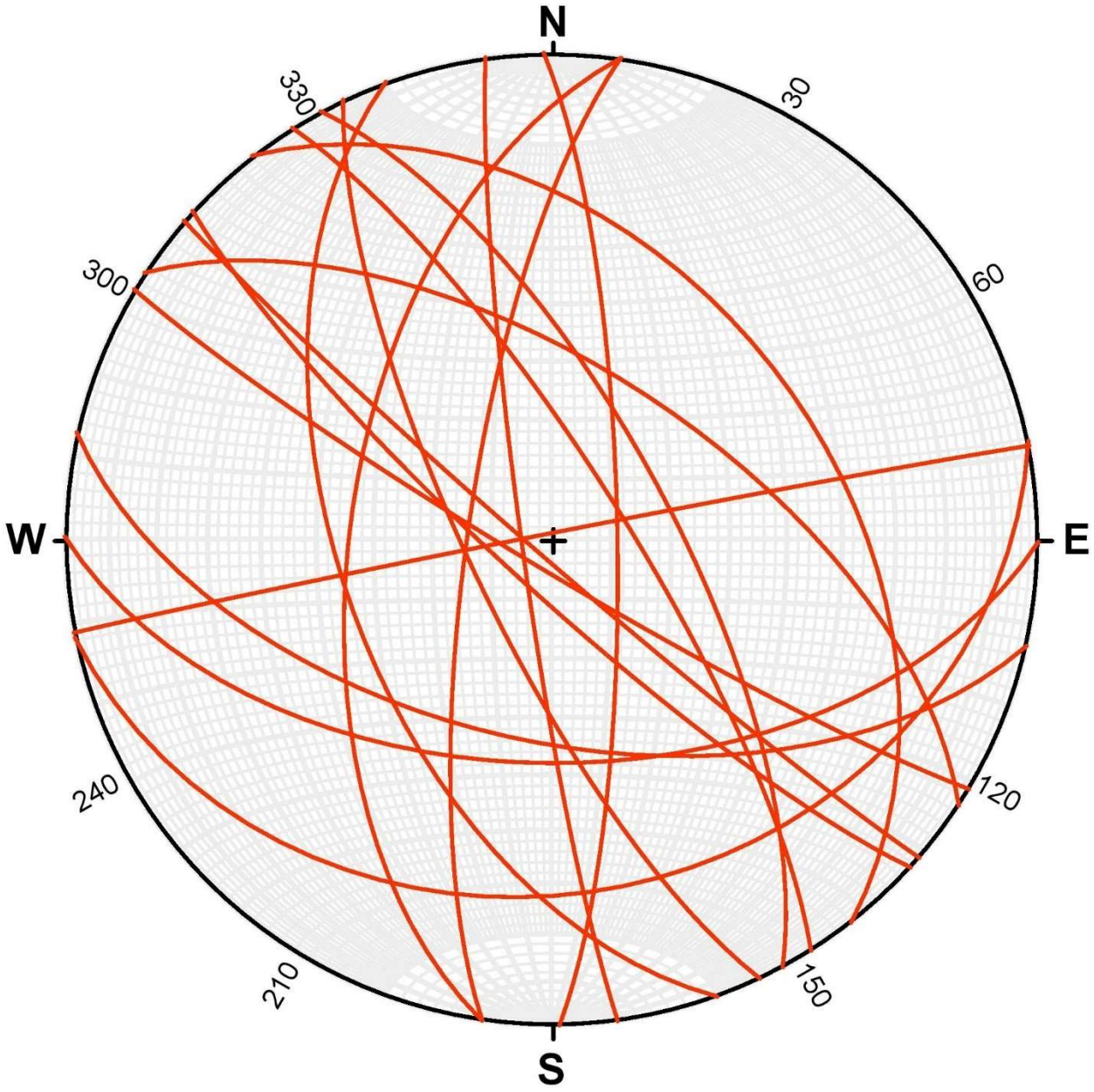

Figure 188 - Fault planes for Riondel Road. N = 17.

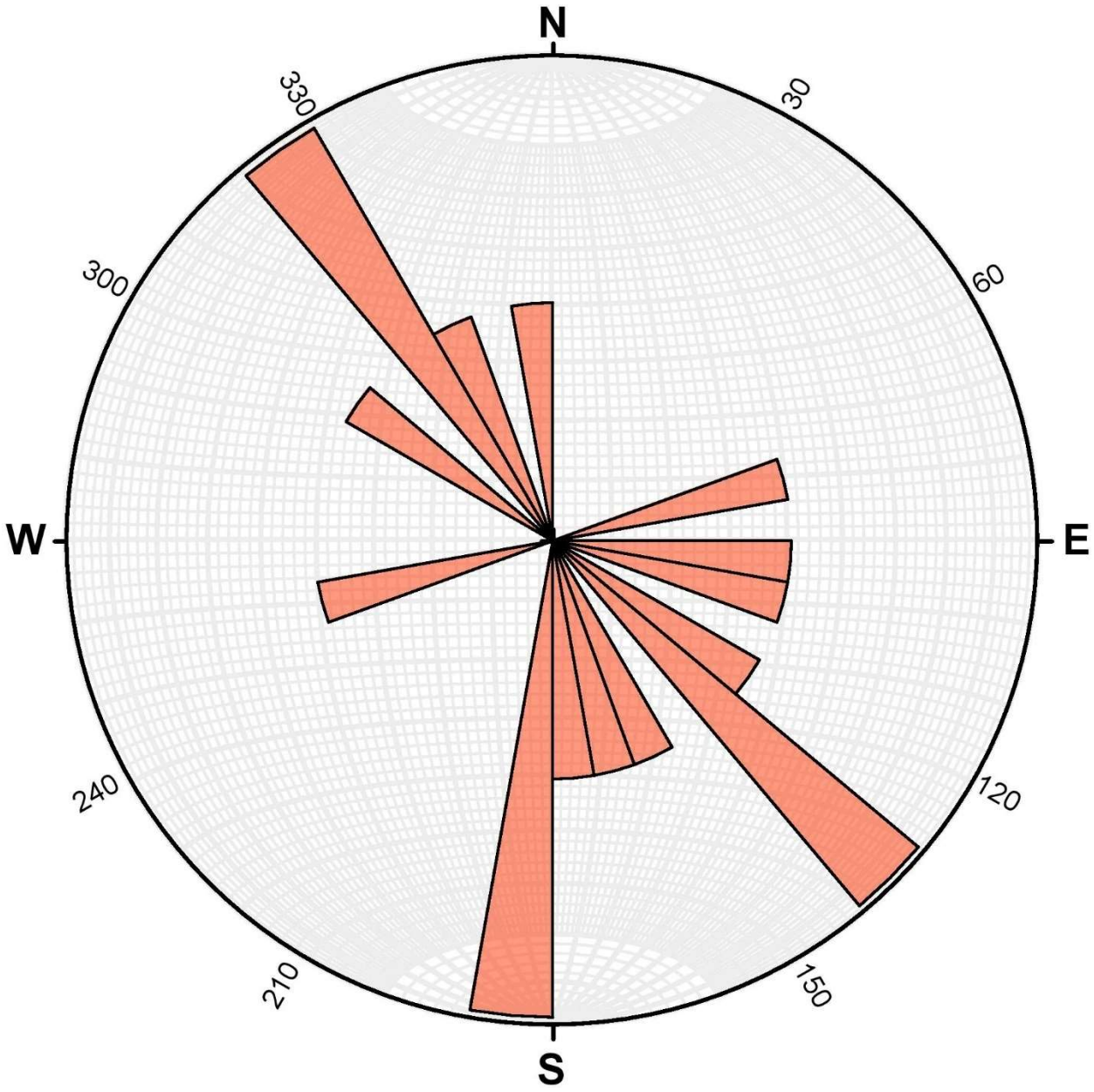

Figure 189 - Rose diagram of fault planes for Riondel Road. N = 17.

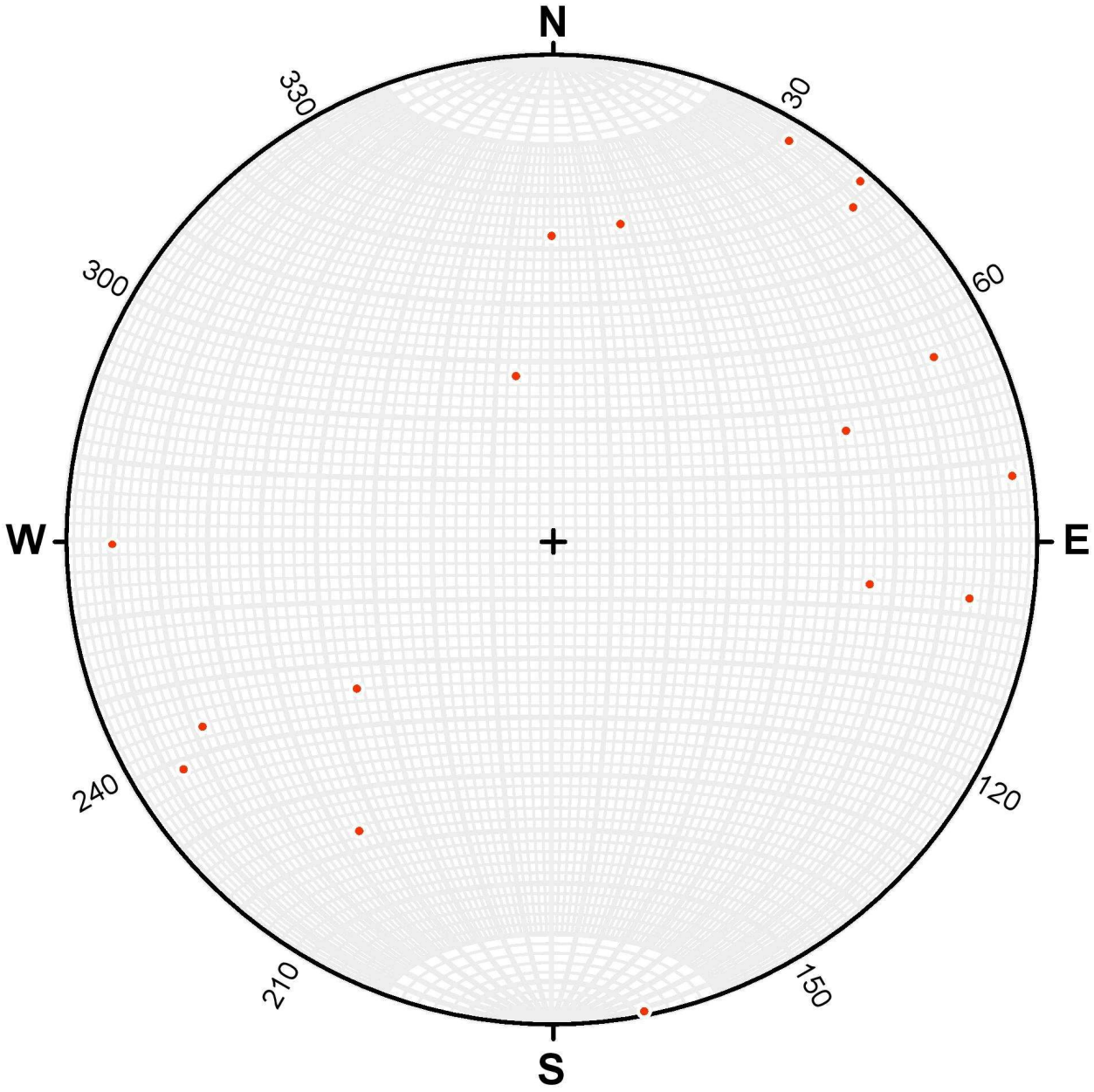

Figure 190 - Fault poles for Riondel Road. N = 17.

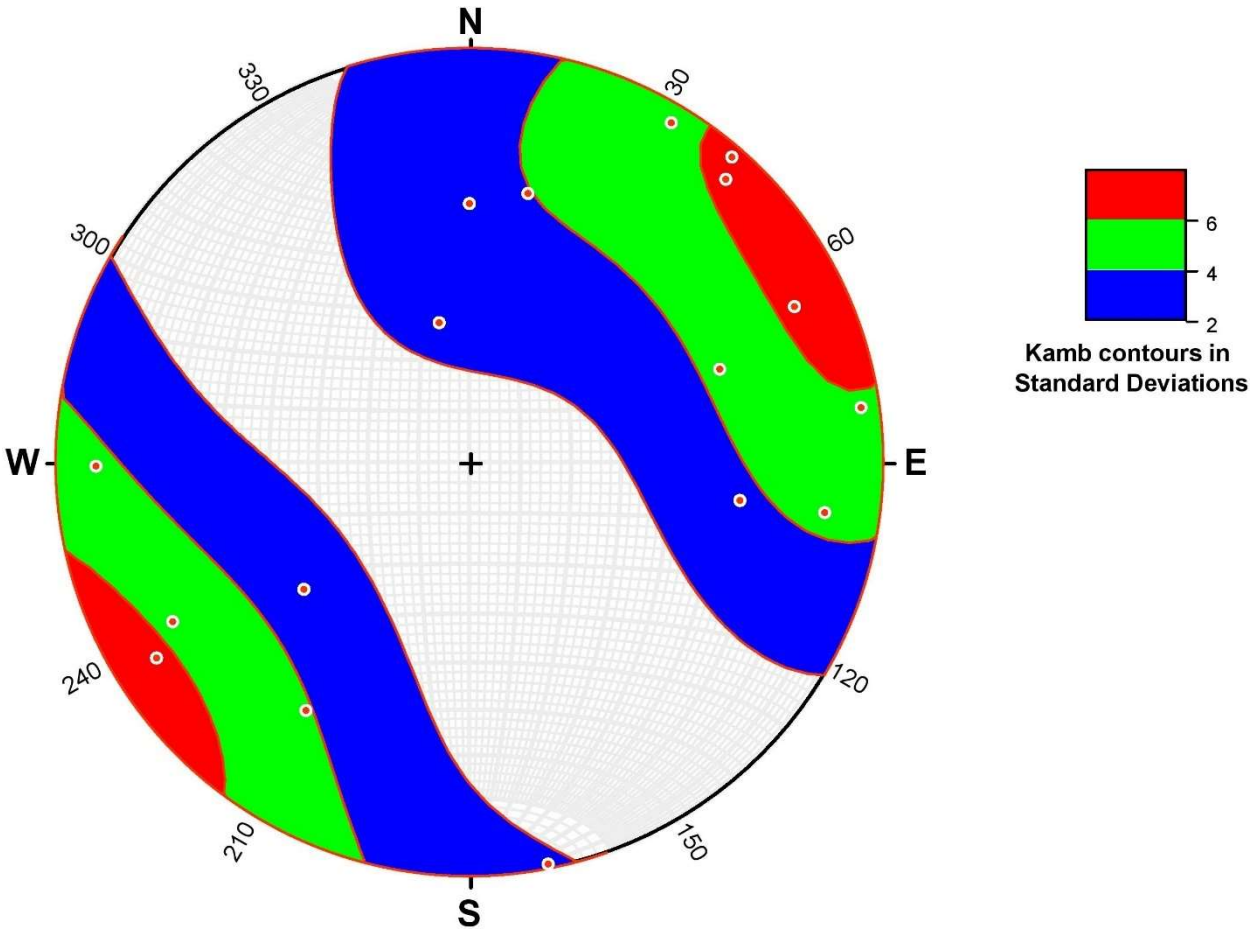

Figure 191 - Kamb contouring of fault poles for Riondel Road. N = 17.

Jointing

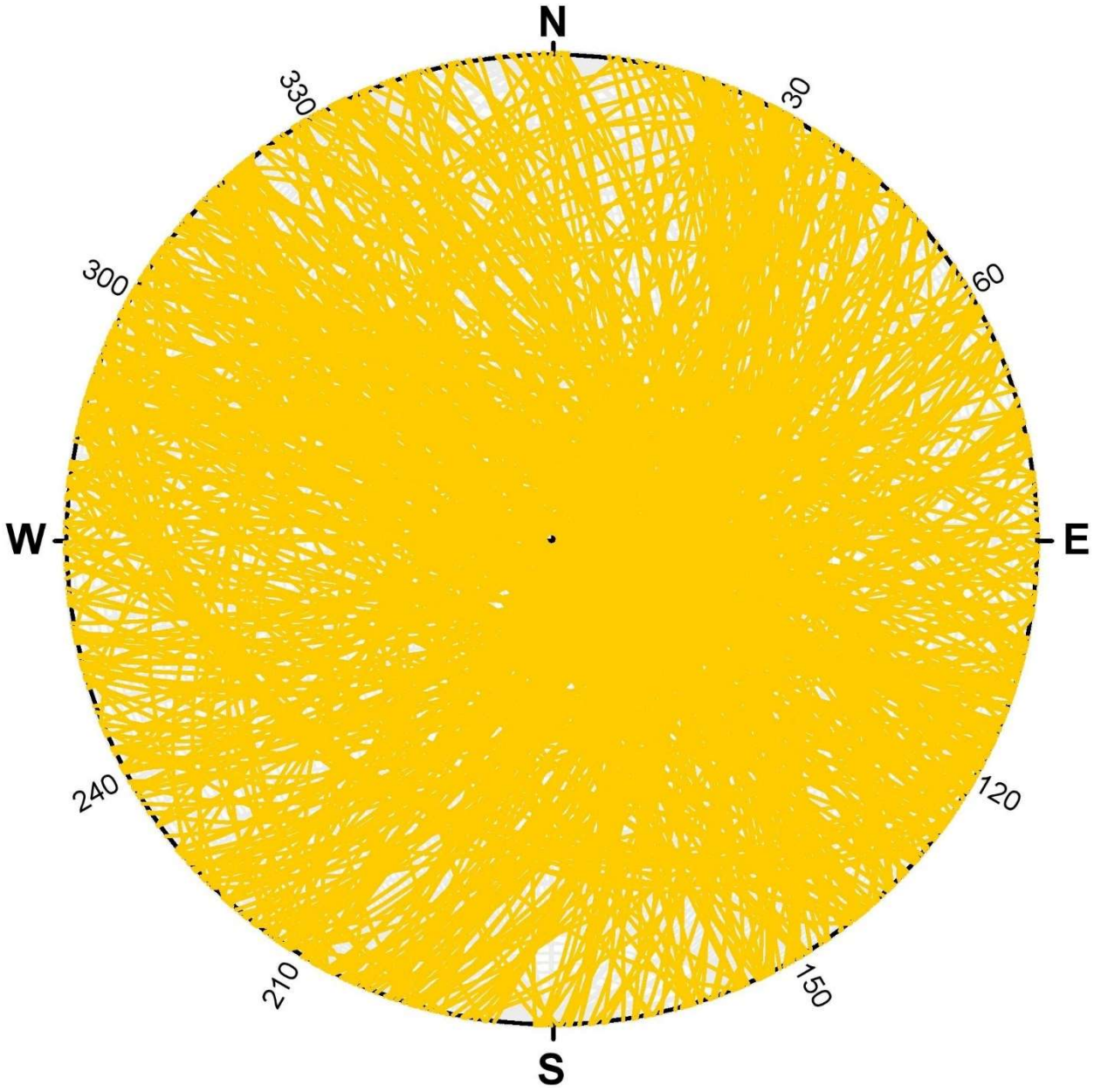

Figure 192 - Joint planes for Riondel Road. N = 482.

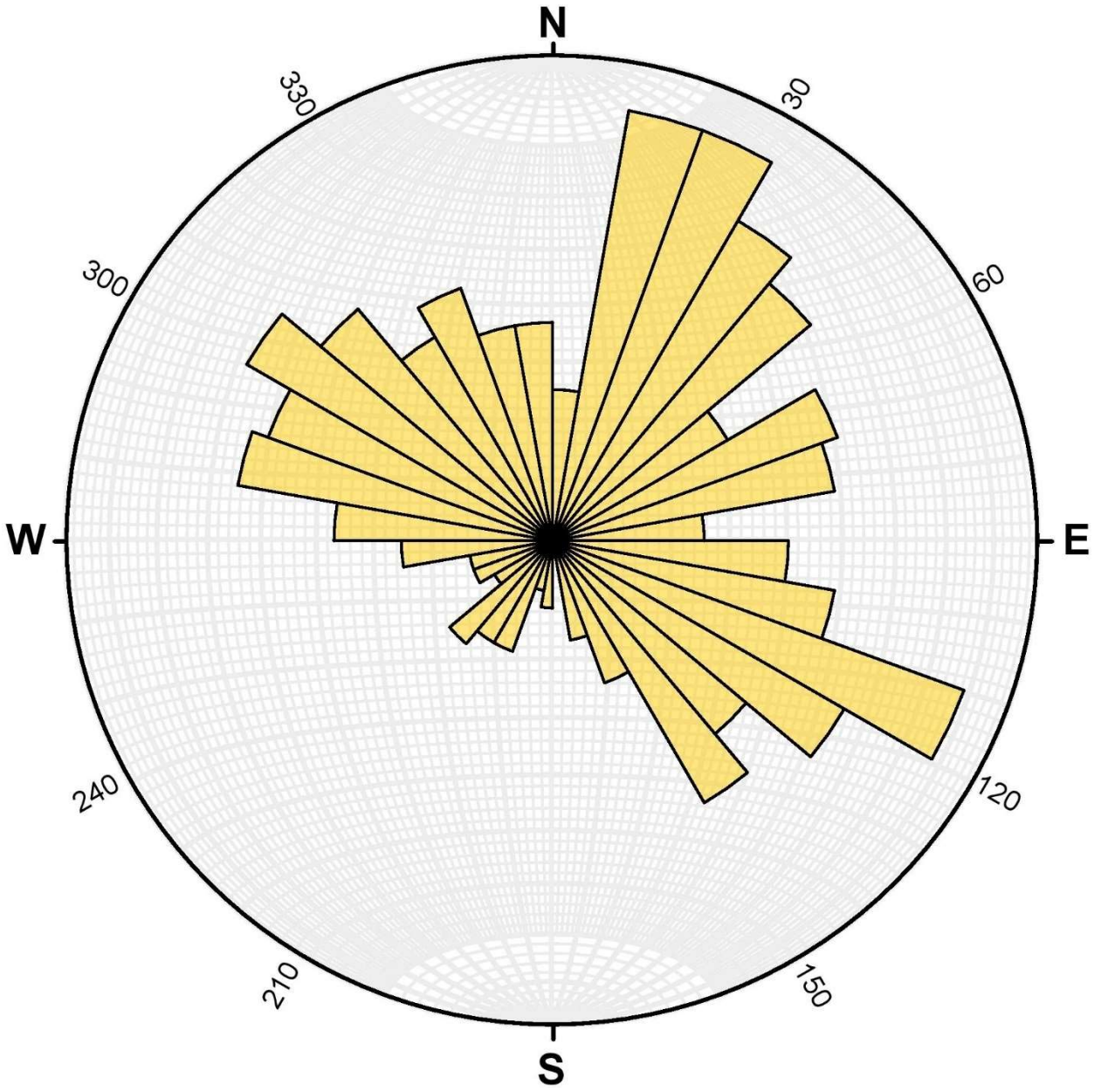

Figure 193 - Rose diagram of joint planes for Riondel Road. N = 482.

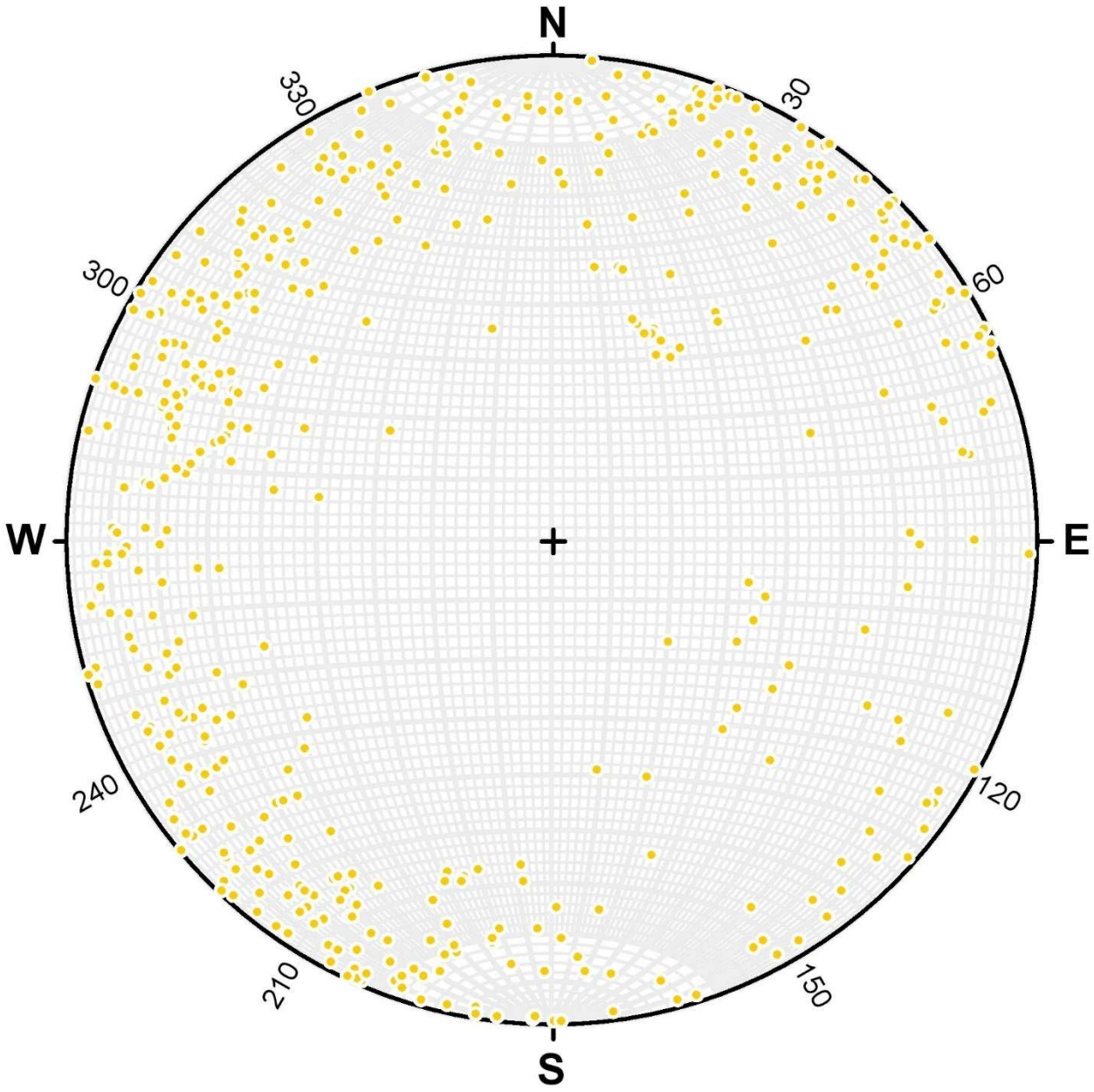

Figure 194 - Joint poles for Riondel Road. N = 482.

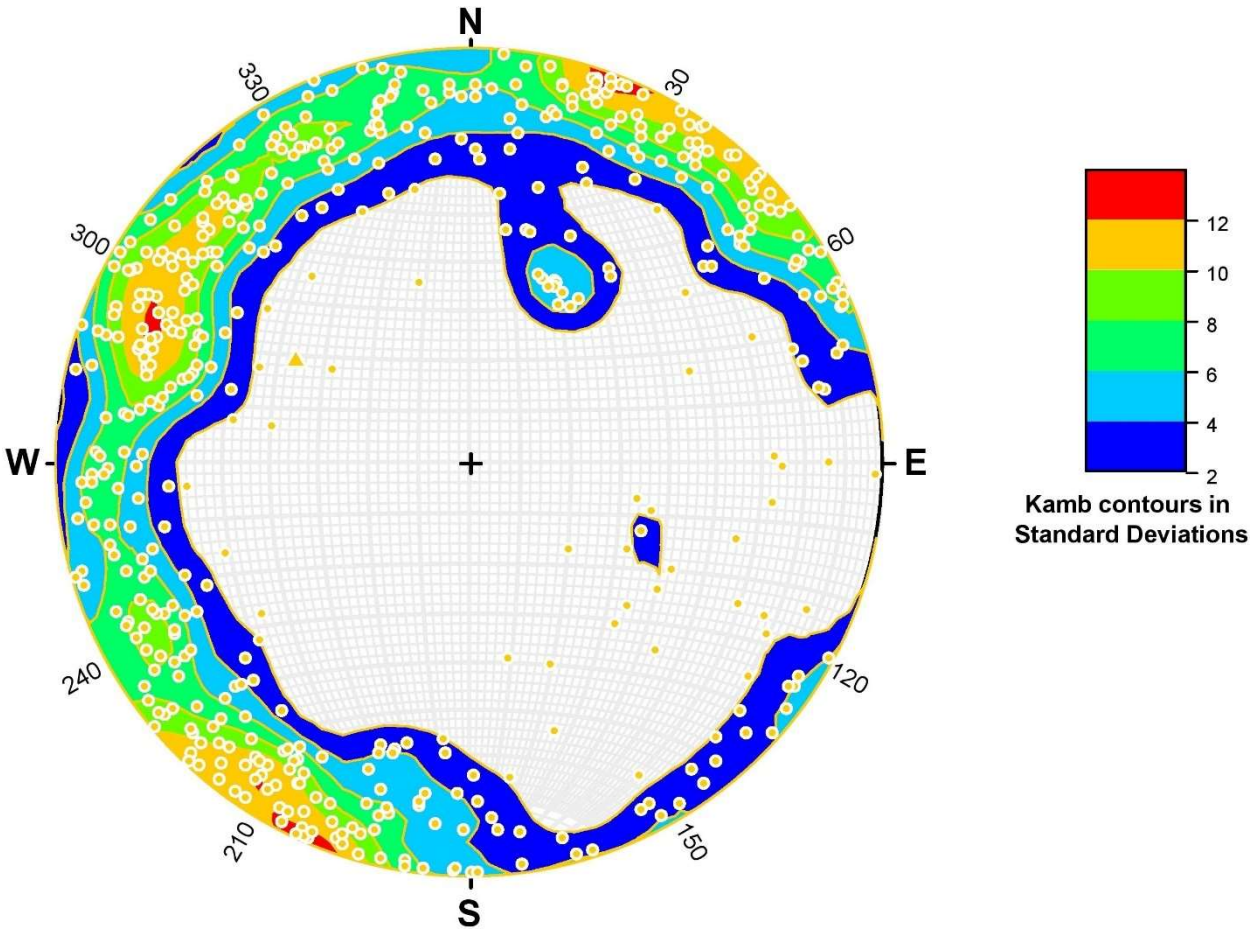

Figure 195 - Kamb contouring of joint poles for Riondel Road. N = 482.

Upper Crawford Creek

Bedding

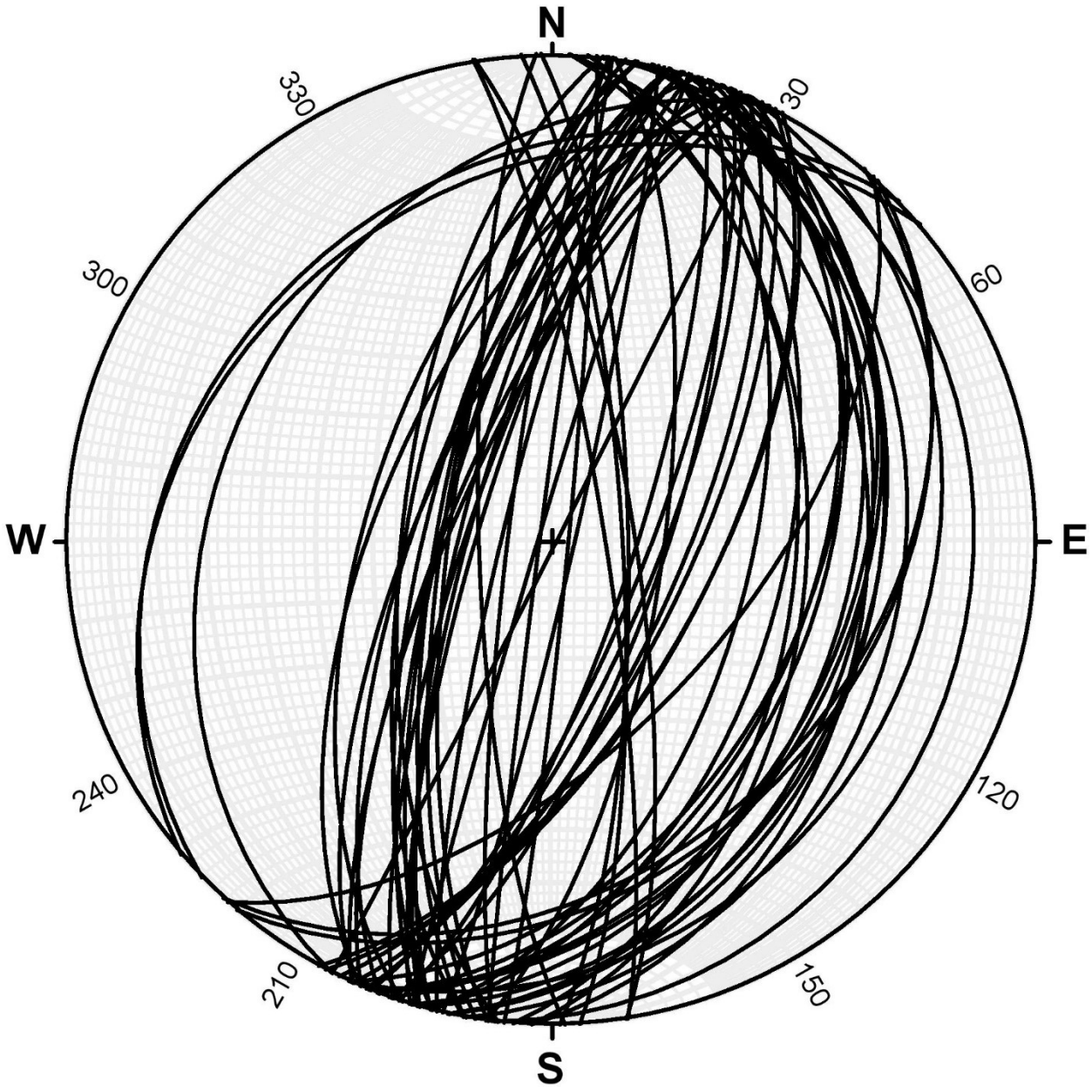

Figure 196 - Bedding planes for Upper Crawford Creek. N = 62.

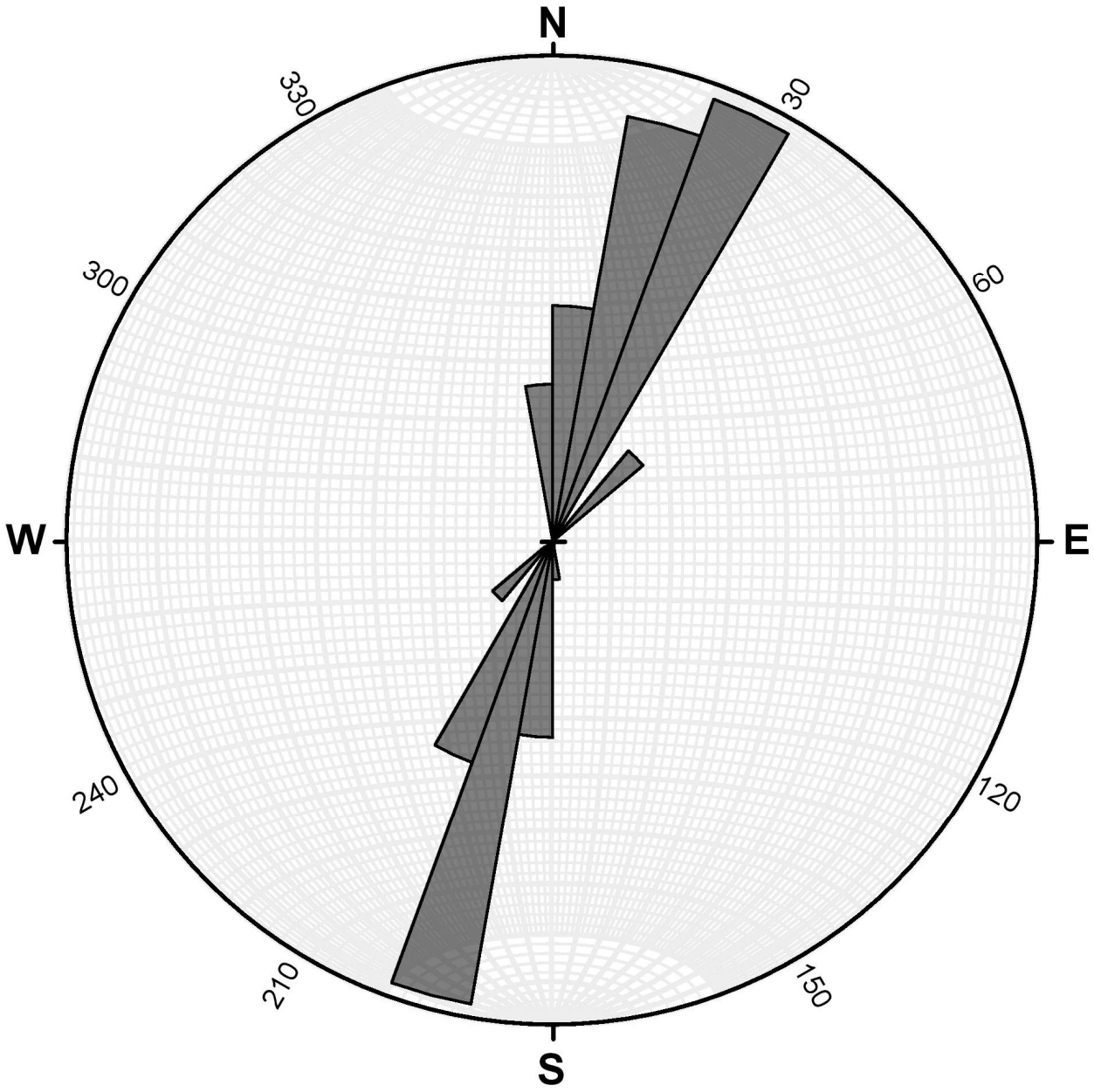

Figure 197 - Rose diagram of bedding planes for Upper Crawford Creek. N = 62.

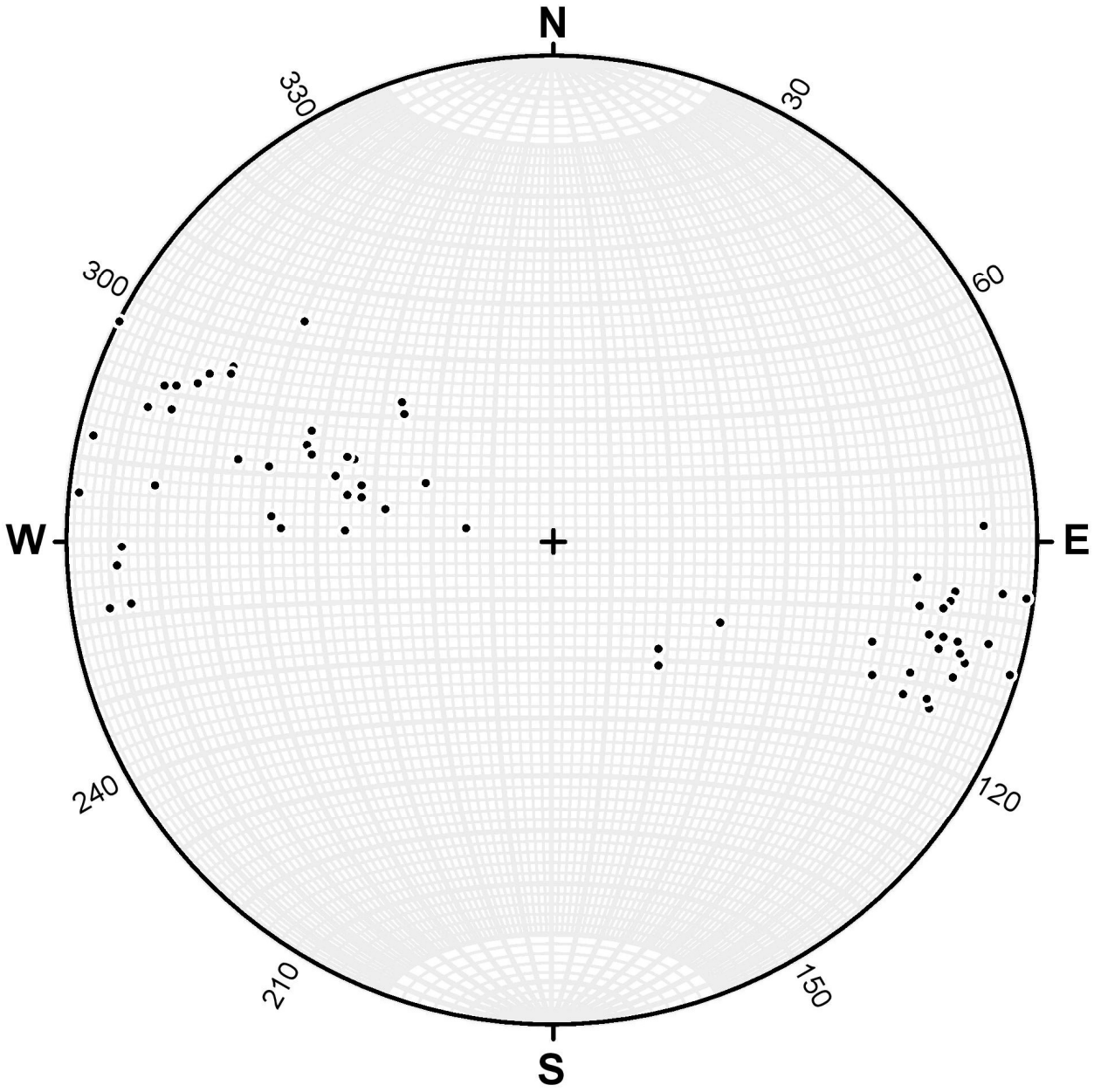

Figure 198 - Bedding poles for Upper Crawford Creek. N = 62.

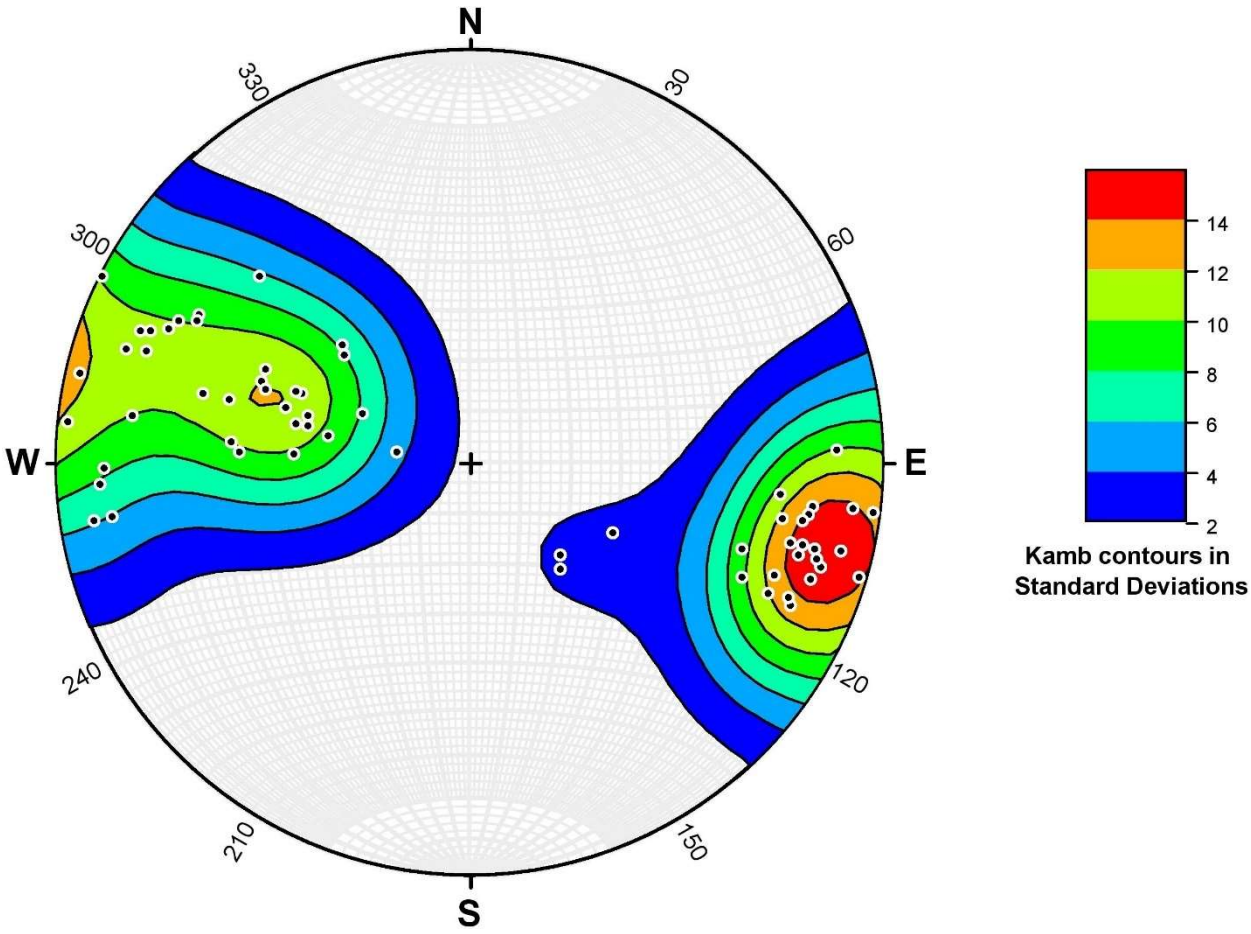

Figure 199 - Kamb contouring of bedding poles for Upper Crawford Creek. N = 62.

Jointing

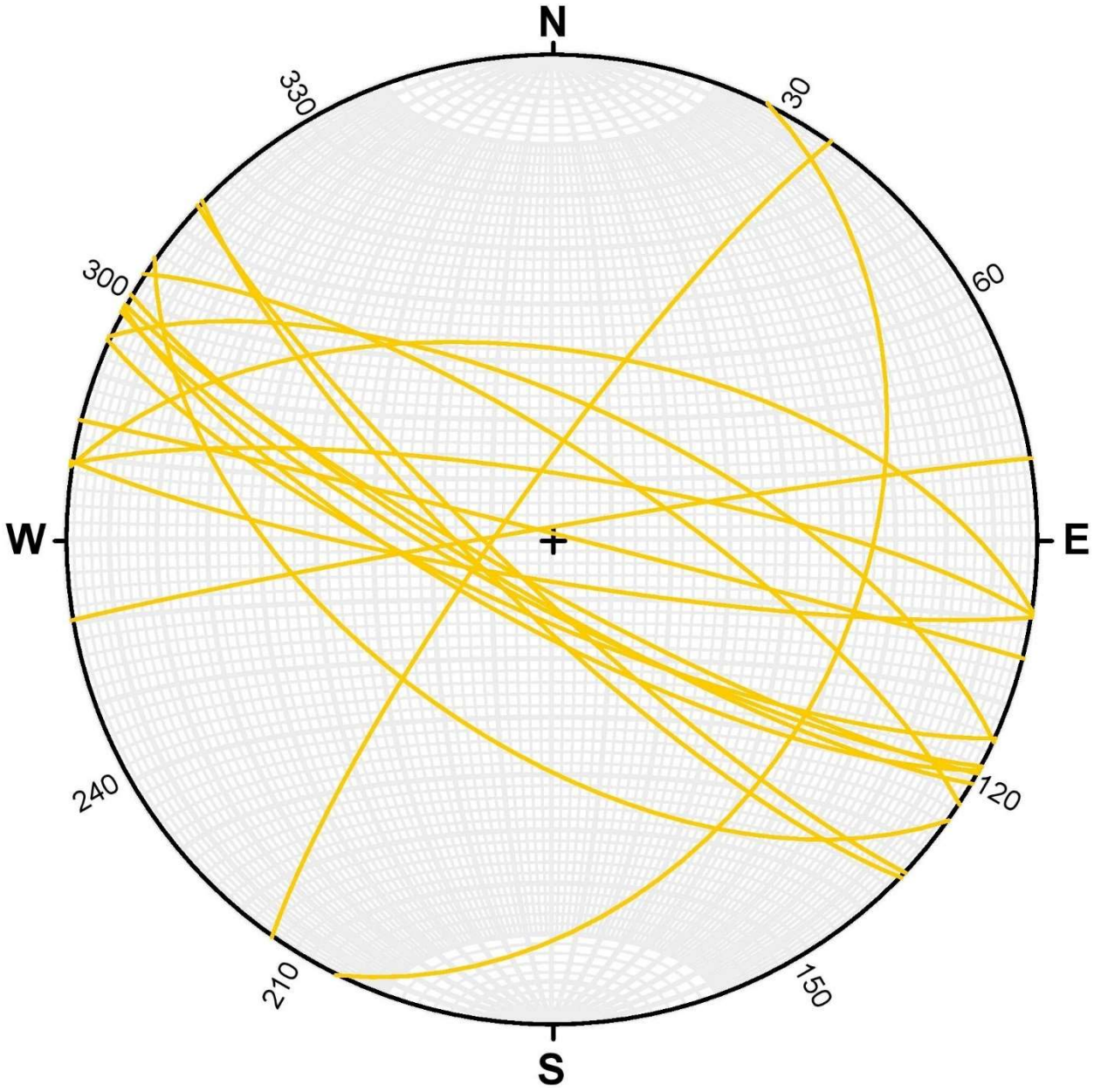

Figure 200 - Joint planes for Upper Crawford Creek. N = 17.

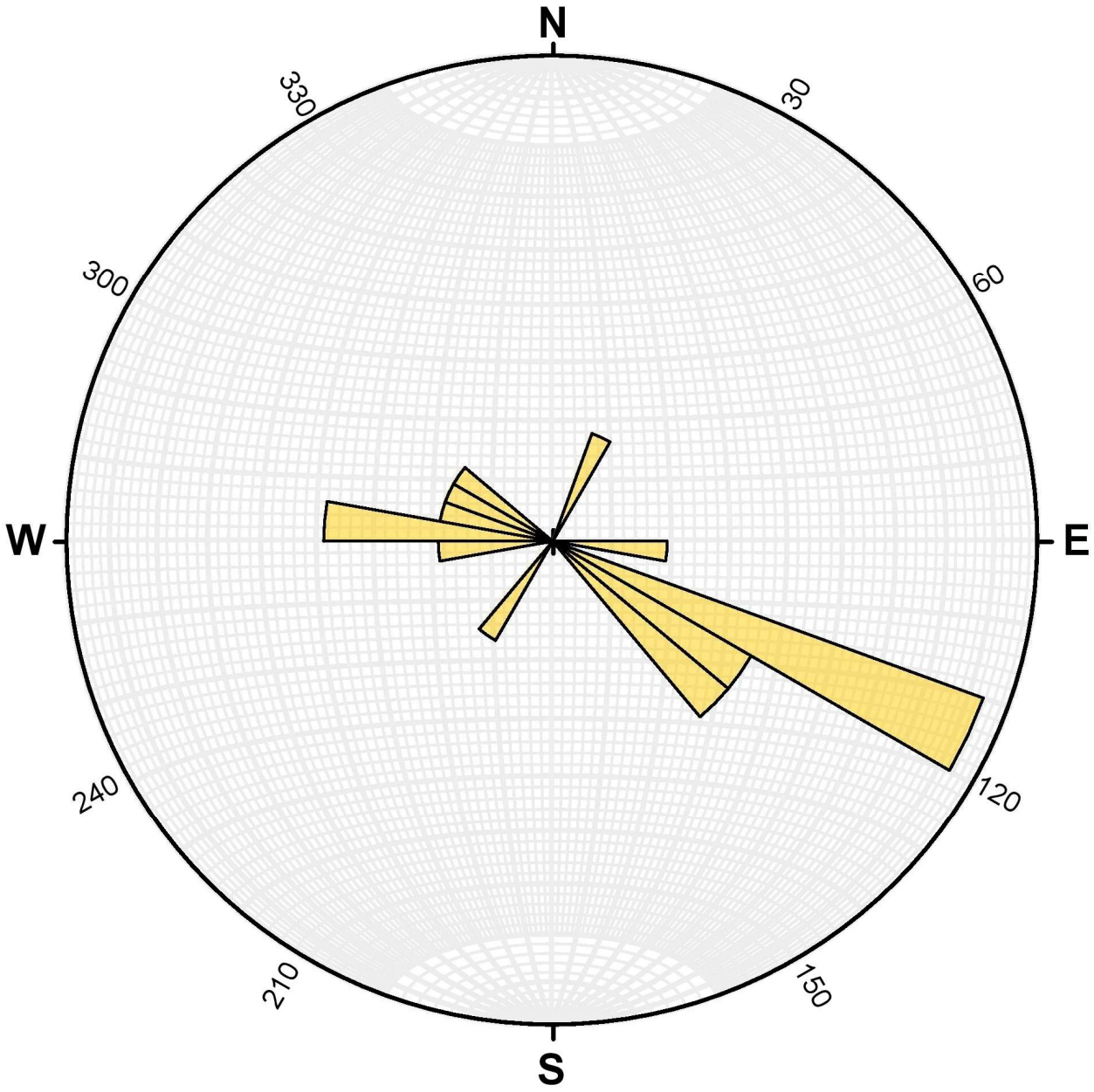

Figure 201 - Rose diagram of joint planes for Upper Crawford Creek. N = 17.

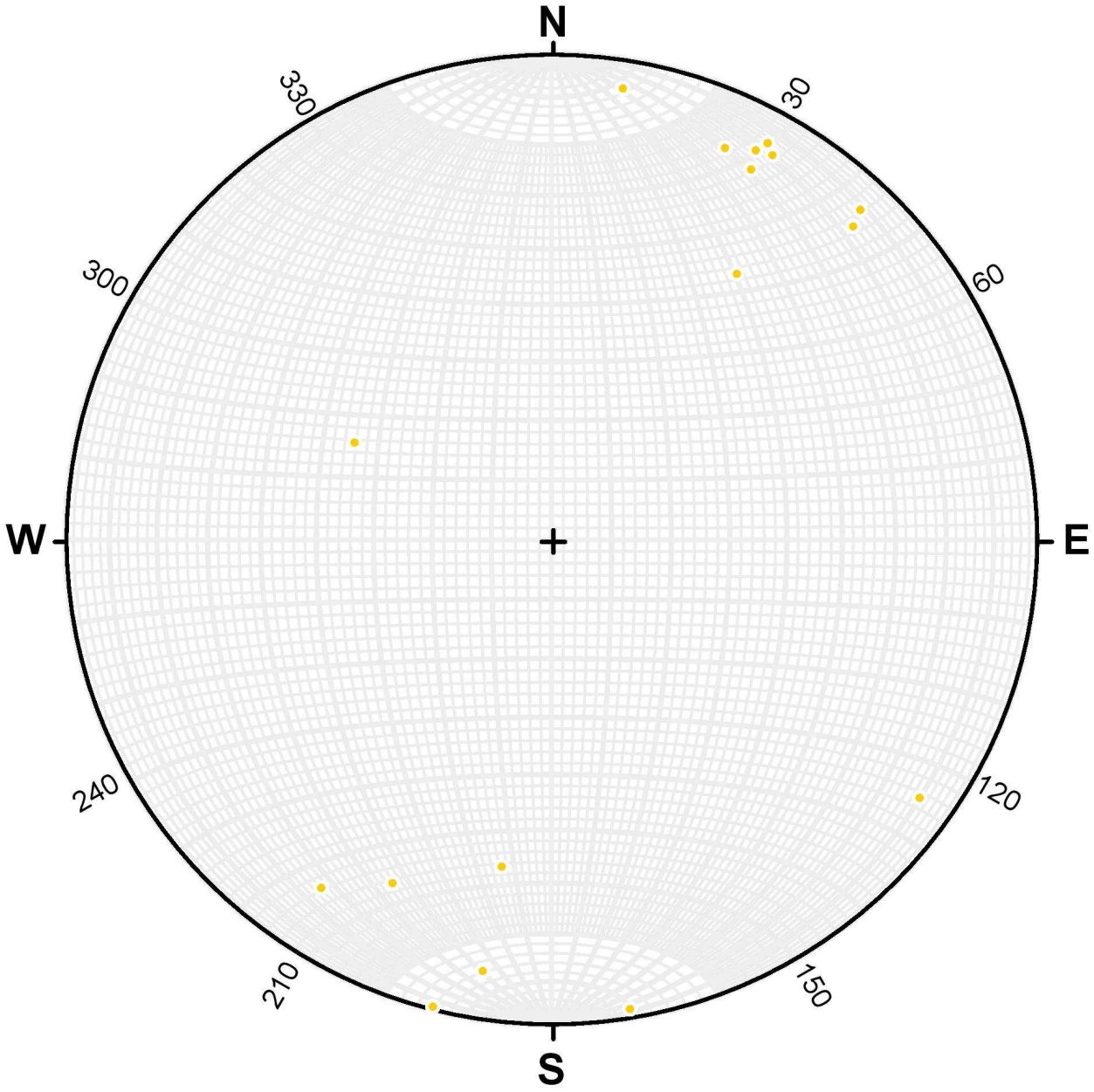

Figure 202 - Joint poles for Upper Crawford Creek. N = 17.

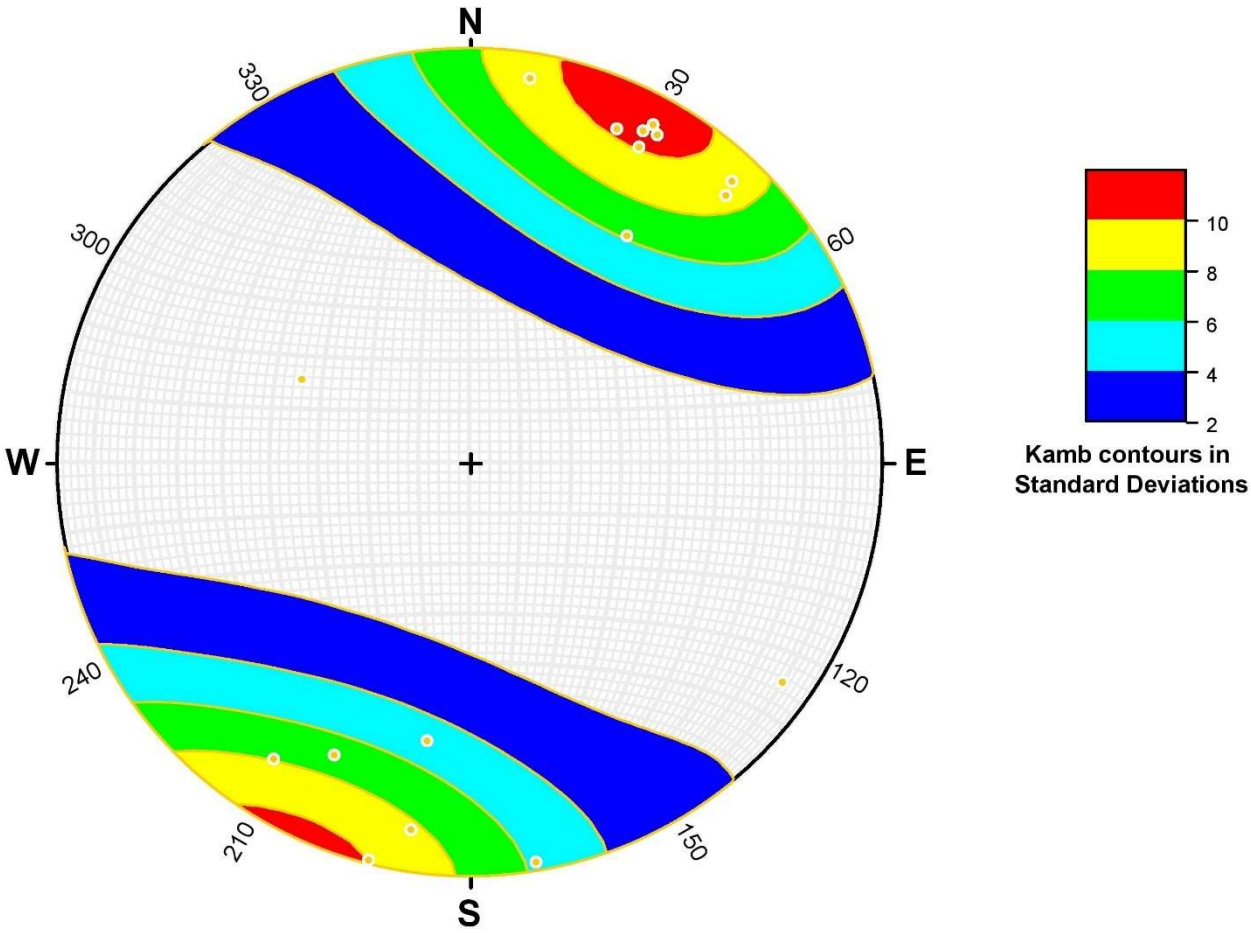

Figure 203 - Kamb contouring of joint poles for Upper Crawford Creek. N = 17.

Plots for All Data

Bedding

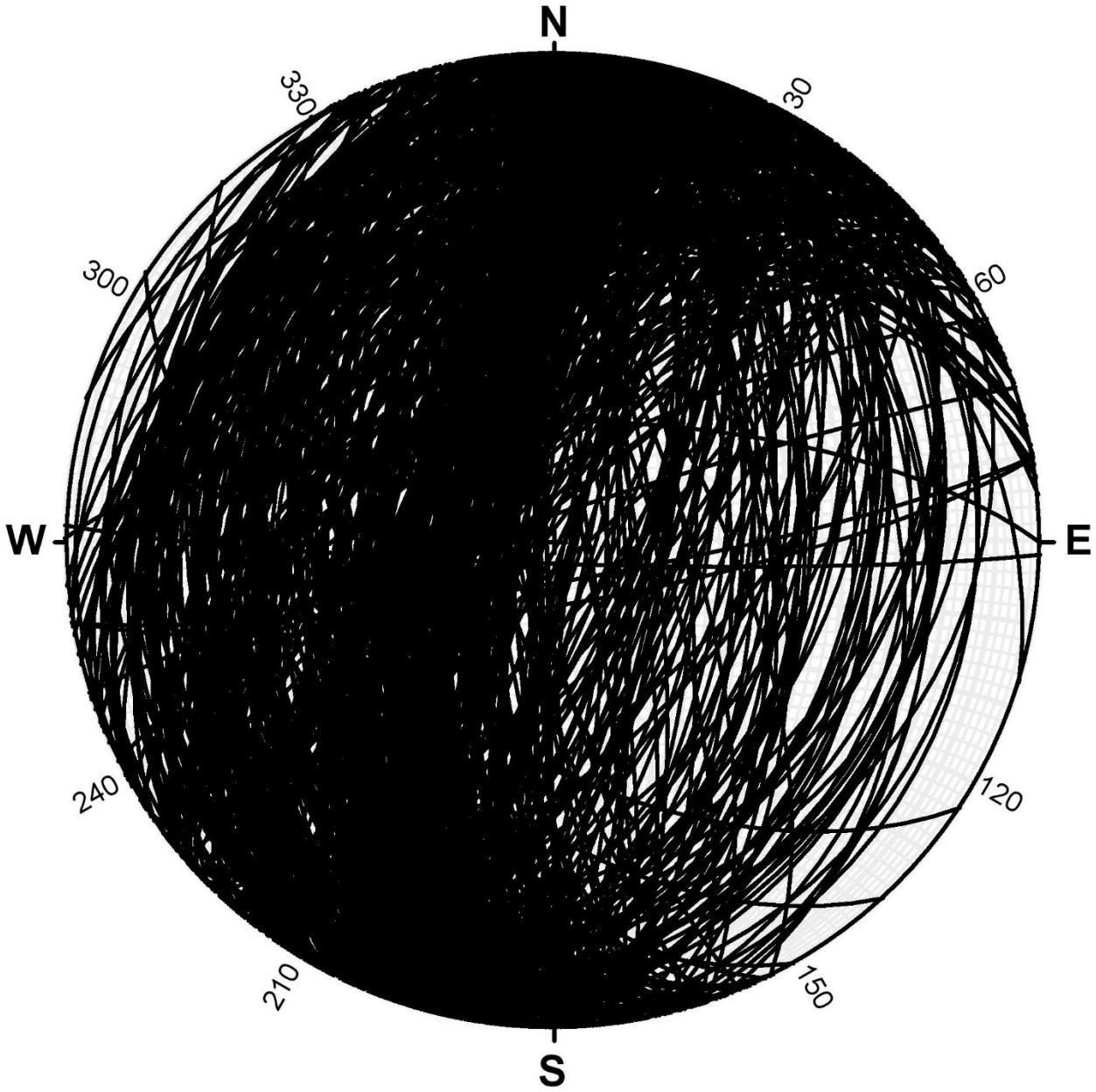

Figure 204 - Bedding planes for all data. N = 538.

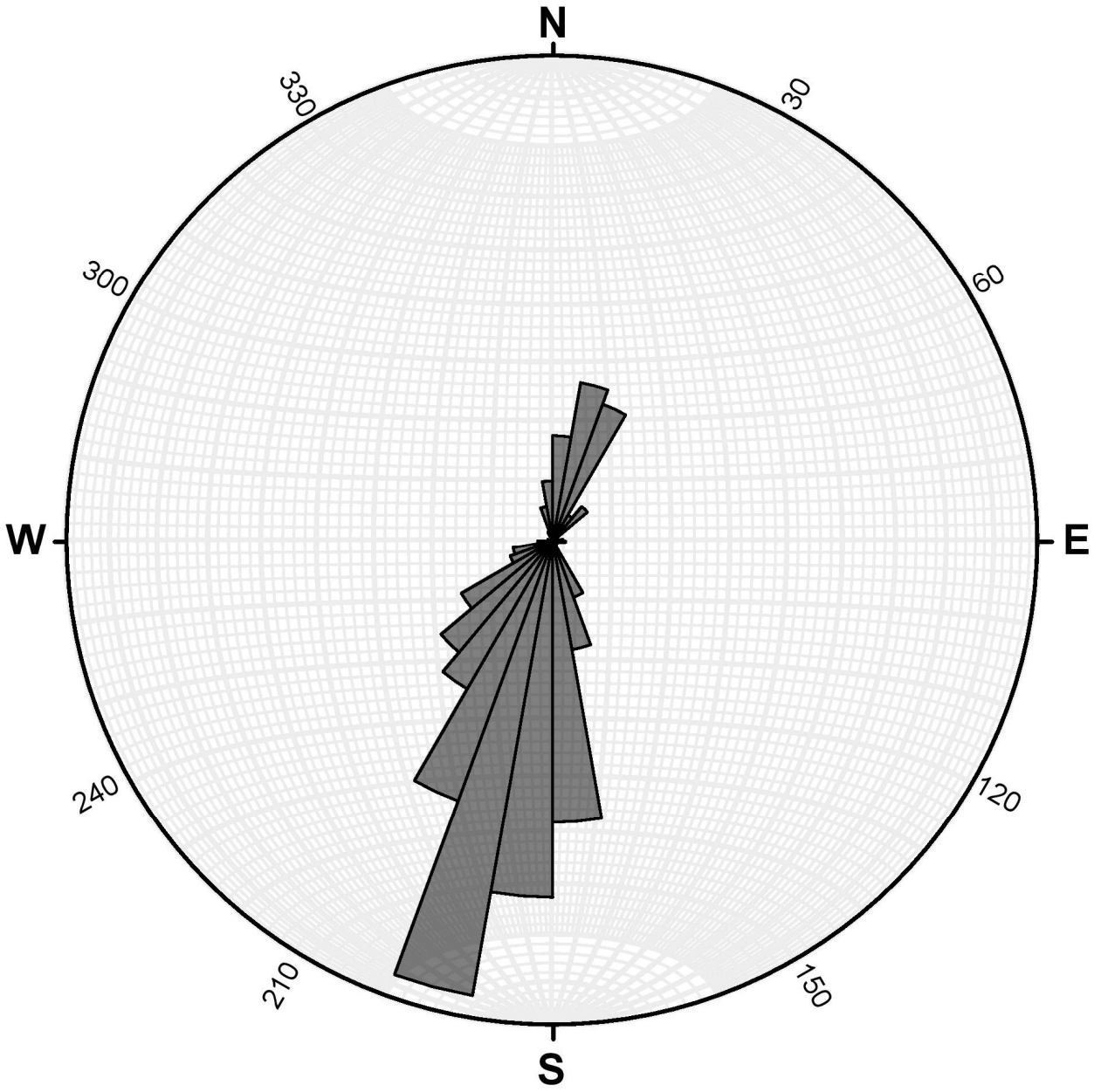

Figure 205 - Rose diagram of bedding planes for all data. N = 538.

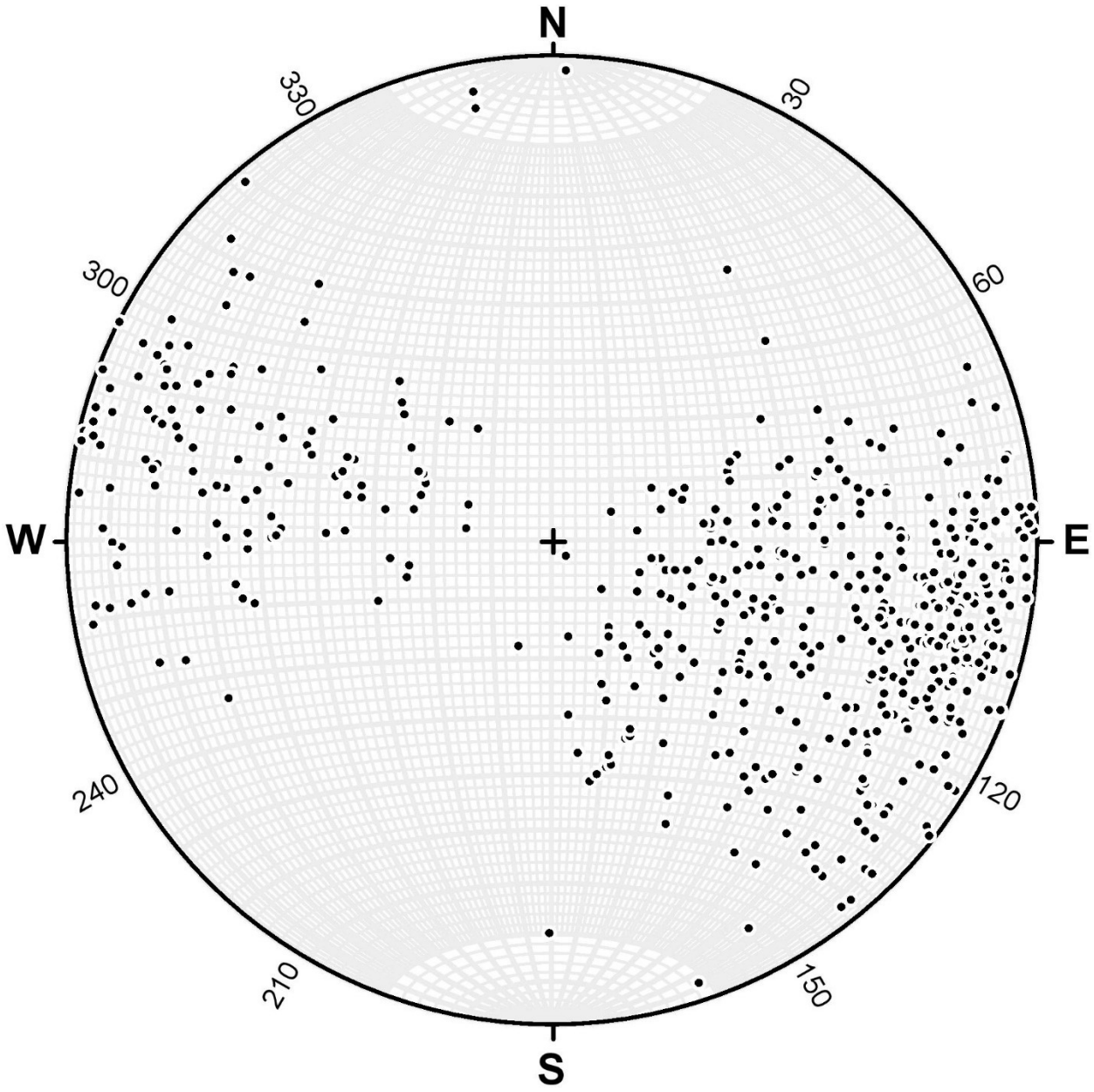

Figure 206 - Bedding poles for all data. N = 538.

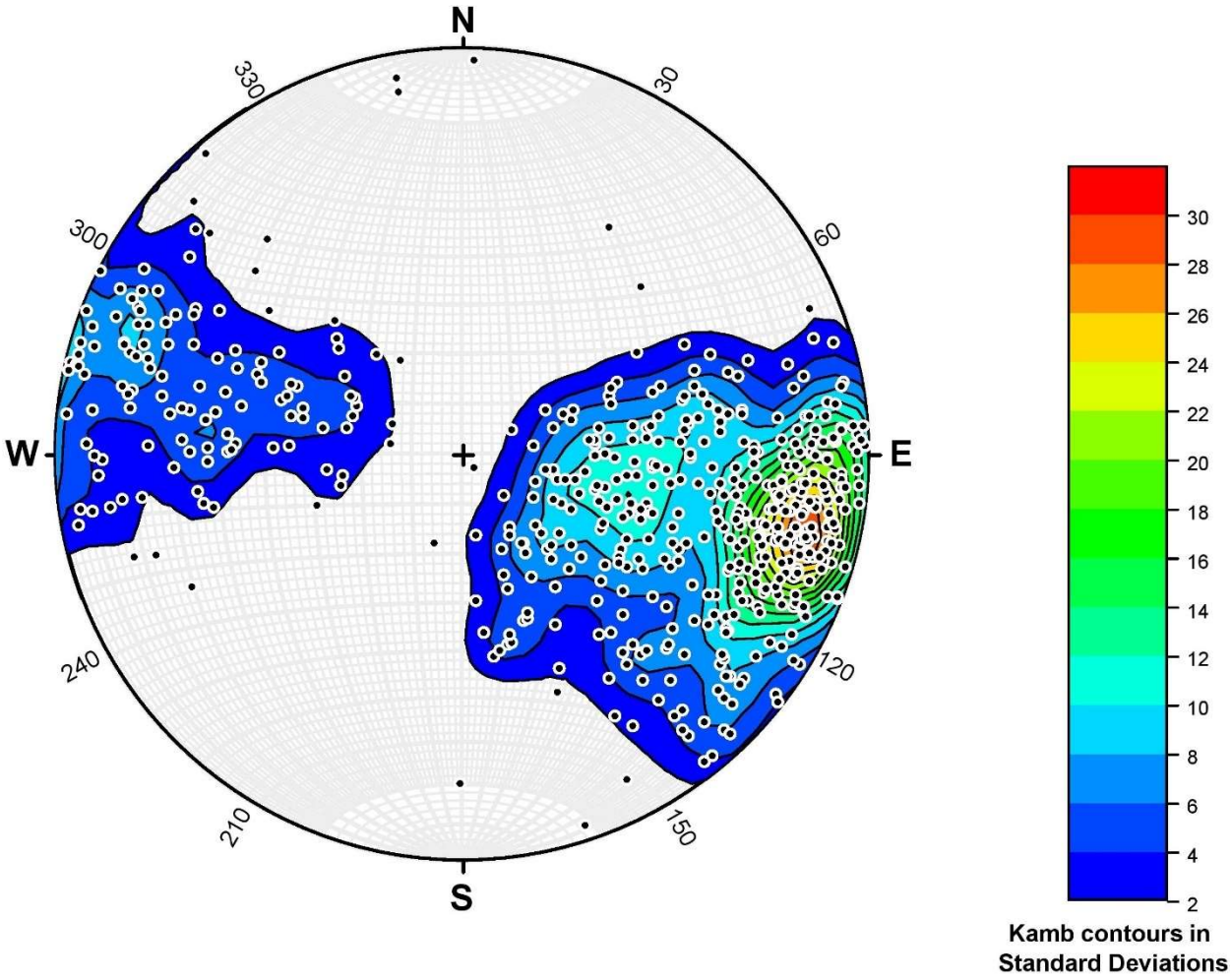

Figure 207 - Kamb contouring of bedding poles for all data. N =538.

Faulting

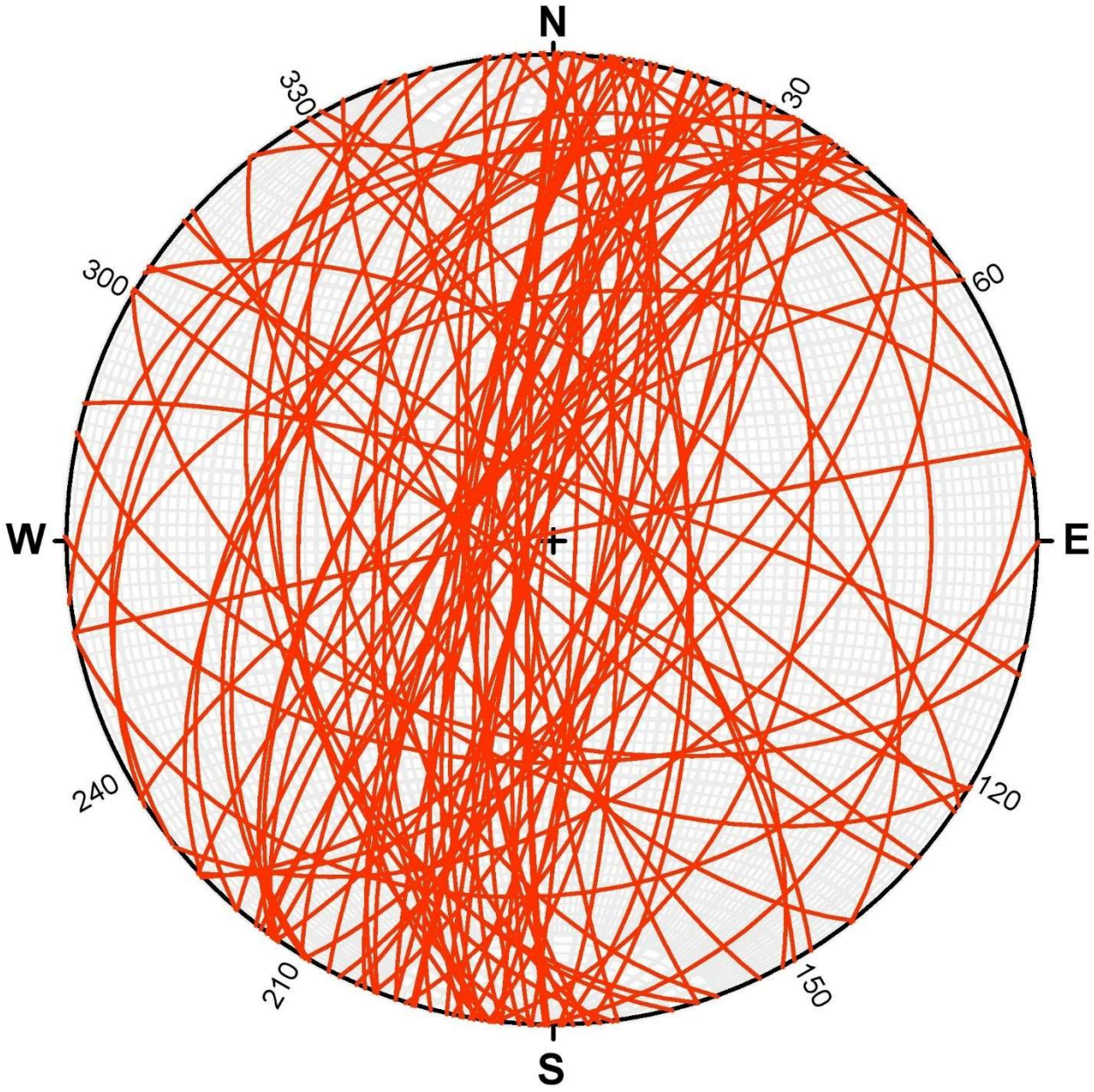

Figure 208 - Fault planes for all data. N = 88.

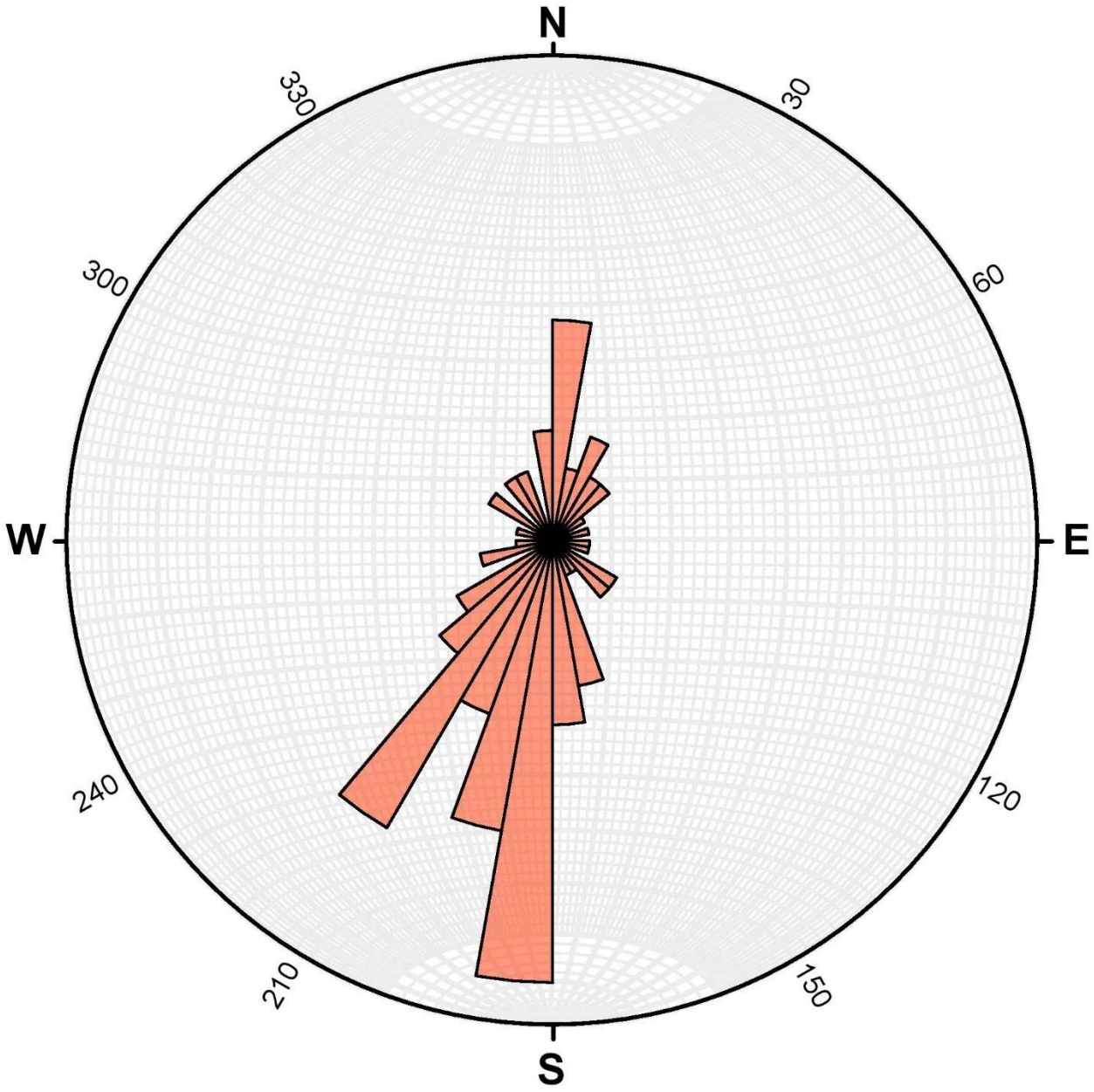

Figure 209 - Rose diagram of fault planes for all data. N = 88.

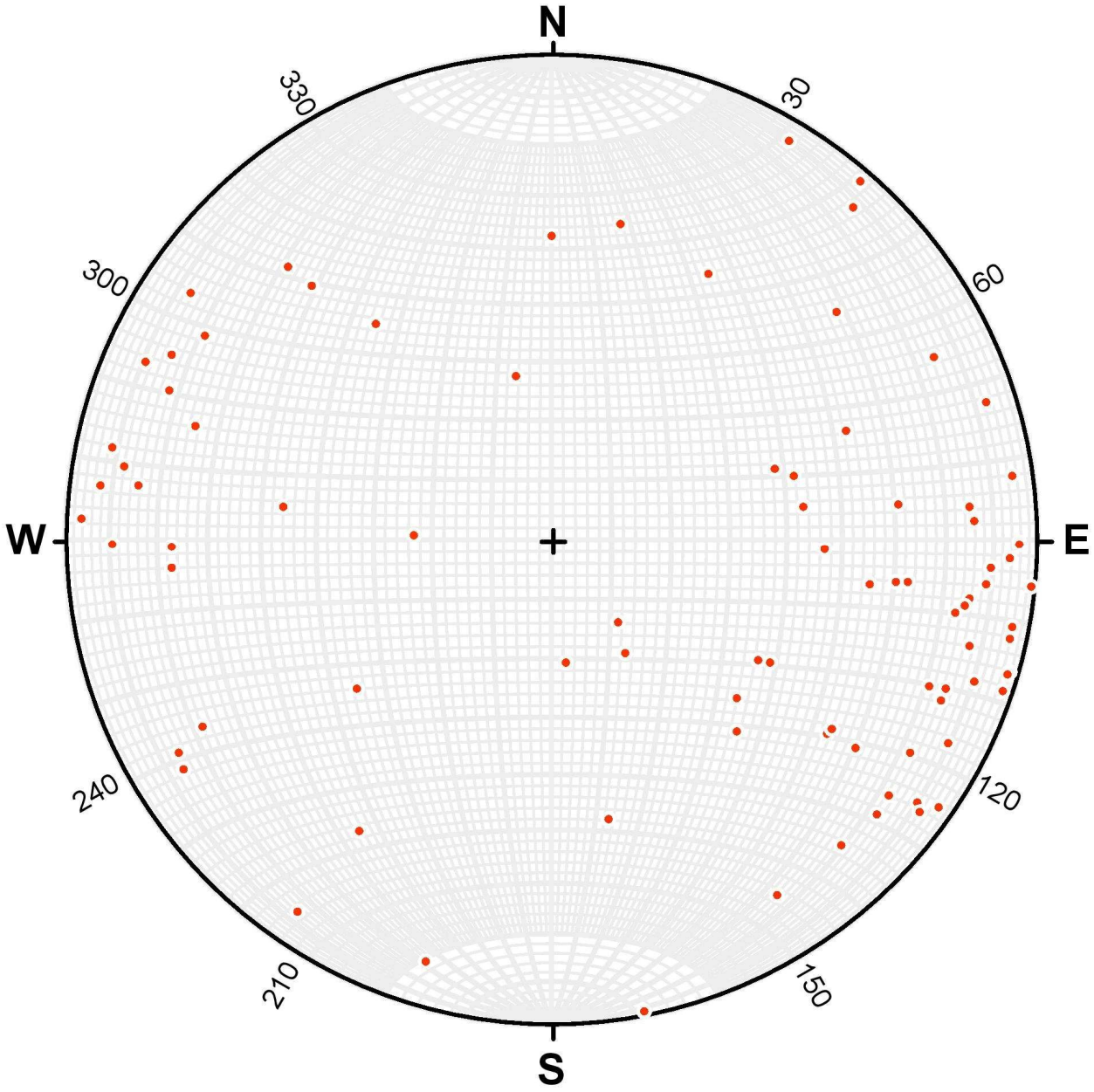

Figure 210 - Fault poles for all data. N = 88.

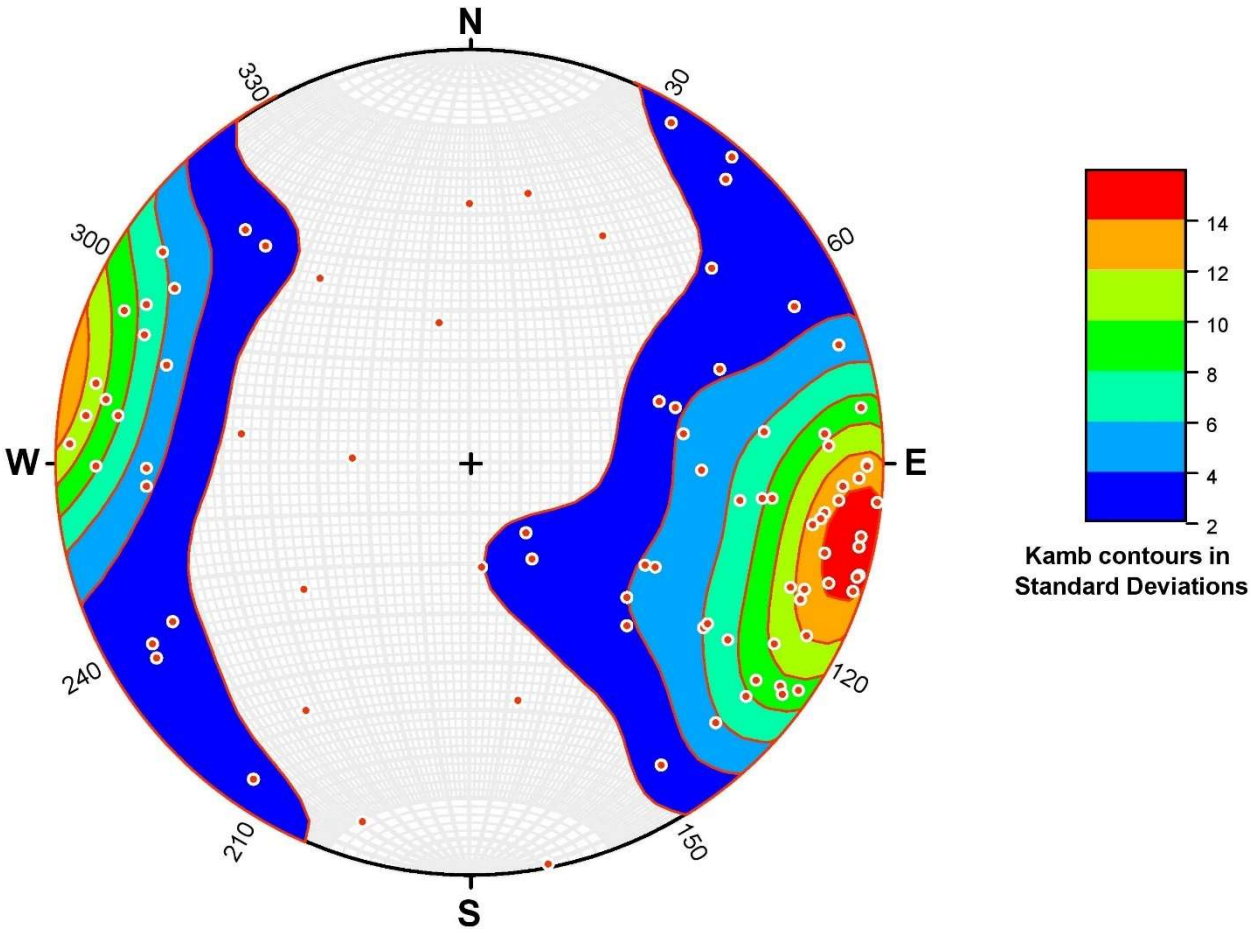

Figure 211 - Kamb contouring of fault poles for all data. N= 88.

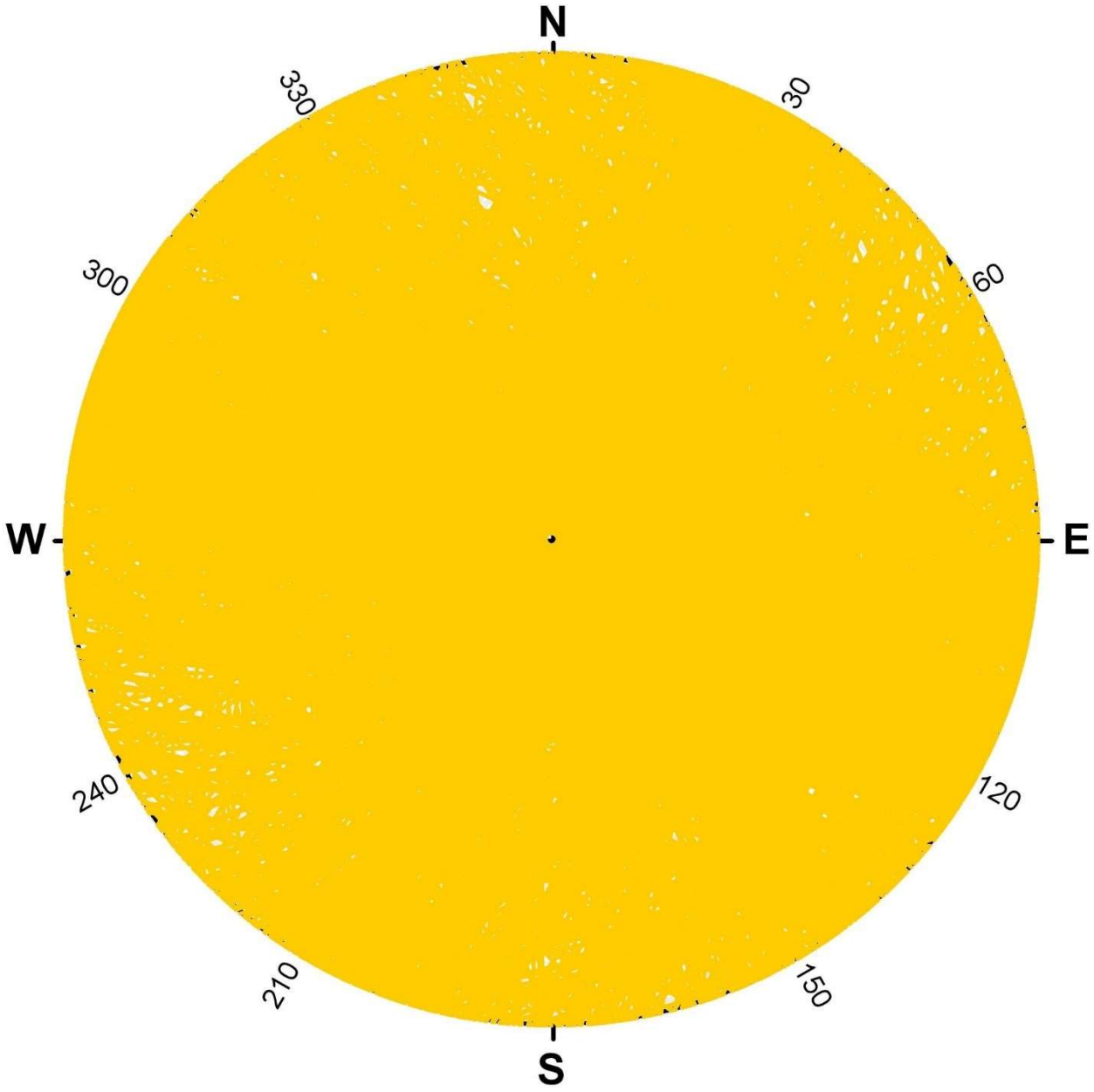

Figure 212 - Joint planes for all data. N = 1133.

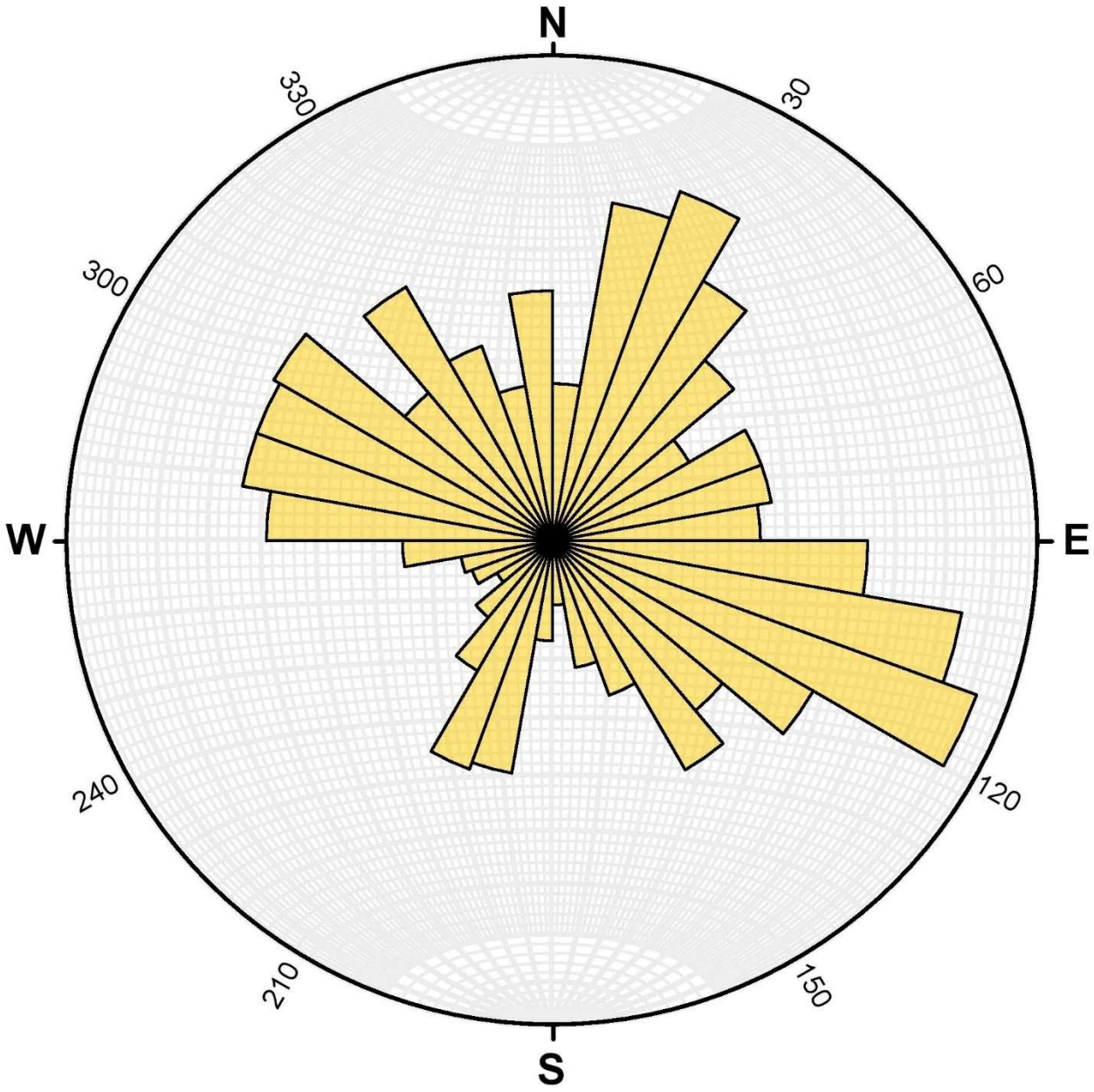

Figure 213 - Rose diagram of joint planes for all data. N = 1133.

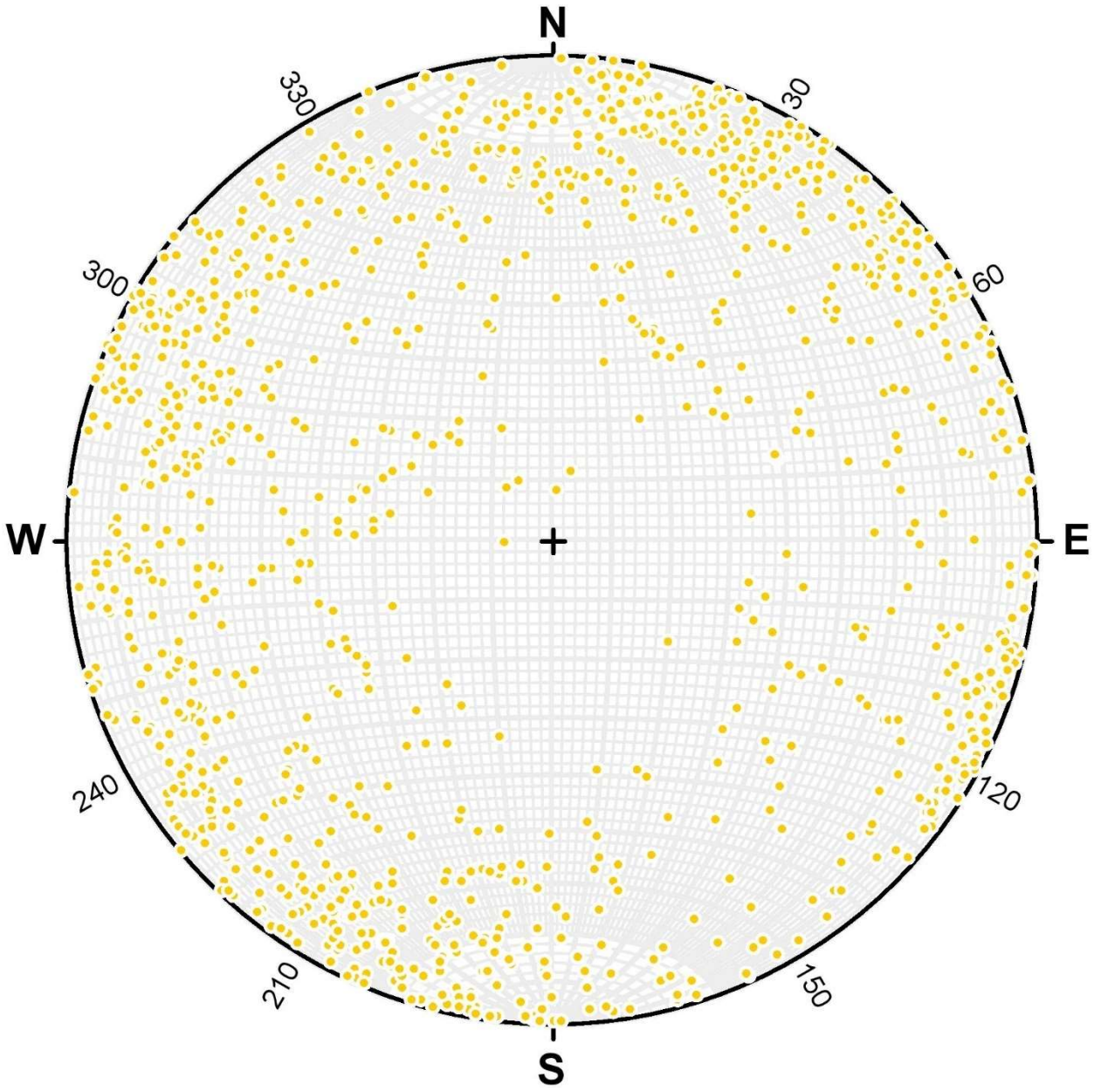

Figure 214 - Joint poles for all data. N = 1133.

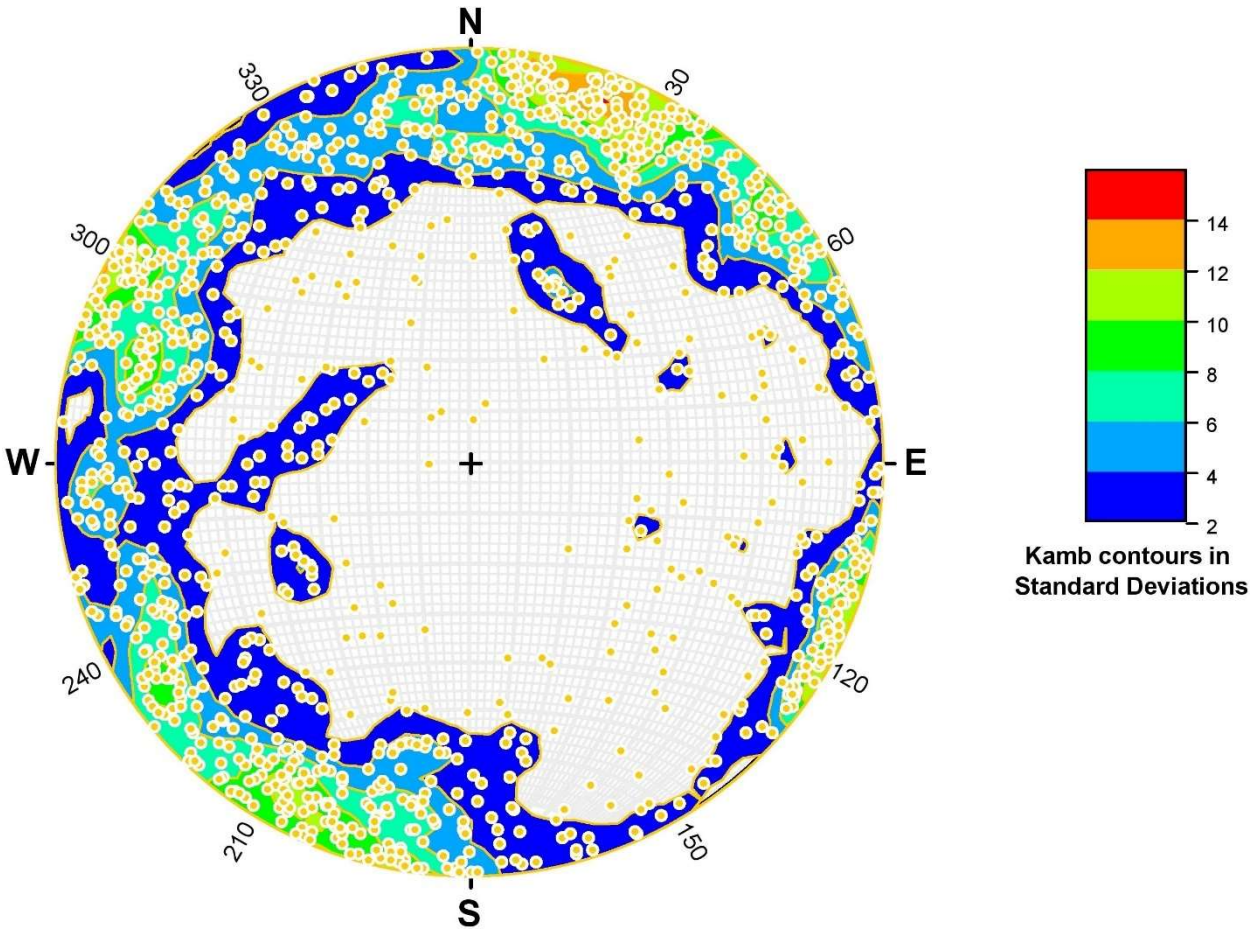

Figure 215 - Kamb contouring of joint poles for all data.

Appendix C: Structural Measurements

The following is a modified version of the dataset created using Stereonet Mobile, with extraneous columns removed for ease of reading.

ID	Longitude	Latitude	Elevation	Strike	Dip	Notes	Type
1	-116.867	49.68803	607.2489	298.7005	84.69355	gneiss	Joint
2	-116.867	49.68806	608.3856	303.4789	76.77778	gneiss	Joint
3	-116.867	49.68812	610.3604	299.7289	72	gneiss	Joint
4	-116.867	49.68812	610.929	300.7283	80.07692	gneiss	Joint
5	-116.867	49.68813	616.2498	308.2264	74	gneiss	Joint
6	-116.867	49.68816	612.3225	59.27677	80	gneiss	Joint
7	-116.867	49.68815	611.9784	53.89444	83.56522	gneiss	Joint
8	-116.867	49.6882	613.9508	334.1051	68.5	gneiss	Joint
9	-116.867	49.68821	611.5074	256.0342	83.04918	gneiss	Joint
10	-116.867	49.68822	614.169	7.937721	72.71795	gneiss	Joint
11	-116.867	49.68821	613.7274	138.5046	87.35	gneiss	Joint
12	-116.867	49.68823	611.827	265.3619	78.29545	gneiss	Joint
13	-116.867	49.68823	611.0335	355.0467	57.8125	gneiss	Joint
14	-116.866	49.69067	606.8689	115.4012	88	gneiss	Joint
15	-116.866	49.69069	610.0199	57.89802	79	gneiss	Joint
16	-116.866	49.69073	609.3578	139.4501	79.14894	gneiss	Joint
17	-116.866	49.69073	609.0384	58.99227	77	gneiss	Joint
18	-116.866	49.69073	608.8654	110.4852	84.23077	gneiss	Joint
19	-116.866	49.69073	608.6712	104.0234	83	gneiss	Joint
20	-116.866	49.69074	608.6768	356.7165	82.75676	gneiss	Joint
21	-116.867	49.69096	604.0304	110.3963	88.15152	gneiss	Joint
22	-116.867	49.69109	608.8701	282.5849	87.94444	gneiss	Joint
23	-116.867	49.69104	605.8809	279.1314	87	gneiss	Joint
24	-116.867	49.69104	605.7573	26.70732	68.775	gneiss	Joint
25	-116.867	49.69114	608.0619	106.0578	80.05	gneiss	Joint
26	-116.867	49.69115	607.6156	293.1713	89	gneiss	Joint
27	-116.867	49.69119	608.1537	297.4021	88	gneiss	Joint
28	-116.867	49.69121	607.9525	18.52818	71	gneiss	Joint
29	-116.867	49.69127	606.6927	111.3537	74	gneiss	Joint
30	-116.867	49.69132	607.3703	161.0298	71.80556	gneiss	Joint
31	-116.867	49.69136	609.7799	116.0131	82.30769	gneiss	Joint
32	-116.867	49.69136	610.2346	148.2382	86	gneiss	Joint
33	-116.867	49.69146	611.8097	269.6327	89	gneiss	Joint
34	-116.867	49.69147	611.7164	66.47648	71	gneiss	Joint
35	-116.867	49.69159	613.7144	149.0799	83.08571	gneiss	Joint
36	-116.867	49.6916	609.4933	78.42379	80	gneiss	Joint

37	-116.867	49.6916	610.1207	297.8091	76.94737	gneiss	Joint
38	-116.863	49.7014	644.6366	30.2942	82	gneiss	Joint
39	-116.863	49.70164	645.3038	16.88122	49.9863	gneiss	Joint
40	-116.863	49.70162	638.9708	47.10964	76	gneiss	Joint
41	-116.863	49.70162	638.9708	124.9996	88.09091	gneiss	Joint
42	-116.863	49.70162	638.9708	55.67949	73	gneiss	Joint
43	-116.863	49.70162	638.9708	19.5998	79	gneiss	Joint
44	-116.863	49.70162	638.9708	192.8177	19	gneiss	Bedding
45	-116.863	49.70162	638.9708	86.9349	77.95238	gneiss	Joint
46	-116.863	49.70162	638.9708	329.5789	71	gneiss	Joint
47	-116.863	49.70162	638.9708	16.21104	70.09091	gneiss	Joint
48	-116.863	49.70162	638.9708	329.6347	79	gneiss	Joint
49	-116.863	49.70162	638.9708	327.8188	77	gneiss	Joint
50	-116.863	49.70162	638.9708	342.2252	87.42105	gneiss	Joint
51	-116.863	49.70162	638.9708	309.8611	79	gneiss	Joint
52	-116.863	49.70162	638.9708	121.4073	89	gneiss	Joint
53	-116.863	49.70162	638.9708	33.14556	70	gneiss	Joint
54	-116.863	49.70162	638.9708	32.90094	78	gneiss	Joint
55	-116.863	49.70162	638.9708	168.5243	77	gneiss	Joint
56	-116.863	49.70162	638.9708	340.2408	72	gneiss	Joint
57	-116.863	49.70162	638.9708	45.66635	60	gneiss	Joint
58	-116.863	49.70162	638.9708	181.4732	27	gneiss	Bedding
59	-116.863	49.70162	638.9708	61.2866	81	gneiss	Joint
60	-116.863	49.70162	638.9708	37.32647	51	gneiss	Joint
61	-116.863	49.70162	638.9708	188.5453	25	gneiss	Bedding
62	-116.863	49.70162	638.9708	171.1807	35	gneiss	Bedding
63	-116.863	49.70162	638.9708	159.3292	32	gneiss	Bedding
64	-116.863	49.70162	638.9708	39.12673	69	gneiss	Joint
65	-116.863	49.70162	638.9708	289.2327	86	gneiss	Joint
66	-116.863	49.70162	638.9708	191.6347	18	gneiss	Bedding
67	-116.863	49.70162	638.9708	18.62807	73	gneiss	Joint
68	-116.863	49.70162	638.9708	241.4599	75	gneiss	Joint
69	-116.863	49.70162	638.9708	181.0678	65	gneiss	Joint
70	-116.863	49.70162	638.9708	325.4498	72	gneiss	Joint
71	-116.863	49.70162	638.9708	49.86875	49	gneiss	Joint
72	-116.863	49.7036	645.268	337.1224	75	gneiss	Joint
73	-116.863	49.7036	645.8841	333.3144	71	gneiss	Joint
74	-116.863	49.70364	645.822	154.0792	89	gneiss	Joint
75	-116.863	49.70364	645.1511	69.15542	67	gneiss	Joint
76	-116.863	49.70366	644.4266	332.0244	80	gneiss	Joint
77	-116.863	49.70367	645.0495	75.93798	78.28571	gneiss	Joint

78	-116.863	49.70368	643.651	333.8706	73	gneiss	Joint
79	-116.863	49.70368	643.8121	242.1252	83	gneiss	Joint
80	-116.863	49.70382	646.2153	225.4063	54	gneiss	Joint
81	-116.863	49.70383	645.8233	358.12	80	gneiss	Joint
82	-116.863	49.704	644.4963	241.3667	87	gneiss	Joint
83	-116.863	49.704	644.3772	180.0266	76	gneiss	Joint
84	-116.862	49.70416	643.4825	353.5103	69	gneiss	Joint
85	-116.862	49.70415	642.9133	344.0082	86.77778	gneiss	Joint
86	-116.862	49.7044	648.2506	303.5691	87	gneiss	Joint
87	-116.86	49.70475	654.6883	25.63393	71.83333	gneiss	Joint
88	-116.86	49.70493	658.5047	311.2093	71	gneiss	Joint
89	-116.86	49.70498	657.0684	17.56811	59.25	gneiss	Joint
90	-116.86	49.70496	655.5523	332.8998	77	gneiss	Joint
91	-116.86	49.70545	658.0537	112.1236	88	gneiss	Joint
92	-116.86	49.70542	657.1573	46.92903	81.66667	gneiss	Joint
93	-116.86	49.70562	657.7398	305.9591	77	gneiss	Joint
94	-116.86	49.70561	654.0601	49.1431	70.7	gneiss	Joint
95	-116.855	49.71938	690.1405	319.6098	56	gneiss	Joint
96	-116.855	49.71941	692.5921	334.6111	80	gneiss	Joint
97	-116.855	49.71946	693.9382	13.04461	87	gneiss	Joint
98	-116.855	49.71946	692.4498	42.08361	75.06667	gneiss	Joint
99	-116.855	49.71958	687.0717	300.2374	73	gneiss	Joint
100	-116.855	49.71958	687.9569	27.14298	76.85714	gneiss	Joint
101	-116.855	49.7196	688.6424	78.94052	56.5	gneiss	Joint
102	-116.854	49.72095	696.6053	75.05717	71	gneiss	Joint
103	-116.854	49.72096	693.4046	351.5326	85	gneiss	Joint
104	-116.854	49.72097	691.6742	79.52689	71	gneiss	Joint
105	-116.854	49.72107	690.1069	254.5246	88	gneiss	Joint
106	-116.854	49.72099	693.9344	169.8227	28	gneiss	Bedding
107	-116.853	49.7275	688.6886	301.3796	82	gneiss	Joint
108	-116.853	49.72748	688.0813	176.1225	27	gneiss	Bedding
109	-116.853	49.72748	689.1168	311.3192	80	gneiss	Joint
110	-116.853	49.72757	689.973	156.1761	89	gneiss	Joint
111	-116.853	49.72762	689.0255	141.5431	89	gneiss	Joint
112	-116.853	49.72762	688.284	323.343	86	gneiss	Joint
113	-116.854	49.73012	667.9286	294.5462	87	gneiss	Joint
114	-116.854	49.73014	666.429	356.743	80	gneiss	Joint
115	-116.854	49.73017	666.1392	162.2122	31.77586	gneiss	Bedding
116	-116.854	49.73021	667.3211	88.93582	77	gneiss	Joint
117	-116.854	49.7302	668.5304	208.1142	46.2	gneiss	Joint
118	-116.854	49.73022	665.6507	293.771	89	gneiss	Joint

119	-116.854	49.73022	665.3675	214.3025	46	gneiss	Joint
120	-116.855	49.73613	655.8133	297.3403	85	pegmatite	Joint
121	-116.854	49.73699	665.0247	111.7898	39.16667	pegmatite	Joint
122	-116.854	49.73699	662.7212	115.291	40	pegmatite	Joint
123	-116.854	49.73699	661.5644	110.6464	40	pegmatite	Joint
124	-116.855	49.73619	658.0499	88.61651	67	pegmatite	Joint
125	-116.854	49.73696	658.2183	116.4317	39.8	pegmatite	Joint
126	-116.854	49.73696	657.5518	119.7703	36	pegmatite	Joint
127	-116.855	49.73631	653.2581	285.4944	88.5	pegmatite	Joint
128	-116.854	49.73696	664.8869	123.649	36.75	pegmatite	Joint
129	-116.854	49.73696	656.0798	119.1595	38.5	pegmatite	Joint
130	-116.855	49.73627	655.733	102.7254	74	pegmatite	Joint
131	-116.855	49.73627	656.442	10.14154	48	pegmatite	Joint
132	-116.854	49.73697	651.7685	140.4817	77	gneiss	Joint
133	-116.854	49.73701	648.3141	163.434	73	gneiss	Joint
134	-116.854	49.73701	653.5553	20.03606	56	gneiss	Joint
135	-116.854	49.73703	654.7608	195.3143	28	gneiss	Bedding
136	-116.854	49.73712	655.69	27.71606	74	gneiss	Joint
137	-116.854	49.73724	654.3278	30.88315	69	gneiss	Joint
138	-116.854	49.7372	655.4134	91.00991	77	gneiss	Joint
139	-116.854	49.73719	655.5055	311.5236	87.8	gneiss	Joint
140	-116.854	49.73721	653.0694	26.62495	65	gneiss	Joint
141	-116.854	49.73721	651.0234	308.1125	87	gneiss	Joint
142	-116.854	49.73723	659.4496	97.10464	81	gneiss	Joint
143	-116.854	49.73724	656.301	24.39438	69	gneiss	Joint
144	-116.855	49.73731	651.5475	174.1487	27	gneiss	Bedding
145	0	0	0	187.8491	34	gneiss	Bedding
146	0	0	0	2.77306	78	gneiss	Joint
147	0	0	0	12.74949	72	gneiss	Joint
148	0	0	0	116.1788	85	gneiss	Joint
149	0	0	0	15.6391	71	gneiss	Joint
150	-116.854	49.7387	648.711	97.01049	72	gneiss	Joint
151	-116.854	49.73961	648.7476	48.28	65	gneiss	Joint
152	-116.854	49.7396	648.8946	316.0967	67.3	gneiss	Joint
153	-116.854	49.7396	650.7104	48.25124	59.1	gneiss	Joint
154	-116.854	49.7396	652.2987	306.7987	64	gneiss	Joint
155	-116.854	49.74067	647.8723	145.832	86	gneiss	Joint
156	-116.854	49.74078	648.9967	353.8775	82	gneiss	Joint
157	-116.854	49.74082	650.6579	149.3514	88.5	gneiss	Joint
158	-116.854	49.74087	649.2755	315.4798	83	gneiss	Joint
159	-116.854	49.74096	653.6632	326.4416	80	gneiss	Joint

160	-116.854	49.74114	654.598	141.171	73	gneiss	Joint
161	-116.854	49.74119	649.5923	148.1644	73	gneiss	Joint
162	-116.854	49.7413	649.702	10.21909	40	gneiss	Joint
163	-116.854	49.7414	646.3567	187.4363	36	gneiss	Bedding
164	-116.854	49.74144	644.3792	67.44268	76	gneiss	Joint
165	-116.854	49.74347	644.9954	116.155	38.7	pegmatite	Joint
166	-116.854	49.74347	643.5603	114.5744	38.16667	pegmatite	Joint
167	-116.854	49.74347	640.2572	124.1229	39	pegmatite	Joint
168	-116.854	49.74319	639.186	50.14523	78	pegmatite	Joint
169	-116.854	49.7435	639.9315	330.294	70.8	gneiss	Joint
170	-116.854	49.74415	634.3969	303.3713	80	gneiss	Joint
171	-116.854	49.74416	630.9959	59.30709	87	gneiss	Joint
172	-116.854	49.74415	630.6591	295.1068	83	gneiss	Joint
173	-116.854	49.74417	630.4774	319.8341	89	gneiss	Joint
174	-116.854	49.74417	631.067	41.28391	85.4	gneiss	Joint
175	-116.854	49.74427	628.6261	98.5777	69	gneiss	Joint
176	-116.854	49.74431	627.8508	66.15169	85.71429	gneiss	Joint
177	-116.854	49.7443	628.6571	149.1727	81	gneiss	Joint
178	-116.854	49.74441	638.8128	180.7831	29	gneiss	Bedding
179	-116.854	49.74505	633.3021	77.64752	87	gneiss	Joint
180	-116.854	49.74506	633.4233	138.9525	83	gneiss	Joint
181	-116.854	49.74513	631.0789	82.34589	69	gneiss	Joint
182	-116.854	49.74517	630.0196	73.57516	72	gneiss	Joint
183	-116.854	49.74517	628.3956	74.51036	73	gneiss	Joint
184	-116.854	49.73638	0	258.9093	89	15 cm rubbly fracture zone with large talus cone of small fragments	Fault
185	-116.863	49.70352	0	331.664	70.15942	3 cm wide gouge filled fracture with significant iron staining and minor chlorite	Fault
186	-116.863	49.70209	0	327.7858	78	low confidence	Fault
187	-116.863	49.70165	0	172.1941	85	low confidence	Fault
188	-116.854	49.74568	636.4563	344.4718	67.96667	gneiss	Joint
189	-116.854	49.74567	621.0202	294.3695	78	gneiss	Joint
190	-116.854	49.74577	626.3299	282.627	76	gneiss	Joint
191	-116.854	49.74584	630.5681	140.5198	62.96703	gneiss	Joint
192	-116.854	49.74611	623.7721	323.6967	52	gneiss	Joint
193	-116.854	49.74609	623.7441	84.20501	76	gneiss	Joint
194	-116.854	49.74617	622.9314	1.211642	67.9434	gneiss	Joint
195	-116.854	49.74622	620.6285	162.8925	84	gneiss	Joint
196	-116.854	49.74623	622.0392	193.6561	30	gneiss	Bedding
197	-116.854	49.74628	620.3248	199.051	29.44	gneiss	Bedding
198	-116.854	49.74646	622.3143	163.6135	82.21154	gneiss	Joint
199	-116.854	49.74655	622.9481	44.20035	62.61538	gneiss	Joint

200	-116.854	49.74661	623.1844	41.58885	73	gneiss	Joint
201	-116.854	49.74675	621.2711	345.27	77.54545	gneiss	Joint
202	-116.854	49.74817	610.6417	103.3932	76	gneiss	Joint
203	-116.854	49.74827	605.4699	126.8958	74.30769	gneiss	Joint
204	-116.854	49.74836	611.9669	199.869	36	gneiss	Bedding
205	-116.854	49.74838	613.3934	45.57084	75.90909	gneiss	Joint
206	-116.854	49.74846	614.1142	112.8874	77.18868	gneiss	Joint
207	-116.854	49.74838	616.5548	46.07479	67	gneiss	Joint
208	-116.854	49.74847	605.1981	67.72765	72	gneiss	Joint
209	-116.853	49.74962	609.6416	338.1698	63	gneiss	Joint
210	-116.853	49.75062	601.2357	14.39676	83	gneiss	Joint
211	-116.853	49.75067	602.2469	157.5923	86.97727	gneiss	Joint
212	-116.853	49.7507	602.2309	340.7727	70	gneiss	Joint
213	-116.853	49.75071	599.7528	355.0856	62	gneiss	Joint
214	-116.853	49.75069	599.4124	358.958	69	gneiss	Joint
215	-116.853	49.75074	597.1764	19.50119	59	gneiss	Joint
216	-116.853	49.75661	579.7282	316.5717	56	gneiss	Joint
217	-116.853	49.75667	572.1985	184.4907	39	gneiss	Bedding
218	-116.853	49.75686	575.0946	245.5006	88.55882	gneiss	Joint
219	-116.861	49.76835	540.6468	26.70176	54.13333	quartzite	Joint
220	-116.861	49.76836	539.8203	288.0172	51	quartzite	Joint
221	-116.861	49.76836	539.8231	44.61805	66.40909	quartzite	Joint
222	-116.861	49.76836	537.37	46.34541	50.625	quartzite	Joint
223	-116.862	49.76853	535.8819	164.8067	72	quartzite	Bedding
224	-116.861	49.76868	538.5876	119.4057	85	quartzite	Joint
225	-116.861	49.76866	532.6097	103.3127	82.15152	quartzite	Joint
226	-116.861	49.76867	533.2551	172.0457	80	quartzite	Bedding
227	-116.861	49.76863	533.2724	172.5929	82.09091	quartzite	Bedding
228	-116.861	49.76863	534.6397	176.2748	83	quartzite	Bedding
229	-116.861	49.76862	533.7963	169.663	85	quartzite	Bedding
230	-116.861	49.76844	536.4519	324.0782	38.62069	quartzite	Joint
231	-116.861	49.7685	536.2741	174.1472	79.125	quartzite	Bedding
232	-116.861	49.76851	534.8515	284.7111	34.5	quartzite	Joint
233	-116.869	49.68273	591.839	148.5273	82	gneiss	Joint
234	-116.869	49.68272	591.5037	320.0062	85	gneiss	Joint
235	-116.869	49.68279	593.9115	130.4698	87	gneiss	Joint
236	-116.869	49.68281	596.0885	213.0358	84.6	gneiss	Joint
237	-116.869	49.68284	595.2708	325.6742	70	gneiss	Joint
238	-116.869	49.68292	595.9843	114.5439	71.05882	gneiss	Joint
239	-116.869	49.68311	594.8495	349.9559	77	gneiss	Joint
240	-116.869	49.68313	595.4703	342.122	76	gneiss	Joint

241	-116.869	49.68318	596.3722	348.9149	72	gneiss	Joint
242	-116.869	49.68319	596.4549	347.0047	78	gneiss	Joint
243	-116.869	49.68321	596.2437	325.2326	85	gneiss	Joint
244	-116.869	49.68318	595.3271	350.3331	81	gneiss	Joint
245	-116.869	49.68324	596.442	258.5474	40.27778	gneiss	Joint
246	-116.869	49.68323	596.0611	247.8551	43.89655	gneiss	Joint
247	-116.869	49.68323	596.8382	126.0725	48	gneiss	Joint
248	-116.868	49.68432	609.5438	262.1329	79.29167	gneiss	Joint
249	-116.868	49.68433	609.096	268.9087	65	gneiss	Joint
250	-116.868	49.68433	607.7962	275.145	56.73077	gneiss	Joint
251	-116.868	49.68433	608.1392	266.4022	75.03571	gneiss	Joint
252	-116.868	49.68432	610.5014	120.7602	80	gneiss	Joint
253	-116.868	49.68434	609.8067	262.5294	66.2069	gneiss	Joint
254	-116.868	49.68437	608.5684	109.6535	81	gneiss	Joint
255	-116.868	49.68426	609.7147	104.0115	82.76471	gneiss	Joint
256	-116.868	49.68432	609.1808	274.6556	59.91667	gneiss	Joint
257	-116.868	49.6844	608.5921	159.2102	21.86792	gneiss	Bedding
258	-116.868	49.68449	607.8026	284.3586	77.23077	gneiss	Joint
259	-116.867	49.6845	608.0245	278.3471	72.78378	gneiss	Joint
260	-116.867	49.68447	607.8763	283.1359	75	gneiss	Joint
261	-116.867	49.68447	607.3514	284.8708	70.76471	gneiss	Joint
262	-116.867	49.68444	606.8012	287.0332	61	gneiss	Joint
263	-116.867	49.68445	605.5868	284.4146	60.78788	gneiss	Joint
264	-116.867	49.68446	605.3475	286.9469	63	gneiss	Joint
265	-116.867	49.68446	605.3243	284.4044	62	gneiss	Joint
266	-116.867	49.68443	606.6558	282.3348	59	gneiss	Joint
267	-116.867	49.68445	604.9408	278.2673	72	gneiss	Joint
268	-116.867	49.68448	602.8868	277.2948	70	gneiss	Joint
269	-116.867	49.68457	609.2346	271.9407	69	gneiss	Joint
270	-116.867	49.68456	608.369	34.21232	75.80769	gneiss	Joint
271	-116.867	49.68456	607.8752	268.3121	71	gneiss	Joint
272	-116.867	49.68454	608.7391	234.0321	81	gneiss	Joint
273	-116.867	49.68466	612.9223	101.675	87	gneiss	Joint
274	-116.867	49.68464	611.3646	294.9478	89	gneiss	Joint
275	-116.866	49.68453	611.8079	315.5582	70.92857	gneiss	Joint
276	-116.866	49.68456	611.2996	120.9311	84.93617	pervasive fracture with lots of rubble at base	Fault
277	-116.867	49.68454	608.2412	130.9314	86.91667	pervasive fracture with rubble at base	Fault
278	-116.865	49.68436	633.3797	66.93349	55	gneiss	Joint
279	-116.865	49.68436	633.3797	62.25283	74.42857	gneiss	Joint
280	-116.865	49.68436	633.3797	358.9488	76	gneiss	Joint
281	-116.865	49.68436	633.3797	292.1091	78	gneiss	Joint

282	-116.865	49.68436	633.3797	322.0285	42	10 cm wide pervasive fracture zone	Fault
283	-116.863	49.68646	645.8145	162.9542	23	gneiss	Bedding
284	-116.861	49.6852	658.5376	196.2241	57	gneiss	Joint
285	-116.861	49.68519	658.0244	23.76631	82	gneiss	Joint
286	-116.861	49.68489	663.235	209.1035	36	gneiss	Joint
287	-116.861	49.68491	662.2837	201.887	37	gneiss	Joint
288	-116.861	49.68492	658.547	192.3834	34.45	gneiss	Joint
289	-116.86	49.68494	656.4818	10.31915	64.90476	gneiss	Joint
290	-116.86	49.68491	656.2147	23.93571	67	gneiss	Joint
291	-116.86	49.6849	655.7772	19.57339	70	gneiss	Joint
292	-116.86	49.68491	656.702	270.785	78	gneiss	Joint
293	-116.86	49.68491	656.5548	19.19921	82	gneiss	Joint
294	-116.86	49.68485	655.9107	10.55436	67	gneiss	Joint
295	-116.86	49.68484	655.453	108.4538	87	gneiss	Joint
296	-116.86	49.68484	654.8713	107.8609	87	gneiss	Joint
297	-116.86	49.68484	655.2503	286.1089	83	gneiss	Joint
298	-116.86	49.68486	654.5933	90.96995	80	gneiss	Joint
299	-116.86	49.68484	654.4621	14.98596	69.40909	gneiss	Joint
300	-116.86	49.68483	654.2926	126.5932	81.27778	gneiss	Joint
301	-116.86	49.68483	655.9867	136.327	84.15	gneiss	Joint
302	-116.86	49.68483	655.2657	139.5656	79.42105	gneiss	Joint
303	-116.863	49.68674	646.6161	94.91719	88.55	gneiss	Joint
304	-116.863	49.68669	645.119	271.9771	88.9375	gneiss	Joint
305	-116.857	49.68569	675.5002	104.1182	75	gneiss	Joint
306	-116.857	49.68592	672.0598	323.4245	76	gneiss	Joint
307	-116.857	49.68594	672.9063	313.4674	83	gneiss	Joint
308	-116.857	49.68598	669.1475	308.0075	74	gneiss	Joint
309	-116.857	49.68596	668.2183	302.3477	72	gneiss	Joint
310	-116.857	49.68595	670.2242	306.2882	80	gneiss	Joint
311	-116.857	49.68599	668.1788	296.4221	68.5	gneiss	Joint
312	-116.857	49.68606	670.7064	288.1538	87	gneiss	Joint
313	-116.857	49.6861	670.4378	188.2321	56	1 to 5 cm wide fault zone with gouge and possible chloritization and some iron staining	Fault
314	-116.857	49.68607	674.0702	314.489	63	gneiss	Joint
315	-116.857	49.68615	674.3787	238.3124	86.65714	gneiss	Joint
316	-116.857	49.6863	677.0208	75.01239	73	gneiss	Joint
317	-116.856	49.68616	683.497	164.8774	19	gneiss	Bedding
318	-116.856	49.68618	680.0699	252.1567	88.33333	gneiss	Joint
319	-116.856	49.68618	679.856	131.7885	82.07143	gneiss	Joint
320	-116.856	49.68618	677.2752	21.87855	70	gneiss	Joint
321	-116.856	49.68619	675.7734	137.0948	80	gneiss	Joint

322	-116.856	49.68621	678.0681	67.90617	89	gneiss	Joint
323	-116.856	49.6862	678.4052	141.2544	86.13333	gneiss	Joint
324	-116.856	49.68609	685.826	83.01385	79.05263	gneiss	Joint
325	-116.856	49.68587	697.0371	154.6412	76	1 cm wide chloritized gouge fracture	Fault
326	-116.854	49.68596	677.466	73.27663	56.91667	gneiss	Joint
327	-116.854	49.68597	678.2359	16.05701	60.875	gneiss	Joint
328	-116.854	49.68589	679.0258	73.19325	64	gneiss	Joint
329	-116.854	49.68592	697.9813	122.7986	75	gneiss	Joint
330	-116.854	49.68577	673.8126	228.0944	78.53846	gneiss	Joint
331	-116.854	49.68533	707.0327	83.59263	62.64706	gneiss	Joint
332	-116.854	49.68555	699.9343	271.8316	88	gneiss	Joint
333	-116.854	49.68558	680.9179	106.3455	78	gneiss	Joint
334	-116.853	49.6855	707.0201	119.1728	73	gneiss	Joint
335	-116.853	49.68506	696.3299	334.6986	59	gneiss	Joint
336	-116.852	49.68482	692.2098	330.8603	64	gneiss	Joint
337	-116.852	49.68475	677.7931	287.5513	82.18182	gneiss	Joint
338	-116.852	49.68468	693.3661	297.7457	74.3125	gneiss	Joint
339	-116.852	49.68452	673.919	50.28892	79	gneiss	Joint
340	-116.852	49.68455	665.9322	299.9865	75	gneiss	Joint
341	-116.851	49.68445	695.482	208.6443	89	gneiss	Joint
342	-116.851	49.6842	690.8701	313.5143	87.07143	gneiss	Joint
343	-116.851	49.68412	686.3028	325.618	74.8125	gneiss	Joint
344	-116.851	49.68407	682.9611	334.4631	81	gneiss	Joint
345	-116.85	49.68383	687.5289	44.8594	70.55556	gneiss	Joint
346	-116.85	49.68383	685.6631	47.39953	72	gneiss	Joint
347	-116.85	49.68382	683.4022	49.64239	72	gneiss	Joint
348	-116.85	49.68381	672.9874	37.71032	66	gneiss	Joint
349	-116.85	49.6838	668.6493	52.34486	70.66667	gneiss	Joint
350	-116.85	49.6838	668.4361	59.97778	60	gneiss	Joint
351	-116.85	49.68376	666.3241	156.2763	64.09091	gneiss	Joint
352	-116.85	49.68374	664.6725	55.91002	61	gneiss	Joint
353	-116.85	49.68367	680.8023	64.35569	69	gneiss	Joint
354	-116.85	49.68365	679.1672	39.68852	68	gneiss	Joint
355	-116.848	49.68328	667.3941	252.2107	57.73333	gneiss	Joint
356	-116.848	49.68329	667.8397	286.6931	75	gneiss	Joint
357	-116.848	49.68333	675.0753	27.49091	76	gneiss	Joint
358	-116.848	49.68332	673.743	303.6344	81.70588	gneiss	Joint
359	-116.848	49.68334	670.5907	64.47253	61.7	gneiss	Joint
360	-116.848	49.68331	668.1189	343.3458	71.09091	gneiss	Joint
361	-116.848	49.68333	671.1422	13.94431	63	gneiss	Joint
362	-116.848	49.68334	664.9229	19.55012	73.18182	gneiss	Joint

363	-116.848	49.68334	662.0848	304.6772	77.33333	gneiss	Joint
364	-116.848	49.68334	661.9312	288.7582	84.2	gneiss	Joint
365	-116.848	49.68333	661.6006	309.3803	83.55556	gneiss	Joint
366	-116.848	49.68334	655.2446	60.13348	74	gneiss	Joint
367	-116.848	49.68334	654.6164	320.1522	82.14286	gneiss	Joint
368	-116.848	49.68337	651.3838	157.3146	88.07143	gneiss	Joint
369	-116.848	49.68335	652.9283	123.2875	87	gneiss	Joint
370	-116.848	49.68333	656.8558	57.0554	69	gneiss	Joint
371	-116.848	49.68331	667.7315	64.24969	67	gneiss	Joint
372	-116.848	49.68332	665.8741	64.51866	74	gneiss	Joint
373	-116.848	49.6833	663.8687	61.84969	75	gneiss	Joint
374	-116.848	49.68329	656.7464	61.64846	78.75	gneiss	Joint
375	-116.848	49.6833	656.9493	64.57464	81	gneiss	Joint
376	-116.848	49.68326	671.4808	33.82373	32.77778	gneiss	Joint
377	-116.848	49.68325	669.0516	224.2433	83	gneiss	Joint
378	-116.848	49.68325	666.2169	78.89625	82	gneiss	Joint
379	-116.848	49.68325	666.1457	313.1035	88.8	gneiss	Joint
380	-116.848	49.68335	642.1778	187.9287	63.14286	gneiss	Joint
381	-116.848	49.68331	671.1344	221.8356	88	gneiss	Joint
382	-116.848	49.68329	665.7458	98.32872	86	gneiss	Joint
383	-116.848	49.68322	655.4121	27.64582	56	gneiss	Joint
384	-116.848	49.6832	654.1467	99.25029	47	gneiss	Joint
385	-116.848	49.68319	654.4591	104.1704	48	gneiss	Joint
386	-116.848	49.68319	656.1113	47.36909	73	gneiss	Joint
387	-116.837	49.68305	642.9239	300.5084	69	gneiss	Joint
388	-116.837	49.68311	635.7917	302.1728	71	gneiss	Joint
389	-116.837	49.68313	644.5306	7.753361	73	gneiss	Joint
390	-116.837	49.68316	642.2293	118.0575	77.5	gneiss	Joint
391	-116.837	49.68324	638.3368	114.563	49.875	gneiss	Joint
392	-116.798	49.59599	0	79.51366	70	phyllite	Joint
393	-116.798	49.59606	0	285.8145	76	phyllite	Joint
394	-116.798	49.59606	0	72.86979	60	phyllite	Joint
395	-116.798	49.59604	563.6444	70.479	66	phyllite	Joint
396	-116.797	49.59605	560.7091	59.94897	65.90909	phyllite	Joint
397	-116.797	49.59607	555.2929	60.12491	66.95	phyllite	Joint
398	-116.797	49.59606	0	0.445229	48	phyllite	Bedding
399	-116.797	49.59606	0	179.1027	56	phyllite	Joint
400	-116.797	49.59609	0	239.4121	56.60606	phyllite	Joint
401	-116.797	49.59613	561.2561	80.73034	70	phyllite	Joint
402	-116.797	49.59611	0	168.2045	89	phyllite	Joint
403	-116.797	49.5961	0	0.153041	56	phyllite	Bedding

404	-116.797	49.59612	0	69.90691	71	phyllite	Joint
405	-116.797	49.5963	570.6098	62.30624	72	phyllite	Joint
406	-116.797	49.59632	563.68	92.55456	81	phyllite	Joint
407	-116.797	49.59634	562.0646	9.361115	51	phyllite	Bedding
408	-116.788	49.61685	559.9715	50.78802	84	granite	Joint
409	-116.788	49.61686	557.733	214.1325	75	granite	Joint
410	-116.788	49.61692	558.8399	214.863	86	granite	Joint
411	-116.788	49.61692	559.5641	33.10921	83	granite	Joint
412	-116.788	49.61694	559.3549	40.63038	80	granite	Joint
413	-116.788	49.61695	559.8543	29.90865	86.21053	granite	Joint
414	-116.788	49.61696	559.3428	216.1525	87	granite	Joint
415	-116.788	49.61703	558.6192	17.75006	83	granite	Joint
416	-116.788	49.6171	558.9241	27.56981	84	granite	Joint
417	-116.788	49.61711	558.812	156.4752	46	granite	Joint
418	-116.788	49.61711	558.8109	152.8041	48	granite	Joint
419	-116.788	49.61714	557.8862	208.713	84.09524	granite	Joint
420	-116.788	49.61721	0	206.088	85	granite	Joint
421	-116.787	49.63645	564.7017	18.44534	85.95238	granite	Joint
422	-116.787	49.63649	563.6038	28.75764	79	granite	Joint
423	-116.787	49.63655	0	198.8432	86.11111	granite	Joint
424	-116.787	49.63659	559.0381	108.5283	83	granite	Joint
425	-116.787	49.63658	559.6468	43.12938	67.97619	granite	Joint
426	-116.787	49.63662	559.0905	211.2275	85	granite	Joint
427	-116.787	49.63664	559.6846	192.4272	75	granite	Joint
428	-116.787	49.63667	557.8194	41.53099	83	granite	Joint
429	-116.787	49.63668	558.4063	65.33232	54	granite	Joint
430	-116.787	49.63674	556.994	30.40426	79.94737	granite	Joint
431	-116.787	49.6368	557.0255	214.3512	84.56	granite	Joint
432	-116.787	49.63685	558.3412	204.011	88	granite	Joint
433	-116.787	49.63689	556.6109	106.7269	78	granite	Joint
434	-116.787	49.63688	556.3819	42.62982	81.76471	granite	Joint
435	-116.788	49.63795	551.9721	22.847	86	granite	Joint
436	-116.788	49.63799	550.1979	29.43139	75	granite	Joint
437	-116.788	49.63804	0	31.92175	86	granite	Joint
438	-116.788	49.63807	551.0526	209.016	87	granite	Joint
439	-116.788	49.63825	556.371	174.2741	61	1 m wide fracture zone with slickenlines, no gouge rubble or other fault characteristics, some chlorite on slickenlines	Fault
440	-116.788	49.63822	549.171	200.6871	34	granite	Joint
441	-116.788	49.63822	548.3572	41.81167	87.52941	granite	Joint
442	-116.788	49.63834	552.837	320.4094	31.55556	granite	Joint
443	-116.788	49.63838	553.6693	298.0077	32	granite	Joint

444	-116.788	49.6384	553.1683	301.3846	41	granite	Joint
445	-116.788	49.63841	552.8953	304.596	43	granite	Joint
446	-116.79	49.63918	557.6607	84.15925	64	granite	Joint
447	-116.79	49.63918	557.6797	38.85977	89	granite	Joint
448	-116.79	49.63925	553.6675	103.0958	78.77419	granite	Joint
449	-116.79	49.63926	550.9659	283.6783	70	granite	Joint
450	-116.79	49.63926	550.963	174.2818	87	granite	Joint
451	-116.79	49.63923	551.1667	281.3432	85.19231	granite	Joint
452	-116.79	49.63923	551.5491	164.1069	85.47059	granite	Joint
453	-116.79	49.63925	552.097	167.341	83	granite	Joint
454	-116.79	49.63925	551.9996	215.093	86	granite	Joint
455	-116.79	49.6393	551.1021	31.62077	80	granite	Joint
456	-116.79	49.63937	547.4537	140.1703	88.17241	granite	Joint
457	-116.792	49.64128	548.4125	205.1236	89	granite	Joint
458	-116.792	49.64175	566.7169	31.89799	78.97059	granite	Joint
459	-116.792	49.64165	554.1434	26.23701	88	granite	Joint
460	-116.792	49.64163	550.1314	24.39432	88	granite	Joint
461	-116.794	49.64279	0	336.4832	59.96667	granite	Joint
462	-116.794	49.64287	0	148.451	89	granite	Joint
463	-116.794	49.64306	547.4053	15.88237	75	granite	Joint
464	-116.795	49.64367	546.7435	202.7577	41	granite	Joint
465	-116.795	49.64374	552.1502	212.6204	86	granite	Joint
466	-116.795	49.64377	551.9317	318.4822	84	granite	Joint
467	-116.795	49.64383	550.0776	355.3738	59	granite	Joint
468	-116.796	49.64396	550.7047	206.6751	84.27273	granite	Joint
469	-116.796	49.64394	550.6358	37.50086	75.72222	granite	Joint
470	-116.796	49.64398	0	307.5522	54	granite	Joint
471	-116.796	49.64403	556.8819	185.7854	84	granite	Joint
472	-116.796	49.64456	559.209	27.56827	82.33333	granite	Joint
473	-116.796	49.64452	0	337.2615	86.46154	granite	Joint
474	-116.796	49.64454	558.121	158.2909	83.09091	granite	Joint
475	-116.796	49.64466	0	217.3958	76.24	5 cm wide fault zone gougey and rubbly and small talus cone	Fault
476	-116.796	49.6448	0	98.14763	8	granite	Joint
477	-116.796	49.64469	554.8271	107.0888	11.96429	granite	Joint
478	-116.796	49.64467	0	202.7632	86	granite	Joint
479	-116.797	49.6447	556.5906	193.7549	89	granite	Joint
480	-116.797	49.6447	556.3565	210.2604	88	granite	Joint
481	-116.797	49.64477	0	23.68105	89	granite	Joint
482	-116.797	49.64477	0	322.1328	77	granite	Joint
483	-116.797	49.64481	554.0479	30.84513	89	granite	Joint
484	-116.797	49.6448	553.8929	207.0965	88	granite	Joint

485	-116.797	49.64481	553.2486	202.937	83	granite	Joint
486	-116.797	49.64483	0	34.27873	70.22222	granite	Joint
487	-116.797	49.64482	552.3489	24.9161	88	granite	Joint
488	-116.797	49.64488	552.335	209.7117	87.42857	granite	Joint
489	-116.797	49.6449	552.4244	200.5555	87	granite	Joint
490	-116.797	49.64494	552.8735	32.71481	87	granite	Joint
491	-116.797	49.64496	552.9323	22.0466	84	granite	Joint
492	-116.797	49.64501	552.5217	212.4821	89	granite	Joint
493	-116.797	49.64506	552.4551	210.5903	82.08333	granite	Joint
494	-116.797	49.64511	0	30.19513	89	granite	Joint
495	-116.797	49.64608	0	292.4397	79	granite	Joint
496	-116.797	49.64619	0	353.3915	79	granite	Joint
497	-116.798	49.64637	556.2186	276.5057	67	granite	Joint
498	-116.797	49.64649	548.895	351.1093	81.47059	granite	Joint
499	-116.798	49.64649	554.3143	341.1522	67.86364	granite	Joint
500	-116.798	49.64655	0	334.4012	69	granite	Joint
501	-116.798	49.64656	554.671	335.4293	70	granite	Joint
502	-116.798	49.64667	555.1364	20.4534	83	granite	Joint
503	-116.798	49.64667	555.3709	31.12489	84.86667	granite	Joint
504	-116.798	49.64672	555.0327	340.3307	78.5	granite	Joint
505	-116.798	49.64686	555.9984	28.39739	81.25	granite	Joint
506	-116.798	49.64702	554.9537	291.4915	82.69231	granite	Joint
507	-116.798	49.64712	551.8377	277.5409	74.88235	granite	Joint
508	-116.798	49.64731	0	181.4052	89	granite	Joint
509	-116.799	49.64789	554.084	247.3633	52.22222	granite	Joint
510	-116.799	49.64789	551.4935	191.6693	85	granite	Joint
511	-116.799	49.64792	0	226.5663	75.71053	fault zone 2 - 5 cm lots of rubble gouge and slickenlines	Fault
512	-116.799	49.64792	0	286.1676	72	granite	Joint
513	-116.799	49.64797	0	355.6398	67	very gougey fault with an uncertain width	Fault
514	-116.799	49.64793	552.918	18.3843	79.8125	granite	Joint
515	-116.799	49.64807	0	237.7314	76	5 cm wide gouge filled fault	Fault
516	-116.799	49.64828	0	181.0072	89	granite	Joint
517	-116.799	49.64831	546.1362	338.1672	87.85714	granite	Joint
518	-116.799	49.64836	544.8193	97.17056	76	granite	Joint
519	-116.799	49.64843	0	224.7842	76	20 cm very gougey and mineralized fault zone	Joint
520	-116.8	49.64876	0	230.8988	61.04167	granite	Joint
521	-116.799	49.64912	542.8251	165.7422	62.65217	granite	Joint
522	-116.799	49.64914	545.4633	163.2938	63.375	granite	Joint
523	-116.799	49.64962	551.6307	192.1041	84	granite	Joint
524	-116.799	49.64964	554.1207	198.7188	75	granite	Joint

525	-116.8	49.6504	555.8254	106.5166	31.27273	marble	Joint
526	-116.8	49.65045	560.8971	115.0262	79	marble	Joint
527	-116.8	49.65083	0	102.6197	41	marble	Joint
528	-116.8	49.6508	0	356.5874	72	marble	Joint
529	-116.801	49.65088	560.2234	142.8043	78.16667	marble	Joint
530	-116.801	49.65088	0	196.7649	84.13333	marble	Joint
531	-116.801	49.65092	0	200.7486	86	marble	Joint
532	-116.801	49.65093	0	254.5481	76	marble	Joint
533	-116.801	49.65125	0	303.264	58	marble	Joint
534	-116.801	49.65127	564.4942	98.03874	78	marble	Joint
535	-116.801	49.65172	562.6512	291.0093	80.125	marble	Joint
536	-116.801	49.65176	0	249.2419	72.78571	marble	Joint
537	-116.801	49.65175	0	262.503	73.73333	marble	Joint
538	-116.801	49.65184	563.1118	197.5951	57	marble	Joint
539	-116.801	49.65192	557.8429	120.4933	87	marble	Joint
540	-116.801	49.65191	559.4908	120.0538	88	marble	Joint
541	-116.801	49.65178	558.2362	105.8477	74	marble	Joint
542	-116.801	49.65178	558.3661	107.68	74	marble	Joint
543	-116.801	49.65176	562.1776	25.86265	82	marble	Bedding
544	-116.8	49.65081	560.087	16.20254	87	marble	Bedding
545	-116.8	49.65042	0	18.79414	85	marble	Bedding
546	-116.802	49.65281	563.5767	136.4869	86	marble	Joint
547	-116.802	49.65293	562.0344	190.9125	44	marble	Joint
548	-116.802	49.65294	560.7332	359.3042	65	marble	Joint
549	-116.802	49.65295	0	150.9329	51	marble	Joint
550	-116.802	49.65299	0	299.9579	77	marble	Joint
551	-116.802	49.65296	559.1107	272.9973	73	marble	Joint
552	-116.802	49.65297	558.4864	106.2796	43	marble	Joint
553	-116.802	49.65295	0	201.5404	86.35294	marble	Bedding
554	-116.802	49.65301	559.426	295.4224	79	marble	Joint
555	-116.802	49.65306	557.8617	70.53371	46	marble	Joint
556	-116.802	49.65305	557.0648	292.721	78.5625	marble	Joint
557	-116.802	49.65274	0	17.45947	65.55172	highly slickensided surface	Fault
558	-116.802	49.65305	0	282.3218	65	marble	Joint
559	-116.802	49.65308	561.4908	227.2669	59	marble	Joint
560	-116.802	49.65308	562.1466	291.3867	72	marble	Joint
561	-116.802	49.65309	560.9908	285.6226	70	marble	Joint
562	-116.802	49.65313	0	281.3401	59	marble	Joint
563	-116.802	49.65346	0	299.5146	80	marble	Joint
564	-116.803	49.65349	562.3636	114.916	59.27273	marble	Joint
565	-116.803	49.65349	563.8426	137.1684	78.625	marble	Joint

566	-116.803	49.65375	0	290.408	83	gneiss	Joint
567	-116.803	49.65409	0	14.82108	87	gneiss	Joint
568	-116.803	49.65423	560.5487	127.2993	65.1	gneiss	Joint
569	-116.803	49.65422	0	185.9904	79	30 cm wide fault gouge zone	Fault
570	-116.801	49.65422	0	2.383753	86	10 cm wide fault zone	Fault
571	-116.803	49.65438	561.5144	326.0164	83.47059	gneiss	Joint
572	-116.803	49.65439	557.4225	231.2474	82	gneiss	Joint
573	-116.803	49.65444	557.4865	222.0794	85	gneiss	Joint
574	-116.803	49.65453	557.1825	101.6267	82.14286	gneiss	Joint
575	-116.803	49.65455	557.3509	12.98894	88	gneiss	Bedding
576	-116.803	49.65469	0	190.8232	86	10 cm wide foliation parallel fault	Fault
577	-116.803	49.65459	558.4312	107.4074	63	gneiss	Joint
578	-116.803	49.65443	562.5773	354.1735	87	gneiss	Joint
579	-116.803	49.6547	556.2535	161.1208	88	gneiss	Joint
580	-116.803	49.65474	556.4561	87.41547	74	gneiss	Joint
581	-116.803	49.65495	0	66.10069	20	gneiss	Joint
582	-116.803	49.65517	0	120.5781	53.2	20 cm wide fracture zone	Fault
583	-116.803	49.65501	0	330.0713	77	very slickensided pervasive fracture	Fault
584	-116.803	49.65503	553.6969	60.40229	11	gneiss	Joint
585	-116.803	49.65508	0	319.8033	73	gneiss	Joint
586	-116.803	49.65505	0	57.92726	42	gneiss	Joint
587	-116.803	49.65595	552.8875	107.0819	65	granite	Joint
588	-116.803	49.65591	559.6345	109.4988	67	granite	Joint
589	-116.803	49.65593	559.4414	355.2919	72	granite	Joint
590	-116.803	49.65593	559.2064	116.557	68	granite	Joint
591	-116.803	49.65593	558.5312	81.50277	76	granite	Joint
592	-116.803	49.65598	560.4058	120.252	74	granite	Joint
593	-116.803	49.65597	558.1253	208.6211	67.11111	granite	Joint
594	-116.803	49.65612	557.0037	96.76595	84	granite	Joint
595	-116.803	49.65611	553.1689	300.1645	78	granite	Joint
596	-116.803	49.65611	0	172.8566	34.15625	granite	Joint
597	-116.804	49.6561	0	258.0969	57.9	granite	Joint
598	-116.804	49.65612	555.8486	87.38175	62	granite	Joint
599	-116.804	49.65618	555.2176	279.9818	84	granite	Joint
600	-116.804	49.65619	555.1383	78.45703	67	granite	Joint
601	-116.804	49.65619	555.901	109.3206	82	granite	Joint
602	-116.804	49.65621	557.5803	279.8669	88	granite	Joint
603	-116.804	49.65624	552.67	345.3836	59	granite	Joint
604	-116.804	49.65632	552.5788	139.2579	64	granite	Joint
605	-116.804	49.65632	550.0387	242.2161	68.25	granite	Joint
606	-116.804	49.65634	553.3933	254.6719	82.6	granite	Joint

607	-116.804	49.65634	552.6898	276.6579	82	granite	Joint
608	-116.804	49.65641	552.1883	231.3941	65.41176	granite	Joint
609	-116.804	49.65641	550.4708	49.0427	11.38462	granite	Joint
610	-116.804	49.65641	551.1131	207.9597	88.08333	granite	Joint
611	-116.804	49.65641	551.2978	142.1507	63	granite	Joint
612	-116.804	49.65645	553.1497	72.47487	75.88235	granite	Joint
613	-116.804	49.6565	0	252.3031	84.81818	granite	Joint
614	-116.804	49.65655	551.4918	297.3918	83.52632	granite	Joint
615	-116.804	49.65681	560.2794	110.1832	66	granite	Joint
616	-116.804	49.65676	555.6017	294.3734	81	granite	Joint
617	-116.804	49.65677	0	9.685379	78	2 m wide highly oxidized and chloritized fault zone	Fault
618	-116.804	49.65678	553.9981	6.923333	82.25	highly oxidized and chloritized slickensided surface	Fault
619	-116.804	49.65678	555.0335	71.53382	60	granite	Joint
620	-116.804	49.65679	554.1532	323.8382	78	granite	Joint
621	-116.804	49.6568	553.9903	284.4933	78	granite	Joint
622	-116.804	49.65683	552.2093	21.84436	65.90909	granite	Joint
623	-116.804	49.65684	0	19.3835	53	granite	Joint
624	-116.804	49.65685	554.7707	5.556674	88	granite	Joint
625	-116.804	49.65683	551.3108	192.9631	87.66667	granite	Joint
626	-116.804	49.65684	552.2325	184.4216	89	granite	Joint
627	-116.804	49.6569	550.8375	93.76576	64	granite	Joint
628	-116.804	49.6569	549.878	84.05919	79	granite	Joint
629	-116.804	49.65692	549.5357	93.91951	72	granite	Joint
630	-116.804	49.65693	550.149	13.05174	72	granite	Joint
631	-116.804	49.65693	0	50.71059	47.40591	highly oxidized chloritized and slickensided fault 1 cm wide	Fault
632	-116.804	49.657	556.1187	138.4311	38	granite	Joint
633	-116.804	49.657	554.346	327.3235	79	granite	Joint
634	-116.804	49.65702	554.3784	104.5566	79	granite	Joint
635	-116.804	49.65705	552.6673	84.16535	87.4	granite	Joint
636	-116.804	49.65705	552.171	23.34464	87.72727	granite	Joint
637	-116.804	49.65706	552.4823	142.0267	35	granite	Joint
638	-116.804	49.65705	552.6307	329.3043	75	granite	Joint
639	-116.804	49.65706	551.7948	329.4031	80.08333	granite	Joint
640	-116.804	49.65708	551.3426	199.3194	88	granite	Joint
641	-116.804	49.65708	551.2691	107.2616	82	granite	Joint
642	-116.804	49.65709	551.7003	100.1414	74	granite	Joint
643	-116.804	49.6571	551.1567	20.06111	88	granite	Joint
644	-116.804	49.65713	551.8128	199.2573	88	granite	Joint
645	-116.804	49.65711	551.9322	136.1782	32	granite	Joint
646	-116.804	49.65711	551.848	354.8786	7.923077	granite	Joint

647	-116.804	49.65713	552.1164	184.4409	88	granite	Joint
648	-116.804	49.65712	551.1212	96.59159	80	granite	Joint
649	-116.804	49.65713	551.8225	195.0086	88.75	granite	Joint
650	-116.804	49.65714	552.508	204.6986	85	granite	Joint
651	-116.804	49.65713	552.8385	202.5245	86	granite	Joint
652	-116.804	49.65737	557.2281	205.3751	86	granite	Joint
653	-116.804	49.65823	563.6698	196.2665	88.09091	significant 3 m wide fault plane highly oxidized chloritized and slickensided	Fault
654	-116.805	49.65845	550.3636	249.5753	42	pegmatite	Joint
655	-116.805	49.65868	555.9443	191.8779	61	pegmatite	Joint
656	-116.805	49.6587	555.9781	320.5007	79	pegmatite	Joint
657	-116.805	49.65957	0	100.4675	68	pegmatite	Joint
658	-116.805	49.65956	556.0108	205.6187	52	pegmatite	Joint
659	-116.805	49.6596	553.7396	207.1989	61	pegmatite	Joint
660	-116.805	49.65971	553.3881	202.4321	74.41667	pegmatite	Joint
661	-116.805	49.65971	553.6451	335.7166	56	pegmatite	Joint
662	-116.805	49.65973	548.6341	334.4685	41.61538	pegmatite	Joint
663	-116.805	49.65984	0	23.64048	80	slickensided rock face	Fault
664	-116.805	49.66005	545.0667	333.7498	39	pegmatite	Joint
665	-116.805	49.65995	551.104	124.4229	66	pegmatite	Joint
666	-116.805	49.65999	556.4106	141.161	75	pegmatite	Joint
667	-116.805	49.66002	556.0501	33.20607	63	pegmatite	Joint
668	-116.805	49.66042	556.3071	325.2377	45.09091	pegmatite	Joint
669	-116.805	49.66037	555.0775	320.9917	57	pegmatite	Joint
670	-116.805	49.66036	555.1212	208.3295	68	pegmatite	Joint
671	-116.805	49.66038	555.7052	118.3057	67	pegmatite	Joint
672	-116.805	49.66006	552.795	325.1384	81	pegmatite	Joint
673	-116.805	49.66045	555.9823	200.6866	80.5	pegmatite	Joint
674	-116.805	49.66048	556.5099	321.438	78.66667	pegmatite	Joint
675	-116.805	49.66048	555.9742	332.3975	70	pegmatite	Joint
676	-116.805	49.66048	556.9273	129.5697	71	pegmatite	Joint
677	-116.806	49.66174	552.8363	138.1425	44	marble	Joint
678	-116.806	49.66153	0	207.2656	81.13333	10 cm gougey and slickensided fault zone	Fault
679	-116.806	49.66178	554.7664	129.0702	66	marble	Joint
680	-116.806	49.66177	0	215.8129	82	2 m wide rubbly and chloritized fault zone	Fault
681	-116.835	49.64947	555.1563	134.8342	80	marble	Joint
682	-116.806	49.66179	557.2613	267.6764	67	marble	Joint
683	-116.806	49.6619	0	214.805	87	5 cm wide highly oxidized and mildly chloritized fault zone	Fault
684	-116.807	49.66182	601.1251	312.3965	88	marble	Joint
685	-116.806	49.66191	556.6955	262.7326	49	marble	Joint
686	-116.806	49.66196	555.6657	136.3964	58	marble	Joint

687	-116.806	49.66172	556.1387	319.6797	80.57143	marble	Joint
688	-116.806	49.66197	553.034	286.2185	80	5 cm wide gougey chloritized fault zone	Fault
689	-116.806	49.66223	559.6095	216.7083	84	4 m wide highly oxidized and chloritized rubbly and gougey fault zone	Fault
690	-116.808	49.66338	554.1805	138.8081	85.25	marble	Joint
691	-116.808	49.6632	552.9415	140.8207	64	marble	Joint
692	-116.808	49.66327	536.0608	341.4245	39	marble	Joint
693	-116.808	49.66349	555.4062	359.0588	44.25	marble	Joint
694	-116.808	49.66337	552.5401	210.8996	75	50 cm incredibly brittle and gougey zone with chlorite and iron oxide	Fault
695	-116.809	49.66423	551.2288	173.0443	89	marble	Joint
696	-116.809	49.66427	0	190.4638	73.55556	20 cm wide highly oxidized brittle zone but small exposure so low confidence	Fault
697	-116.807	49.6612	0	30.89598	73.21053	marble	Joint
698	-116.81	49.66427	549.1313	324.4548	76.58824	marble	Joint
699	-116.809	49.6644	558.0376	209.0549	61	marble	Bedding
700	-116.809	49.66443	551.4771	219.1076	71	marble	Bedding
701	-116.81	49.66441	550.6888	205.3368	76	marble	Bedding
702	-116.81	49.66441	0	261.1502	56	marble	Joint
703	-116.809	49.66451	0	220.2604	76.58333	5 m wide highly oxidized highly chloritized rubble and gougey fault zone	Fault
704	-116.81	49.66459	553.3919	171.7719	81	marble	Joint
705	-116.81	49.66462	554.2715	227.3408	65	marble	Bedding
706	-116.81	49.66461	0	209.8149	43	1 m highly oxidized highly chloritized fault zone	Fault
707	-116.809	49.66316	0	215.0965	59	partially obscured highly oxidized and chloritized fault 1 m	Fault
708	-116.81	49.66502	553.816	350.6949	43.81818	marble	Joint
709	-116.809	49.66508	549.359	123.7926	61.14286	marble	Joint
710	-116.809	49.6652	0	216.7689	53	marble	Bedding
711	-116.874	49.66491	560.6405	357.7953	77	granite	Joint
712	-116.874	49.66491	560.5709	243.7156	83	granite	Joint
713	-116.874	49.6649	560.5865	23.17322	61	granite	Joint
714	-116.874	49.6649	560.5835	355.5021	74	granite	Joint
715	-116.874	49.6649	560.54	76.20348	78.55263	granite	Joint
716	-116.874	49.66492	559.4456	1.353855	79	granite	Joint
717	-116.874	49.66482	565.2188	13.6461	57	granite	Joint
718	-116.874	49.66486	559.4449	343.4213	89	granite	Joint
719	-116.873	49.66347	0	220.787	32	gneiss	Bedding
720	-116.872	49.66269	548.4395	117.4323	80.08696	gneiss	Joint
721	-116.872	49.66263	0	339.5505	52.87902	gneiss	Joint
722	-116.872	49.66265	0	11.71656	64.73684	gneiss	Joint
723	-116.872	49.66267	551.4847	331.398	67.21053	gneiss	Joint
724	-116.873	49.66183	549.2634	196.3481	36	gneiss	Bedding
725	-116.873	49.66175	554.4289	24.45242	45.94444	gneiss	Joint
726	-116.873	49.66186	550.7384	127.5983	79.0625	gneiss	Joint

727	-116.873	49.66187	549.8116	121.2237	83	gneiss	Joint
728	-116.873	49.6619	546.5759	124.8193	83.04348	gneiss	Joint
729	-116.873	49.6619	547.0538	125.3964	79.09524	gneiss	Joint
730	-116.873	49.66181	551.1137	26.77616	77.86957	gneiss	Joint
731	-116.873	49.66188	551.6226	288.1956	67	gneiss	Joint
732	-116.873	49.6618	0	74.57646	37	gneiss	Joint
733	-116.873	49.66189	548.9901	200.4779	39	gneiss	Bedding
734	-116.873	49.66194	549.1034	25.11347	76.97778	gneiss	Joint
735	-116.873	49.66187	549.6853	290.6719	82.16667	gneiss	Joint
736	-116.873	49.66229	0	201.8137	35.05714	gneiss	Bedding
737	-116.873	49.66222	557.8095	315.6823	66	gneiss	Joint
738	-116.873	49.66203	562.2187	16.98094	69	gneiss	Joint
739	-116.873	49.66204	0	126.9673	65.07895	gneiss	Joint
740	-116.873	49.66133	562.3534	28.9099	87.41667	gneiss	Joint
741	-116.873	49.66145	565.0207	29.57111	83	gneiss	Joint
742	-116.873	49.66149	562.2127	104.1423	57.46667	gneiss	Joint
743	-116.873	49.66151	562.2763	29.26749	83.3	gneiss	Joint
744	-116.873	49.6615	562.9705	113.8357	80.2	gneiss	Joint
745	-116.873	49.66167	0	102.6832	55.81481	slickensides with minor chlorite fracture surface	Fault
746	-116.874	49.66178	560.6395	19.52464	89	gneiss	Joint
747	-116.873	49.66147	564.5001	98.63227	76	gneiss	Joint
748	-116.873	49.66148	565.1668	22.34824	82	gneiss	Joint
749	-116.874	49.66056	569.9057	210.2504	72	granite	Joint
750	-116.874	49.66052	565.9013	207.3706	69.53333	granite	Joint
751	-116.875	49.65908	568.0034	316.1521	82.2	granite	Joint
752	-116.875	49.65905	568.9425	233.8335	86	granite	Joint
753	-116.875	49.65898	0	217.5434	74	granite	Joint
754	-116.875	49.659	565.3189	74.89626	88	granite	Joint
755	-116.875	49.65899	0	308.1355	87.46154	granite	Joint
756	-116.875	49.65915	568.6494	127.6418	84	granite	Joint
757	-116.875	49.65913	568.5289	37.25721	86.08333	granite	Joint
758	-116.876	49.65894	563.4713	222.5161	78	granite	Joint
759	-116.875	49.65425	559.9928	203.802	78.35294	gneiss	Joint
760	-116.876	49.65423	556.3399	125.1925	89	gneiss	Joint
761	-116.875	49.6542	556.3526	168.0942	75.25	gneiss	Joint
762	-116.875	49.65418	555.9823	181.9546	88	gneiss	Joint
763	-116.875	49.65415	555.5711	93.56495	79.11111	gneiss	Joint
764	-116.875	49.65414	555.7953	228.3818	26	gneiss	Bedding
765	-116.875	49.65411	555.7967	313.869	78	gneiss	Joint
766	-116.875	49.65409	555.9216	141.29	73	gneiss	Joint
767	-116.875	49.6541	556.3687	140.3045	74	gneiss	Joint

768	-116.875	49.65408	555.5731	105.2171	48	gneiss	Joint
769	-116.875	49.654	556.2951	118.0157	74	gneiss	Joint
770	-116.875	49.65402	555.9012	107.873	82.25	gneiss	Joint
771	-116.875	49.65396	0	303.2045	61	fracture with minor oxidation and chlorite and some slickenlines	Fault
772	-116.876	49.65387	551.7703	268.6289	89	granite	Joint
773	-116.875	49.65399	559.3216	21.08935	71.11765	granite	Joint
774	-116.875	49.65398	559.5484	87.15987	80.33333	granite	Joint
775	-116.875	49.65338	562.8204	32.65881	55.9	gneiss	Joint
776	-116.875	49.65334	562.8272	347.8662	64	gneiss	Joint
777	-116.875	49.65332	563.2314	0.629529	78	gneiss	Joint
778	-116.875	49.65328	560.3541	154.9365	83	gneiss	Joint
779	-116.875	49.65328	560.3421	214.6386	85.1	gneiss	Joint
780	-116.875	49.65328	560.2428	153.5919	80	gneiss	Joint
781	-116.875	49.65328	560.1849	215.2591	84	gneiss	Joint
782	-116.875	49.65328	559.7147	336.8467	82	gneiss	Joint
783	-116.876	49.65318	558.6168	207.0836	22.71429	gneiss	Bedding
784	-116.875	49.65161	561.597	166.9974	85	gneiss	Joint
785	-116.875	49.65157	561.1535	169.0504	85	gneiss	Joint
786	-116.875	49.65153	0	130.7744	39	gneiss	Joint
787	-116.875	49.65154	561.489	322.1826	86	gneiss	Joint
788	-116.875	49.65149	560.8072	110.522	80	gneiss	Joint
789	-116.878	49.64607	545.3993	196.9058	83.85714	gneiss	Joint
790	-116.877	49.64623	545.9522	199.3484	83	gneiss	Joint
791	-116.878	49.64619	545.0145	193.6425	72.3	gneiss	Joint
792	-116.878	49.6462	544.0631	189.6633	86	gneiss	Joint
793	-116.878	49.64618	543.9163	199.7275	82	gneiss	Joint
794	-116.878	49.64582	543.5091	141.4163	81	gneiss	Joint
795	-116.878	49.64587	542.6129	45.32259	48	gneiss	Joint
796	-116.878	49.64587	543.7364	216.9656	88	gneiss	Joint
797	-116.878	49.6459	543.1776	50.23101	81	gneiss	Joint
798	-116.878	49.64611	548.7353	141.6967	64	5 cm thick fracture zone	Fault
799	-116.877	49.64578	546.5059	20.91673	89	gneiss	Joint
800	-116.878	49.64608	547.61	198.0942	87	gneiss	Joint
801	-116.878	49.64607	546.4962	193.8777	87	gneiss	Joint
802	-116.878	49.64605	546.1997	194.6718	86	gneiss	Joint
803	-116.878	49.64607	546.1312	196.0233	87.57143	gneiss	Joint
804	-116.878	49.64607	546.7381	119.2187	66	gneiss	Joint
805	-116.878	49.64615	560.8968	17.85883	65	gneiss	Joint
806	-116.878	49.64612	559.0118	313.2943	75	gneiss	Joint
807	-116.878	49.64633	555.9567	216.1126	85	gneiss	Joint
808	-116.878	49.64617	561.3493	139.1085	74	gneiss	Joint

809	-116.878	49.64613	563.885	237.191	24	gneiss	Bedding
810	-116.879	49.64631	569.6964	325.9858	75	gneiss	Joint
811	-116.878	49.64625	566.3624	324.268	79	gneiss	Joint
812	-116.878	49.64623	566.9813	320.1093	76	gneiss	Joint
813	-116.878	49.64623	566.6662	192.8028	71	gneiss	Joint
814	-116.878	49.64622	567.0274	1.855283	61	gneiss	Joint
815	-116.878	49.64622	567.1534	68.79886	67	gneiss	Joint
816	-116.878	49.6462	566.8663	322.1071	70.25	gneiss	Joint
817	-116.878	49.64638	566.2335	305.1305	30	gneiss	Joint
818	-116.878	49.64626	566.9973	157.3826	68	gneiss	Joint
819	-116.879	49.64619	560.7547	156.2479	66	gneiss	Joint
820	-116.875	49.64676	547.1787	250.8582	26	gneiss	Bedding
821	-116.874	49.64564	575.7945	240.4969	28.85714	gneiss	Bedding
822	-116.874	49.64564	581.9764	197.5552	76.24242	gneiss	Joint
823	-116.874	49.64564	581.3954	121.0714	77.72727	gneiss	Joint
824	-116.874	49.6453	550.2879	146.7602	63	gneiss	Joint
825	-116.874	49.64513	552.8929	224.1551	21	gneiss	Bedding
826	-116.874	49.64438	563.3752	192.7457	85.29032	gneiss	Joint
827	-116.874	49.64439	563.4829	271.0998	86.66667	gneiss	Joint
828	-116.874	49.6444	561.0423	188.3842	87.97059	gneiss	Joint
829	-116.874	49.64442	561.127	262.8592	73	gneiss	Joint
830	-116.874	49.64455	568.2147	195.64	71	gneiss	Joint
831	-116.874	49.64453	566.7342	338.2539	68	gneiss	Joint
832	-116.873	49.64376	566.7617	221.6659	77.52381	gneiss	Joint
833	-116.872	49.64375	565.287	205.2235	80	gneiss	Joint
834	-116.872	49.64378	558.1672	309.9181	59	gneiss	Joint
835	-116.872	49.64363	580.589	259.7393	16.55556	gneiss	Bedding
836	-116.872	49.64345	0	262.3977	21	2 cm minor chloritized fault zone	Fault
837	-116.872	49.64355	561.1007	235.3916	22	gneiss	Bedding
838	-116.867	49.63639	550.1703	287.9479	49	gneiss	Joint
839	-116.867	49.63639	546.5907	278.8548	59	gneiss	Joint
840	-116.855	49.62572	566.4037	123.2502	78.625	gneiss	Joint
841	-116.854	49.62533	554.2723	71.1234	59	gneiss	Joint
842	-116.854	49.62515	546.2913	351.4833	76.625	gneiss	Joint
843	-116.854	49.62515	546.2745	264.5762	30.04545	gneiss	Bedding
844	-116.864	49.63546	544.8471	53.26134	75	marble	Joint
845	-116.864	49.63546	544.8471	41.46294	76	marble	Joint
846	-116.847	49.62164	0	286.9865	19	marble	Bedding
847	-116.864	49.63546	585.564	237.7132	68	schist	Bedding
848	-116.842	49.61825	0	214.7382	65	10 m super fault zone	Fault
849	-116.842	49.61798	536.1474	214.1101	59.18182	10 m super fault zone	Fault

850	-116.842	49.61839	551.242	226.0104	46	10 m super fault zone	Fault
851	-116.842	49.61834	540.612	220.4486	41.90909	10 m super fault zone	Fault
852	-116.84	49.61871	0	246.7444	21	schist	Bedding
853	-116.84	49.61902	0	231.2088	18	possible continuation of the super fault width uncertain but multiple meters.	Fault
854	-116.839	49.61883	0	218.1781	37	schist	Bedding
855	-116.827	49.60932	540.6738	137.3753	50.2	schist	Bedding
856	-116.827	49.60918	540.992	158.3813	55.71429	schist	Bedding
857	-116.827	49.60917	0	162.0047	63.23529	schist	Bedding
858	-116.825	49.6067	541.1483	214.8515	63	schist	Bedding
859	-116.824	49.60665	546.4295	222.6203	75	schist	Bedding
860	-116.824	49.60615	539.5142	219.9434	57	schist	Bedding
861	-116.825	49.60603	534.8151	17.52028	61	schist	Joint
862	-116.825	49.60605	535.854	22.69009	64	schist	Joint
863	-116.821	49.60445	525.9893	245.9314	88	quartzite	Joint
864	-116.821	49.60413	564.6903	247.6037	79	quartzite	Joint
865	-116.82	49.60394	550.1175	183.2468	39	schist	Bedding
866	-116.819	49.60304	0	100.3911	85	granite	Joint
867	-116.819	49.60264	0	209.7598	55	schist	Bedding
868	-116.831	49.669	556.7794	141.2177	64.27778	marble	Joint
869	-116.831	49.66904	552.1783	276.2587	89	marble	Joint
870	-116.831	49.66906	547.1923	157.8211	48	marble	Joint
871	-116.831	49.66906	544.6837	17.73798	71	marble	Joint
872	-116.831	49.66904	546.8692	292.8576	87	marble	Joint
873	-116.831	49.66904	546.8036	262.4799	88	marble	Joint
874	-116.831	49.66904	543.2757	275.2256	77	marble	Joint
875	-116.832	49.65843	0	232.0659	4	gneiss	Bedding
876	-116.841	49.66549	633.5682	32.85292	87	gneiss	Joint
877	-116.832	49.65834	639.4303	25.21184	61	gneiss	Joint
878	-116.832	49.65831	0	156.1457	11	gneiss	Bedding
879	-116.856	49.67794	639.8137	318.4952	61	gneiss	Joint
880	-116.836	49.65326	663.465	34.28716	78.66667	gneiss	Joint
881	-116.836	49.65314	759.7425	219.0848	25.64516	gneiss	Bedding
882	-116.836	49.65305	756.932	33.49543	74.44444	gneiss	Joint
883	-116.836	49.65305	755.5025	320.7909	86	gneiss	Joint
884	-116.837	49.65443	764.311	110.7443	86.5	gneiss	Joint
885	-116.837	49.65443	764.2275	179.1717	63	gneiss	Joint
886	-116.839	49.65628	767.9493	181.8518	30.95455	gneiss	Bedding
887	-116.839	49.65628	764.7121	317.8454	77.33333	gneiss	Joint
888	-116.839	49.65854	0	236.8193	18	gneiss	Bedding
889	-116.839	49.65876	772.408	359.0757	79	20 cm pervasive fracture zone with water coming out	Fault
890	-116.839	49.65876	770.0435	111.3529	65	gneiss	Joint

891	-116.84	49.65989	780.865	212.2632	17	gneiss	Bedding
892	-116.842	49.66152	786.877	32.91113	82	gneiss	Joint
893	-116.842	49.66144	787.8658	225.3412	12	gneiss	Bedding
894	-116.841	49.65791	0	160.0974	54.28571	20 cm very oxidized fault zone	Fault
895	-116.846	49.65921	841.4008	150.3971	41	gneiss	Bedding
896	-116.846	49.65874	0	188.1791	76	10 cm minor rubbly oxidized fault	Fault
897	-116.848	49.65928	851.2935	78.36711	28	3 cm minor fault	Fault
898	-116.848	49.65934	841.9617	23.9136	65	granite	Joint
899	-116.849	49.65908	847.4034	142.2382	56	granite	Joint
900	-116.849	49.65914	844.44	7.718753	72	granite	Joint
901	-116.849	49.65913	0	90.31039	52	3 cm gougey fault	Fault
902	-116.85	49.65875	843.5792	138.0402	67	granite	Joint
903	-116.85	49.65872	837.6788	112.9907	88	granite	Joint
904	-116.85	49.65874	834.2359	279.0276	89	granite	Joint
905	-116.85	49.65876	835.4209	207.9049	63	granite	Joint
906	-116.85	49.65875	835.5733	108.9455	84	granite	Joint
907	-116.852	49.65915	838.0063	334.7184	73.2	granite	Joint
908	-116.852	49.65915	835.948	69.91529	85	granite	Joint
909	-116.852	49.65916	835.3092	142.0188	73.25	granite	Joint
910	-116.852	49.65915	834.5183	297.5943	77	granite	Joint
911	-116.852	49.65915	841.8358	220.9691	26.4	gneiss	Joint
912	-116.852	49.65917	836.8224	32.47625	68	gneiss	Joint
913	-116.852	49.65916	836.3689	75.38704	76	gneiss	Joint
914	-116.852	49.65916	837.5321	16.60749	60	gneiss	Joint
915	-116.852	49.65912	836.9964	38.77151	80	gneiss	Joint
916	-116.852	49.65913	836.6539	92.08716	62	gneiss	Joint
917	-116.852	49.65913	837.4427	42.36875	76	gneiss	Joint
918	-116.852	49.65914	837.828	201.0771	16	gneiss	Bedding
919	-116.852	49.65923	836.4134	195.8159	20	gneiss	Bedding
920	-116.852	49.65903	842.4791	195.4364	37.75	granite	Joint
921	-116.852	49.65908	838.1855	135.5225	89	granite	Joint
922	-116.852	49.65908	835.87	36.06737	74	granite	Joint
923	-116.853	49.65905	832.701	91.16902	64.22222	granite	Joint
924	-116.853	49.65906	831.2374	222.1606	43	granite	Joint
925	-116.853	49.65905	832.8341	21.88782	74	granite	Joint
926	-116.853	49.65905	832.5916	228.2432	43.89474	granite	Joint
927	-116.853	49.65905	830.9751	40.3668	73	granite	Joint
928	-116.853	49.65904	831.1051	305.2199	87	granite	Joint
929	-116.853	49.659	830.7999	45.5977	80	granite	Joint
930	-116.853	49.65898	831.839	24.93575	60	granite	Joint
931	-116.853	49.65891	832.5544	37.71492	70.25	granite	Joint

932	-116.853	49.65891	831.863	35.91566	71	granite	Joint
933	-116.854	49.66092	835.3175	77.96991	79	granite	Joint
934	-116.854	49.66091	834.1875	27.59894	63.1875	granite	Joint
935	-116.854	49.66096	830.494	97.40178	65	granite	Joint
936	-116.853	49.66161	831.9068	138.3095	73	gneiss	Joint
937	-116.853	49.66153	834.1436	135.2288	85	gneiss	Joint
938	-116.853	49.66158	831.8355	6.772072	77	gneiss	Joint
939	-116.854	49.66173	827.0006	1.651099	72	gneiss	Joint
940	-116.853	49.66174	821.4398	131.1124	77	gneiss	Joint
941	-116.854	49.66173	823.556	220.2845	29	gneiss	Bedding
942	-116.854	49.66193	831.2457	132.4646	81.58824	10 cm minor oxidized fault zone	Fault
943	-116.854	49.66187	834.4037	9.052227	69	gneiss	Joint
944	-116.854	49.6623	833.2509	190.7819	18.81818	gneiss	Bedding
945	-116.856	49.66349	828.4427	174.7738	14.58065	gneiss	Bedding
946	-116.856	49.66049	815.1949	226.8557	32	gneiss	Bedding
947	-116.856	49.66052	814.7595	120.4423	68	gneiss	Joint
948	-116.856	49.66062	817.0355	127.8243	47	gneiss	Joint
949	-116.857	49.66181	796.2978	230.32	83.16667	gneiss	Joint
950	-116.857	49.6619	797.4669	313.912	75	gneiss	Joint
951	-116.857	49.66193	799.0241	199.424	25	gneiss	Bedding
952	-116.857	49.66197	799.2705	125.6345	84	gneiss	Joint
953	-116.859	49.66258	779.1657	236.4552	21.66667	gneiss	Bedding
954	-116.855	49.65617	851.8669	217.9145	87	gneiss	Joint
955	-116.855	49.65613	850.2811	30.81201	88	gneiss	Joint
956	-116.855	49.65615	863.7152	284.2253	81	granite	Joint
957	-116.855	49.65611	869.0675	80.04056	85	granite	Joint
958	-116.855	49.65611	865.5433	19.26855	84	granite	Joint
959	-116.855	49.65608	865.0758	108.7124	86	granite	Joint
960	-116.841	49.65573	0	239.557	19	gneiss	Bedding
961	-116.837	49.64895	0	222.4976	38.29412	gneiss	Bedding
962	-116.838	49.64722	859.0266	208.8149	32	marble	Bedding
963	-116.834	49.6473	844.5833	208.7097	49	gneiss	Bedding
964	-116.834	49.64735	846.1226	203.8687	49	gneiss	Bedding
965	-116.834	49.64731	844.6217	122.4099	87.92857	gneiss	Joint
966	-116.834	49.64731	0	91.21138	41	gneiss	Joint
967	-116.836	49.6465	865.3233	228.0175	53	marble	Bedding
968	-116.836	49.64648	866.2149	227.6957	56	marble	Bedding
969	-116.836	49.64644	869.075	231.7501	55.61538	marble	Bedding
970	-116.836	49.64646	868.2841	130.3521	84	marble	Joint
971	-116.836	49.64647	867.7204	139.6283	78	marble	Joint
972	-116.836	49.64658	865.9452	206.7021	49.88	gneiss	Bedding

973	-116.837	49.64688	856.9774	198.9998	53	gneiss	Bedding
974	-116.838	49.64694	864.3629	214.222	41	marble	Bedding
975	-116.838	49.64697	862.6298	336.265	82	marble	Joint
976	-116.838	49.64694	860.9388	343.2971	72	marble	Joint
977	-116.84	49.64576	881.2608	234.7591	33	marble	Bedding
978	-116.844	49.64539	906.9044	307.8692	86	gneiss	Joint
979	-116.844	49.64544	908.0772	283.4517	60	gneiss	Joint
980	-116.845	49.64724	909.524	355.7156	83	gneiss	Joint
981	-116.845	49.64712	921.9201	53.36598	44	diorite	Joint
982	-116.845	49.647	927.1368	76.96005	42	diorite	Joint
983	-116.845	49.64704	922.9818	295.9587	72	diorite	Joint
984	-116.845	49.64703	923.6334	306.415	75	diorite	Joint
985	-116.845	49.64701	925.9747	60.02267	48	diorite	Joint
986	-116.845	49.64702	925.4935	106.173	49	diorite	Joint
987	-116.845	49.64702	926.5203	65.07312	52	diorite	Joint
988	-116.841	49.64447	896.3553	195.5228	46	marble	Bedding
989	-116.841	49.64457	895.5747	195.1859	39	marble	Bedding
990	-116.841	49.64459	893.3996	177.5844	64	marble	Joint
991	-116.839	49.64523	887.8495	207.3997	38	schist	Bedding
992	-116.839	49.6452	887.4049	211.2554	38	schist	Bedding
993	-116.839	49.64519	886.4774	211.0358	42	schist	Bedding
994	-116.842	49.64117	934.6449	258.5167	49.16667	50 cm wide highly oxidized zone	Fault
995	-116.842	49.64098	939.7581	247.9756	53.21429	schist	Bedding
996	-116.842	49.64066	943.0995	217.8703	71	schist	Bedding
997	-116.84	49.6405	959.7379	227.7281	78	marble	Bedding
998	-116.84	49.64053	956.5894	231.3119	78.36842	marble	Bedding
999	-116.84	49.64045	958.9752	226.1456	85	marble	Bedding
1000	-116.84	49.64038	962.7353	231.3552	76	schist	Bedding
1001	-116.84	49.64047	960.1262	222.8769	77.25	marble	Bedding
1002	-116.84	49.64036	956.1703	230.3176	86	marble	Bedding
1003	-116.839	49.63983	969.5601	228.3568	55.9	marble	Bedding
1004	-116.84	49.63977	969.3165	49.48853	86	marble	Bedding
1005	-116.839	49.63946	0	34.43638	78.36364	2 m wide rubbly rusty zone	Fault
1006	-116.837	49.64013	962.712	45.93164	66.72727	5 m wide very brittle and rubbly oxidized fault zone	Fault
1007	-116.837	49.64085	958.7037	231.7237	86	marble	Bedding
1008	-116.837	49.64073	956.7234	219.6117	74.75	marble	Bedding
1009	-116.838	49.63986	0	162.4628	40	30 cm wide limited exposure so low confidence	Fault
1010	-116.832	49.64903	800.8492	220.2939	43.44444	gneiss	Bedding
1011	-116.832	49.64901	799.7445	210.4326	41	50 cm very gougey and oxidized fault zone	Fault
1012	-116.83	49.64924	774.3704	213.5354	38.63636	gneiss	Bedding

1013	-116.831	49.64897	782.7783	21.8707	73	gneiss	Joint
1014	-116.831	49.64856	802.471	11.95236	74	gneiss	Joint
1015	-116.831	49.64879	789.7948	280.1673	59	gneiss	Joint
1016	-116.831	49.64884	788.6681	294.2317	70.85714	gneiss	Joint
1017	-116.831	49.64883	788.9515	326.2322	84	gneiss	Joint
1018	-116.831	49.64879	790.5829	212.8353	44	gneiss	Bedding
1019	-116.831	49.64875	786.8147	155.5786	79	gneiss	Joint
1020	-116.831	49.6487	793.7464	357.2911	76	gneiss	Joint
1021	-116.831	49.64872	790.5036	214.7118	39	gneiss	Bedding
1022	-116.83	49.64825	792.2796	200.5037	31.2	marble	Bedding
1023	-116.829	49.6477	769.7652	192.4643	61	schist	Bedding
1024	-116.829	49.64751	769.4132	202.55	76	possible 5 m fault zone very brittle and rusty but low confidence	Fault
1025	-116.828	49.64744	770.5648	10.7817	72	marble	Joint
1026	-116.828	49.64744	766.201	227.5228	41	schist	Bedding
1027	-116.828	49.64721	767.5145	277.2805	89	diorite	Joint
1028	-116.828	49.6472	771.6825	46.5339	22	diorite	Joint
1029	-116.828	49.64714	772.4002	13.07878	66	diorite	Joint
1030	-116.828	49.64714	772.6927	307.601	37	diorite	Joint
1031	-116.828	49.64713	772.0067	20.332	83	diorite	Joint
1032	-116.828	49.64667	774.0872	21.40307	73	10 cm gougey rusty fault	Fault
1033	-116.828	49.64716	0	25.84811	75.13333	10 cm gougey rusty fault	Fault
1034	-116.828	49.6472	766.6578	13.86189	71	diorite	Joint
1035	-116.828	49.64715	769.8547	30.92148	57	diorite	Joint
1036	-116.828	49.64717	0	30.47318	71.42857	10 cm gougey rusty fault	Fault
1037	-116.83	49.6406	854.0604	217.4918	87	marble	Bedding
1038	-116.84	49.63479	0	236.7637	56.07143	marble	Bedding
1039	-116.843	49.63734	869.4688	45.92133	37	gneiss	Bedding
1040	-116.843	49.6372	862.9871	36.76812	49	gneiss	Bedding
1041	-116.843	49.63714	860.2393	47.61014	60	gneiss	Bedding
1042	-116.843	49.63716	858.7058	298.6019	83	gneiss	Joint
1043	-116.843	49.63717	858.7519	292.1705	79	gneiss	Joint
1044	-116.846	49.63807	843.941	231.3432	67	marble	Bedding
1045	-116.846	49.63805	841.5799	230.9203	72	marble	Bedding
1046	-116.846	49.63848	839.1634	80.13438	82.81818	marble	Bedding
1047	-116.846	49.63866	845.1778	230.9731	52.86667	marble	Bedding
1048	-116.846	49.63914	846.7359	241.0885	40	schist	Bedding
1049	-116.846	49.63909	844.6085	261.0296	41.92593	schist	Bedding
1050	-116.846	49.63909	845.252	258.7171	41	schist	Bedding
1051	-116.846	49.63909	844.1287	249.624	36.2	schist	Bedding
1052	-116.846	49.6391	845.2867	248.089	36.28571	schist	Bedding
1053	-116.846	49.63923	852.5053	216.8495	49	schist	Bedding

1054	-116.846	49.6393	849.1214	224.996	47	schist	Bedding
1055	-116.846	49.63936	849.4212	232.9865	46.6875	schist	Bedding
1056	-116.846	49.63943	849.5059	245.4235	48.75	schist	Bedding
1057	-116.846	49.6406	848.5704	256.3745	40.2	schist	Bedding
1058	-116.846	49.64063	851.4892	255.1897	40	schist	Bedding
1059	-116.846	49.64061	849.8197	323.9755	45	schist	Joint
1060	-116.846	49.64075	854.0213	320.9459	59	schist	Joint
1061	-116.846	49.64049	852.5374	247.5294	34.82353	schist	Bedding
1062	-116.846	49.64051	852.286	255.1507	38	schist	Bedding
1063	-116.847	49.64252	0	224.8221	23	gneiss	Bedding
1064	-116.848	49.64068	804.5042	56.37666	56	gneiss	Joint
1065	-116.848	49.6407	806.6781	283.6583	52	gneiss	Joint
1066	-116.848	49.64071	806.63	53.51653	82	gneiss	Joint
1067	-116.848	49.64072	807.9798	119.147	71.13333	gneiss	Joint
1068	-116.848	49.64071	806.707	13.08581	64	gneiss	Joint
1069	-116.849	49.64121	803.059	251.1588	29	gneiss	Bedding
1070	-116.84	49.63484	867.1407	46.55618	60.77273	50 cm gougey oxidized fault zone	Fault
1071	-116.84	49.63505	867.066	358.6793	67	50 cm gougey oxidized fault zone	Fault
1072	-116.825	49.64081	783.1679	12.92726	86.53333	schist	Bedding
1073	-116.823	49.62745	779.1289	296.9298	39.0303	quartzite	Joint
1074	-116.823	49.6274	780.3506	123.3927	56	quartzite	Bedding
1075	-116.824	49.6272	806.5904	342.3795	73	quartzite	Bedding
1076	-116.825	49.62632	0	270.261	70	quartzite	Bedding
1077	-116.784	49.53993	824.034	183.5252	84	quartzite	Joint
1078	-116.825	49.62427	840.4841	183.6145	70	quartzite	Joint
1079	-116.825	49.62427	838.3932	284.5441	79	quartzite	Joint
1080	-116.826	49.62326	0	91.77155	86	quartzite	Bedding
1081	-116.826	49.62309	879.0719	162.2301	89	quartzite	Joint
1082	-116.818	49.62874	792.1847	80.25457	79	quartzite	Bedding
1083	-116.818	49.62881	0	7.42072	74	1 m wide very rusty gouge zone	Fault
1084	-116.818	49.63101	785.7821	160.8205	41	schist	Joint
1085	-116.817	49.63098	772.9466	159.8695	40.6875	schist	Joint
1086	-116.817	49.63099	769.4537	11.6666	84	schist	Bedding
1087	-116.817	49.63024	774.3309	259.6222	61	quartzite	Joint
1088	-116.817	49.63026	773.4454	208.6102	49	quartzite	Joint
1089	-116.817	49.63022	774.8582	118.5551	84	quartzite	Joint
1090	-116.817	49.63045	764.972	230.4915	48	quartzite	Bedding
1091	-116.817	49.63048	770.7232	150.3579	82.625	quartzite	Joint
1092	-116.817	49.63048	770.4159	147.1992	83	quartzite	Joint
1093	-116.817	49.63048	770.6335	142.9235	84	quartzite	Joint
1094	-116.817	49.63046	770.8819	153.6378	80	quartzite	Joint

1095	-116.817	49.63049	771.591	150.3904	82	quartzite	Joint
1096	-116.817	49.63048	771.9	341.6665	89	quartzite	Joint
1097	-116.827	49.64587	801.3023	262.5109	36.84211	marble	Bedding
1098	-116.829	49.66063	0	207.1446	25	marble	Bedding
1099	-116.829	49.66081	583.7066	196.5647	33	marble	Bedding
1100	-116.829	49.66077	0	207.0777	20.75	marble	Bedding
1101	-116.829	49.66092	589.838	140.1837	84	marble	Joint
1102	-116.829	49.66093	583.6053	131.043	88	marble	Joint
1103	-116.829	49.66083	584.9504	135.3866	87	marble	Joint
1104	-116.829	49.66074	585.6676	112.894	62	marble	Joint
1105	-116.829	49.66074	585.2223	96.62692	55	marble	Joint
1106	-116.824	49.65532	537.0371	41.23429	71	marble	Bedding
1107	-116.824	49.65538	569.0439	43.11461	79	marble	Bedding
1108	-116.824	49.6554	568.7745	154.5521	87	marble	Joint
1109	-116.825	49.656	580.7288	251.7123	86	marble	Bedding
1110	-116.826	49.65676	561.604	242.9506	79	schist	Bedding
1111	-116.825	49.65626	569.8089	229.2133	72	schist	Bedding
1112	-116.845	49.62052	0	211.5708	65.56	marble	Bedding
1113	-116.845	49.62069	540.0587	8.804988	56.92	marble	Bedding
1114	-116.846	49.62077	547.5144	10.71081	71	marble	Bedding
1115	-116.846	49.62074	544.8697	9.979313	72	marble	Bedding
1116	-116.845	49.62053	0	207.5644	71	marble	Bedding
1117	-116.845	49.62049	563.6567	231.3159	60.53333	marble	Bedding
1118	-116.839	49.61717	541.9215	151.0272	79	schist	Joint
1119	-116.839	49.61716	540.481	144.8756	83	schist	Joint
1120	-116.839	49.61715	541.1314	145.7405	79	schist	Joint
1121	-116.839	49.61726	592.2422	148.1911	66	schist	Joint
1122	-116.839	49.61718	546.4007	150.8396	76	schist	Joint
1123	-116.839	49.61718	546.7225	149.169	86	schist	Joint
1124	-116.838	49.61709	0	49.32533	26	schist	Bedding
1125	-116.838	49.61694	539.6463	56.69279	22	schist	Bedding
1126	-116.809	49.64012	548.0406	187.5406	49	marble	Bedding
1127	-116.809	49.64012	546.2374	181.9916	61	marble	Bedding
1128	-116.785	49.7126	779.3283	193.4814	60	quartzite	Bedding
1129	-116.785	49.71259	773.0093	193.7131	63	quartzite	Bedding
1130	-116.786	49.71295	770.3239	300.5443	59	quartzite	Joint
1131	-116.785	49.7128	769.3069	14.89934	33	quartzite	Joint
1132	-116.785	49.71292	783.4892	11.14782	34	quartzite	Joint
1133	-116.785	49.71293	778.7517	6.032514	30	quartzite	Joint
1134	-116.785	49.71292	775.6018	28.02892	26.2381	quartzite	Joint
1135	-116.785	49.71296	768.9725	19.75207	30	quartzite	Joint

1136	-116.785	49.7129	772.5036	2.510866	30	quartzite	Joint
1137	-116.785	49.71285	775.1104	354.317	41	quartzite	Joint
1138	-116.785	49.71286	772.4956	14.80179	32	quartzite	Joint
1139	-116.785	49.7129	775.3852	306.7261	58	quartzite	Joint
1140	-116.785	49.71291	777.4189	37.75488	28.3	quartzite	Joint
1141	-116.785	49.71291	778.0349	184.9599	62	quartzite	Bedding
1142	-116.785	49.71305	784.3341	38.46181	25	quartzite	Joint
1143	-116.785	49.71293	784.4533	307.0718	67.625	quartzite	Joint
1144	-116.785	49.71282	781.393	318.1303	62	quartzite	Joint
1145	-116.785	49.71287	781.4258	203.935	61.04	quartzite	Bedding
1146	-116.785	49.71287	771.0889	295.0236	57	quartzite	Joint
1147	-116.785	49.71267	781.3239	305.1458	59	quartzite	Joint
1148	-116.785	49.71266	783.9458	191.2182	59	quartzite	Bedding
1149	-116.785	49.71263	778.6856	21.05693	22	quartzite	Joint
1150	-116.785	49.71241	776.5102	194.6653	60	quartzite	Bedding
1151	-116.77	49.7128	819.5683	191.9357	61	schist	Bedding
1152	-116.77	49.71275	818.7114	84.99024	49	schist	Joint
1153	-116.77	49.71278	819.706	80.81973	48	schist	Joint
1154	-116.77	49.71279	816.7698	120.6906	63	schist	Joint
1155	-116.77	49.71279	816.967	85.13317	64.27273	schist	Joint
1156	-116.77	49.71294	0	182.3052	69	schist	Bedding
1157	-116.771	49.71267	0	198.8675	61	schist	Bedding
1158	-116.764	49.71331	0	194.2425	76	quartzite	Bedding
1159	-116.764	49.71341	0	205.0021	64.6	quartzite	Bedding
1160	-116.764	49.71359	0	180.3571	86	30 m orebin creek fault	Fault
1161	-116.764	49.71373	0	180.8299	86	30 m orebin creek fault	Fault
1162	-116.764	49.71362	0	187.3121	80	quartzite	Bedding
1163	-116.764	49.71343	840.5981	210.5677	67	quartzite	Bedding
1164	-116.764	49.71353	843.3603	118.4565	69	quartzite	Joint
1165	-116.764	49.71352	841.8779	119.8331	73	quartzite	Joint
1166	-116.764	49.71345	829.2556	204.9086	78.9	quartzite	Bedding
1167	-116.764	49.71337	830.0383	193.8677	85	quartzite	Bedding
1168	-116.764	49.71338	830.4269	205.1338	82	quartzite	Bedding
1169	-116.764	49.7134	829.3281	112.4182	83	quartzite	Joint
1170	-116.764	49.71341	830.9442	112.7157	81.41176	quartzite	Joint
1171	-116.764	49.7134	833.0008	144.3415	77	quartzite	Joint
1172	-116.764	49.71333	0	186.1519	79	quartzite	Bedding
1173	-116.737	49.71026	0	200.046	76	gritstone	Bedding
1174	-116.737	49.71046	868.7002	121.6791	87	gritstone	Joint
1175	-116.737	49.71038	864.6684	124.6055	89	gritstone	Joint
1176	-116.728	49.7093	0	196.8359	78	phyllite	Bedding

1177	-116.728	49.70954	0	200.6292	67.78571	phyllite	Bedding
1178	-116.726	49.70896	0	284.1935	89	phyllite	Joint
1179	-116.726	49.70905	0	25.79689	66.64706	phyllite	Bedding
1180	-116.722	49.70962	0	186.8996	82.89474	phyllite	Bedding
1181	-116.721	49.70931	0	178.2996	78	phyllite	Bedding
1182	-116.721	49.70966	0	198.9187	76.32911	phyllite	Bedding
1183	-116.709	49.72159	1192.179	187.4539	73	phyllite	Bedding
1184	-116.716	49.72073	0	204.196	74	gritstone	Bedding
1185	-116.72	49.71872	1343.149	188.8921	72	phyllite	Bedding
1186	-116.72	49.71865	0	190.2434	71	phyllite	Bedding
1187	-116.72	49.71876	1341.215	26.29774	37	phyllite	Joint
1188	-116.722	49.72075	0	190.3241	65.84211	phyllite	Bedding
1189	-116.722	49.72091	0	202.9874	73	phyllite	Bedding
1190	-116.721	49.72198	0	197.714	59	phyllite	Bedding
1191	-116.719	49.7256	0	186.1927	65	phyllite	Bedding
1192	-116.72	49.72405	0	203.9208	68	phyllite	Bedding
1193	-116.69	49.72453	1003.302	187.34	88.2069	phyllite	Bedding
1194	-116.69	49.72464	0	193.5159	82	phyllite	Bedding
1195	-116.686	49.72632	1001.65	278.9191	79	phyllite	Joint
1196	-116.687	49.72626	1005.47	12.842	86	phyllite	Bedding
1197	-116.684	49.72755	0	195.9185	72	phyllite	Bedding
1198	-116.683	49.72895	0	194.1956	69.11111	phyllite	Bedding
1199	-116.682	49.72867	986.3196	118.8253	82	phyllite	Joint
1200	-116.683	49.72882	998.0652	303.049	75	phyllite	Joint
1201	-116.682	49.72884	999.473	125.3393	56	phyllite	Joint
1202	-116.683	49.72882	999.1848	133.3332	82	phyllite	Joint
1203	-116.683	49.7292	1005.358	134.1008	78.5	phyllite	Joint
1204	-116.677	49.73126	1010.938	120.1966	80	phyllite	Joint
1205	-116.677	49.73132	1011.217	114.1868	77	phyllite	Joint
1206	-116.677	49.73133	1011.129	117.8695	79	phyllite	Joint
1207	-116.677	49.73154	0	5.472632	87	phyllite	Bedding
1208	-116.673	49.73462	1025.091	206.7453	32	phyllite	Bedding
1209	-116.673	49.73447	1024.151	229.4845	28	phyllite	Bedding
1210	-116.673	49.73447	0	225.8582	26	phyllite	Bedding
1211	-116.677	49.73114	1009.588	356.5256	78	phyllite	Bedding
1212	-116.677	49.73117	0	194.2452	72	phyllite	Bedding
1213	-116.694	49.69421	0	195.6165	76.55882	phyllite	Bedding
1214	-116.694	49.6942	0	196.5436	88	phyllite	Bedding
1215	-116.694	49.69418	1230.241	26.66573	88.97436	phyllite	Bedding
1216	-116.694	49.69408	0	20.88028	44.55556	phyllite	Bedding
1217	-116.693	49.694	0	21.72574	74	phyllite	Bedding

1218	-116.693	49.69403	0	18.14142	76	phyllite	Bedding
1219	-116.692	49.6938	0	19.03199	71	phyllite	Bedding
1220	-116.692	49.6938	0	7.648326	71	phyllite	Bedding
1221	-116.691	49.69398	0	350.833	81	phyllite	Bedding
1222	-116.691	49.69404	1287.669	294.6665	67	phyllite	Joint
1223	-116.691	49.6939	0	278.582	58	phyllite	Joint
1224	-116.692	49.69414	1284.423	350.9937	76	phyllite	Bedding
1225	-116.691	49.69395	0	358.8929	77	phyllite	Bedding
1226	-116.701	49.70848	1227.641	22.27164	71.9	phyllite	Bedding
1227	-116.701	49.70863	1227.229	41.65198	57	phyllite	Bedding
1228	-116.701	49.70845	1219.612	14.12613	56	phyllite	Bedding
1229	-116.702	49.70637	0	14.28221	50	phyllite	Bedding
1230	-116.703	49.70085	0	15.77905	33	phyllite	Bedding
1231	-116.703	49.70086	0	21.87127	35.81818	phyllite	Bedding
1232	-116.702	49.70589	0	24.39193	44.82759	phyllite	Bedding
1233	-116.702	49.70558	0	40.22884	32.51429	phyllite	Bedding
1234	-116.695	49.70706	0	28.48672	63	phyllite	Bedding
1235	-116.694	49.70701	0	27.55754	62.90625	phyllite	Bedding
1236	-116.694	49.70712	0	23.96879	68	phyllite	Bedding
1237	-116.698	49.70594	1414.374	4.400943	48	phyllite	Bedding
1238	-116.698	49.7057	1429.24	19.36221	43	phyllite	Bedding
1239	-116.698	49.70535	1434.515	16.53455	38	phyllite	Bedding
1240	-116.699	49.70445	1457.057	12.06107	32.76	phyllite	Bedding
1241	-116.699	49.70449	1444.146	118.3815	75.11538	phyllite	Joint
1242	-116.699	49.70429	0	42.35068	34	phyllite	Bedding
1243	-116.696	49.70487	1481.339	99.26109	83	phyllite	Joint
1244	-116.696	49.70485	0	24.50186	23.02128	phyllite	Bedding
1245	-116.669	49.73278	0	12.19953	35.04545	phyllite	Bedding
1246	-116.666	49.73525	0	6.606859	14	phyllite	Bedding
1247	-116.666	49.73569	0	2.219771	34.875	phyllite	Bedding
1248	-116.661	49.73169	1426.65	2.238401	46.10811	phyllite	Bedding
1249	-116.662	49.72746	0	10.01991	28	gritstone	Bedding
1250	-116.662	49.7275	0	215.0771	82	gritstone	Joint
1251	-116.662	49.72754	1399.243	260.3982	88	gritstone	Joint
1252	-116.662	49.72745	0	22.20533	37	gritstone	Bedding
1253	-116.766	49.70393	0	183.798	80	5 m weak zone possible continuation of orebin creek	Fault
1254	-116.766	49.70384	987.2756	196.475	84.5	quartzite	Bedding
1255	-116.766	49.70387	988.6328	196.5588	82	quartzite	Bedding
1256	-116.766	49.70386	989.9524	281.2734	86.04348	quartzite	Joint
1257	-116.766	49.70386	989.123	281.657	84	quartzite	Joint
1258	-116.766	49.70391	0	187.8879	77	quartzite	Bedding

1259	-116.765	49.70396	0	189.2319	81	quartzite	Bedding
1260	-116.766	49.70411	0	195.1497	74	quartzite	Bedding
1261	-116.766	49.70414	0	269.7324	84	quartzite	Joint
1262	-116.765	49.70413	0	190.9187	81.15152	quartzite	Bedding
1263	-116.765	49.70421	987.9038	101.5689	81.77273	quartzite	Joint
1264	-116.765	49.70423	984.5459	115.3511	87	quartzite	Joint
1265	-116.766	49.70443	995.0078	96.42875	86	quartzite	Joint
1266	-116.765	49.70439	997.4406	193.1406	76	quartzite	Bedding
1267	-116.765	49.70439	982.394	194.2756	76	quartzite	Bedding
1268	-116.765	49.70439	994.6562	280.8599	72.04167	quartzite	Joint
1269	-116.765	49.70463	991.6645	119.5872	65.82353	quartzite	Joint
1270	-116.765	49.70467	986.1245	196.9279	76	quartzite	Bedding
1271	-116.762	49.70726	983.8462	100.992	89	quartzite	Joint
1272	-116.762	49.707	993.8204	202.0421	65	quartzite	Bedding
1273	-116.761	49.70692	999.6374	93.40567	86	quartzite	Joint
1274	-116.76	49.70736	1008.019	197.0821	66.0625	quartzite	Bedding
1275	-116.76	49.70719	995.0481	272.8731	87.97561	quartzite	Joint
1276	-116.758	49.70719	0	188.6593	58	quartzite	Bedding
1277	-116.758	49.707	1009.314	197.2117	62	quartzite	Bedding
1278	-116.758	49.70704	1010.015	95.67037	84	quartzite	Joint
1279	-116.758	49.70675	984.8653	189.3668	51.96875	quartzite	Bedding
1280	-116.757	49.70701	999.9832	109.4418	82	quartzite	Joint
1281	-116.757	49.70677	0	187.3599	60.925	2 m wide gouge zone with lots of water coming out	Fault
1282	-116.757	49.70668	998.3189	103.7969	83	quartzite	Joint
1283	-116.757	49.70672	1005.271	183.2141	51.85185	quartzite	Bedding
1284	-116.756	49.70657	1029.502	350.2756	61.42308	quartzite	Joint
1285	-116.756	49.70655	1026.575	350.7822	59.31579	quartzite	Joint
1286	-116.756	49.7065	1032.324	351.597	52	quartzite	Joint
1287	-116.756	49.70654	1032.257	9.175024	27.38636	quartzite	Joint
1288	-116.756	49.70648	1034.033	95.12359	84	quartzite	Joint
1289	-116.756	49.70618	1013.733	184.9461	42	quartzite	Bedding
1290	-116.755	49.70607	1027.616	271.3608	89	quartzite	Joint
1291	-116.755	49.70629	1044.319	279.2653	72	quartzite	Joint
1292	-116.755	49.70629	1044.155	166.2283	51	quartzite	Bedding
1293	-116.755	49.70605	1040.031	100.9154	85	quartzite	Joint
1294	-116.755	49.70599	1015.213	181.0687	47	quartzite	Bedding
1295	-116.758	49.70725	1014.465	352.5336	62.02857	quartzite	Joint
1296	-116.753	49.70539	1054.334	326.6826	38	quartzite	Joint
1297	-116.753	49.70562	1065.658	65.87558	86	quartzite	Joint
1298	-116.753	49.70546	1050.096	171.6574	56	quartzite	Bedding
1299	-116.753	49.70526	1050.398	325.2277	38	quartzite	Joint

1300	-116.753	49.70538	1050.138	354.0651	48	quartzite	Joint
1301	-116.753	49.70535	1051.786	289.3047	83	quartzite	Joint
1302	-116.753	49.70535	1057.389	165.6441	43	50 cm gouge and fracture zone	Fault
1303	-116.752	49.70523	0	182.1785	46.88	2 m fracture zone with lots of water	Fault
1304	-116.752	49.70517	1044.633	169.7658	41	quartzite	Bedding
1305	-116.752	49.70518	1047.165	277.46	72	quartzite	Joint
1306	-116.752	49.70508	1053.302	178.4494	80.96296	phyllite	Bedding
1307	-116.752	49.70512	1055.531	177.1129	76	phyllite	Bedding
1308	-116.752	49.70516	1049.028	180.777	79	phyllite	Bedding
1309	-116.752	49.7051	1046.706	195.0751	82	phyllite	Bedding
1310	-116.751	49.70468	1044.439	110.6596	74	phyllite	Joint
1311	-116.75	49.70486	1073.354	262.5784	57.83871	phyllite	Joint
1312	-116.75	49.7047	1047.924	162.5271	83	10 cm rusty gouge zone	Fault
1313	-116.75	49.70498	1034.636	172.9195	47	phyllite	Bedding
1314	-116.749	49.70474	1065.211	185.6797	57	phyllite	Bedding
1315	-116.749	49.70471	1068.615	170.5737	54	phyllite	Bedding
1316	-116.748	49.70466	1043.865	164.2545	50	phyllite	Bedding
1317	-116.747	49.70452	1045.097	187.2012	63	20 m fracture zone with lots of water	Fault
1318	-116.747	49.70451	1031.562	185.9294	66	phyllite	Bedding
1319	-116.746	49.70446	1037.946	96.76706	86	phyllite	Joint
1320	-116.748	49.70457	1038.603	176.4246	70	2 m zone	Joint
1321	-116.74	49.70455	1032.861	183.2316	57	phyllite	Bedding
1322	-116.738	49.70495	1032.495	195.2186	75.03226	phyllite	Bedding
1323	-116.738	49.70522	1018.461	198.0969	74	phyllite	Bedding
1324	-116.752	49.70493	1019.363	161.7348	43	gritstone	Bedding
1325	-116.752	49.70525	1037.932	162.5029	41	gritstone	Bedding
1326	-116.753	49.70526	1032.373	155.5111	34.66667	gritstone	Bedding
1327	-116.753	49.70533	1029.674	177.4408	50	gritstone	Bedding
1328	-116.753	49.70539	1029.587	179.6658	62	gritstone	Bedding
1329	-116.754	49.70572	1059.576	163.2694	58	gritstone	Bedding
1330	-116.754	49.70566	1055.607	175.6513	37.75	gritstone	Bedding
1331	-116.768	49.69987	0	351.8741	68	schist	Bedding
1332	-116.768	49.69996	0	270.7002	57	schist	Joint
1333	-116.768	49.69992	1013.534	275.637	75.875	schist	Joint
1334	-116.768	49.70002	1028.526	349.0384	54	quartzite	Bedding
1335	-116.768	49.70041	1023.304	198.6666	81	surface possible continuation of orebin creek	Fault
1336	-116.768	49.70042	1027.605	163.4631	85	quartzite	Bedding
1337	-116.768	49.7006	1022.425	182.7485	72	quartzite	Bedding
1338	-116.768	49.70064	1019.118	279.9593	51	quartzite	Joint
1339	-116.766	49.70271	1025.104	341.5294	68	quartzite	Bedding
1340	-116.766	49.70283	1033.801	333.4994	63	quartzite	Bedding

1341	-116.766	49.70266	1023.966	173.9981	74	quartzite	Bedding
1342	-116.766	49.70268	1031.688	180.2051	75	quartzite	Bedding
1343	-116.766	49.7027	1033.415	108.3334	80.68421	quartzite	Joint
1344	-116.766	49.70269	1033.093	189.5847	74	quartzite	Bedding
1345	-116.766	49.70275	1034.441	179.7986	75	quartzite	Bedding
1346	-116.766	49.70277	1034.21	96.38773	85.6	quartzite	Joint
1347	-116.766	49.70277	1035.798	308.1021	87.4	quartzite	Joint
1348	-116.766	49.70293	1053.627	109.9264	78	quartzite	Joint
1349	-116.766	49.70282	1040.885	103.5035	74.61111	quartzite	Joint
1350	-116.766	49.7028	1041.407	186.4031	73.28571	quartzite	Bedding
1351	-116.766	49.70279	1040.674	185.1942	73	quartzite	Bedding
1352	-116.766	49.70278	1036.357	281.1544	86	quartzite	Joint
1353	-116.766	49.70278	1036.817	278.2521	79	quartzite	Joint
1354	-116.766	49.7032	1040.463	331.502	39.07407	quartzite	Joint
1355	-116.766	49.70303	1045.72	190.2626	74	quartzite	Bedding
1356	-116.766	49.70306	1043.047	183.7474	40.17391	quartzite	Joint
1357	-116.766	49.70309	1034.082	87.89712	66	quartzite	Joint
1358	-116.765	49.70343	1055.746	188.6768	77.2381	quartzite	Bedding
1359	-116.765	49.70336	1050.055	188.4393	85	quartzite	Bedding
1360	-116.765	49.70337	1047.011	114.7805	73	quartzite	Joint
1361	-116.765	49.70337	1046.953	328.7621	38.4	quartzite	Joint
1362	-116.765	49.7036	1045.115	101.4948	75	quartzite	Joint
1363	-116.765	49.70365	1060.994	208.0747	72.16667	quartzite	Bedding
1364	-116.765	49.70343	1057.808	97.58845	89	quartzite	Joint
1365	-116.764	49.70364	1066.645	84.84527	69	quartzite	Joint
1366	-116.765	49.70358	1050.703	192.5013	73	quartzite	Bedding
1367	-116.764	49.70355	1057.599	184.9012	68	quartzite	Bedding
1368	-116.764	49.70364	1058.252	272.0517	61	quartzite	Joint
1369	-116.764	49.70352	1048.532	108.6565	73	quartzite	Joint
1370	-116.764	49.70364	1061.502	112.5679	75	quartzite	Joint
1371	-116.764	49.70364	1057.726	183.4957	75.625	quartzite	Bedding
1372	-116.764	49.70364	1054.241	186.8481	70	quartzite	Bedding
1373	-116.764	49.70372	1073.271	186.4325	71	quartzite	Bedding
1374	-116.764	49.70371	1065.9	116.3162	74	quartzite	Joint
1375	-116.764	49.70325	1003.258	113.9772	71.53846	quartzite	Joint
1376	-116.764	49.70421	1071.082	107.9659	77	quartzite	Joint
1377	-116.764	49.70409	1060.068	185.2127	78.36364	quartzite	Bedding
1378	-116.763	49.70424	1067.388	275.868	60	quartzite	Joint
1379	-116.764	49.70383	1069.921	11.64828	81	20 cm rubble zone	Fault
1380	-116.761	49.70507	1114.309	207.2596	68	quartzite	Bedding
1381	-116.761	49.70502	1106.932	113.3109	78.4	quartzite	Joint

1382	-116.761	49.70512	1116.384	110.0247	59	quartzite	Joint
1383	-116.761	49.7051	1106.85	193.4886	78	quartzite	Bedding
1384	-116.761	49.70516	1116.497	109.0956	63	quartzite	Joint
1385	-116.76	49.70507	1103.892	103.1008	63	quartzite	Joint
1386	-116.76	49.70509	1108.676	187.2581	67	quartzite	Bedding
1387	-116.76	49.70517	1111.645	176.0192	72	quartzite	Bedding
1388	-116.76	49.70517	1109.145	281.1483	88	quartzite	Joint
1389	-116.759	49.70562	1121.662	118.1401	68	quartzite	Joint
1390	-116.759	49.7052	1122.513	193.3344	65	quartzite	Bedding
1391	-116.759	49.70559	1122.209	189.9077	68	quartzite	Bedding
1392	-116.759	49.70545	1119.769	101.978	62.8	quartzite	Joint
1393	-116.757	49.70465	1145.403	177.7234	59	quartzite	Bedding
1394	-116.757	49.70459	1147.553	99.6753	86	quartzite	Joint
1395	-116.757	49.70431	1170.713	173.6696	67	quartzite	Bedding
1396	-116.754	49.70357	1179.022	197.3419	40	quartzite	Bedding
1397	-116.754	49.70358	1169.637	5.108343	36	quartzite	Joint
1398	-116.754	49.70355	1172.553	89.73113	57.04348	quartzite	Joint
1399	-116.754	49.70343	1181.765	102.5712	60	quartzite	Joint
1400	-116.754	49.70346	1181.611	195.5663	65	quartzite	Bedding
1401	-116.753	49.70334	1182.553	7.039259	63.47059	quartzite	Joint
1402	-116.753	49.70336	1191.976	178.6301	61	quartzite	Bedding
1403	-116.754	49.70287	1226.317	298.3427	81	quartzite	Joint
1404	-116.752	49.70287	1196.503	171.5199	59	quartzite	Bedding
1405	-116.752	49.70277	1208.479	186.9286	54	gritstone	Bedding
1406	-116.751	49.70285	1200.889	125.1528	87	gritstone	Joint
1407	-116.751	49.70276	1187.749	171.7755	46.47619	gritstone	Bedding
1408	-116.751	49.7026	1245.532	173.2978	54	gritstone	Bedding
1409	-116.751	49.70274	1188.669	177.7788	68	gritstone	Bedding
1410	-116.748	49.70252	1198.255	193.0906	69	phyllite	Bedding
1411	-116.748	49.70237	1194.965	193.3047	66	phyllite	Bedding
1412	-116.748	49.70242	1192.622	304.1075	82	phyllite	Fault
1413	-116.747	49.70237	1205.476	123.5768	80	phyllite	Joint
1414	-116.747	49.70225	0	195.7359	67.96	phyllite	Bedding
1415	-116.747	49.7023	1200.624	187.9365	67.35	phyllite	Bedding
1416	-116.747	49.70226	1183.609	66.57501	61	phyllite	Joint
1417	-116.745	49.70202	1191.979	192.3752	76	phyllite	Bedding
1418	-116.745	49.70205	1190.62	110.5181	79.25	phyllite	Joint
1419	-116.742	49.70211	0	175.2603	53.58974	phyllite	Bedding
1420	-116.764	49.70251	1199.357	193.993	72	quartzite	Bedding
1421	-116.757	49.75055	0	16.96278	74	schist	Bedding
1422	-116.757	49.75063	2147.765	22.14117	60	schist	Bedding

1423	-116.756	49.75047	2130.78	20.9331	88	schist	Bedding
1424	-116.754	49.74966	2144.092	30.40566	58	schist	Bedding
1425	-116.75	49.74914	2161.507	24.41128	51	schist	Bedding
1426	-116.75	49.74912	2162.687	144.9864	41	schist	Joint
1427	-116.75	49.74912	2161.319	159.2379	40.84615	schist	Joint
1428	-116.75	49.74899	2156.914	14.33989	86.56	schist	Bedding
1429	-116.749	49.74889	2150.966	144.7722	36	schist	Joint
1430	-116.749	49.74911	0	177.4378	76	15 m zone possible continuation of orebin creek	Fault
1431	-116.749	49.74881	0	16.27201	83	quartzite	Bedding
1432	-116.749	49.74884	2164.937	302.0112	88	quartzite	Joint
1433	-116.749	49.74888	2161.599	284.9809	68.93333	quartzite	Joint
1434	-116.749	49.74892	2163.538	126.4553	25	quartzite	Joint
1435	-116.749	49.74892	2164.053	279.4235	73	quartzite	Joint
1436	-116.748	49.7487	2167.023	39.95038	74	schist	Bedding
1437	-116.747	49.74873	2172.234	176.1568	89	quartzite	Bedding
1438	-116.747	49.74864	0	183.1391	83	quartzite	Bedding
1439	-116.747	49.74859	2171.994	100.0637	74	quartzite	Joint
1440	-116.747	49.74863	2175.43	115.7428	71	quartzite	Joint
1441	-116.746	49.74824	0	16.6632	69	schist	Bedding
1442	-116.746	49.74805	2139.572	125.9923	50.10526	schist	Joint
1443	-116.746	49.74788	2149.482	10.83052	64	schist	Bedding
1444	-116.745	49.74651	0	24.33315	76	schist	Bedding
1445	-116.745	49.74645	2091.817	127.7917	73.05263	schist	Joint
1446	-116.745	49.74646	2093.519	111.2163	59	schist	Joint
1447	-116.744	49.74414	2095.635	17.91178	75.57143	schist	Bedding
1448	-116.741	49.73972	0	206.8823	65.03571	quartzite	Bedding
1449	-116.741	49.73958	2168.483	73.94151	38	quartzite	Joint
1450	-116.741	49.73957	0	97.02065	83	quartzite	Joint
1451	-116.741	49.73957	0	212.6739	63	quartzite	Bedding
1452	-116.741	49.73953	0	202.804	63	quartzite	Bedding
1453	-116.741	49.73953	2173.764	336.6512	29	quartzite	Joint
1454	-116.741	49.73951	2175.065	67.51556	29.56667	quartzite	Joint
1455	-116.741	49.7394	2183.584	195.8514	56.95652	quartzite	Bedding
1456	-116.741	49.73556	0	207.5326	46.92857	quartzite	Bedding
1457	-116.741	49.73504	2104.177	192.1938	59.16667	quartzite	Bedding
1458	-116.74	49.73301	0	192.9183	54	phyllite	Bedding
1459	-116.74	49.73305	0	200.6442	76	phyllite	Bedding
1460	-116.739	49.73147	0	199.1427	66.78571	quartzite	Bedding
1461	-116.736	49.73015	0	203.058	61	gritstone	Bedding
1462	-116.733	49.72921	0	194.283	75	gritstone	Bedding
1463	-116.809	49.6644	574.8867	198.9465	68	marble	Bedding

1464	-116.808	49.66451	583.3167	191.3884	81	marble	Bedding
1465	-116.808	49.66447	584.1212	205.3705	82.73684	marble	Bedding
1466	-116.808	49.66447	584.9588	204.1384	79	marble	Bedding
1467	-116.808	49.66443	584.7013	51.79619	25	marble	Joint
1468	-116.808	49.66444	583.4275	113.1578	88	marble	Joint
1469	-116.808	49.66446	583.6351	33.39865	34	marble	Joint
1470	-116.808	49.66468	587.8822	23.54685	29	marble	Joint
1471	-116.808	49.66456	586.4012	53.49296	41	marble	Joint
1472	-116.809	49.6649	585.0067	45.51537	24	marble	Joint
1473	-116.805	49.66217	562.3269	218.5595	78	marble	Bedding
1474	-116.805	49.66142	557.0161	213.6101	67.46154	marble	Bedding
1475	-116.805	49.66024	0	211.9447	87.54902	marble	Bedding
1476	-116.803	49.65495	0	177.3213	87.35714	marble	Bedding
1477	-116.802	49.65319	563.9803	1.424235	66	marble	Bedding
1478	-116.802	49.65299	562.6637	26.89218	77	marble	Bedding
1479	-116.802	49.65301	0	182.5039	87.11429	marble	Bedding
1480	-116.801	49.65167	574.623	203.0913	78.09524	marble	Bedding
1481	-116.8	49.65125	579.2611	201.072	89	marble	Bedding
1482	-116.8	49.65084	583.4424	200.9883	89	marble	Bedding
1483	-116.8	49.6507	574.6529	204.0884	81.25806	marble	Bedding
1484	-116.799	49.65039	588.5765	196.4527	79.34783	marble	Bedding
1485	-116.799	49.65051	594.9193	189.5179	69	marble	Bedding
1486	-116.8	49.65185	627.1129	187.591	68	gneiss	Bedding
1487	-116.799	49.65193	611.2393	179.7312	72	gneiss	Bedding
1488	-116.799	49.6519	611.6999	180.3766	68	gneiss	Bedding
1489	-116.799	49.6521	627.4799	184.0554	83	marble	Bedding
1490	-116.799	49.65219	615.7374	179.096	86	marble	Bedding
1491	-116.799	49.65245	623.1563	204.8329	71	marble	Bedding
1492	-116.799	49.65272	636.0499	195.6218	69	marble	Bedding
1493	-116.799	49.65325	632.7197	194.1468	76	marble	Bedding
1494	-116.799	49.65337	635.1998	199.7423	77	marble	Bedding
1495	-116.799	49.65394	651.1978	185.0962	74	marble	Bedding
1496	-116.799	49.65384	642.8306	192.4339	86	10 m very rusty brittle chloritized zone	Fault
1497	-116.8	49.65395	646.3437	178.4501	88	marble	Bedding
1498	-116.8	49.65725	671.1381	194.3748	78	50 m very rusty brittle chloritized zone	Fault
1499	-116.8	49.65768	673.8448	201.3465	72.42105	50 m super fault	Fault
1500	-116.8	49.6584	681.9801	200.9584	76	50 m super fault	Fault
1501	-116.8	49.65948	674.4908	208.8938	82	marble	Bedding
1502	-116.8	49.65986	680.8839	196.6655	88	10 m rusty brittle very chloritized zone	Fault
1503	-116.801	49.66028	684.4953	221.9992	63.125	marble	Bedding
1504	-116.801	49.66164	700.1944	226.5579	83	marble	Bedding

1505	-116.803	49.66389	671.8371	214.5966	77	marble	Bedding
1506	-116.803	49.66282	662.3562	215.6112	60	marble	Bedding
1507	-116.803	49.66273	643.8265	178.5743	75.05556	marble	Bedding
1508	-116.804	49.66271	641.5746	219.9401	74	marble	Bedding
1509	-116.804	49.66339	648.3715	219.5741	78	marble	Bedding
1510	-116.801	49.66302	0	201.6937	63	marble	Bedding
1511	-116.8	49.66287	722.3839	226.1706	85	marble	Bedding
1512	-116.799	49.6632	762.9963	222.8965	80	gneiss	Bedding
1513	-116.794	49.65756	809.7515	190.3112	70	marble	Bedding
1514	-116.794	49.65748	809.8624	176.1584	76	marble	Bedding
1515	-116.794	49.65741	804.5411	193.3744	59	marble	Bedding
1516	-116.794	49.65915	824.6829	185.1107	67.96296	marble	Bedding
1517	-116.794	49.66009	843.421	195.2087	70.04	marble	Bedding
1518	-116.794	49.66027	855.918	194.907	55	marble	Bedding
1519	-116.795	49.66143	855.7506	191.4507	83	marble	Bedding
1520	-116.795	49.66246	873.439	162.0649	80	schist	Bedding
1521	-116.796	49.66338	890.5101	211.4655	78	marble	Bedding
1522	-116.796	49.66329	887.4632	218.1347	89	marble	Bedding
1523	-116.796	49.66318	0	175.7386	75.13333	10 m rusty brittle very chloritized zone	Fault
1524	-116.796	49.66397	923.5056	217.6894	70	marble	Bedding
1525	-116.796	49.664	898.5027	194.3539	77	marble	Bedding
1526	-116.796	49.66441	909.0176	207.9279	67	marble	Bedding
1527	-116.795	49.66643	932.9163	183.4679	81	marble	Bedding
1528	-116.795	49.66545	958.273	211.1711	81.5	marble	Bedding
1529	-116.795	49.66544	954.2513	256.2922	78	marble	Joint
1530	-116.793	49.66439	1003.567	200.1578	80.16667	marble	Bedding
1531	-116.789	49.66215	1105.294	209.2272	61	marble	Bedding
1532	-116.788	49.66177	1096.984	185.2826	83	marble	Bedding
1533	-116.788	49.66193	0	189.158	75	3 m rusty chloritized rubble zone	Fault
1534	-116.787	49.66209	1114.734	197.889	82	schist	Bedding
1535	-116.787	49.66142	1121.025	178.1248	81	schist	Bedding
1536	-116.789	49.6619	1082.587	185.2336	84	schist	Bedding
1537	-116.789	49.66161	1080.459	204.1506	71	schist	Bedding
1538	-116.789	49.66144	1069.383	195.6596	71.92857	schist	Bedding
1539	-116.788	49.66135	1095.784	211.941	86	schist	Bedding
1540	-116.787	49.66046	1090.435	198.9459	72	schist	Bedding
1541	-116.787	49.66056	0	185.8517	89	50 cm rusty rubbly zone with water coming out	Fault
1542	-116.787	49.66057	0	198.7127	88	30 cm rusty rubbly zone	Fault
1543	-116.794	49.66376	954.6671	186.6978	59	marble	Bedding
1544	-116.794	49.66345	958.1005	200.2196	74.03922	gneiss	Bedding
1545	-116.793	49.66333	0	192.0039	77	marble	Bedding

1546	-116.793	49.66274	0	195.748	64.86792	marble	Bedding
1547	-116.791	49.66079	960.6468	190.7483	82.53846	marble	Bedding
1548	-116.794	49.66416	961.4991	172.7226	43.57895	5 m rusted and chloritized zone	Fault
1549	-116.794	49.65663	802.4909	300.7755	77	granite	Joint
1550	-116.794	49.65676	801.1451	307.6365	80	granite	Joint
1551	-116.794	49.65687	800.8133	304.476	70	granite	Joint
1552	-116.794	49.65692	802.9632	172.0512	62	granite	Joint
1553	-116.794	49.65691	801.763	196.2145	55	granite	Joint
1554	-116.794	49.65677	805.003	354.1477	71	granite	Joint
1555	-116.794	49.65677	0	13.99445	71.54545	granite	Joint
1556	-116.793	49.65659	0	179.8259	87	schist	Bedding
1557	-116.793	49.65646	813.7889	177.762	80.77419	schist	Bedding
1558	-116.792	49.65559	0	176.4277	83.02941	schist	Bedding
1559	-116.789	49.65195	0	220.7832	55.21053	granite	Joint
1560	-116.789	49.65194	0	223.4764	50.77778	granite	Joint
1561	-116.788	49.63915	0	261.0888	52	granite	Joint
1562	-116.788	49.6391	0	270.2882	51	granite	Joint
1563	-116.791	49.64314	0	30.55631	85	granite	Joint
1564	-116.791	49.64311	0	326.4511	82	granite	Joint
1565	-116.791	49.64311	0	36.13416	88	granite	Joint
1566	-116.791	49.64309	0	254.4674	87	granite	Joint
1567	-116.786	49.6218	0	1.150299	33.13333	granite	Joint
1568	-116.786	49.62185	0	1.347535	36	granite	Joint
1569	-116.786	49.62185	590.9739	1.180393	42	granite	Joint
1570	-116.786	49.62187	0	354.2336	43	granite	Joint
1571	-116.784	49.62215	593.8945	197.9732	82	granite	Joint
1572	-116.784	49.62246	602.3621	199.1016	79	granite	Joint
1573	-116.784	49.62249	0	194.2521	82	granite	Joint
1574	-116.784	49.62247	0	215.8898	86	granite	Joint
1575	-116.769	49.60023	877.0494	190.2868	67	phyllite	Bedding
1576	-116.77	49.60017	968.2415	201.5	73	phyllite	Bedding
1577	-116.77	49.60018	967.5104	202.0682	67	phyllite	Bedding
1578	-116.77	49.60017	971.7719	295.4155	65	phyllite	Joint
1579	-116.77	49.60027	969.1995	259.2399	63	phyllite	Joint
1580	-116.769	49.60067	1011.363	196.3202	81	phyllite	Bedding
1581	-116.769	49.60067	1010.991	193.6207	83	phyllite	Bedding
1582	-116.769	49.60063	1012.23	196.0541	78	phyllite	Bedding
1583	-116.769	49.60063	1012.25	303.0917	51	phyllite	Joint
1584	-116.767	49.6059	1053.191	339.9218	31	gritstone	Bedding
1585	-116.765	49.60664	1071.233	15.14178	68	gritstone	Bedding
1586	-116.767	49.60646	1059.889	16.5184	72.3125	gritstone	Bedding

1587	-116.766	49.60644	0	21.28261	54	gritstone	Bedding
1588	-116.766	49.60645	0	358.1714	52	gritstone	Bedding
1589	-116.767	49.60657	1064.121	28.09214	73	gritstone	Bedding
1590	-116.765	49.60485	1110.403	21.67699	80	phyllite	Bedding
1591	-116.765	49.60481	1107.023	25.17289	78	phyllite	Bedding
1592	-116.765	49.60485	1106.022	35.8265	71	phyllite	Bedding
1593	-116.765	49.60486	1109.782	30.0143	79	phyllite	Bedding
1594	-116.763	49.60567	1133.541	12.03949	46	phyllite	Bedding
1595	-116.762	49.60609	0	20.79698	49	phyllite	Bedding
1596	-116.762	49.60624	0	0.925849	47	phyllite	Bedding
1597	-116.762	49.60624	0	6.790666	46	30 cm gouge zone with extensive rusting in surrounding area	Fault
1598	-116.761	49.6067	1159.153	184.7074	88	phyllite	Bedding
1599	-116.76	49.60699	1169.476	14.21822	65	phyllite	Bedding
1600	-116.76	49.60698	1163.908	206.5314	56	phyllite	Joint
1601	-116.761	49.60407	1235.959	9.016402	59	phyllite	Bedding
1602	-116.762	49.60165	1278.006	1.251016	52	phyllite	Bedding
1603	-116.761	49.60114	1325.647	351.4431	55	phyllite	Bedding
1604	-116.758	49.60376	0	11.16145	73.57143	phyllite	Bedding
1605	-116.758	49.6038	0	20.18629	65.68182	phyllite	Bedding
1606	-116.76	49.6078	1136.584	23.95019	75	phyllite	Bedding
1607	-116.76	49.60797	0	1.564459	23	30 cm gouge zone cross cutting foliation	Fault
1608	-116.761	49.60956	0	7.413429	61.17391	phyllite	Bedding
1609	-116.76	49.60963	1125.449	167.2589	60	phyllite	Joint
1610	-116.76	49.60964	0	165.451	53.125	phyllite	Joint
1611	-116.761	49.60955	0	7.213103	53	phyllite	Bedding
1612	-116.761	49.60978	1108.044	1.328043	81	phyllite	Bedding
1613	-116.762	49.6141	0	12.68777	23.26316	gritstone	Bedding
1614	-116.762	49.61419	0	27.61194	24	gritstone	Bedding
1615	-116.762	49.61456	0	22.26283	14.85714	gritstone	Bedding
1616	-116.761	49.61568	0	27.32009	25	gritstone	Bedding
1617	-116.761	49.61589	1166.072	33.23779	27.9	gritstone	Bedding
1618	-116.76	49.61645	0	28.86944	42.21053	phyllite	Bedding
1619	-116.757	49.6178	1183.498	352.5049	27	phyllite	Bedding
1620	-116.757	49.61789	1176.849	344.8939	25	phyllite	Bedding
1621	-116.757	49.61793	1179.415	348.82	24	phyllite	Bedding
1622	-116.757	49.61813	1187.051	18.47103	23	phyllite	Bedding
1623	-116.753	49.61883	0	17.88961	36.975	phyllite	Bedding
1624	-116.753	49.61882	1195.706	116.5443	76.3125	phyllite	Joint
1625	-116.751	49.61916	1203.054	226.7316	56.16667	gritstone	Bedding
1626	-116.751	49.61913	1201.469	223.7766	59	gritstone	Bedding
1627	-116.751	49.61912	1201.487	239.6166	64	gritstone	Bedding

1628	-116.751	49.61914	1200.766	97.38218	69.46154	gritstone	Joint
1629	-116.749	49.61907	1199.182	164.7424	60	phyllite	Bedding
1630	-116.749	49.61886	1181.539	180.6289	75.91667	phyllite	Bedding
1631	-116.749	49.61889	1194.101	178.5121	71	phyllite	Bedding
1632	-116.751	49.61903	1177.061	11.9001	88	phyllite	Bedding
1633	-116.746	49.61878	1212.773	193.8064	76	phyllite	Bedding
1634	-116.743	49.61752	1206.016	180.9916	79	gritstone	Bedding
1635	-116.77	49.62273	0	154.1689	51	phyllite	Bedding
1636	-116.735	49.6261	0	2.670927	58	phyllite	Bedding
1637	-116.735	49.62597	0	347.7772	52.25	phyllite	Bedding
1638	-116.734	49.62572	0	6.479476	80	phyllite	Bedding
1639	-116.734	49.62583	1019.421	99.16552	63.4375	phyllite	Joint
1640	-116.734	49.62578	1013.893	102.714	66	phyllite	Joint
1641	-116.732	49.62552	1022.292	176.1074	86	phyllite	Bedding
1642	-116.729	49.62527	1055.742	95.29285	64	phyllite	Joint
1643	-116.729	49.62527	1057.584	88.7722	59	phyllite	Joint
1644	-116.729	49.62529	1058.858	89.88113	60	phyllite	Joint
1645	-116.729	49.62528	1057.008	88.83028	64	phyllite	Joint
1646	-116.729	49.62527	1055.593	359.4634	79	phyllite	Bedding
1647	-116.777	49.5403	1061.572	178.9889	89	phyllite	Bedding
1648	-116.734	49.62763	0	357.1905	60	phyllite	Bedding
1649	-116.734	49.62749	1126.505	120.3954	75	phyllite	Joint
1650	-116.734	49.62772	0	1.752373	38	phyllite	Bedding
1651	-116.735	49.62828	1127.456	93.31881	61.61538	phyllite	Joint
1652	-116.735	49.6281	0	82.76864	70	phyllite	Joint
1653	-116.735	49.6281	1150.184	79.29549	64.24138	phyllite	Joint
1654	-116.735	49.6281	0	157.4363	82	phyllite	Bedding
1655	-116.735	49.62806	0	167.3563	75	phyllite	Bedding
1656	-116.732	49.62765	1181.54	92.69321	65.125	phyllite	Joint
1657	-116.732	49.62767	0	351.6278	84	phyllite	Bedding
1658	-116.732	49.62763	1182.279	95.67915	59	phyllite	Joint
1659	-116.731	49.6276	1182.104	94.07494	70	phyllite	Joint
1660	-116.731	49.62757	1182.883	352.2701	73	phyllite	Bedding
1661	-116.801	49.78228	0	182.135	71	gneiss	Bedding
1662	-116.801	49.78205	0	270.6669	76	gneiss	Joint
1663	-116.8	49.78148	0	159.0687	22	marble	Bedding
1664	-116.8	49.78153	1610.863	349.3799	85	schist	Bedding
1665	-116.799	49.78155	1629.755	73.02726	87	schist	Joint
1666	-116.798	49.78156	1629.308	265.2719	87	schist	Joint
1667	-116.798	49.78173	1623.772	273.5631	85	schist	Joint
1668	-116.798	49.7817	1615.264	178.0939	88	schist	Bedding

1669	-116.798	49.78184	0	170.1456	84	schist	Bedding
1670	-116.797	49.78174	0	160.403	51	gneiss	Bedding
1671	-116.793	49.78103	0	171.6315	49.05556	gneiss	Bedding
1672	-116.792	49.77987	0	183.2185	35.30769	marble	Bedding
1673	-116.792	49.77986	1606.155	6.142717	59.92308	marble	Joint
1674	-116.792	49.7799	1601.879	286.7202	89	marble	Joint
1675	-116.792	49.77956	0	193.5282	28	marble	Bedding
1676	-116.792	49.77944	1618.089	6.068135	46	marble	Joint
1677	-116.792	49.77951	1605.741	295.2939	71	marble	Joint
1678	-116.792	49.77918	0	174.148	46	schist	Bedding
1679	-116.794	49.78127	0	189.1843	55	gneiss	Bedding
1680	-116.796	49.78108	1638.146	169.0349	72.09091	schist	Bedding
1681	-116.799	49.78178	1639.412	182.6454	84.09524	major regional fault displacing units	Fault
1682	-116.8	49.78158	1620.321	156.5955	33	marble	Bedding
1683	-116.8	49.78184	1646.998	172.5376	38	marble	Bedding
1684	-116.801	49.78192	0	166.6682	46.73913	gneiss	Bedding
1685	-116.801	49.78199	1646.597	270.56	79	gneiss	Joint
1686	-116.801	49.78195	1643.316	265.2615	82	gneiss	Joint
1687	-116.801	49.78193	1636.371	91.33173	88.88889	gneiss	Joint
1688	-116.834	49.78842	721.1727	153.0787	19	gneiss	Bedding
1689	-116.834	49.78847	723.7426	172.0625	39	gneiss	Bedding
1690	-116.858	49.75431	0	159.3907	24	marble	Bedding
1691	-116.861	49.75495	550.1532	233.1737	48	marble	Joint
1692	-116.861	49.75863	0	173.963	26	quartzite	Bedding
1693	-116.861	49.75855	0	193.1636	23.3	quartzite	Bedding
1694	-116.861	49.757	604.5078	291.9691	71	quartzite	Joint
1695	-116.861	49.75615	612.2933	76.91467	75.47297	quartzite	Joint
1696	-116.862	49.75581	612.67	189.6872	39.54839	quartzite	Bedding
1697	-116.862	49.75574	615.0179	175.8625	35	quartzite	Bedding
1698	-116.862	49.75578	607.7086	305.5974	88.125	quartzite	Joint
1699	-116.862	49.75578	610.2472	296.27	75	quartzite	Joint
1700	-116.861	49.7583	610.6639	174.4332	30	quartzite	Bedding
1701	-116.861	49.7583	611.0916	84.47448	65	quartzite	Joint
1702	-116.861	49.75827	612.3471	145.7238	89	quartzite	Joint
1703	-116.861	49.75854	0	193.9836	21.7037	marble	Bedding
1704	-116.861	49.75854	605.0445	314.9313	62.10714	marble	Joint
1705	-116.861	49.75861	604.6646	64.31637	75	marble	Joint
1706	-116.859	49.75764	0	176.786	40.10345	marble	Bedding
1707	-116.859	49.75761	552.6324	85.30375	77	marble	Joint
1708	-116.859	49.7576	553.3319	101.1669	81	marble	Joint
1709	-116.859	49.75766	553.9181	95.03241	77.05263	marble	Joint

1710	-116.862	49.75968	0	172.0118	59.05405	quartzite	Bedding
1711	-116.862	49.75984	563.1558	304.4915	87	quartzite	Joint
1712	-116.864	49.75905	566.8031	177.2778	45	quartzite	Bedding
1713	-116.864	49.759	0	83.39442	74	quartzite	Joint
1714	-116.86	49.76407	0	90.3529	75	quartzite	Joint
1715	-116.86	49.76404	566.1663	283.187	86	quartzite	Joint
1716	-116.86	49.76406	564.9351	290.8353	75	quartzite	Joint
1717	-116.861	49.7641	0	191.1862	17	quartzite	Bedding
1718	-116.857	49.7636	561.637	311.2331	75	quartzite	Joint
1719	-116.86	49.76365	559.5907	292.7971	89	quartzite	Joint
1720	-116.86	49.76328	562.5977	189.6553	32	quartzite	Bedding
1721	-116.86	49.76323	563.6649	304.3174	83.17143	quartzite	Joint
1722	-116.86	49.76324	557.3918	279.8034	85	quartzite	Joint
1723	-116.86	49.76323	557.5167	263.1147	86.57692	quartzite	Joint
1724	-116.862	49.76932	538.4248	173.842	75	quartzite	Bedding
1725	-116.863	49.76886	539.357	180.1786	47	quartzite	Bedding
1726	-116.863	49.76888	541.9278	49.94262	58	quartzite	Joint
1727	-116.863	49.76888	541.1872	344.2359	41	quartzite	Joint
1728	-116.787	49.71338	656.9998	201.7501	50	marble	Bedding
1729	-116.787	49.71338	804.011	203.4064	47	marble	Bedding
1730	-116.788	49.71385	802.5615	204.8097	42.0625	marble	Bedding
1731	-116.788	49.71385	816.6673	118.7417	72	marble	Joint
1732	-116.788	49.71385	809.9589	197.3054	38	marble	Bedding
1733	-116.788	49.715	856.511	183.6624	39.78261	quartzite	Bedding
1734	-116.788	49.71458	837.5374	188.5118	43	quartzite	Bedding
1735	-116.787	49.7147	839.1302	340.567	67	quartzite	Joint
1736	-116.787	49.7147	838.8247	341.8834	69	quartzite	Joint
1737	-116.787	49.7147	837.6035	99.19759	79.59524	quartzite	Joint
1738	-116.787	49.7147	834.7152	74.01773	54	quartzite	Joint
1739	-116.787	49.7147	835.6867	102.8835	76	quartzite	Joint
1740	-116.787	49.7147	834.7954	108.406	81	quartzite	Joint
1741	-116.788	49.71445	839.699	186.7761	45	quartzite	Bedding
1742	-116.788	49.71445	833.4123	11.66492	63	quartzite	Joint
1743	-116.788	49.71445	833.1972	114.9822	84.10526	quartzite	Joint
1744	-116.788	49.7146	838.1947	354.1208	50	quartzite	Joint
1745	-116.788	49.7146	838.6903	111.3431	86.125	quartzite	Joint
1746	-116.785	49.7118	0	209.6549	59.44118	schist	Bedding
1747	-116.785	49.71172	771.781	320.4567	40	schist	Joint
1748	-116.775	49.71241	818.2783	213.75	67	schist	Bedding
1749	-116.775	49.71241	821.4189	136.5515	69.83784	schist	Joint
1750	-116.766	49.71322	0	188.038	75.23077	schist	Bedding

1751	-116.767	49.71322	0	168.7757	51.82759	schist	Bedding
1752	-116.784	49.70625	0	214.1887	67.70588	schist	Bedding
1753	-116.785	49.70705	0	222.7077	59	schist	Bedding
1754	-116.804	49.69633	632.4701	179.9537	61	marble	Bedding
1755	-116.804	49.69646	0	24.65386	48	marble	Joint
1756	-116.804	49.69646	636.5381	165.957	47	marble	Bedding
1757	-116.848	49.63856	0	236.6382	23	rusty fracture	Fault
1758	-116.802	49.68518	708.6125	197.6453	41	marble	Bedding
1759	-116.802	49.68518	707.6829	199.4592	46	marble	Bedding

Appendix D: Water Chemistry Measurements

ID	Name	Type	Easting	Northing	Temperature (°C)	pH	Conductivity (µS/cm)	TDS (ppm)	Salinity (ppt)
1	preacher creek	2	515335	5506584	10.8	8.29	121	85.9	0
2	preacher spring	1	515332	5506811	8.1	8.43	205	146	0
3	white quartzite spring	1	515496	5506744	13.2	8.32	279	201	0.1
4	riondel road 1	2	510414	5507241	12.6	8.29	95.8	67.9	0
5	riondel road 2	2	510557	5507726	12	8.27	117.6	85.9	0
6	riondel road 3	2	510571	5508551	10.9	8.42	158.3	112	0
7	riondel road 4	2	510543	5508622	13.3	8.27	151.5	110	0
8	riondel road 5	2	510538	5510379	12.6	8.23	235	167	0.1
9	riondel road 6	2	510552	5510765	11.5	7.8	205	146	0.1
10	riondel	2	510381	5512625	11.5	8.25	167.2	119	0
11	riondel north 1	1	510358	5512987	14.4	7.61	318	222	0.1
12	riondel north 2	1	510456	5513149	12.7	7.76	348	248	0.1
13	riondel north 3	2	510715	5513534	9.8	8.44	208	148	0.1
14	riondel north 4	1	510828	5513733	13.8	8.3	374	268	0.1
15	riondel north 5	1	510948	5514583	21.6	8.17	384	279	0.2
16	riondel north 6	1	510920	5514875	15.3	8.51	264	193	0.1
17	tam o shanter creek	2	510928	5515558	11.6	8.25	103.6	73.5	0
18	pilot peninsula trailhead	2	508919	5499451	13.9	7.25	243	171	0.1
19	pilot road 1	1	508985	5499721	13.8	7.25	133.4	94.9	0
20	pilot road 2	1	509021	5500727	13.8	8.28	261	185	0.1
21	pilot road 3	1	509080	5500790	10.7	7.46	123.5	88.7	0
22	pilot road 4	2	509196	5501188	12.4	7.94	123	87.3	0
23	pilot road 5	2	509276	5502127	11.5	7.82	80.5	57.3	0
24	boccalinos	2	509365	5502981	15	7.59	131.3	92.9	0
25	grey creek red spring	1	519356	5497270	16.1	7.59	152.5	108	0
26	grey creek	2	515273	5496740	11.7	7.92	88.4	63	0
27	grey creek store	2	515384	5497190	11.6	7.06	160.2	114	0
28	east shore creek 1	2	515302	5497506	11.6	7.32	56.4	40.5	0
29	east shore creek 2	2	515344	5497988	15.2	7.54	46.5	33.1	0
30	east shore creek 3	2	515215	5498503	10.1	7.57	84.4	59.9	0
31	east shore creek 4	2	515074	5498662	12.1	7.5	25.6	18.3	0
32	east shore granite	2	514952	5498880	14.6	7.66	117.3	83.7	0
33	east shore creek 5	2	514806	5499015	10.8	7.72	50.2	35.7	0
34	granite boundary creek	2	514462	5499735	13.8	8.2	283	201	0.1
35	east shore marble seep 1	1	514446	5499758	24.8	8.03	480	340	0.2
36	east shore marble seep 2	1	514355	5499922	19.7	7.55	515	364	0.2

37	east shore dirty seep	1	514150	5500565	13.9	7.19	470	330	0.2
38	crawford creek road 1 creek	2	513577	5501984	11.5	8.2	168.6	118	0
39	crawford creek road 2	1	513740	5502368	17.7	8.16	192.3	136	0.1
40	crawford creek road 3	1	513749	5502453	12.8	8.01	169.1	120	0
41	crawford creek road 4	1	513919	5503520	17.7	8.36	440	312	0.1
42	crawford creek road 5	1	514081	5503982	22.5	8.07	509	360	0.2
43	crawford creek road 6	1	514178	5504667	14.3	8.09	226	160	0.1
44	secret selkirk road spring	1	514178	5503515	7.7	7.24	605	428	0.3
45	picnic table beach creek	2	512598	5495209	9.7	7.85	294	209	0.1
46	red spring	1	512201	5495458	9.5	7.14	626	442	0.3
47	mega fault	1	511437	5496208	16.2	7.4	517	370	0.2
48	sawmill bay creek	2	509877	5498604	14.6	8.25	385	273	0.2
49	sawmill bay creek 2	2	509783	5498698	13.2	8.12	318	227	0.1
50	sawmill bay creek spur	2	509786	5498712	13.8	7.93	271	192	0.1
51	muddy seep	1	509389	5498918	13.9	7.31	299	209	0.1
52	crawford creek bridge	2	523823	5509460	9.5	7.71	92.6	65.8	0
53	crawford 1 creek	2	523735	5509381	9.7	7.81	67.6	48.4	0
54	crawford 2 seep	1	523538	5509170	8.9	7.67	242	172	0.1
55	crawford 3 creek	2	523213	5508751	11	7.62	118.2	83.8	0
56	crawford 4 creek	2	523009	5508655	12.1	7.76	97.4	69.2	0
57	crawford 5 seep	1	522822	5508494	7.1	7.36	59.6	42.2	0
58	crawford 6 seep	1	522618	5508302	9.1	7.66	104.8	74.1	0
59	crawford 7 seep	1	522521	5508236	8.5	7.68	118.8	87.6	0
60	crawford 8 creek	2	522471	5508214	7.7	7.71	171.1	121	0
61	crawford 9 creek	2	522380	5508125	7.6	7.92	129.3	91.8	0
62	crawford 10 creek	2	522269	5508042	9.6	7.85	102.3	72.6	0
63	crawford 11 seep	1	521841	5507610	8.2	7.27	33	23.4	0
64	spring creek	2	521554	5507429	12.5	7.55	60.9	43.2	0
65	crawford 12 creek	2	520652	5506775	11	7.77	114.1	81.2	0
66	crawford 13 seep	1	520440	5506592	13.6	7.84	128.9	91.7	0
67	crawford 14 creek	2	519956	5506346	14.6	7.86	69.5	49.2	0
68	johnson creek	2	519296	5506358	13.2	7.81	89.1	63.4	0
69	crawford 15 creek	2	518480	5506568	13.4	7.9	106	74.7	0
70	crawford 16 creek	2	518312	5506601	10.9	7.78	81	57.3	0
71	orebin creek	2	517286	5506808	11.2	7.78	63.7	44.8	0
72	hot spring	1	517100	5506597	30.1	6.59	68.8	49.1	0
73	washout creek	2	516188	5506697	15.2	7.95	115.4	80	0
74	crawford 17 creek	2	515957	5506701	11.6	7.71	238	167	0.1

75	crawford 18 creek	2	515911	5506688	12.8	7.96	230	164	0.1
76	crawford 19 creek	2	514936	5506184	9.4	8.26	196.1	139	0
77	russ' driveway	2	514042	5505259	12.7	8.1	201	142	0.1
78	two dogs creek	2	513499	5504715	12.3	8.27	221	157	0.1
79	mcgregor lake	2	511378	5499802	21.6	7.99	171.1	122	0
80	crystal lake road 1 seep	1	511821	5500013	12.5	8.14	325	240	0.1
81	crystal lake road 2 seep	1	512205	5501398	13.9	7.81	210	149	0.1
82	road zone 1 creek	2	512236	5502684	14.4	7.98	174.1	123	0
83	fraser lake	2	510866	5503403	24.6	7.55	143.1	101	0
84	houghton creek	2	515525	5506054	12.9	7.93	66.7	47.3	0
85	quartzite 1 seep	1	517544	5506102	9.7	7.13	9.9	7	0
86	quartzite 2 seep	1	518246	5505794	11.7	7.3	43.3	30.9	0
87	quartzite 3 creek	2	518371	5505797	12.8	7.58	46.7	33.2	0
88	quartzite 4 seep	1	518693	5505797	13	7.85	87.6	62.2	0
89	preacher spring 2	1	515519	5507260	11	8.03	324	229	0.1
90	quartzite 4 creek	2	515526	5506938	11.5	8.29	273	195	0.1
91	krishna spring	1	510228	5506108	11.3	6.86	150.4	108	0
92	sonni well	1	509536	5503034	11.1	7.58	459	325	0.2
93	marble zone 1 seep	1	514380	5500984	13	7.89	515	365	0.2
94	marble zone 2 spring	1	514571	5501100	8.6	7.93	597	424	0.3
95	marble zone 3 seep	1	514814	5500669	12.6	7.94	486	345	0.2
96	marble zone 4 seep	1	514919	5500477	20.3	7.8	432	305	0.2
97	marble zone 5 seep	1	514968	5500346	9.1	8.02	281	201	0.1
98	marble zone 6 spring	1	515085	5500146	11.3	7.91	210	148	0.1
99	marble zone 7 seep	1	515156	5501296	16.3	7.55	201	141	0.1
100	big ditch spring	1	515304	5501001	18.5	7.11	88.7	63.1	0
101	marble zone 9 spring	1	515382	5500915	12.4	7.28	221	156	0.1
102	marble zone 10 spring	1	515402	5500897	11	7.35	235	166	0.1
103	eco village well	1	509703	5504985	16	7.97	332	229	0.1

EOS 490 Final Report: Assessing the Geothermal Reservoir or Resource Potential of the Kootenay Lake Region Through Structural, and Geochemical Analysis

December 21st, 2022

By:
Aidan McQuarrie

Submitted to:
Dr. Edwin Nissen
Theron Findley, Ph.D. Candidate

INTRODUCTION

The Kootenay Lake Geothermal Project is an ongoing geoscience reconnaissance project which aims to summarize geologic evidence in order to characterize a possible geothermal reservoir or resource in the Kootenay Lake region. The study area is in the southeastern corner of the Canadian province of British Columbia (Figure 1), within the high-grade metamorphic Omineca Belt (Monger et al., 1982) – one of the 5 physiographic belts which comprise the Canadian Cordillera. The Kootenay Lake Geothermal Project is founded on the thinking that meteoric surface waters penetrate ~0.9-2.2km (Allen et al., 2006) within the lithosphere via brittle faults and fractures where they are heated, and then circulate back to the surface/near-surface where that geothermally heated fluid can be harnessed for heating or electrical generation. Several hot springs are found along structurally controlled features within the study area, providing justification for further examination of the hypothesis of this project.

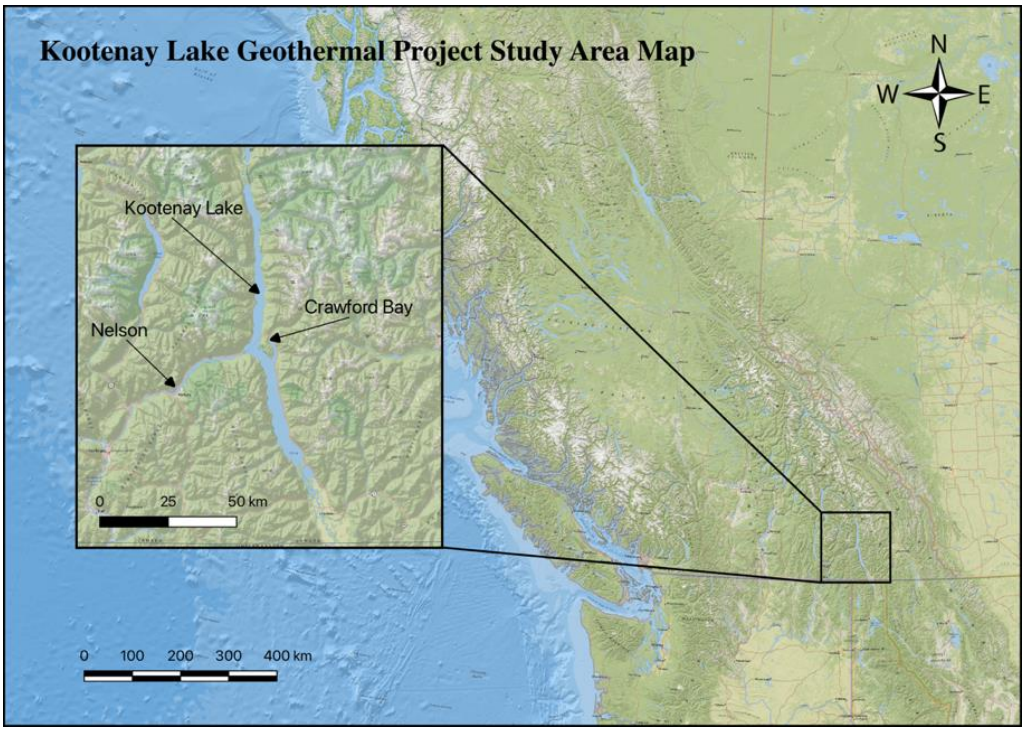

Figure 1:Kootenay Lake Geothermal Project Study Area Map

The Kootenay Lake Geothermal Project is currently in phase 2 of the 3 planned phases. Phase 1 of the project involved the compilation of remote sensing, geophysical, geologic, and other open-source data to delineate evidence of geothermal resources in the broader Kootenay Lake region (Sabutsch, 2021). Phase 2 builds on the results of phase 1 by targeting areas identified as high interest with geochemical sampling, geologic mapping, and high-resolution remote sensing. The ongoing phase 2 attempts to find evidence of a fault/fracture-controlled fluid flow model which could theoretically provide a circulation conduit for geothermal fluid. Phase 3 and beyond will likely consist of drilling one or more temperature gradient wells in locations that are deemed suitable based on the results of the prior phases. The results of drilling test wells will ultimately inform the economic feasibility of extracting the geothermal resource. The current long-term objective and use-case of the Kootenay Lake Geothermal Project is the development of a geothermally heated greenhouse, which would increase local food security, provide a case study for the successful development of a small-scale geothermal project in Canada, and contribute to the local green economy. Locating a renewable geothermal fluid source that exceeds 38°C, with a flow rate of at least 53.6 liters/second, would be sufficient to fulfill the heating requirements of a 4000m^2 commercial greenhouse complex (Desrochers, 1992).

Phases 1 and 2 have thus far been completed in collaboration with the not-for-profit South Kootenay Lake Community Services Society (SKLCSS), with the financial support of Geoscience BC, NSERC Applied Research & Development, CiCAN Career Launcher - Natural Resources Internship Program, and the Regional District of Central Kootenay. The project is coordinated by Volunteer Project Lead Gord MacMahon (Geologist/Project Manager), with assistance from Volunteer Technical Advisors Dan Gatto (Geologist) and Sonni Greene (Geologist). Funding was utilized in part to hire fourth year Simon Fraser University Geology student Colin Vandenbrink to undertake a large portion of the summer 2022 field program, under the direct supervision of Gord MacMahon. Additional funds were allocated to undertake a drone hosted high resolution LiDAR survey and Thermal Imaging survey of the Orebin Creek area, a zone of particular promise within the broader study area. The drone survey was carried out in October 2022 by students and faculty of Selkirk College's GIS department. Unfortunately, the processing time of these surveys prevented their inclusion in this report. The analysis undertaken for this report was chiefly aimed at synthesizing the geologic data obtained from a number of techniques to support the feasibility of a third stage of geothermal resource exploration. The geologic data in this analysis report considers 2 broad fields – Structural geology and Geochemistry.

Structural geology considerations of this report included the construction of a geologic cross sections based on existing geologic maps. The cross section explores a plausible subsurface geometry that is consistent with geologic mapping of the area with the aim of better understanding the potential fluid pathways of a geothermal resource in the Kootenay Lake region, while acknowledging the uncertainty associated with predicting the subsurface. Understanding the lithology of a potential geothermal reservoir can guide future exploration programs, such as in selecting an appropriate geothermometer (Allen et al., 2006; Grasby et al., 2000; Bruhn et al., 2010) for that area's reservoir rock type in a geochemical survey. Additionally, cross sections may be used in conjunction with measured parameters such as permeability, heat flow, or conductivity to create geothermal reservoir models.

The geochemical considerations of this report examined the results of lab-tested water samples that were obtained as part of the field work program during the summer of 2022 (Vandenbrink, 2022). A preliminary aqueous chemistry dataset obtained for the Kootenay Lake study area of 103 samples contained temperature, pH, conductivity, total dissolved solids (TDS), and salinity measurements. From this preliminary dataset, 20 samples were selected to undergo analytical testing by Caro Analytical Services, located in Kelowna, BC. A much more comprehensive dataset including ion concentrations of each sample could then be analyzed using AqQA software by Rockworks. The AqQA program enabled preliminary insight into geothermometry for samples suspected to originate from a geothermal/hydrothermal source. Stiff diagrams which visually represent ion concentrations were also generated, allowing comparison between water samples collected, and known geothermal waters such as Ainsworth Hot spring.

The overarching objective of these analyses are to begin to quantify the four parameters required for a geothermal resource: a heat source to heat the fluid, fluid flow (meteoric water), permeability, and orientation of the stress field in relation to the permeability. The Kootenay Lake Geothermal Project has identified the Crawford Bay area as its highest priority exploration area; thus, the remainder of this report focuses on this area.

GEOLOGIC SETTING

Cordillera and relevant tectonic domains

Western Canada, including British Columbia (B.C.), is thought to be made up of an accumulation of island arc terranes that collided with continental North America over the course of some ~150 million years, from the Jurassic to the Paleogene (Monger, 2008). This accumulation of welded-on terranes onto the western margin of North America is known as the Cordillera, which itself is comprised of five distinct morphological belts. Most westward is the Insular Belt which makes up BC's west coast, followed eastward by the Coast Belt, Intermontane Belt, Omineca Belt, and Foreland Belt. The Canadian Cordillera is a relatively young and tectonically active system of interconnected mountain ranges, plateaus, and valleys (Monger, 2008), and plays host to several clusters of thermal springs in different regions of high to low heat flow (Majorowicz and Grasby, 2010; Grasby et al., 2005).

Within the Canadian Cordillera, the study area is located within the Omineca Belt, which hosts the adjacent Purcell Anticlinorium and Kootenay Arc tectonic domains. The Purcell Anticlinorium is comprised of Mesoproterozoic to Neoproterozoic strata that are broadly folded (Moynihan & Pattison, 2008), situated east of the study area. The Kootenay Arc is a narrow metamorphosed and polydeformed region west of the Purcell Anticlinorium, and overlaps continental North American rocks and rocks from exotic island arc terranes.

Structural setting

Formed following the mid-Jurassic, the Omineca Belt is composed of autochthonous North American continent as well as allochthonous terranes that amalgamated and accreted to the western margin of North America (Monger et al., 1982). The intense compressional forces of suturing these exotic terranes with continental North America initiated a first generation of regional deformation, developing high-amplitude westward-closing recumbent anticlines, likely including the Riondel nappe (Moynihan & Pattison, 2008). A secondary phase of folding initiated from compressional deformation is interpreted to have deformed the Riondel Nappe (Höy, 1980). Rioseco et al. (2022) proposed that during this early-Cretaceous period of compressional orogeny, the rigid Mesoproterozoic rocks of the Purcell Anticlinorium to the east of the study area acted as a buttress upon which the ductile rocks of the Kootenay Arc deformed against. Intense compressional deformation likely led to peak metamorphic conditions in the mid-Cretaceous (Moynihan & Pattison, 2008), continuing until the early Eocene.

In the Eocene (55 Mya), a slight change in the direction of the subducting oceanic plate underneath the Cordillera likely caused a shift from regional compression to transtension (Monger, 2008). The subducting ocean-floor may have rotated towards the north to northeast, causing the oblique convergence of oceanic and continental plates. This oblique tectonic force may have caused extensive dextral (right-lateral) strike slip faulting, as well as extension, leading to stretching/thinning of the crust (Monger, 2008). Crawford Bay is situated along a major fault related to Eocene extension, the Purcell Trench Fault, (Doughty & Price, 2000). Finley et al (2022) suggest that the Purcell Trench Fault and other structures in the region have been reactivated as dextral strike slip faults in the present day as a result of far-field forces due to the subduction of the Juan de Fuca plate under continental North America.

Regional Stress Orientation

The southern Cordillera (including Crawford Bay) sees relatively low seismic activity compared to the northern Cordillera and the coast region. The United States Geologic Survey (USGS) earthquake database reports a low magnitude (M 2.8) earthquake in 2004 within Kootenay Lake, along the Purcell Trench Fault immediately adjacent to the town of Crawford Bay (USGS, 2022). Ristau et al. (2007) used regional moment tensor analysis to estimate the focal mechanisms from magnitude >4 earthquakes in order to constrain the regional stress orientation ($\sigma 1$) of the Cordillera. They found an overall regional stress orientation today of NE-SW. Building on these findings, Finley et al. (2022), presents novel structural evidence of post-Eocene dextral strike slip faulting with kinematics agreeing with the NE-SW stress orientation. These findings suggest faults in the southeastern Cordillera are active today. Finley et al. (2022), concludes that within the Cordillera, thermal springs may be associated with areas of increased seismicity, and that fault zones correlate well to thermal springs. The structural analysis included in this report aims to place the structural data collected around Crawford Bay into this regional context.

Stratigraphy

Moynihan & Pattison (2011) compiles several publications regarding the stratigraphy of the Kootenay region, comprising of Neoproterozoic to Triassic aged rocks. The Horsethief Creek Group are Neoproterozoic in age and act as basement rock composed of metapelite, quartzite, limestone and amphibolite. The Hamill Group overlies the Horsethief Creek Group and a regional unconformity separates Neoproterozoic age Hamill from Cambrian aged Hamill of micaceous quartzite, mica schist, marble, and calc-silicate. The Mohican formation is Cambrian in age and is composed of mica schist, marble, and quartzite. The Badshot Formation overlies the Mohican, comprised of limestone/marble and is thought to have been deposited on a shallow- marine shelf during a period of relative tectonic quiescency (Moynihan & Pattison, 2011). The Lardeau Group is Cambrian to Ordovician in age, and conformably follows the Badshot Formation, and its lowest unit is demarcated by a black metapelite that is thought to have been deposited in deep water anoxic conditions. The Lardeau Group is typically associated with black-grey-green calc-schist to gneissic metamorphic rocks that evolved from a sedimentary protolith. Metavolcanic rocks within the Lardeau signal a return to active rifting post-Cambrian, while amphibolite, calc-silicate, marble, and conglomerate rocks are also present. Though not observed in the Crawford Bay area, The Milford and Kaslo groups are unconformably laid on top of Lardeau, followed by the Triassic aged Slocan Group. Cretaceous plutonic suites called the Crawford Bay Stock and the Shoreline Intrusions are composed of biotite-muscovite granite and pegmatite plutons, and may have been emplaced during the height of regional metamorphism, but not following the last event of regional deformation (Hoy, 1980). Figure 2 below, from Moynihan & Pattison (2011), summarizes the stratigraphy of the Kootenay region. Vandenbrink (2022) simplifies the lithology into seven broad categories (Table 1) for the benefit of focusing on the geothermal potential of Crawford Bay, rather than the complex geology.

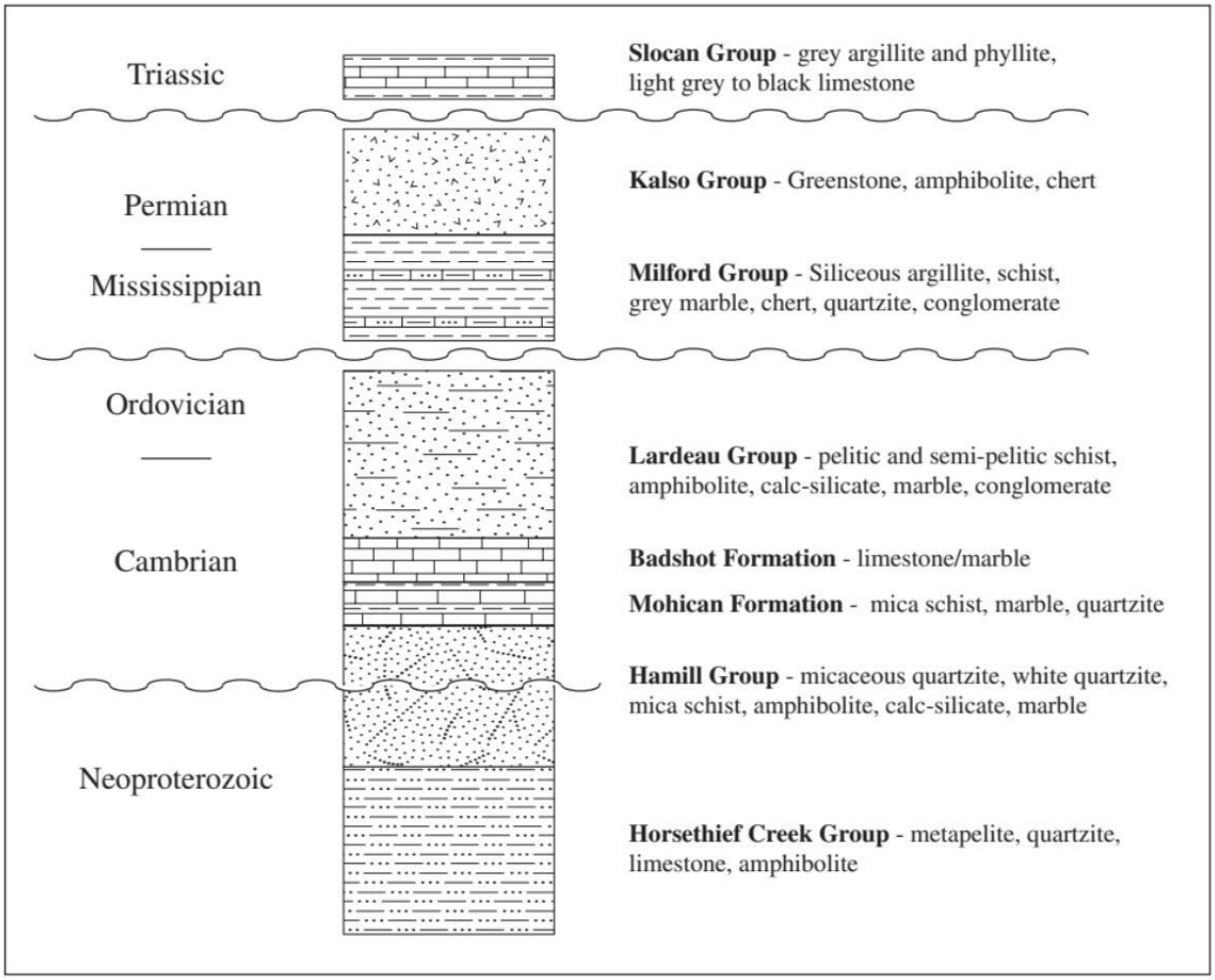

Figure 2: Summary of Kootenay's regional stratigraphy. Figure from Moynihan & Pattison (2011).

Table 1: Simplified Crawford Bay lithology from Vandenbrink, (2022). Colours correlate to the colour scheme adopted on the Geological Survey of Canada (GSC) surficial geology map of the Crawford Bay area.

Lithology	Stratigraphy	Age
Granite	Crawford Bay Stock / Shoreline Intrusions	Cretaceous
Schist-Gneiss	Index formation (Lardeau Group)	Cambrian to Ordovician
Marble	Badshot and Mohican formation (Lardeau Group)	Cambrian
Quartzite	Hamill Group	Neoproterozoic to Cambrian
Schist	Hamill Group	Neoproterozoic to Cambrian
Gritstone	Three Sisters Formation / Lower Hamill Group	Neoproterozoic
Phyllite	Horsetheif Creek Group (Windermere supergroup)	Neoproterozoic

GEOTHERMAL SETTING

Background geothermal resource information

The primordial heat of Earth's formation and the breakdown of radiogenic isotopes in the crust and mantle both contribute to a consistent loss of heat energy from Earth's interior. However, this heat loss is anything but uniform across the planet. Concentrations of this heat within the crust are referred to as geothermal reservoirs or resources, depending on the usability or applicability of the heat source - which in turn depends on the extent and magnitude of heat, as well as the presence and flow of fluid within the reservoir/resource. Areas of the crust that are thinned (and therefore less insulating of the mantle), or have experienced recent volcanism or plutonism, tend to host these concentrations of escaping heat. Heat flow is a measure of the amount of heat energy that's escaping from a reservoir/resource, and is reported in milli Watts per m^2 (mWm^{-2}). The Southeastern Cordillera is one such area of concentrated heat loss, or elevated heat flow, due in part to Eocene age extension discussed above. Elevated heat flow is typically associated with elevated geothermal gradient, which is a measure of how rapidly temperature increases with depth in the crust. Elevated geothermal gradients are preferential for geothermal developments, as accessing anomalous geothermal heat reservoirs is cheaper and easier when these reservoirs are closer to the surface. According to Majorowicz & Grasby (2010**)** the Cordillera hosts some of the highest heat flow and geothermal gradients in Canada. In addition to the volcanic centres of Mt. Meager and Mt. Caley located within the Coast Belt near Squamish and Whistler BC, Southeastern BC sees some of the highest heat flow values and geothermal gradients in the Cordillera with average heat flows ranging from ~100-150 mWm^{-2}, and temperature gradients from ~25-55°C/km (Allen et al., 2005; Finley et al., 2022; Majorowicz & Grasby, 2010; Grasby et al., 2012).

Geothermal resource classification types

Moeck, 2014, proposes a classification scheme that summarizes the geologic controls of geothermal systems around the world. It is broadly separated into *convection* dominated, and *conduction* dominated geothermal plays, as these heat transfer mechanisms are responsible for the migration of heat from great depth to human accessibility. These broad categories are further divided into six characteristic play types, where 1-3 are convection driven, while 4-6 are conduction driven.

1. *Active volcanic fields* are characterized by high enthalpy and high potential for power generation, with fluid heated adjacent to molten magma. Mount Meager, B.C. and Java-Kamojang exemplify the volcanic, convection dominated geothermal play type.

2. *Plutonic belts* are associated with emplaced batholiths, plutons, sills, and laccoliths as a heat source. The age of the emplaced body can determine the heat mechanism; recent plutonism will generate geothermal heat through the cooling of the rock body, whereas an old igneous body will generate heat from radioactive decay in granitic rock. The heat production of plutonic belts can thus range from lots of heat to very little. Larderello, Italy, exemplifies this play type as hot steam is trapped in the subsurface, heated by recent plutonism rather than active volcanism. The geothermally heated steam vents of Ladrerello have been exploited since Roman times, when geothermal steam was employed to heat baths (Minissale, A., 1991).

3. *Extensional settings* are characterized by permeable layers and faulting, which act as conduits for heated meteoric water to rise to the surface. Crustal extension can lead to elevated geothermal gradients, meaning circulating fluids can be sufficiently heated at relatively shallow depths. Nevada's Basin and Range geothermal province exemplifies the extensional geothermal setting (Grasby et al., 2012).

4. *Sedimentary Basins* are characterized by low to absent tectonic activity with near normal geothermal gradient. However, the sedimentary nature of these basins makes them a geothermal exploration target due to their high porosity, which is a natural *reservoir* for interstitial subsurface fluid, despite generally low enthalpy. Direct use applications may be most suitable for sedimentary basin geothermal play types, in many circumstances. The Williston Basin of Saskatchewan and North Dakota hosts highly permeable and porous sandstone, serving as an example of the sedimentary basin play type (Moeck, 2014).

5. *Orogenic belt type* is characterized by low to moderate heat flow in a mountainous region with deep rooted fault systems and high permeability. Hot springs are often associated with this play type as deep, complex, crustal scale faulting is generally present, acting as a conduit for meteoric waters. Recharge areas are generally at high elevations, and meteoric water is circulated through faults and any permeable beds to discharge in valley bottoms. Despite this advective heat transport, the orogenic belt geothermal play type is still considered by Moeck (2014) to be a conduction dominated geothermal play type. Temperature gradients somewhat follow topography, thus circulating meteoric water that enters the system at high elevations passes through higher isotherms before reaching valley bottoms, or seeping out into hot springs. However, the transit time for this circulation can range from decades to millennia, depending on porosity and permeability. This slow recharge rate could pose a challenge for the longevity of a geothermal project, unless a reinjection strategy is determined. The Molasse Basin of Southern Germany is characteristic of the orogenic belt type (Moeck, 2014).

6. *Basement type* geothermal plays aim to take advantage of deep-seated crystalline (e.g. granitic) rocks that host immense heat resources, underlying large portions of many continents. The Cooper Basin of Australia is an example of the Basement type geothermal play system.

Geothermal characteristics of the Kootenay Arc / Crawford Bay area

Canada is made up of a diverse array of geologic settings from old-cold craton to active volcanic arcs, plutonic belts and sedimentary basins, and thus possesses a wide spectrum of the geothermal play types noted above. The geothermal system near Crawford Bay cannot be easily confined to a single distinctive play type – rather this geologic setting has characteristics of the Plutonic Belt type, Extensional Setting type, and Orogenic Belt type. The Cretaceous age Shoreline Intrusions are pervasive plutons emplaced in the study area due to partial melting of a subducting oceanic plate. Composed of biotite-muscovite granite and pegmatites, these felsic bodies may act as a heat source for circulating meteoric water as a product of the radiogenic decay of ^{40}K, (a constituent of alkali feldspars), ^{232}Th, and possibly a component of ^{238}U. Lewis et al. (1992) reports that the Omineca Belt hosts several plutons of elevated heat flow, including the Crawford Bay Stock, with a heat flow of 2.69 $\mu W/m^3$, averaged from 7 observations with a standard deviation of 0.29 $\mu W/m^3$. In addition to the Plutonic Belt geothermal play type, the study area also shares characteristics of the Extensional Setting geothermal play type. Numerous studies conducted in the Cordillera report the presence of an extensional structural setting dating back to the Eocene in the Omineca Belt in the Southeastern Cordillera, which is potentially active today (Majorowicz and Grasby, 2010; Finley et al., 2022; Allen et al., 2005). Prolific faulting, crustal thinning, and elevated heat flow (Majorowicz and Grasby, 2010) all point to the extensional geothermal play type – it should be noted that seismicity in the area may be related to reactivation of ancient normal faults as dextral strike slip faults (Finley et al., 2022), rather than faults generating extension. However, the nearby presence of hot springs, high topographic relief, and deep crustal scale faulting point to the Orogenic Belt geothermal play type. Regardless of definition, this combination of ancient arc plutonism and extensional faulting in the Southern Cordillera (Allen, 2005) could provide a favourable geothermal setting for an accessible geothermal resource in Crawford Bay. Nevada's Basin and Range province may prove to be similar in nature to the geothermal system at Crawford Bay (Grasby et al., 2012) – Notably, Nevada

contains the highest number of geothermal power plants in of any state in the U.S. (Finley, 2020). Nevada has an elevated geothermal gradient due to its extensional structural setting, hosts a complex series of overlapping faulting which can accommodate the circulation of geothermal fluid, topped off with the superposition of late Cenozoic volcanism/intrusions (Finley, 2020; Blackwell. 1983). Typical heat-flow for Nevada's Basin and Range provinces averages ~85 ± 10 mWm^{-2} (Blackwell, 1983), whereas the regional average heat-flow for the southeastern Cordillera is comparable at >70 mWm^{-2} (Grasby et al., 2012). Lewis et al. (1992) reports that the heat flow of the Omineca Belt is 86.3 mW/m^2, averaging from 26 sample sites, with a standard deviation of 20 mW/m^2.

A final compelling argument for the presence of a substantial geothermal system near Crawford Bay are the hot and warm springs in the area including the Ainsworth and Dewar Creek hot springs, the Crawford Creek warm spring, and the intersection of hot water within the nearby, now abandoned Bluebell Mine in Riondel. The Ainsworth and Dewar Creek hot springs reach measured surface temperatures of 45°C and 83°C, respectively (Grasby et al., 2000), while the Crawford Creek warm spring sits on the Orebin Creek fault and reaches at least 30°C (Vandenbrink, 2022). Grasby et al. (2000) performed geothermometry on a suite of thermal springs in the Cordillera, including the Ainsworth and Dewar Creek hot springs to constrain the maximum temperature that spring water was heated to at depth. Ainsworth and Dewar Creek Geothermometry results indicate maximum temperatures of 147°C and 163°C, respectively (Grasby, 2000). Knowing the geothermal gradient of the area where these hot springs are located can give an estimate of the depth that water was heated at, and ultimately the required depth for a geothermal well to intercept. According to Allen et al. (2005), thermal spring water circulation depths range from 0.9-2.2km for thermal springs located just to the East of the Crawford Bay study area, near the Rocky Mountain Trench, which may be a somewhat similar environment to the Crawford Bay study area. Furthermore, Finley et al. (2022) suggests fault hosted circulation depths may reach greater than 2km in the southeastern Canadian Cordillera.

The Bluebell Mine located ~10km north of Crawford Bay in the community of Riondel operated from the late 1800's until 1971, producing lead, zinc, copper, and silver. In 1956, at a depth of 260m below ground (elevation of 292m a.s.l.), warm (21°C), slightly acidic water with a high flow rate of 90L/s was initially encountered. At lower levels (elevation of 212m), the temperature increased, ranging 23-40°C at the lowest workings (Desrochers, 1992). This interception of warm water caused engineering problems for the remainder of the mine life, as high volumes of thermal water and dissolved CO_2 gas had to be pumped from the mine. $CaMgCO_3$ precipitation caused rapid scale build-up within the pipes installed to remove the hydrothermal fluid, making it difficult to remove the hydrothermal fluid for the remainder of the mine-life. At one point, 110,000 bags of cement were pumped into the thermal conduits in an attempt to plug the leak, however this proved ineffective (Desrochers, 1992). When the mine closed in 1972, the mine was allowed to flood, reaching an equilibrium elevation of 451m a.s.l., which also stopped the leakage of CO_2 gas from the mine workings (Desrochers, 1992). It has been proposed that the source of the thermal water is from great depth, travelling upward along open faults and intersecting the Badshot Limestone unit that was the target of the Bluebell Mine operation. It's postulated that the fluid is fault hosted, as the thermal fluid would neutralize if it spends any significant amount of time in contact with the Badshot limestone unit. An internal report written by the mine operator, Cominco, conservatively estimates 150L/s of 37.8°C thermal fluid is available for extraction to the surface from the lower workings (Desrochers, 1992).

METHODS

Structural Analysis:

Data sources

Structural data considered in this report was sourced from Höy, 1980, the Geological Survey of Canada (GSC) Crawford Bay Geology map (Brown et al. (2011), which is based on Höy, 1980), Moynihan, 2008, and structural measurements and mapping from Vandenbrink, 2022.

Metamorphism indicating intense structural deformation

Crawford Bay is located within the Omineca Crystalline Belt in southeastern BC, hosting high grade metamorphism, intense folding, and major fault zones as a result of intense, large scale structural deformation, in addition to granitic magmatism, uplift, and significant erosion (Monger et al., 1982; Moynihan and Pattison, 2008; Webster & Pattison, 2018). Anomalously high-grade metamorphic rocks of the Amphibolite facies are observed running parallel to Kootenay Lake (Moynihan & Pattison, 2008), as shown in Figure 3. Pressures of at least 7kb are required to generate kyanite-bearing Barrovian rocks, which translates to at least 25km of burial (Moynihan & Pattison, 2008). These highly deformed rocks are thought to have undergone at least 3 (if not more) deformation events, including during exhumation throughout the mid-Cretaceous (~80-120Ma) (Moynihan & Pattison, 2008; Höy, 1980). The presence of these rocks at the surface today indicates extensive erosion has removed kilometers of overlying material. Höy (1980) proposed that this series of major deformation events may have generated a nappe structure that extends from the Meadow Creek Anticline of the Duncan Lake area (~70km north), in order to explain the inverted age sequence that is observed near Crawford Bay. Just east of Crawford Bay, older Hamill quartzite occupies the cores of synform folds, while younger Lardeau schist-gneiss occupies the cores of antiforms. This zone of complex deformation near Kootenay Lake and Crawford Bay is juxtaposed with a zone of relatively coherent stratigraphy to the east of the Orebin Creek Fault, with the broadly folded Neoproterozoic Windermere Supergroup overlying the Mesoproterozoic Purcell Supergroup. Höy, 1980, proposes a décollement zone as an explanation for this contrast.

Figure 3:Relatively high-grade metamorphic rock, possibly Amphibolite facies. Observed near Crawford Bay Ferry Terminal on Oct. 5, 2022. Thanks to Gord MacMahon for the geologic familiarization tour.

Cross section methodology

To conceptualize the complicated structure of the Crawford Bay area, and to hypothesize possible subsurface geometries in the vicinity of the Crawford Creek warm spring, several geologically plausible cross sections were constructed based on Höy's (1980) mapping of the area, and the Geological Survey of Canada Crawford Bay Geology map (Brown et al. 2011). At least 6 iterations of cross-sections representing the Riondel nappe hypothesis were produced, in addition to several attempts to produce a cross-section without a nappe structure that still adheres to Höy's (1980) map pattern. Ultimately, only the nappe cross section interpretation is included in this report, as other interpretations were unsuccessful in adhering to surficial mapping. While constructing a geologic cross section, it was assumed that bed thicknesses remain constant and that measurements taken perpendicular to the section line can be projected along strike. Considering the high degree of ductile deformation in the study area, these basic assumptions are likely not entirely valid, however they are necessary to reduce the degrees of freedom while fitting the subsurface structure to the observations at the surface. Due to the wide spectrum of reliability and proximity of structural measurements to the cross-section line, no correction of apparent dips to true dips were executed. The cross-section line (A-A') runs directly East-West, perpendicular to the regional structural grain, through the Crawford Creek warm spring (geochemical sample 72). The cross-section also intercepts the West Bernard Fault, and the Orebin Creek fault. Vandenbrink, 2022, reports a very large (n = 1759) catalog of structural measurements (Joints, Bedding, and Faults) in the Crawford Bay area, which were used to assign dip angles of strata and faults in the cross section, in addition to mapping by Höy (1980).

Geochemical Analysis:

Stiff diagrams

Geochemical data considered in this report was sourced from Grasby (2000), (Ainsworth and Dewar Creek), Desrochers (1992), (Riondel), and from Vandenbrink (2022) (all other samples). Vandenbrink (2022) initially collected geochemical data including temperature, pH, conductivity, total dissolved solids (TDS), salinity, and location from 103 sample sites within the Crawford Bay study area. These measurements were collected using an Oakton PCTSTestr 50 multiparameter meter over the course of the summer of 2022. Using this preliminary data, 20 high interest sites were identified for further testing. These sample sites were revisited at the end of August 2022, at which point samples were collected and shipped to Caro Analytical Services. The comprehensive dataset including ion concentrations of each sample was then analyzed using AqQA software by Rockworks. A map representing the water sample locations and each sample's corresponding composition (using Stiff diagrams) is shown in Figure 7. This diagram is useful in making a rapid visual comparison between water from different sources and the corresponding lithology mapped at the surface of each sample site. An example Stiff diagram is shown in Figure 4, where a polygon is generated based on the abundance of Magnesium, Calcium, and Sodium + Potassium Cations on the left side of the diagram, and Sulfate, Bicarbonate, and Chloride Anions on the right side of the diagram. Displaying a sample's major ion composition, combined with the surface lithology in a visual manor, allows interpretation of similar water types throughout the study area, which could aid in locating a geothermal reservoir or resource.

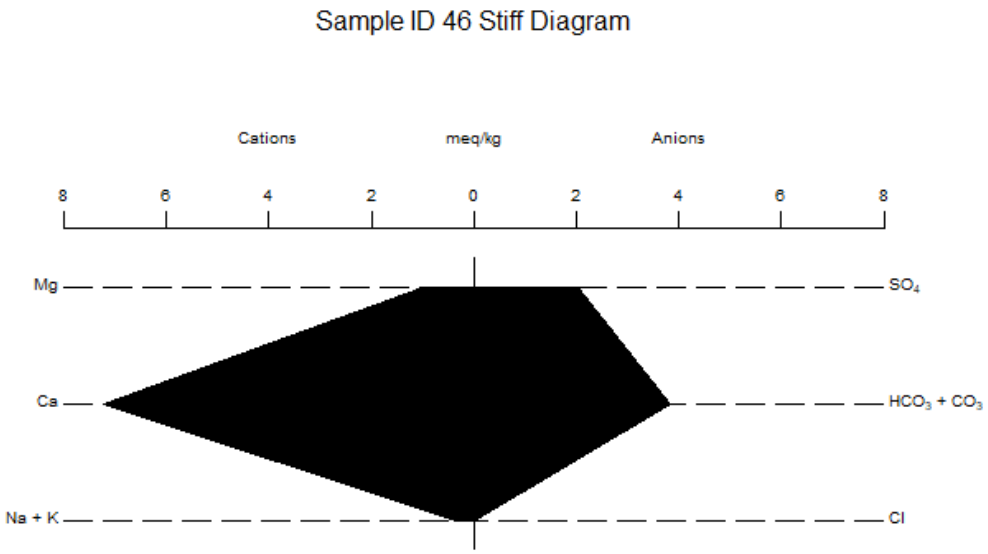

Figure 4: Example Stiff diagram generated using AqQA software by Rockworks

Series plot

A series plot displaying the Chloride (Cl^-), Sulfate (SO^4), Calcium (Ca), Manganese*, Sodium (Na), and Bicarbonate (HCO_3) ion concentrations of each sample was also produced, as a series plot allows comparison of individual ion concentrations from one sample to another (Figure 8). Notably, the ions displayed on the series plot are the same as those on the Stiff diagrams of each sample, however, the series plot gives an alternate view of the data. Another outcome of the geochemistry component of this report is an investigation into geothermometry, which attempts to constrain the maximum temperature a fluid reaches at depth. Geothermometry is not meant to sample meteoric or near surface water and is only applicable to hydrothermal/geothermal waters. Therefore, not every sample analyzed by Caro Analytical Services is applicable for geothermometry. Vandenbrink, 2022, has divided samples into 2 classes: 1, samples that are likely to have a greater thermal fluid component (seeps, springs and wells), and 2, samples that were retrieved from the surface (stream, lake, creeks, etc). Class 1 samples are applicable for geothermometry, whereas class 2 samples are not.

*Note: Manganese was displayed on the series plot in error, when Magnesium was intended to be displayed. AqQA licencing time constraints made correction of this issue untenable.

Justification

The only reliable way to determine subsurface temperatures is to drill a well and record a direct, physical measurement. In lieu of such wells in the study area, geothermometry is applied to infer the temperature of the subsurface at the study site using the solubility of various ions in a thermal fluid, depending on the composition of the host rock. Geothermometers constrain temperature at depth based on chemical changes that occur when a mineral or solution is exposed to temperatures at or exceeding a threshold temperature for that reaction to occur. There are several geothermometers, all of which are subject to a series of assumptions: The geothermal fluid is in equilibrium with hydrothermal minerals precipitated in the reservoir; the pressure in the reservoir is fixed by coexistence of liquid and steam; the geothermal liquid cools adiabatically or conductively through steam separation at 100°C; the geothermal fluid of interest does not mix with cold ground water during its ascent towards the surface (this assumption is quite bold); the geothermal liquid does not precipitate/lose any relevant mineral phases

during ascent. The silica geothermometer takes advantage of the fact that silica can occur in various forms (quartz, cristobalite, chalcedony, amorphous silica) depending on the pressure/temperature conditions. At low temperatures, quartz is less soluble and amorphous silica is more soluble. This relationship has been quantified by several authors (Fournier, 1977; Arnorsson et al., 1983), allowing the temperature of the fluid to be constrained based on the abundance of each silica polymorph. This method is reliable until 300°C, however the effects of pH, steam separation, and possible mixing of hot and cold water can increase the complexity of this method tremendously (Verma, 2000; Bruhn et. al., 2010). Other geothermometers include the gas (steam) geothermometers, Ionic Solute, and isotope geothermometers. (Arnorsson, 2000; Bruhn et. al., 2010).

Grasby et al. (2000) used a host rock-based classification scheme proposed by Souther (1992), which categorizes geothermal fluids by the host rock that thermal fluid was collected from. Grasby et al. (2000) analyzed thermal fluids from a variety of thermal springs in the Canadian Cordillera, and divided these thermal springs into 3 host rock categories: 1. Carbonate rocks, 2. Silicate (igneous and metamorphic) rocks, and 3. Quaternary volcanic belts. Maximum temperatures of thermal fluids discharging from carbonate rocks were determined to be most accurately estimated by the Chalcedony geothermometer, while the temperatures of silicate rock-hosted thermal fluids were best estimated by taking the average between the quartz and Na-K-Ca geothermometer.

For this report, two geothermometer classification schemes are proposed. The first assigns geothermometers based on the surface lithology where the sample was collected, or the host rock of the thermal water, similar to Grasby et al. (2000). However, all of the samples in this report discharge from surficial silicate rocks, thus an average between the quartz and Na-K-Ca geothermometer was used to constrain temperatures at depth for these silicate hosted springs. The second scheme is based on the pH of each sample. In the Crawford Bay study area, the Badshot-Mohican formation is the only major carbonate unit (composed of calcite, marble, and dolomite) excluding the Purcell Supergroup to the East. As the Badshot-Mohican formation is suspected to influence the subsurface (see cross section), assuming all thermal spring host rocks are silicates from the surface expression alone may be misleading. Because acidic fluids react and neutralize on contact with carbonates, considering the potential of hydrogen (pH) could reveal if thermal waters interacted with carbonates in the subsurface. Acidic ($pH < 7$) samples are very likely to have silicate host rocks with little to no interaction with carbonates, which would neutralize the pH to at least 7.0. These samples were assigned the same silicate hosted geothermometer scheme as above, an average temperature between the quartz and Na-K-Ca geothermometrs. Samples with a $pH > 7$ may have interacted with carbonate host rocks (eg. Badshot-Mohican marble) on their ascent to the surface. Grasby et al. (2000) uses the chalcedony geothermometer for carbonate hosted springs, which was adopted for this report.

RESULTS / DISCUSSION

Structural Results:

Cross section

Of primary interest to the assessment of the geothermal potential of Crawford Creek is the warm-spring (geochemical sample 72) situated on strike with the Orebin Creek fault, which runs ~N/S through the fractured quartzite of the Hamill Formation. A cross section was constructed in an attempt to better understand and characterize the rocks in the study area, especially those which underlie the Orebin Creek fault, to resolve which geothermometer should be applied (see geochemistry section). The geologic cross section exercise also contributes to an appreciation of the geologic history, including numerous regional scale deformation events which have occurred in the study area.

Constructing a cross section of the study area reveals a somewhat complex structural puzzle of various faulting and folding events. Figure 5 is a map of the Crawford Bay area with the cross-section line shown overlaying the GSC geologic map by Brown et al., 2011, which the cross-section and cross-section color scheme are based off of. Resolving the inverted stratigraphy of the Bluebell Mountain Synform and the Preacher Creek Antiform proved to be the crux of the cross-section exercise. A labelling discrepancy between Höy, 1980, and GSC (Brown et al., 2011), adds confusion as the GSC map has labelled the inclined Bluebell Mountain *Synform* as the Bluebell Mountain *Syncline*, and the Preacher Creek *Antiform* as the Preacher Creek *Anticline*. As older material does in-fact overlie younger material, Synform and Antiform nomenclature is correct, as is stated in Höy, 1980. However, as the younging direction is known, these features may be labeled as the Bluebell Mountain Synformal Anticline, and the Preacher Creek Antiformal Syncline, respectively. A recumbent fold (such as a highly deformed nappe structure) is needed to generate synformal anticline and anticlinal synform structures, which lends support to Höy's (1980) proposition of the Riondel Nappe. Though not shown on the cross section, the Bluebell mine in Riondel has inverted surface geology, with Hamil quartzite overlying Badshot-Mohican carbonates - Höy proposes this structure is the remnant part of a limb of the now largely eroded Nappe. The Crawford Bay area is thought to have undergone several deformation events (Höy, 1980; Moynihan & Pattison, 2008), which together may have generated the Riondel Nappe structure, however, this nappe structure is in stark contrast to the relatively undeformed stratigraphy to the east, the Windermere Super Group (WSG) and the Purcell Supergroup (of the Purcell Anticlinorium (Moynihan and Pattison, 2008)). To explain this contrast, Höy (1980) proposes a décollement surface at the base of the Hamill Formation, separating the Hamil Formation from the Three Sisters Formation (indicated on cross section). This décollement surface may act as a large scale, nearly horizontal fault where overlying strata have been highly deformed, where beneath this décollement surface, within the Three Sisters Formation, the strata remain somewhat undeformed.

The very steeply dipping Orebin Creek fault was assigned dextral strike-slip symbology, as evidenced by kinematic indicators observed during a field visit, and the overall NE-SW regional stress orientation described by Ristau et al., 2007. However, Höy (1980) proposes that the Orebin Creek fault formed as a normal fault due to the third deformation event, the Eocene extension, and may have been reactivated recently as a dextral strike slip fault. These observations are consistent with the observations presented by Finley et al., (2022).

Though somewhat unrelated to the investigation of a potential geothermal system in Crawford Bay, stratigraphy east of the Orebin Creek fault was considered. The Windermere Supergroup (WSG) is bound by the Three Sisters Formation above, and the Toby formation below. However, the Three Sisters Formation dips to the west, whereas the toby formation dips to the east following the axial plane of an inclined fold. In order to maintain a constant thickness of the Windermere Supergroup, it was assumed

that the Three Sisters, WSG, Toby, and Purcell Supergroup contacts were squished, thus making use of the change in elevation to explain the opposing dip directions.

Unresolved questions and discussion

Though the geologic cross section constructed for this report successfully honors surficial mapping by Höy (1980), Brown et al., 1982, and Vandenbrink, 2022, it nonetheless leaves many questions unanswered. Chiefly, the highly deformed rocks that are found west of the Orebin Creek Fault seemingly end at the Hamil Formation, at which point the rocks are faulted and fractured due to brittle deformation, and do not display the intense ductile deformation observed to the west. This is problematic, as these rocks are located to the west of the Three Sisters Formation where décollement is thought to have occurred (Höy, 1980), and thus should have undergone intense ductile deformation according to the presented cross section. It may therefore be reasonable to conclude that the décollement surface is in fact located to the west of the presented décollement surface.

The West Bernard fault separates the deformed, inverted stratigraphy to the west, with the right-side-up panel of rocks to the east. Exposures of the West Bernard fault in the study area are unavailable, which has led to a lack of conclusive evidence regarding the direction of displacement of the fault. The West Bernard Fault is presented as a thrust fault rather than a normal fault because if the west Bernard Fault is a normal fault, the root of the Riondel nappe should be exposed to the east of the fault, which has not been shown. Instead, the root of the Riondel nappe is interpreted to reside below the West Bernard fault, within the Hamill formation east of the West Bernard fault (Höy, 1980). However, this is potentially problematic as the Hamil formation observed at the surface does not display significant ductile deformation which could be expected if the root of the nappe was buried beneath. Another line of evidence that the West Bernard fault is a thrust fault is the increasing metamorphic grade to the west of the fault. As a thrust fault, the West Bernard fault could have brought Kootenay Arc metamorphic rocks up to the surface rather than burying them further.

The proposed cross section above is one interpretation that agrees with Höy's (1980) mapping, however may not represent the real structural setting of the area. Other structural interpretations are likely plausible, and should be considered.

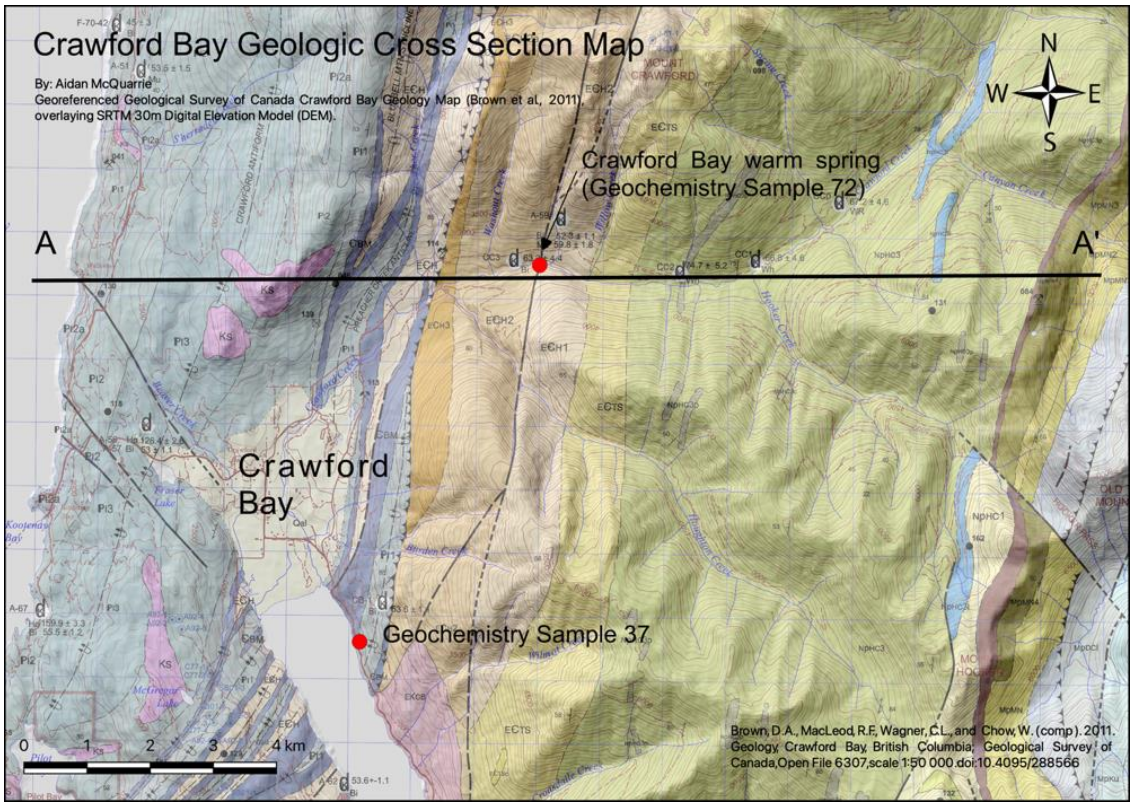

Figure 5: Plan view map of geologic cross section showing surficial mapping from Brown et al., 2011 Notable geochemical sample locations are noted, however, geochemistry sample 46 is not shown within the extent of the map.

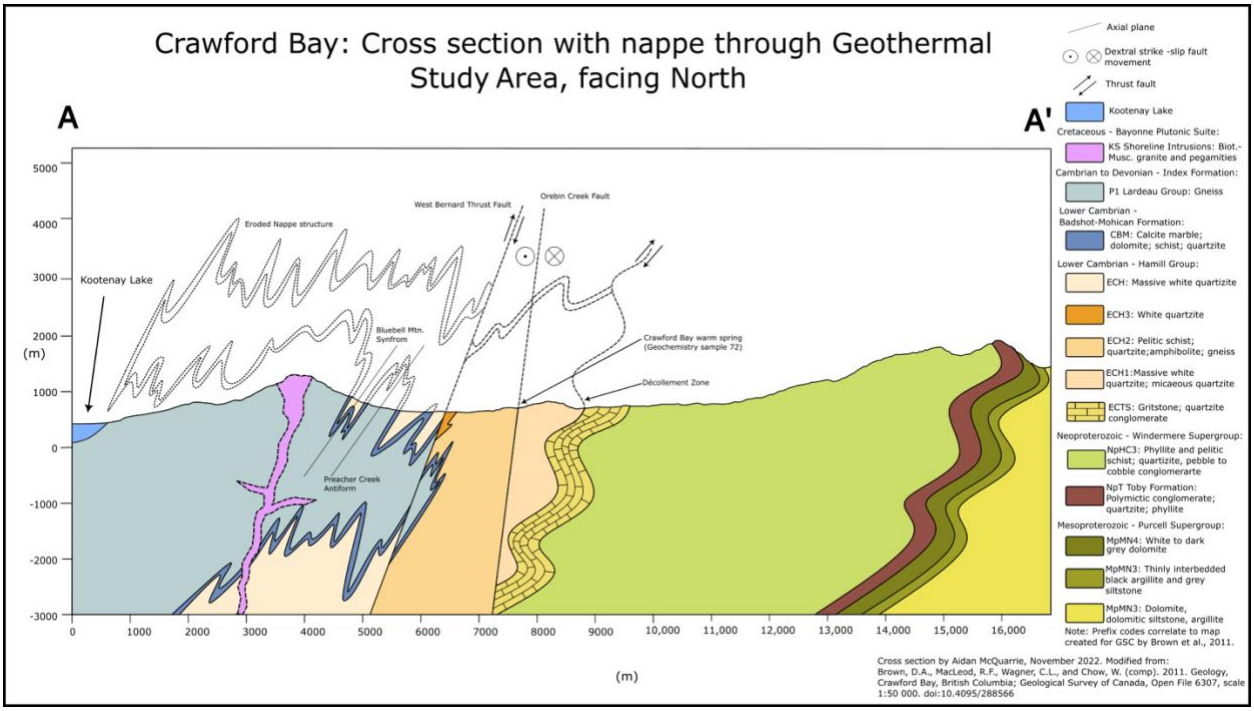

Figure 6: Geologic cross section of Crawford Bay study area

Geochemistry Results:

Geothermometry results

Table 2 represents the results of both geothermometry methods, with anomalous samples 37 and 46 highlighted. Both methods (surface lithology and pH) result in anomalously high theoretical maximum temperatures at depth. As shown in Figure 7, samples 37 and 46 are separated by Crawford Bay, thus it's unlikely these sample locations are hydrologically connected at the surface, though they may be connected at depth via deep faulting pathways. Notably, these samples are situated within a highly deformed, folded and faulted area of Crawford Peninsula, that stretches across Kootenay Lake to the West, and extends towards the North East, intersecting the West Bernard Fault. It is conceivable that these samples are less affected by groundwater infiltration than other samples, and are thus providing a somewhat accurate estimate of subsurface maximum temperatures, whereas other samples in the study area may have been contaminated by groundwater and are thus inaccurate, providing geothermometry results that are too low. However, the influence of ground water is inherently unpredictable, thus the only reliable method of determining subsurface temperatures is through in situ measurements via drilling. Only samples that were categorized as "class 1" by Vandenbrink, 2022, are listed in Table 2, as geothermometry is only applicable to geothermal waters.

Table 2: Geothermometry results.

Sample	Quartz Geothermometer (°)	Chalcedony Geothermometer (°)	Na-K-Ca Geothermometer (°)	pH	Host Rock	Geothermometry Lithology Control (°)	Geothermometry pH Control (°)	Average Geothermometry
3	31.027	<0	<0	8.32	Silicate	31.027	<0	31.027
37	154.38	129.7	17.191	7.19	Silicate	85.7855	129.7	107.74275
44	47.56	14.992	3.8479	7.24	Silicate	25.70395	14.992	20.347975
46	181.98	161.18	13.353	7.14	Silicate	97.6665	161.18	129.42325
47	49.777	17.264	13.494	7.4	Silicate	31.6355	17.264	24.44975
63	31.027	<0	<0	7.27	Silicate	31.027	<0	31.027
72	68.595	36.728	29.034	6.59	Silicate	48.8145	36.728	42.77125
85	24.531	<0	26.966	7.13	Silicate	25.7485	<0	25.7485
86	20.23	<0	<0	7.3	Silicate	20.23	<0	20.23
91	44.004	11.357	0.21211	6.86	Silicate	22.108055	22.108055	22.108055
91w	57.231	24.935	2.3502	6.86	Silicate	29.7906	29.7906	29.7906
94	50.315	17.816	<0	7.93	Silicate	50.315	17.816	34.0655
101	47.56	14.992	<0	7.28	Silicate	47.56	14.992	31.276
Ainsworth[1]	203.58	186.38	88.682	6.5	Silicate	146.131	186.38	166.2555
Dewar Creek[1]	208.68	192.41	148.86	6.4	Silicate	178.77	192.41	185.59
Riondel[2]	191.31	172	186.94	7.2	Silicate	189.125	172	180.5625

Samples 3-101: Data sourced from Caro Analytical Services Ion Concentration data, and pH values from Vandenbrink, 2022. [1] Ainsworth and Dewar Creek data obtained from Grasby et al., 2000. [2] Riondel data obtained from Desrochers, 1992. Geothermometry calculations were carried out in Rock Works AqQA software.

Stiff diagrams and water sample location diagram

Figure 7 displays the locations of water samples that underwent laboratory ion concentration analysis, with corresponding Stiff diagrams for each sample location. The shapes of these Stiff diagrams appear weakly correlated – Samples within the Lardeau Group, found in near the Western side of the study area, appear to be enriched in Calcium and Bicarbonate, with minimal Mg, Na +K, SO_4, or Cl. Hamil Group hosted samples appear somewhat less alike, with a somewhat wider range of ion concentration relationships, however, Calcium and Bicarbonate ions still appear enriched. Notably, sample 72 represents the Crawford Creek warm spring, and appears enriched in Mg to a similar extent as the Riondel thermal waters. Sample 63 is the only sample hosted in the Windermere Supergroup;

however, this sample appears to demonstrate a similar shape as sample 72 with enriched Mg concentration. These similarities could indicate a subsurface connection between these 3 geographically distinct sample locations. Hot springs Ainsworth and Dewar Creek, along with Riondel thermal waters, all show significantly different Stiff ion concentration diagrams, despite all of these locations presenting anomalous surface temperatures. These samples were collected directly from the heated water itself, and therefore likely have not been significantly contaminated with near-surface groundwater. However, the other samples (though considered "class 1", Vandenbrink, 2022), may have a significant groundwater component that could obscure any real ion concentration pattern, as interacting thermal fluid with ground water could result in the sampled water taking on the ion concentration attributes of the ground water. It may be advisable to submit a reference standard representing groundwater or meteoric water to the lab for ion concentration analysis, in order to compare this to the other collected samples.

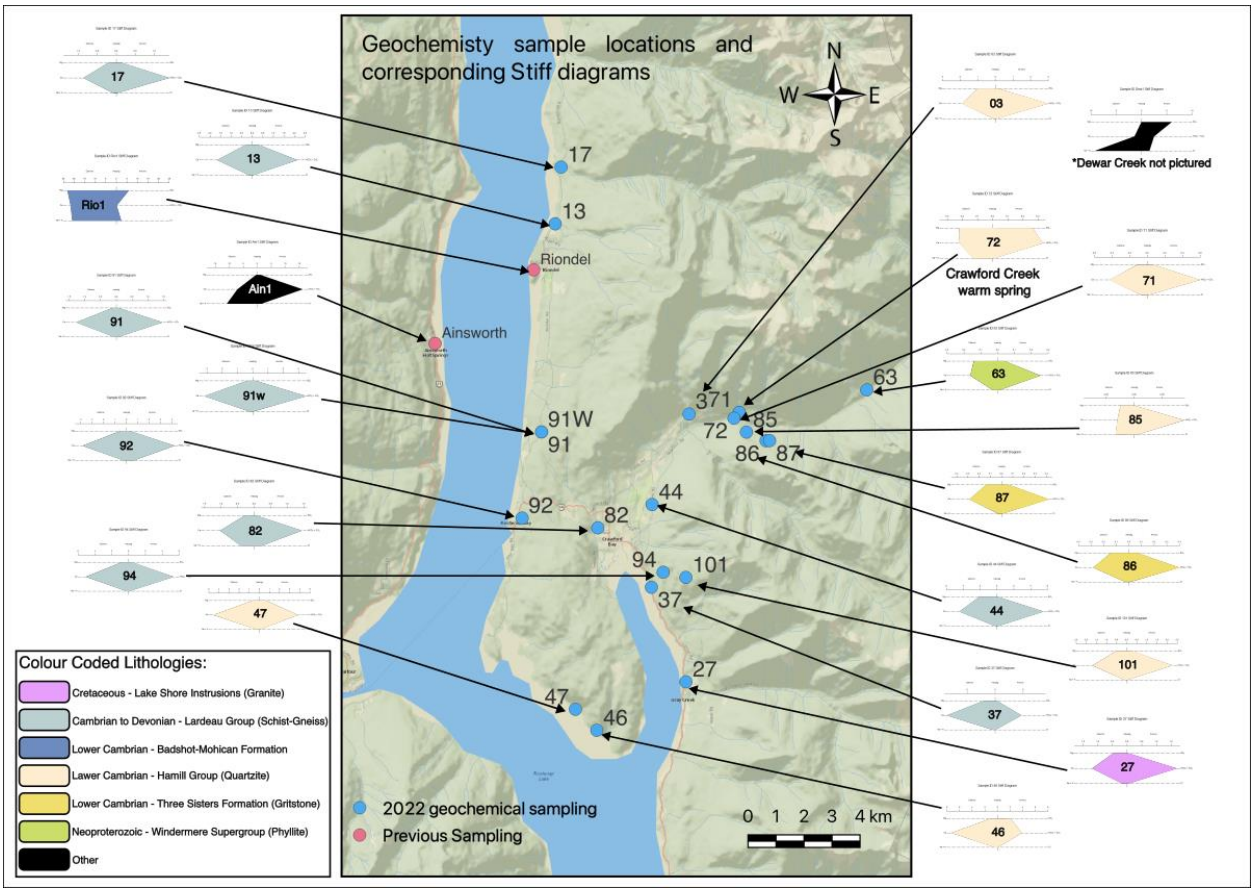

Figure 7: 2022 Geochemistry sample locations with associated ion concentrations represented by Stiff Diagrams. Produced using QGIS software and AqQA software by Rock Works. Sample 72 is the Crawford Creek warm spring sample.

Ion concentration series plot

Figure 9 directly compares the ion concentrations of each sample. Unfortunately, bicarbonate is significantly more concentrated than other ions, skewing the diagram and making the other ions difficult to interpret. The ion concentration series plot may be worth re-visiting when AqQA licensing has been rectified. Another issue with the ion concentration series plot is that Manganese was plotted in error instead of Magnesium, which is unfortunate as Magnesium may have displayed a notable relationship between samples 72, 63, and Riondel respective Stiff diagrams. Intriguingly, Sample 72, the Crawford

Creek warm spring sample, appears depleted in all ions displayed on the ion concentration series plot. Considering the significance of this sample as a highly prospective geothermal site, this may warrant further investigation. Desrochers, 1992, notes the difficulty raised by calcification of pumping pipes at the Bluebell Mine in Riondel due to the $CaMgCO_3$ rich fluid (shown on the ion concentration series plot) – perhaps this depletion of bicarbonate and other ions is a positive indication that a future geothermal well will not encounter the same calcification problem. Other notable samples include 37 and 46 due to their anomalous geothermometry heat values – however, on the ion concentration series plot, these samples show no obvious distinction between other samples.

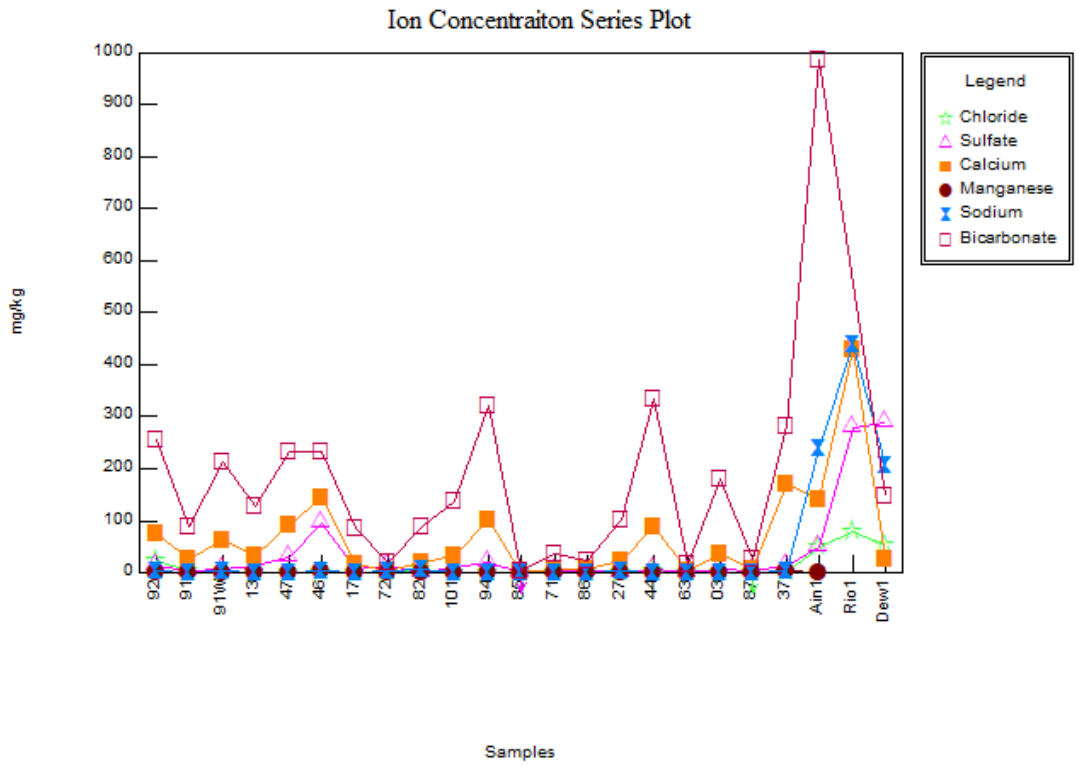

Figure 9: Ion concentration series plot showing major cations and anions for each sample. Figure generated using AqQA software by Rockworks.

RECOMENDATIONS

Geochemistry

Several recommendations are made for future investigations into the geothermal potential of the Crawford Bay area. Relating to future geochemical samples, submitting a meteoric water reference standard with potential geothermally sourced water may help in identifying which samples have been contaminated with surface water, and thus are not displaying accurate geothermometry results. Detailed descriptions and photos of geochemical sample collection locations may assist future geothermometry studies chose an appropriate geothermometer, and may allow for some kind of quantification of ground water contamination. Additionally, considering which ions are relevant to geothermal processes when analyzing ion concentrations may reveal previously unnoticed spatial or compositional correlations. Investigation into any natural CO^2 release of a geothermal system should be investigated, as Desrochers (1992) reports CO^2 leakage related to the geothermal fluids at the Bluebell Mine in Riondel.

GIS analysis

Lineament analysis was intended to be included in this report. Analyzing open-source and LiDAR and the drone data collected during phase 2 of this project for visual surface lineaments could provide a large data set from which to identify the preferred regional strain direction. Comparing this data set to other works (Risteau et al., 2007; Finley et al., 2022) could place the Crawford Bay study area in the context of regional stress orientation. Additionally, drone borne thermal imaging may be advisable to verify the anomalous temperature values generated in samples 37 and 46.

Field work

Related to future field work, further investigation into the West Bernard fault may provide further evidence of either normal or thrust movement, which would subsequently aid in interpreting the subsurface rocks of the study area. Measuring slickenlines and noting slikenfibres could help characterize fault movement in the area, thereby determining the regional stress pattern, and whether fluid pathways are actively opening or closing. Though not discussed in this report, mafic dykes can be found throughout the study area, and may warrant investigation. Finally, a geophysics survey, such as an electrical resistivity survey, may be useful for determining depths and extents of fluid reservoirs in the subsurface.

Economics

An economically focused investigation into the feasibility of a geothermally heated green house, similar to Desrocher (1992), is recommended. This investigation could provide a technical or non-technical overview of current geothermal heat exchange technology and techniques, in order to determine the minimal temperature and flow rate required to heat a certain sized greenhouse economically. In the event geothermal drilling at Crawford Bay is conducted, this report could inform future steps after determining the actual temperature and flow rate of a potential Crawford Bay geothermal system.

CONCLUSION

From metamorphic petrology, structural geology, plate tectonics, economic geology, geochemistry, seismicity, and hydrogeology, this report employs a wide spectrum of geologic disciplines and tools in an effort to characterize and better understand the geothermal potential of the Crawford Bay area. Crawford Bay's elevated heat flow/geothermal gradient, abundant fluid pathways in the form of faults and fractures, ideal regional stress field, and presence of hot springs in the vicinity all indicate the possible existence of a geothermal reservoir or resource in the Crawford Bay area. Special attention should be paid to geochemical samples 37 and 46, as these samples record elevated geothermometry estimated maximum temperatures, while siting within a continuous zone of major deformation. The Crawford Creek warm spring (geochemical sample 72) may be a favorable location for further geothermal exploration due to its highly fractured fluid flow network within Hamill quartzite, the beneficial orientation of the regional stress field, and proximity to major faults including the Purcell Trench fault, West Bernard Fault, and Orebin Creek fault.

REFERENCES

Allen, D. M., Grasby, S., & Voormeij, D. (2006). Determining the circulation depth of thermal springs in the southern Rocky Mountain Trench, south-eastern British Columbia, Canada using geothermometry and borehole temperature logs. *Hydrogeology Journal*, *14*(1-2), 159–172. https://doi.org/10.1007/s10040-004-0428-z

Arnórsson, S., Gunnlaugsson, E., & Svavarsson, H. (1983). The chemistry of geothermal waters in Iceland. III. Chemical geothermometry in geothermal investigations. *Geochimica et Cosmochimica Acta*, *47*(3), 567–577. https://doi.org/10.1016/0016-7037(83)90278-8

Arnórsson, S. (ed.). (2000). *Isotopic and Chemical Techniques in Geothermal Exploration, Development and Use*, International Atomic Energy Agency, Vienna, p. 351

Brown, D.A., MacLeod, R.F., Wagner, C.L., and Chow, W. (comp). 2011. Geology, Crawford Bay, British Columbia; Geological Survey of Canada, Open File 6307, scale 1:50 000. doi:10.4095/288566

Bruhn, D., Manzella, A., Vuataz, F., Faulds, J., Moeck, I., & Erbas, K. (2010). Exploration Methods. In E. Huenges (Eds.), *Geothermal Energy Systems* (pp. 37-112). Wiley-VCH. https://doi.org/10.1002/9783527630479.ch1

Desrochers, D. T. (1992). Geothermal feasibility study for the use of hot water near Riondel, B.C. *Geological Survey of Canada, Open File 2502, 108 pages;* 10.4095/133452. https://doi.org/10.4095/133452

Doughty, P. T., & Price, R. A. (2000). Geology of the Purcell Trench rift valley and Sandpoint Conglomerate; Eocene en echelon normal faulting and synrift sedimentation along the eastern flank of the Priest River metamorphic complex, northern Idaho. *Geological Society of America Bulletin*, *112*(9), 1356–1374. https://doi.org/10.1130/0016-7606(2000)112<1356:GOTPTR>2.0.CO;2

Finley, T. (2020). Fault-hosted geothermal systems in southeastern British Columbia. https://doi.org/10.7939/r3-r87x-jt83

Finley, T. D., Johnston, S. T., Unsworth, M. J., Banks, J., & Pana, D. I. (2022). Modern dextral strain controls active hydrothermal systems in the southeastern Canadian Cordillera. *GSA Bulletin*. https://doi.org/10.1130/B36500.1

Fournier R.O. (1977) Chemical geothermometers and mixing models for geothermal systems: Geothermics, Vol. 5, 41-50.

Grasby, S. E., Hutcheon, I., & Krouse, H. R. (2000). The influence of water–rock interaction on the chemistry of thermal springs in western Canada. *Applied Geochemistry*, *15*(4), 439–454. https://doi.org/10.1016/S0883-2927(99)00066-9

Hadlari, T., Arnott, R. W. C., Matthews, W. A., Poulton, T. P., Root, K., & Madronich, L. I. (2021). Provenance of the incipient passive margin of NW Laurentia (Neoproterozoic); detrital zircon from continental slope and basin floor deposits of the Windermere Supergroup, southern Canadian Cordillera. Lithosphere, 2021(1). https://doi.org/10.2113/2021/8356327

Höy, T. (1980). *Geology of the Riondel area, central Kootenay Arc, southeastern British Columbia* (p. 89). Ministry of Energy, Mines, and Petroleum Resources. https://cmscontent.nrs.gov.bc.ca/geoscience/PublicationCatalogue/Bulletin/BCGS_B073.pdf

Lewis, T. J., Bentkowski, W. H., & Hyndman, R. D. (1992). Crustal Temperatures near the Lithoprobe southern Canadian Cordillera Transect. In *Canadian Journal of Earth Sciences vol. 29, no. 6, p. 1197-1214; 10.1139/e92-096*. Canadian Science Publishing. https://doi.org/10.1139/e92-096

Ristau, J., Rogers, G. C., & Cassidy, J. F. (2007). Stress in Western Canada from regional moment tensor analysis. *Canadian Journal of Earth Sciences*, *44*(2), 127–148. https://doi.org/10.1139/e06-057

Ross, G. M. (1991). Tectonic setting of the Windermere Supergroup revisited. Geology (Boulder), 19(11), 1125–1128. https://doi.org/10.1130/0091-7613(1991)0192.3.CO;2

Majorowicz, J., and Grasby, S.E. (2010). Heat flow, depth– temperature variations and stored thermal energy for enhanced geothermal systems in Canada. *Journal of Geophysics and Engineering*, v. 7, p. 232–241, https:// doi.org/10.1088/1742-2132/7/3/002.

Monger, J. W. H. (2008). Evolution of Canada's western mountains. In *Geological Survey of Canada, Open File 5804*; 1 sheet; 10.4095/225581. https://doi.org/10.4095/225581

Monger, J. W. H., Price R. A., Templeman-Kluit D.J. (1982) Tectonic accretion and the origin of the two major metamorphic and plutonic belts in the Canadian Cordillera. *Geology*, 10:70–75.

Monger JWH, Price RA, Templeman-Kluit DJ (1982) Tectonic accretion and the origin of the two major metamorphic and plutonic belts in the Canadian Cordillera. Geology 10:70–75

Moynihan, D. P., & Pattison, D. R. (2011). The origin of mineralized fractures at the Bluebell Mine site, Riondel, British Columbia. *Economic Geology*, *106*(6), 1043-1058.

Sabutsch, J. (2021). *Community Geothermal Assessment 2021 Report*. Selkirk Innovates.

USGS. (2022). Earthquake Catalog. Accessed on December 8, 2022, from: https://earthquake.usgs.gov/earthquakes/search/

Verma, M. P. (2000). Limitations in applying silica geothermometers for geothermal reservoir evaluation. *Proceedings, Twenty-Fifth Workshop on Geothermal Reservoir Engineering.* https://pangea.stanford.edu/ERE/pdf/IGAstandard/SGW/2000/Verma3.pdf

Webster, E. R., & Pattison, D. R. M. (2018). Spatially overlapping episodes of deformation, metamorphism, and magmatism in the southern Omineca Belt, southeastern British Columbia. *Canadian Journal of Earth Sciences*, *55*(1), 84–110. https://doi.org/10.1139/CJES-2017-0036